The University Of Sheffield.

The mechanistic function of BICC1: its role in ADPKD pathogenesis

By:

Devon Caira Smith

A thesis submitted in partial fulfilment of the requirements for the degree of Doctor of Philosophy

The University of Sheffield
Faculty of Medicine, Dentistry and Health
Department of Immunity, Infection and Cardiovascular Disease

May 2019

Acknowledgments

I would like to thank and recognise those who helped me throughout my PhD journey, and whom without I would not have reached this great achievement.

Firstly, I would like to thank Professor Albert Ong and Dr Andrew Streets for their guidance, advice and support throughout my time at the University of Sheffield. I would like to express my sincere gratitude to my primary supervisor, Prof. Ong, for the continuous encouragement of my research, for his patience, motivation, and immense knowledge. His guidance helped me to reach great heights in my research and writing of this thesis. I could not have imagined having a better advisor and mentor for my PhD study. I would also like to express my gratitude to Dr Streets who has taught me many molecular science techniques. I appreciate all his contributions of time, ideas, and troubleshooting to make my PhD experience productive and stimulating.

Besides my supervisors, I would thank the members of the Ong lab who helped me on a day-to-day basis, whether that be with laboratory techniques, or just by making Co-IPs that little bit more bearable. Lijun (Lisa) Chang, thank you for sharing your molecular wisdom and helping me with bacterial cloning and preparing plasmids. Morgane Lannoy, thank you for the in-depth kidney discussions and showing me how to perform cyst assays – and for never taking over my lab bench space. Laura Vergoz, thank you for being my office next-door neighbour and qPCR buddy, and for showing me how to properly design primers.

I would like to acknowledge Professor Stuart Wilson and Dr Nicolas Viphakone for taking time out of their busy schedules to provide me with their wisdom and guidance when it came to designing fRIP experiments.

I greatly appreciate the support I received from the Faculty of Medicine, Dentistry and Health during my PhD. They provided fantastic training modules and also provided many opportunities to get involved in various aspects of the department, which I thoroughly enjoyed. I also gratefully acknowledge the funding I received towards my PhD from the Faculty Scholarship programme.

I would like to thank the brilliant members of the PGRS for always being there for me and providing friendly support outside of the lab. I especially thank Emily Fisk for being my SciComm and PubhD partner-in-crime and for making my time outside of the lab extra special and fun – but always still full of science!

I would like to thank my family for always supporting me throughout my research and in my life in general. To my father, for always taking an interest and supporting me in many ways. Thank you to my sister, Evie, for always listening to me after a long and stressful day and knowing how to turn my mood around. Thank you to my Nan, my aunty Nic, Helen and Barbara for always having the right remedy just when I needed it.

Lastly, I would like to thank my amazing husband Tom. Without him I wouldn't have made it to the end of this long, hard and challenging period of my life. His guidance, advice, and support were my rock. We started the PhD process together and we finished it together.

I would like to dedicate this thesis to my mother, Christina, who always saw my passion for science and always supported me in my studies.

Abstract

Autosomal dominant polycystic kidney disease (ADPKD) is the most common form of polycystic kidney disease (PKD), whose cardinal feature is the formation of fluid-filled renal and extrarenal cysts. It is the most common hereditary nephropathy and leads to 10% of end-stage renal disease (ESRD) in man. Bicaudal-C family RNA binding protein 1 (BICC1) was first identified in *Drosophila melanogaster* and is a highly evolutionarily-conserved RNA binding protein (RBP), with homologs throughout the taxonomic hierarchy. BICC1 mutant models across various species share many common phenotypes with ADPKD, including polycystic kidneys, dysfunction of multiple cellular functions and the misregulation of different signalling pathways. Several known functions of BICC1 are also shared with ADPKD-related proteins (cystoproteins). Furthermore, BICC1 shares common pathways and complexes that have a function in ADPKD, indicating that BICC1 may have a role within these interactions. The hypothesis of this study stated that BICC1 is a major interacting effector protein of the polycystin protein complex and is somehow involved in the pathogenesis of ADPKD. Using RNA immunoprecipitation and deep sequencing (RIP-Seq), mass spectrometry, co-immunoprecipitation, and *in vitro* cyst assays, it was found that BICC1 post-transcriptionally regulates its RNA targets, including *PKD2* and *ANKS3*, through forming protein interactions with translation initiation complexes, to promote mRNA translation, as well as with deadenylation complexes, to inhibit mRNA degradation and protect mRNA stability. BICC1 directly interacts with the 3' untranslated regions (UTRs) of *PKD2* and *ANKS3*, and also forms interactions with their protein counterparts in a cystoprotein complex. In summary, BICC1 is a central regulator of the major cystoproteins encoded by *PKD1* and *PKD2*, related protein networks, cellular organisation and vital signalling pathways, through direct interactions and modulation of both protein and RNA. Through its action, BICC1 contributes to the normal homeostasis of human kidney epithelial cells.

List of Figures and Tables

Chapter 1

Chapter 2

Chapter 3

Chapter 7

Abbreviations

ACDY6:	adenylate cyclase 6
ACE:	angiotensin-converting enzyme
ACTB:	beta-actin
ActD:	actinomyosin D
ADCY6:	adenylate cyclase 6
ADPKD:	autosomal dominant polycystic kidney disease
AGO:	argonaute
ANK:	ankyrin
AP-1:	activator protein 1
APF:	antiproliferative factor
ARB:	angiotensin-2 receptor blockers
ARE:	AU-rich element
ARPKD:	autosomal recessive polycystic kidney disease
ATP:	adenosine trisphosphate
BICC1:	bicaudal-C family RNA binding protein 1
bp:	base pair
BSA:	bovine serum albumin
C. elegans:	*Caenorhabditis elegans*
cAMP:	cyclic adenosine monophosphate
CC:	coiled-coil
cDNA:	complementary DNA
CEP164:	centrosomal protein 164
CFTR:	cystic fibrosis transmembrane conductance regulator
Co-IP:	co-immunoprecipitation
CT:	C-terminal tail
CT1:	PC1 C-terminal tail
CT2:	PC2 C-terminal tail
CTLH:	C-Terminal Lis-Homology domain
CTP:	C-terminal product
D. melanogaster:	*Drosophila melanogaster*
DCP1A:	decapping mRNA 1A
DCP2:	decapping mRNA 2
DMEM-F12:	Dulbecco's Modified Eagles Medium-Ham's 12
DNA:	deoxyribonucleic acid
E:	exon
ECM:	extracellular matrix
EGF:	epidermal growth factor
eGFR:	estimated glomerular filtration rate
eIF3:	eukaryotic translation initiation factor 3
eIF4F:	eukaryotic initiation factor
eIF4G:	eukaryotic initiation factor 4G
ER:	endoplasmic reticulum
ESRD:	end stage renal disease
ESWL:	extracorporeal shock wave lithotripsy
FBS:	fetal bovine serum
FDR:	false discovery rate
FRET:	Förster resonance energy transfer
fRIP:	fragmented RIP
GAIN:	GPCR-autoproteolysis inducing
GAPDH:	glyceraldehyde 3-phosphate dehydrogenase

GDP:	guanosine diphosphate
gfp:	green fluorescent protein
GFR:	glomerular filtration rate
GLD-3:	germline development defective 3
GM3S:	GM3 synthase
GO:	gene ontology
GPCR:	G protein-coupled receptor
GPS:	G-protein-coupled receptor proteolysis site
grk:	*gurken*
Gsc:	*goosecoid homeobox*
GSK3:	glycogen synthase kinase 3
GST:	glutathione S-transferases
GTP:	guanosine triphosphate
HEK:	human embryonic kidney
HIF1AN:	hypoxia inducible factor 1 alpha inhibitor
HIF1α:	HIF1-alpha
HLH:	helix-loop-helix
hnRNP K:	heterogeneous nuclear ribonucleoprotein K
HPA:	human protein atlas
I:	intron
IC:	inversin compartment
IGF:	insulin-like growth factors
IMCD:	inner medullary collecting duct
IP:	immunoprecipitation
IVS:	intervening sequence
KH:	K-homology
LIPs:	linear interacting peptides
logFC:	log fold change
MAP:	mitogen-activated protein
MEK:	mouse embryonic kidney
miRNA:	micro RNA
MMP:	matrix metalloproteinase
mRNA:	messenger RNA
MS:	mass spectrometry
mTOR:	mammalian target of rapamycin
N:	number
N. lugens:	*Nilaparvata lugens*
NEF:	nucleotide-exchange factor
negGFP:	negative gfp
NEK:	NIMA-related kinase
NHS:	national health service
NMD:	no mutation detected
NME3:	NME/NM23 nucleoside-diphosphate kinase 3
Nog:	*noggin*
NPHP:	nephronophthisis
ns:	not significant
NT2:	PC2 N-terminal tail
NTP:	N-terminal product
osk:	*oskar*
OST:	N-oligosaccharyl transferase
Ox161c1:	ADPKD epithelial cell line
P:	passage

PABP:	poly(A)-binding protein
PBS:	phosphate buffered saline
PC1:	polycystin 1
PC2:	polycystin 2
PCA:	principal component analysis
PCL1:	polycystin-like 1
PCL2:	polycystin-like 2
PCP:	planar cell polarity
PCR:	polymerase chain reaction
PDI:	protein disulphide isomerase
PI3K:	phosphoinositide-3-kinase
PIC:	preinitiation complex
PKA:	protein kinase A
PKD:	polycystic kidney disease
PKDB:	PKD database
PKI-α:	PKI-alpha
PLAT:	polycystin-1, lipoxygenase, alpha-toxin
PTEC:	proximal tubular epithelial cells
QC:	quality control
qPCR:	quantitative reverse transcriptase-PCR
RBP:	RNA binding protein
RCC1:	regulator of chromosome condensation 1
RIP:	RNA immunoprecipitation
RISC:	RNA-inducing silencing
RNA-Seq:	RNA deep sequencing
RNP:	ribonucleoprotein
RT-qPCR:	reverse-transcriptase quantitative PCR
SAM:	sterile alpha motif
SEM:	scanning electron microscope
sgRNA:	single guide RNA
shRNA:	short hairpin RNA
sia:	*siamois homeodomain1*
smFISH:	single molecule fluorescent *in situ* hybridisation
snRNA:	small nuclear RNA
SNX3:	sorting nexin 3
TAP:	tandem affinity purification
tet:	tetracycline
TKV:	total kidney volume
TMP:	transcripts per million
tral:	*trailer hitch*
TRiC:	chaperonin-containing T-complex
TRK:	tropomyosin receptor kinase
TRP:	transient receptor potential
UP_Keywords:	UniProtKB Keywords
UTR:	untranslated region
V2 receptor:	vasopressin receptor 2
wt:	*wildtype*
Xnr3:	*nodal3.1*
Y2H:	yeast two hybrid

Table of Contents

Chapter 1

Introduction

1.0 Introduction

1.1 Autosomal Dominant Polycystic Kidney Disease

Autosomal dominant polycystic kidney disease (ADPKD) is a monogenic form of polycystic kidney disease (PKD) exemplified by fluid-filled renal and extrarenal cysts (Iglesias *et al*., 1983). It is the most common hereditary nephropathy, with a prevalence of 1:400-1:1000 live births, accounting for 10% of end-stage renal diseases (ESRD) (UK Renal Registry). It is estimated that approximately 60,000 individuals in the UK suffer from the condition (UK Renal Registry), with approximately 50% of patients requiring a kidney transplant, as well as intervening treatment for pain or infection, by the age of 60 (Stengel, 2003). The characteristic nature of ADPKD begins with the formation and expansion of multiple, bilateral cysts throughout the kidneys (Iglesias *et al*., 1983), causing vast enlargement and disruption of normal function (Figures 1.1.1.1 and 1.1.1.2).

The kidneys, with a normal weight of 500 g, increase their weight by up to 15 times and expand from approximately 10 cm in length to 40 cm. ADPKD causes several extrarenal manifestations, which add to the impact of the disease (Iglesias *et al*., 1983; Torres *et al*., 2007). These include liver and pancreatic cysts, heart defects and intracerebral aneurysms. Dependent upon the severity of the disease, renal survival varies between the fifth and eighth decade of life. The disease severity can be estimated by assessing total kidney volume (TKV) while the decline of kidney function is measured clinically by changes in estimated glomerular filtration rate (eGFR) (Chang and Ong, 2008). Unsurprisingly, ADPKD puts a great burden and financial affliction on the UK National Health Service (NHS) and health companies worldwide, and therefore requires a more extensive molecular understanding to enable the development of successful treatments.

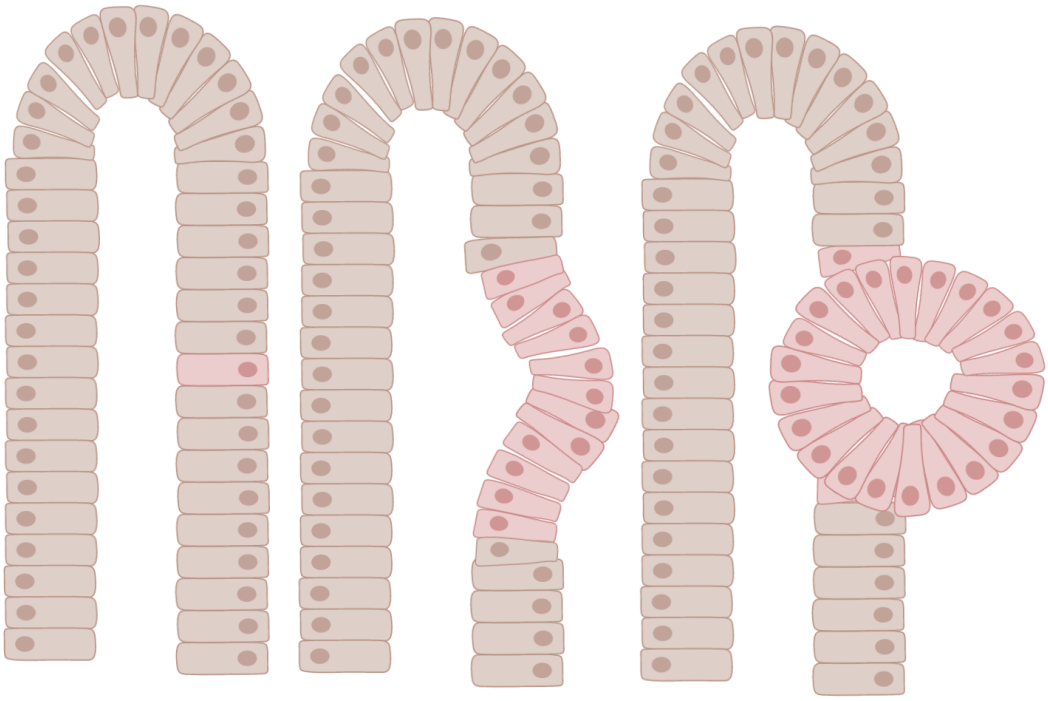

Figure 1.1.1.1. A schematic of cyst establishment and formation in ADPKD. The germline mutation allele could be either *PKD1* or *PKD2*. The 'second hit' (red epithelial cell) refers to either a second somatic mutation in the same allele, or the level of corresponding polycystin protein falls below a required threshold. The second hit leads to the growth and expansion of cysts, exacerbated by the formation of fibrosis and infiltration of inflammatory cells, as well as the collapse of some cysts and vast cell death. This schematic was generated using Biorender and adapted from Happé and Peters (2014).

ADPKD is currently incurable and treatment has been limited to that for symptoms and complications. Many ADPKD patients experience pain from urinary tract infections, burst cysts, cyst infection, pressure from the enlarged kidneys and kidney stones. Kidney stones can be removed if required by an ureteroscope or extracorporeal shock wave lithotripsy (ESWL) to dislocate and fracture the accumulated protein mass (Chang and Ong, 2008). Non-steroidal anti-inflammatory drugs can be administered to control pain relief for short periods of time, while anticonvulsants or antidepressants can be used for long-term pain relief (Chang and Ong, 2008). The majority of ADPKD patients also develop hypertension which can lead to heart attacks and aneurysm rupture. There are two widely used medications to reduce the effects of hypertension: angiotensin-converting enzyme (ACE) inhibitors and angiotensin-2 receptor blockers (ARB) (Chang and Ong, 2008).

Several clinical trials to investigate the effectiveness of new therapies to treat ADPKD have been completed. The main trials include inhibitors of mammalian

target of rapamycin (mTOR), somatostatin analogues and vasopressin receptor 2 (V2 receptor) antagonists to reduce changes in TKV and to slow the decline of glomerular filtration rates (GFR) (Chang and Ong, 2008; Torres *et al*., 2007). The TEMPO 3:4 (Tolvaptan) study (NCT00428948), which tested the efficacy of a V2 receptor antagonist, was the first successful trial. Tolvaptan was approved as a treatment for ADPKD in Europe in 2015 and in the USA in 2018. V2 receptors are G protein-coupled receptors (GPCRs) that regulate the movement of fluid from the inner medulla through the basolateral membrane of the collecting ducts. This process occurs in response to the pituitary hormone vasopressin, which acts on the collecting ducts to increase urine osmolarity by activating the secondary messenger cyclic adenosine monophosphate (cAMP) (Torres *et al*., 2007). Increased levels of cAMP activate aquaporin-2 vesicles to insert into the apical membrane of the collecting ducts, increasing water reabsorption in the kidneys, and also activate other genetic programmes which contribute to the formation of renal cysts (Katsura *et al*., 1997; Moeller *et al*., 2009).

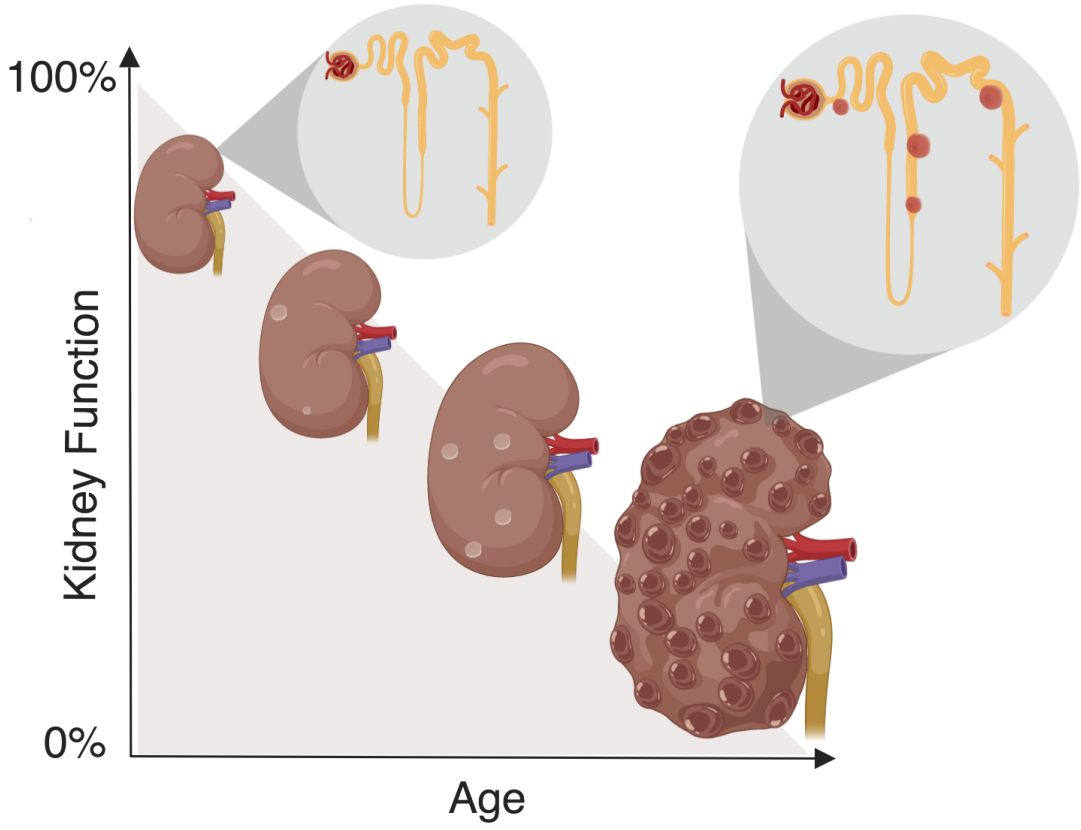

Figure 1.1.1.2. A schematic of ADPKD progression over time. In ADPKD, cystogenesis increases as a patient ages causing their kidney function to decrease. The grey circles highlight the difference between a normal kidney nephron and an ADPKD nephron that has developed several cysts. This schematic was generated using Biorender and adapted from the PKD Foundation (2019).

1.2. PKD genes

ADPKD is a genetically heterogeneous disease with two major disease-causing loci: *PKD1* and *PKD2*. Although the majority of ADPKD patients have a mutation in either of these loci, approximately 9% of cases have no detectable mutation (NMD). This has led to the postulate of a third locus, or additional undetected mutations at the known loci (Audrézet *et al*., 2012; Rossetti *et al*., 2007). Despite various research groups publishing regarding the third locus, referred to as *PKD3,* a recent collaborative study by Paul and colleagues has disregarded this notion (Paul *et al*., 2014). After re-analysis of data used by the previous studies regarding five ADPKD families with no apparent *PKD1* or *PKD2* linkage, it was discovered that each of the families did have either a *PKD1* or *PKD2* mutation. This event has highlighted the vital requirement for accurate and comprehensive mutation screening for ADPKD patients, as this was not originally completed for these five families.

1.2.1 *PKD1*

PKD1 was first identified as the causative gene locus for ADPKD (The European Polycystic Kidney Disease Consortium 1994). The gene is located on chromosome 16p13.3 and encodes polycystin 1 (PC1). In its uncleaved and glycosylated form, PC1 is a 4303 amino acid protein with a molecular weight of around 600 kDa. It is predicted to be a 11-transmembrane receptor, with a large 3074 amino acid ectodomain, which extends into the extracellular matrix or space. PC1 is believed to form a complex with polycystin 2 (PC2) through its C-terminal (CT) tail to regulate the influx of calcium ions in renal epithelial cells. The formation of the polycystin complex is also believed to be necessary to traffic the polycystins to the plasma membrane of the epithelial cell and primary cilia, where they are thought to function (Nauli *et al*., 2003; Xu *et al*., 2003; Yoder, 2002). Recent studies have demonstrated that the levels of PC2, as well as complex formation, is essential for the trafficking of PC1 to the cilia membrane (Cai *et al*., 2014; Gainullin *et al*., 2015; Su *et al*., 2015).

PC1 has a phosphorylated CT tail and a 200 amino acid coiled-coil domain, which binds PC2 (Newby *et al*. 2002; Streets *et al*. 2013). This domain also contains a G-protein motif, which binds and thus activates G-proteins. It can

also bind protein phosphatases, and this interaction could regulate polycystin phosphorylation as well as the phosphorylation of other signalling pathways, including Wnt signalling (Streets *et al*., 2013). Of interest, the extracellular domain of PC1 contains 16 multiple copies of a unique domain which can undergo folding and unfolding. This domain is referred to as the PKD domain (Bycroft *et al*., 1999). PC1 contains a G-protein-coupled receptor (GPCR)-autoproteolysis inducing (GAIN) domain linked to a G-protein-coupled receptor proteolysis site (GPS) motif (Araç *et al*., 2012). The GAIN domain induces cis-acting autoproteolysis of PC1 to create two halves: a N-terminal product (NTP) and C-terminal product (CTP), which remain attached by non-covalent bonds (Yu *et al*., 2007; Araç *et al*., 2012). The functional role of GPS cleavage is unclear but may be essential for the protein to traffic from the endoplasmic reticulum (ER) and the Golgi after processing or stabilise the protein for its function (Yu *et al*., 2007). The polycystin-1, lipoxygenase, alpha-toxin (PLAT) domain of PC1 binds Ca^{2+} and phospholipids, whilst forming a stable scaffold to enable cell signaling and PC1 retrograde trafficking (Xu *et al*., 2016). A representative structure of PC1 is illustrated in Figure 1.2.1.1.

Mutations within this gene locus are found in 78% of pedigrees and account for up to 85% of all ADPKD cases (Audrézet *et al*., 2012; Rossetti *et al*., 2007). The specific nature of the mutations can vary between patients and family members, but *PKD1* mutations lead to the most severe form of the disease with the probability of developing ESRD at 58.1 years. Examination of the PKD database (PKDB) (accessed 27th March 2019) has demonstrated that in the 1874 families reported, there were 1271 different mutations in the *PKD1* gene. 65% of the mutations produce a truncated PC1 protein, believed to cause the most severe disease outcomes, while the remaining 35% produce a non-truncated protein (Cornec-Le Gall *et al*., 2013).

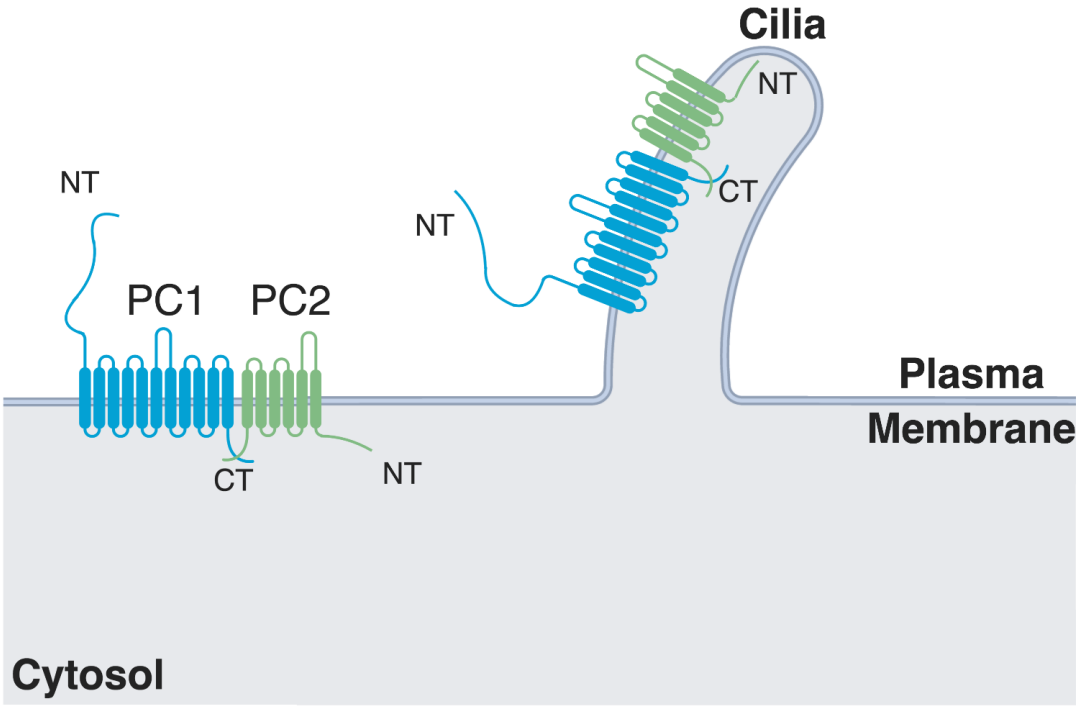

Figure 1.2.1.1. The polycystin protein complex. The polycystin proteins are predicted to form a complex through an interaction of their C-terminal tails. Research has demonstrated the polycystin complex to be present on both the plasma membrane and the cilia. This schematic was generated using Biorender.

1.2.2 *PKD2*

PKD2 was identified after the discovery of *PKD1* as a second locus for ADPKD (Mochizuki *et al*., 1996). The gene is located on chromosome 4q22 and encodes for PC2. PC2 has a predicted molecular weight of approximately 110 kDa comprising 968 amino acids. It is a 6-transmembrane Ca^{2+}-responsive permeable cation channel (Figure 1.2.1.1) with high conductance and is a member of the transient receptor potential (TRP) channel superfamily. Hence, PC2 is often referred to as TRPP2. PC2 is predominately localised to primary cilia, apical and basolateral membranes and exosomes, but it is also strongly localised to the ER to regulate intracellular calcium release and calcium stores (Koulen *et al*., 2002; Nauli *et al*., 2003; Xu *et al*., 2003; Yoder, 2002).

Similarly to PC1, PC2 contains two coiled-coil (CC) domains, CC1 and CC2, in its C-terminal domain (CT2). CC2 forms oligomers of PC2 which is essential to facilitate the binding of PC1 at its C-terminus (CT1) (Giamarchi *et al*., 2010). Upstream of CC2 is the EF-hand domain, which encompasses a Ca^{2+} binding

motif (Petri *et al*., 2010). PC2 has been shown to form high order structures such as tetramers, a function common to other TRP family members (Feng *et al*., 2008; Zhang *et al*., 2009; Feng *et al*., 2011). Membrane-targeting motifs have also been identified in PC2 proteins, specific for cilium (^{6}RVxP^{9}) and the plasma membrane (^{572}KxxxF^{576}) (Geng *et al*., 2006). Recent studies have suggested that glycogen synthase kinase 3 (GSK3) and PKA-cAMP-mediated pathways, possibly independent of PC1, may control the trafficking of PC2 to the cilia and plasma membrane (Streets *et al*., 2006, 2013).

Mutations within this gene locus are found in 13% of ADPKD pedigrees and account for up to 15% of all cases (Audrézet *et al*., 2012; Consugar *et al*., 2008; Rossetti *et al*., 2007). The specific nature of the mutations can vary between patients and family members, but *PKD2* mutations are associated with a less severe renal phenotype than *PKD1* mutations, with the probability of developing ESRD at 79.7 years. Examination of the PKDB (accessed 27th March 2019) has demonstrated that in 438 reported families, there were 202 different mutations in *PKD2*. 87% of the mutations produce a truncated PC2 protein, while the remaining 13% of reported mutations produce a non-truncated protein (Consugar *et al*., 2008). Mutation in PC2 induces cyst formation and kidney disease probably through decreasing intracellular Ca^{2+} leading to an increase in total cAMP and consequent downstream signalling (Gonzalez-Perrett, 2000).

1.2.3. Protein-protein interactions of PC1 and PC2

As previously mentioned in section 1.2.1, PC1 has a phosphorylated CT tail which binds PC2 (Newby *et al*. 2002; Streets *et al*. 2013). PC1 also binds to other proteins and carbohydrate ligands through its various domains, a function thought to localise the protein to basolateral and apical membranes of the cell (Tritarelli *et al*. 2004). Malhas and colleagues (2002) have reported protein interactions between the extracellular leucine-rich repeats of PC1 and various components of the extracellular matrix including collagen I, fibronectin and laminin. The G-protein activating sequence of PC1 binds and activates heterotrimeric G-proteins and other G-protein regulators such as RGS7 (Kim *et al*., 1999). Through glutathione S-transferases (GST) pull-down and *in vitro* filament assembly assays, Xu and colleagues (2001) have demonstrated

interactions between CT1 and the intermediate filament proteins vimentin, cytokeratin K8, cytokeratin K18, and desmin. In addition, CT1 was found to interact with Siah-1, a protein believed to regulate PC1 through the ubiquitin-dependent proteasome pathway (Kim *et al*., 2004). Although less studied, the PLAT domain of PC1 binds Ca^{2+} and phospholipids, whilst forming a stable scaffold to enable localised cell signaling and PC1 retrograde trafficking (Xu *et al*., 2016). The known protein interactions of PC1 are summarised in Figure 1.2.3.1.

PC2 has been reported to interact with multiple proteins including, alpha-actinins, actin-binding and actin-bundling proteins (Li *et al*., 2005). Alpha-actinin binds the N-terminus and C-terminus of PC2 and stimulates its channel activity. Interestingly, alpha-actinins have a role in regulating cytoskeleton organisation, cell adhesion, proliferation and migration. More recently, others have discovered an interaction between PC2 and the retromer complex. Specifically, an interaction was observed with retromer-associated protein sorting nexin 3 (SNX3), a component of a complex of proteins involved in the endo-lysosomal network and responsible for the sorting of integral membrane proteins (Feng *et al*., 2017; Tilley *et al*., 2018). This interaction occurs through the N-terminus of PC2 and the researchers suggest that this confirms PC2 as a retromer cargo protein. The known protein interactions of PC2 are summarised in Figure 1.2.3.2.

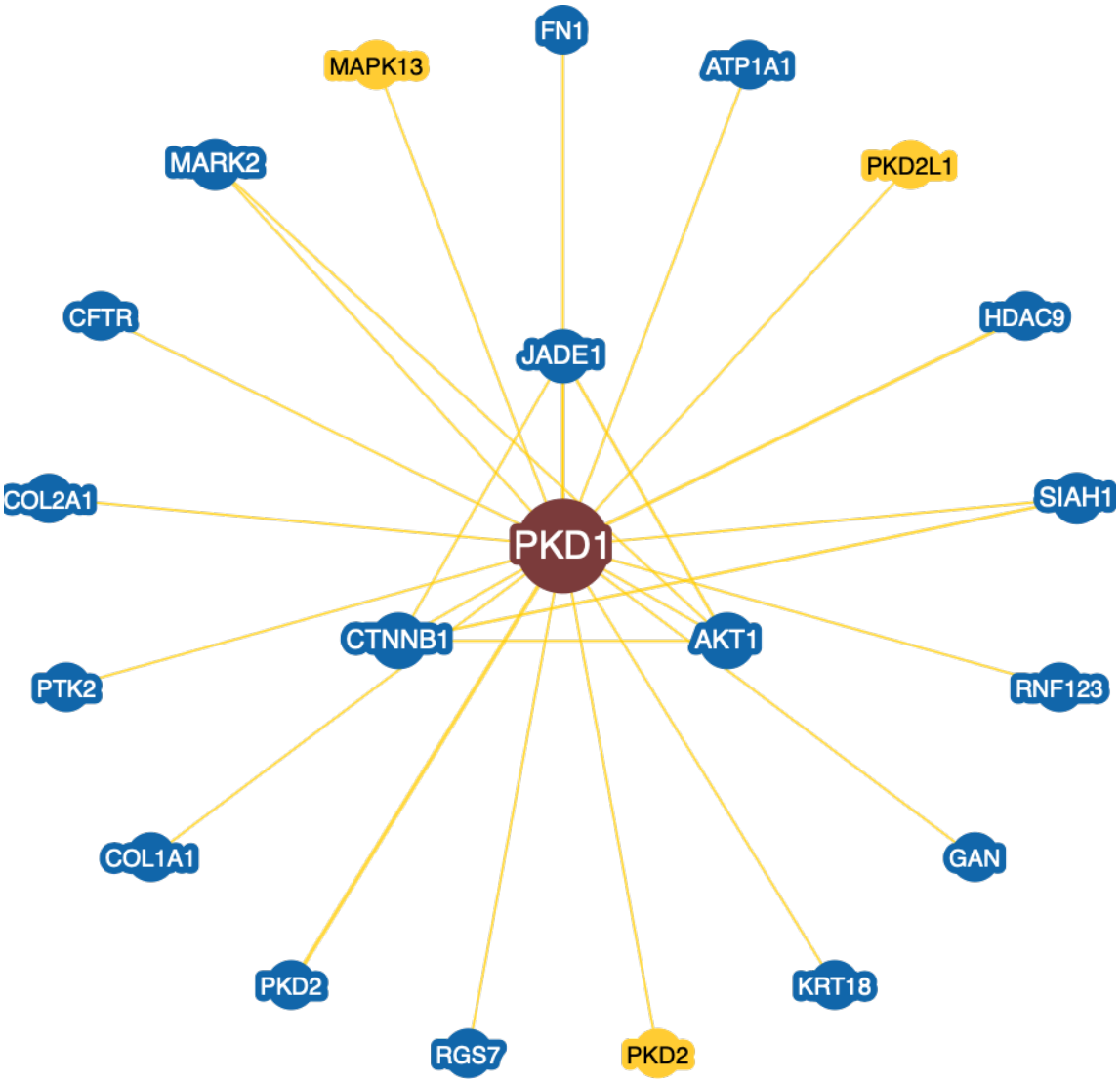

Figure 1.2.3.1. The protein network of *PKD1*. Interactions of polycystin 1 were explored using BIOGRID (accessed 20th April 2019). All the proteins represented have been validated experimentally (highlighted by yellow connecting lines). Proteins highlighted in blue represent associations within the same organism, while proteins highlighted in yellow represent associations from a different organism. Proteins positioned towards the centre are more closely associated.

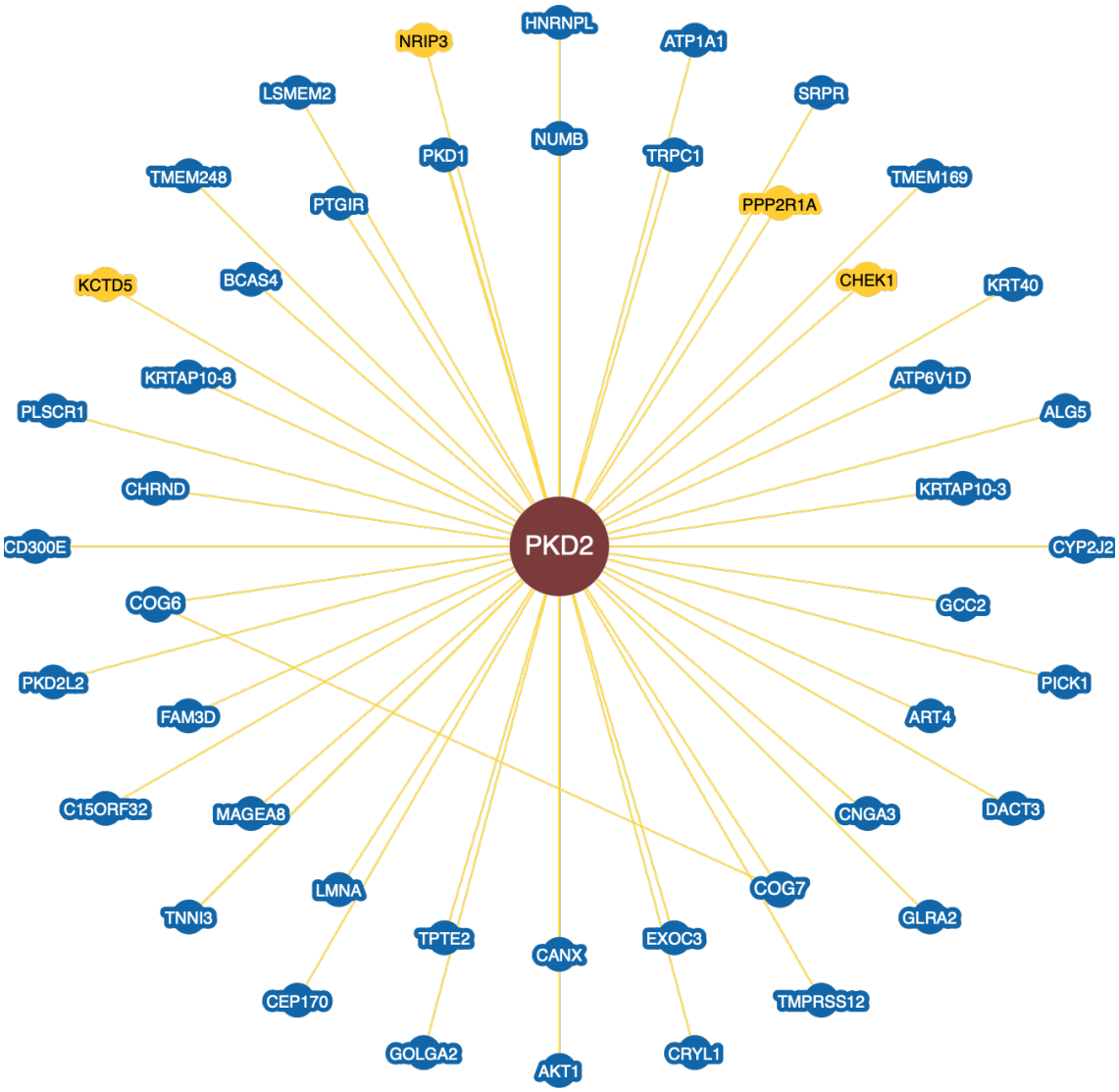

Figure 1.2.3.2. The protein network of *PKD2*. Interactions of polycystin 2 were explored using BIOGRID (accessed 20th April 2019). All the proteins represented have been validated experimentally (highlighted by yellow connecting lines). Proteins highlighted in blue represent associations within the same organism, while proteins highlighted in yellow represent associations from a different organism. Proteins positioned towards the centre are more closely associated.

1.3 Cystogenesis in ADPKD: the dosage model

As discussed above, ADPKD has great allelic heterogeneity. However, due to technological advancements, the genetics, phenotypic variability and disease course is becoming apparent. Still, the nature of the disease is complex and complete understanding of exactly how cysts form and why there is such variability between patients, family members and the effects of PKD mutations has not been attained. Consequently, there has been widespread debate over the precise establishment and expansion of cysts in ADPKD. Five main

concepts have been proposed, all of which could contribute to the formation of cysts. They include an increase in cellular proliferation, apoptosis and fluid secretion; abnormal cell polarity; defective cilia (discussed further below) and malfunctioning cell-matrix cross talk (Torres *et al*., 2007; Ong and Harris, 2015).

Although the precise mechanisms linking proliferation and apoptosis in ADPKD remain to be elucidated, there is some evidence that they both play a crucial role in cystogenesis. Cyst expansion has been closely linked to abnormal proliferation in tubular epithelial cells and was detected in young cysts and dilated tubules from human ADPKD samples and mouse models of sporadic ADPKD (Lantinga-van Leeuwen *et al*., 2007). Furthermore, combinations of increased apoptosis and cell proliferation has been observed in ADPKD kidney tissues samples, including renal tubular epithelial cells (Edelstein, 2005). Interestingly, dysregulation of proliferation and apoptosis has also been shown to disrupt PCP (Patel *et al*., 2008).

A disconnection from the glomerular filtrate has been observed for several tubular cystic lesions. Researchers suggest this may be due to dysregulation of net transepithelial fluid secretion through a loss of efferent and afferent tubule connections (Davidow *et al*., 1996), Moreover, cell division of cysts was shown to be stimulated by the swelling and stretching of cysts due to fluid accumulation (Li *et al*., 2004). These data demonstrate the importance of fluid secretion on cyst formation and expansion.

Various integrin-related cell-cell and cell-matrix interactions are disrupted in ADPKD. Two examples include the overexpression of extracellular matrix proteins in several ADPKD models and an increase in cyst lining epithelial cells demonstrating elevated adhesiveness to type I and type IV collagen in response to growth factors (Drummond, 2011). On another note, renal cilia are mechanosensors and function in response to fluid flow. However, this function is lost in PC1 mutant models, which leads to abnormal calcium signals in response to fluid flow (Nauli *et al*., 2003).

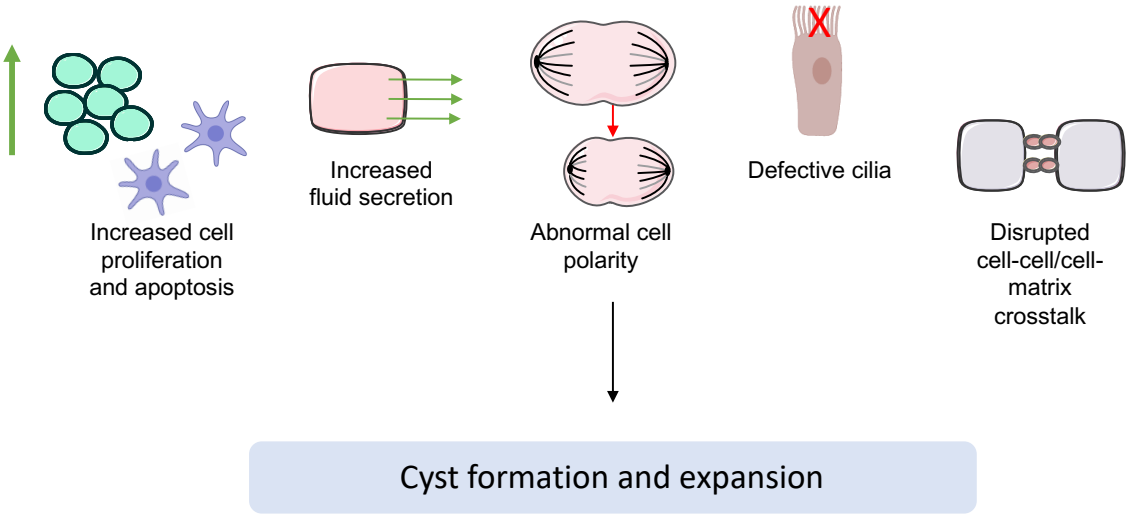

Figure 1.3.1.1. The five main concepts driving cysts expansion in ADPKD. Increased cellular proliferation, apoptosis and fluid secretion; abnormal cell polarity; defective cilia and disrupted cell-cell/cell-matrix crosstalk have been theorised to lead to cyst formation and expansion in ADPKD (Edelstein, 2005; Lantinga-van Leeuwen *et al*., 2007; Patel *et al*., 2008; Drummond, 2011; Ong and Harris, 2015).

Another idea that has been investigated is that of a phenotypic switch of the normal function of renal tubular epithelial cells from being primarily absorptive to primarily secretory. In ADPKD patients, increased secretion of the anion chloride has been observed with the passive movement of water and sodium into the cyst lumen (Sullivan *et al*., 1998). Chloride secretion is mainly mediated by the chloride membrane channel cystic fibrosis transmembrane conductance regulator (CFTR), although a role for other calcium activated chloride channels has been reported (Sullivan *et al*., 1998). Intracellular cAMP and extracellular adenosine trisphosphate (ATP) can both increase chloride secretion (Wallace *et al*., 1996).

Cell polarity is essential to maintain normal tubular cell structure and function. In cystic cells acquired from ADPKD patients, the transmembrane protein E-cadherin was relocated to the apical surface in some studies. The resulting loss of polarity may lead to the mislocalisation of other basement membrane proteins, for example laminin and type IV collagen, required to maintain the basement membrane structure (Charron, 2000). Abnormalities in planar cell polarity (PCP) and oriented cell division has also been observed in cystic cells and tubules (Charron, 2000; Fischer *et al*., 2006). These changes are believed to lead to an increase in tubular epithelial cell number and tubular diameter,

leading to the eventual loss of tubular architecture in cystic cells (Figure 1.1.1.1).

1.4. Signalling pathways and mechanisms altered in ADPKD

The complexity and variability of ADPKD has led scientists to believe that various influencing factors and/or pathways are involved in the establishment and disease development. Some of these factors are illustrated in Figure 1.4.1.1 and are discussed below.

In normal renal epithelial cells, the polycystin complex acts as a flow detector; assessing and measuring the flow and pressure of urine, as it is known that cilia are able to detect flow. The polycystin complex induces Ca^{2+} influx in response to the presence of flow, which triggers downstream signalling pathways for normal cilia function and the differentiation of renal cells. Research supporting this idea demonstrates that a decrease in PC1 and PC2 levels results in a decrease in Ca^{2+} influx (Chebib *et al*., 2015). However, the sole function of the polycystin complex in Ca^{2+} regulation in renal epithelial cells is debated. Whether changes in Ca^{2+} levels in renal epithelial cells affect the kidneys on a large scale, or whether the polycystin complex solely regulates Ca^{2+} levels in the cilia is unclear. It has also been suggested that the polycystin complex may function in a cilia-based signalling pathway, unrelated to calcium-related regulation of cAMP (Chebib *et al*., 2015). It is possible that a ligand or a stimulus is required to activate the polycystin complex.

In 2016, Kim *et al*. identified WNT9B, a Wnt ligand, to bind and interact with the extracellular domain of PC1 to activate *PKD2*-dependent Ca^{2+} influx and induce whole cell currents. Wnt ligands induce Ca^{2+} signalling on target cells, which regulates essential cellular functions. Wnt signalling has become an important focus within ADPKD research, as it is comprised of a variety of signalling cascades that can be activated by secreted Wnt ligands. Two major signalling cascades include the canonical or β-catenin pathway and the PCP pathway, previously discussed in section 1.3. Both of these pathways are important for kidney development and homeostasis, and their disruption can cause PKD. More recently, two Wnt inhibitors successfully suppressed cystogenesis and

extended the survival of mice with ADPKD (Li *et al*., 2018). The researchers suggest that inhibiting the production of Wnt proteins, disrupting the stability of β-catenin or genetically altering its expression reverse the effects caused by elevated β-catenin signalling in *Pkd2* deficient models (Li *et al*., 2018).

It is likely that mutations in *PKD1* and *PKD2* result in abnormal downstream signalling in renal epithelial cells leading to cyst formation, cyst growth and disease progression. A major pathway altered in ADPKD patients is the mTORC1 pathway, where mTOR is over-activated (Shillingford *et al*., 2006; Distefano *et al*., 2009). mTOR is thought to be a master regulator, controlling many cellular processes including proliferation, survival and transcription. Another common pathway disrupted in ADPKD is the MAPK/ERK pathway. In this deregulated pathway, tyrosine receptor kinase (TRK) and protein kinase A (PKA) are activated, concurrently activating MEK/ERK through the induction of Src/Ras/BRAF (Yamaguchi *et al*., 2003). Furthermore, ERK signalling is also stimulated by GPCRs as well as intracellular calcium (Yamaguchi *et al*., 2003).

C- MYC, a nuclear phosphoprotein transcription factor, vital for transcriptional regulation, is also overexpressed in ADPKD (Trudel *et al*., 1997; Couillard *et al*., 2002). In turn, this can lead to an increase in both apoptosis and proliferation, as well as an increase in the cell survival deacetylation protein SIRT1 (Trudel *et al*., 1997; Couillard *et al*., 2002). This occurs despite an equal increase in the tumour-suppressor gene p53 and the anti-apoptotic Bcl-2 protein. A possible treatment target for ADPKD is the transcription factor STAT3 (Weimbs *et al*., 2013). In normal adult kidneys STAT3 levels are low, whereas the level is much increased in the epithelial cells that line ADPKD cysts (Takakura *et al*., 2011). The abnormal activation of STAT3 leads to increased activation of growth factors, cytokines and chemokines, which consequently activate macrophages. This could result in an increased inflammatory response through factors secreted by the cystic cells (Karihaloo *et al*., 2011; Swenson-Fields *et al*., 2013). Proposed alterations in signalling pathways and mechanisms in ADPKD are demonstrated in Figure 1.4.1.1.

A major topic of debate in the ADPKD field is the effect of *PKD1* and *PKD2* mutations on Ca^{2+} signalling, especially regarding the idea of the polycystin

complex in the cilia. Research has suggested that mutations in *PKD1* and *PKD2* cause upregulated expression of renal developmental genes, inducing an increase and decrease in the expression of proto-oncogenes and tumour-suppressor genes respectively. This mis-regulation of vital regulatory genes leads to over proliferation of renal epithelial cells. The mutations have also been linked to mis-regulation between intracellular Ca^{2+} and cAMP interactions (Gattone *et al*., 2003; Wang *et al*., 2010; Yamaguchi *et al*., 2006). A study has identified PC1 and PC2 localisation to the cilium (Yoder, 2002). However, its exact function is still unclear. It is believed that the Ca^{2+}-responsive channel PC2 becomes defective; lowering the intracellular Ca^{2+} levels whilst increasing both PKA signalling and cAMP. Ca^{2+} stores in the ER have also been observed to decrease when *PKD2* is mutated (Gattone *et al*., 2003; Wang *et al*., 2010; Yamaguchi *et al*., 2006).

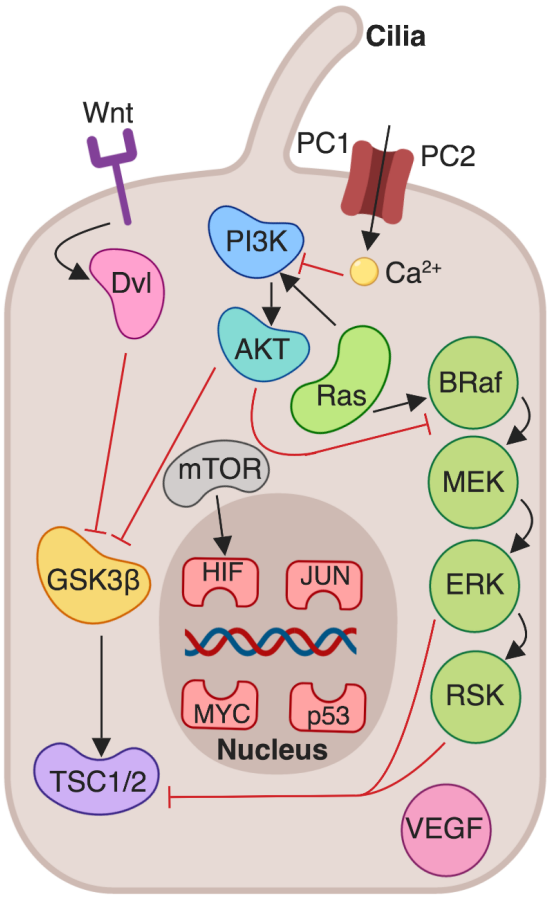

Figure 1.4.1.1. A simplified representation of some of the major pathways mis-regulated in ADPKD. Research has demonstrated various important cellular pathways to be implicated in ADPKD, including calcium, cAMP, MAPK/ERK, Wnt, and mTOR. This schematic was generated using Biorender and adapted from Floege *et al*., (2015). Note: the colouring used has no importance and was just used to differentiate between different pathways.

1.5 Bicaudal-C Family RNA Binding Protein 1

1.5.1 Introduction to Bicaudal-C family RNA binding protein 1

Bicaudal-C family RNA binding protein 1 (BICC1) is an evolutionarily conserved RNA binding protein (RBP) with homologs throughout the taxonomic hierarchy (Figure 1.5.1.2). The human *BICC1* gene is located on chromosome 10q21.3 and encodes a 974 amino acid protein, with a molecular weight of approximately 110 kDa (Uniprot, release 2019_02). The human BICC1 protein consists of two sets of functional domains and a central intervening sequence (IVS) of unknown function. Two eukaryotic type I K-homology (KH) domains are located towards its N-terminus, while a single sterile alpha motif (SAM) domain is located towards its C-terminus (Figure 1.5.1.1). The number of KH domains differs across species. For example, as previously stated, human BICC1 contains two KH domains, mouse and rat BICC1 homologs contain three KH domains, while in flies, insects and worms, BICC1 has five KH domains (Uniprot, release 2019_02). However, all homologs contain at least the last two KH domains and a single SAM domain (Figure 1.5.1.3).

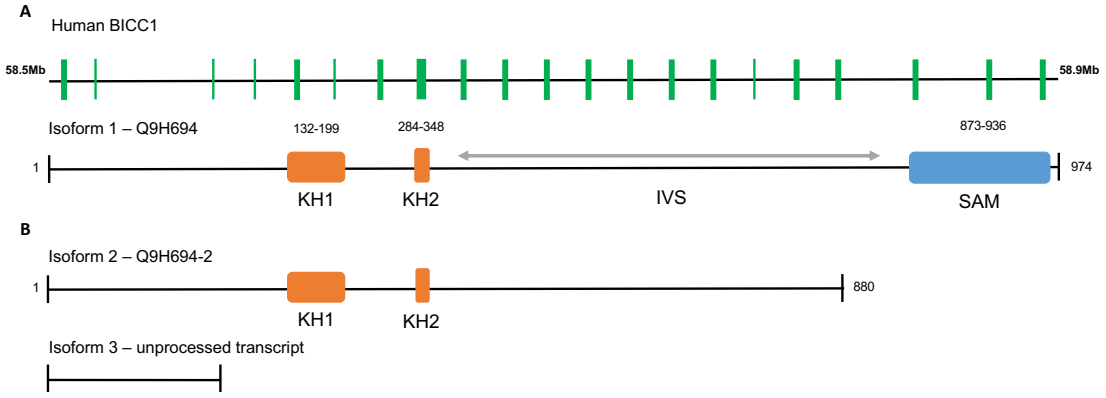

Figure 1.5.1.1. Schematic representation of human BICC1. A) A representation of the human BICC1 gene. The black line represents the introns, while the green boxes represent the 21 exons. The protein domains of Isoform 1 (Q9H694), the canonical sequence, are also represented, overlapping the exons from which they are encoded. **B)** The protein domains of Isoform 2 (Q9H694-2), lacking the SAM domain, and Isoform 3 which is an unprocessed transcript. The amino acid position of the protein domains is denoted above the domains. The isoforms were accessed from Uniprot (release 2019_02). KH1= K homology 1 (orange), KH2= K homology 2 (orange), IVS= intervening sequence, SAM= sterile alpha domain (blue).

KH domains were first discovered in the ribonucleoprotein, heterogeneous nuclear ribonucleoprotein K (hnRNP K), a protein responsible for mRNA processing (Siomi *et al*., 1993). The KH domain of hnRNP K recognises and binds to pre-mRNA through the formation of a hydrophobic cleft, in order to

process messenger RNA (mRNA), either by promoting translation or mRNA degradation (Siomi *et al*., 1993). Globally, KH domains function to bind RNA molecules. SAM domains have been shown to mediate several diverse biological processes, including the binding of RNA. However, they frequently self-associate or form SAM-SAM interfaces, commonly in a head-to-tail manner, with other SAM-containing proteins to form multi-protein complexes for particular functions, depending on the proteins involved. Due to its functional domains and initial experimentation, BICC1 has been classified as an RBP responsible for the post-transcriptional regulation of target mRNA transcripts.

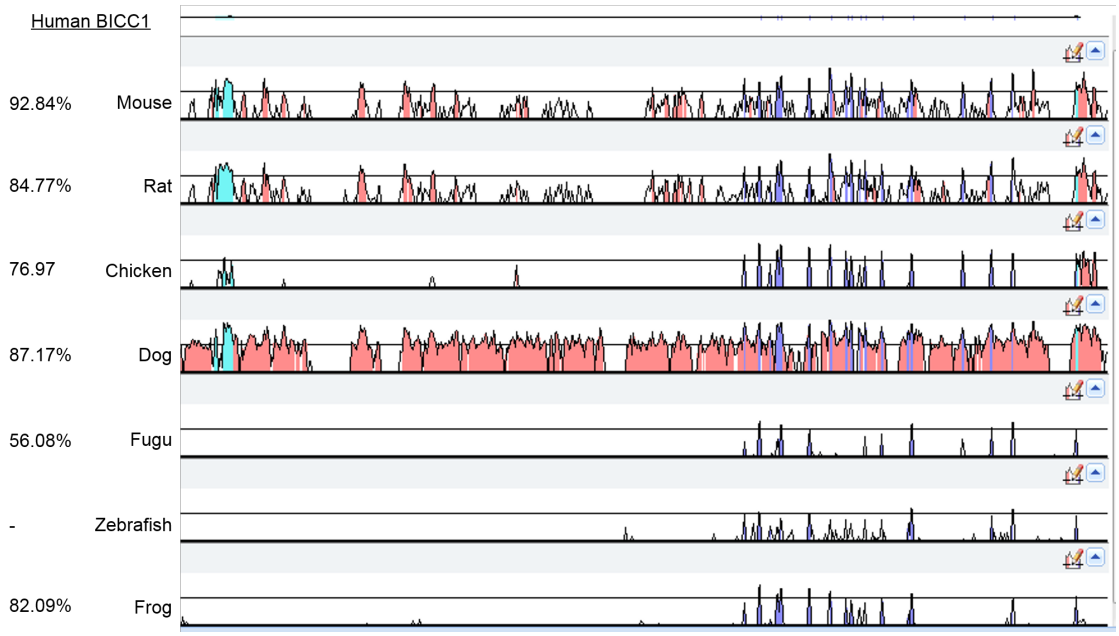

Figure 1.5.1.2. BICC1 is evolutionarily conserved across species. The peaks that are coloured demonstrate a region that has a minimum of 50% conservation to the human BICC1 gene. The wider the peak, the larger the conserved area, in terms of base pairs. The blue peaks represent 5' and 3' UTRs (from left to right), the purple peaks represent exons and the pink peaks represent non-coding regions. The percentage of conservation to human BICC1 was obtained from the UniProt database (release 2019_02) and the graph was generated using Vista Genome Browser (accessed 28th March 2019). Note that *C. elegans* was not available for comparison. BICC1 accession numbers included Q9H694 (Human), Q99MQ1 (Mouse), P0C0T2 (Rat), A0A1D5PXG4 (Chicken), F1PUI0 (Dog), H2T9W2 (Fugu), X1WGP5 (*Zebrafish*), Q9IA00 (*Xenopus*).

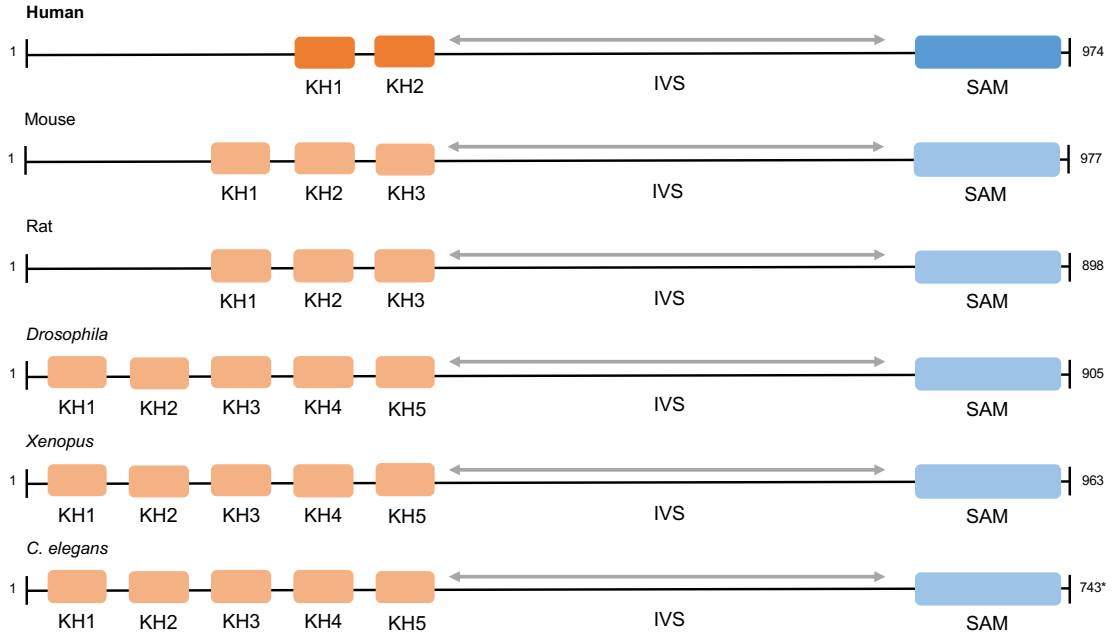

Figure 1.5.1.3. Schematic representation of the number of functional BICC1 domains across different species. Human BICC1 contains two KH domains, mouse and rat Bicc1 contain three KH domains, *Drosophila*, *Xenopus* and *C. elegans BicC* contain five KH domains, and all BICC1 species contain one SAM domain. The protein sequences were accessed from Uniprot (release 2019_02). BICC1 accession numbers included Q9H694 (Human), Q99MQ1 (Mouse), P0C0T2 (Rat), Q24009 (*Drosophila*), Q9IA00 (*Xenopus*), Q95ZK7 (*C.elegans*). KH= K homology (orange), IVS= intervening sequence, SAM= sterile alpha domain (blue).

BICC1 was first identified in *Drosophila melanogaster* (*D. melanogaster*) by Lasko and colleagues in 1995, and was referred to as *BicC* (Mahone *et al*., 1995). The researchers discovered *BicC* by a mutagenic screen during investigations of anterior patterning and oocyte development. Further studies established a requirement of *BicC* for proper anterior-posterior patterning, as *in vivo* mutations within the second and third KH domains prevented normal localisation and translation of *oskar* (*osk*), an essential RNA required for posterior embryonic development. *BicC* sequestered *osk* to the posterior pole (Saffman *et al*., 1998). The *BicC* protein and its RNA also accumulated within the early oocyte, suggesting a vital role in oocyte development (Saffman *et al*., 1998). *BicC* also plays an essential role in the metamorphosis of *Nilaparvata lugens* (*N. lugens*), a planthopper insect pest (Zhang *et al*., 2015). This study confirms a role for *BicC* as a post-transcriptional regulator of developmental processes in a second insect model.

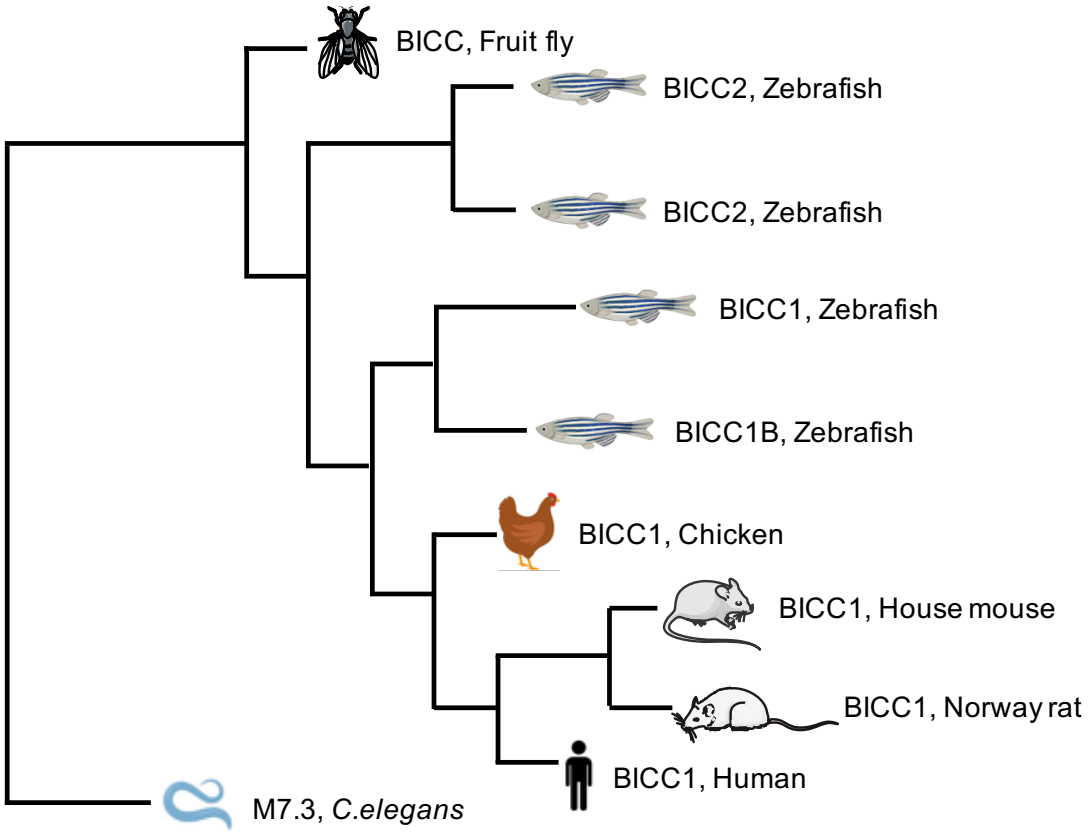

Figure 1.5.1.4. Phylogenetic tree of BICC1. The phylogenetic tree was produced using TreeFam (EMBL-EBI, accessed 20th April 2019). BICC, Fruit fly: FBgn0000182; BICC2, Zebrafish: ENSDARP00000098252.1; BICC1, Zebrafish: ENSDARP00000082675.4; BICC1B, Zebrafish: ENSDART00000103526.6; BICC1, Chicken: ENSGALP00000002859.4; BICC1, House mouse: ENSMUST00000143791.7; BICC1, Norway rat: ENSRNOT00000000754.6; BICC1, Human: ENST00000373886.8; M7.3, *C.elegans*: WBGene00000246.

A homolog of BICC1, Gld-3, has also been identified in *Caenorhabditis elegans* (*C. elegans*) (Figure 1.5.1.4). Gld-3 controls germline sex determination by binding to another RBP, Fbf, to inhibit its repressive function on target mRNAs (Nakel *et al*., 2010). In this way, Gld-3 promotes spermatogenesis, determining the fate of the developing oocyte. A BICC1 homolog, referred to as Bicc1, was also found in *Xenopus* models and is responsible for regulating oogenesis and embryogenesis through the initiation of endoderm formation by specifying mRNA localisation (Wessely and De Robertis, 2000). The researchers reported that loss of all five of the RNA-binding domains inhibited endoderm formation, highlighting the requirement of the KH domains for proper Bicc1 function (Wessely and De Robertis, 2000). Additional research in *Xenopus* has demonstrated that Bicc1 controls the transformation of the pronephros into mesonephros, thereby initiating kidney development, as well as embryonic development (Tran *et al*., 2007).

More recently, Park *et al*., (2016) have identified a novel role for maternal Bicc1 in regulating vertebrate embryogenesis. A reduction in the level of maternal Bicc1 in *Xenopus* embryos disrupted normal embryonic patterning, due to an over-expression of organiser-specific genes including *siamois homeodomain1 (sia1), goosecoid homeobox (gsc), nodal3.1 (xnr3) and noggin (nog)*, which control the formation of the dorsal and anterior structures (Park *et al*., 2016). Furthermore, loss of Bicc1 led to a repression of the Cripto-1 protein and a reduction in the expression of the *WNT11*b protein (Zhang *et al*. 2013; Park *et al*. 2016).

1.5.2. BICC1 and ADPKD

While it is clear that mutations in the *BICC1* gene lead to the mis-regulation of patterning in embryogenesis and developmental defects in various models, a link between BICC1 and PKD was not made until 2003 when mutations in *Bicc1* were identified in in two spontaneous mouse models of PKD: *jcpk* and *bpk* (Bouvrette *et al*., 2003). In the *jcpk* allele, a single point mutation within the third exon of *Bicc1* led to the exon to be skipped during transcription, thus inducing a frameshift (Figure 1.5.2.1). This in turn resulted in a premature stop codon within exon 4 and the subsequent loss of the KH domains and a predicted non-functional truncated protein unable to bind RNA (Bouvrette *et al*., 2003). In the *bpk* allele, a two-base pair insertion was identified within exon 22 of one of the two splice variants of *Bicc1* (Figure 1.5.2.1). This mutation led to an extension of the exon by 149 amino acids, but it was predicted that it would have no effect on the final protein product, as the normal stop codon is located upstream within exon 21 (Bouvrette *et al*., 2003). However, the researchers do not discuss the possible effect it might have upon the regulation of the *Bicc1* gene, as the elongation might disrupt it's 3' UTR, a common site for regulatory activities for many genes.

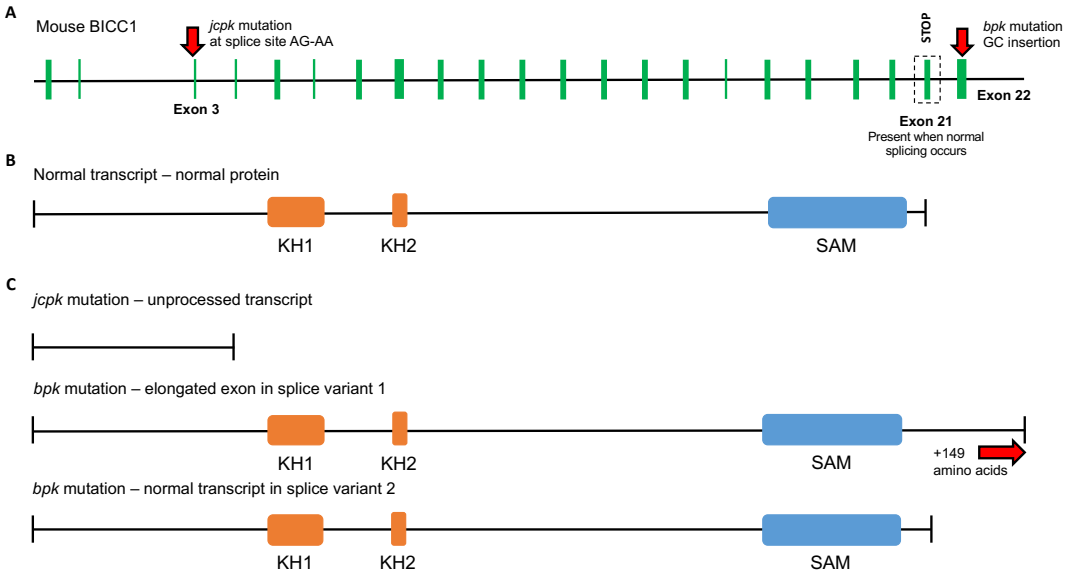

Figure 1.5.2.1. The genetics of the *jcpk* and *bpk* murine models of the mouse BICC1 gene locus. A) A representation of the mouse BICC1 gene. The black line represents the introns, while the green boxes represent the 21 exons. The *jcpk* point mutation was identified in exon 3 at the splice acceptor site AG The *bpk* GC insertion mutation was identified in exon 22. **B)** The functional protein domains of the canonical mouse sequence overlapping the exons from which they are encoded. **C)** The *jcpk* mutation caused exon skipping of exon 3 leading to a premature stop codon in exon 4 and likely an unprocessed transcript, while the *bpk* mutation extended the protein by 149 amino acids. Schematic adapted from Bouvrette *et al*., (2003).

A link between BICC1 and PKD was additionally identified by gene knockdown of *bicc1* in a *Xenopus* model, which resulted in a PKD-associated phenotype (Tran *et al*., 2007). Defective differentiation of epithelial tissues, including the collecting ducts and tubules, was observed. Tran *et al*., (2007) noted that the length of the primary cilia was not affected by loss of *bicc1*, a phenotype commonly observed in PKD cases, indicating a possible distinct role for Bicc1 to cilia-mediated signalling. The link between BICC1 and PKD was also confirmed in zebrafish. Using antisense morpholinos, knockdown of *Bicc1* resulted in pronephric cysts. However, no defects in kidney structures or pronephric cilia were observed, as is the case for mammalian models (Tran *et al*., 2010).

More recently, a tangible link between BICC1 and human kidney disease was established, as two heterozygous mutations in the *BICC1* gene locus were identified in a screen of 137 patients with various renal abnormalities, some of which had PKD (Kraus *et al*., 2012). The first mutation identified was a nonsense mutation located in exon 3, which is predicted by the Interpro database to encode an additional KH domain, a domain that is not represented on the Uniprot database. This mutation inhibited BICC1 from binding known

mRNA targets previously identified in mammalian models, including *DVL2* (discussed further in section 1.5.3 and 1.5.5). The second mutation was identified as a missense mutation in the last exon (exon 21) of BICC1, which encodes the SAM domain (Kraus *et al*., 2012). The mutation led to the exon to be skipped and resulted in loss of the SAM domain. This disabled the capability of BICC1 to localise to P-bodies in the cytoplasm, a function vital for the silencing of *DVL2* and consequent inhibition of the Wnt signalling pathway (discussed further in section 1.5.3 and 1.5.5). These results highlight the functional aspects of the BICC1 domains, confirming that the KH domains are required to bind RNA, while the SAM domain is required to localise BICC1 to cytoplasmic P-bodies to facilitate mRNA silencing.

1.5.3. Loss of BICC1 causes a range of cellular defects observed in PKD models

In models of PKD, a range of cellular defects including cilia dysfunction, loss of planar cell polarity (PCP) and defective cell-cell communication have been reported. BICC1 mutations in various models have been reported to cause similar phenotypes. Experiments in HEK293T$^{Bicc1-/-}$ cells and mutant *Bicc1* murine models demonstrated that loss of *Bicc1* had negative effects on cilia orientation, cilia fluid flow and normal cilia function (Maisonneuve *et al*., 2009). With the use of TOPFLASH reporter assays, video microscopy and scanning electron microscopy (SEM), *Bicc1* was shown to interact with a known mRNA target, *DVL2,* through its SAM domain (discussed further in section 1.5.5) (Maisonneuve *et al*., 2009). The interaction sequestered *DVL2* within P-bodies in the cytoplasm, thus disrupting its normal localisation to the plasma membrane and preventing Wnt signalling (Maisonneuve *et al*., 2009). The inhibition of this signalling pathway negatively affected PCP and randomised the LR axis by altering Nodal expression, the earliest signal determining the establishment of LR asymmetry. Similarly, normal renal development was altered, and cysts developed.

However, the role of BICC1 in primary cilia function remains controversial. Research from the Constam group opposes a global role for BICC1 in regulating or controlling PCP in all cilium, since in cochlear hair cells, loss of

BICC1 resulted in no significant effects on cilia length (Piazzon *et al*., 2012). These results could suggest that BICC1-mediated PCP establishment is kidney-specific and is regulated by an unknown mechanism in kidney epithelial cells. Alternatively, these researchers have discovered that BICC1 is also required to maintain the actin cytoskeleton (discussed further below) (Piazzon *et al*., 2012).

Conversely, Bicc1 expression has been colocalised with PC2 and GM3 synthase (GM3S) to ciliary bulbs in LLCPK cells (Mohieldin *et al*., 2015). GM3S is a monosialodihexosylganglioside, a type of ganglioside, which transduces signals from plasma membrane lipids. Interestingly, GM3 expression had been previously found to be elevated in both human and mouse PKD models, possibly indicating a causal link between BICC1, PC2 and GM3 in ADPKD (Natoli *et al*., 2010). The co-localisation of these three proteins in the ciliary bulb could imply a functional role within cilia. However, this is the only report of BICC1 localisation to primary cilia so far, so these findings need to be replicated.

Loss of BICC1 may lead to a range of cellular and intracellular defects. Short hairpin RNA (shRNA) knockdown of *Bicc1* in murine IMCD cells resulted in defects of the actin cytoskeleton and cell-to-cell contacts, whilst increased cell proliferation and apoptosis was also observed (Fu *et al*., 2010). For example, *Bicc1* shRNA knockdown cells exhibited thick and enriched stress fibers and developed an irregular shape compared to wild type cells. Moreover, loss of *Bicc1* disrupted normal tubular morphogenesis and induced cystogenesis in IMCD cells grown in 3D culture. Interestingly, a loss of E-cadherin based cell-cell adhesion and a redistribution of the tight junction marker, ZO-1, was observed, resulting in altered epithelial polarity, a common phenotype found in ADPKD (Fu *et al*., 2010). No significant change in the overall protein expression of E-cadherin or ZO-1 was observed suggesting that BICC1 may be involved in their correct cellular localisation in this model rather than as a post-transcriptional regulator of translation.

Table 1.5.3.1. A summary of the cellular phenotypes caused by loss of BICC1.

BICC1 Model	Cell Type/Organism	Cilia manifestation	Extra-cilia manifestation
Cogswell *et al*. 2003	Mouse		Cystogenesis
Tran *et al*. 2007	*Xenopus*		Defective differentiation of epithelial tissues
Maisonneuve *et al*. 2009	HEK293 Mouse	Loss of orientation Loss of flow Loss of normal function	Inhibition of Wnt signalling Altered Nodal expression Loss of PCP Randomised LR axis
Bouvrette *et al*. 2010	Mouse		Pronephric cysts
Fu *et al*. 2010	IMCD		Enriched stress fibers Irregular cell shape Disrupted tubulogenesis Cystogenesis Loss of E-cadherin cell-cell adhesion Redistribution of ZO-1 Altered PCP
Piazzon *et al*. 2012	Mouse		Defective actin cytoskeleton Increased cAMP Increased PKA signalling
Rothe *et al*. 2015	HEK293T		Inhibition of Wnt signalling

1.5.4 The role of BICC1 in mRNA stability and translation: poly(A) tail length

Studies in several animal models suggest a role for BICC1 as a post-transcriptional regulator of mRNA stability and translation in kidney epithelial cells. However, precise details of how it binds to regulate different individual mRNA targets remain inconclusive. The action of the KH and SAM domains of BICC1, and their role in the repressive function of BICC1 upon certain mRNA

targets, however, is becoming better understood. Various studies have demonstrated that the KH domains are required for mRNA targeting and binding, while the SAM domain is required to repress or inhibit mRNA translation. For example, Chicoine and colleagues (2007) have shown *Bic-C* to bind *cis*-elements in the 5' UTR of its own RNA through its KH domains *in vitro* in *Drosophila* models.

Through this mechanism, *Bic-C* negatively regulates the stability of its own RNA by recruiting and directly binding the *NOT3/5* subunit of the CCR4 deadenylation complex to shorten its poly(A) tail length (Chicoine *et al*., 2007). This would suggest a role for *Bic-C* as an activator of the CCR4 deadenylation complex. Interestingly, the researchers note that mRNA regulation in this way is uncommon, as the CCR4 deadenylation complex is usually found associated with the 3' UTR of mRNA targets. However, 5' UTRs and 3' UTRs are often in close proximity to each other during mRNA translation, as circularisation of mRNA is common due to frequent associations between the eukaryotic initiation factor 4G (eIF4G) of the 5' cap and the poly(A)-binding protein (PABP) (Wells *et al*., 1998; Kahvejian *et al*., 2005; Hong *et al*., 2017). Consequently, some 3' UTR RBPs may stimulate translation initiation as well as inhibit translation, negatively impacting mRNA stability. Therefore, it is plausible for *Bic-C* to bind its own 5' UTR to regulate its poly(A) tail length.

The recruitment of the CCR4 deadenylation complex by *Bic-C* to deadenylate target mRNAs and subsequently decrease their translational efficiency is supported by research conducted by Snee and Macdonald (2009). Their study demonstrated that *Bic-C* interacts with trailer hitch (*tral*), a gene also involved in anterior-posterior patterning and as discussed previously for the germline gene *osk*. Mutations of either *Bic-C* or *tral* genes led to the incorrect localisation of gurken (*grk*) and *osk,* mRNAs required for correct oocyte patterning (Snee and Macdonald, 2009). Furthermore, the organisation of microtubules was altered, and the formation of ectopic actin cages was observed towards the anterior region of the oocyte. Gurken was found to be sequestered within these actin cages, preventing its normal secretion as well as follicular signalling (Snee and Macdonald, 2009). Interestingly, these results suggest that *tral* may act as a scaffold to induce ribonucleoprotein (RNP) complexes with *Bic-C*, including the

CCR4 complex and target mRNAs. Conversely, *tral* may induce *Bic-C* to regulate the deadenylation of poly(A) tails and repress translation of target mRNAs, a theory similarly proposed by Chicoine and colleagues.

The homolog of BICC1 found in *C. elegans*, Gld-3, has also been observed to regulate the poly(A) tails of target germline mRNAs, but in a translationally active manner, through forming a KH domain tertiary structure (Nakel *et al*., 2010). It was discovered that four of the five KH domains (KH2-5) form a structural scaffold, while KH1 protrudes from the unit to interact with Gld-2, a non-canonical cytoplasmic poly(A) polymerase (Figure 1.5.4.1). Gld-2 functions to extend the poly(A) tail length of mRNAs with short poly(A) tails, consequently inducing their translation and releasing them from their dormant state (Nakel *et al*., 2010). The two proteins cooperatively function to bind mRNA targets, polyadenylate their poly(A) tails and induce translation. However, the researchers stated that their study was unable to demonstrate an RNA binding function for the KH scaffold in isolation (Nakel *et al*., 2010). Therefore, this could suggest that the KH scaffold may mediate protein-protein interactions instead. Nevertheless, it is possible that an RNA intermediate is involved in the interaction and that in the isolation studies the proper environmental conditions for RNA binding were not present.

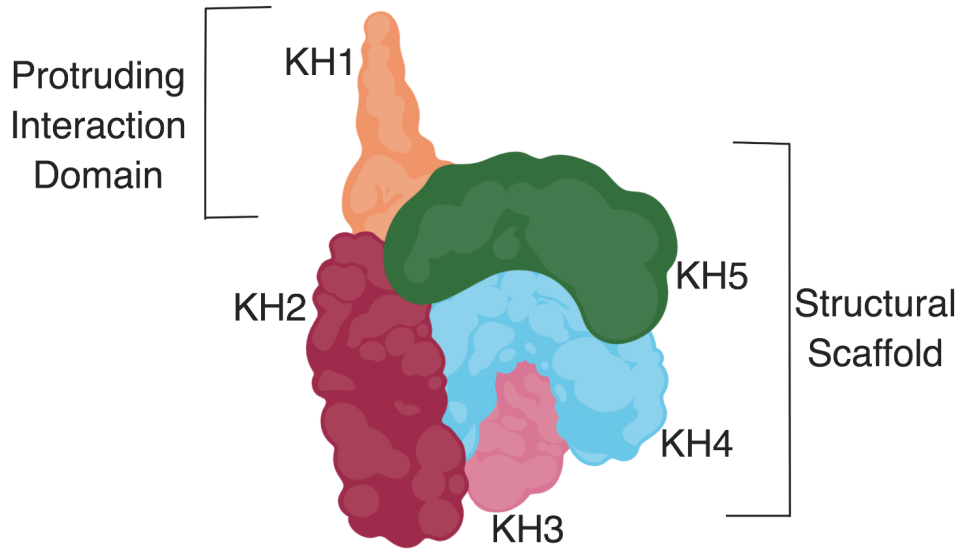

Figure 1.5.4.1. A representation of the KH1-KH5 model structure. KH2-5 form a structural scaffold, while KH1 protrudes from the unit to interact with Gld-2. This schematic was generated using Biorender and adapted from Nakel *et al*., (2010).

Nakel and colleagues (2015) have gone on to identify specific mRNAs binding to the KH tertiary scaffold that promote meiotic progression in *C. elegans*. They discovered that Gld-2 alone is unable to bind mRNAs to extend their poly(A) tails; therefore, its ability to switch the translational states of mRNAs depends upon its association with Gld-3 (Nakel *et al*., 2015). To further elucidate this interaction and its mechanistic function, the researchers demonstrated that the protruding KH1 domain of Gld-3 activates the Gld-2/3 complex through the addition of positively charged residues to a nearby RNA-binding site on Gld-2, a function not previously observed for BICC1 (Nakel *et al*., 2015).

Based on our current knowledge, it can be concluded that BICC1 can initiate both poly(A) tail elongation and deadenylation, possibly through a novel switch mechanism. It is possible that BICC1 auto-regulation controls the switch between poly(A) tail polyadenylation or deadenylation, therefore maintaining a vital equilibrium to fine-tune gene expression for kidney epithelial cell homeostasis. Furthermore, specific protein interactions might also be involved in determining the type of regulation upon poly(A) tails, as well as directing the targeting of particular mRNAs, whether they be translationally active or repressed.

1.5.5 The role of BICC1 in mRNA stability and translation: P-bodies

Developmental studies in *D. melanogaster*, *Xenopus*, *C. elegans* and *N. lugens*, have revealed that BICC1 regulates developmental patterning through altering the poly(A) tails of target mRNAs, whilst highlighting the importance of the BICC1-KH domains to interact and bind RNA for this function. Alternatively, other studies have suggested that BICC1 could utilise P-bodies, or be a P-body protein itself, to direct and enable mRNA repression. As discussed previously, Maisonneuve and colleagues (2009) identified *Bic-C* to regulate PCP and LR asymmetry in *Xenopus* models. The researchers suggest that one method in which *Bic-C* regulates PCP is through mediating the sequestration of *DVL2* in cytoplasmic P-bodies. In this study, *Bic-C* was localised to the periphery of P-bodies, identified by co-staining with the decapping enzyme *Dcp1a*, a known P-body protein. They also established that the SAM domain of *Bic-C* was required for this function, as a truncated version of *Bic-C* lacking the SAM domain, but

not the KH domains, was unable to localise to P-bodies (Maisonneuve *et al*., 2009). Surprisingly, *Bic-C* did not interact with *DVL2* in immunoprecipitation experiments in this study, indicating an indirect interaction. However, Tran *et al*., (2010) have also observed Bicc1 to be localised to cytoplasmic P-bodies with markers for GW182 and HEDLS (discussed further in section 1.5.8).

1.5.6 The role of BICC1 in mRNA stability and translation: miRNA

In 2012, new RNA binding partners of BICC1 were identified by Constam and colleagues, linking its involvement to other genes implicated in cyst formation (Piazzon *et al*., 2012). In PKD models, cAMP accumulation is a common feature linked to cyst formation and expansion. In *Bicc1* mouse mutants, levels of cAMP, and adenylate cyclase 6 (*ADCY6*), are increased due to the loss of Bicc1-mediated inhibition of *ADCY6* mRNA (Piazzon *et al*., 2012). In this study, Bicc1 was shown to interact with the 3' UTR of *ADCY6* mRNA through its KH domains, whilst Co-IP experiments demonstrated interactions between Bicc1 and miR-125a and BICC1 and Dicer. Therefore, the researchers concluded that Bicc1 binds and recruits miR-125a and the endoribonuclease, Dicer, thus activating the formation of the RNA-inducing silencing (RISC) complex (Piazzon *et al*., 2012). The researchers also found that the SAM domain was required to coordinate the formation of the RISC complex, through recruiting and binding the catalytic enzyme of the RISC complex, Argonaute (AGO). Bicc1-SAM was observed to interact with the TNRC6A/GW182 P-body, where AGO proteins are commonly bound (Piazzon *et al*., 2012). In this way, Bicc1 repressed *ADCY6* mRNA expression. In a similar manner, BICC1 also silenced PKI-alpha (PKI-α), a member of the PKA signalling pathway, by binding and recruiting miR-27a.

However, it is still unclear how Bicc1 KH domains binds and interacts with mRNA targets, and whether this is a direct or indirect interaction (this study did not conduct definitive experiments to prove direct or indirect mRNA binding). One could theorise that it is possible for BICC1 to bind a miRNA, which then recruits the RISC complex through interactions with Dicer and AGO, therefore functioning as a guide to target specific mRNA. Such a theory is plausible as seed sequences targeting specific mRNAs have been identified in miRNA molecules. Conversely, it could also be plausible that the Bicc1 KH domains

also contain a miRNA seed sequence, however, this requires further experimentation. In addition, one could theorise that BICC1 may be required to form a complex, or a specific structure, in association with other RBPs in order to bind RNA and to perform its repressive function upon mRNA targets.

1.5.7 The role of BICC1 in mRNA stability and translation: protein-protein interactions

The structure and interaction of BICC1 with other proteins has been investigated to define whether the formation of a homologous or heterologous protein complex is required for BICC1 function, especially regarding its role in repressing mRNA translation and stability (Rothé *et al*., 2015). Previous research discussed in sections 1.5.5. and 1.5.6, has highlighted the requirement of the SAM domain for cytoplasmic localisation and interaction with P-bodies to locate bound mRNA for silencing. Such research would suggest that a function of BICC1 is to identify mRNA targets and transport them to a certain location, with the help of other cytoplasmic proteins. In this way, BICC1 localises mRNAs to P-bodies specifically for repression. However, BICC1 can also bind mRNAs to positively regulate their expression by promoting or stabilising them. Yet, the mechanism behind how BICC1 is regulated to localise and regulate mRNA targets remains unknown. One could theorise that the formation of protein complexes has a role in this.

Crystal structures, electron microscopy and model simulations have demonstrated that BICC1-SAM can self-polymerise, a structural conformation which is essential for the localisation of BICC1 to P-bodies (Rothé *et al*., 2015). To confirm this observation, the SAM domain was mutated, which caused BICC1 to form a left-handed helix and cytoplasmic P-body localisation was lost (Rothé *et al*., 2015). Wnt signalling was also assessed in this study due to the reports of dysregulation by other research groups (Maisonneuve *et al*., 2009; Tran *et al*., 2010; Kraus *et al*., 2012; Lian *et al*., 2014), however, no dysregulation was observed. Therefore, these results suggest that the polymerisation of BICC1 contributes to its own stability as well as contributing specificity to its function.

More recently, it was shown that Bicc1 can cooperate with a centrosomal protein, OFD1, which has been previously shown to localise to primary cilia with PC1, PC2 and EDGF (Jerman *et al*., 2014). BICC1 interacts with OFD1 to positively regulate mRNA targets by interacting with members of the preinitiation complex (PIC) of translation and the eukaryotic initiation factor (eIF4F) complex (Iaconis *et al*., 2017). The study demonstrated that OFD1 does not physically interact with its mRNA targets, instead, Bicc1 bound some of the mRNA targets of OFD1 (Iaconis *et al*., 2017). Therefore, the research suggests that OFD1 may recruit BICC1 to regulate its mRNA targets to enable proper regulation. However, it must be noted that this study did not demonstrate an interaction between OFD1 and BICC1. Furthermore, the researchers state that the method in which Bicc1 regulates mRNA, either in a positive or negative manner, might depend on its subcellular localisation and the availability of interacting partners and/or mRNA targets, as BICC1 has frequently been shown to negatively regulate mRNA targets (Iaconis *et al*., 2017). However, in this model, BICC1 positively regulates mRNA targets, possibly through specific recruitment by OFD1 and localisation to the centrosome. Further experimentation is required to confirm this theory.

A novel role of Bicc1 protein interactions in altering glucose and lipid metabolism in polycystic kidneys has been reported which could drive cystic growth (Leal-Esteban *et al*., 2018). Using a tandem affinity purification (TAP) assay followed by mass spec, Leal-Esteban and colleagues (2018) discovered that several subunits of the C-Terminal Lis-Homology domain (CTLH) complex were novel protein partners of Bicc1. They suggest that Bicc1 regulates the expression of FBP1 and PEPCK, two gluconeogenic enzymes, through interactions with the CTLH complex to sustain normoglycemia in the kidneys (Leal-Esteban *et al*., 2018).

1.5.8 Links between BICC1 and the polycystins

As discussed above, Tran *et al* (2010) discovered that BICC1 post-transcriptionally regulates the mRNA expression of *PKD2* in a *Bicc1*$^{-/-}$ mouse model, by binding the 3' UTR of *PKD2* through its KH domains (Tran *et al*., 2010). In this way, Bicc1 competitively inhibits miR-17, a repressive oncomir

from the miR-17/92 gene cluster, from binding to the 3' UTR of *PKD2* to destabilise it, thereby increasing *PKD2* translation (Tran *et al*., 2010). Bicc1 has also been observed to regulate *PKD2* in the ducts of pancreatic progenitor cells (Lemaire *et al*., 2015). Loss of Bicc1 within pancreatic progenitor cells leads to increased cellular proliferation and the formation of cysts from pancreatic ductal cells.

Bicc1 also regulates osteoblast differentiation through *PKD2* expression in the *Bicc1*$^{jcpk/jcpk}$ mouse model (Mesner *et al*., 2014). Interestingly, the interaction between Bicc1 and *PKD2* at the RNA level occurs through the 3' UTR of *PKD2*, which differs from the interaction of Bicc1 and target mRNA molecules, including its own RNA, that are regulated by poly(A) tail modulation, as discussed in section 1.5.4. This would suggest that Bicc1 binds different regions of mRNA to perform differing regulatory functions.

Other groups have also reported a potential link between Bicc1 and Pc1 (Lian *et al*., 2014). Loss of *PKD1* by shRNA in mIMCD3 cells, as well as in the *PKD1*$^{-/-}$ mouse model, resulted in a reduction of Bicc1 mRNA and protein expression levels by 50% (Wu *et al*. 2001, Lian *et al*. 2014). To confirm a regulatory role of Pc1 upon Bicc1, *PKD1* was re-introduced into mIMCD3 cells and Bicc1 levels were restored. In summary, this research confirms a functional link of Bicc1 with the polycystins and suggests a likely role for Bicc1 in a polycystin cystogenesis pathway.

1.5.9 The relationship between BICC1 and other ADPKD-related proteins

There are several non-orthologous *in vivo* models of ADPKD, including the Han:SPRD-*Cy* rat model, first described by Kaspareit-Rittinghausen and colleaugues (1991). Schäfer *et al*. (1994) then characterised the model and described the enlarged renal manifestation observed in depth, with cysts arising from the proximal tubules. The gene locus, named *Pkdr1*, was distinct from *Pkd1* or *Pkd2* (Bihoreau *et al*., 1997). Utilising positional cloning and mutation techniques, a pathogenic missense mutation at amino acid 823, in the SAM domain, was identified in a new protein named SamCystin (Brown *et al*., 2005). The missense mutation caused a C to T transition in the nucleotide sequence,

which altered the amino acid sequence from a charged, aliphatic arginine to a non-polar, aromatic tryptophan (R823W). The *Pkdr1* locus, now known as *Anks6*, is commonly referred to as a PKD-related protein or 'cystoprotein'.

Mutations in *Bicc1* and *Anks6* cause very similar phenotypes in several PKD models, leading researchers to investigate possible interactions between Bicc1, Anks6 and other cystoproteins. In 2009, the Bryda research group demonstrated a protein interaction between Bicc1 and SamCystin (referred to as Anks6 hereafter) (Stagner *et al*., 2009). Anks6 proteins were observed to self-interact, as well as bind Bicc1 in co-transfected mIMCD3 cells (Stagner *et al*., 2009). The missense mutation R823W in the SAM domain of Anks6, identified in the Han:SPRD-*Cy* rat model, prevented the self-association ability of Anks6, but did not affect its interaction with Bicc1.

This data indicates that the SAM domain is a vital element for Anks6 self-polymerisation, but not for its interaction with Bicc1, suggesting that Anks6 and Bicc1 interact independently of their SAM domains. In addition, Stagner *et al*. (2009) suggested that this interaction could be indirect and mediated by a protein complex or RNA molecule. In this way, several Anks6 proteins may form a SAM-SAM interface, in a head-tail formation, and connect with another SAM domain containing protein or a protein complex with an RNA molecule bound (Figure 1.5.9.1).

In theory, Anks6 acts as a molecular scaffold to bind several proteins or complexes to perform a currently unknown function. This model might explain why the SAM domains of Bicc1 and Anks6 are not required for an interaction to occur. Instead, the KH domain of Bicc1 might be the key element. In summary, this research suggests that Bicc1 and Anks6 cooperatively function in a common cystogenesis pathway, as when either gene is altered, molecular changes occur which ultimately cause renal cystogenesis and ADPKD-like phenotypes.

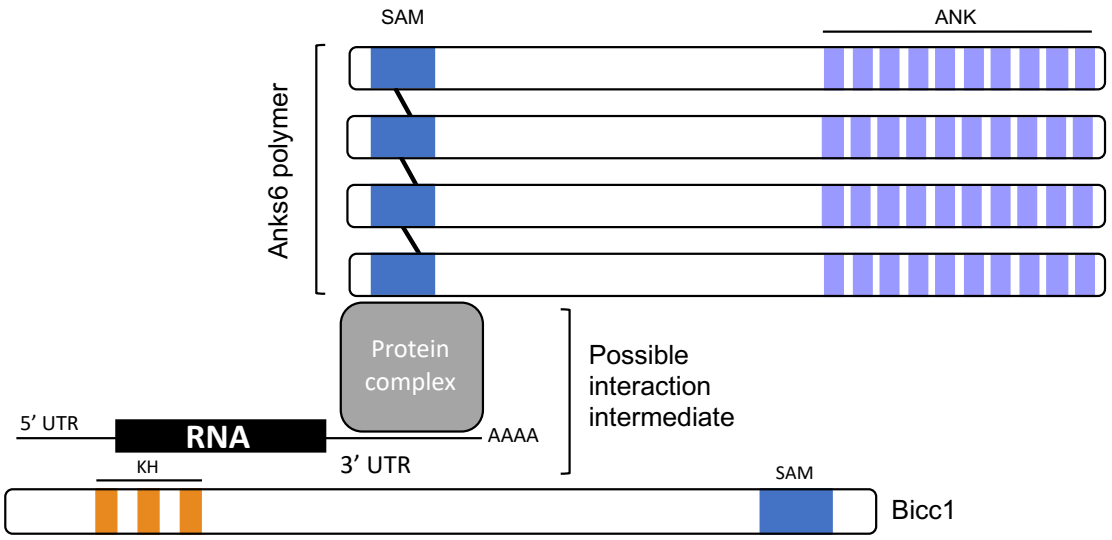

Figure 1.5.9.1. Anks6 and Bicc1 interact indirectly. The SAM domain of Anks6 is required for an interaction with Bicc1. In this mouse model, Anks6 forms SAM-SAM interface with addition Anks6 proteins in a head-tail formation, represented by the black diagonal lines in-between the SAM domains. This polymer then connects with another SAM domain-containing protein (or a protein complex with an RNA molecule bound), which forms an interaction with Bicc1 through its KH domains. Schematic adapted from Stagner *et al*. (2009).

SAM domains mediate several diverse biological processes through forming large protein structures or matrices within cells (Knight *et al*., 2011). They frequently self-associate to form polymers, they form heterodimers through SAM-SAM interfaces with other SAM-containing proteins, and they also form heterotypic complexes with other proteins (Knight *et al*., 2011). SAM domains also have the potential to bind RNA. Anks6 from *Rattus norvegicus* and *Mus musculus* contains a SAM domain at its C-terminal and 10 ankyrin (ANK) repeats at its N-terminal, while human Anks6 contains 11 ANK repeats.

Stagner *et al*. (2009) demonstrated the importance of the Anks6-SAM domain in mediating self-association and possibly other protein interactions. Further research has also discovered an important function of the SAM domain of the Anks6-related protein, Anks3. Like Anks6, Anks3 has a C-terminal SAM domain, 6 N-terminal ANK repeats and can also self-polymerise through its SAM domain (Knight *et al*., 2011). Data from TAP experiments revealed an interaction between Anks3 and Anks6 (Hoff *et al*., 2013), and additional research has established that they interact through their SAM domains (Leettola *et al*., 2014; Yakulov *et al*., 2015; Bakey *et al*., 2015; Delestré *et al*., 2015; Kan *et al*., 2016). Negative GFP (negGFP) native gel binding assays, crystal structures and yeast two hybrid (Y2H) systems have demonstrated a direct

interaction between Anks3-SAM and Anks6-SAM, wherein Anks6 can bind to one end of an Anks3 polymer (Leettola *et al*., 2014; Delestré *et al*., 2015). This action prevents Anks3 polymerisation (Figure 1.5.9.2).

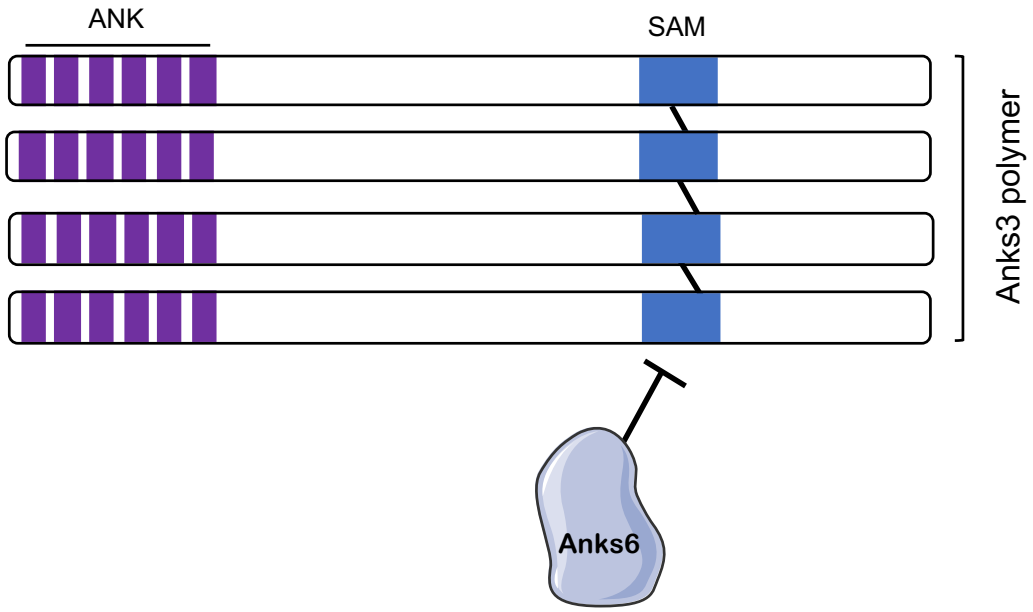

Figure 1.5.9.2. A schematic of Anks3 self-polymerisation and the inhibitory effect of Anks6. Anks3 can self-polymerise (represented by the black diagonal lines in-between the SAM domains), however the presence of Anks6 prevents the formation of this polymer (Leettola *et al*., 2014; Delestre *et al*., 2015). ANK = ankyrin, SAM = sterile alpha motif.

While the R823W mutation does not affect the ability of Anks6 to interact with Bicc1, the mutation disrupts the interaction between Anks6 and Anks3 (Figure 1.5.9.3) (Leettola *et al*., 2014). Interestingly, another missense mutation found in a screen of N-ethyl-N-nitrosourea-treated mice disrupts the interaction between Anks6 and Bicc1, but not between Anks6 and Anks3 (Figure 1.5.9.3) (Bakey *et al*., 2015). The mutation occurs only 6 amino acids upstream of the R823W rat mutation, where a T to A transition changes a non-polar, uncharged aliphatic isoleucine to a polar, aliphatic asparagine (I747N). Through molecular dynamics simulations and free energy analysis, Kan *et al*. (2016) have demonstrated that mutations in Anks6-SAM negatively disrupt its structure, consequently preventing its protein-protein binding ability. However, the R823W mutation only affects the interaction between Anks6 and Anks3, suggesting the structural integrity of Anks6-SAM is vital for its interaction with Anks3, while its interaction with Bicc1 must involve other structural elements and/or motifs.

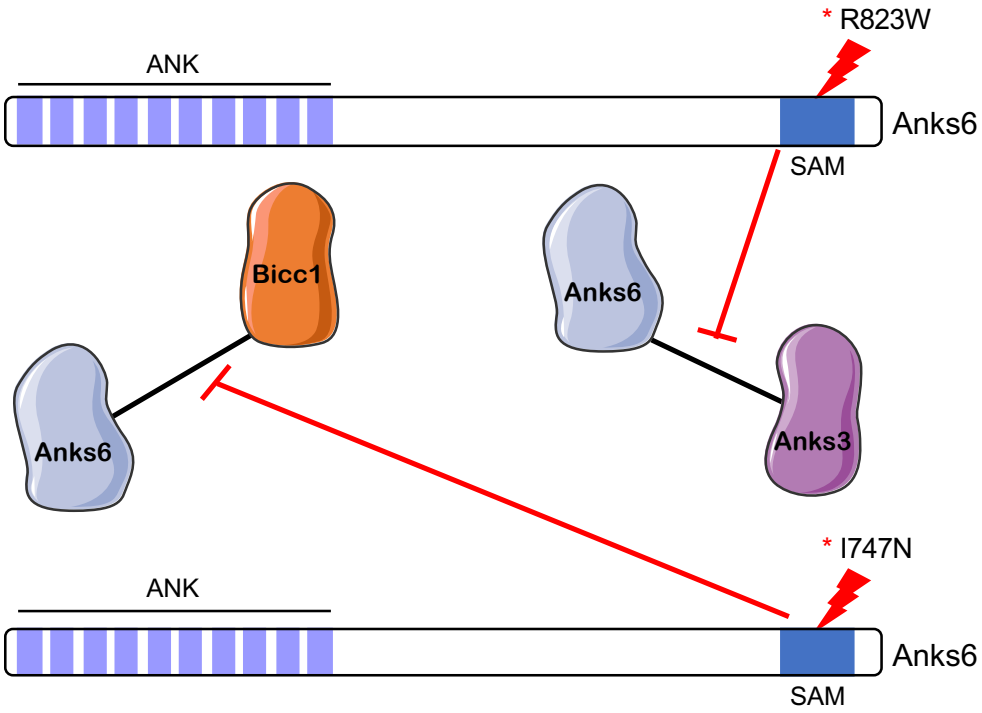

Figure 1.5.9.3. The effect of the R823W and I747N mutations on the Anks6-Anks3 and Anks6-Bicc1 interactions. The R823W mutation disrupts the Anks6-Anks3 interaction, but not the Anks6-Bicc1 interaction, while the I747N mutation disrupts the Anks6-Bicc1 interaction, but not the Anks6-Anks3 interaction (Leettola *et al*., 2014; Bakey *et al*., 2015). Interactions are represented by black lines between two proteins. ANK = ankyrin, SAM = sterile alpha motif.

Previous interaction and mutational analysis suggest that BICC1, ANKS6 and ANKS3 form a protein interaction network. Furthermore, genetic alterations in BICC1 and ANKS6 cause ADPKD-like phenotypes in various cellular and animal models, as well as in patients with cystic kidneys, suggesting they all function in a common ADPKD pathway. However, a molecular link has not been fully established between BICC1 and ANKS3, and interactions between ANKS6 and BICC1 have not been comprehensively confirmed. In 2015, an interaction between BICC1 and ANKS3 was demonstrated through Co-IP experiments for the first time in transfected HEK293T cells (Yakulov *et al*., 2015), while in 2018 Rothe and colleagues mapped precise interactions between BICC1, ANKS6 and ANKS3, through Y2H studies using full-length and truncated constructs. The results demonstrated that BICC1 and ANKS3 and ANKS3 and ANKS6 interact strongly (Figure 1.5.9.4). However, interactions between BICC1 and ANKS6 were either very weak or undetected, which differs from previous observations discussed in the literature (Stagner *et al*., 2009; Bakey *et al*., 2015). Instead, Rothe and colleagues (2018) suggest ANKS3 is required to stabilise an interaction between BICC1 and ANKS6, although further experimentation is required to confirm this theory.

BICC1-ANKS3 and ANKS3-ANKS6 complexes both relied on SAM-SAM interactions, as well as additional binding surfaces involving the ANK repeats and KH domains (Rothé *et al*., 2018). Interestingly, BICC1-SAM preferably bound the SAM domain of ANKS3 not ANKS6. Despite Rothe and colleagues (2018) providing a complex network map of interacting proteins and domains, they also discovered certain domains that failed to interact, including BICC1-KH and ANKS3-ANK. In agreement with the results presented by Stagner and colleagues (2009), this data suggests additional determinants are required for stable interactions, adding importance to domains previously overlooked. In summary, an intricate and complex molecular interaction network between BICC1, ANKS6 and ANKS3 has been uncovered.

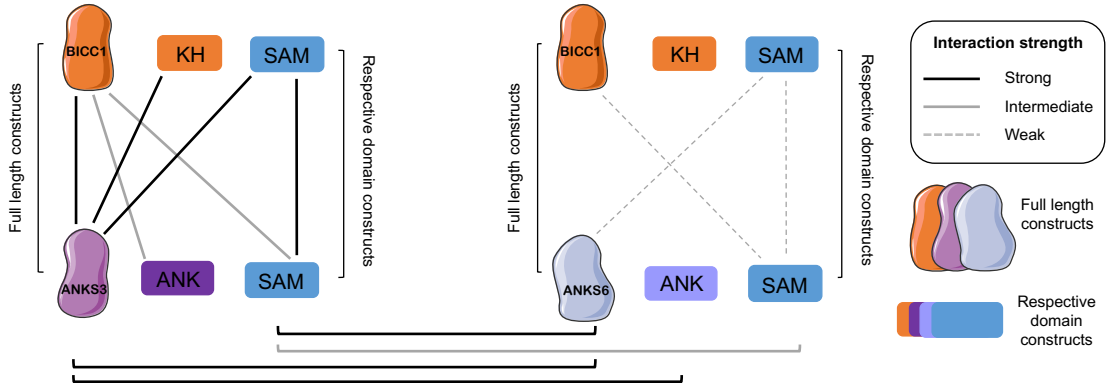

Figure 1.5.9.4. The interaction network of BICC1, ANKS3 and ANKS6. Interactions observed between BICC1 and ANKS3: Bicc1-FL + ANKS3-FL, Bicc1-FL + ANKS3-SAM, Bicc1-SAM + ANKS3-FL, Bicc1-SAM + ANKS3-SAM and KH + ANK. Interactions observed between ANKS3 and ANKS6: ANKS3-FL + ANKS6-FL, ANKS3-SAM + ANKS6-FL, ANKS3-SAM + ANKS6-SAM and ANKS3-FL + ANKS6-ANK. Outcomes where weak or no interaction was observed: Bicc1-FL + ANKS6-FL, Bicc1-SAM + ANKS6-SAM and Bicc1-KH and ANKS3-ANK. The strength of the interactions was determined by the addition of 3-Amino-1,2, 4-triazol (3-AT), a competitive inhibitor of histidine synthesis, to evaluate the strength of the interactions. FL = full-length, SAM = sterile alpha motif, KH = K-homology and ANK = ankyrin repeat. Schematic adapted from Rothe *et al*. (2018).

1.5.10 ANKS6 and ANKS3 interact with NPHP proteins associated with nephronophthisis and ciliopathies

Some features of the phenotype observed in animal models of ADPKD overlap with other cystic diseases affecting the kidneys such as nephronophthisis (NPHP). Unsurprisingly, the proteins identified to have a role in these disease pathways also overlap (Olbrich *et al*., 2003; Mollet *et al*., 2005; Delous *et al*., 2007; Bergmann *et al*., 2008). Apart from the link with ADPKD, ANKS6 has been classified as a member of the NPHP family (NPHP16, see Table 1.5.10.1). NPHP, like ADPKD, is a genetic disorder mainly localised to the kidneys which

causes cystic kidney disease but with prominent renal fibrosis and early-onset ESRD (Badano *et al*., 2006). NPHP mainly affects children and adolescents and is classified as a renal ciliopathy due to expression of the 20 or more identified gene products being in the primary cilia and their compartments or appendages (Badano *et al*., 2006).

The affected signalling pathways in NPHP and ADPKD also overlap and include the hedgehog, mTOR and Wnt pathways, to name but a few (Simons *et al*., 2005; Bergmann *et al*., 2008). Previous data has demonstrated that NPHP is closely linked to the related Joubert and the Meckel-Gruber syndromes, also referred to as the NPHP-JBS-MKS network (Srivastava *et al*., 2018). Research into the NPHP gene products has shown that they form large molecular systems to perform particular functions, usually involving proteins containing domains that function in protein-protein interactions (Srivastava *et al*., 2018). Currently, four main NPHP modules have been identified, including the NPHP1-4-8, the NPHP5-6, the NPHP2-3-9 and the MKS modules (Srivastava *et al*., 2018). How these modules assemble, how they are regulated, and their function, however, remain elusive.

ANKS6 was identified as a binding partner of the serine/threonine protein kinase NEK8 (also known as NPHP9, see Table 1.5.10.1) following Co-IP experiments and mass spectrometry (MS) analysis in HEK293T cells using NEK8 as bait (Hoff *et al*., 2013). NEK8 has been shown to be important for ciliogenesis, through both its activation and degradation (Zalli *et al*., 2012). Furthermore, ANKS6 was observed to form a new network with the NPHP2-3-9 module by connecting NEK8 to Inversin (INVS, also known as NPHP2) and NPHP3 in primary cilia (Hoff *et al*., 2013). ANKS6 is responsible for assembling this module and activates NEK8 by binding to its kinase domain and the proceeding amino acids (259-312) through its ANK domain, a function discovered through analysis of the *Anks6*^{Streaker} model (Figure 1.5.10.1) (Czarnecki *et al*., 2015). The activation of NEK8 by ANKS6 causes NEK8 to phosphorylate ANKS6, demonstrating that ANKS6 regulates its own phosphorylation and possible activation. As observed previously, an interaction is mediated through a recognised domain and additional surrounding motifs. The *Anks6*^{Streaker} model contains a missense mutation in the ANK domain of

ANKS6 which substitutes the highly conserved methionine-187 to a lysine, disrupting the interaction between ANKS6 and NEK8 and thus preventing NEK8 activation. In summary, ANKS6 recruits and assembles the NPHP2-3-9 module, while INVS localises it to the axoneme of primary cilia.

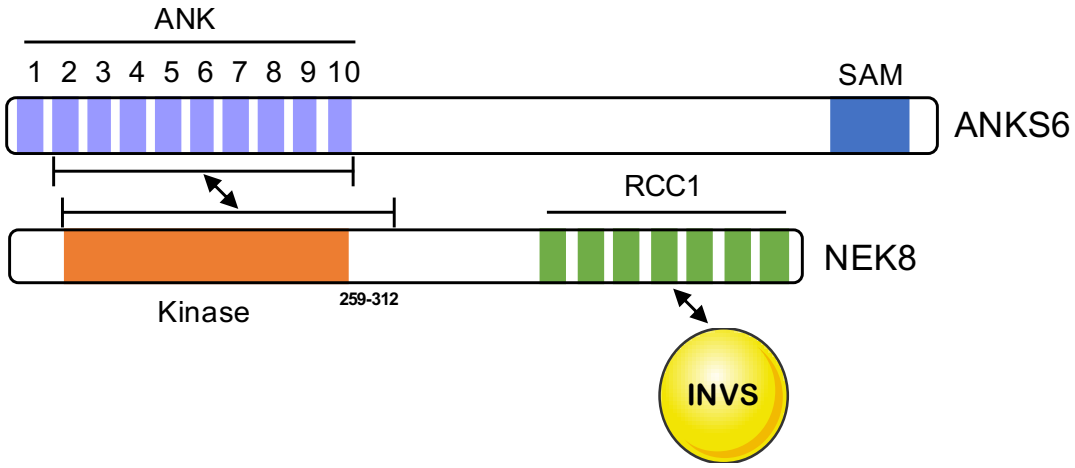

Figure 1.5.10.1. ANKS6 interacts with NEK8 and connects INVS. The interaction between ANKS6 and NEK8 requires ANK repeats 2-10 of ANKS6 and the kinase domain of NEK8 followed by amino acids 259-312 of NEK8. The interaction between NEK8 and INVS requires the C-terminal RCC1 repeat of NEK8. Required binding domains/motifs were not investigated for INVS (Czarnecki *et al*., 2015). ANK = ankyrin, SAM = sterile alpha motif, RCC1 = regulator of chromosome condensation 1.

The MS screen also revealed an association of the asparaginyl-hydroxylase hypoxia inducible factor 1 alpha inhibitor (HIF1AN) to ANKS6, which was confirmed by follow-up Co-IPs, where an interaction with INVS was also observed. HIF1AN is an oxygen sensor responsible for the hydroxylation of HIF1-alpha (HIF1α) and proteins containing ANK domains (Wilkins *et al*., 2012). Hoff *et al*. (2013) discovered HIF1AN hydroxylates ANKS6 and INVS at their conserved hydroxylation recognition motifs, asparagine N129 and N75 respectively. HIF1AN also alters the organisation of the module, as mutations in the hydroxylation site of ANKS6 were responsible for a loss of interaction with NEK8. Hoff and colleagues suggest that HIF1AN facilitates ANKS6-NPHP2-3-9 module formation through hydroxylation of ANKS6, which consequently modifies its ability to interact with protein targets. Of note, knockdown of HIF1AN in *Xenopus* phenocopied other NPHP disease models, and expression levels of HIF1AN targets including HO-1, Glut-1, and VEGF, were increased in the Han:SPRD-*Cy* rat model, suggesting hydroxylation or its regulation might play a role in cystogenesis (Bernhardt *et al*., 2007; Stagner *et al*., 2009; Hoff *et al*., 2013).

In a similar manner to ANKS6, ANKS3 interacts with several NPHP proteins. Data obtained from Co-IP experiments in HEK293T cells demonstrates that ANKS3, but not ANKS6, partners with the NPHP1-4-8 module through a direct interaction with NPHP1 (Yakulov *et al*., 2015). Furthermore, NPHP8 demonstrated an association with ANKS3, but not ANKS6, when co-expressed with NPHP1 or NPHP4. However, ANKS3 was also observed to interact with NPHP9 (NEK8), suggesting that ANKS3 is also able to connect with the ANKS6-NPHP2-3-9 module (Figure 1.5.10.2). However, this connection is likely made through the direct interaction ANKS3 has with ANKS6. As ANKS3 contains two conserved hydroxylation sites, Yakulov and colleagues (2015) investigated whether ANKS3 could be hydroxylated by HIF1AN, as observed by Hoff *et al*. (2013) for ANKS6 and INVS (NPHP2). Co-IP experiments demonstrated an interaction between ANKS3 and HIF1AN, while MS analysis in the presence or absence of HIF1AN suggested asparagine N96 to be the active hydroxylation site of ANKS3. Mutation of this site confirmed this theory.

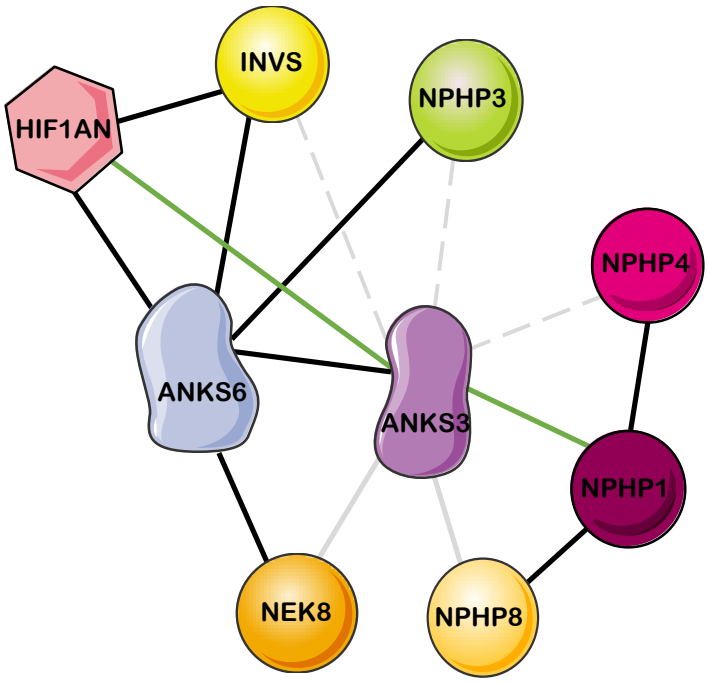

Figure 1.5.10.2. Schematic representation of ANKS3 protein interactions. The black, solid lines represent interactions previously confirmed by other research groups. The green lines represent new interactions observed in this study. The dashed, grey lines represent weak interactions that were observed, while the light, grey lines represent interactions observed only when NPHP1 and NPHP4 were co-expressed (Yakulov *et al*., 2015).

As well as interacting with the NPHP1-4-8 module, ANKS3 also interacts with NEK7 through its ANK domain (Figure 1.5.10.3) (Ramachandran *et al*., 2015). Interestingly, this interaction also requires the following amino acids up to 421,

suggesting the functional domain requires additional elements to maintain a stable interaction, a feature also observed in the interaction between ANKS6-NEK8, ANKS6-BICC1 and ANKS3-BICC1. The binding motif of NEK7 required for the interaction was not investigated in this study. NEK7 was also identified in MS analysis following an ANKS6 Co-IP but was not explored further (Hoff *et al*., 2013). Ramachandran and colleagues (2015) confirmed the interaction between ANKS3 and NEK7 and established that it was specific, as NEK7 did not interact with INVS, another protein containing ANK repeats.

As well as interacting with NEK7, analysis of western blots demonstrated an increase in the molecular weight of ANKS3 by 20 kDa in the presence of NEK7, suggesting NEK7 modifies ANKS3 in some manner (Ramachandran *et al*., 2015). Further investigation demonstrated that the modification of ANKS3 was specific to NEK7, as no change in molecular weight was observed in the presence of NEK8. However, Ramachandran and colleagues (2015) discovered that although the modification required NEK7, this did not result in phosphorylation of ANKS3. MS analysis of serine and threonine phosphorylation sites, as well as mutation analysis and probing for mono-ubiquitination, demonstrated that neither phosphorylation nor mono-ubiquitination was responsible for the modification, although ANKS3 was poly-ubiquitinated in the presence of NEK7. In addition, co-expression of ANKS3, ANKS6 and NEK7 followed by Co-IP experiments demonstrated that modified ANKS3 can still bind ANKS6 (Ramachandran *et al*., 2015). Therefore, the modification of ANKS3 has no effect on its interaction with ANKS6.

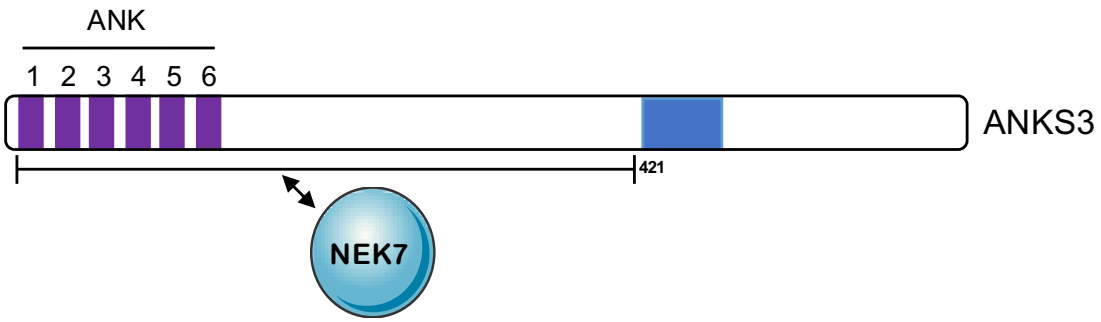

Figure 1.5.10.3. ANKS3 interacts with NEK7. NEK7 interacts with ANKS3 through the ANK domain of and the following amino acids up to 421 (Ramachandran *et al*., 2015). ANK = ankyrin, SAM = sterile alpha motif.

Investigations by Lažetić and Fay (2017) and Lažetić *et al*. (2018) also observed interactions between ANKS6 and the NPHP2-3-9 module and ANKS3 and NEK7 in a *C. elegans* model. Research into molting and the associated apical extracellular matrix remodelling discovered that MLT-2/ANKS6, MLT-3/ANKS3 and MLT-4/INVS were the central genes regulating this process. MLT proteins co-localise with NEKL proteins and form clear, sizeable apical foci to promote cuticle shedding, and therefore regulate molting. NEKL-2/NEK8, MLT-2/ANKS6 and MLT-4/INVS were observed to co-localise, while NEKL-3/NEK6/NEK7 and MLT-3/ANKS3 were observed to co-localise. Furthermore, MLT-2/ANKS6 and NEKL-3/NEK6/NEK7 co-localised with CDC-42 and its effector protein kinase SID-3/ACK1, proteins known to regulate actin dynamics. Together, this data suggests that the MLT-NEKL network regulates actin and therefore apical extracellular matrix remodelling, through interactions with CDC-42 and SID-3/ACK. Based on these results, they proposed a model where MLT proteins serve as molecular scaffolds for NEKL kinases, a network that could apply to mammalian models.

Another recent finding has been the discovery that NME/NM23 nucleoside-diphosphate kinase 3 (NME3), a kinase involved in DNA-repair mechanisms, interacts with several NPHP proteins, including centrosomal protein 164 (CEP164 or NPHP15), NEK8, and ANKS6 (Figure 1.5.10.4) (Hoff *et al*., 2018). The former two proteins have recently been linked to regulating genome stability through functioning in a DNA-damage response pathway (Sivasubramaniam *et al*., 2008; Chaki *et al*., 2012; Choi *et al*., 2013; Abeyta *et al*., 2017). These Co-IP experiments also demonstrated a link between NME3 and NPHP1, 3 and 4. Further Co-IP experiments found that NEK6, a centrosomal protein kinase known to regulate cell cycle arrest following DNA damage, could interact with NME3 as well as INVS, NPHP3, ANKS6, NEK8, NEK9 (Figure 1.5.10.4).

The data suggest that NME3 connects the ANKS6-NPHP2-3-9 and NPHP1-4-8 modules and could function in DNA-repair pathways involving NEK6 and its upstream activator NEK9. Whether the NPHP modules are directly linked to DNA-repair mechanisms, possibly through NME3 and other proteins, requires further investigation. Following immunofluorescent staining and confocal

imaging, Hoff *et al*. (2018) observed NME3 to localise at the basal body and centrioles of centrosomes of primary cilia. Like many other NPHP- or ADPKD-related proteins, loss of NME3 in *Xenopus* and zebrafish models causes phenotypes observed in ciliopathies.

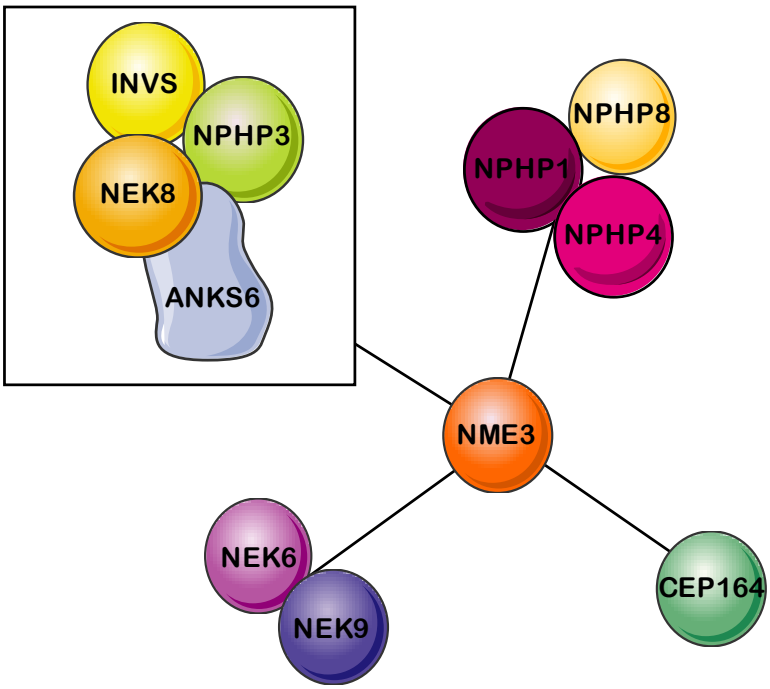

Figure 1.5.10.4. Schematic representation of NME3 protein interactions. NME3 directly interacts with members of the ANKS6-NPHP2-3-9 module, and NPHP1 of the NPHP1-4-8 module. NME3 also binds CEP164 and NEK9 and co-localises with NEK6. Adapted from Hoff *et al*. (2018).

Table 1.5.10.1. The gene aliases of the NPHP proteins.

Gene Name 1	Gene Name 2	Gene Name 3
NPHP1		
NPHP2	*INVS*	
NPHP3		
NPHP4		
NPHP5	*IQCB1*	
NPHP6	*CEP290*	
NPHP7	*GLIS2*	
NPHP8	*RPGRIP1L*	
NPHP9	*NEK8*	
NPHP10	*SDCCAG8*	
NPHP11	*TMEM67*	*MKS3*
NPHP12	*TTC21B*	
NPHP13	*WDR19*	*IFT44*
NPHP14	*ZNF423*	
NPHP15	*CEP164*	
NPHP16	*ANKS6*	*ANKRD14*
NPHP17	*IFT172*	
NPHP18	*CEP83*	
NPHP19	*DCDC2*	
NPHP20	*MAPKBP1*	*JNKBP1*
N/A	*ANKS3*	

1.5.11 BICC1, ANKS6 and ANKS3 co-localise to primary cilia

The localisation of BICC1 and other cystoproteins has been debated over the years, but more recently researchers have shown BICC1, ANKS6 and ANKS3 to localise in the primary cilia of kidneys in various models (Hoff *et al*., 2013, Yakulov *et al*., 2015, Bakey *et al*., 2015; Delestre *et al*., 2015). Moreover, ANKS6 and ANKS3 co-localise in primary cilia, along with various NPHP proteins, in specific compartments. (Figure 1.5.11.2). ANKS3 has also been observed to localise in ciliary basal bodies, individually or as large aggregates, in the epidermal cells of *Xenopus* (Yakulov *et al*., 2015). As previously discussed, Czarnecki *et al*. (2015) described how ANKS6 interacts with and activates NEK8, but ANKS6 requires NEK8 for localisation to the ciliary inversin compartment (IC). INVS, NPHP3 and NEK8 are known proteins of the IC, however its biological function remains elusive (Yokoyama *et al*., 1993; Bergmann *et al*., 2008; Manning *et al*., 2012). Ramachandran and colleagues (2015) demonstrated that ANKS3 and NEK7 interact, and that NEK7 can modify ANKS3. Moreover, ANKS3 can retain NEK7 in the cytoplasm, preventing its normal localisation to the nucleus (Ramachandran *et al*., 2015). This data suggests NEK7 initiates modification of ANKS3 to enable ANKS3 to arrest NEK7 in the cytoplasm, thus inhibiting its function in the nucleus and/or promoting a different function to occur in the cytoplasm (Figure 1.5.11.1).

Research by Lazetic and Fay (2017) have made similar observations in *C. elegans*. Loss of MLT-ANKS3 caused a strong localisation of NEKL-3/NEK6/NEK7 to the nucleus, suggesting MLT-3/ANKS3 retains NEKL-3/NEK6/NEK7 in the cytoplasm and prevents its nuclear localisation (Figure 1.5.11.1). Furthermore, the loss of MLT-2/ANKS6 caused NEKL-2/NEK8 to accumulate in the nucleus, while loss of MLT-4/INVS reduced its normal localisation at hyp7–seam cell boundary in *C. elegan* animals. Loss of either NEKL-3/NEK6/NEK7 or NEKL-2/NEK8 did not affect the localisation of MLT-3/ANKS3 or MLT-2/ANKS6-MLT-4/INVS respectively. This data suggests that not only do MLT proteins serve as molecular scaffolds for NEKL kinases, they also control their localisation, possibly to regulate a particular function.

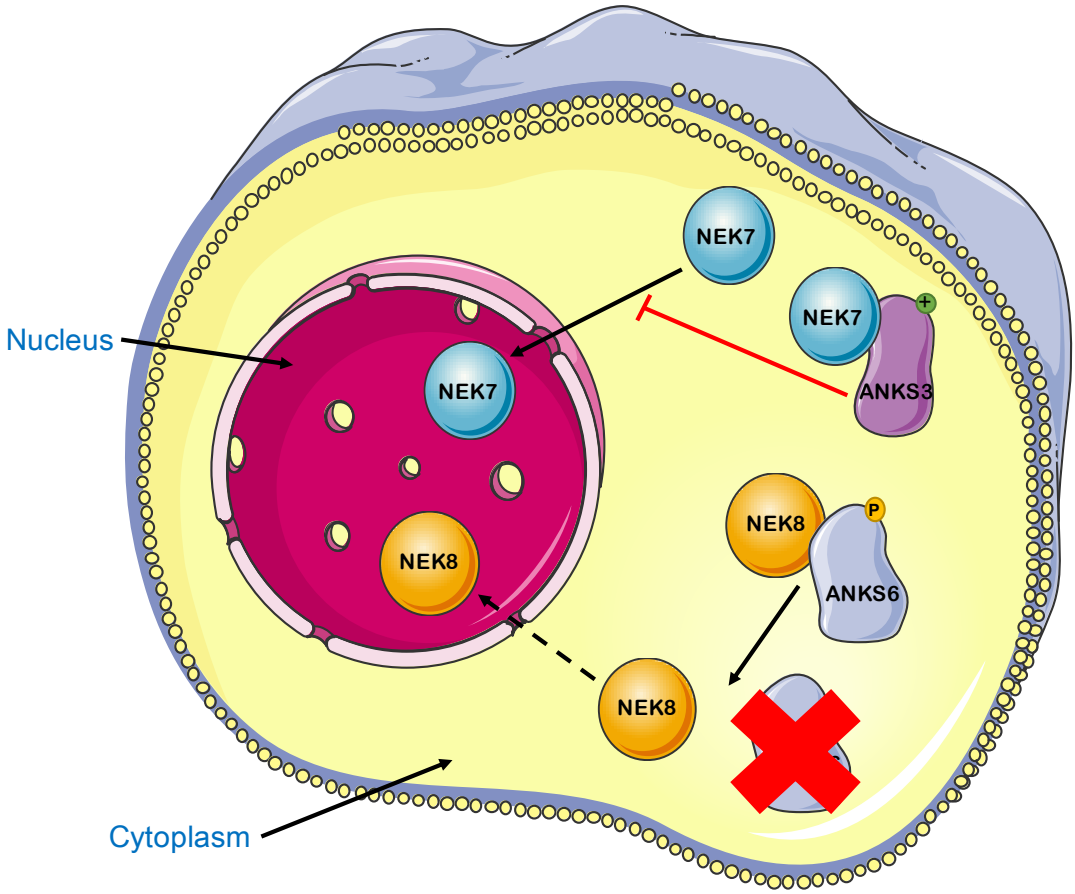

Figure 1.5.11.1. ANKS3 and ANKS6 regulate the localisation of NEK7 and NEK8. ANKS3 retains NEK7 in the cytoplasm, preventing its normal localisation to the nucleus (Ramachandran *et al.*, 2015; Lazetic and Fay 2017). Loss of ANSK6 causes NEK8 to localise to the nucleus from the cytoplasm (Lazetic and Fay 2017).

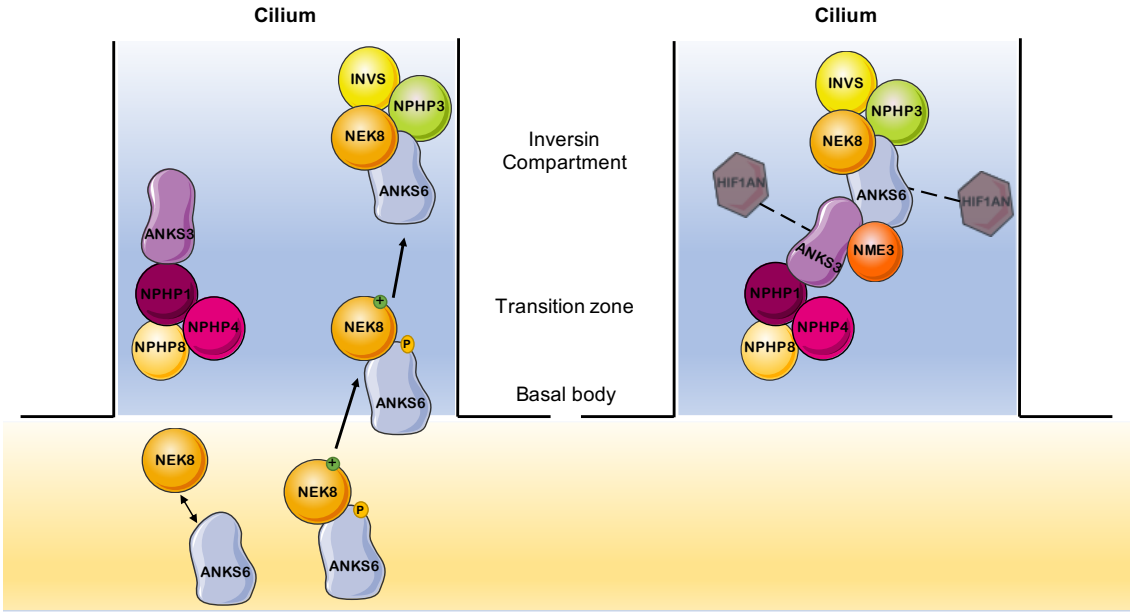

Figure 1.5.11.2. A summary schematic representing the co-localisation of ANKS3, ANKS6 and the NPHP proteins in various compartments of primary cilia.

1.6 Project Overview

BICC1 mutant models in various species are known to share common phenotypes with ADPKD models. BICC1 also shares several functions with ADPKD-related proteins and is found in common pathways and complexes with these proteins in ADPKD models, indicating that BICC1 may have an important and functional role within the disease.

The hypothesis of this study states that BICC1 is a major interacting protein of the polycystin protein complex and is somehow involved in the pathogenesis of ADPKD. Since BICC1 is an RBP whose protein and RNA binding partners have not been fully elucidated in human kidney, the main aims of this thesis were:

1. To confirm a functional link between BICC1 and the polycystin proteins
    a. Confirm loss of BICC1 causes ADPKD-like phenotypes using 3D cellular cyst assays
    b. Explore interactions between BICC1 and the polycystin proteins and define their likely binding domains using Co-IP and protein domain deletion experiments
    c. Confirm a role for BICC1 as a regulator of *PKD2* and investigate whether BICC1 also regulates the mRNA expression of *PKD1* using CRISPR-Cas9 generated *BICC1 KO* models and qPCR
    d. Investigate whether BICC1 regulates the protein expression levels of PC1 and PC2 using the *BICC1 KO* models and western blotting
2. To discover global, novel protein binding partners of BICC1 in human kidney epithelial cells
    a. Identify novel protein interacting partners of BICC1 using Co-IP experiments followed by mass spectrometry
    b. Validate a novel interacting partner through Co-IP and domain-deletion experiments
    c. Investigate whether the novel interacting partner of BICC1 also interacts with the polycystins using Co-IP, mutagenesis and western blotting

   d. Investigate whether BICC1 regulates the expression of its novel binding partner in kidney epithelial cells using the CRISPR Cas9 *BICC1 KO* models

3. To discover global, novel RNA binding partners of BICC1 in human kidney cells
   a. Identify novel RNA targets of BICC1 using an optimised endogenous RNA-IP followed by deep sequencing (RNA-Seq)
   b. Investigate whether BICC1 interacts with its RNA targets using a fragmented RNA-IP approach
   c. Analyse the effect of loss of BICC1 on global transcriptome expression using the *BICC1 KO* model and compare to WT human epithelial cells through RNA-Seq
   d. Investigate how BICC1 regulates the expression of its identified RNA targets by assessing mRNA stability or other methods of mRNA regulation

Chapter 2

Materials and Methods

2.0 Material and Methods

2.1 Cell Culture

All cells were maintained in Dulbecco's Modified Eagles Medium-Ham's 12 (DMEM-F12, Invitrogen) supplemented with either 10% fetal bovine serum (FBS) or 5% Nu serum (a growth medium supplement which provides a low-serum alternative to FBS), 1% penicillin/streptomycin (antibiotic/antimycotic, Invitrogen) solution and 1% L-glutamine (Invitrogen). Some cells required additional supplements including interferon gamma, insulin-transferrin-sodium selenite and 3,3',5-triiodo-L-thyronine sodium salt, a thyroid hormone. The cell lines were grown at either 37°C or 33°C, depending on their immortalisation. Cell lines used in this study are listed in Table 2.1.1. All the cell lines used in this study are of human origin.

Table 2.1.1. Cell lines used in this study.

Cell line	Cell type	Media/Temp	Immortalisation	Alterations	Phenotype	Source
HEK293	Embryonic kidney	FBS/37°C	Sheared human Ad5 DNA	-	Embryonic kidney	ETCC
HA-BICC1	Embryonic kidney	FBS/37°C	Sheared human Ad5 DNA	Transfected with tet-inducible BICC1 plasmid	BICC1 over-expression	Wessely Lab
UCL93	Kidney epithelial	Nu/33°C	Temperature sensitive large T antigen	-	Wild-type	Parker *et al*. 2007
Ox161c1	Kidney epithelial	Nu/33°C	Temperature sensitive large T antigen	-	*PKD1* mutation	Parker *et al*. 2007
BICC1 KO	Kidney epithelial	Nu/33°C	Derived from UCL93 cell line	*BICC1* gene *KO*	No *BICC1* expression	Ong Lab
PKD1 KO	Kidney epithelial	Nu/33°C	Derived from UCL93 cell line	*PKD1* gene *KO*	No *PKD1* expression	Ong Lab
PKD2 KO	Kidney epithelial	Nu/33°C	Derived from UCL93 cell line	*PKD2* gene *KO*	No *PKD2* expression	Ong Lab

The 3D cyst assay in collagen was performed by plating UCL93 cells and *BICC1 KO* cells at $1.4x10^5$ cell/mL in 96-well plates. Collagen gels were prepared as follows: 70% collagen, 10% $NaHCO_3$, 20x MEM media. The cells were mixed with the collagen and 60 µL of collagen/cells mixture was plated in each well and incubated with 5% Nu serum media at 33°C for 48 hours. The assay was incubated at 33°C for 14 days, with fresh media changes every 2 days, to allow for structural formation. Tubular formation or cystogenesis was determined in 10 randomly selected microscopy fields for each experimental

condition and the number of different structures were counted and compared between cell lines.

2.2 Quantitative Reverse Transcriptase-PCR (qPCR)

RNA was extracted using the TRIzol Reagent method (Ambion). Briefly, cells were plated at $1x10^6$ cells/mL in 10 cm^2 plates and incubated overnight until approximately 80% confluent. Cells were washed with media containing no serum and incubated with media containing no serum for 24 hours to synchronise the cell cycle. The media was then replaced with media containing serum, to allow the cells to re-enter the cell cycle, and incubated for 24 hours. Cells were removed from the incubator and 1 mL TRIzol per 10 cm^2 plate was added, transferred to a 1.5 mL Eppendorf, and incubated at room temperature to lyse the cells.

After 5 minutes, 200 µL chloroform was added and the tubes were shaken vigorously for 15 seconds, before incubation at room temperature for 5 minutes. The tubes were centrifuged at 12,000 *g* at 4°C for 15 minutes before the upper, clear aqueous phase containing RNA was removed and placed in a clean 1.5 mL Eppendorf. A volume of 500 µL of isopropanol (100%) was added and incubated at room temperature for 5 minutes before centrifugation at 12,000 *g* at 4°C for 10 minutes. The centrifugation time was increased to 20-30 minutes if the RNA yield was expected to be low. The supernatant was removed, and the pellet was washed in 1 mL 75% ethanol. The pellet was centrifuged at 7,500 *g* at 4°C for 5 minutes, the ethanol was removed and then the pellet was allowed to air dry for 5 minutes. The RNA was resuspended in 20 µL RNase-free water and heated at 60°C for 10 minutes. The RNA concentration was measured using the ND-100 programme on the Nanodrop 2000c (Thermo Scientific) and was either stored at -80°C or treated with DNase I before proceeding with complementary DNA (cDNA) synthesis.

RNA samples were treated with DNase-I following the standard protocol from the DNA-free™ Kit (Ambion). Briefly, 2 µL 10x DNase I Buffer and 1 µL rDNase I was added to the RNA sample and incubated at 37°C for 30 minutes. After incubation, 2 µL DNase Inactivation Reagent was added and incubated at room

temperature for 2 minutes before centrifugation at 10,000 *g* for 90 seconds. The DNase I-treated RNA samples were then transferred to a clean 1.5 mL Eppendorf and the RNA concentration re-measured. To convert RNA to 2 µg cDNA, the High Capacity RNA-to-cDNA protocol (Applied Biosystems) was followed. RNA was reverse transcribed in a Thermal Cycler at 37°C for 60 minutes, followed by 95°C for 5 minutes, with a final 4°C hold. The cDNA was diluted 1/25 for downstream qPCR procedures.

The acquired cDNA (100 ng) and The Power SYBR Green PCR Master Mix (Applied Biosystems) components were used for qPCR procedures. Primers prepared at 10 nM (Table 2.2.1) were used to measure specific mRNA expression. Beta-actin (*ACTB*) and glyceraldehyde 3-phosphate dehydrogenase (*GAPDH*) were used as reference genes. PCR reactions were performed for 35 amplification cycles at an annealing temperature of 60°C (ABI 7900, Applied Biosystems). Results were processed and analysed using the SDS 2.4 and Data Assist programmes. All primers were obtained from Eurofins Genomics.

Table 2.2.1. Oligo sequences designed for qPCR procedures. The primers were designed using NCBI Primer Blast and tested for specificity across the *Homo sapiens* organism genome using Primer3. *F: forward primer, R: reverse primer*, *e: exon, i: intron.*

Oligo	**Sequence (5'-3')**
BICC1 F	AACAGCCAAGCAAGTCTGTG
BICC1 R	ACTGCTTTCAAGTCCGAGGA
ACTB F	AGGATTCCTATGTGGGCGAC
ACTB R	ATAGCACAGCCTGGATAGCAA
GAPDH F	CCATCTTCCAGGAGCGAGAT
GAPDH R	TGCTGATGATCTTGAGGCTG
PKD1 F	TCTGAGGAACCTGAGCCCTA
PKD1 R	AGTGGCTGGAGAGGTTCAGA
PKD2 F	AGCCTGGATGACTCTGAGGA
PKD2 R	TGGCTCGCTCCATAATCTCT
ANKS3 F	GCTGGCCATGAGATAATCGT
ANKS3 R	GCAGAGAGGGCGAGTAAGTG
ANKS6 F	CTCAGGTGGCAGCATAGACA
ANKS6 R	AGTTCCAGATGGAGGCCTTT
CDC42 F	CGTGACCTGAAGGCTGTCAA
CDC42 R	GGGCAGCCAATATTGCTTCG
ACK1 F	CCTGGAGTCCAAGCGCTTTA
ACK1 R	GGAGAAGGTGCGTGTCTTCA
NPHP3 F	GCCCTGAGTTTGCCCATAGT
NPHP3 R	AGATCCATCTCAGGCTGGGT

INVS F	ACACAGAACCCAAGGCCAAA
INVS R	TGTACGATGGTGGGGAGGAT
NEK1 F	AGTGACATTTGGGCTCTGGG
NEK1 R	GAGACACCAAACTGCGGAGA
NEK2 F	TGGCTCCATGACAGAAGCTG
NEK2 R	CACTAGCCAGATCCCCTCCT
NEK3 F	TCAAGGGTGCATCAGTCCAC
NEK3 R	GGGGGTAAGCACTTCTGGAC
NEK4 F	GAGCTATGGAGAGGTGACGC
NEK4 R	TGTGCCAATGAGGGTGCTAG
NEK6 F	CCCAACACGCTGTCTTTTCG
NEK6 R	CTGCACCTTCTTCAGAGCCA
NEK7 F	CCTTACGACCGGATATGGGC
NEK7 R	CATCCAAGAGACAGGCTGCT
NEK8 F	AGATCCTGCTTGCACTGCAT
NEK8 R	CATGCGGTGTTTGTCAAGCA
NEK9 F	TGAGGGTCAGCTCTATGCCT
NEK9 R	TGCTCCACTGGATTGCTGAG
NEK11 F	CCAACTCCTCTCCAAGCTGG
NEK11 R	ATCTCGGCCCTCACAGTACT
HK1 F	CCCTAAATGCTGGGAAACAA
HK1 R	TCATCGCAGGTGCTATTCAG
PGK1 F	GTGCCAAATGGAACACGGAG
PGK1 R	TGCCAAGTGGAGATGCAGAA
ANKS3 e7-i7 F	GACACATGAAGATCGTGGCC
ANKS3 e7-i7 R	AAGCTCAAGGCAACCAGAGA
ANKS3 polyA 1 F	TGGGACCTTAGGAATGAGGAC
ANKS3 polyA 1 R	GTGCCTCATGTCATGTGACC
ANKS3 polyA 2 F	ACCTTAGGAATGAGGACTGGG
ANKS3 polyA 2 R	CCAGTGCCTCATGTCATGTG
ANKS6 e12-i12 F	CTTCCTCGTCATCCCATCGG
ANKS6 e12-i12 R	TCACCTTGCAGTTCCTTGCT

2.3 Western blot

Cells were plated at $1x10^5$ cells/mL in 10 cm^2 plates and incubated for at least 48 hours until approximately 80-90% confluent. Cells were washed twice with ice-cold phosphate buffered saline (PBS) and transferred to a 1.5 mL Eppendorf. The cells were resuspended in 50-100 µL lysis buffer (150 mM NaCl, 25 mM PO_4 pH 7.0, 1% Triton X-100, 0.5% NP40, protease inhibitor at 1x concentration) dependent on expected protein concentration and incubated at 4°C with rotation for 30 minutes to lyse the cells. The lysate was centrifuged at maximum speed for 10 minutes and the supernatant was transferred to a clean 1.5 mL Eppendorf. Protein concentration was measured using the Biorad DC protein Assay Kit, and lysates were diluted to a standard concentration of 30 µg.

An equal volume of 2x Laemmli buffer was added to the protein lysates and incubated at 37°C for 30 minutes.

Proteins were separated by 7% SDS acrylamide gel electrophoresis and transferred to a PVDF membrane (Immobilon®, Millipore) before blocking in 10% milk, or bovine serum albumin (BSA) if stated on antibody datasheets. The membranes were probed by primary and secondary antibodies (section 2.9) prepared in 5% milk or BSA and developed using the Biorad ECL reagent. The Biorad ChemiDoc™ XRS+ and Image Lab 5.1 software were used for visualisation and quantification of proteins of interest.

2.4 Co-Immunoprecipitation (Co-IP)

Cells were plated at $1x10^5$ cells/mL in $10cm^2$ plates or $2.5x10^5$ in 12-well plates and cell lysates were prepared as standard (section 2.3). Pierce™ anti-HA mouse conjugated magnetic beads and Pierce™ Protein G Magnetic Beads (Thermo Scientific) were resuspended and washed in triplicate in 1 mL immunoprecipitation (IP) buffer (150 mM NaCl, 25 mM PO_4 pH 7.0, 1% Triton X-100, 0.5% NP40, 1x protease inhibitor). The washed HA-conjugated beads were added to the cell lysate and incubated at 4°C for 90 minutes with rotation. Before the Protein G beads were added to the cell lysate, an antibody of interest was added at 1 µg and incubated at 4°C for 90 minutes with rotation. Following this, the Protein G beads were added and incubated at 4°C for 15 minutes with rotation. The protein-antibody complex was washed on a magnet four times in 1 mL IP buffer, with a final wash in PBS. The complex was resuspended in 2x Laemmli buffer and incubated at 37°C for 30 minutes. The samples were either ran on SDS-PAGE gel (section 2.3), to assess the efficiency of the Co-IP, or sent for analysis by mass spectrometry (MS) (section 2.5).

2.5 Mass Spectrometry

Samples were run on a 1D SDS-PAGE gel, cut into 10 sections and processed in a laminar flow cabinet, using an optimised in-gel digestion protocol conducted by the FingerPrints Proteomics department at the University of Dundee. This process was to minimise contamination (i.e. keratin). The trypsinised digests of each gel section were run on a 1D NanoLC ESI MS/MS instrument. This system required the loading of the samples onto a Capillary LC system, which is coupled to a MS/MS instrument. The sample peptides were separated within the Capillary LC system, using a reverse phase C18 column. The peptides were then eluted directly into the MS/MS instrument and detected as ions in the MS mode, or further fragmented and detected in MS/MS mode. The resulting peptides were inputted into the Mascot database to search and identify the proteins, and the identified proteins were analysed using the DAVID, KEGG pathway, PANTHER databases and statistical programmes (Figure 2.5.1).

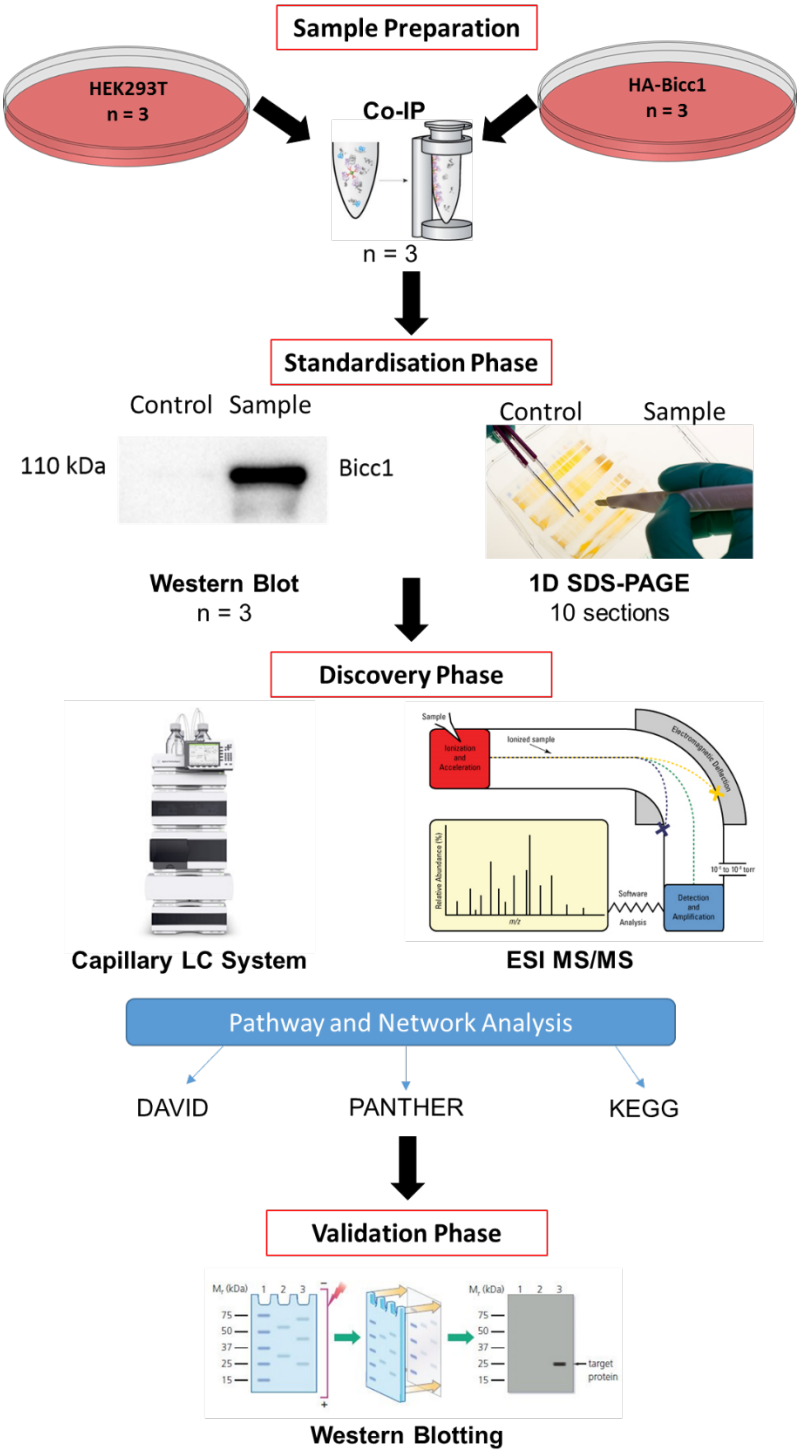

Figure 2.5.1. A flowchart depicting the experimental plan for proteomic analysis of BICC1 protein binding partners. During the sample preparation phase, HEK293 and HA-BICC1 cells were plated at 1x10^5 cells/mL and grown to 90% confluency. Protein was extracted from the cells and a Co-IP was performed to immunoprecipitate BICC1 and its proten binding partners. To test the efficiciency of the Co-IP, a western blot experiment was performed during the standardisation phase. Once this was verified, the samples were run on a 1D SDS-PAGE gel in preparation for mass spectrometery analysis. Ten sections were cut and digested with trypsin, before being applied to the LC Capillary system. The samples were then directly eluted onto the ESI MS/MS intrument. The spectra was inputted into the Mascott database and matched against library spectra to identify the proteins detected in the discovery phase. The identified proteins were then analysed using bioinformatic tools, and will be validated by western blotting.

2.6 Site-Directed Mutagenesis

To introduce mutations in ANKS3 and ANKS6 plasmid DNA constructs, site-directed mutagenesis was performed using either the *gfp*-ANKS3 or the *gfp*-ANKS6 construct as templates (Table 2.6.1). To induce the desired mutation (Figure 2.6.1), mutagenic primers were designed 15 base pairs (bp) either side of the mutation site (Table 2.6.2). The mutagenic PCR was set up as follows:

Component	**Amount per reaction**
ddH_2O	37.5 µL
10x Pfu Turbo Buffer	5 µL
Template DNA vector (50-100 ng/µL)	1 µL
Primer #1 (100 ng/µL)	1 µL
Primer #2 (100 ng/µL)	1 µL
dNTP Mix (10 µM)	1 µL
DMSO	2.5 µL
Pfu Turbo Enzyme (DNA polymerase)	1 µL

The PCR cycle was as follows:

Temperature	**Time**	**Repeats**
95°C	30 sec	
95°C	30 sec	X16
50°C to 68°C	1 min	
68°C	1 min/kb	
4°C	∞	

Before the mutagenic product was assessed by digestion, 10 µL of the PCR product was taken to be run on a 1% agarose gel. Then, 1 µL DpnI (Promega) was added to the PCR product to digest the methylated, un-mutated parental DNA template and to select for mutation-containing synthesized DNA. The reaction was incubated at 37°C for 30 minutes and then assessed on a 1% agarose gel, along with the un-digested RT-PCR product.

The DpnI-digested product (2 µL) was then transformed in 40 µL competent DH5-α cells and incubated at 37°C for 1 hour. Approximately 200 µL SOC media was added and the cells were plated onto ampicillin resistant agar plates and incubated at 37°C overnight. The following day, individual colonies were selected and added to 2 mL of LB broth with 100 µg mL^{-1} ampicillin and incubated at 37°C with shaking overnight. A negative control was included to assess for proper bacterial growth. Following incubation, a miniprep procedure was performed using the Omega E.Z.N.A. Plasmid DNA Mini Kit to isolate the

mutagenic plasmid DNA and the desired mutation was assessed by DNA sequencing.

Table 2.6.1. DNA constructs used in this study.

DNA Construct	Species Origin	Tag	Source
gfp-ANKS3	*Mus musculus*	*gfp*	Walz Lab
gfp-ANKS3-ΔSAM	*Mus musculus*	*gfp*	Ong Lab
gfp-ANKS6	*Rattus norvegicus*	*gfp*	Walz Lab
gfp-ANKS6-ΔSAM	*Rattus norvegicus*	*gfp*	Ong Lab
myc-mBICC1	*Mus musculus*	myc	Wessely Lab
myc-mBICC1-ΔKH	*Mus musculus*	myc	Ong Lab
myc-mBICC1-ΔSAM	*Mus musculus*	myc	Ong Lab
myc-mBICC1-del133-691	*Mus musculus*	myc	Ong Lab
PC1-HA	*Homo sapiens*	HA	Ong Lab
HA-PC1-R4227X	*Homo sapiens*	HA	Ong Lab
PC2-HA	*Homo sapiens*	HA	Ong Lab
HA-PC2-R742X	*Homo sapiens*	HA	Ong Lab
NT2-HA	*Homo sapiens*	HA	Ong Lab
GST-CT1	*Homo sapiens*	GST	Ong Lab
GST-CT1-4227X	*Homo sapiens*	GST	Ong Lab
GST-NT2	*Homo sapiens*	GST	Ong Lab
GST-CT2	*Homo sapiens*	GST	Ong Lab

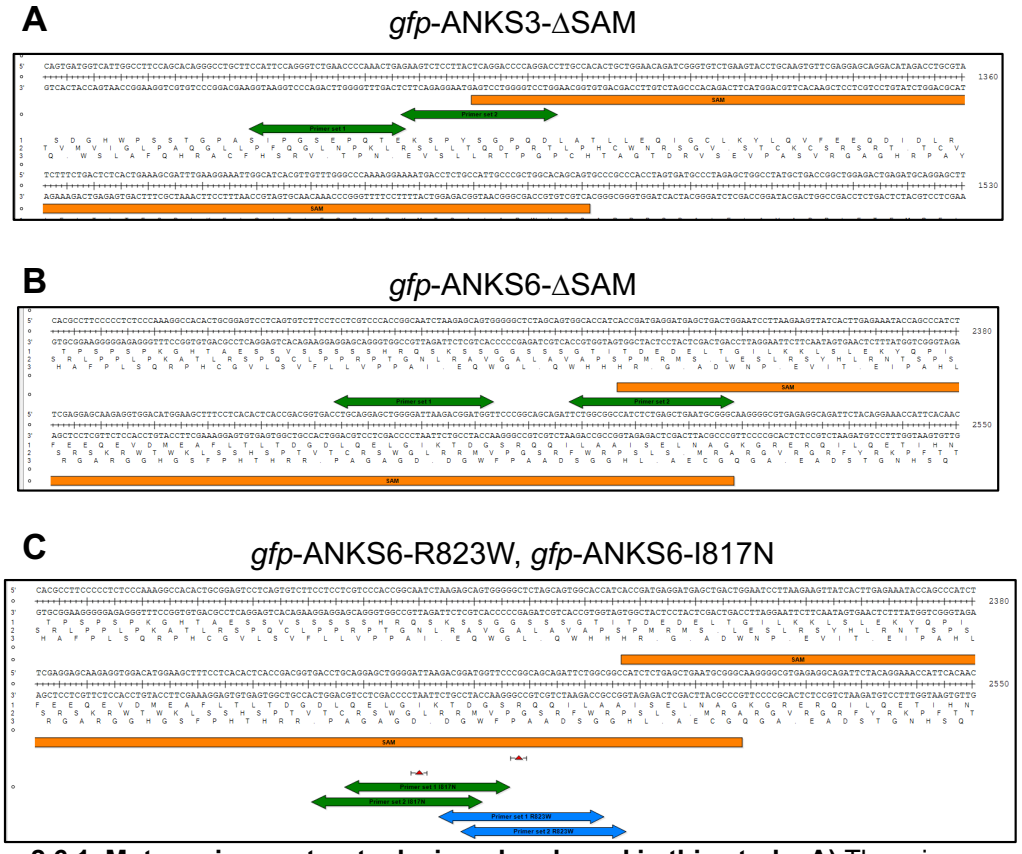

Figure 2.6.1. Mutagenic constructs designed and used in this study. A) The primers were designed to induce a STOP upstream of the ANKS3-SAM domain in order to create a construct with the ANKS3-SAM domain deleted. **B)** The primers were designed to induce a STOP upstream of the ANKS6-SAM domain in order to create a construct with the ANKS6-SAM domain deleted. **C)** The primers were designed to induce a two different point mutation within the ANKS6-SAM domain in order to create the constructs ANKS6-R823W (green) and ANKS6-I817N (blue). Two sets of primers were designed for each mutagenesis experiment. The sequence upstream and downstream of the ANKS3- and ANKS6-SAM domains is shown. SAM = sterile alpha motif (orange).

Table 2.6.2. Mutagenic primers used in this study. The nucleotide highlighted in red was the nucleotide changed in order to either produce a STOP codon or induce a point mutation depending on the experimental procedure. Two sets of primers were designed for each experimental condition and the primers used to successfully generate the mutagenic constructs are displayed.

Construct	Sequence (5'-3')
gfp-ANKS3-ΔSAM F	CC ATT CCA GGG TCT TAA CCC CAA ACT GAG
gfp-ANKS3-ΔSAM R	CTC AGT TTG GGG TTA AGA CCC TGG AAT GG
gfp-ANKS6-ΔSAM F	CC TCG TCC CAC CGG TAA TCT AAG AGC AGT G
gfp-ANKS6-ΔSAM R	C ACT GCT CTT AGA TTA CCG GTG GGA CGA GG
gfp-ANKS6-R823W F	G ACG GAT GGT TCC TGG CAG CAG ATT CTG GC
gfp-ANKS6-R823W R	GC CAG AAT CTG CTG CCA GGA ACC ATC CGT C
gfp-ANKS6-I817N F	CAG GAG CTG GGG AAT AAG ACG GAT GGT TCC
gfp-ANKS6-I817N R	GGA ACC ATC CGT CTT ATT CCC CAG CTC CTG

2.7 CRISPR-Cas9

To create a stable *KO* cell line, single guide RNAs (sgRNA) were designed using Benchling to the first exon of the target gene followed by a PAM sequence and ordered from Eurofins (Table 2.7.1). The cloning of the sgRNA oligos into a pSpCas9 (BB) vector for co-expression with Cas9 was adapted from Ran *et al*. (2013). Briefly, the sgRNAs were mixed with 1 µL 10x T4 ligation buffer, 1 µL T4 PNK enzyme and 6 µL ddH_2O and incubated in a thermocycler to align the oligos. The reaction was as follows: 37°C for 30 minutes, 95°C for 5 minutes, ramp down to 25°C at 5°C min^{-1}. The sgRNA oligos were diluted 1:200 and a ligation reaction was performed to clone the oligos into the pSpCas9 (BB) vector. The reaction was as follows: 100 ng pSpCas9 (BB), 2 µL diluted sgRNA oligos, 2 µL 10x Tango buffer, 1 µL 10 mM ATP, 1 µL FastDigest Bbsl or Bpil, 0.5 µL T7 of T4 DNA ligase and ddH_2O to make to reaction volume up to 20 µL. The ligation reaction was incubated in a thermocycler as follows: 37°C for 5 minutes, 21°C for 5 mins, repeat for 10 cycles, end of 65°C for 30 minutes and hold at 12°C. The ligation product was then transformed into competent cells, stocks were produced, and the ligation was assessed by DNA sequencing as performed in section 2.6. An example of the sgRNA guide vector generated for the *BICC1* gene is shown in Figure 2.7.1.

Once confirmed, 1 µg of the plasmid DNA construct was co-transfected into UCL93 cells at a concentration of $1x10^6$ cells/mL using 3 µL Lipofectamine 3000 and 50 µL Opti-MEM reduced serum media. The final volume was 2 mL. The cells were incubated at 37°C for 7 hours before the media was removed

and replaced with fresh Nu serum media. A GFP transfection control was included to check for successful transfection. If successful, the cells were trypsinised and media with 3.5 µg/mL puromycin (10 mg/mL) was added to select for puromycin resistant clones (as the pSpCas9 (BB) vector contains a puromycin resistant gene). The cells were incubated at 33°C for at least 72 hours before the assessment of puromycin resistant clones. After 72 hours, the media was replaced, and cells were allowed to recover and expand for 1 week with regular media replacements.

After 1 week the cells were observed to be about approximately 10-20% confluent, so they were trypsinised and plated as single cells into a 96-well plate. The cells were incubated at 33°C for 2-3 weeks and then expanded into 12-well plates for functional assessment. The *KO* was tested by western blotting and any successful clones were validated by DNA sequencing. The successful clones were used for any downstream experiments.

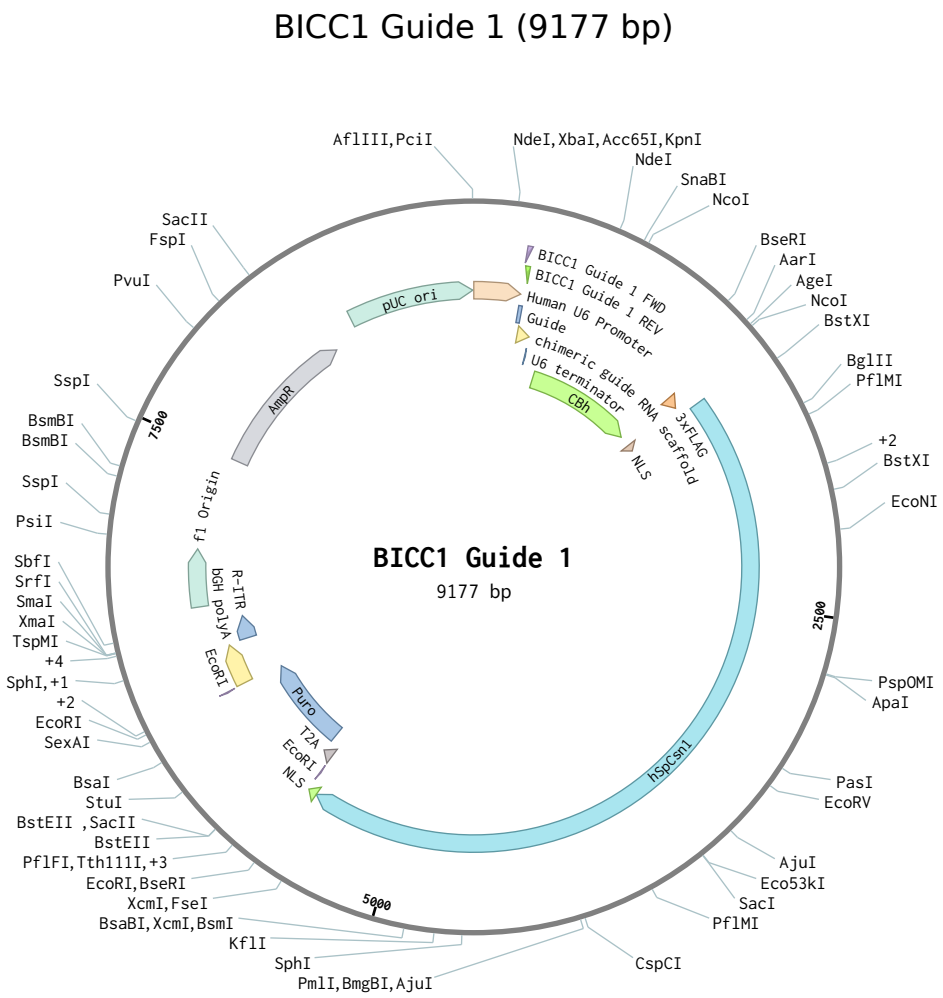

Figure 2.7.1. The *BICC1 KO* sgRNA sequencing vector generated for this study.

Table 2.7.1. The sgRNA guide oligos designed and used in this study. The sgRNA guides were designed to the first exon of the target gene.

sgRNA	Sequence (5'-3')
BICC1 sgRNA F	CACCGGGAGAGCCCGGCTACCTGG
BICC1 sgRNA R	AAACCCAGGTAGCCGGGCTCTCCC
PKD1 sgRNA F	CACCGCGCCGGGCGCTGGGCCGCAG
PKD1 sgRNA R	AAACCTGCGGCCCAGCGCCCGGCGC
PKD2 sgRNA F	CACCGCGTGGAGCCGCGATAACCC
PKD2 sgRNA R	AAACGGGTTATCGCGGCTCCACGC

2.8 Low Formaldehyde RNA Immunoprecipitation (RIP)

UCL93 and *BICC1 KO* cells were plated at $5x10^5$ cells/mL in 10 mL in 10 cm^2 plates and incubated at 33°C until 90% confluency was achieved. Once confluent, the cells were fixed with 0.1% formaldehyde to cross-link protein-RNA interactions (Hendrickson *et al*., 2016). After 10 minutes 1x glycine (0.125 M) was added to stop the fixation and the cells were rocked at room temperature for 5 minutes. The cells were then harvested, washed with ice cold PBS and prepared for cell lysis. The cells were suspended in 400 µL lysis buffer 2 (lysis buffer, 1/25 protease inhibitor cocktail (SigmaFast), 1 mM DTT, RNase inhibitor) and transferred to ice-chilled Eppendorfs. The cells were homogenised through the addition of 2 µL Turbo DNase and left on ice for 5 minutes. The cells were then subjected to sonication (10x 30s ON – 30s OFF) to generate short RNA fragments of approximately 300-400 nucleotides in length. Following sonication, the cells were centrifuged at 16100 xg for 10 minutes at 4°C to clear the lysate. An 10% input sample (30 µL) was retained, snap-frozen and kept at -80°C for downstream procedures.

Dynabeads Protein G (Novex by Life Technologies) were used in this study to immunoprecipitate endogenous BICC1. 100 µL of the beads were used per condition and were washed twice with 900 µL lysis buffer (50 mM HEPES-HCl pH 7.5, 150 mM NaCl, 10% glycerol, 1% NP-40, 0.1% SDS, 0.5% sodium deoxycholate) and then resuspended in 300 µL lysis buffer supplemented with 1% BSA and 4 µg of anti-mouse BICC1 antibody (Santa Cruz Biotechnology Inc). The beads/antibody suspension was incubated at room temperature for 1 hour before being washed twice with 900 µL lysis buffer. The remaining volume of the cleared lysate (approximately 300 µL) was added to the beads and the sample were rotated at 4°C for 2 hours.

The samples were washed twice with 900 µL lysis buffer followed by washes with 900 µL high salt lysis buffer (0.5 M NaCl) and then washes with 900 µL normal lysis buffer. Following these washes, 56 µL ice-cold RNase free H_2O was added to the beads and 26 µL to the inputs, before 33 µL of the 3X reverse-crosslinking buffer (3X PBS, 6% N-lauroylsarcosine, 30 mM EDTA, 15 mM DTT), 10 µL proteinase K (Roche 19 mg/uL) and 1 µL RNase inhibitor was added. The beads were resuspended by flicking the tube gently and were then incubated at 42°C for 1 hour followed by 55°C for 1 hour with shaking at 1100rpm (for both hours). The samples were placed on a magnet and the eluates were collected and the total volume was made to 250 µL (addition of approximately 150 µL) with ice-cold RNase free H_2O. RNA was isolated and treated with DNase I following the same procedure described in section 2.2. Depending on the downstream experiment required, the treated RNA was subjected to RT and qPCR or sent for deep sequencing with Novogene. Primers were designed to assess the regional binding of BICC1 upon RNA targets and are listed in Table 2.8.1.

Table 2.8.1. RIP primers used in this study.

Oligo	Sequence (5'-3')
PKD1 5' UTR F	CGCTAGACGTCTCCCACAA
PKD1 5' UTR R	CGGGTTCCCACTCAGGTTTA
PKD1 3' UTR F	TGGACGGTTTCTAGCCTCTG
PKD1 3' UTR R	GGGAGTACGGTAGGAACTGG
PKD2 5' UTR F	GGAAAGCAGCACTAACCGAG
PKD2 5' UTR R	TTGGAGCTCATCATGCCGTA
PKD2 3' UTR F	TGCCACCATGACTGAGTCTT
PKD2 3' UTR R	GCCAGAGTGGAAAGGAATGC
ANKS3 5' UTR F	GTGCAGCGGAGAGAGTTAGA
ANKS3 5' UTR R	GATTGTGTCGTGGCCAATGT
ANKS3 3' UTR F	GGAGGACAGTGAGCAGGTAG
ANKS3 3' UTR R	ATGAACTCTGGGCCTCACC

2.9 Antibodies

Primary antibodies used in this study include anti-mouse BICC1 (sc-514846, Santa Cruz), anti-mouse ANKS6 (sc-515124 Santa Cruz), anti-rabbit ANKS3 (24058-1-AP, Proteintech), anti-mouse PC1 (sc-130554, Santa Cruz), anti-goat PC2 (sc-10376, Santa Cruz), anti-mouse ACTB (ab6276, Abcam), anti-HA High Affinity (rat monoclonal clone 3F10, Roche) and anti-rabbit GFP (ab6556, Abcam). All primary antibodies were used at 1:1000 unless otherwise stated in

the results section. Secondary antibodies used in this study include goat anti-mouse IgG (1030-05, Southern Biotech), goat anti-rabbit IgG (4050-01, Southern Biotech), goat anti-rat IgG (3050-01, Southern Biotech) and rabbit anti-goat IgG (P 0449, Dako). All secondary antibodies were used at 1:10,000, unless otherwise stated in the results section.

2.10 Statistical analysis

Data generated was entered into the Prism software to produce grouped bar charts and separated scatter graphs, with standard error of the mean plotted. Statistical analysis, including paired T-tests and ANOVA, were also performed using the Prism software and statistically significant p-values were represented on the graphs.

2.11 Figure Drawing

Figures throughout the thesis were drawn using templates from Smart - Servier Medical Art: https://smart.servier.com under the Creative Commons Attribution 3.0 Unported License. Where cited, some figures were designed using Biorender: https://biorender.com with my student, individual license.

Chapter 3

BICC1 FORMS AN INTERACTION COMPLEX WITH PC1 AND PC2

3.0 BICC1 forms an interaction complex with PC1 and PC2

3.1 Introduction and Aims

BICC1 post-transcriptionally regulates the mRNA expression of *PKD2* in a *Bicc1*$^{-/-}$ mouse model (Tran *et al*., 2010). Furthermore, BICC1 has also been observed to regulate *PKD2* expression in the ducts of pancreatic progenitor cells (Lemaire *et al*., 2015). In addition, BICC1 regulates osteoblast differentiation through the regulation of *PKD2* expression, as observed in the *Bicc1*$^{jcpk/jcpk}$ mouse (Mesner *et al*., 2014). However, the mechanism underlying these functions are unknown, although clearly *PKD2* is a downstream target of BICC1 in osteogenesis. Researchers have also reported a potential link between BICC1 and PC1, as loss of *Pc1* by shRNA in mIMCD3 cells and in the *PKD1*$^{-/-}$ mouse model resulted in a reduction of *Bicc1* mRNA and protein expression levels by 50% (Lian *et al*., 2014). To confirm a regulatory role of *Pc1* upon *Bicc1*, *Pc1* was re-introduced into mIMCD3 cells and *Bicc1* levels were restored. This research suggests a functional link of BICC1 with PC1 and suggests that PC1 is upstream of BICC1 in a cystogenesis pathway.

Despite a functional relationship forming between BICC1 and the polycystins, how they interact, why this is important, and the downstream ramifications are not clear. Therefore, this chapter aimed to further understand this relationship through protein-protein interactions, as a link between BICC1 and the polycystins at the protein level has never been previously established. Moreover, this chapter aimed to further elucidate whether BICC1 regulates the expression of the polycystins at the mRNA and protein level.

Chapter Aims:

1. Confirm that loss of BICC1 causes ADPKD-like phenotypes
2. Investigate whether BICC1 and the polycystins interact at the protein level
3. Confirm that BICC1 regulates the mRNA expression of *PKD2* and examine whether BICC1 also regulates the mRNA expression of *PKD1*
4. Investigate whether BICC1 regulates the protein expression levels of PC1 and PC2

3.2.1 Loss of BICC1 causes ADPKD-like phenotypes

Published data has demonstrated a link between loss of BICC1 and cystogenesis. Therefore, a 3D collagen cyst assay was performed upon the UCL93 (a non-cystic human control immortalised kidney epithelial cell line) and *BICC1 KO* cell lines to assess cyst formation (see section 2.1 for methods). After 14 days culture in 3D matrigel, *BICC1 KO* cells (*BICC1 KO* C4 is displayed below as a representative image) developed more cysts than tubule structures compared to the UCL93 cells (Figure 3.2.1.1). *BICC1 KO* cells produced ~70% cysts compared to ~30% tubules, while UCL93 cells produced ~15% cysts compared to ~85% tubules. This assay confirms that loss of BICC1 leads to a cystic phenotype in vitro.

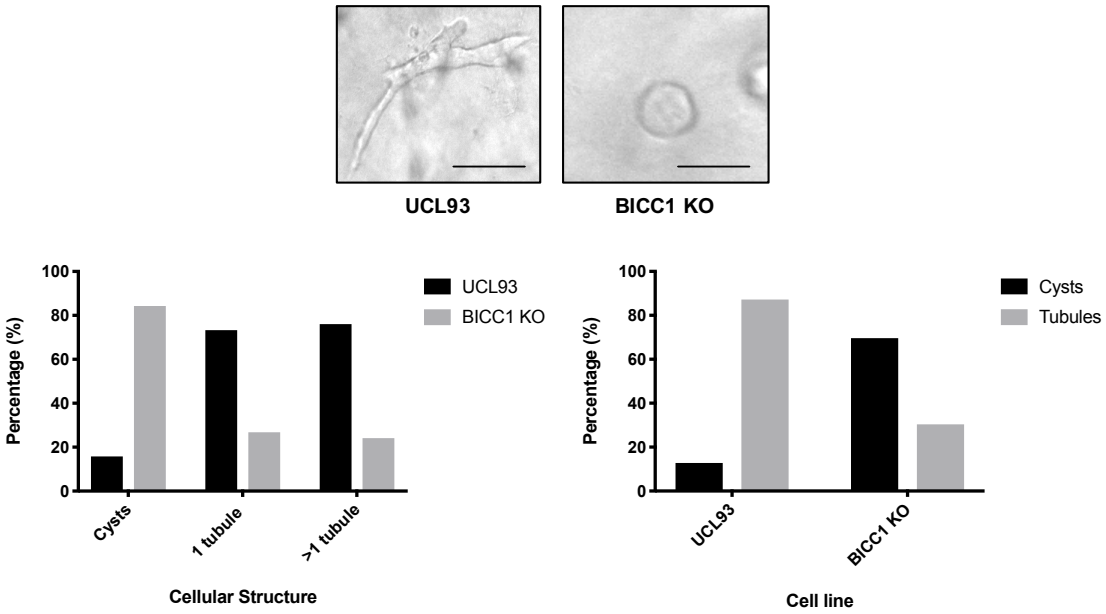

Figure 3.2.1.1. Loss of BICC1 causes cystogenesis in 3D culture. A cyst assay was performed to assess tubule formation in UCL93 and *BICC1 KO* cell lines. In this representative experiment, *BICC1 KO* C4 was used (n=1). The number of tubules, branching tubules and cysts were counted and plotted. Scale bar represents 5 μM. Images were taken at x60 magnification.

To assess whether cellular growth rates were affected in *BICC1 KO* cell lines compared to UCL93 cells, cell counts were taken every 24 hours following initial plating at a density of $1x10^5$ cells/mL. No significant changes were observed between UCL93 cells and *BICC1 KO* cell lines, except for *BICC1 KO* C35, which appears to be an outlier (Figure 3.2.1.2).

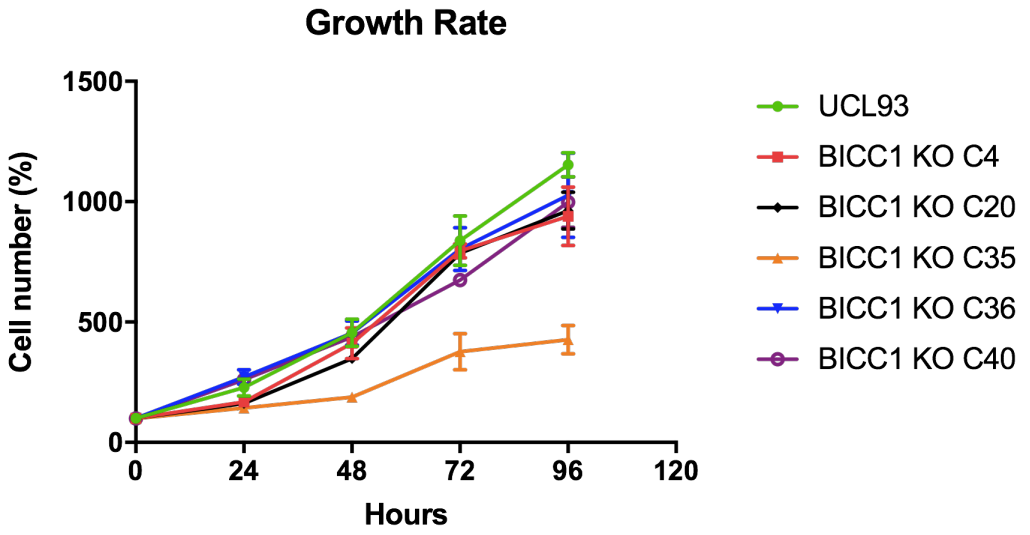

Figure 3.2.1.2. Loss of BICC1 does not affect cellular growth rate. Cell counts were performed for UCL93 and *BICC1 KO* cell lines every 24 hours following an initial cell plating density of $1x10^5$ cells/mL (n=3). A value of 1.0 was assigned to 0 hours and the cell number at all other time points was expressed relative to this value as a percentage.

3.2.2 PC1 regulates the expression of BICC1 in human kidney epithelial cells

To confirm a regulatory link between PC1 and BICC1 in the kidneys, BICC1 expression levels were assessed in healthy (UCL93) and ADPKD (Ox161c1) human patient kidney epithelial cells. The Ox161c1 cell line has reduced *PKD1* expression (see section 2.1 for more details regarding the cell lines). As observed in published data, BICC1 expression was significantly decreased at both the mRNA and protein level by 60% and 80% respectively (Figure 3.2.2.1 A and B).

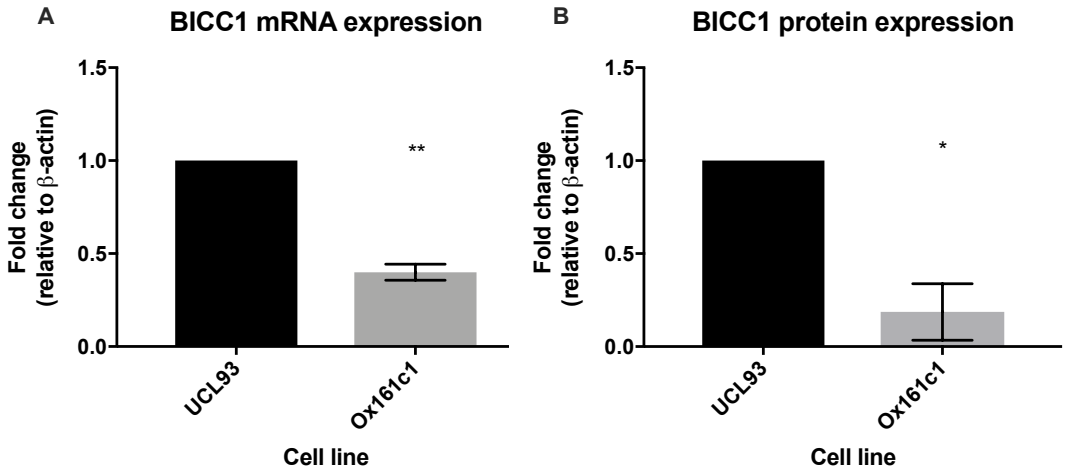

Figure 3.2.2.1. PC1 regulates the expression of BICC1. A) qPCR was used to measure the mRNA expression level of BICC1 in UCL93 and Ox161c1 patient kidney epithelial cell lines (n=3). **B)** Western blot analysis was used to measure protein expression levels of BICC1 between UCL93 and Ox161c1 patient kidney epithelial cell lines (n=3). Paired t-tests were performed (p values * ≤0.05, ** = ≤0.01, *** = ≤0.001 and **** = ≤0.0001). Error bars represent standard error of the mean.

3.2.3 PC1 and BICC1 interact

As discussed in section 3.1, loss of PC1 is associated with lower expression of BICC1 both *in vitro* and *in vivo*, but the molecular link and mechanism responsible for this regulatory function has not been fully investigated. Furthermore, BICC1 regulates the expression of *PKD2* in various cellular and animal models. However, an interaction between BICC1, PC1 and PC2 at the protein level has never been explored. Therefore, this study investigated whether BICC1 directly interacts with PC1 or PC2 proteins. To explore a possible interaction between PC1 and BICC1, various BICC1 constructs were designed and transfected into HEK293 cells along with a full-length PC1 construct (Figure 3.2.3.1 and Figure 3.2.5.2).

Figure 3.2.3.1. Schematic diagram of BICC1 constructs used in this study. The myc-mBICC1 construct represents full length BICC1, while myc-mBICC1-ΔSAM has the SAM domain and the following 39 amino acids deleted and myc-mBICC1-ΔKH has the KH domains and the preceding 132 amino acids deleted. KH= K-homology, SAM= sterile alpha motif.

A Co-IP experiment was performed to investigate whether PC1 and BICC1 interact *in vitro*, and which protein domains could be responsible. HEK293 cells were co-transfected with a full-length PC1 construct containing a HA-tag (PC1-HA) and either full-length BICC1 (myc-mBICC1) or deletion constructs of BICC1 i.e. with its SAM domain deleted (myc-mBICC1-ΔSAM) or with its KH domain deleted (myc-mBICC1-ΔKH) (Figure 3.2.3.1 and Figure 3.2.5.2). Western blot analysis demonstrated that full-length PC1 interacts with full-length BICC1 (Figure 3.2.3.2 A).

Full-length PC1 was also observed to interact with the deletion constructs assessed. Moreover, a significantly stronger interaction was observed between full-length PC1 and myc-mBICC1-ΔKH (8-fold) compared to myc-mBICC1 and myc-mBICC1-ΔSAM, suggesting the interaction between PC1 and BICC1 does not require the KH domain or the first 132 amino acids of BICC1 (Figure 3.2.3.2 B). The interaction with myc-mBICC1-ΔSAM suggests that the interaction between PC1 and BICC1 does not require the SAM domain or the terminal 39 amino acids of BICC1 also. However, the SAM domain may be involved in stabilising the protein interaction, as the association of PC1 with myc-mBICC1-ΔSAM was approximately 55% lower compared to its association with full-length BICC1, although this was not statistically significant (Figure 3.2.3.2 B). No interaction was observed with the pcDNA3 negative control.

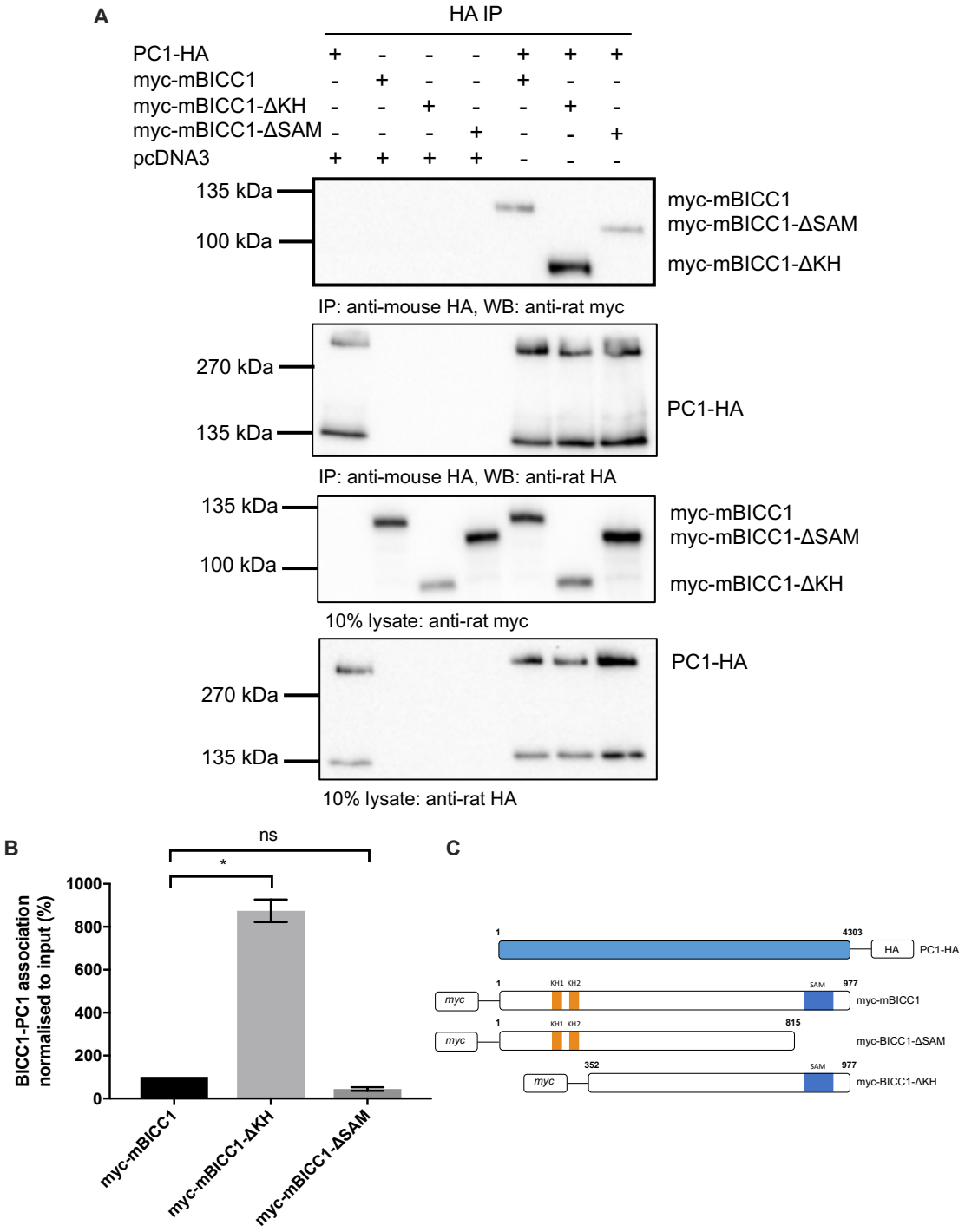

Figure 3.2.3.2. PC1 and BICC1 interact. A) Western blot analysis following Co-IP experiments, using a PC1-HA tagged construct as bait, were used to assess protein interactions between PC1 and BICC1. pcDNA3 was included as a negative control. **B)** Quantification of the Co-IP experiments (n=3). Paired t-tests were performed to assess significance (p values * ≤0.05, ** = ≤0.01, *** = ≤0.001, **** = ≤0.0001 and ns = not significant). Error bars represent standard error of the mean. **C)** Schematic diagram of the constructs used in this experiment.

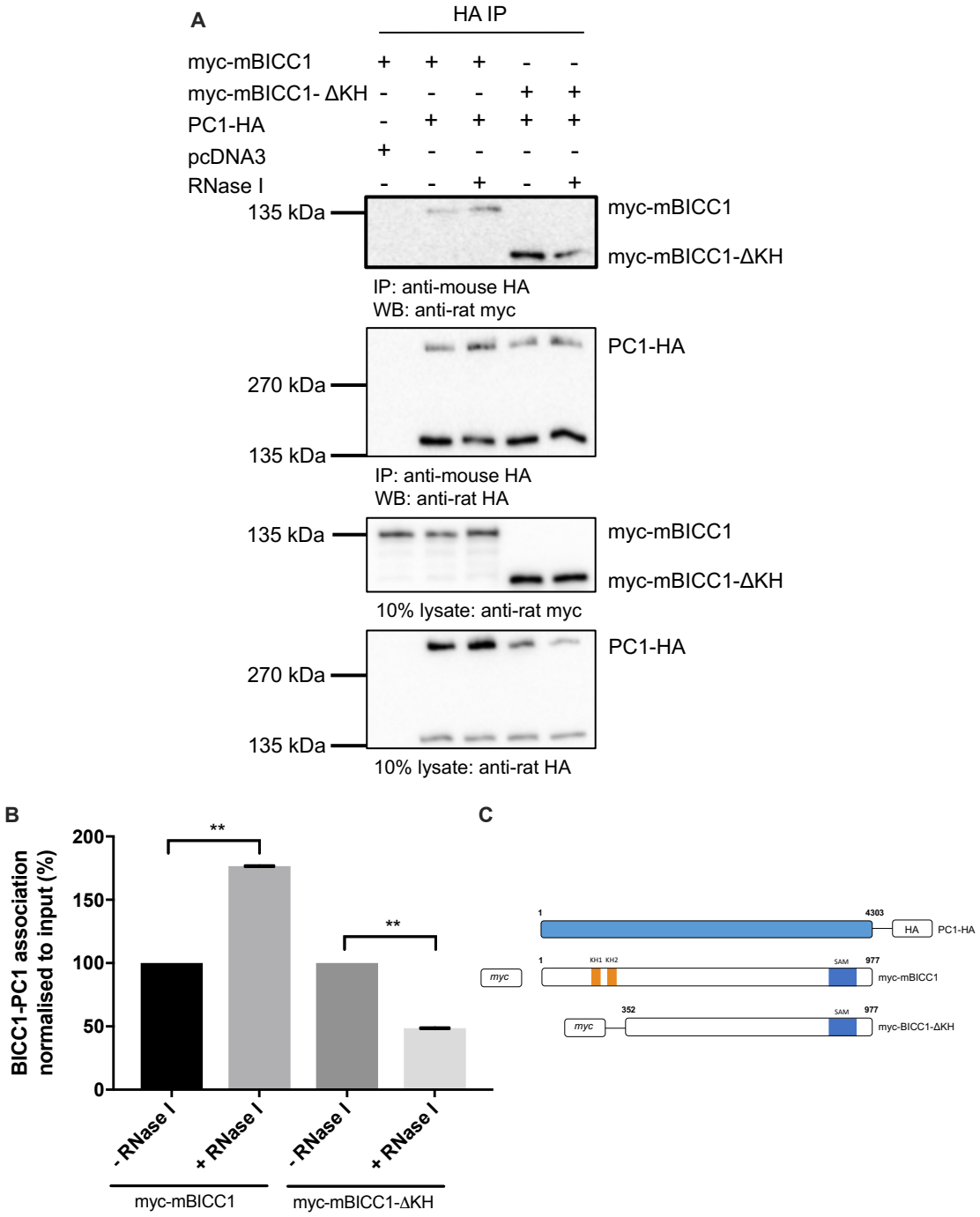

Figure 3.2.3.3. The interaction between PC1 and BICC1 is affected by RNase treatment. **A)** Western blot analysis following Co-IP experiments, using a PC1-HA tagged construct as bait, were used to assess protein interactions between PC1 and BICC1. RNase I was introduced to the Co-IP experiments in lane 3 and 5. pcDNA3 was included as a negative control. **B)** Quantification of the Co-IP experiments, with comparisons drawn between no RNase I treatment (-RNase I) and RNase I treatment (+RNase I) (n=3). Paired t-tests were performed to assess significance (p values * ≤0.05, ** = ≤0.01, *** = ≤0.001 and **** = ≤0.0001). Error bars represent standard error of the mean. **C)** Schematic diagram of the constructs used in this experiment.

Further Co-IPs were performed to investigate whether treatment with RNase I affects the interaction between full-length PC1 and myc-mBICC1 and myc-mBICC1-ΔKH. As before, HEK293 cells were co-transfected with the stated constructs and lysates were extracted. Western blot analysis demonstrated that RNase I treatment significantly increased the interaction between full-length PC1 and full-length BICC1 by nearly 2-fold (Figure 3.2.3.3). In contrast, RNase I treatment significantly decreased the interaction between full-length PC1 and myc-mBICC1-ΔKH by 50%. No interaction was observed with the pcDNA3 negative control.

Based on these results, a Co-IP was next performed to investigate whether PC1 and BICC1 interact endogenously, and whether treatment with RNase I would have an effect. Lysates were extracted from UCL93 cells and western blot analysis demonstrated that PC1 interacts with BICC1 endogenously (Figure 3.2.3.4 A). Furthermore, treatment with RNase I had no effect on the interaction, which suggests that there is no RNA intermediate required for the endogenous interaction between PC1 and BICC1 (Figure 3.2.3.4 B). This data also validates previous work perform in our lab by Dr Andrew Streets, who demonstrated a direct interaction between PC1 and BICC1 through *in vitro* binding assays (Streets, unpublished). No interaction was observed with the anti-mouse IgG negative control.

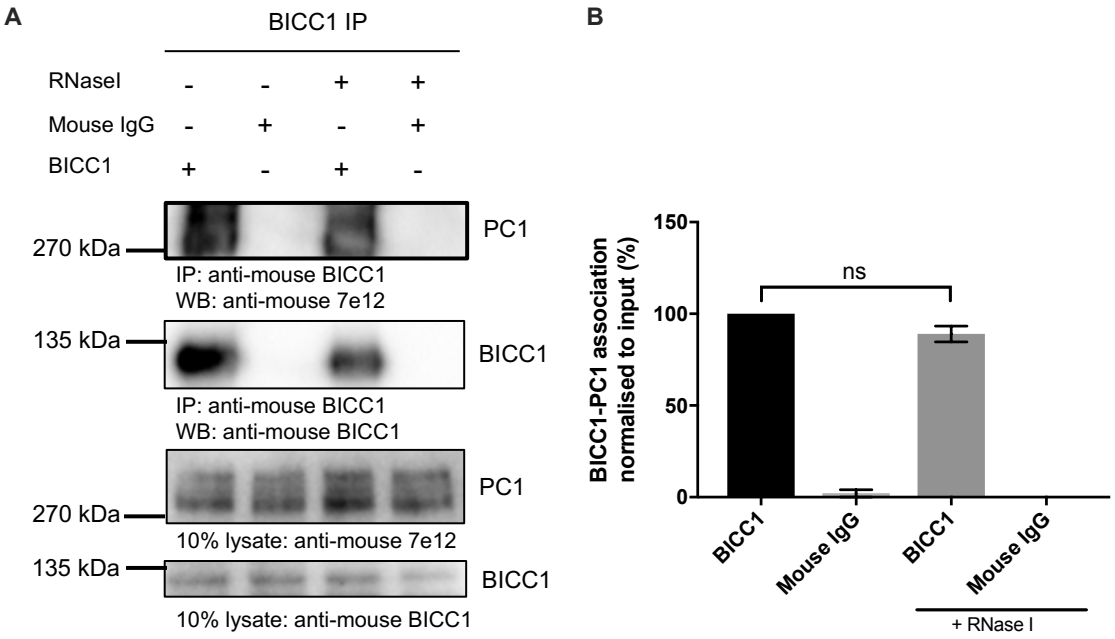

Figure 3.2.3.4. PC1 and BICC1 interact endogenously. A) Western blot analysis following Co-IPs experiments, using an anti-mouse BICC1 antibody as bait, were used to assess endogenous protein interactions between PC1 and BICC1. A mouse IgG antibody was included as a negative control. **B)** Quantification of the Co-IP experiments (n=3). Paired t-tests were performed to assess significance (ns = not significant, p value = >0.05). Error bars represent standard error of the mean.

3.2.4 PC2 and BICC1 interact

A Co-IP was performed to investigate whether PC2 and BICC1 interact *in vitro*, and which protein domain may be responsible. HEK293 cells were co-transfected with a full-length PC2 construct containing a HA-tag (PC2-HA) and either full-length BICC1 (myc-mBICC1), BICC1 with its SAM domain deleted (myc-mBICC1-ΔSAM) or BICC1 with its KH domain deleted (myc-mBICC1-ΔKH) constructs (Figure 3.2.3.1 and Figure 3.2.5.2). Western blot analysis demonstrated that full-length PC2 interacts with full-length BICC1 (Figure 3.2.4.1 A). Full-length PC2 was also observed to interact with myc-mBICC1-ΔSAM, but not with myc-mBICC1-ΔKH, suggesting that unlike PC1, the interaction between PC2 and BICC1 is through the KH domain of BICC1 (Figure 3.2.4.1 B). No interaction was observed with the pcDNA3 negative control.

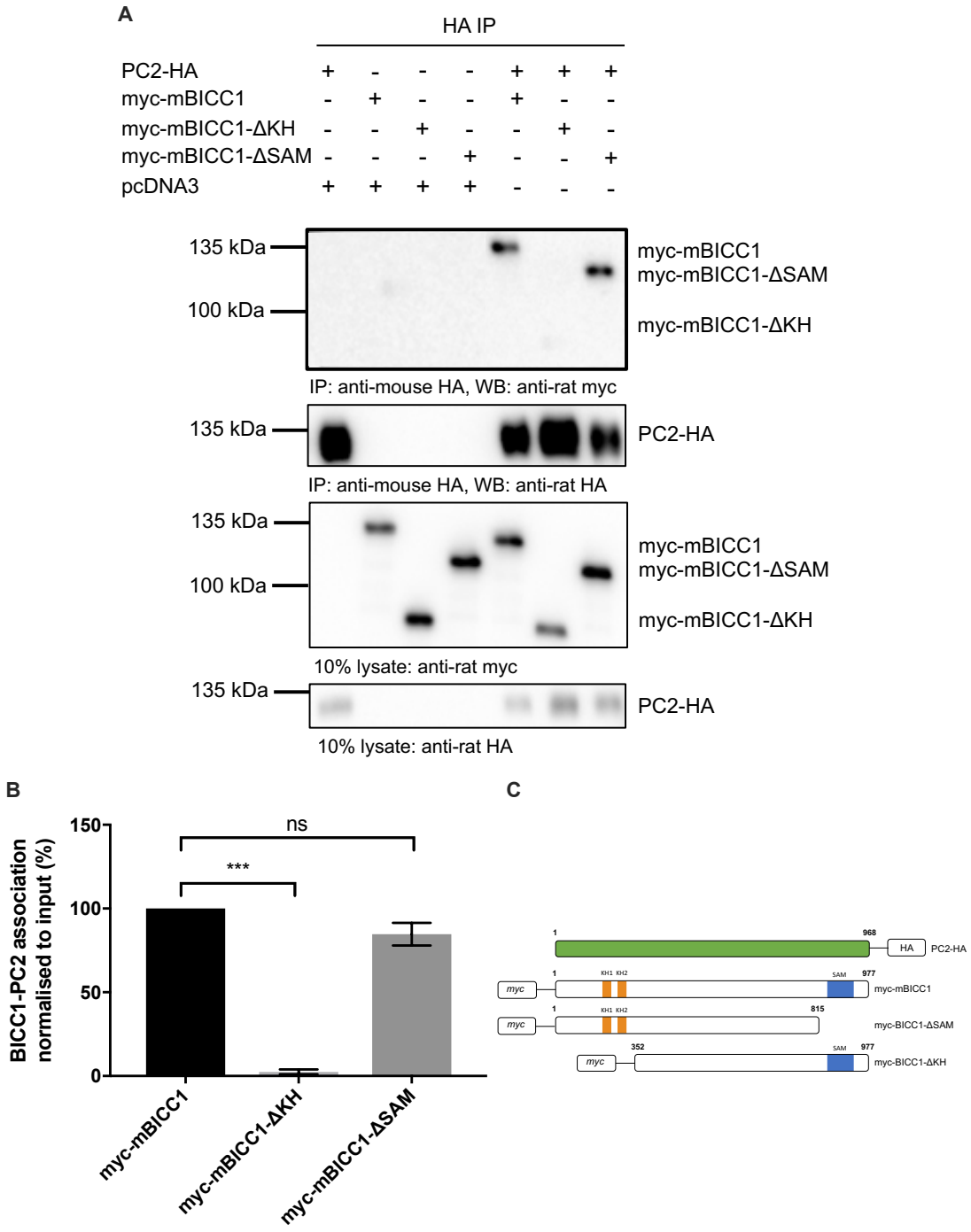

Figure 3.2.4.1. PC2 and BICC1 interact. A) Western blot analysis following Co-IP experiments, using a PC2-HA tagged construct as bait, were used to assess protein interactions between PC2 and BICC1. pcDNA3 was included as a negative control. **B)** Quantification of the Co-IP experiments (n=3). Paired t-tests were performed to assess significance (p values * ≤0.05, ** = ≤0.01, *** = ≤0.001, **** = ≤0.0001 and ns = not significant). Error bars represent standard error of the mean. **C)** Schematic diagram of the constructs used in this experiment.

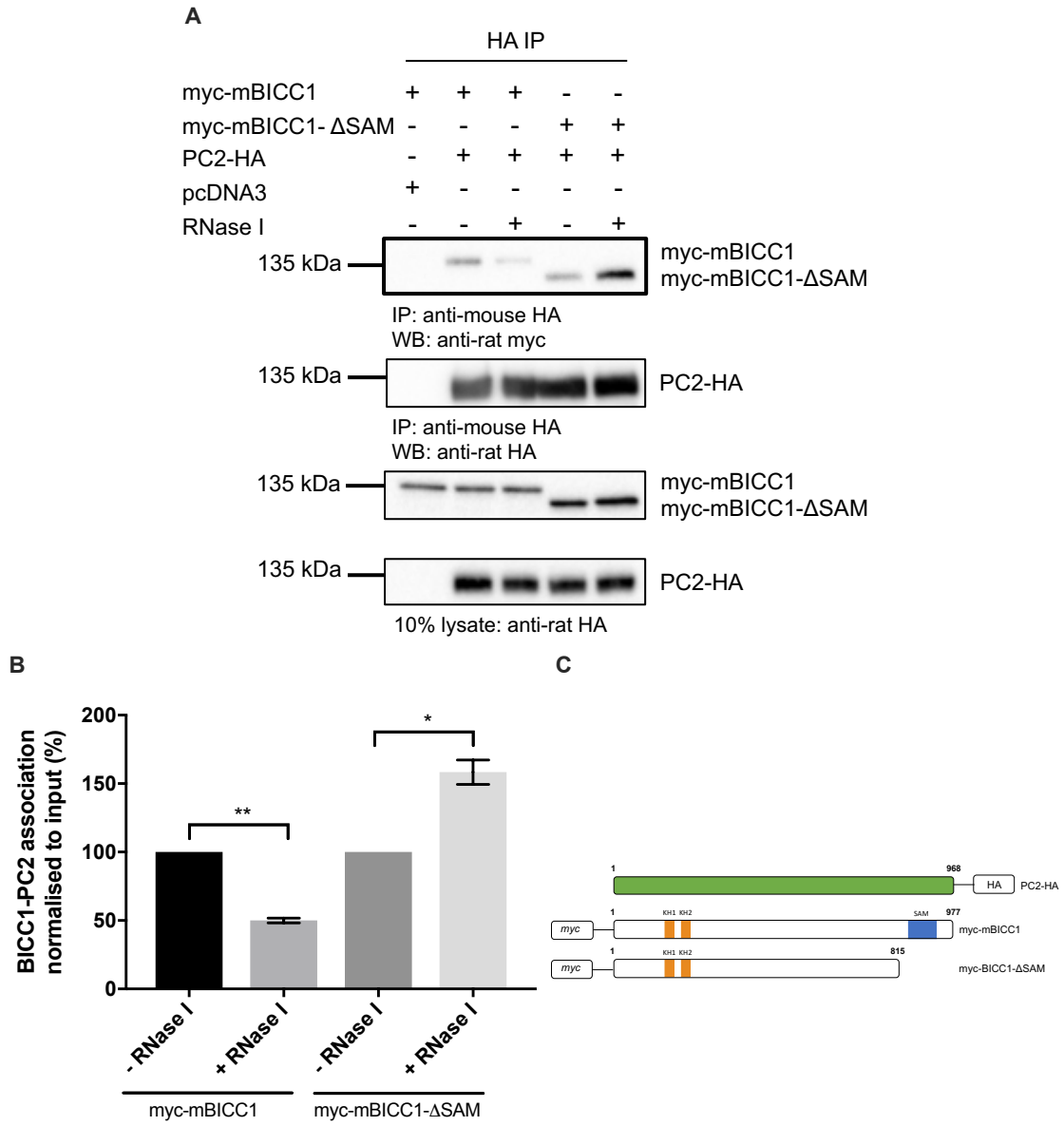

Figure 3.2.4.2 The interaction between PC2 and BICC1 is affected by RNase treatment. **A)** Western blot analysis following Co-IP experiments, using a PC2-HA tagged construct as bait, were used to assess protein interactions between PC2 and BICC1. RNase I was introduced to the Co-IP experiments in lane 3 and 5. pcDNA3 was included as a negative control. **B)** Quantification of the Co-IP experiments, with comparisons drawn between no RNase I treatment (-RNase I) and RNase I treatment (+RNase I) (n=3). Paired t-tests were performed to assess significance (p values * ≤0.05, ** = ≤0.01, *** = ≤0.001 and **** = ≤0.0001). Error bars represent standard error of the mean. **C)** Schematic diagram of the constructs used in this experiment.

Further Co-IPs were performed to investigate whether treatment with RNase I effects the interaction between full-length PC2 and myc-mBICC1 and myc-mBICC1-ΔSAM. As before, HEK293 cells were co-transfected with the stated constructs and lysates were extracted. Western blot analysis demonstrated that RNase I treatment significantly decreased the interaction between full-length PC2 and full-length BICC1 by 50% (Figure 3.2.4.2). In contrast, RNase I

treatment significantly increased the interaction between full-length PC2 and myc-mBICC1-ΔSAM by 1.5-fold. No interaction was observed with the pcDNA3 negative control.

Following results from the previous data, a Co-IP was performed to investigate whether PC2 and BICC1 interacted endogenously, and whether treatment with RNase I would have an effect. Lysates were extracted from UCL93 cells and western blot analysis demonstrated that PC2 interacts with BICC1 endogenously (Figure 3.2.4.3 A). Furthermore, treatment with RNase I increased the interaction by approximately 45%, although this did not reach statistical significance (Figure 3.2.4.3 B). No interaction was observed with the anti-mouse IgG negative control.

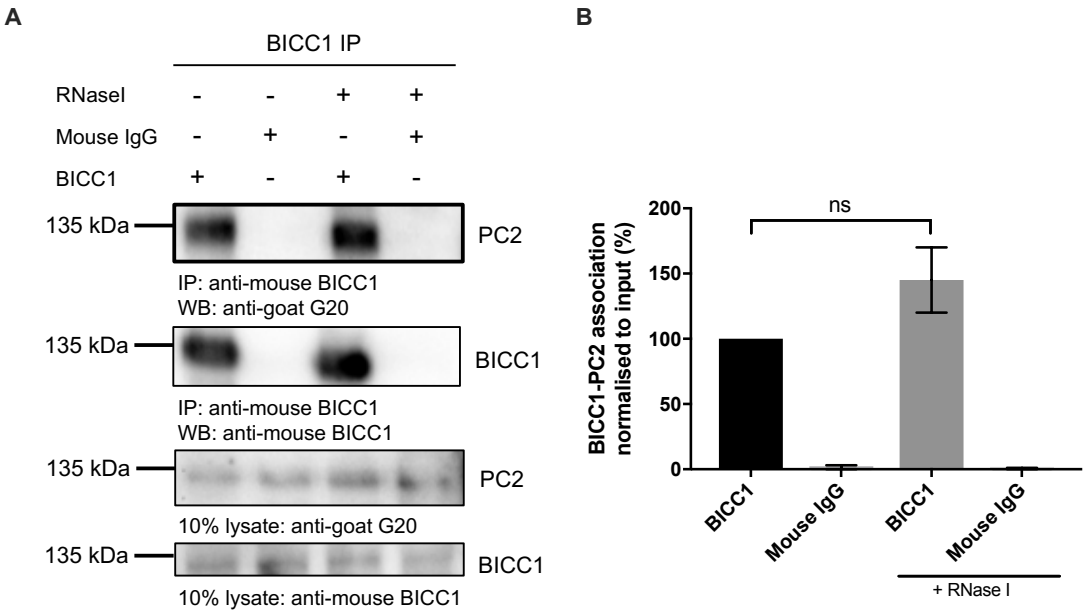

Figure 3.2.4.3. PC2 and BICC1 interact endogenously. A) Western blot analysis following Co-IP experiments, using an anti-mouse BICC1 antibody as bait, were used to assess protein interactions between PC2 and BICC1. A mouse IgG antibody was included as a negative control. **B)** Quantification of the Co-IP experiments (n=3). Paired t-tests were performed to assess significance (p values * ≤0.05, ** = ≤0.01, *** = ≤0.001, **** = ≤0.0001 and ns = not significant). Error bars represent standard error of the mean.

3.2.5 Interactions between PC1 and BICC1 and PC2 and BICC1 require different binding motifs

Data from the previous Co-IPs suggests that PC1 and PC2 require different binding domains to interact with BICC1. To investigate this further, HEK293 cells were co-transfected with either full-length PC1 (PC1-HA) or full-length PC2 (PC2-HA) constructs and either full-length BICC1 (myc-mBICC1) or BICC1 with amino acids 133-691 deleted (myc-mBICC1-del133-691) constructs. Lysates were extracted, and western blot analysis demonstrated that both full-length PC1 and PC2 interact with full-length BICC1 (as previously observed) and myc-mBICC1-del133-691 (Figure 3.2.5.1 A).

This data suggests that PC1 has a binding affinity for BICC1 between amino acids 693 and 815, which will be referred to as binding motif 2 (Figure 3.3.1 A and C) but may still require the SAM domain for a more stable interaction. However, as the expression of the PC1-HA construct was much lower when co-expressed with the BICC1 constructs a conclusive interpretation cannot be made. This experiment requires repeating, with a different PC1 construct, which produces improved expression levels when co-expressed with other DNA constructs.

In contrast, PC2 has a binding affinity for BICC1 between amino acids 1 and 132, which will be referred to as binding motif 1 (Figure 3.3.1 B and C) and may require the KH domains for a more stable interaction. A statistically significant difference was observed for the interaction between PC1 and full-length BICC1 and myc-mBICC1-del133-691 (Figure 3.2.5.1 B), which might relate to differences in baseline expression of PC1. No interaction was observed with the pcDNA3 negative control.

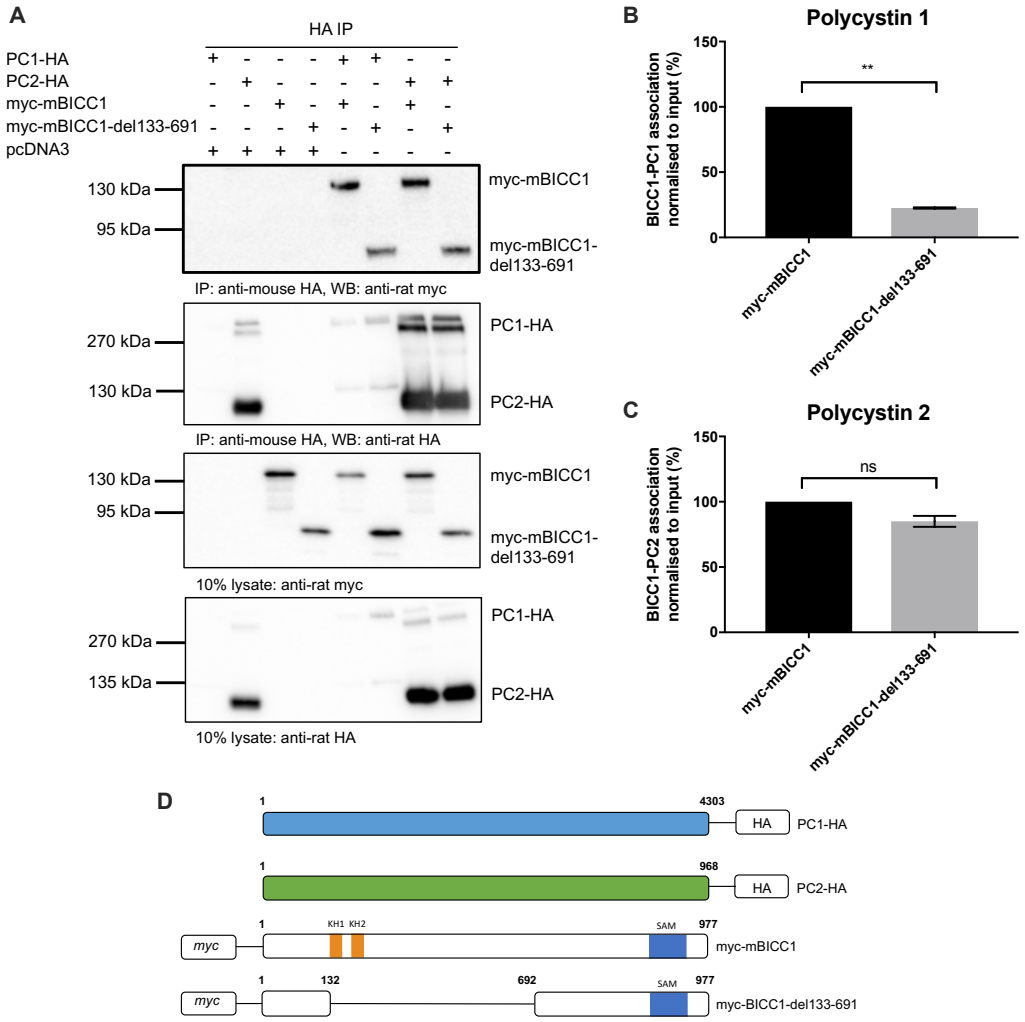

Figure 3.2.5.1. The interactions between PC1 and BICC1 and PC2 and BICC1 require different binding motifs. A) Western blot analysis following Co-IP experiments, using PC1-HA and PC2-HA tagged constructs as bait, were used to assess protein interactions between PC1 and BICC1 and PC2 and BICC1. pcDNA3 was included as a negative control. Quantification of the Co-IP experiments for PC1 (**B**) and PC2 (**C**) (n=3). Paired t-tests were performed to assess significance (p values * ≤0.05, ** = ≤0.01, *** = ≤0.001, **** = ≤0.0001 and ns = not significant). Error bars represent standard error of the mean. **D)** Schematic diagram of the constructs used in this experiment. Of note, the myc-mBICC1-del133-691 construct has the two KH domains with an additional section of the intervening sequence, from amino acids 352-691, deleted.

Following the identification of the required BICC1 binding motifs for interactions with PC1 and PC2, various PC1 and PC2 constructs were obtained and transfected into HEK293 cells to identify the required binding regions of PC1 and PC2 for an interaction with BICC1 (Figure 3.2.5.2). HEK293 cells were co-transfected with the constructs listed in Figure 3.2.5.2 and full-length BICC1 (myc-mBICC1), lysates were extracted, and a Co-IP was performed. Western blot analysis demonstrated that full-length BICC1 interacts with the C-terminus of PC1 (Figure 3.2.5.2). Interestingly, full-length BICC1 interacts with both the N-terminus and C-terminus of PC2. No interaction was observed with the pcDNA3 negative control.

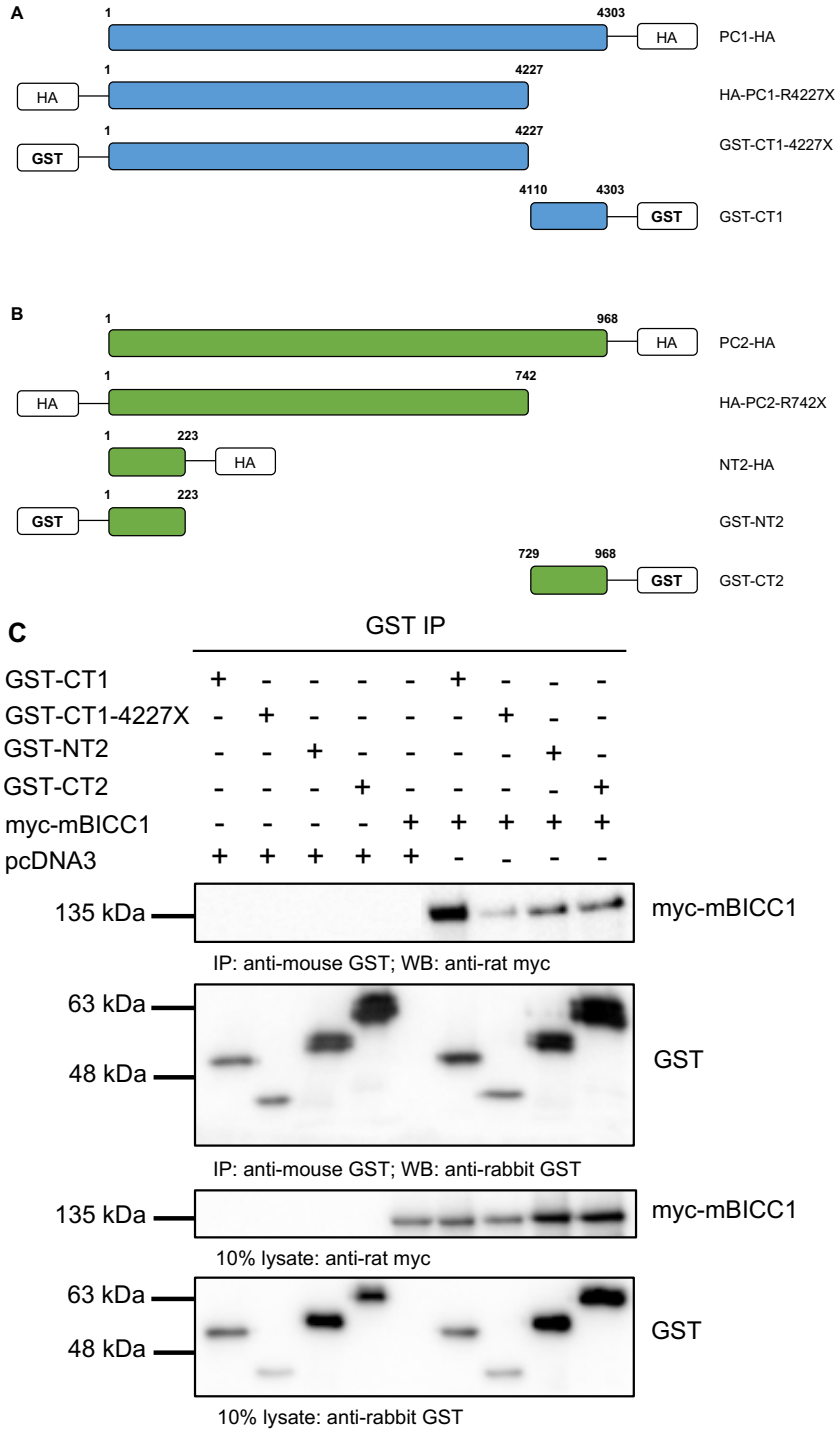

Figure 3.2.5.2. BICC1 interacts with PC1 and PC2 at different protein terminals. A) Schematic diagram of the PC1 constructs used in this study. The PC1-HA construct represents full length PC1 with a C-terminal HA tag, while the HA-PC1-R4227X construct has a N-terminal HA tag and the C-terminus of PC1 deleted. The GST-CT1-4227X construct also has the C-terminus of PC1 deleted, but a N-terminal GST tag. The GST-CT1 construct is the C-terminus of PC1 with a C-terminal GST tag. **B)** Schematic diagram of the PC1 constructs used in this study. The PC2-HA construct represents full length PC2 with a C-terminal HA tag, while the HA-PC2-R742X construct has a N-terminal HA tag and the C-terminus of PC2 deleted. The NT2-HA construct is the N-terminus of PC2 with a C-terminus HA tag, while the GST-NT2 construct also is the N-terminus of PC2 but with a N-terminal GST tag. The GST-CT2 construct is the C-terminus of PC2 with a C-terminal GST tag. The numbers on the constructs represent the amino acids.. **C)** Western blot analysis following Co-IP experiments, using GST tagged constructs as bait, were used to assess protein interactions between PC1 and BICC1 and PC2 and BICC1. pcDNA3 was included as a negative control. CT = C-terminus, NT = N-terminus, GST = Glutathione S-Transferase.

3.2.6 Generation of a stable BICC1 knock-out cell line using CRISPR/Cas9

This study has demonstrated that BICC1 interacts with both PC1 and PC2, the main proteins known to be defective in ADPKD. As BICC1 is an RNA binding protein, it was hypothesised that BICC1 might regulate the polycystin proteins at the RNA level. To assess the effects of BICC1 on *PKD1* (PC1) and *PKD2* (PC2), a stable BICC1 knock-out (*KO*) cell line was generated using CRISPR/Cas9 techniques (see section 2.7 for methods). Following the successful generation *BICC1 KO* clones, several single cell populations were expanded and sequenced to ensure the correct nucleotides were targeted (Figure 3.2.6.1 A and B). The *BICC1 KO* clones (from now on shortened to C) were also expanded through several passages to ensure the *KO* was stable (Figure 3.2.6.1 C). The clones highlighted in bold were then used for follow-on experiments.

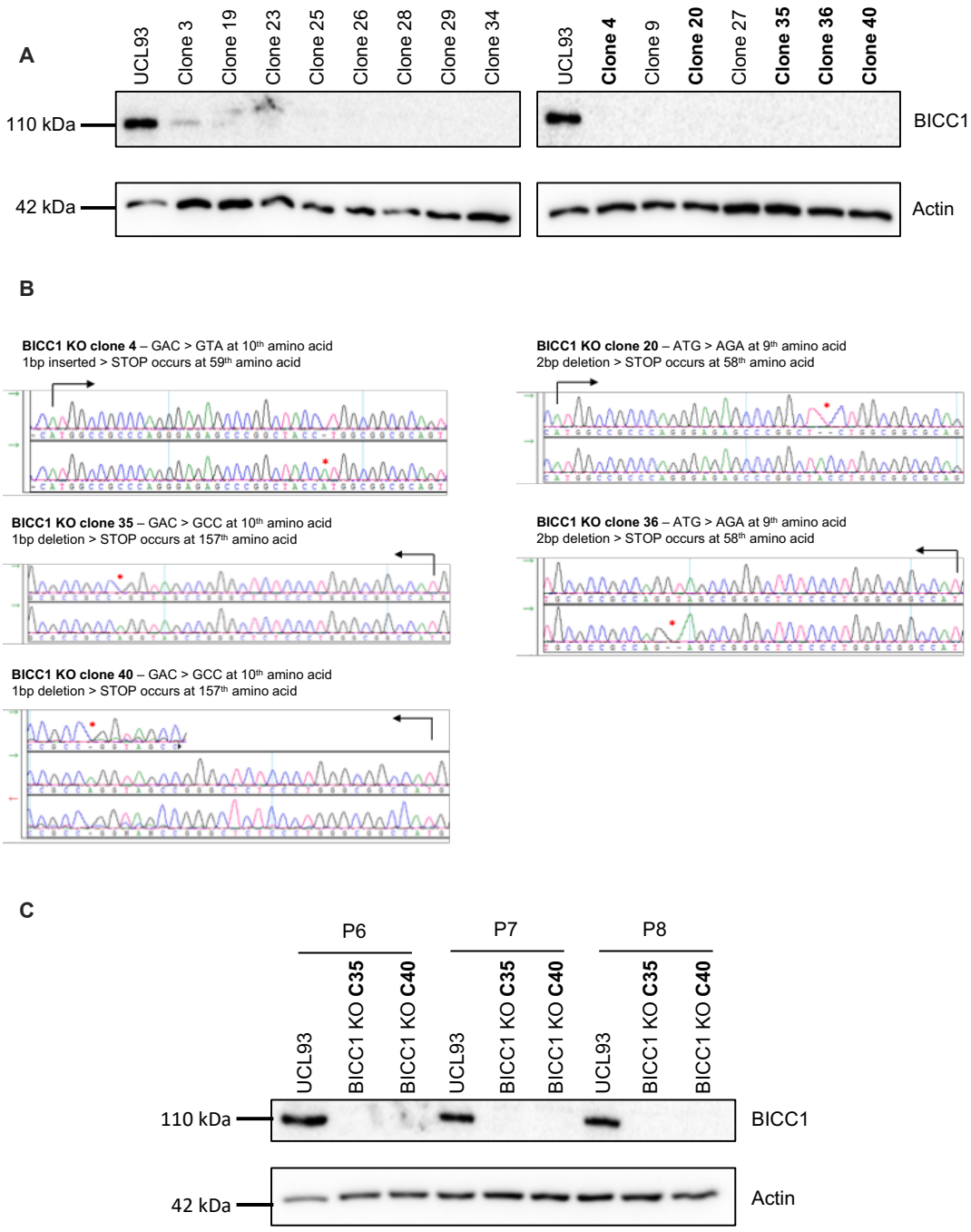

Figure 3.2.6.1. Generation of a stable *BICC1 KO* cell line using CRISPR/Cas9. A) Western blot analysis was used to evaluate 15 *BICC1 KO* clones established following transfection of BICC1 gRNA into UCL93 cells. The clones highlighted in bold were selected for further analysis and DNA sequencing. **B)** DNA chromatograms for each selected clone. The red star illustrates the place of DNA disruption, while the black arrow represents the direction of the open reading frame. Details of the DNA disruption are described above the chromatograms. **C)** Western blotting was used to assess the increasing passage numbers of selected *BICC1 KO* cell lines.

3.2.7 Loss of BICC1 through CRISPR-Cas9 *KO* downregulates *PKD1* mRNA expression, but has no effect on PC1 protein expression

As a molecular link has been observed between PC1 and BICC1, as well as observing a developing protein interaction network through Co-IP experiments, it was speculated whether loss of BICC1 would affect the expression levels of PC1. Therefore, mRNA and protein expression levels were measured by qPCR and western blotting respectively in established *BICC1 KO* cell lines. Loss of BICC1 significantly reduced *PKD1* mRNA expression in all *BICC1 KO* clones, by approximately 25-35% (Figure 3.2.7.1 A). In contrast, loss of BICC1 had no significant effect of PC1 protein expression (Figure 3.2.7.1 B, C). This data suggests that BICC1 may positively regulate *PKD1* mRNA but did not have a detectable effect on protein translation.

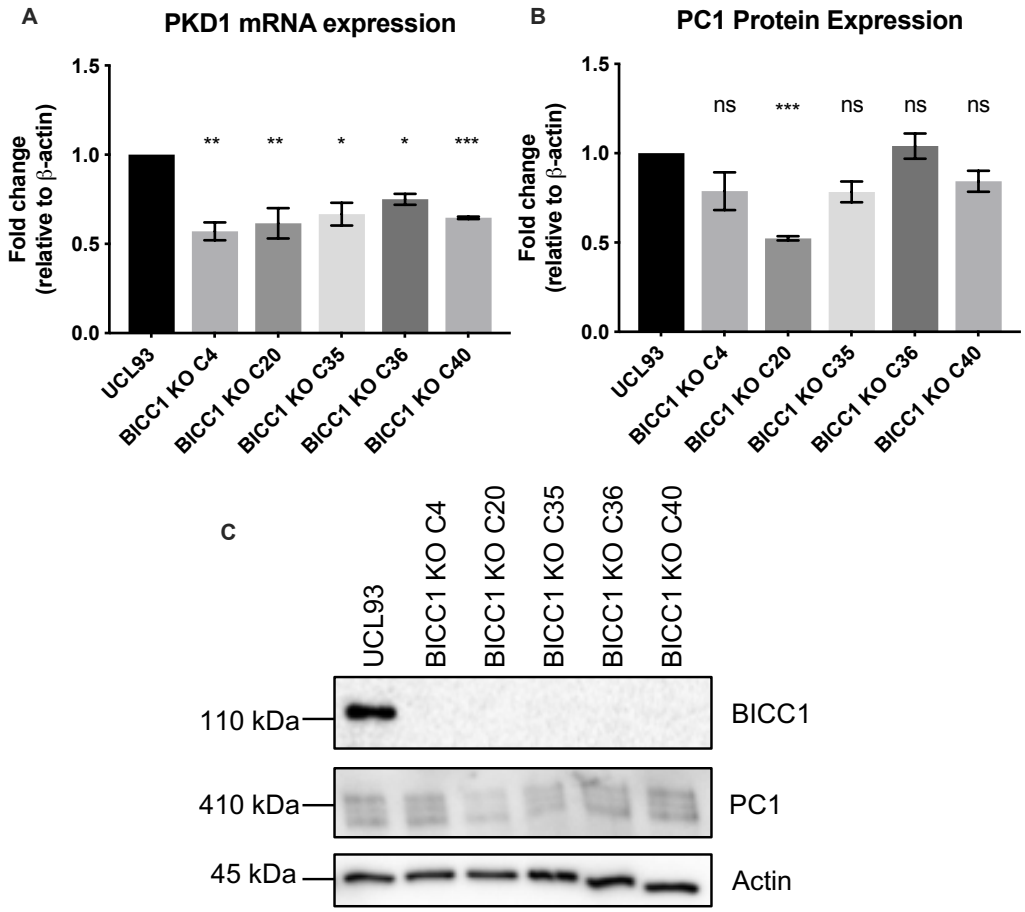

Figure 3.2.7.1. Loss of BICC1 downregulates *PKD1* mRNA expression. A) qPCR was used to measure the mRNA expression level of *PKD1* in the selected *BICC1 KO* clones (n=3). **B, C)** Western blot analysis was used to measure the protein expression level of PC1 in the selected *BICC1 KO* clones (n=3). The western blots were quantified and normalised to actin. Paired t-tests were performed to assess significance (p values * ≤0.05, ** = ≤0.01, *** = ≤0.001, **** = ≤0.0001 and ns = not significant). Error bars represent standard error of the mean.

3.2.8 Loss of BICC1 downregulates polycystin 2 expression

As performed in section 3.2.6, mRNA and protein expression levels were measured by qPCR and western blotting respectively in established *BICC1 KO* cell lines. Loss of BICC1 significantly reduced *PKD2* mRNA and PC2 protein expression in all *BICC1 KO* clones, by approximately 50% (Figure 3.2.8.1). This data suggests that BICC1 positively regulates polycystin 2 expression levels.

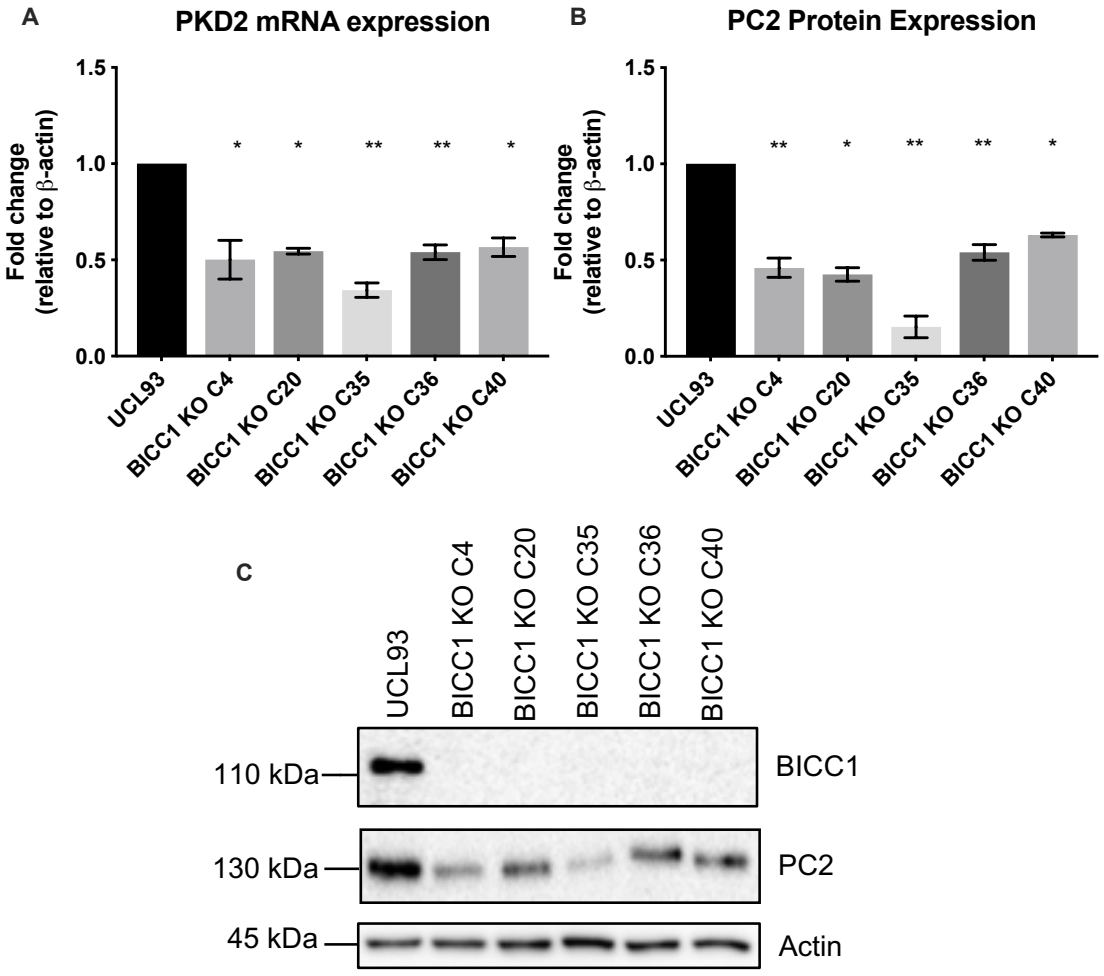

Figure 3.2.8.1. Loss of BICC1 downregulates *PKD2* mRNA and PC2 protein expression. **A)** qPCR was used to measure the mRNA expression level of *PKD2* in the selected *BICC1 KO* clones (n=3). **B, C)** Western blot analysis was used to measure the protein expression level of PC2 in the selected *BICC1 KO* clones (n=3). The western blots were quantified and normalised to actin. Paired t-tests were performed to assess significance (p values * ≤0.05, ** = ≤0.01, *** = ≤0.001 and **** = ≤0.0001). Error bars represent standard error of the mean.

3.2.9 Loss of *PKD1* through CRISPR-Cas9 *KO* downregulates BICC1 expression

As a molecular link has been observed between PC1 and BICC1, as well as observing a developing protein interaction network between BICC1, PC1 and PC2, it was speculated whether loss of PC1 would affect the expression levels of BICC1, as previously observed in published data and section 3.2.2. Therefore, stable *PKD1* CRISPR-Cas9 *KO* cell lines were established in the same manner as discussed in section 3.2.6. mRNA and protein expression levels were measured by qPCR and western blotting respectively in established *PKD1 KO* cell lines. Loss of *PKD1* significantly reduced BICC1 mRNA and protein expression in nearly all of the *PKD1 KO* clones, by approximately 40-70% and 50-90% respectively (Figure 3.2.9.1). *PKD1 KO* C11 appears to be an outlier in the protein expression analysis. This data validates and confirms previous data that PC1 positively regulates BICC1 expression levels.

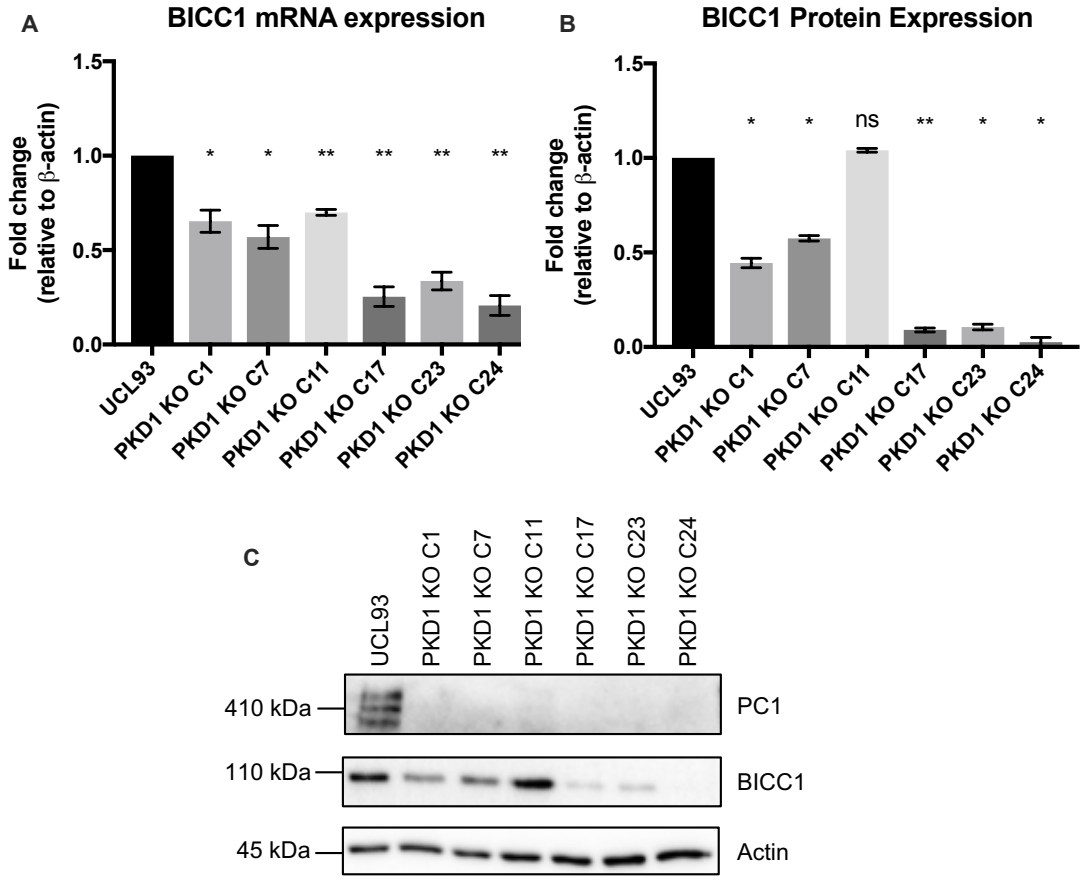

Figure 3.2.9.1. Loss of *PKD1* downregulates BICC1 expression. A) qPCR was used to measure the mRNA expression level of BICC1 in the selected *PKD1 KO* clones (n=3). **B, C)** Western blot analysis was used to measure the protein expression level of BICC1 in the selected *PKD1 KO* clones (n=3). The western blots were quantified and normalised to actin. Paired t-tests were performed to assess significance (p values * ≤0.05, ** = ≤0.01, *** = ≤0.001, **** = ≤0.0001 and ns = not significant). Error bars represent standard error of the mean.

3.2.10 Loss of *PKD2* through CRISPR-Cas9 *KO* upregulates BICC1 expression

As a molecular link has been observed between PC1 and BICC1, as well as observing a developing protein interaction network between BICC1, PC1 and PC2, it was speculated whether loss of PC2 would also affect the expression levels of BICC1. Therefore, stable *PKD2* CRISPR-Cas9 *KO* cell lines were established in the same manner as discussed in section 3.2.6. mRNA and protein expression levels were measured by qPCR and western blotting respectively in selected *PKD2 KO* cell lines. Loss of *PKD2* significantly increased BICC1 mRNA and protein expression in nearly all of the *PKD2 KO* clones, by approximately 5-fold and 2-fold respectively (Figure 3.2.10.1). This data suggests that PC2 is likely to be downstream of BICC1.

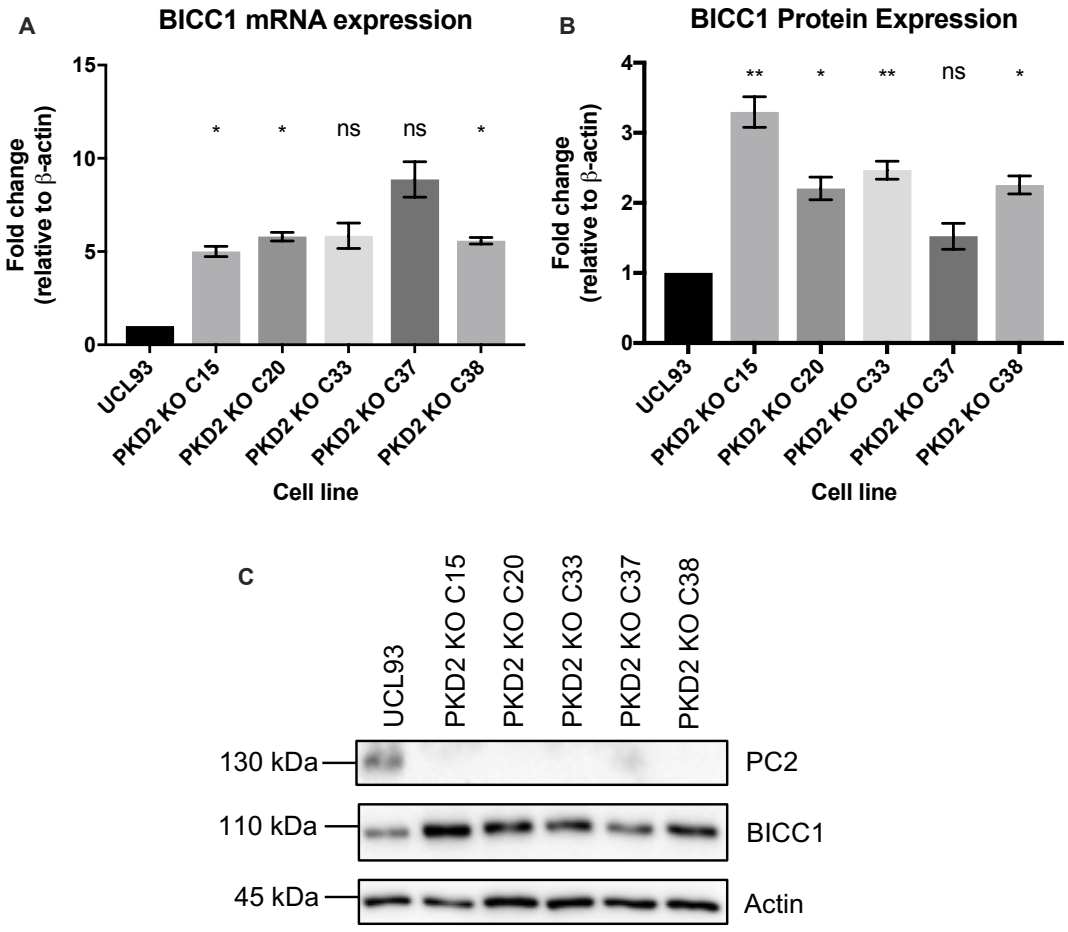

Figure 3.2.10.1. Loss of *PKD2* upregulates BICC1 expression. A) qPCR was used to measure the mRNA expression level of BICC1 in the selected *PKD2 KO* clones (n=3). **B, C)** Western blot analysis was used to measure the protein expression level of BICC1 in the selected *PKD2 KO* clones (n=3). The western blots were quantified and normalised to actin. Paired t-tests were performed to assess significance (p values * ≤0.05, ** = ≤0.01, *** = ≤0.001, **** = ≤0.0001 and ns = not significant). Error bars represent standard error of the mean.

3.2.11 Loss of *PKD1* downregulates polycystin 2 expression

As a molecular link and protein interaction network has been observed between PC1, PC2 and BICC1, it was speculated whether loss of PC1 would affect the expression levels of PC2. mRNA and protein expression levels were measured by qPCR and western blotting respectively in selected *PKD1 KO* cell lines. Loss of *PKD1* significantly reduced *PKD2* mRNA and PC2 protein expression in 4 out of the 6 *PKD1 KO* clones, by approximately 40% and 50-70% respectively (Figure 3.2.11.1). *PKD1 KO* C17 appears to be an outlier in the expression analysis. This data suggests that PC1 is upstream of PC2.

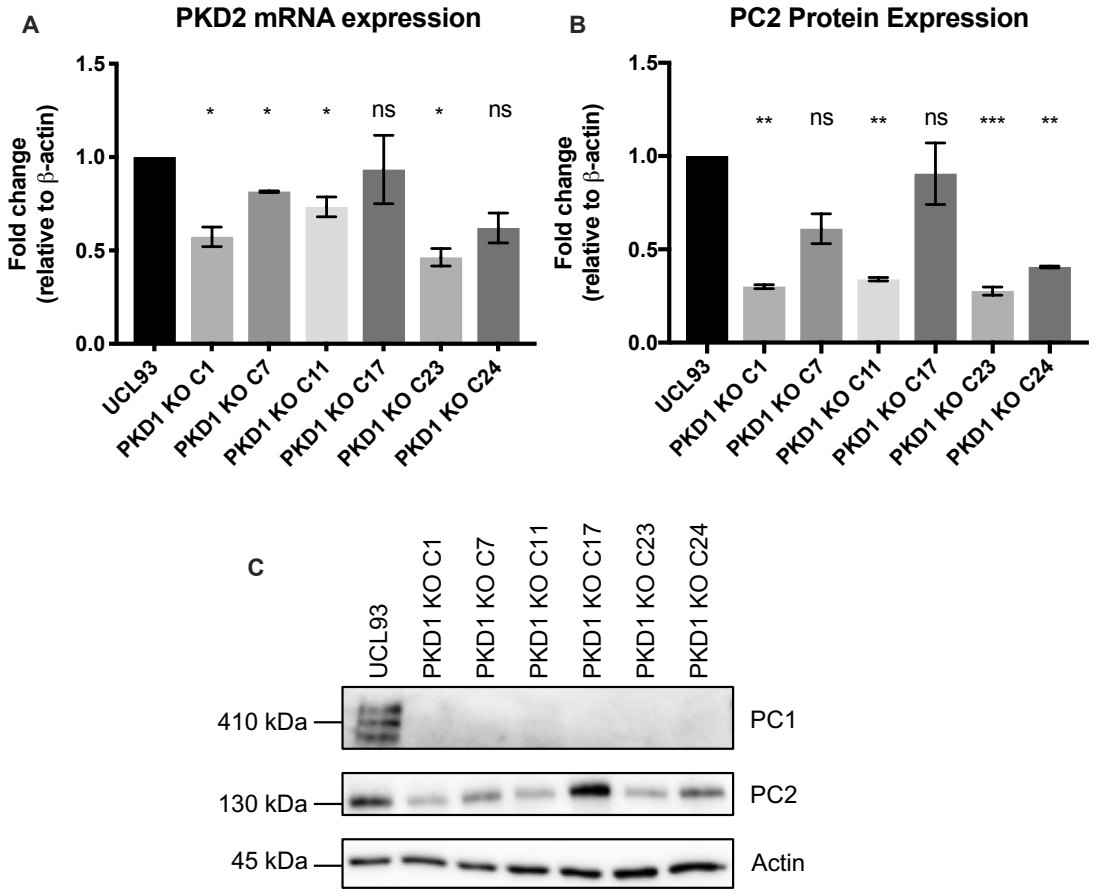

Figure 3.2.11.1. Loss of *PKD1* downregulates PC2 expression. A) qPCR was used to measure the mRNA expression level of *PKD2* in the selected *PKD1 KO* clones (n=3). **B, C)** Western blot analysis was used to measure the protein expression level of PC2 in the selected *PKD1 KO* clones (n=3). The western blots were quantified and normalised to actin. Paired t-tests were performed to assess significance (p values * ≤0.05, ** = ≤0.01, *** = ≤0.001, **** = ≤0.0001 and ns = not significant). Error bars represent standard error of the mean.

3.2.12 Loss of *PKD2* has no effect on polycystin 1 expression

As a molecular link and protein interaction network has been observed between PC1, PC2 and BICC1, it was speculated whether loss of PC2 would affect the expression levels of PC1. mRNA and protein expression levels were measured by qPCR and western blotting respectively in selected *PKD2 KO* cell lines. Loss of *PKD2* had no significant effect on *PKD1* mRNA and PC1 protein expression in all of the *PKD2 KO* clones (Figure 3.2.12.1). As expected, loss of *PKD2* caused a loss of the top band of PC1, known to be its mature form, as PC2 is required for the proper glycosylation of PC1 (Gainullin *et al*., 2015). However, this data suggests that PC2 has no effect on PC1 expression levels.

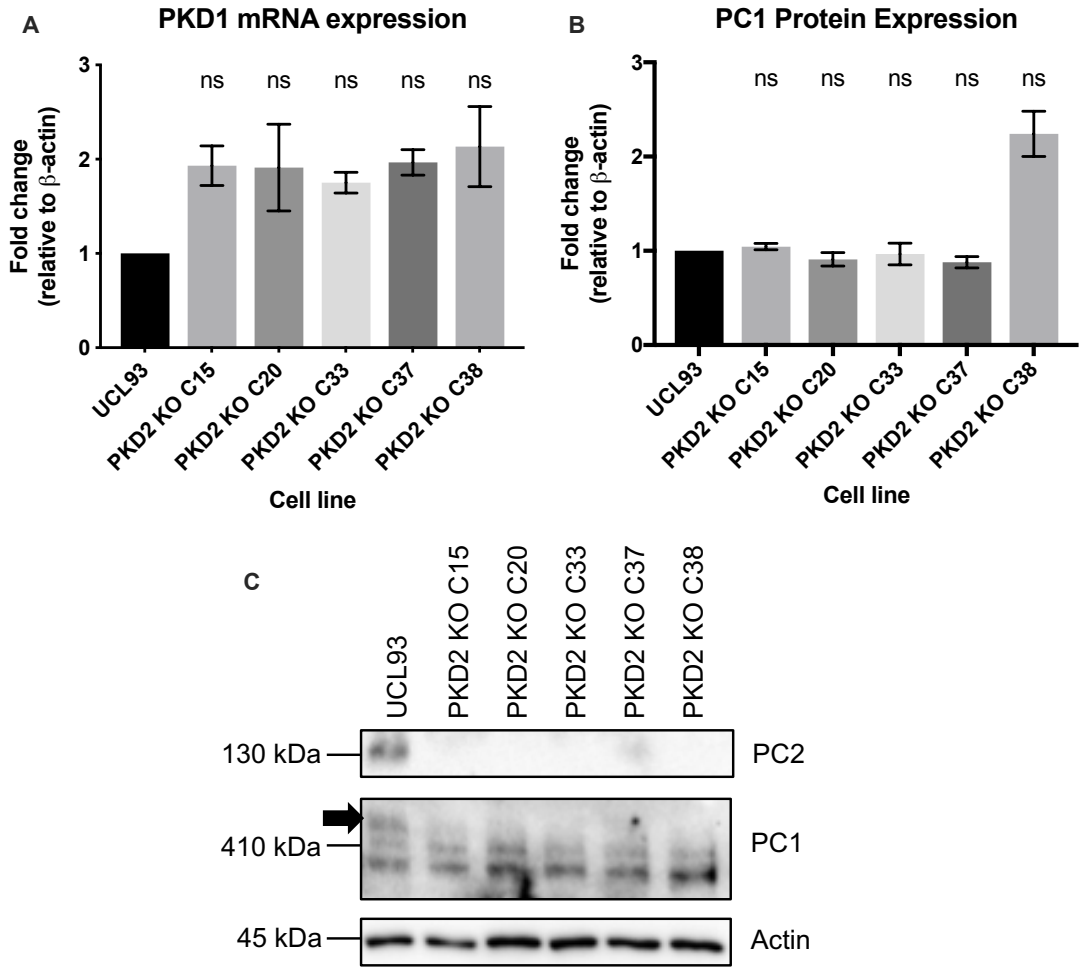

Figure 3.2.12.1. Loss of *PKD2* has no effect on PC1 expression. A) qPCR was used to measure the mRNA expression level of *PKD1* in the selected *PKD2 KO* clones (n=3). **B, C)** Western blot analysis was used to measure the protein expression level of PC1 in the selected *PKD2 KO* clones (n=3). The black arrow shows the upper, mature band of PC1. The western blots were quantified and normalised to actin. Paired t-tests were performed to assess significance (ns = not significant, p value = >0.05). Error bars represent standard error of the mean.

3.2.13 Overexpression of BICC1 upregulates *PKD1* expression but has no effect on *PKD2* expression

To further assess the role of BICC1 in the polycystin network, tetracycline was added to HA-BICC1 cells to induce BICC1 expression. Following 24 hours of incubation, RNA was extracted, and a qPCR was performed. *PKD1* mRNA expression was significantly increased in HA-BICC1 cells compared to HEK293 cells by 2.5-fold, whereas there was no significant change in the mRNA expression levels of *PKD2* (Figure 3.2.13.1). This data suggests that the levels of BICC1 present in kidney cells is very important, as loss of BICC1 causes a downregulation of *PKD2* (Figure 3.2.8.1), but an overexpression of BICC1 causes an upregulation of *PKD1*. Overall, the results suggest that BICC1 regulates *PKD1* mRNA expression and that PC2 is likely to lie downstream of both PC1 and BICC1.

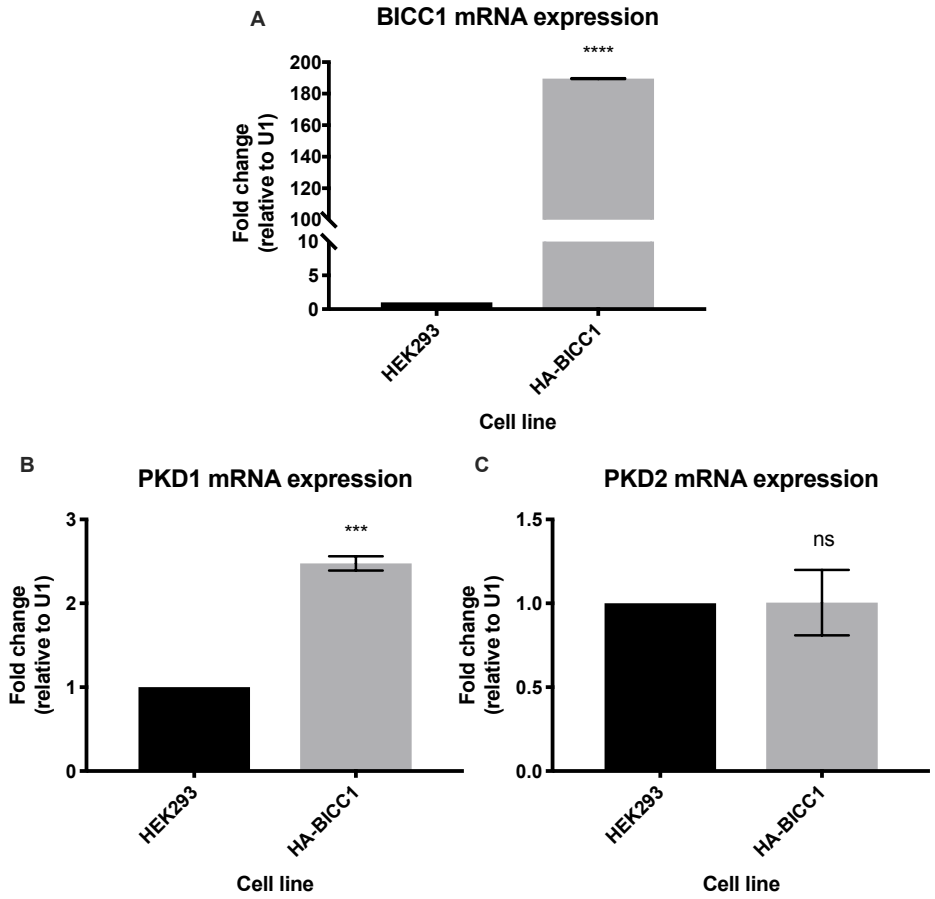

Figure 3.2.13.1. Overexpression of BICC1 upregulates the expression of *PKD1*, but not *PKD2*. A) qPCR was used to measure the mRNA expression level of BICC1 in HA-BICC1 cells (n=3). qPCR was used to measure the mRNA expression levels of *PKD1* **(B)** and *PKD2* **(C)** in HA-BICC1 cells (n=3). Paired t-tests were performed to assess significance (p values * ≤0.05, ** = ≤0.01, *** = ≤0.001, **** = ≤0.0001 and ns = not significant). Error bars represent standard error of the mean.

3.3 Discussion

Published data has demonstrated a functional relationship between BICC1 with the polycystins, through loss of expression of BICC1 in *PKD1 KO* models and the reduction in *PKD2* expression due to loss of BICC1 in other disease models. Such data suggests a likely role for BICC1 in a polycystin cystogenesis pathway. In addition, published data has demonstrated a link between loss of BICC1 and cystogenesis leading to ADPKD-like phenotypes. Despite a functional relationship forming between BICC1 and the polycystins; how they interact, why this is important, and the downstream ramifications are not clear. Therefore, this chapter aimed to further understand this relationship through protein-protein interactions and to further elucidate whether BICC1 regulates the expression of the polycystin proteins.

To begin, the first aim of this chapter sought to confirm that a loss of BICC1 causes ADPKD-like phenotypes. To investigate this further, a CRISPR-Cas9 *BICC1 KO* 3D cell model system was generated (see Chapter 3, section 3.2.6 for further details regarding the CRISPR-Cas9 *BICC1 KO* system). A loss of BICC1 in these cells caused cystogenesis, while a wild-type control cell line, with normal BICC1 expression, formed normal branching tubules. Moreover, our study confirmed that BICC1 expression is reduced by approximately 50% in kidney epithelial cells due to loss of PC1.

The second aim of this chapter sought to identify whether PC1 and PC2 can interact with BICC1 at the protein level. Co-immunoprecipitation experiments using BICC1 as bait were performed, and the data revealed novel protein-protein interactions between BICC1 and PC1 and BICC1 and PC2. Furthermore, through deletion domain Co-IP experiments, novel binding sites within the BICC1 protein were discovered. Figure 3.3.1 summarises our findings. In brief, PC1 does not require either the KH or SAM domains of BICC1 to interact, however, the SAM domain may still be necessary for a more stable interaction. PC2 requires the KH domains but not the SAM domain of BICC1 to interact. However, our data demonstrated that PC1 had a greater binding affinity for BICC1 between C-terminal amino acids 693 and 815 (termed binding motif 2), while in contrast, PC2 had a greater binding affinity for BICC1 between

N-terminal amino acids 1 and 132 (termed binding motif 1) and may require the KH domains and an RNA intermediate for a more stable interaction.

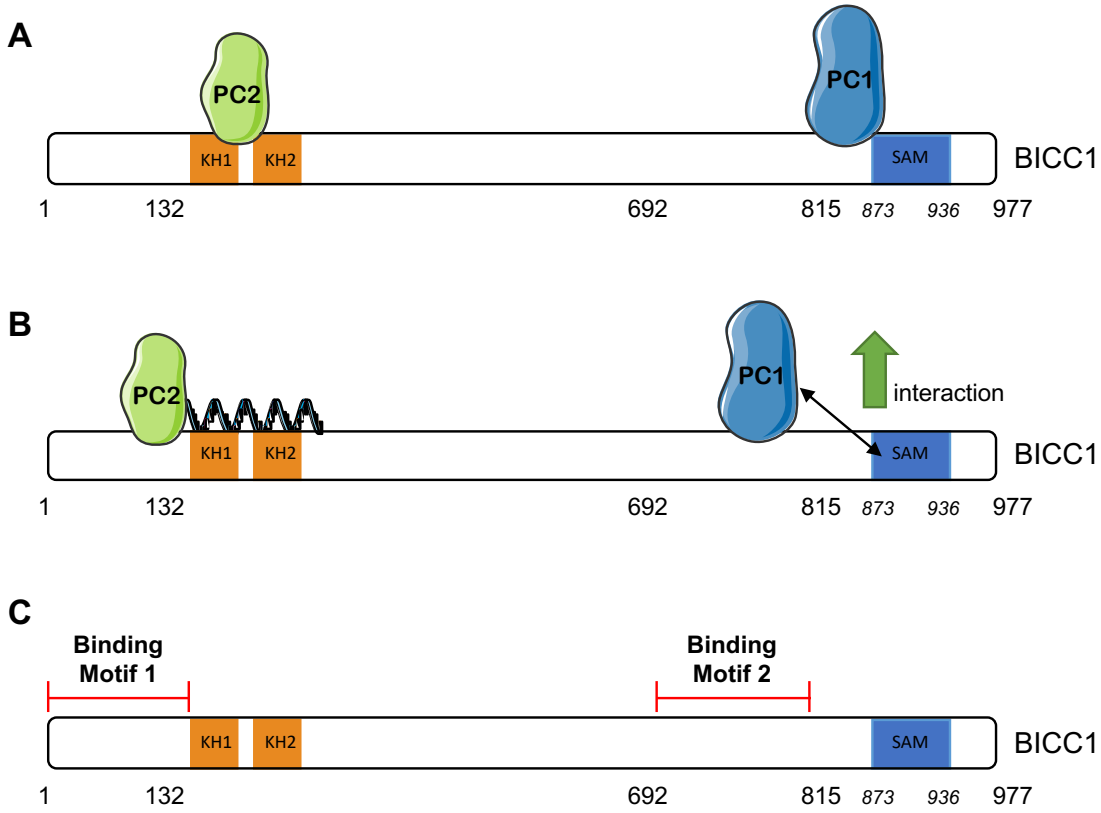

Figure 3.3.1. Schematic summary of the novel BICC1 binding motifs discovered to bind PC1 and PC2. A) PC1 can interact with the SAM domain but not the KH domains of BICC1. PC2 can interact with the KH domains but not the SAM domain of BICC1. **B)** PC1 has a greater binding affinity for BICC1 between amino acids 693 and 815 (binding motif 2) but may still require the SAM domain for a more stable interaction. PC2 has a greater binding affinity for BICC1 between amino acids 1 and 132 (binding motif 1) and may require the KH domains and an RNA intermediate for a more stable interaction. **C)** Binding motif 1 is found towards to N-terminus of BICC1, while binding motif 2 is found towards the C-terminus of BICC1. The amino acid sequences are depicted below the proteins. KH = K homolog. SAM = sterile alpha motif. The SAM domain spans amino acids 873-936.

As neither the KH or SAM domains mediated the interactions between BICC1 and PC1 and BICC1 and PC2, we performed additional analysis on the new binding sites and used bioinformatic databases to further elucidate the motifs. First, we discovered that there is a high chance that the human BICC1 protein has a third KH domain located upstream of the two documented KH domains displayed in Figure 3.3.1. This discovery was made when investigating the BICC1 protein sequence using the InterPro database (v.72). This database predicts that BICC1 contains another KH domain between amino acids 45-130, although there is not a consensus on the specific start and end of the domain. This differs from information present on the Uniprot, database, which states that

BICC1 contains only two KH domains from amino acids 132-199 and 284-348 (see the red arrows in Figure 3.3.2 A).

However, through sequence similarity and prediction software, Interpro suggests there are three KH domains present in the human BICC1 protein, and that these domains are all KH-type 1 domains. This prediction aligns with our data, as well as the number of KH domains found in other mammalians such as mice and rats, therefore we conclude that another binding domain, with potential RNA binding capability, is present between amino acids 1 and 132 of the BICC1 protein.

Despite all three of the KH domains containing the RNA binding motif GXXG (see Figure 3.3.2 B), the data from our Co-IP experiments suggest that only the first KH domain (or binding motif 1) is required for PC2 to interact with BICC1, as an interaction between BICC1 and PC2 is strongest in the presence of the KH1 domain. Furthermore, following RNase treatment, the interaction between PC2 and BICC1 was decreased, suggesting an RNA intermediate is required.

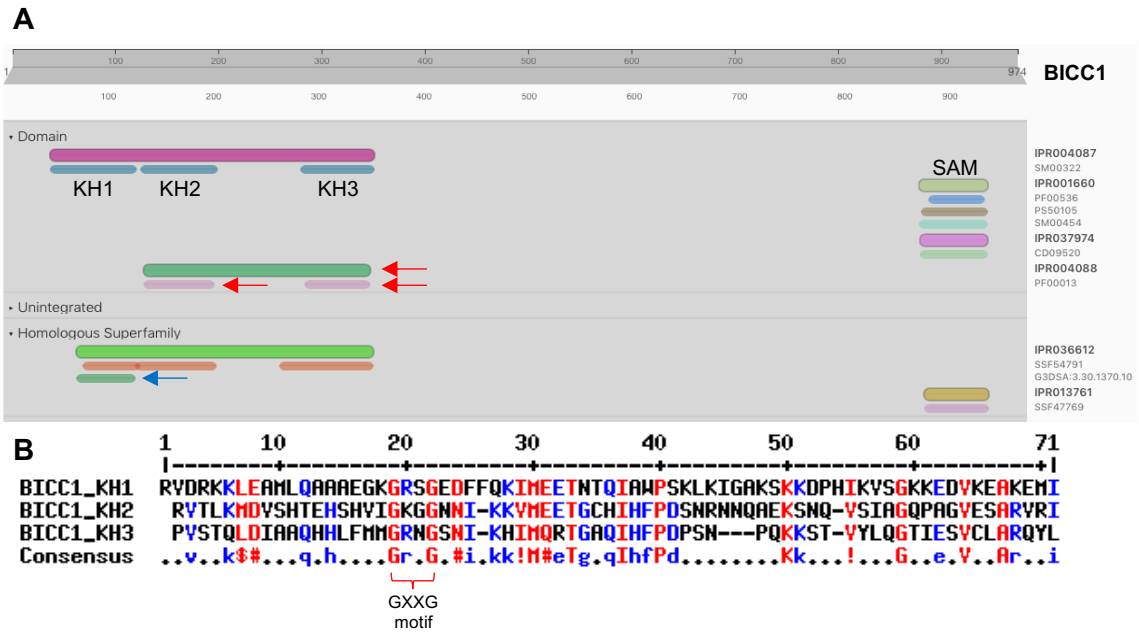

Figure 3.3.2. BICC1 contains three KH domains with RNA binding capability. A) A screenshot of the BICC1 protein from Interpro, with predicted binding domains shown. The red arrows represent the KH domains predicted by Uniprot. The blue arrow represents the sequence homology between the documented KH domains and the newly predicted KH domain (KH1). **B)** A sequence alignment using MultAlin of the three BICC1 KH domains. Each KH domains contains a GXXG RNA binding motif, highlighted with a red bracket. Amino acids highlighted red show high consensus (90%), while amino acids highlight blue show low consensus (50%) and amino acids highlight black are neutral. The amino acid position of the KH domains is depicted on the righthand side of the image.

Second, we discovered two potential new binding sites upstream of the documented SAM domain. Again, this discovery was made when investigating the BICC1 protein sequence using the InterPro database (v.72). This database predicts that BICC1 contains motifs between amino acids 665-719 and 783-846 (red * in Figure 3.3.3 A). These predictions were made using MobiDB, a database of protein disorder and mobility annotations (v.3.0.0). MobiDB highlights different intrinsic protein disorder aspects including, 'disorder', 'linear interacting peptides (LIPs)', and 'dynamic structure' (Piovesan *et al*., 2018). Disorder refers to regions predicted to lack a fixed 3D structure, LIPs refer to regions that interact with other proteins or DNA/RNA and dynamic structure refers to the propensity of a residue or region to form a secondary structure.

As shown in Figure 3.3.3 C, the potential new binding motifs, labelled 1 and 2, display high levels of disorder (highlighted in orange), while regions upstream and downstream of each motif have LIPs propensity (highlighted in green). The binding motif labelled 1 has two LIP regions, a and b, upstream and downstream of its region; however, the region of LIP b has very low 'disorder', therefore suggesting that this region has greater protein binding affinity than LIP a, as well as the binding motif labelled 2. The LIP b sequence is 32 amino acids in length and is as follows: HLAPRSSYVNMQAFDYEQKKLLATKAMLKKPV. The stretch of FDYEQKKLLATKAML suggests the presence of a helix formation, while the stretch of APRSS at the start of the motif and the stretch KKPV at the end of the motif suggests the presence of coil formation. In addition, two prolines in succession are usually helix breakers and there are also charged residues (K) present in the sequence, which may help to bind negative charges in CT-tail of PC1 (also referred to as CT1). Overall, this suggests the possibility of a secondary formation to which a protein binding partner could interact. This prediction aligns with our own data and we can therefore conclude the presence of another binding domain between amino acids 716 and 747 of the BICC1 protein to which PC1 interacts.

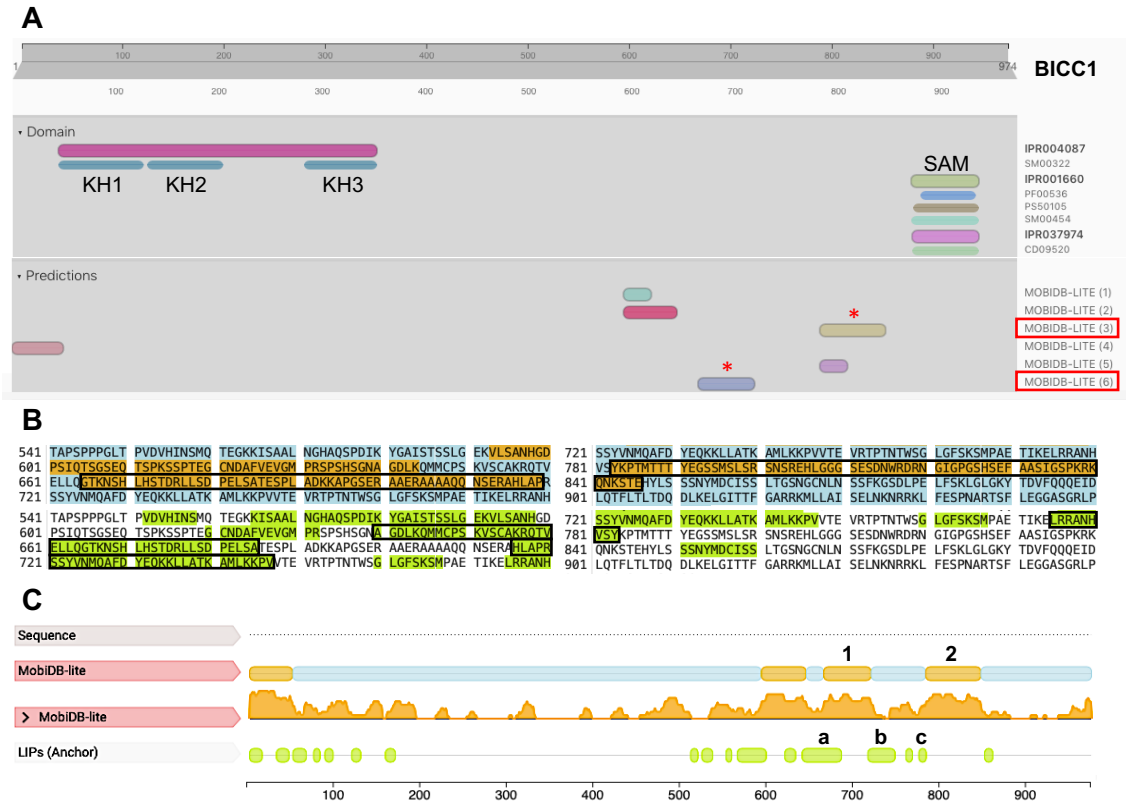

Figure 3.3.3. BICC1 contains a new protein binding domain upstream of its SAM domain. **A)** A screenshot of the BICC1 protein from Interpro, with predicted binding domains shown. The red * represent the new binding regions predicted by MobiDB. **B)** The BICC1 sequence between amino acids 541 and 901. The sequence of the domains predicted by MobiDB 'disorder' are highlighted in orange, while the sequence of the MobiDB LIP regions are highlighted in green. The sequence of the predicted 'binding motif 2' to which PC1 interacts is highlighted with a black bow. **C)** A screenshot of the ModiDB protein motif predictions in the BICC1 protein sequence.

To confirm previous interactions observed between BICC1 and PC1 and BICC1 and PC2 using BICC1 as bait, additional co-immunoprecipitation experiments were performed using either PC1 or PC2 as bait. These interactions were confirmed and through deletion domain Co-IP experiments, BICC1 was shown to interact with the C-terminus of PC1 but with both termini of PC2. Figure 3.3.4 summarises our findings.

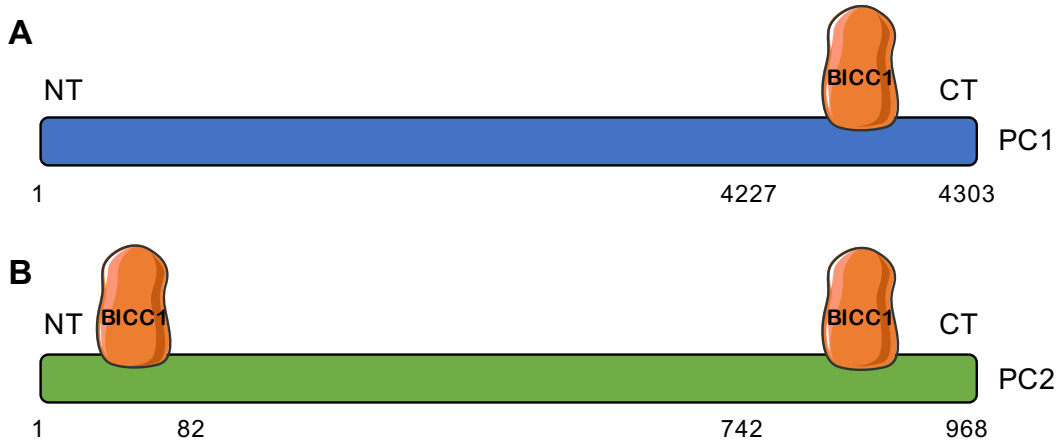

Figure 3.3.4. Schematic summary of the regions of PC1 and PC2 that interact with BICC1. **A)** BICC1 interacts with the C-terminus of PC1. **B)** BICC1 interact with both the N-terminus and C-terminus of PC2. The amino acid sequences are depicted below the proteins. NT = N-terminus. CT = C-terminus.

The final aims of this chapter sought to investigate whether BICC1 regulates the expression of PC1 and PC2, as we have demonstrated novel protein-protein interactions between BICC1 and both PC1 and PC2, the main proteins known to be defective in ADPKD. As BICC1 is a known RNA binding protein, it is plausible to hypothesise that BICC1 might also regulate the polycystin proteins at the RNA level. To assess the regulatory effects of BICC1 on PC1 and PC2, a stable *BICC1 KO* cell line was generated using CRISPR/Cas9 techniques. Following the successful generation of *BICC1 KO* clones, qPCR and western blot experiments were performed to assess the expression levels of PC1 and PC2. Table 3.3.1 summarises our findings. In brief, loss of BICC1 caused an approximate 50% downregulation in both PC2 mRNA and protein expression. Loss of BICC1 also caused an approximate 30% downregulation in PC1 mRNA expression, however, there was no change in the protein expression level of PC1.

CRISPR-Cas9 techniques were also used to generate stable *PKD1* and *PKD2 KO* cell lines, and the expression levels of BICC1, as well as PC1 or PC2 (depending on the cell line used), were assessed. In summary, loss of PC1 caused an approximate 60% downregulation in both BICC1 mRNA and protein expression, which correlates with published data. Loss of PC1 also caused an approximate 50% reduction in PC2 mRNA and protein expression. Conversely, loss of PC2 caused an approximate 5-fold increase in BICC1 mRNA expression

and a 2-fold increase in BICC1 protein expression. In contrast, loss of PC2 has no effect on the expression levels of PC1.

Overexpression studies were also performed, and the data demonstrated that an overexpression of BICC1 caused a 2-fold increase in PC1 mRNA expression but had no effect on the mRNA expression level of PC2. Overall, this data suggests that the levels of BICC1 present in kidney epithelial cells is very important, as loss of BICC1 causes a downregulation of PC2, while overexpression of BICC1 causes an upregulation of PC1.

Table 3.3.1. Summary of the gene expression analysis from the CRISPR-Cas9 experiments.

GENE	BICC1	PKD1	PKD2
BICC1 KO	-	DOWN	DOWN
PKD1 KO	DOWN	-	DOWN
PKD2 KO	UP	NO CHANGE	-
BICC1 OVER	-	UP	NO CHANGE

Chapter 3 Summary:

- ⇒ Loss of *BICC1* causes an ADPKD-phenotype in 3D cyst assay model
- ⇒ PC1 regulates the expression of BICC1 in human kidney epithelial cells
- ⇒ PC1 and BICC1 interact through a sequence distinct from the KH and SAM domains
- ⇒ PC2 and BICC1 interact through a sequence containing a novel KH domain
- ⇒ BICC1 positively regulates PC1 expression at the mRNA but not protein level
- ⇒ BICC1 positively regulates PC2 expression at the mRNA and protein level
- ⇒ Loss of *PKD1* downregulates the expression of BICC1
- ⇒ Loss of *PKD1* downregulates the expression of PC2
- ⇒ Loss of *PKD2* upregulates the expression of BICC1
- ⇒ Loss of *PKD2* has no effect on the expression of PC1
- ⇒ Overexpression of *BICC1* upregulates *PKD1* expression but has no effect on the expression of *PKD2*

Chapter 4

BICC1 FORMS AN INTERACTION COMPLEX WITH OTHER ADPKD-RELATED PROTEINS

4.0 BICC1 forms an interaction complex with other ADPKD-related proteins

4.1 Introduction and Aims

BICC1 is classified as a RBP, however, published data have demonstrated that certain protein interactions are also required for BICC1 to regulate its known mRNA targets (Rothé *et al*., 2015; Iaconis *et al*., 2017). Data presented in Chapter 3 has demonstrated that BICC1 interacts with the polycystins at the protein level, as well as regulating their mRNA expression levels. Therefore, this chapter sought to identify additional novel BICC1-protein binding partners, in an unbiased manner, to further understand the BICC1-dependent processes and mechanistic functions required to maintain normal kidney function in kidney epithelial cells and that could also have a role in preventing ADPKD. Through the identification of novel associations within its proteome, we can begin to develop an improved understanding of the role of BICC1 in kidney epithelial cells and in the pathogenesis of ADPKD.

Chapter Aims

1. Identify novel protein interacting partners of BICC1 in kidney epithelial cells using an unbiased approach
2. Validate a novel interacting partner through Co-IP and domain-deletion experiments
3. Investigate whether the novel interacting partner of BICC1 also interacts with the polycystins
4. Investigate whether BICC1 regulates the expression of its novel binding partner in kidney epithelial cells

4.2 Results

4.2.1 Identification of novel binding partners of BICC1

To identify novel BICC1-interacting proteins, co-immunoprecipitation (Co-IP) experiments were performed in HEK293 cells and HEK293 cells stably transfected with a HA-BICC1 construct (referred to as HA-BICC1 cells). Interacting proteins were analysed by LC-MS/MS and the resulting peptides were identified by the Mascot database (see section 2.5 for methods). A total of 3289 proteins were identified, of which 427 proteins were enriched in all three Co-IPs performed (Figure 4.2.1.1), these proteins were taken forward for further analysis using the DAVID, KEGG pathway, PANTHER databases (see section 2.5 for methods).

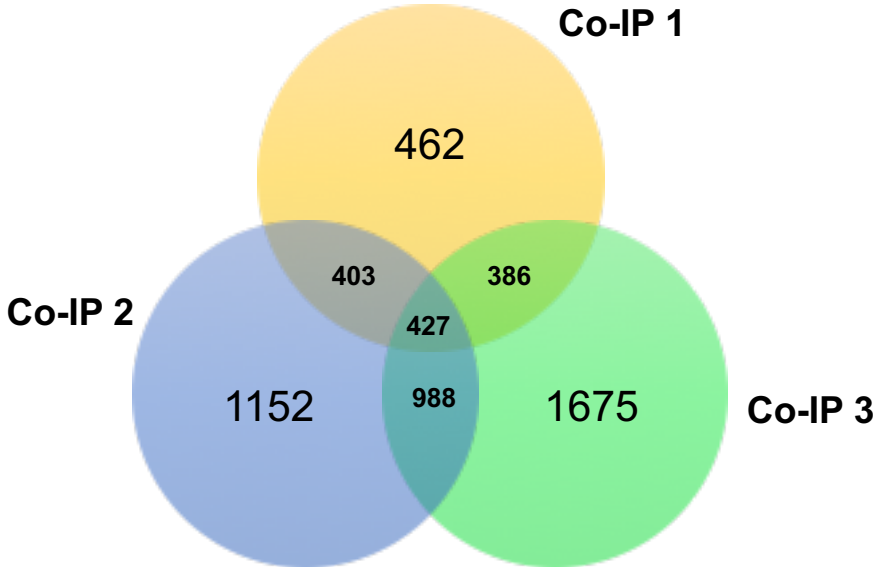

Figure 4.2.1.1. The identified BICC1-interacting proteins following Co-IP and LC-MS/MS analysis in HA-BICC1 cells. Following normalisation to the proteins pulled-down in the control HEK293 cells, 462 proteins were identified in Co-IP 1, while 1152 and 1675 proteins were identified in Co-IP 2 and 3 respectively. 427 proteins were enriched in all 3 Co-IP experiments and these proteins were taken forward for further analysis.

To further understand the BICC1 protein interactome, the identified list of 427 proteins were analysed by DAVID and enriched pathways and processes were analysed using the functional tools within the KEGG, PANTHER and Enricher databases. The data presented is taken from the analysis performed in DAVID; however, the results are comparable to the results from both PANTHER and Enricher. First, enriched UniProtKB Keywords (UP_Keywords) were explored, and the data revealed that BICC1 bound proteins are modified, found in

different cellular locations and function in important biological pathways. For example, nearly 77% of all the enriched proteins are phosphoproteins; proteins post-translationally modified by the addition of a phosphate group. In addition, 67% of the enriched RNAs are acetylated, another form of post-translational modification. Therefore, it can be stated with confidence that the majority of BICC1 bound proteins can be post-translationally modified. Several other significant, biologically relevant UP_Keywords can be viewed in Table 4.2.1.1.

Table 4.2.1.1. The top 20 UniProtKB keywords, ranked by p-value, identified from DAVID analysis of our enriched proteins associated with BICC1. The count refers to the number of proteins enriched in function to the relevant UP_Keyword Term, and this number is also presented as a percentage of the total number of transcripts assessed (%). Significant keywords are displayed with a p-value and Benjamini (adjusted p-value) value cut off of 0.05.

UP Keyword Term	Count	%	P-Value	Benjamini
Acetylation	284	66.7	9.80E-120	3.20E-117
Phosphoprotein	327	76.8	1.80E-54	3.00E-52
RNA-binding	85	20	4.30E-42	4.70E-40
Ribonucleoprotein	56	13.1	2.20E-36	1.80E-34
Isopeptide bond	91	21.4	2.80E-29	1.90E-27
Ribosomal protein	40	9.4	3.50E-28	1.90E-26
Cytoplasm	190	44.6	2.40E-22	1.10E-20
Methylation	75	17.6	4.20E-22	1.70E-20
Mitochondrion	77	18.1	1.60E-20	6.00E-19
Ubl conjugation	97	22.8	3.60E-20	1.20E-18
Nucleotide-binding	96	22.5	2.90E-18	8.60E-17
Protein biosynthesis	27	6.3	8.30E-17	3.10E-15
Helicase	25	5.9	2.20E-15	5.70E-14
Transit peptide	45	10.6	6.30E-15	1.50E-13
ATP-binding	76	17.8	1.30E-14	2.90E-13
Mitochondrion inner membrane	30	7	4.30E-13	8.80E-12
Translation regulation	19	4.5	5.00E-12	9.80E-11
mRNA splicing	26	6.1	2.00E-10	3.70E-09
Host-virus interaction	31	7.3	5.40E-10	9.40E-09
mRNA processing	28	6.6	1.60E-09	2.60E-08

Second, enriched gene ontology (GO) terms in relation to biological processes were explored, and the data revealed that BICC1 bound proteins are involved in important biological pathways. For example, the most significantly enriched (p-value and Benjamini value <0.05) BICC1 bound proteins are involved in translation initiation. In addition, BICC1 bound proteins are involved in several other important, biological processes including the nuclear-transcribed mRNA catabolic process (nonsense-mediated decay) and rRNA processing.

Interestingly, the GO biological processes which contain the largest percentage of enriched BICC1 bound proteins are the process of translation (42 count, 9.9%) and cell-cell adhesion (42 count, 9.9%). Several other significantly relevant GO biological processes can be viewed in Table 4.2.1.2.

Table 4.2.1.2. The top 20 GO biological processes, ranked by p-value, identified from DAVID analysis of our enriched proteins associated with BICC1. The count refers to the number of proteins enriched in function to the relevant GO biological processes, and this number is also presented as a percentage of the total number of transcripts assessed (%). Significant keywords are displayed with a p-value and Benjamini (adjusted p-value) value cut off of 0.05.

GO Biological Process	Count	%	P-Value	Benjamini
translational initiation	34	8	7.60E-24	1.40E-20
SRP-dependent cotranslational protein targeting to membrane	29	6.8	3.60E-23	3.20E-20
nuclear-transcribed mRNA catabolic process, nonsense-mediated decay	31	7.3	2.10E-22	1.30E-19
translation	42	9.9	2.40E-22	1.10E-19
rRNA processing	39	9.2	3.20E-22	1.10E-19
cell-cell adhesion	42	9.9	3.50E-21	1.00E-18
viral transcription	26	6.1	1.70E-17	4.30E-15
negative regulation of translation	17	4	3.50E-13	7.80E-11
protein folding	25	5.9	1.20E-11	2.40E-09
tRNA aminoacylation for protein translation	13	3.1	1.10E-10	2.00E-08
mitochondrial translational elongation	17	4	1.90E-10	3.10E-08
mRNA splicing, via spliceosome	26	6.1	1.90E-10	2.80E-08
regulation of mRNA stability	18	4.2	4.40E-10	6.00E-08
mitochondrial translational termination	16	3.8	2.10E-09	2.70E-07
RNA processing	16	3.8	1.20E-08	1.40E-06
gene expression	11	2.6	1.80E-07	2.10E-05
osteoblast differentiation	15	3.5	2.20E-07	2.30E-05
nuclear-transcribed mRNA poly(A) tail shortening	9	2.1	3.10E-07	3.10E-05
viral process	24	5.6	1.20E-06	1.10E-04
mRNA transport	10	2.3	1.60E-06	1.50E-04

Third, enriched GO terms in relation to molecular function were explored, and the data revealed that BICC1 bound proteins are involved in various important biological functions. For example, the majority of the proteins function in protein binding (331 count, 77.7%). In addition, BICC1-related proteins have poly(A) RNA binding function (196 count, 46%). Interestingly, BICC1 bound proteins are also significantly required in cadherin binding involved in cell-cell adhesion (49 count, 11.5%). Furthermore, ATP binding was highly significant (80 count, 18.8%). Several other significantly relevant GO molecular functions can be viewed in Table 4.2.1.3.

Table 4.2.1.3. The top 20 GO molecular functions, ranked by p-value, identified from DAVID analysis of our enriched proteins associated with BICC1. The count refers to the number of proteins enriched in function to the relevant GO molecular functions, and this number is also presented as a percentage of the total number of transcripts assessed (%). Significant keywords are displayed with a p-value and Benjamini (adjusted p-value) value cut off of 0.05.

GO Molecular Function	Count	%	P-Value	Benjamini
poly(A) RNA binding	196	46	3.90E-119	2.60E-116
protein binding	331	77.7	1.10E-31	3.50E-29
cadherin binding involved in cell-cell adhesion	49	11.5	3.80E-26	8.30E-24
RNA binding	64	15	4.30E-25	7.10E-23
structural constituent of ribosome	40	9.4	2.20E-22	2.90E-20
ATP-dependent RNA helicase activity	17	4	3.00E-12	3.30E-10
ATP binding	80	18.8	5.20E-11	4.90E-09
GTPase binding	10	2.3	6.60E-09	5.50E-07
mRNA binding	18	4.2	1.20E-08	8.50E-07
protein domain specific binding	22	5.2	4.90E-08	3.20E-06
nucleotide binding	28	6.6	1.60E-07	9.40E-06
double-stranded RNA binding	12	2.8	2.50E-07	1.40E-05
mRNA 3'-UTR binding	11	2.6	2.60E-07	1.30E-05
Ran GTPase binding	9	2.1	4.60E-07	2.20E-05
unfolded protein binding	15	3.5	5.20E-07	2.30E-05
aminoacyl-tRNA ligase activity	7	1.6	2.10E-06	8.80E-05
rRNA binding	9	2.1	4.90E-06	1.90E-04
helicase activity	12	2.8	7.40E-06	2.70E-04
GTPase activity	19	4.5	2.10E-05	7.30E-04
tRNA binding	9	2.1	3.20E-05	1.10E-03

Fourth, enriched GO terms in relation to cellular compartments were explored, and the data revealed that of interest, some of the BICC1 bound proteins are in focal adhesions (46 count, 10.8%). In addition, BICC1-associated RNAs encode proteins found in the membrane (211 count, 49.5%), extracellular exosomes (183 count, 43%) and the cytosol (189 count, 44.4%). Interestingly, BICC1-related proteins are also found within intracellular ribonucleoprotein complexes (35 count, 8.2%) and cell-cell adherens junctions (49 count, 11.5%). Several other significantly relevant GO cellular compartments can be viewed in Table 4.2.1.4.

Table 4.2.1.4. The top 20 GO cellular compartments, ranked by p-value, identified from DAVID analysis of our enriched proteins associated with BICC1. The count refers to the number of proteins enriched in function to the relevant GO cellular compartments, and this number is also presented as a percentage of the total number of transcripts assessed (%). Significant keywords are displayed with a p-value and Benjamini (adjusted p-value) value cut off of 0.05.

GO Cellular Compartment	Count	%	P-Value	Benjamini
membrane	211	49.5	1.80E-83	9.00E-81
extracellular exosome	183	43	7.50E-44	1.90E-41
cytosol	189	44.4	2.80E-37	4.70E-35
intracellular ribonucleoprotein complex	35	8.2	7.40E-26	9.30E-24
cell-cell adherens junction	49	11.5	2.70E-25	2.70E-23
mitochondrial inner membrane	56	13.1	5.00E-25	4.20E-23
mitochondrion	96	22.5	5.00E-24	3.60E-22
ribosome	36	8.5	6.70E-24	4.20E-22
myelin sheath	32	7.5	7.60E-21	4.30E-19
focal adhesion	46	10.8	3.20E-19	1.60E-17
melanosome	25	5.9	4.80E-18	2.20E-16
nucleoplasm	133	31.2	1.60E-17	6.70E-16
nucleolus	65	15.3	3.90E-17	1.50E-15
cytoplasm	192	45.1	7.60E-14	2.70E-12
nucleus	195	45.8	3.40E-13	1.10E-11
mitochondrial small ribosomal subunit	12	2.8	2.80E-12	8.80E-11
cytoplasmic stress granule	13	3.1	1.40E-11	4.20E-10
extracellular matrix	29	6.8	2.70E-10	7.40E-09
mitochondrial nucleoid	13	3.1	2.70E-10	7.20E-09
catalytic step 2 spliceosome	17	4	2.90E-10	7.40E-09

Fifth, enriched Interpro terms were explored, and the data revealed that BICC1 bound proteins contain various functional domains or are part of important protein super-families. For example, the most significantly enriched BICC1-associated proteins are P-loop containing nucleoside triphosphate hydrolases, DNA/RNA helicases (DEAD/DEAH box type, N-terminal) and contain K homology domains. In addition, some of the enriched proteins are part of the helicase, C-terminal and helicase superfamily 1 or 2 with an ATP-binding domain, which is in line with observing ATP binding as a significant GO molecular function in table 4.2.1.3. Several other significant and biologically relevant Interpro terms can be viewed in Table 4.2.1.5.

Table 4.2.1.5. The top Interpro terms, ranked by p-value, identified from DAVID analysis of our enriched proteins associated with BICC1. The count refers to the number of proteins enriched in function to the relevant Interpro Term, and this number is also presented as a percentage of the total number of transcripts assessed (%). Significant keywords are displayed with a p-value and Benjamini (adjusted p-value) value cut off of 0.05.

Interpro	Count	%	P-Value	Benjamini
P-loop containing nucleoside triphosphate hydrolase	54	12.7	7.30E-11	7.30E-08
DNA/RNA helicase, DEAD/DEAH box type, N-terminal	15	3.5	3.70E-10	1.80E-07
K Homology domain	11	2.6	8.50E-09	2.80E-06
Nucleic acid-binding, OB-fold	14	3.3	1.70E-08	4.20E-06
Nucleotide-binding, alpha-beta plait	24	5.6	3.80E-08	7.60E-06
K Homology domain, type 1	11	2.6	4.00E-08	6.50E-06
Helicase, C-terminal	15	3.5	1.50E-07	2.10E-05
Helicase, superfamily 1/2, ATP-binding domain	15	3.5	1.90E-07	2.40E-05
RNA recognition motif domain	21	4.9	2.30E-07	2.50E-05
Aminoacyl-tRNA synthetase, class I, conserved site	7	1.6	5.50E-07	5.40E-05
Importin-beta, N-terminal	7	1.6	1.30E-06	1.20E-04
14-3-3 protein, conserved site	5	1.2	8.60E-06	7.10E-04
14-3-3 domain	5	1.2	8.60E-06	7.10E-04
14-3-3 protein	5	1.2	8.60E-06	7.10E-04
RNA helicase, DEAD-box type, Q motif	8	1.9	1.70E-05	1.30E-03
Rossmann-like alpha/beta/alpha sandwich fold	8	1.9	3.90E-05	2.80E-03
G-protein beta WD-40 repeat	11	2.6	4.80E-05	3.20E-03
Ribosomal protein S5 domain 2-type fold	8	1.9	5.40E-05	3.30E-03
Armadillo-type fold	22	5.2	5.50E-05	3.20E-03
Aminoacyl-tRNA synthetase, class 1a, anticodon-binding	5	1.2	1.60E-04	8.60E-03

Finally, enriched KEGG pathways were explored, and the data revealed that BICC1 bound proteins are involved in several pathways related to protein and RNA processing. For example, BICC1-associated proteins are enriched in the following pathways; ribosome, protein processing in the endoplasmic reticulum, RNA transport and RNA degradation. Several other significant, biologically relevant KEGG pathways can be viewed in Table 4.2.1.6.

Table 4.2.1.6. The top 20 KEGG pathways, ranked by p-value, identified from DAVID analysis of our enriched proteins associated with BICC1. The count refers to the number of proteins enriched in function to the relevant KEGG pathway, and this number is also presented as a percentage of the total number of transcripts assessed (%). Significant keywords are displayed with a p-value and Benjamini (adjusted p-value) value cut off of 0.05.

KEGG Pathways	Gene Count	%	P-Value	Benjamini
Ribosome	31	7.3	3.70E-16	7.10E-14
Protein processing in endoplasmic reticulum	25	5.9	6.70E-09	7.20E-07
RNA transport	23	5.4	2.00E-07	1.40E-05
RNA degradation	14	3.3	3.10E-06	1.70E-04
Aminoacyl-tRNA biosynthesis	11	2.6	1.10E-04	4.80E-03
Biosynthesis of antibiotics	20	4.7	2.20E-04	7.90E-03
Epstein-Barr virus infection	18	4.2	4.90E-04	1.50E-02
Carbon metabolism	12	2.8	2.50E-03	6.40E-02
Biosynthesis of amino acids	9	2.1	5.00E-03	1.10E-01
Fatty acid metabolism	7	1.6	7.20E-03	1.40E-01

Following the analysis of enriched pathways and processes of novel BICC1-interacting partners, semi-quantitative analysis of the MS data was performed. Peptide scores and fold enrichment was calculated by comparison against the background found in the control HEK293 cells. The values were normalised over the fold enrichment obtained for the bait protein. The presented values in the tables below correspond to the average of the normalised fold enrichments obtained in the two replicates, as Co-IP 1 continuously demonstrated lower peptide scores compared to Co-IP 2 and 3. However, the listed proteins were identified in all three of the Co-IP experiments performed.

Highly enriched proteins comprised the CNOT1 subunit of the CCR4-NOT deadenylation complex and FASN and FLNA, indicating that our screen detected known BICC1-interacting factors (Tables 4.2.1.7, 4.2.1.8 and Appendix Tables 7.1 and 7.2). Furthermore, both the average peptide scores and fold enrichment analysis presented similar protein lists (highlighted in bold). Interestingly, ENO1, or alpha-endolase, was highly enriched in both tables. ENO1 is a glycolytic enzyme and alternative splicing of its gene results in a shorter isoform that binds to the C-MYC promoter to function as a tumour suppressor (Feo *et al*., 2000). More recently, ENO1 has been identified as an RBP and may play a role in the deadenylation-dependent mRNA decay pathway (Castello *et al*., 2012; Strein *et al*., 2014).

As previously discussed, this study wished to explore the hypothesis that BICC1 is part of a multi-protein complex with other cystoproteins. Therefore, an unbiased proteomic screen was performed which identified several novel BICC1-interacting partners. Among the 20 proteins that were enriched at least 20-fold or had an average score greater than 700, this study chose to focus on an interaction of BICC1 with ANKS3, as at the start of this project ANKS3 was identified as a new binding partner of ANKS6, and possible links to ADPKD were developing.

Table 4.2.1.7. The novel BICC1-interacting partners identified and presented as fold change. Proteins highlighted in bold are presented in both analytical methods (see Table 4.2.1.2).

Gene	Identified Protein	Accession Number	Ctr_IP 2	IP 2	Ctr_IP 3	IP 3	Fold change
BICC1	Protein bicaudal C homolog 1	Q9H694	0	61	0	66	**64.50**
FASN	Fatty acid synthase	P49327	0	45	0	64	**55.50**
CNOT1	CCR4-NOT transcription complex subunit 1	A5YKK6	0	43	0	34	**39.50**
CLTC	Clathrin heavy chain 1	Q00610	0	32	0	42	**38.00**
LRPPRC	Leucine-rich PPR motif-containing protein, mitochondrial	P42704	0	26	0	46	**37.00**
FLNA	Filamin-A	P21333	0	27	0	40	**34.50**
DHX9	ATP-dependent RNA helicase A	Q08211	0	34	0	29	**32.50**
MYH9	Myosin-9	P35579	0	26	0	37	**32.50**
ENO1	Alpha-enolase	P06733	0	30	0	33	**32.50**
PKM	Pyruvate kinase PKM	P14618	0	30	0	33	**32.50**
ANKS3	Ankyrin repeat and SAM domain-containing protein 3	Q6ZW76	0	32	0	29	**31.50**
CCT8	T-complex protein 1 subunit theta	P50990	0	23	0	33	**29.00**
UBA1	Ubiquitin-like modifier-activating enzyme 1	P22314	0	22	0	32	**28.00**
EPRS	Bifunctional glutamate/proline--tRNA ligase	P07814	0	16	0	33	**25.50**

Table 4.2.1.8. The unique peptides identified as novel BICC1-interacting partners. Proteins highlighted in bold are presented in both analytical methods (see Table 4.2.1.1).

Gene	Identified Protein	Accession Number	Ctr_IP 2	IP_2	Ctr_IP 3	IP_3	Average
BICC1	Protein bicaudal C homolog 1	Q9H694	0	11708	0	10788	**11247.80**
ENO1	Alpha-enolase	P06733	0	1784	0	5781	**3782.41**
PKM	Pyruvate kinase PKM	P14618	0	1149	0	2746	**1947.89**
FASN	Fatty acid synthase	P49327	0	1207	0	2441	**1824.23**
UBA1	Ubiquitin-like modifier-activating enzyme 1	P22314	0	916	0	1950	**1433.02**
CKB	Creatine kinase B-type OS=Homo sapiens	P12277	0	774	0	2057	**1415.62**
VDAC1	Voltage-dependent anion-selective channel protein 1	P21796	0	690	0	2005	**1347.53**
FLNA	Filamin-A OS=Homo sapiens	P21333	0	820	0	1836	**1327.86**
MYH9	Myosin-9	P35579	0	1002	0	1597	**1299.28**
CLTC	Clathrin heavy chain 1	Q00610	0	1025	0	1559	**1291.88**
LRPPRC	Leucine-rich PPR motif-containing protein, mitochondrial	P42704	0	754	0	1479	**1116.75**
CCT8	T-complex protein 1 subunit theta	P50990	0	730	0	1408	**1069.35**
1433E	14-3-3 protein epsilon	P62258	0	615	0	1429	**1022.06**
DHX9	ATP-dependent RNA helicase A	Q08211	0	1128	0	897	**1012.70**
TRIM28	Transcription intermediary factor 1-beta	Q13263	0	725	0	1285	**1004.70**
ANKS3	Ankyrin repeat and SAM domain-containing protein 3	Q6ZW76	0	1029	0	977	**1003.04**
CNOT1	CCR4-NOT transcription complex subunit 1	A5YKK6	0	1297	0	685	**990.96**
HNRNPA2B1	Heterogeneous nuclear ribonucleoproteins A2/B1	P22626	0	659	0	1244	**951.62**
CSE1L	Exportin-2 OS=Homo sapiens	P55060	0	639	0	1217	**927.92**
PABPC1	Polyadenylate-binding protein 1	P11940	0	681	0	880	**780.63**

4.2.2 BICC1 interacts with ANKS3

To confirm a physical interaction between BICC1 and ANKS3, various constructs were designed and transfected into HEK293 cells (see section 2.6 for methodology). ANKS6 constructs were also designed to confirm interactions observed in published literature, as well as to explore the ANKS3-ANKS6 interaction further (Figure 4.2.2.1).

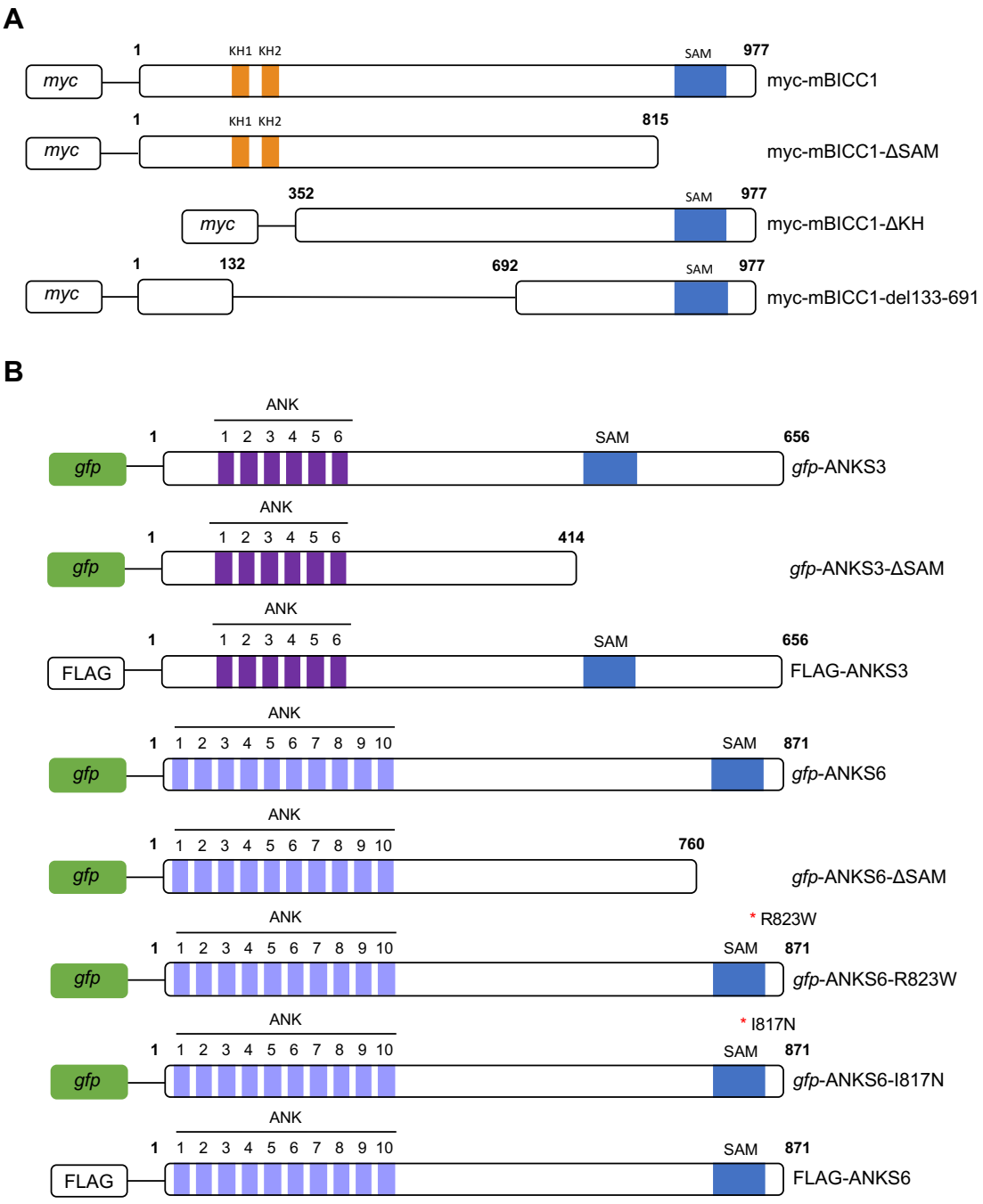

Figure 4.2.2.1. Schematic diagram of the BICC1, ANKS3 and ANKS6 constructs used in this study. A) The myc-mBICC1 construct represents full length BICC1 with an N-terminal myc tag, while myc-mBICC1-ΔSAM has the SAM domain and the following 39 amino acids deleted. The myc-mBICC1-ΔKH construct has the two KH domains and the preceding 132 amino acids deleted, while the myc-mBICC1-del133-691 construct has the two KH domains with an additional section of the intervening sequence, from amino acids 352-691, deleted. The BICC1 constructs contain mouse cDNA. **B)** The *gfp*-ANKS3 construct represents full length ANKS3 with a N-terminal *gfp* tag, while the *gfp*-ANKS3-ΔSAM construct has the SAM domain deleted. The FLAG-ANKS3 construct represents full length ANKS3 with a N-terminal FLAG tag. The *gfp*-ANKS6 construct represents full length ANKS6 with a N-terminal *gfp* tag, while the *gfp*-ANKS6-ΔSAM construct has the SAM domain deleted. The *gfp*-ANKS6-R823W and *gfp*-ANKS6-I817N constructs were altered to produce a missense mutation at amino acid 823 and 817 respectively in the SAM domain of ANKS6. The FLAG-ANKS6 construct represents full length ANKS6 with a N-terminal FLAG tag. The ANKS3 constructs contain mouse cDNA, while the ANKS6 constructs contain rat cDNA. KH = K-homology, SAM = sterile alpha motif, ANK = ankyrin repeat.

To investigate whether BICC1 and ANKS3 interact *in vitro*, and whether this interaction is specific to ANKS3 or whether BICC1 can bind other proteins containing ANK repeats and SAM domains, HA-BICC1 cells (previously described in section 3.2.12) were induced to express BICC1 with tetracycline and transfected with either a full-length ANKS3 construct containing a *gfp*-tag (*gfp*-ANKS3), a full-length ANKS6 construct containing a *gfp*-tag (*gfp*-ANKS6) or both (Figure 4.2.2.1). HA-BICC1 was used as bait in Co-IP experiments and western blot analysis demonstrated that full-length BICC1 interacts with full-length ANKS3, but not full-length ANKS6 or the pcDNA3 of *gfp* negative controls (Figure 4.2.2.2). Moreover, when ANKS6 was co-transfected with ANKS3 in the HA-BICC1 cells, the interaction between BICC1 and ANKS3 was lost. This data suggests ANKS6 competes with BICC1 for ANKS3 binding, and ANKS6 has the greater affinity over BICC1.

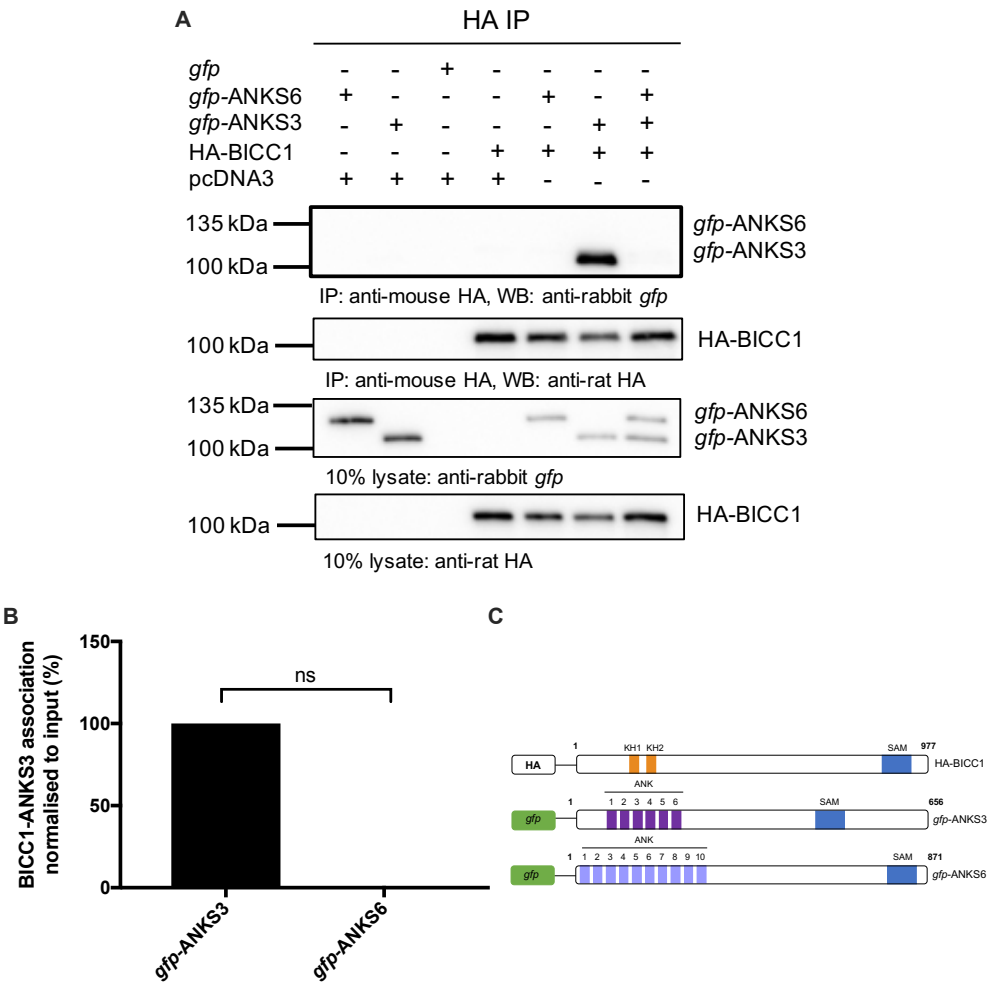

Figure 4.2.2.2. BICC1 interacts with ANKS3, but not ANKS6. A) Western blot analysis following Co-IP experiments, using HA-tagged BICC1 as bait, were used to assess protein interactions between BICC1, ANKS3 and ANKS6. pcDNA3 and a *gfp* construct were included as a negative control. **B)** Quantification of the Co-IP experiments (n=3). Paired t-tests were performed to assess significance (ns = not significant, p value = >0.05). Error bars represent standard error of the mean. **C)** Schematic diagram of the constructs used in this experiment.

To further explore the interaction between BICC1 and ANKS3 and investigate which of the protein domains of BICC1 were responsible for the interaction, HEK293 cells were co-transfected with *gfp*-ANKS3 and either a full-length BICC1 construct (myc-mBICC1), a BICC1 construct with the SAM domain deleted (myc-mBICC1-ΔSAM) or the KH domain deleted (myc-mBICC1-ΔKH) (Figure 4.2.2.1). *gfp*-ANKS3 was used as bait and Co-IP experiments confirmed ANKS3 interacts with full-length BICC1 (Figure 4.2.2.3 A). A significantly stronger interaction was observed between ANKS3 and myc-mBICC1-ΔKH (15-fold) compared to myc-mBICC1 and myc-mBICC1-ΔSAM, suggesting the interaction between ANKS3 and BICC1 does not require the KH domain or the first 132 amino acids of BICC1 (Figure 4.2.2.3 B). Furthermore, an interaction with myc-mBICC1-ΔSAM suggests that the interaction between ANKS3 and BICC1 does not require the SAM domain or the following 39 amino acids of BICC1 also. Therefore, the interaction between ANKS3 and BICC1 does not require the KH or SAM domains of BICC1. These interactions were specific as no interaction was observed with the pcDNA3 negative control.

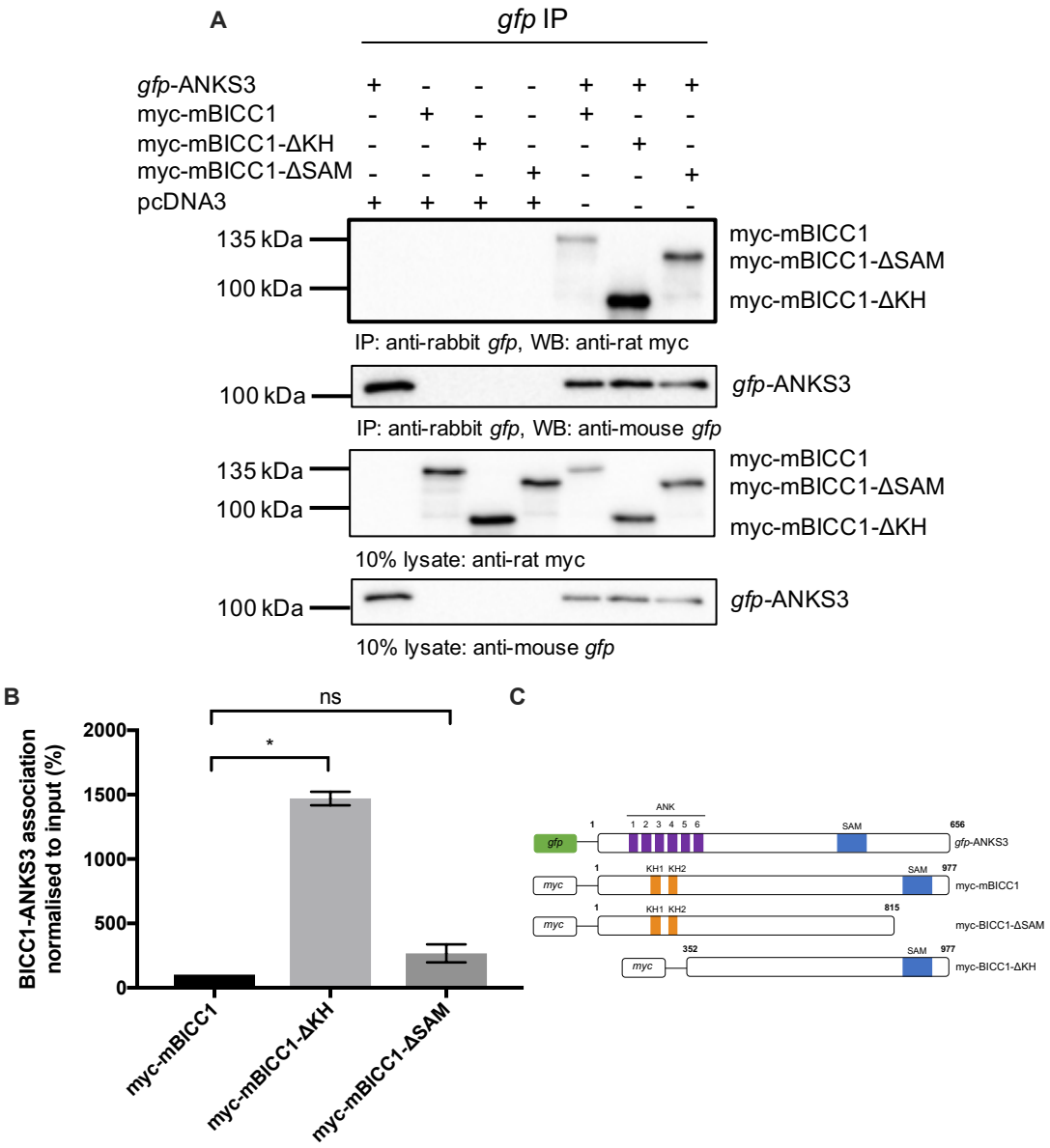

Figure 4.2.2.3. The interaction between ANKS3 and BICC1 does not require either the KH or SAM domain of BICC1. A) Western blot analysis following Co-IP experiments, using a *gfp*-ANKS3 tagged construct as bait, were used to assess protein interactions between ANKS3 and BICC1. pcDNA3 was included as a negative control. **B)** Quantification of the Co-IP experiments (n=3). Paired t-tests were performed to assess significance (p values * ≤0.05, ** = ≤0.01, *** = ≤0.001, **** = ≤0.0001 and ns = not significant). Error bars represent standard error of the mean. **C)** Schematic diagram of the constructs used in this experiment.

Data from the previous Co-IPs suggests that ANKS3 does not require either the KH or SAM domains of BICC1 to interact. To discover where ANKS3 interacts with BICC1, HEK293 cells were co-transfected with an additional BICC1 construct where amino acids 133-691 were deleted (myc-mBICC1-del133-691). Using *gfp*-ANKS3 as bait, Co-IP experiments demonstrated that ANKS3 interacts BICC1, as previously observed in Figure 4.2.2.3, as well as with myc-mBICC1-del133-691 (Figure 4.2.2.4 A). This data confirms that ANKS3 does not require either the KH or SAM domains of BICC1 to interact and also

suggests that ANKS3 has a binding affinity for BICC1 between amino acids 693 and 815, or the newly identified binding motif 2 (Figure 3.3.1) as identified for PC1 in section 3.2.4. These interactions were specific as no interaction was observed with the pcDNA3 negative control.

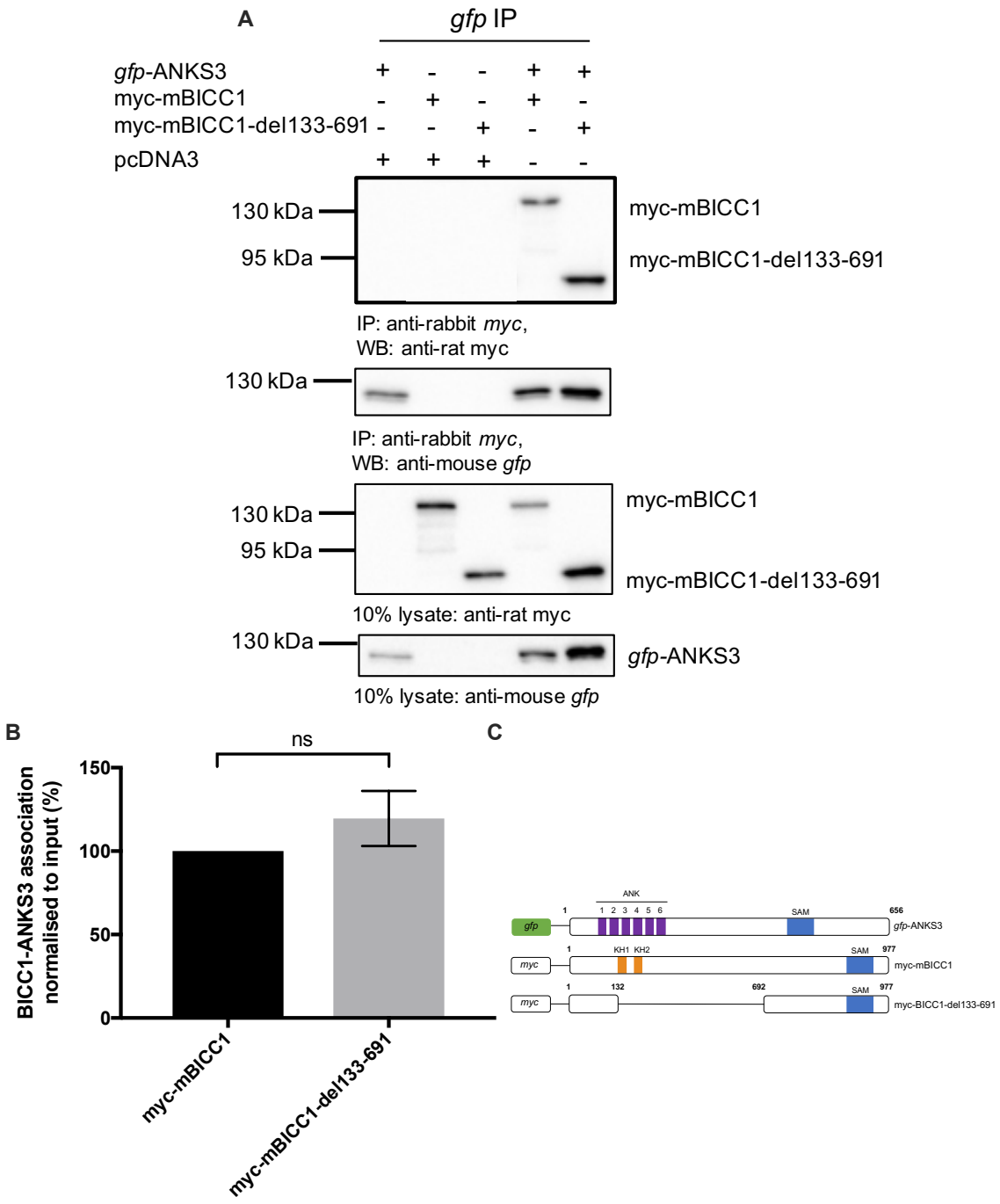

Figure 4.2.2.4. ANKS3 interacts with BICC1 between amino acids 693-815. A) Western blot analysis following Co-IP experiments, using a *gfp*-ANKS3 tagged construct as bait, were used to assess protein interactions between ANKS3 and BICC1. pcDNA3 was included as a negative control. **B)** Quantification of the Co-IP experiments (n=3). Paired t-tests were performed to assess significance (ns = not significant, p value = >0.05). Error bars represent standard error of the mean. **C)** Schematic diagram of the constructs used in this experiment.

To confirm the interaction observed between ANKS3 and BICC1 was not due to an artefact of overexpression, an endogenous Co-IP was performed. RNase I treatment was also included to investigate whether RNA was involved in mediating the interaction. Lysates were extracted from UCL93 cells and an anti-rabbit ANKS3 antibody was used as bait. The Co-IP demonstrated that ANKS3 and BICC1 interact endogenously (Figure 4.2.2.5 A). Furthermore, RNase I treatment had no significant effect on the interaction, suggesting RNA does not mediate the interaction (Figure 4.2.2.5 B). This interaction was specific as no interaction was observed with the anti-rabbit IgG negative control.

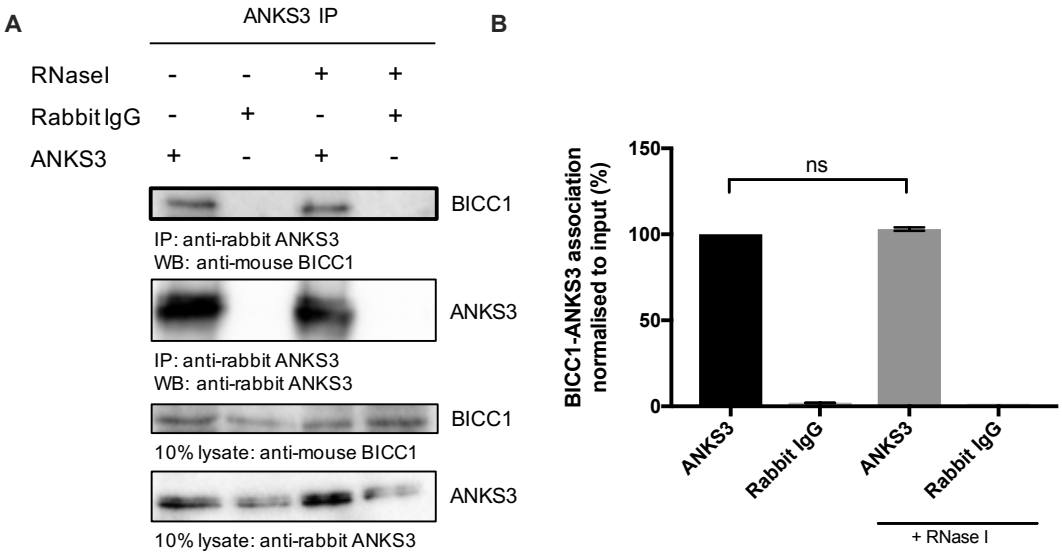

Figure 4.2.2.5. ANKS3 interacts with BICC1 endogenously. A) Western blot analysis following Co-IPs experiments, using an anti-rabbit ANKS3 antibody as bait, were used to assess endogenous protein interactions between ANKS3 and BICC1. RNase I was introduced to the Co-IP experiments in lane 3 and 4. A rabbit IgG antibody was included as a negative control. **B)** Quantification of the Co-IP experiments (n=3). Paired t-tests were performed to assess significance (ns = not significant, p value = >0.05). Error bars represent standard error of the mean. **C)** Schematic diagram of the constructs used in this experiment.

Previous data highlighted competition between BICC1 and ANKS6 for ANKS3 binding (Figure 4.2.2.2). Furthermore, the protein binding domains of BICC1 are not responsible for the interaction observed between ANKS3 and BICC1. Instead a section of amino acids upstream of the BICC1-SAM binds ANKS3. To further investigate these interactions, the required binding domains or motifs of ANKS3 and why ANKS6 is able to interact with ANKS3 over BICC1, deletion constructs of

ANKS3 and ANKS6 were designed (Figure 4.2.2.1) and they were transfected into HA-BICC1 cells (see section 2.6 for methods).

Using HA-BICC1 as bait, Co-IPs were performed, and western blot analysis demonstrated that BICC1 interacts with full-length ANKS3, as previously observed in Figure 4.2.2.2, as well as with *gfp*-ANKS3-ΔSAM (Figure 4.2.2.6 A). However, this interaction was significantly weaker (60%), suggesting that the SAM domain of ANKS3 is a vital, but not exclusive, element involved in mediating an interaction between BICC1 and ANKS3 (Figure 4.2.2.6 B). As observed in Figure 4.2.2.2, BICC1 did not interact with full-length ANKS6, and co-transfection of *gfp*-ANKS3 and *gfp*-ANKS6 disrupted the interaction between BICC1 and ANKS3. Furthermore, no interaction was observed between BICC1 and *gfp*-ANKS6-ΔSAM. Moreover, co-transfection of *gfp*-ANKS3-ΔSAM and *gfp*-ANKS6-ΔSAM did not rescue the interaction between ANKS3 and BICC1 (Figure 4.2.2.6 B). However, an interaction between BICC1 and ANKS3 was re-established after co-transfection of *gfp*-ANKS6 and *gfp*-ANKS3-ΔSAM (Figure 4.2.2.7 A). Co-transfection of *gfp*-ANKS3 and *gfp*-ANKS6-ΔSAM also rescued the interaction between BICC1 and ANKS3. These interactions were specific as no interaction was observed with the pcDNA3 negative control.

Together, this data demonstrates the importance of the SAM domain of ANKS3 for initiating, but not stabilising, any interaction with BICC1, as well as controlling its interaction with ANKS6 (see section 4.2.3). Likewise, it also highlights the importance of the SAM domain of ANKS6 for its interaction with ANKS3, as when ANKS6-SAM is lost, ANKS6 is unable to interact with ANKS3, with or without its own SAM domain. Consequently, BICC1 is now able to re-establish its interaction with ANKS3, through ANKS3-SAM. It is interesting to note that deletion of both of the SAM domains of ANKS3 and ANKS6 does not restore an interaction between BICC1 and ANKS3.

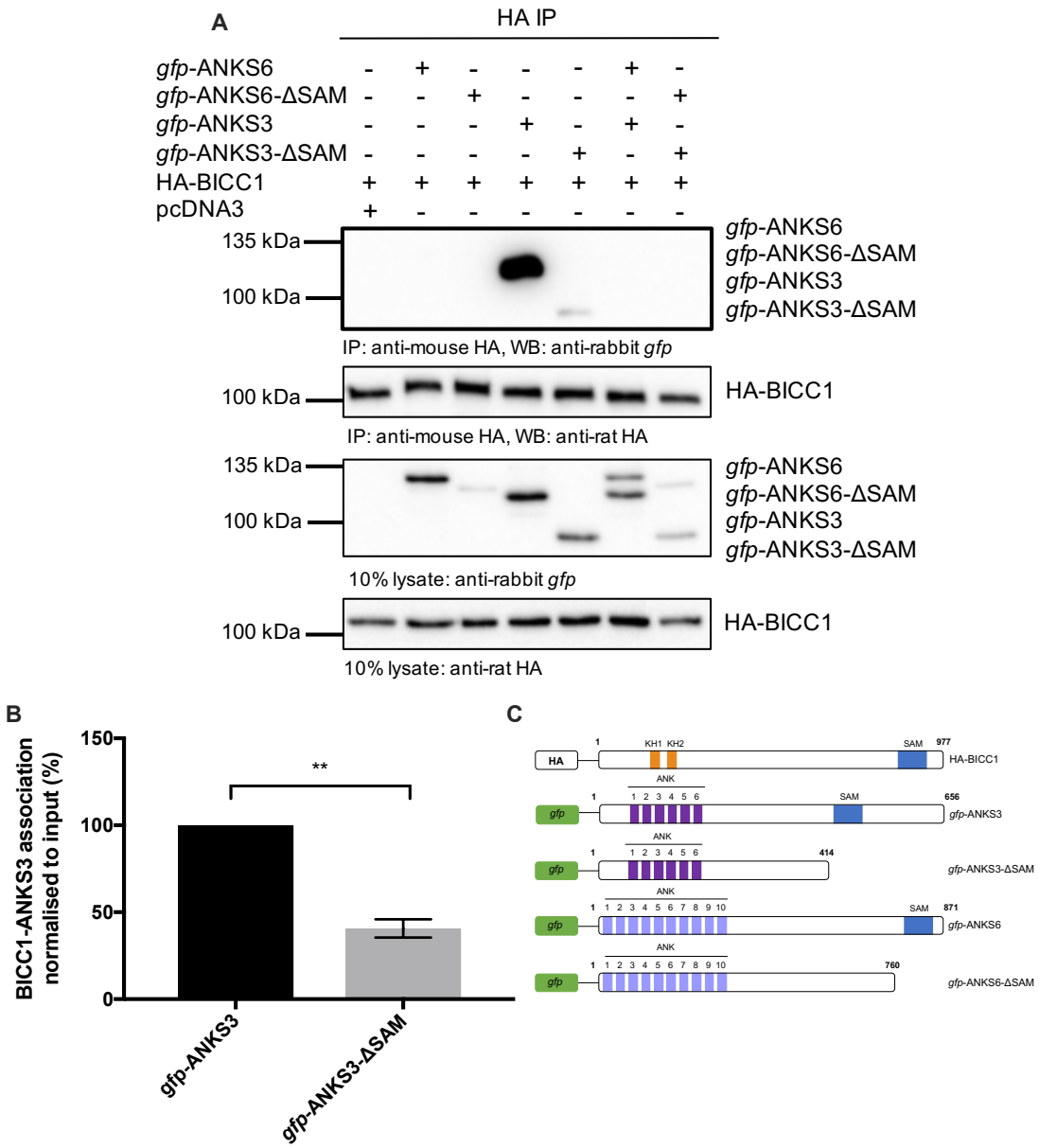

Figure 4.2.2.6. The interaction between BICC1 and ANKS3 requires the SAM domain of ANKS3. A) Western blot analysis following Co-IP experiments, using a HA-tagged BICC1 as bait, were used to assess protein interactions between BICC1, ANKS3 and ANKS6. pcDNA3 was included as a negative control. **B)** Quantification of the Co-IP experiments (n=3). Paired t-tests were performed to assess significance (p values * ≤0.05, ** = ≤0.01, *** = ≤0.001, **** = ≤0.0001 and ns = not significant). Error bars represent standard error of the mean. **C)** Schematic diagram of the constructs used in this experiment.

As discussed in section 4.1.1, a missense mutation in the SAM domain of ANKS6 (R823W) has been shown to disrupt its interaction with ANKS3, while another missense mutation 6 amino acids upstream (I747N) was reported to have no effect on its interaction with ANKS3, but disrupted its interaction with BICC1. To confirm this observation, the R823W and I747N mutations were recreated in the rat *gfp*-ANKS6 construct and so-called *gfp*-ANKS6-R823W and *gfp*-ANKS6-I817N (Figure 4.2.2.1). Note the R823W mutation was in a rat

model, while the I747N mutation was in a mouse model. The amino acid sequences differ slightly between these models, hence the different between the notation of I747N and the *gfp*-ANKS6-I817N construct used in this study. HA-BICC1 cells were co-transfected with these constructs and HA-BICC1 was used as bait. The Co-IP experiments demonstrated that BICC1 does not interact with full-length ANKS6, as previously observed, as well as with *gfp*-ANKS6-R823W or *gfp*-ANKS6-I817N (Figure 4.2.2.7 C). Neither the point mutation of R823W or I817N re-established an interaction between BICC1 and ANKS3, suggesting a complete loss of ANKS6-SAM is required to reinstate this interaction. It must be noted, however, that the expression of the *gfp*-ANKS6-R823W and the *gfp*-ANKS6-I817N plasmids was much lower than the *gfp*-ANKS6 and the *gfp*-ANKS6-ΔSAM plasmids, which suggests that the point mutations within the SAM domain might destabilise the protein. These interactions observed were specific as no interaction was observed with the pcDNA3 negative control.

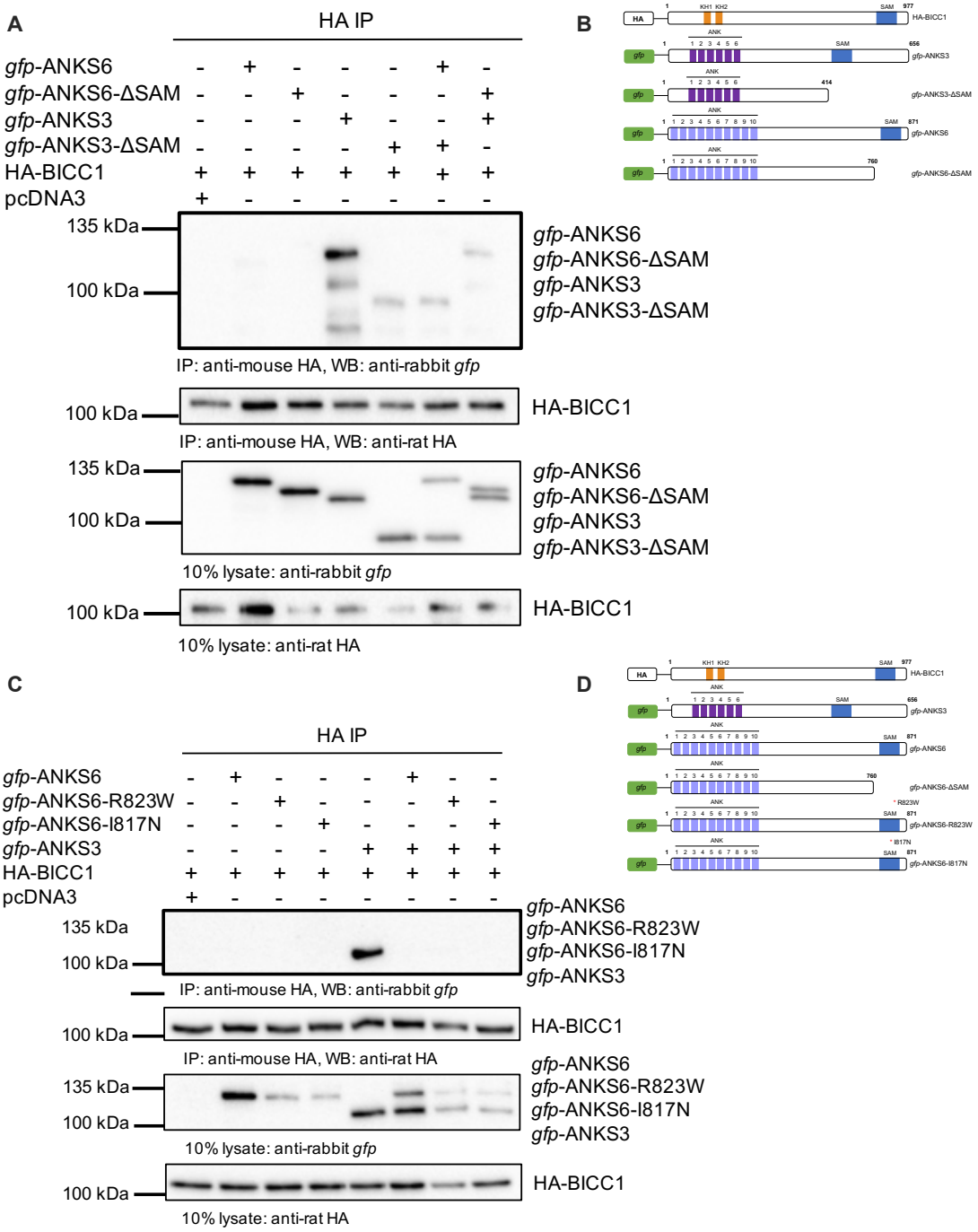

Figure 4.2.2.7. The interaction between BICC1 and ANKS3 is restored following deletion of the SAM domain of ANKS3 and ANKS6. A, C) Western blot analysis following Co-IP experiments, using a HA-tagged BICC1 as bait, were used to assess protein interactions between BICC1, ANKS3 and ANKS6. pcDNA3 was included as a negative control. **B, D)** Schematic diagrams of the constructs used in these experiments.

4.2.3 ANKS3 interacts with ANKS6

Published data has demonstrated that ANKS3 and ANKS6 interact. To confirm this observation and investigate whether RNA has any role in the interaction, lysates were extracted from UCL93 cells and an anti-rabbit ANKS3 antibody

was used as bait for endogenous Co-IP experiments. Western blot analysis confirmed an interaction between ANKS3 and ANKS6 (Figure 4.2.3.1 A). Surprisingly, RNase I treatment significantly decreased the interaction (60%), suggesting that an RNA intermediate is required for the endogenous interaction (Figure 4.2.3.1 B). These interactions were specific as no interaction was observed with the anti-rabbit IgG negative control.

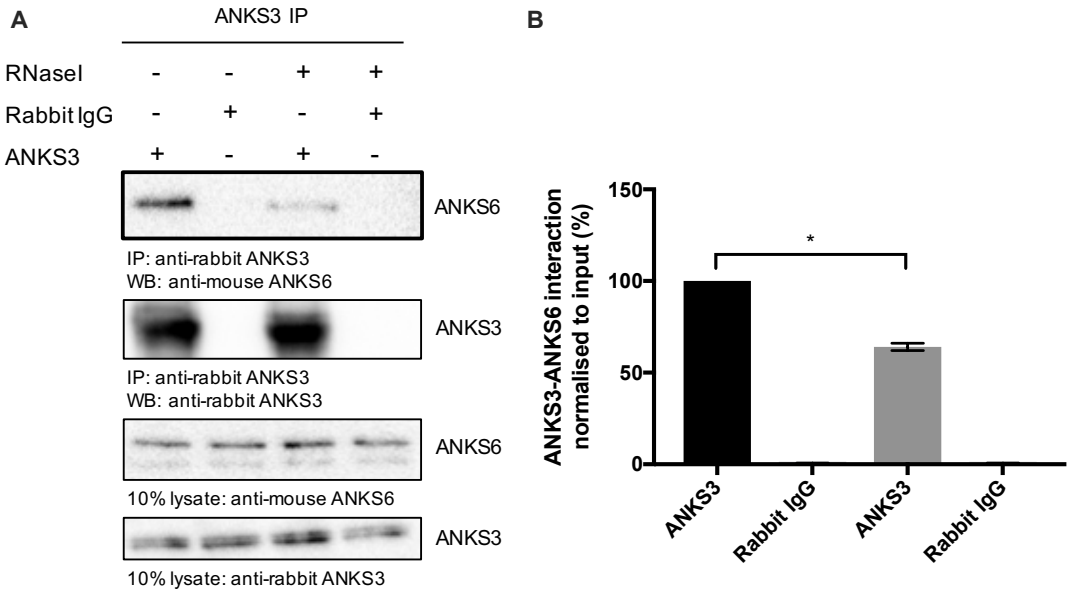

Figure 4.2.3.1. ANKS3 and ANKS6 interact endogenously. A) Western blot analysis following Co-IPs experiments, using an anti-rabbit ANKS3 antibody as bait, were used to assess endogenous protein interactions between ANKS3 and ANKS6. RNase I was introduced to the Co-IP experiments in lane 3 and 4. A rabbit IgG antibody was included as a negative control. **B)** Quantification of the Co-IP experiments (n=3). Paired t-tests were performed to assess significance (p values * ≤0.05, ** = ≤0.01, *** = ≤0.001, **** = ≤0.0001 and ns = not significant). Error bars represent standard error of the mean.

ANKS3 and ANKS6 interact endogenously. Furthermore, previous Co-IP experiments in this study and in published literature have highlighted the importance of the SAM domains of both ANKS3 and ANKS6 in mediating interactions (section 4.2.2). To further confirm this observation, HEK293 cells were co-transfected with variations ANKS3 and ANKS6 constructs (Figure 4.2.2.1). *Gfp*-tagged constructs were used as bait in the Co-IP experiments, which demonstrated that full-length ANKS3 interacts with full-length ANKS6 (Figure 4.2.3.2 A). Furthermore, ANKS3 interacts with ANKS6 when its SAM domain has been deleted, although this interaction is significantly weaker (80%) (Figure 4.2.3.2 B). In contrast, the interaction between ANKS3 and ANKS6 is lost when the SAM domain of ANKS3 is deleted. This data confirms the

importance of ANKS3-SAM in mediating the interaction between ANKS3 and ANKS6.

As observed in Figure 4.2.2.7 C, neither the point mutation of R823W or I817N re-establish an interaction between BICC1 and ANKS3, which also suggests that these mutations would not disrupt the ability of ANKS6 to interact with ANKS3. To confirm this theory, HEK293 cells were co-transfected with the *gfp*-ANKS6-R823W and *gfp*-ANKS6-I817N constructs, as well as with FLAG-ANKS3. Lysates were extracted, Co-IPs were performed, and western blot analysis demonstrated that ANKS3 is still able to interact with ANKS6 despite the point mutations in its SAM domain, although the interaction is significantly weaker (80-85%) (Figure 4.2.3.2).

This data suggests that the R823W and I817N point mutations must modify ANKS6-SAM in a way that it reduces its protein binding ability, as well as potentially affecting the structure or confirmation of the protein as a whole. However, the mutations alone are not enough to completely disrupt the ability of ANKS6 to form protein interactions. These interactions are specific as no interaction was observed with the pcDNA3 negative control.

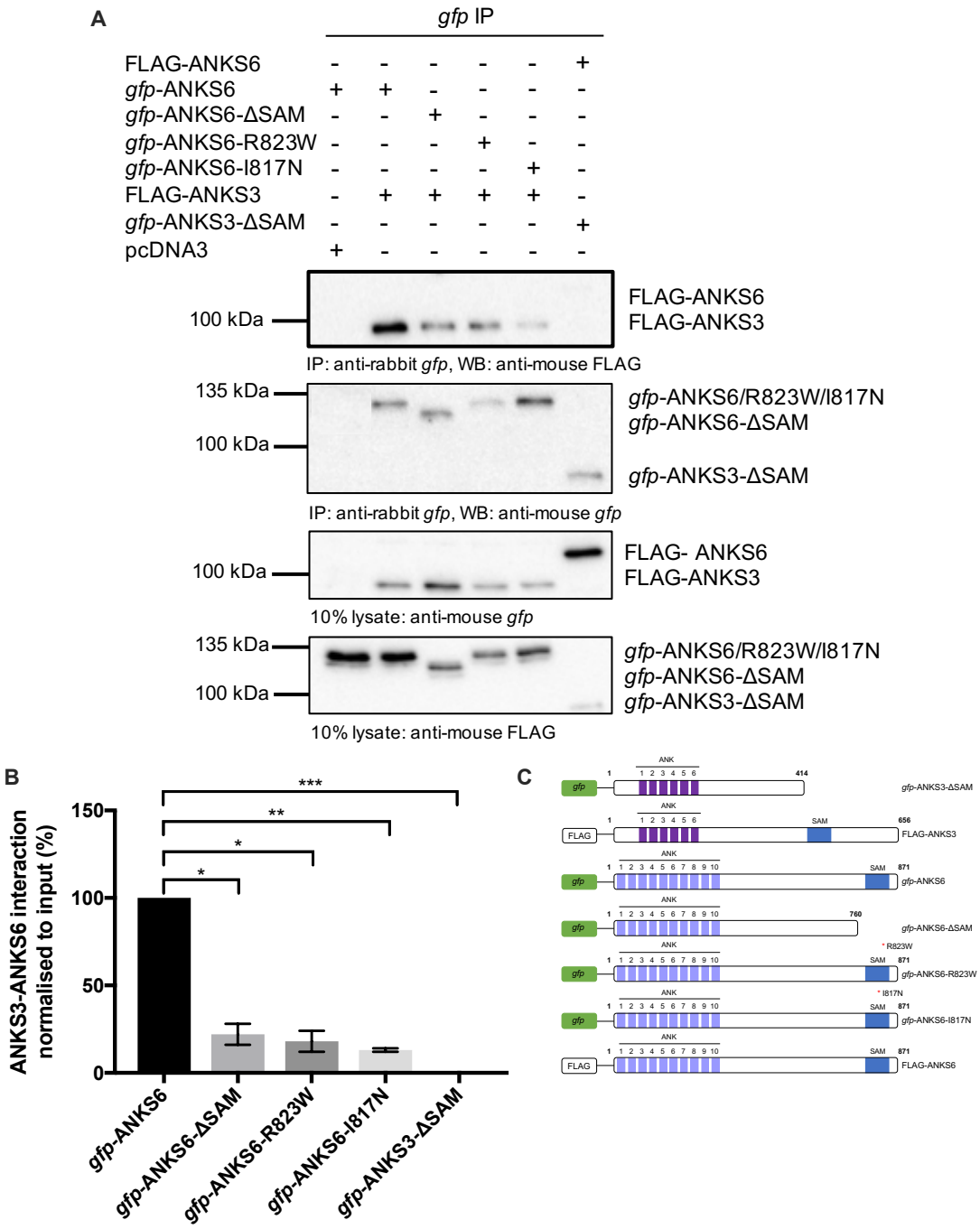

Figure 4.2.3.2. The interaction between ANKS3 and ANKS6 requires the SAM domain of ANKS3 but not the SAM domain of ANKS6. A) Western blot analysis following Co-IP experiments, using a *gfp*-ANKS3 tagged construct as bait, were used to assess protein interactions between ANKS3 and ANKS6. pcDNA3 was included as a negative control. **B)** Quantification of the Co-IP experiments (n=3). Paired t-tests were performed to assess significance (p values * ≤0.05, ** = ≤0.01, *** = ≤0.001, **** = ≤0.0001 and ns = not significant). Error bars represent standard error of the mean. **C)** Schematic diagram of the constructs used in this experiment.

4.2.4 ANKS3 interacts with the polycystin proteins

This study has demonstrated that BICC1 can interact with the polycystin proteins PC1 and PC2, as well as with the cystoprotein ANKS3, which could lead one to hypothesise that BICC1 can form multiprotein complexes. If this hypothesis were to be true, it is conceivable to hypothesise that ANKS3 also interacts with the polycystin proteins. To investigate whether ANKS3 interacts with PC1, HEK293 cells were transfected with the *gfp*-ANKS3 and *gfp*-ANKS3-ΔSAM construct, as well as the PC1-HA construct described in Figure 3.2.4.2.

Using PC1-HA as bait Co-IP experiments demonstrated that PC1 interacts with full-length ANKS3, as well as with *gfp*-ANKS3-ΔSAM (Figure 4.2.4.1 A). However, this interaction was significantly weaker (60%), suggesting that the SAM domain of ANKS3 is a vital, but not exclusive, element involved in mediating an interaction between PC1 and ANKS3 (Figure 4.2.4.1 B). HEK293 were also co-transfected with PC1-HA and the *gfp*-ANKS6 and *gfp*-ANKS6-ΔSAM constructs, to assess whether the interaction of PC1 to ANKS3 was specific. Western blot analysis demonstrated that PC1 did not interact with either full-length ANKS6 or ANKS6-ΔSAM (Figure 4.2.4.1). These interactions are specific as no interaction was observed with the pcDNA3 negative control. As competition for ANKS3 binding has been observed between ANKS6 and BICC1, the presence of ANKS6 and its effect on the interaction between PC1 and ANKS3 was assessed. However, the expression of PC1-HA was observed to be decreased when the three constructs were simultaneously transfected. Therefore, an accurate assessment of any possible effects could not be made.

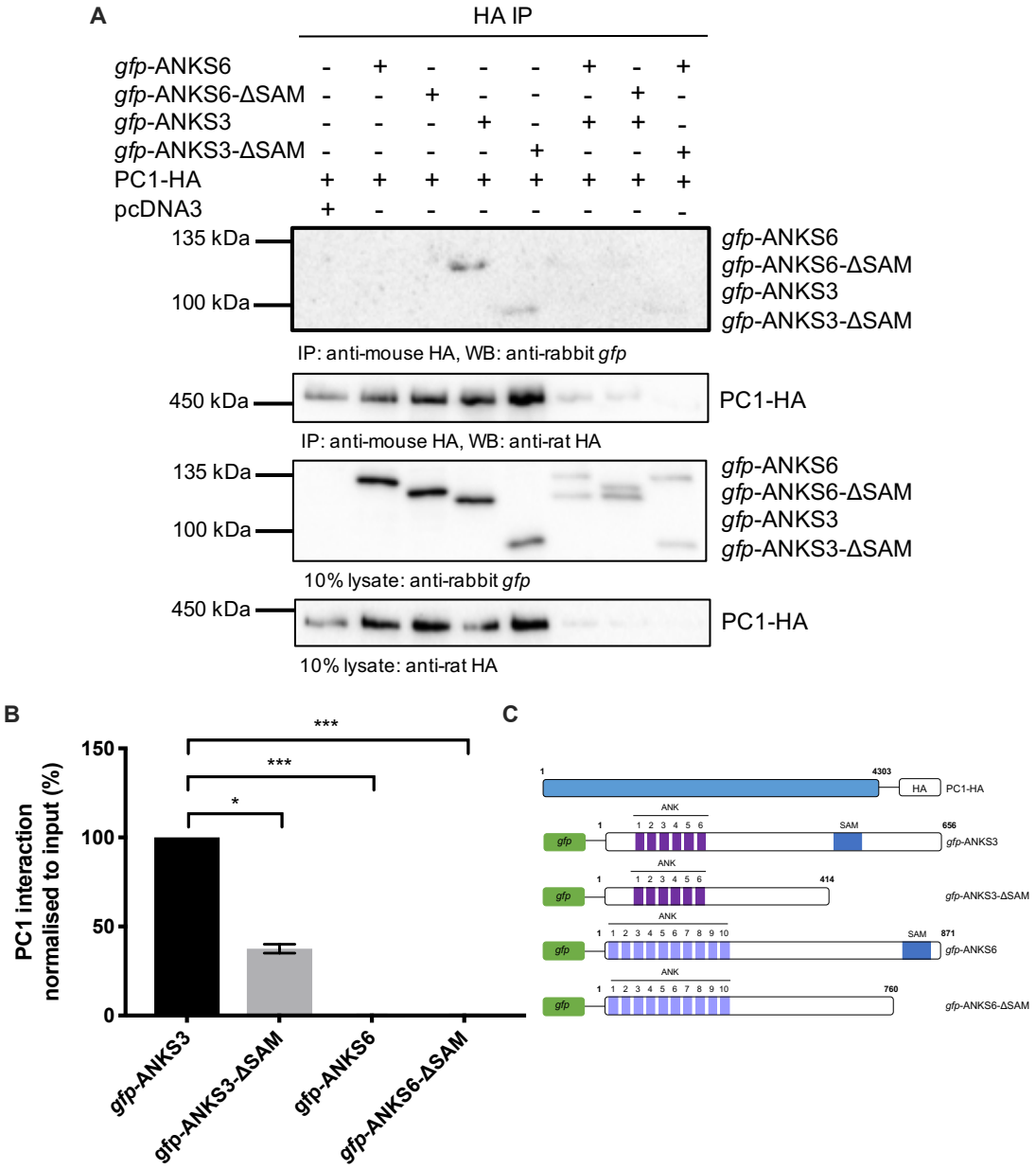

Figure 4.2.4.1. PC1 interacts with ANKS3 and the interaction requires the SAM domain of ANKS3. A) Western blot analysis following Co-IP experiments, using a PC1-HA tagged construct as bait, were used to assess protein interactions between a PC1, ANKS3 and ANKS6. pcDNA3 was included as a negative control. **B)** Quantification of the Co-IP experiments (n=3). Paired t-tests were performed to assess significance (p values * ≤0.05, ** = ≤0.01, *** = ≤0.001, **** = ≤0.0001 and ns = not significant). Error bars represent standard error of the mean. **C)** Schematic diagram of the constructs used in this experiment.

To validate the interaction observed between PC1 and ANKS3 and investigate whether RNA has any role in the interaction, lysates were extracted from UCL93 cells and endogenous Co-IPs were performed using an anti-rabbit ANKS3 antibody as bait. Western blot analysis demonstrated that ANKS3 and PC1 interact endogenously (Figure 4.2.4.2 A). Furthermore, treatment with RNase I had no significant effect, suggesting RNA does not mediate the

interaction (Figure 4.2.4.2 B). These interactions are specific as no interaction was observed with the anti-rabbit IgG negative control.

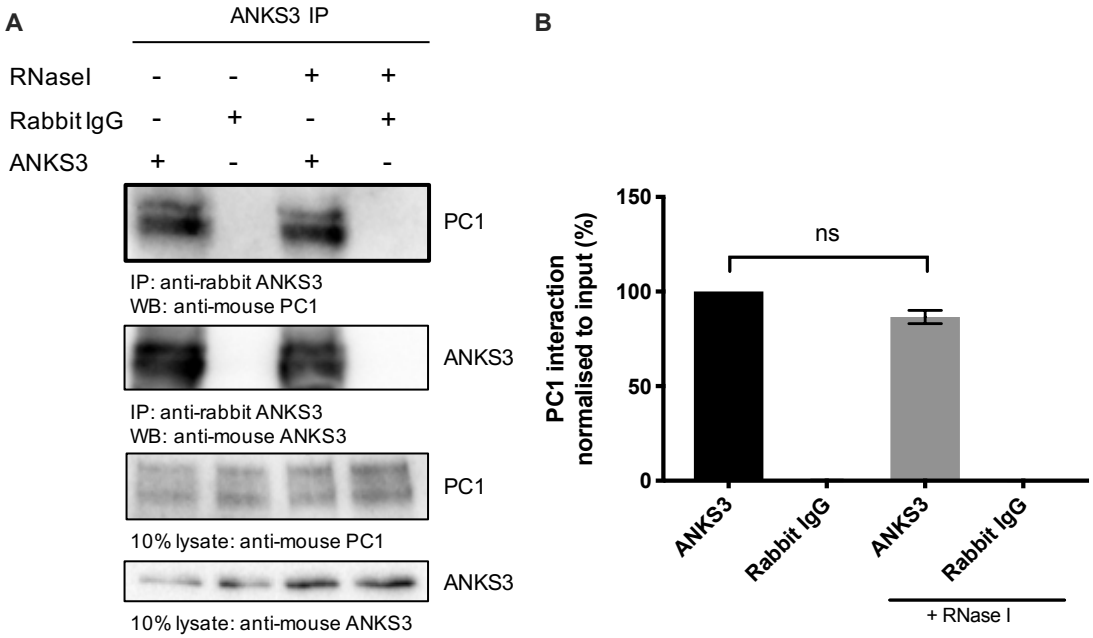

Figure 4.2.4.2. ANKS3 and PC1 interacts endogenously. A) Western blot analysis following Co-IPs experiments, using an anti-rabbit ANKS3 antibody as bait, were used to assess endogenous protein interactions between ANKS3 and PC1. RNase I was introduced to the Co-IP experiments in lane 3 and 4. A rabbit IgG antibody was included as a negative control. **B)** Quantification of the Co-IP experiments (n=3). Paired t-tests were performed to assess significance (ns = not significant, p value = >0.05). Error bars represent standard error of the mean.

To investigate whether ANKS3 interacts with PC2, HEK293 cells were transfected with the *gfp*-ANKS3 and *gfp*-ANKS3-ΔSAM construct, as well as the PC2-HA construct described in Figure 3.2.4.2. Using PC2-HA as bait the Co-IPs experiments demonstrated that PC2 interacts with full-length ANKS3, as well as with the *gfp*-ANKS3-ΔSAM construct (Figure 4.2.4.3 A). However, this interaction was significantly weaker (75%), suggesting that the SAM domain of ANKS3 is a vital, but not exclusive, element involved in mediating an interaction between PC2 and ANKS3 (Figure 4.2.4.3 B). HEK293 were also co-transfected with PC2-HA and the *gfp*-ANKS6 and *gfp*-ANKS6-ΔSAM constructs, to assess whether the interaction of PC2 to ANKS3 was specific. Western blot analysis demonstrated that PC2 did not interact with either full-length ANKS6 or ANKS6-ΔSAM (Figure 4.2.4.3).

As competition for ANKS3 binding has been observed between ANKS6 and BICC1, the presence of ANKS6 and its effect on the interaction between PC2 and ANKS3 was assessed. Co-transfection of ANKS6 disrupts the interaction between PC2 and ANKS3 (Figure 4.2.4.3). However, when the SAM domain of ANKS6, but not the SAM domain of ANKS3, is deleted the interaction between ANKS3 and PC2 is restored, albeit very weakly. These interactions are specific as no interaction was observed with the pcDNA3 negative control.

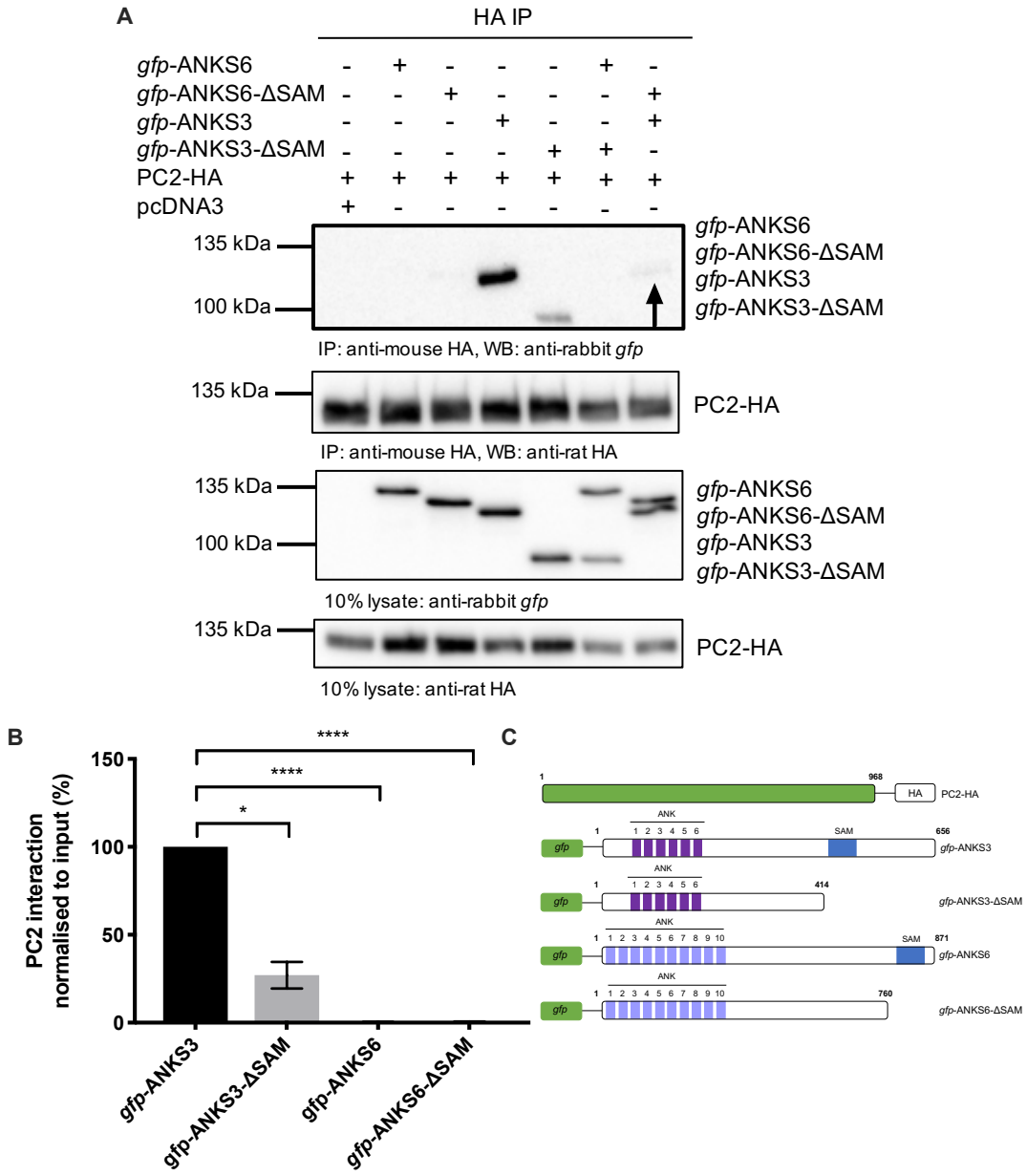

Figure 4.2.4.3. PC2 interacts with ANKS3 and the interaction requires the SAM domain of ANKS3. A) Western blot analysis following Co-IP experiments, using a PC2-HA tagged construct as bait, were used to assess protein interactions between a PC2, ANKS3 and ANKS6. pcDNA3 was included as a negative control. The black arrow highlights the presence of a faint band. **B)** Quantification of the Co-IP experiments (n=3). Paired t-tests were performed to assess significance (p values * ≤0.05, ** = ≤0.01, *** = ≤0.001, **** = ≤0.0001 and ns = not significant). Error bars represent standard error of the mean. **C)** Schematic diagram of the constructs used in this experiment.

To validate the interaction observed between PC2 and ANKS3 and investigate whether RNA has any role in the interaction, lysates were extracted from UCL93 cells and endogenous Co-IPs were performed using an anti-rabbit ANKS3 antibody as bait. Western blot analysis demonstrated that ANKS3 and PC2 interact endogenously (Figure 4.2.4.4 A). Furthermore, treatment with RNase I had a small significant effect, suggesting RNA could be involved in mediating the interaction (Figure 4.2.4.4 B). These interactions are specific a no interaction was observed with the anti-rabbit IgG negative control.

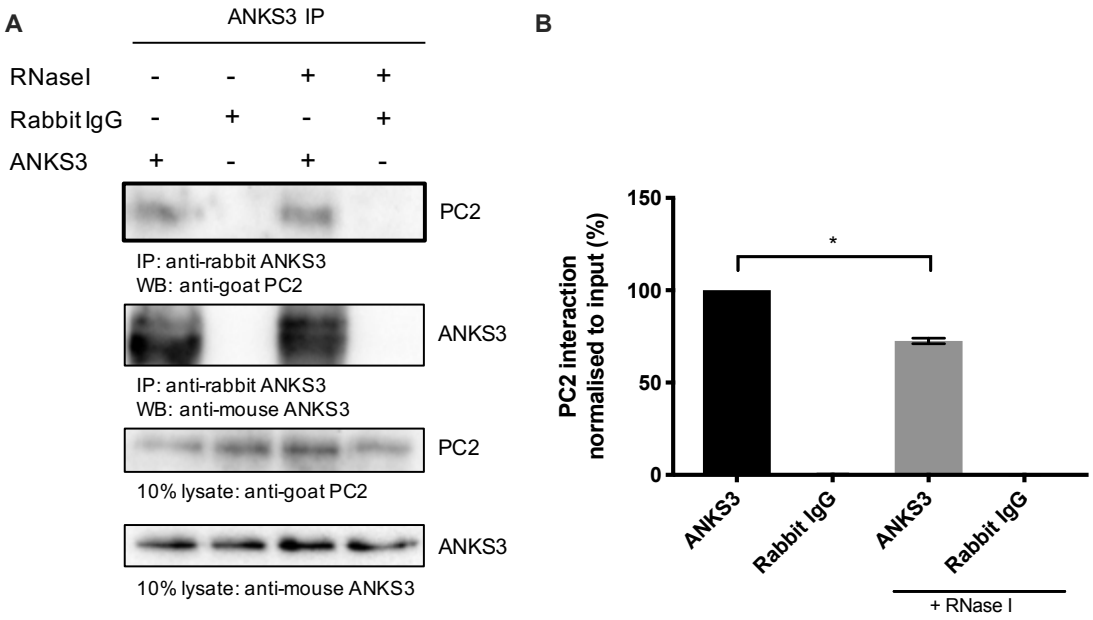

Figure 4.2.4.4. ANKS3 and PC2 interact endogenously. A) Western blot analysis following Co-IPs experiments, using an anti-rabbit ANKS3 antibody as bait, were used to assess endogenous protein interactions between ANKS3 and PC2. RNase I was introduced to the Co-IP experiments in lane 3 and 4. A rabbit IgG antibody was included as a negative control. **B)** Quantification of the Co-IP experiments (n=3). Paired t-tests were performed to assess significance (ns = not significant, p value = >0.05). Error bars represent standard error of the mean.

4.2.5 The cellular localisation of the polycystins and their related cystoproteins

To investigate where the proteins of the PC1-PC2-BICC1-ANKS3-ANKS6 complex localise, cellular fractionation was performed on UCL93 cells to obtain cytoplasmic and nuclear fractions. All proteins were observed in the cytoplasmic fraction, while BICC1 and ANKS6 were also observed in the nuclear fraction (Figure 4.2.5.1. A). However, both BICC1 and ANKS6 were more strongly expressed in the cytoplasmic fraction, by 4-fold and 7-fold respectively, when their expression was normalised to the relative controls for each fraction (Figure 4.2.5.1. B). It is interesting to note the ANKS6 nuclear band migrated slower than its cytoplasmic band. Actin was used as a positive control for the cytoplasmic fraction, while Alyref was used as a positive control for the nuclear fraction. Alyref, or Aly/REF Export Factor, was used as a positive control as it is a well-known, abundant protein in the nucleus.

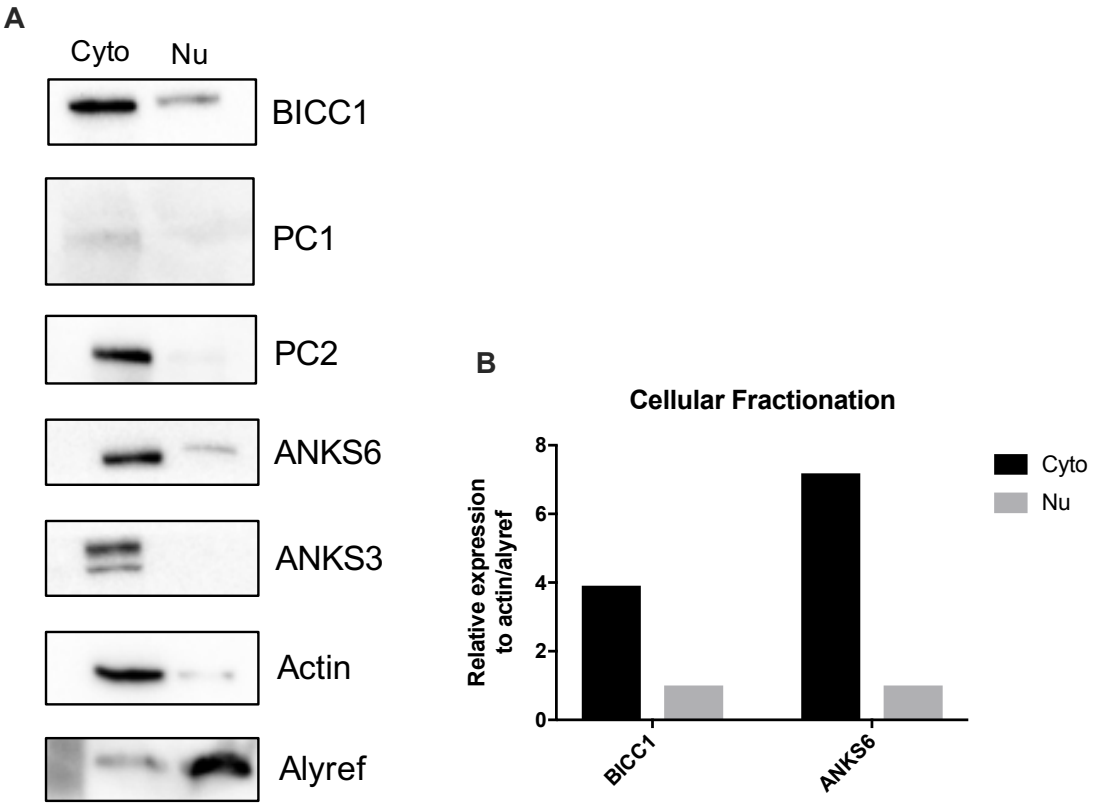

Figure 4.2.5.1. Cellular localisation of polycystins and cystoproteins. A) Following cellular fractionation into cytoplasmic (Cyto) and nuclear (Nu) fractions, western blots were performed to assess the localisation of BICC1, PC1, PC2, ANKS6 and ANKS3. Actin was included as a positive control for the cytoplasmic fraction, while Alyref was included as a positive control for the nuclear fraction. **B)** BICC1 and ANKS6 were observed in both fractions, therefore the relative expression of both proteins was normalised to Actin for the cytoplasmic fraction and Alyref for the nuclear fraction.

4.2.6 Loss of BICC1 downregulates ANKS3 expression

This study has established a link between BICC1 and ANKS3 through protein-protein interactions. As BICC1 is an RNA-binding protein known to regulate gene expression, it was hypothesised that BICC1 could regulate ANKS3 expression. The mRNA and protein expression levels of ANKS3 were measured by qPCR and western blotting respectively in established *BICC1 KO* cell lines. Loss of BICC1 significantly reduced *ANKS3 mRNA* expression in all of the *BICC1 KO* clones, by approximately 50-80% (Figure 4.2.6.1 A). Furthermore, loss of BICC1 completely inhibited ANKS3 protein expression (Figure 4.2.6.1 B, C). This data suggests that BICC1 positively regulates ANKS3. ANKS3 displayed two bands when blotted, however, following ANKS3-targeted siRNA transfection, only the upper band was reduced (Figure 4.2.6.1 D). Therefore, the lower band is a non-specific band.

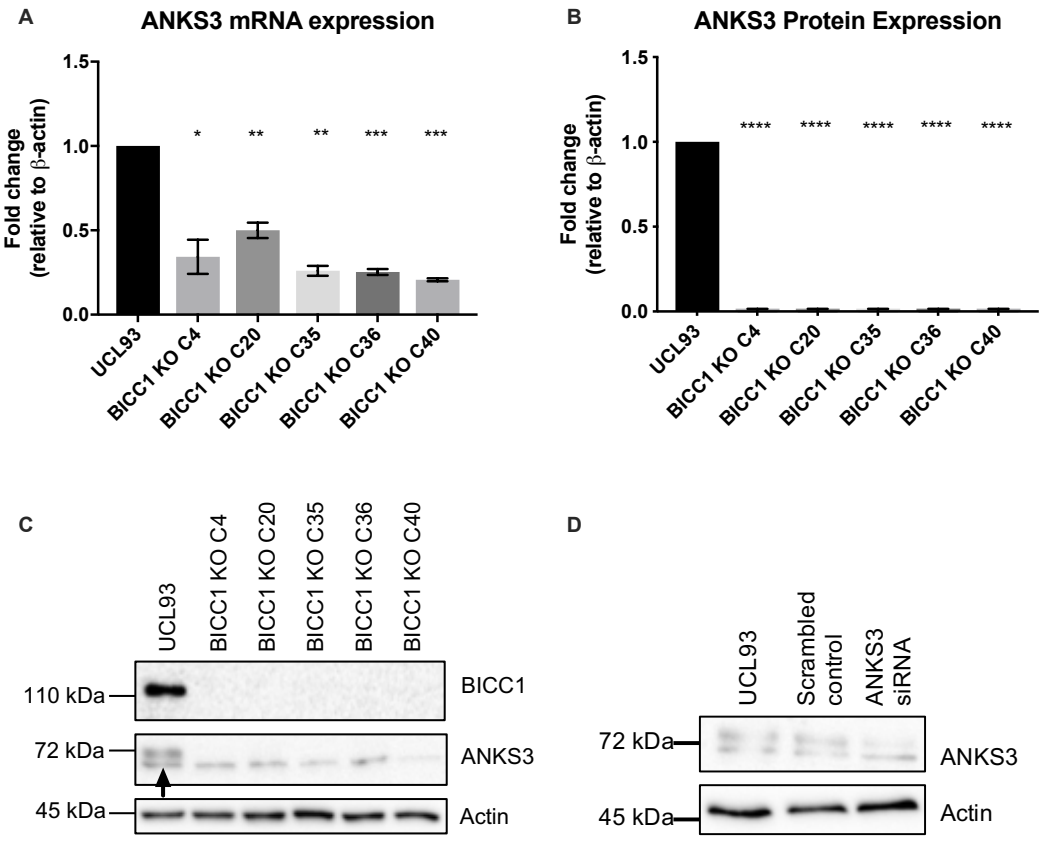

Figure 4.2.6.1. Loss of BICC1 downregulates ANKS3 expression. A) qPCR was used to measure the mRNA expression level of *ANKS3* in the selected *BICC1 KO* clones (n=3). **B, C)** Western blot analysis was used to measure the protein expression level of ANKS3 in the selected *BICC1 KO* clones (n=3). The western blots were quantified and normalised to actin. Paired t-tests were performed to assess significance (p values * ≤0.05, ** = ≤0.01, *** = ≤0.001 and **** = ≤0.0001). Error bars represent standard error of the mean. **D)** UCL93 cells were transfected with siRNA specific to ANKS3 or a scrambled siRNA control. The upper band of ANKS3 was dramatically reduced, suggesting the lower band of ANKS3 is unspecific.

4.2.7 Loss of BICC1 has no effect on ANKS6 expression

As a link has been observed between ANKS3 and ANKS6 through a developing protein interaction network, and the significant effect ANKS6 has on the interaction between BICC1 and ANKS3, it was speculated whether BICC1 regulates the expression levels of ANKS6. Therefore, *ANKS6 mRNA* and protein expression levels were measured by qPCR and western blotting respectively in established *BICC1 KO* cell lines. Loss of BICC1 has no significant effect on *ANKS6 mRNA* expression in 4 out of the 5 *BICC1 KO* clones (Figure 4.2.7.1 A). Furthermore, loss of BICC1 had no significant effect on ANKS6 protein expression in 3 out of the 5 *BICC1 KO* clones (Figure 4.2.7.1 B, D). *BICC1 KO* C35 appears to be an outlier at both expression levels, while *BICC1 KO* C40 appears to be an outlier in the protein expression analysis of the upper, phosphorylated band of ANKS6 (ANKS6*U*).

Nakajima *et al*. (2018) first demonstrated that the upper band of ANKS6 (ANKS6*U*) is a phosphorylated form, as phosphatase treatment decreased the intensity of the upper band but had no effect of the lower band of ANKS6 (ANKS6*L*). This upper band of ANKS6 is likely to be the nuclear band we previously observed in Figure 4.2.5.1. However, the remaining *BICC1 KO* clones displayed no significant changes in the phosphorylation of ANKS6, although the general trend is slightly increased. Overall, this data suggests that BICC1 has no effect on the expression of ANKS6.

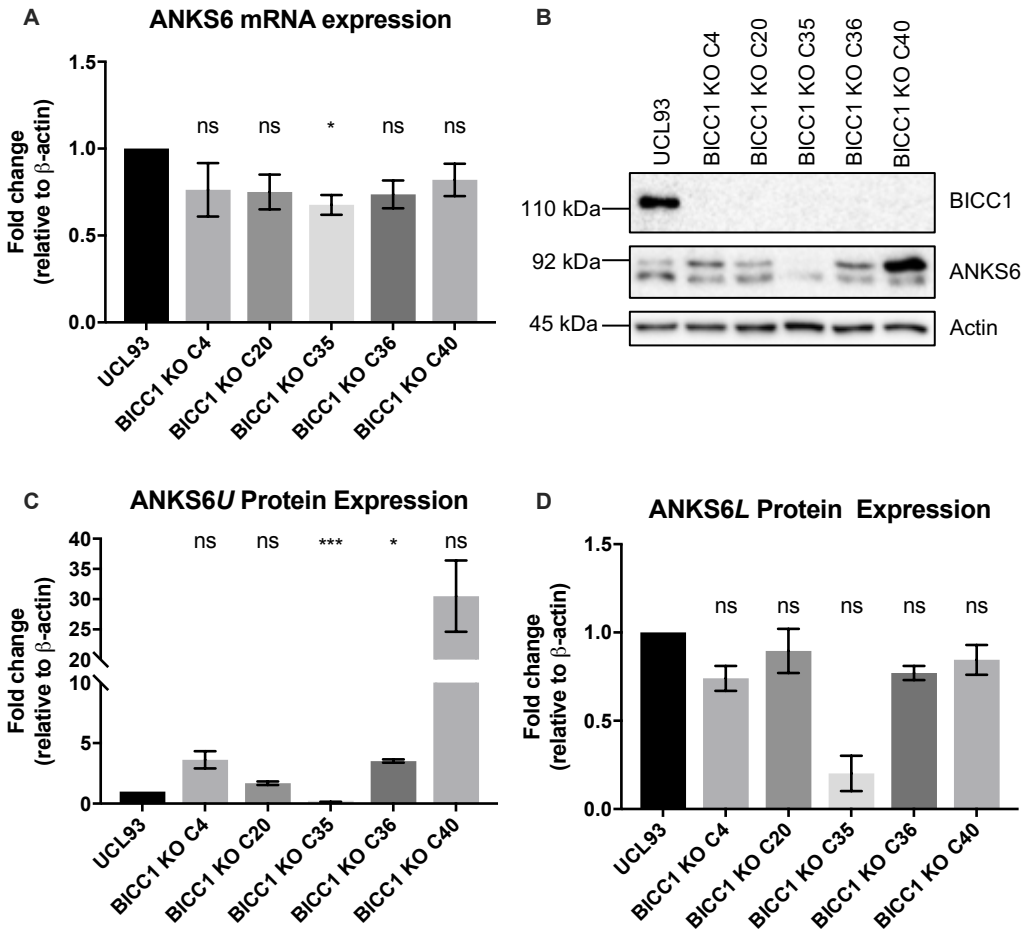

Figure 4.2.7.1. Loss of BICC1 has no effect on ANKS6 expression. A) qPCR was used to measure the mRNA expression level of *ANKS6* in the selected *BICC1 KO* clones (n=3). **B)** Western blot analysis was used to measure the protein expression level of the **C)** upper band of ANKS6 (ANKS6*U*) and the **D)** lower band of ANKS6 (ANKS6*L*) in the selected *BICC1 KO* clones (n=3). The western blots were quantified and normalised to actin. Paired t-tests were performed to assess significance (p values * ≤0.05, ** = ≤0.01, *** = ≤0.001, **** = ≤0.0001 and ns = not significant). Error bars represent standard error of the mean.

4.2.8 Loss of *PKD1* downregulates ANKS3 expression

As a link has been observed between PC1 and BICC1, as well as observing a developing protein interaction network between BICC1, PC1, PC2 and ANKS3 it was speculated whether loss of *PKD1* (PC1) would affect the expression levels of ANKS3. Therefore, *ANKS3 mRNA* and protein expression levels were measured by qPCR and western blotting respectively in established *PKD1 KO* cell lines. Loss of *PKD1* significantly reduced *ANKS3 mRNA* and protein expression in nearly all of the *PKD1 KO* clones, by approximately 25-50% and 50-90% respectively (Figure 4.2.8.1). *PKD1 KO* clone 11 appears to be an outlier, as observed for BICC1 in Figure 3.2.9.1. *PKD1 KO* clones 23 and 24 were observed to blot very weakly for ANKS3, but this is not thought to be

caused by loss of *PKD1* but a clonal variation. Overall, this data suggests PC1 positively regulates ANKS3 expression levels, possibly through regulating BICC1, as loss of *PKD1* significantly reduced BICC1 expression, while loss of BICC1 dramatically reduces the expression of ANKS3 (Figures 3.2.9 and 4.2.6).

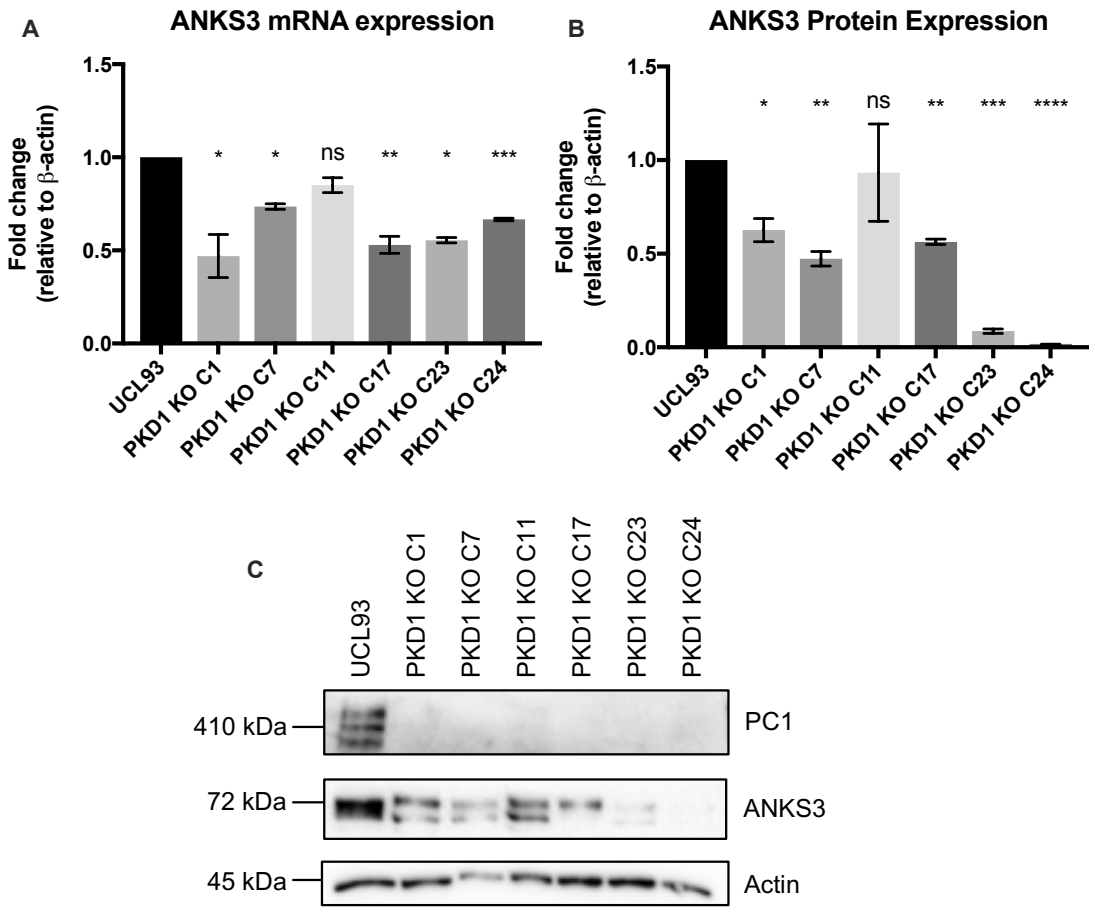

Figure 4.2.8.1. Loss of *PKD1* downregulates ANKS3 expression. A) qPCR was used to measure the mRNA expression level of *ANKS3* in the selected *PKD1 KO* clones (n=3). **B, C)** Western blot analysis was used to measure the protein expression level of ANKS3 in the selected *PKD1 KO* clones (n=3). The western blots were quantified and normalised to actin. Paired t-tests were performed to assess significance (p values * ≤0.05, ** = ≤0.01, *** = ≤0.001, **** = ≤0.0001 and ns = not significant). Error bars represent standard error of the mean.

4.2.9 Loss of *PKD1* downregulates ANKS6 protein expression but has no effect on *ANKS6 mRNA* expression

As performed in section 4.2.7, *ANKS6 mRNA* and protein expression levels were measured by qPCR and western blotting respectively in established *PKD1 KO* cell lines. Loss of *PKD1* has no significant effect on *ANKS6 mRNA* expression, but significantly downregulates ANKS6 protein expression (Figure 4.2.9.1). Furthermore, 3 out of the 6 *PKD1 KO* clones displayed no significant changes in the phosphorylation of ANKS6. *PKD1 KO* C17 appears to be an

outlier in the protein analysis. *PKD1 KO* clones 23 and 24 were observed to blot very weakly for ANKS6, as was observed for ANKS3, but this is not thought to be caused by loss of *PKD1* but a clonal variation. Overall, this data suggests that PC1 positively regulates ANKS6 protein expression levels but has no effect on the phosphorylation of ANKS6.

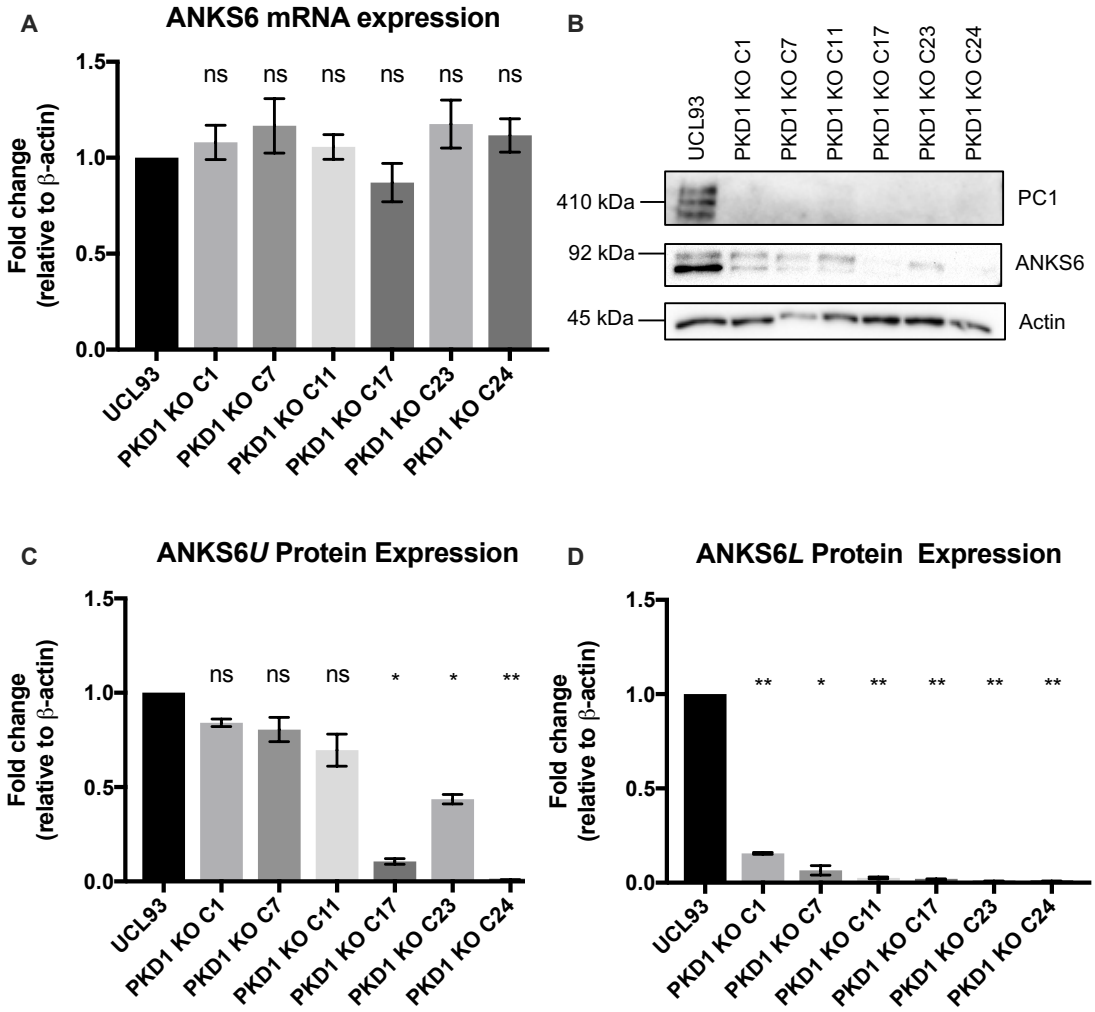

Figure 4.2.9.1. Loss of *PKD1* downregulates ANKS6 protein expression but has no effect on *ANKS6 mRNA* expression. A) qPCR was used to measure the mRNA expression level of *ANKS6* in the selected *PKD1 KO* clones (n=3). **B)** Western blot analysis was used to measure the protein expression level of the **C)** upper band of ANKS6 (*U*ANKS6) and the **D)** lower band of ANKS6 (*L*ANKS6) in the selected *PKD1 KO* clones (n=3). The western blots were quantified and normalised to actin. Paired t-tests were performed to assess significance (p values * ≤0.05, ** = ≤0.01, *** = ≤0.001, **** = ≤0.0001 and ns = not significant). Error bars represent standard error of the mean.

4.2.10 Loss of *PKD2* upregulates ANKS3 expression

As a link has been observed between PC2 and BICC1, as well as observing a developing protein interaction network between BICC1, PC1, PC2 and ANKS3 it was speculated whether loss of *PKD2* (PC2) would affect the expression levels of ANKS3. Therefore, *ANKS3 mRNA* and protein expression levels were measured by qPCR and western blotting respectively in established *PKD2 KO* cell lines. Loss of *PKD2* has no significant effect on *ANKS3 mRNA* expression, although an increase of approximately 1.5-fold was observed (Figure 4.2.10.1 A). In contrast, loss of *PKD2* significantly upregulated ANKS3 protein expression by an average of 3-fold (Figure 4.2.10.1. B, C). This data suggests PC2 negatively regulates ANKS3 expression levels, possibly through the regulating the expression of BICC1, as loss of *PKD2* significantly upregulated BICC1 expression (Figure 3.2.9).

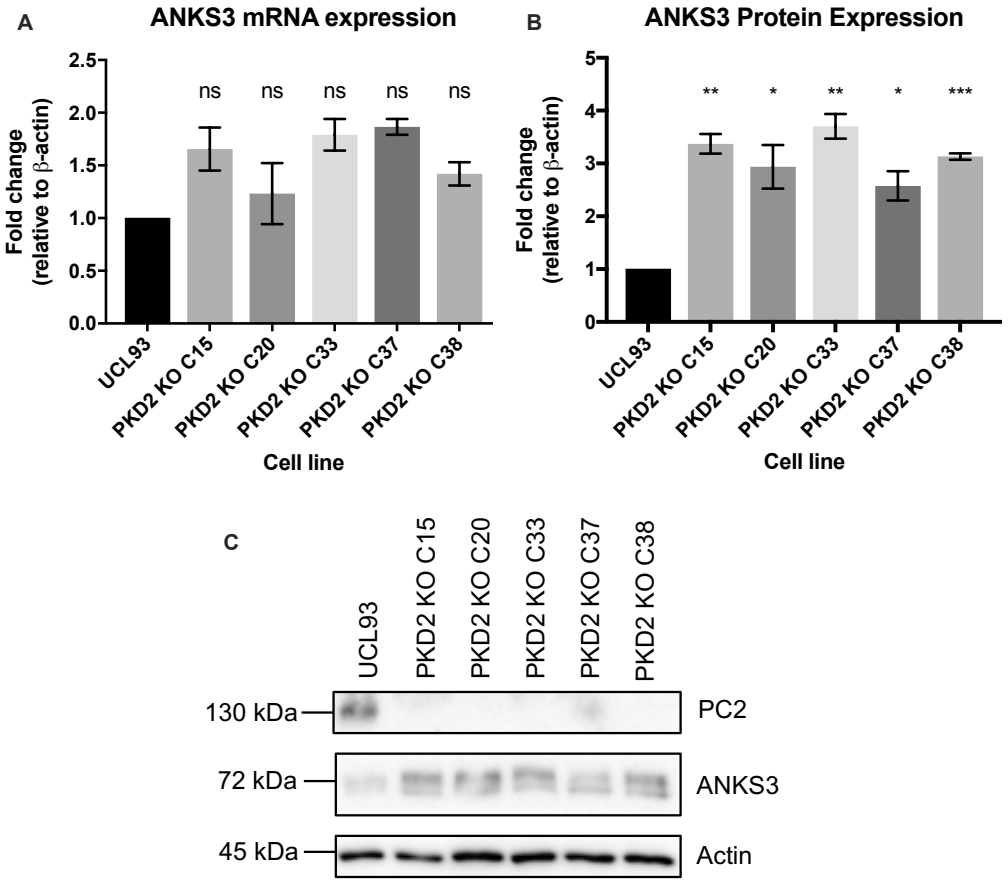

Figure 4.2.10.1. Loss of *PKD2* upregulates ANKS3 protein expression but has no effect on mRNA expression. A) qPCR was used to measure the mRNA expression level of *ANKS3* in the selected *PKD2 KO* clones (n=3). **B, C)** Western blot analysis measured the protein expression level of ANKS3 in the selected *PKD2 KO* clones (n=3). The western blots were quantified and normalised to actin. Paired t-tests were performed to assess significance (p values * ≤0.05, ** = ≤0.01, *** = ≤0.001, **** = ≤0.0001 and ns = not significant). Error bars represent standard error of the mean.

4.2.11 Loss of *PKD2* has no effect on ANKS6 expression

As performed in section 4.2.9, *ANKS6 mRNA* and protein expression levels were measured by qPCR and western blotting respectively in established *PKD2 KO* cell lines. Loss of *PKD2* has no significant effect on *ANKS6 mRNA* or protein expression, however *PKD2 KO* C37 appears to be an outlier in the protein analysis (Figure 4.2.11.1). Loss of *PKD2* also had no effect on the phosphorylation of ANKS6. This data suggests PC2 does not regulate ANKS6 expression.

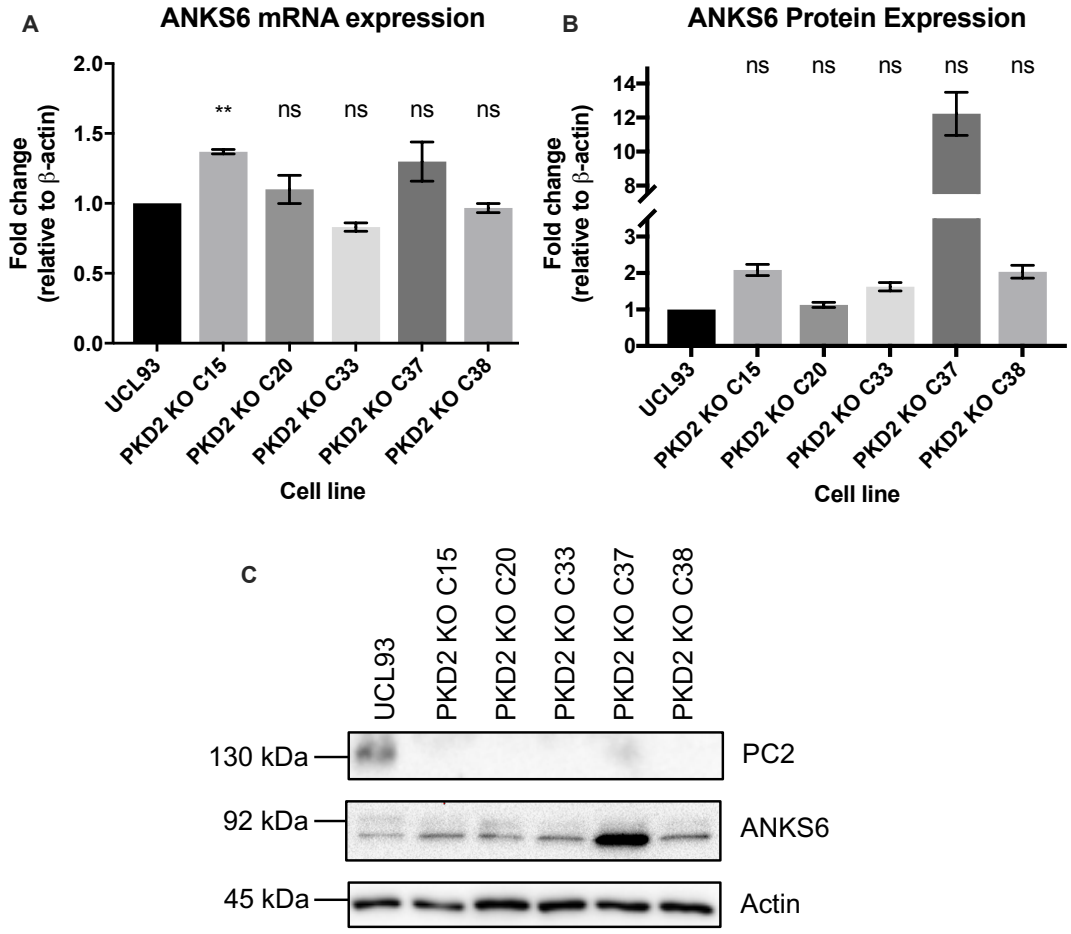

Figure 4.2.11.1. Loss of *PKD2* has no effect on ANKS6 expression. A) qPCR was used to measure the mRNA expression level of *ANKS6* in the selected *PKD2 KO* clones (n=3). **B, C)** Western blot analysis was used to measure the protein expression level of ANKS6 in the selected *PKD2 KO* clones (n=3). The western blots were quantified and normalised to actin. Paired t-tests were performed to assess significance (p values * ≤0.05, ** = ≤0.01, *** = ≤0.001, **** = ≤0.0001 and ns = not significant). Error bars represent standard error of the mean.

4.2.12 Overexpression of BICC1 upregulates the expression of *ANKS3* but not *ANKS6*

Following the induction of BICC1 through the addition of tetracycline to HA-BICC1 cells for 24 hours, RNA was extracted, and a qPCR was performed. *ANKS3 mRNA* expression was significantly increased in HA-BICC1 cells compared to HEK293 cells by 2.5-fold, whereas there was no significant change in the mRNA expression levels of *ANKS6* (Figure 4.2.12.1). This data suggests that the levels of BICC1 present in kidney cells is very important and tightly regulated, as loss of BICC1 causes a downregulation of *ANKS3*, but an overexpression of BICC1 causes an upregulation of *ANKS3*. This data also demonstrates a complex molecular, regulatory network between BICC1 and these cystoproteins, alongside the interaction network observed at the protein level.

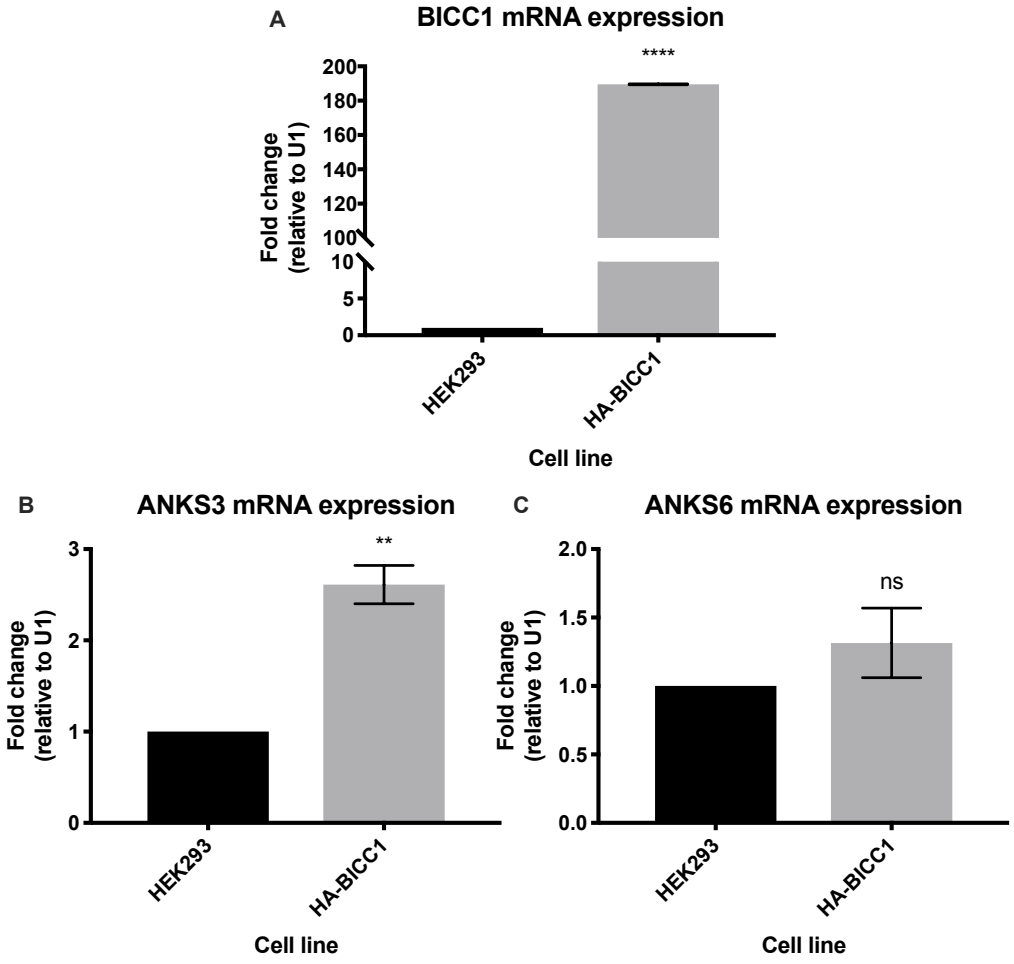

Figure 4.2.12.1. Overexpression of BICC1 upregulates the expression of *ANKS3* but not *ANKS6*. A) qPCR was used to measure the mRNA expression level of BICC1 in HA-BICC1 cells (n=3). qPCR was used to measure the mRNA expression levels of *ANKS3* **(B)** and *ANKS6* **(C)** in HA-BICC1 cells (n=3). Paired t-tests were performed to assess significance (p values * ≤0.05, ** = ≤0.01, *** = ≤0.001, **** = ≤0.0001 and ns = not significant). Error bars represent standard error of the mean.

4.2.13 Loss of BICC1 downregulates the expression of NEK and NEK protein partners

An interaction between BICC1 and NEK7 was identified in the MS analysis (Table 4.2.13.1) and various published research has demonstrated interactions between cystoproteins (or NPHP proteins) NEK kinases and their effector proteins (section 4.1). Combining the known function of BICC1 with the interaction link between BICC1 and cystoproteins, one could hypothesis that BICC1 regulates NEK kinases and/or their effector proteins to control their interactions and subsequent function with the cystoproteins. Therefore, the mRNA expression levels of *NEK* kinases and their effector proteins were measured by qPCR in established *BICC1 KO* cell lines. Loss of BICC1 significantly reduced the mRNA expression levels of *NEK1* (40-50%), *NEK2* (40-50%), *NEK4* (50-75%), *NEK6* (40-50%), *NEK7* (40-50%), *NEK8* (50%), *NEK9* (60-70%) and *NEK11* (50%) (Figure 4.2.13.1).

The most significant decrease was observed for *NEK9*. The mRNA expression levels of *NEK5* and *NEK10* were not measured as functional primers could not be designed. Furthermore, loss of BICC1 significantly decreased the mRNA expression levels of NPHP-related proteins *NPHP3* (40-60%) and *INVS/NPHP2* (40-50%), two proteins of the ANKS6-NPHP2-3-9 module (Figure 4.2.13.2). Moreover, loss of BICC1 also significantly reduced the mRNA expression levels of *ACK1* (50%) but not *CDC42.* ACK1 is the effector protein kinase of CDC42, and CDC42 is known to regulate the cell cycle and actin dynamics through interactions with MLT-2/ANKS6 and NEKL-3/NEK6/NEK7 of the NEKL-MLT network in *C. elegans* (section 4.1). This data suggests that BICC1 positively regulate certain NPHP modules, NEK kinases and their effector proteins.

Table 4.2.13.1. NEK7 is a novel binding partner of BICC1.

Gene	Identified Protein	Accession Number	Fold change	Average Score
NEK7	Serine/threonine-protein kinase Nek7	Q8TDX7	14.33	390.83
NEK1	Serine/threonine-protein kinase Nek1	Q96PY6	-	0.00
NEK2	Serine/threonine-protein kinase Nek2	P51955	-	0.00
NEK3	Serine/threonine-protein kinase Nek3	P51956	-	0.00
NEK4	Serine/threonine-protein kinase Nek4	P51957	-	0.00
NEK5	Serine/threonine-protein kinase Nek5	Q6P3R8	-	0.00
NEK6	Serine/threonine-protein kinase Nek6	Q9HV98	-	0.00
NEK8	Serine/threonine-protein kinase Nek8	Q86SG6	-	0.00
NEK9	Serine/threonine-protein kinase Nek9	Q8TD19	-	0.00
NEK10	Serine/threonine-protein kinase Nek10	Q6ZWH5	-	0.00
NEK11	Serine/threonine-protein kinase Nek11	Q8NG66	-	0.00
CDC42	Cell division control protein 42 homolog	P60953	-	0.00
ACK1	Activated CDC42 kinase 1	Q07912	-	0.00
INVS	Inversin (NPHP2)	Q9Y283	-	0.00
NPHP3	Nephrocystin-3	Q7Z494	-	0.00

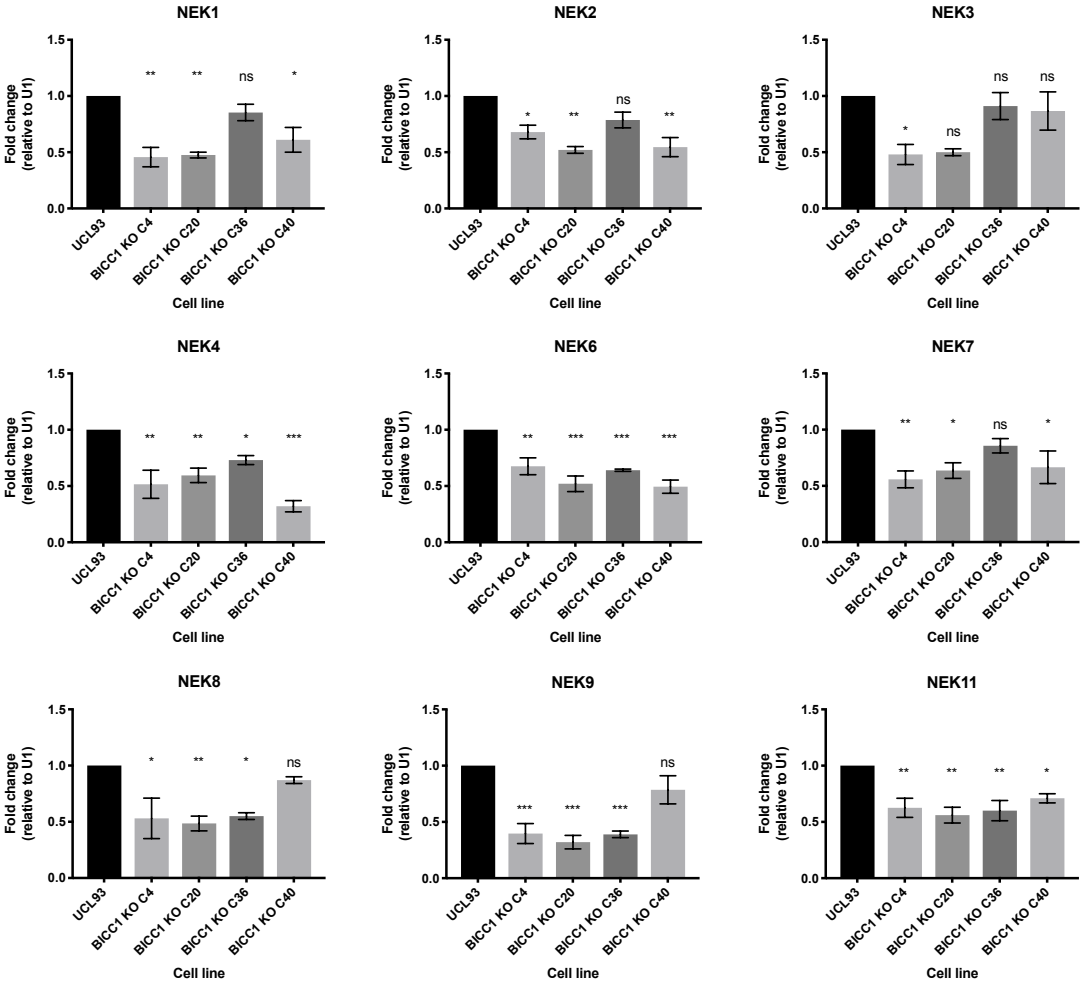

Figure 4.2.13.1. Loss of BICC1 downregulates the mRNA expression of *NEK* genes. qPCR was used to measure the mRNA expression level of *NEK* genes in the selected *BICC1 KO* clones (n=3). Paired t-tests were performed to assess significance (p values * ≤0.05, ** = ≤0.01, *** = ≤0.001, **** = ≤0.0001 and ns = not significant). Error bars represent standard error of the mean.

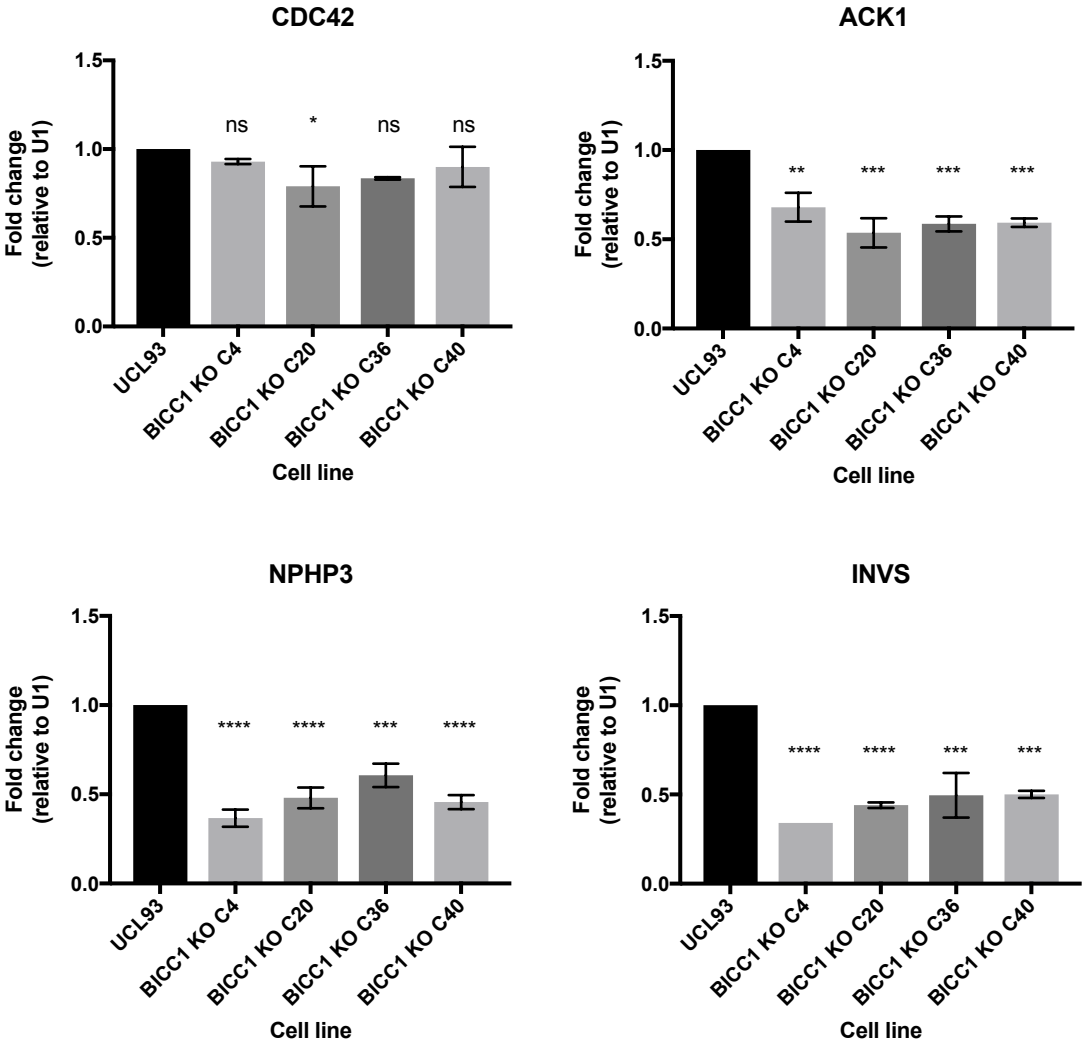

Figure 4.2.13.2. Loss of BICC1 downregulates the mRNA expression of *ACK1, NPHP3* and *INVS*. qPCR was used to measure the mRNA expression level of *NEK*-effector and *NPHP* genes in the selected *BICC1 KO* clones (n=3). Paired t-tests were performed to assess significance (p values * ≤0.05, ** = ≤0.01, *** = ≤0.001, **** = ≤0.0001 and ns = not significant). Error bars represent standard error of the mean.

4.3 Discussion

Data from this study has demonstrated that BICC1 interacts with the polycystins at the protein level, as well as regulating their mRNA expression levels. Therefore, the first aim of this chapter sought to identify additional novel BICC1-protein binding partners that could play a role in the pathogenesis of ADPKD, in an unbiased manner, by performing BICC1 Co-IP experiments followed by mass spectrometry (MS). The results demonstrate that BICC1 binds several novel proteins in kidney epithelial cells. Through functional annotation analysis, several BICC1-associated proteins were identified, which are mainly involved in translation initiation, deadenylation and poly(A) binding, RNA transport and degradation and protein processing. The proteins that were most significantly enriched with BICC1 were CNOT1, FASN, FLNA and ANKS3.

To ensure specificity and reliability, the protein dataset obtained from the MS analysis was compared to another BICC1-protein binding mass spectrometry dataset generated by the Constam research laboratory. A TAP-tag method was used and performed in a doxycycline-inducible, MmBicc1-SH stable cell line originally produced in HEK293 cells (Leal-Esteban *et al*., 2018). Each data set was analysed using DAVID and a cut off value of 0.05 was applied to the Benajmini value (adjusted p-value) to assess for significant and comparable protein hits between the two datasets.

Table 4.3.1 demonstrates that both datasets have significant hits in common pathways. For example, the Constam MS dataset contained RNA transcripts that encode proteins that function as phosphoproteins and in acetylation and isopeptide bonds, comparable to our MS dataset. Furthermore, both datasets contained significant hits in the GO biological process of translation initiation, SRP-dependent co-translational protein targeting to the membrane and nuclear-transcribed mRNA catabolic process (nonsense-mediated decay), to name but a few. Moreover, both datasets encoded proteins that are involved in poly(A) RNA binding, protein binding, and RNA binding, as well as being involved in the structural constituent of the ribosome. The Constam MS dataset presented proteins that are mainly localised to the membrane, extracellular exosome and the cytosol, similar to our MS dataset. Of interest, KEGG pathways analysis

was performed and both datasets displayed protein hits involved in the following pathways: the ribosome, protein processing in the endoplasmic reticulum, RNA transport, RNA degradation and aminoacyl-tRNA biosynthesis. The full list of pathways and biological functions can be viewed in Table 4.3.1.

Table 4.3.1. The comparison of enriched protein binding partners between our MS dataset and the Constam laboratory MS datasets. A cut off value of 0.05 was set for the Benjamini value (adjusted p-value) and the top keywords, GO terms and pathways are listed.

Term	Smith Mass Spec		Constam Mass Spec	
UP_Keywords	*p-value*	*Benjamini*	*p-value*	*Benjamini*
Acetylation	9.80E-120	3.20E-117	3.10E-89	7.50E-87
Phosphoprotein	1.80E-54	3.00E-52	1.20E-45	1.50E-43
Isopeptide bond	2.80E-29	1.90E-27	1.90E-30	1.50E-28
GO Biological Process	*p-value*	*Benjamini*	*p-value*	*Benjamini*
translational initiation	7.60E-24	1.40E-20	3.80E-24	2.20E-21
SRP-dependent cotranslational protein targeting to membrane	3.60E-23	3.20E-20	3.20E-20	1.30E-17
nuclear-transcribed mRNA catabolic process, nonsense-mediated decay	2.10E-22	1.30E-19	3.10E-19	9.30E-17
translation	2.40E-22	1.10E-19	5.40E-17	1.30E-14
GO Molecular Function	*p-value*	*Benjamini*	*p-value*	*Benjamini*
poly(A) RNA binding	3.90E-119	2.60E-116	8.30E-48	3.20E-45
protein binding	1.10E-31	3.50E-29	2.20E-32	4.20E-30
RNA binding	4.30E-25	7.10E-23	5.00E-17	6.50E-15
structural constituent of ribosome	2.20E-22	2.90E-20	2.80E-16	3.20E-14
GO Cellular Compartment	*p-value*	*Benjamini*	*p-value*	*Benjamini*
membrane	1.80E-83	9.00E-81	2.20E-44	3.90E-42
extracellular exosome	7.50E-44	1.90E-41	7.20E-22	8.50E-20
cytosol	2.80E-37	4.70E-35	2.60E-46	9.10E-44
Interpro	*p-value*	*Benjamini*	*p-value*	*Benjamini*
RNA recognition motif domain	2.30E-07	2.50E-05	2.90E-05	1.30E-03
KEGG Pathways	*p-value*	*Benjamini*	*p-value*	*Benjamini*
Ribosome	3.70E-16	7.10E-14	9.20E-13	1.30E-10
Protein processing in endoplasmic reticulum	6.80E-09	7.20E-07	7.40E-05	2.60E-03
RNA transport	2.00E-07	1.40E-05	2.70E-08	1.90E-06
RNA degradation	3.10E-06	1.70E-04	5.60E-06	2.60E-04
Aminoacyl-tRNA biosynthesis	1.10E-04	4.80E-03	3.00E-03	4.60E-02

To further understand the common KEGG pathways, and the types of transcripts BICC1 may regulate, the individual enriched proteins were explored. As displayed in Figure 4.3.1, there were several common transcripts that encode ribosomal proteins enriched in the ribosome pathway. RPL10, RPL10A, RPL18A, RPL31, RPL35A, RPL7, RPLP0 are components of the large 60S ribosomal subunit, responsible for proper mRNA translation. In contrast, RPS15 and RPS16 are components of the small 40S ribosomal subunit.

The common proteins enriched in protein processing in the ER included BAG2, CANX, HSPA4L and HSPH1 (Figure 4.3.1). Of interest is CANX, a molecular chaperone, which interacts with N-linked glycoproteins in the ER. CANX is a calcium-binding protein that has been linked to protein assembly and protein retention of improperly assembled proteins. BAG2, also known as the BCL2 associated athanogene 2, is a co-chaperone for HSP70 and HSC70 and acts as a nucleotide-exchange factor (NEF) to promote substrate protein release.

HSPA4L protects a heat-shocked cell from the effects of aggregated proteins, such as citrate synthase. HSPH1, on the other hand, is a NEF for HSC70, similarly to BAG2.

Several common, enriched proteins were observed in the RNA transport pathway including DDX20, EIF3A and PABPC1 (Figure 4.3.1). DDX20 is a DEAD box-containing RNA helicase. EIF3A, eukaryotic translation initiation factor 3 subunit A, is the RNA-binding component of the eIF3 complex responsible for the initiation of protein synthesis. The eIF3 complex is involved in several steps including binding the pre-initiation complex, mRNA recruitment to the pre-initiation complex and the scanning of mRNA for the UAG start codon. PABPC1 binds the 3' poly(A) tails of mRNAs and, as well as promoting translation initiation, PABPC1 is also involved in the deadenylation of poly(A) tails; therefore, promoting mRNA degradation.

The common proteins observed in the RNA degradation pathway were mostly members of the CCR4-CNOT deadenylation complex (Figure 4.3.1). Of interest is CNOT1 (identified as the most enriched protein of the complex in our MS dataset) and CNOT3 (identified as the most enriched protein of the complex in the Constam MS dataset). CNOT1 is the core subunit of the CCR4-CNOT complex and is responsible for providing a scaffold for the other subunits to bind to. CNOT3 binds to CNOT1 as well as CNOT2 to regulate RNA targeting and repression. Furthermore, EDC4, or enhancer of mRNA decapping 4, was enriched. EDC4 has been linked to the decapping of AU-rich element (ARE)-containing mRNAs and subsequent degradation through the formation of a complex with DCP1A (decapping mRNA 1A) and DCP2 (decapping mRNA 2), whilst stimulating the catalytic activity of the latter.

The common proteins enriched in aminoacyl-tRNA biosynthesis included several synthetases; RARS, DARS and QARS, to name but a few (Figure 4.3.1). RARS is an arginyl-tRNA synthetase responsible for catalysing the aminoacylation of tRNA and linking them to their relevant nucleotide triplet. Similarly, DARS is an aspartly-tRNA synthetase which enables the attachment of specific amino acids to its cognate tRNA. QARS is a glutaminyl-tRNA

synthase, while EPRS is a glutaminyl-prolyl-tRNA synthase, KARS is a lysyl-tRNA synthase and MARS is a methionyl-tRNA synthase.

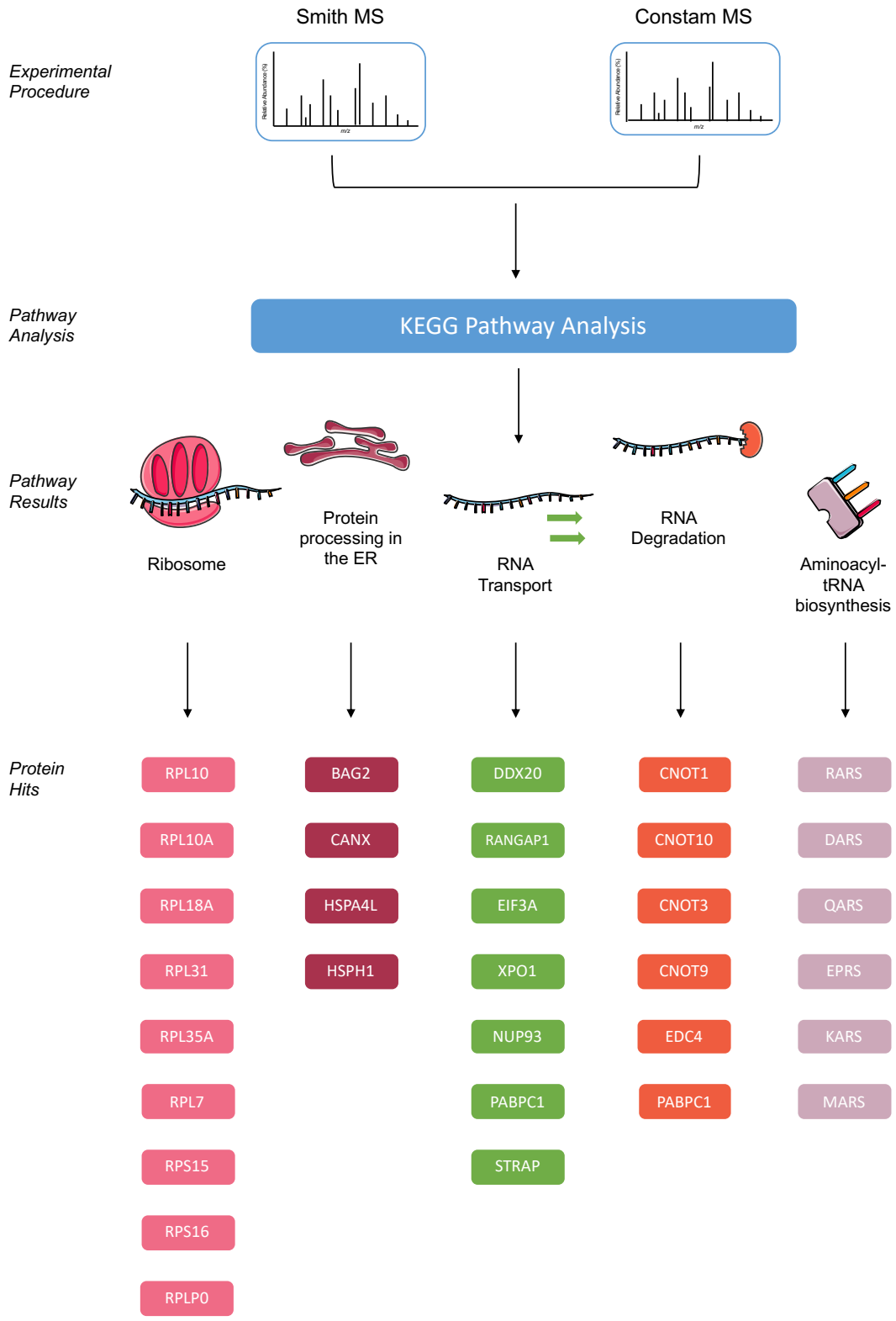

Figure 4.3.1. The common enriched binding partners identified in our BICC1 MS dataset and the Constam MS dataset. Significantly enriched binding partners from our MS dataset and the Constam MS dataset were compared and the common KEGG pathways were analysed by DAVID. The individual transcripts enriched within analysed pathways were further assessed and displayed according to their functional relationship.

Next, we analysed the individual proteins identified in our BICC1 MS dataset and the Constam MS dataset in regard to their enrichment with BICC1 by measurement of peptide fold change. Figure 4.3.2 displays the 6 most significantly BICC1-enriched proteins identified in both datasets, with their fold-change values for each dataset presented below each transcript. CNOT1, previously discussed, is the core subunit of the CCR4-CNOT complex and is responsible for providing a scaffold for the other subunits to bind to (Albert *et al*., 2000). FLNA, or filamin A, is an actin-binding protein that promotes the branching of actin filaments as well as linking actin filaments to membrane glycoproteins. FLNA has been linked to regulation of cell shape and migration through reorganisation of the cytoskeleton (Maestrini *et al*., 1990; Fox *et al*., 1998).

FASN, or fatty acid synthase, is a multifunctional protein involved in catalysing the conversion of acetyl-CoA and malonyl-CoA to palmitate for energy production; therefore, when overexpressed it can lead to the development of malignant cells (Wakil, 1989). ANKS3 is a newly identified protein that functions in protein complexes with its related family protein ANKS6, as well as with NEK kinases including NEK7, as discussed in Chapter 1 (Knight *et al*., 2011, Hoff *et al*., 2013; Leettola *et al*., 2014; Bakey *et al*., 2015; Delestre *et al*., 2015; Yakulov *et al*., 2015; Kan *et al*., 2016). CCT8, or chaperone containing TCP1 subunit 8, is a member of the chaperonin-containing T-complex (TRiC) which is involved in the folding of proteins upon ATP hydrolysis (Kubota *et al*., 1995). CCT8 may also be involved in the transport and assembly of newly synthesised proteins in the cytoplasm. EPRS, previously discussed is a glutaminyl-prolyl-tRNA synthase which enables the attachment of specific amino acids to its cognate tRNA (Cerini *et al*., 1991). In summary, BICC1 is enriched with proteins that function in mRNA degradation, organisation of the cytoskeleton, energy production, protein complex formation, protein folding and tRNA synthetase activity.

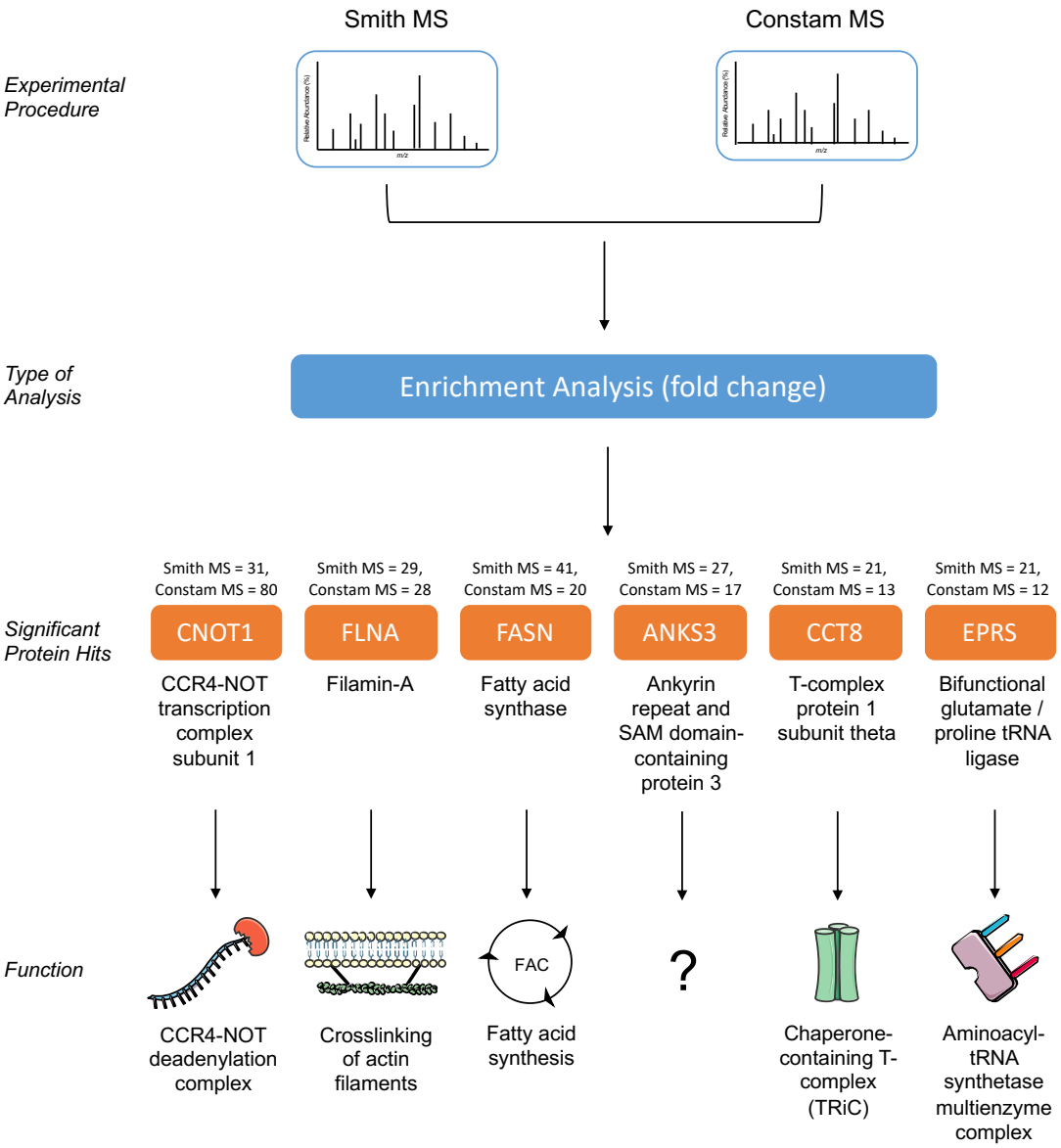

Figure 4.3.2. The most significantly enriched binding partners identified in our BICC1 MS dataset and the Constam MS dataset. Significantly enriched binding partners identified from our BICC1 MS dataset (Smith MS) and the Constam MS dataset were compared and the common transcripts were analysed by DAVID. Significance was measured by peptide fold change and the values were rounded up to the nearest whole number. The most significantly enriched transcripts were then manually analysed and displayed according to their function. A cut off value of 10 was applied to the fold change analysis.

Following the identification of novel protein binding partners of BICC1, a second aim was set to confirm whether BICC1 interacts with ANKS3, one of the highest enriched protein from the MS analysis and a protein recently implicated in PKD. Co-IP experiments using ANKS3 as bait were performed, and the data revealed novel protein-protein interactions between BICC1 and ANKS3. Furthermore, through deletion domain Co-IP experiments, we discovered ANKS3 also binds to the new binding motif 2 of BICC1. Figure 4.3.3 A and B summarise our findings. In brief, ANKS3 does not require either the KH or SAM domains of

BICC1 to interact but has a greater binding affinity for BICC1 between C-terminal amino acids 693 and 815 (termed binding motif 2). However, ANKS3 may still require the SAM domain for a more stable interaction. A similar observation was made for PC1 in chapter 3.

Co-IP experiments using BICC1 as bait were also performed, and the data confirmed protein-protein interactions between BICC1 and ANKS3. Furthermore, through additional deletion domain Co-IP experiments, we discovered BICC1 required the SAM domain of ANKS3 for a stable interaction. Figure 4.3.3 C and D summarise our findings. In brief, BICC1 interacts with ANKS3 and our data suggests that BICC1 requires ANKS3-SAM to stabilise the interaction, as when ANKS3-SAM was deleted, the interaction between BICC1 and ANKS3 was greatly reduced. Therefore, this data suggests that the SAM domain of ANKS3 is a vital, but not exclusive, element involved in mediating an interaction between BICC1 and ANKS3. Therefore, BICC1 might bind upstream or downstream of the SAM domain and link with the SAM domain in some manner to mediate an interaction, but further experimentation is required to confirm this theory.

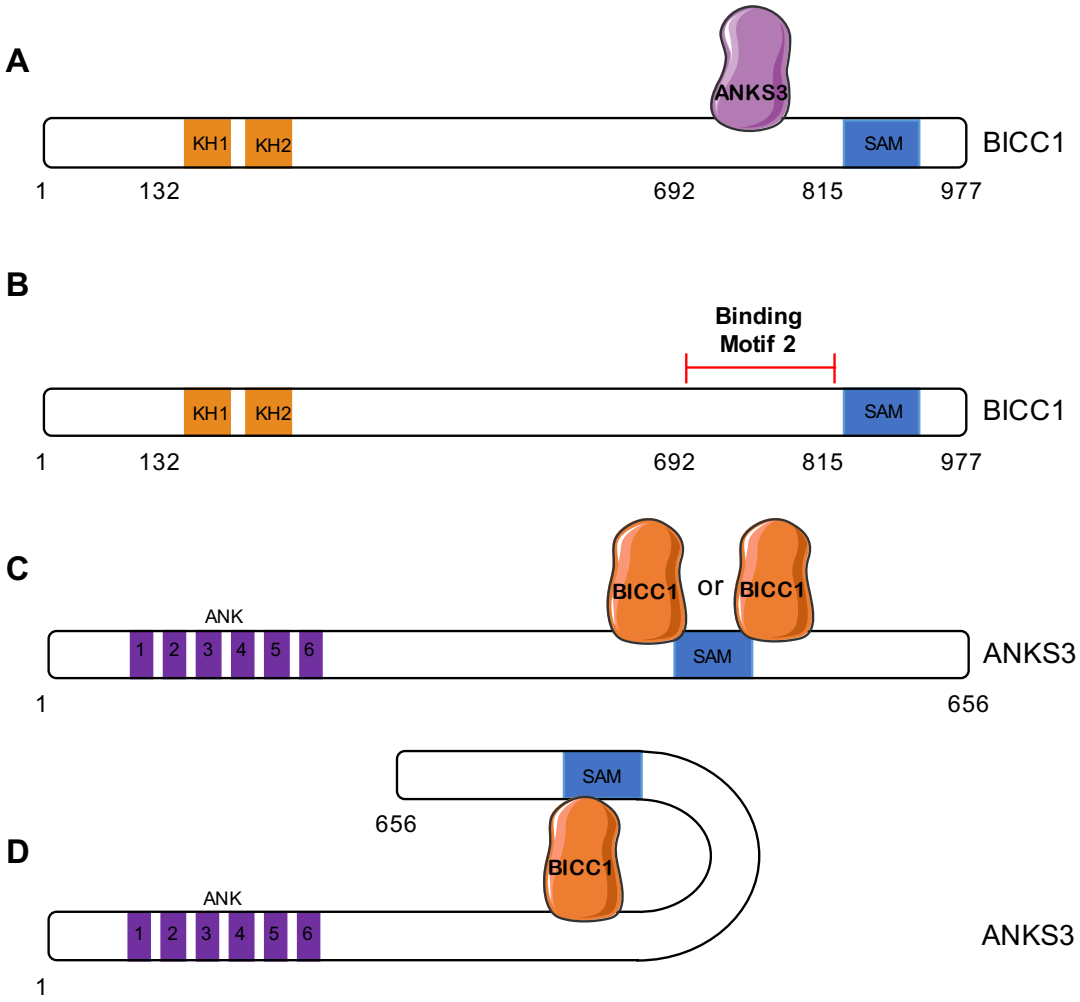

Figure 4.3.3 Schematic summary of the binding domains required for an interaction between BICC1 and ANKS3. A, B) ANKS3 has a greater binding affinity for BICC1 between amino acids 693 and 815 (binding motif 2) but may still require the SAM domain for a more stable interaction. **C)** The SAM domain of ANKS3 is a vital, but not exclusive, element involved in mediating an interaction between BICC1 and ANKS3, therefore, BICC1 may bind upstream or downstream of ANKS3-SAM. However, the SAM domain may be involved in stabilising the interaction. **D)** A hypothesised method of binding. BICC1 binds to ANKS3 upstream of the SAM domain. The SAM domain bends to interact with BICC1 to stabilise its interaction with ANKS3. KH = K-homology domain, SAM = sterile-alpha motif, ANK = ankyrin repeats.

Following the confirmed interaction between BICC1 and ANKS3, Co-IP experiments were performed to assess the interaction relationship between BICC1, ANKS3 and its published interacting partner, ANKS6. Analysis of the co-expression Co-IP experiments revealed competition between BICC1 and ANKS6 for binding with ANKS3, as when ANKS3 and ANKS6 were co-expressed in HA-BICC1 cells, the interaction previously observed between BICC1 and ANKS3 was lost (Figure 4.3.4). This data suggests that ANKS6 has a higher binding affinity for ANKS3 over BICC1, or perhaps inhibits BICC1 from binding to its ANKS3 binding site, however the reason behind this function is not clear.

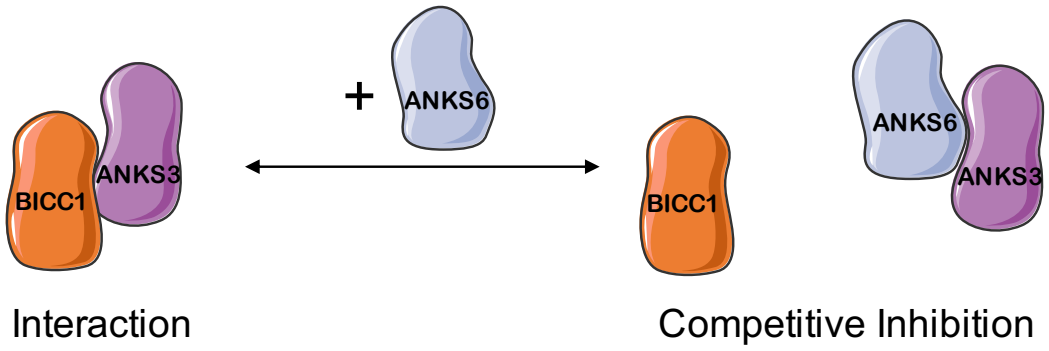

Figure 4.3.4. ANKS6 competitively inhibits BICC1 from interacting with ANKS3 *in vitro*.

As our previous data highlighted competition between BICC1 and ANKS6 for ANKS3 binding, additional Co-IPs were performed to further investigate these interactions, the required binding domains or motifs of ANKS3 for its protein interactions, and why ANKS6 is able to competitively interact with ANKS3 over BICC1. Using BICC1 as bait, the data demonstrated that BICC1 interacts with full-length ANKS3 as well as ANKS3-ΔSAM. However, this interaction was significantly weaker by approximately 60%, confirming that the SAM domain of ANKS3 is a vital, but not exclusive, element involved in mediating an interaction between BICC1 and ANKS3, as previously discussed.

BICC1 did not interact with ANKS6, and co-transfection of ANKS3 and ANKS6 disrupted the interaction between BICC1 and ANKS3, as formerly observed. Furthermore, no interaction was observed between BICC1 and ANKS6-ΔSAM. Moreover, co-transfection of ANKS3-ΔSAM and ANKS6-ΔSAM with BICC1 did not rescue the interaction between ANKS3 and BICC1. However, an interaction between BICC1 and ANKS3 was re-established after co-transfection of ANKS6 and ANKS3-ΔSAM. Co-transfection of ANKS3 and ANKS6-ΔSAM also rescued the interaction between BICC1 and ANKS3.

Together, this data demonstrates the importance of the SAM domain of ANKS3 for initiating, but not stabilising, any interaction with BICC1, as well as controlling its interaction with ANKS6 (discussed further in the next section). Likewise, it also highlights the importance of the SAM domain of ANKS6 for its interaction with ANKS3, as when ANKS6-SAM is lost, ANKS6 is unable to interact with ANKS3, with or without its own SAM domain. Consequently, BICC1 is now able to re-establish its interaction with ANKS3, through ANKS3-SAM. It

is interesting to note that deletion of both of the SAM domains of ANKS3 and ANKS6 does not restore an interaction between BICC1 and ANKS3, which again confirms the necessity of the SAM domain of ANKS3 for its interaction with BICC1. These observations are summarised in the schematic displayed in Figure 4.3.5.

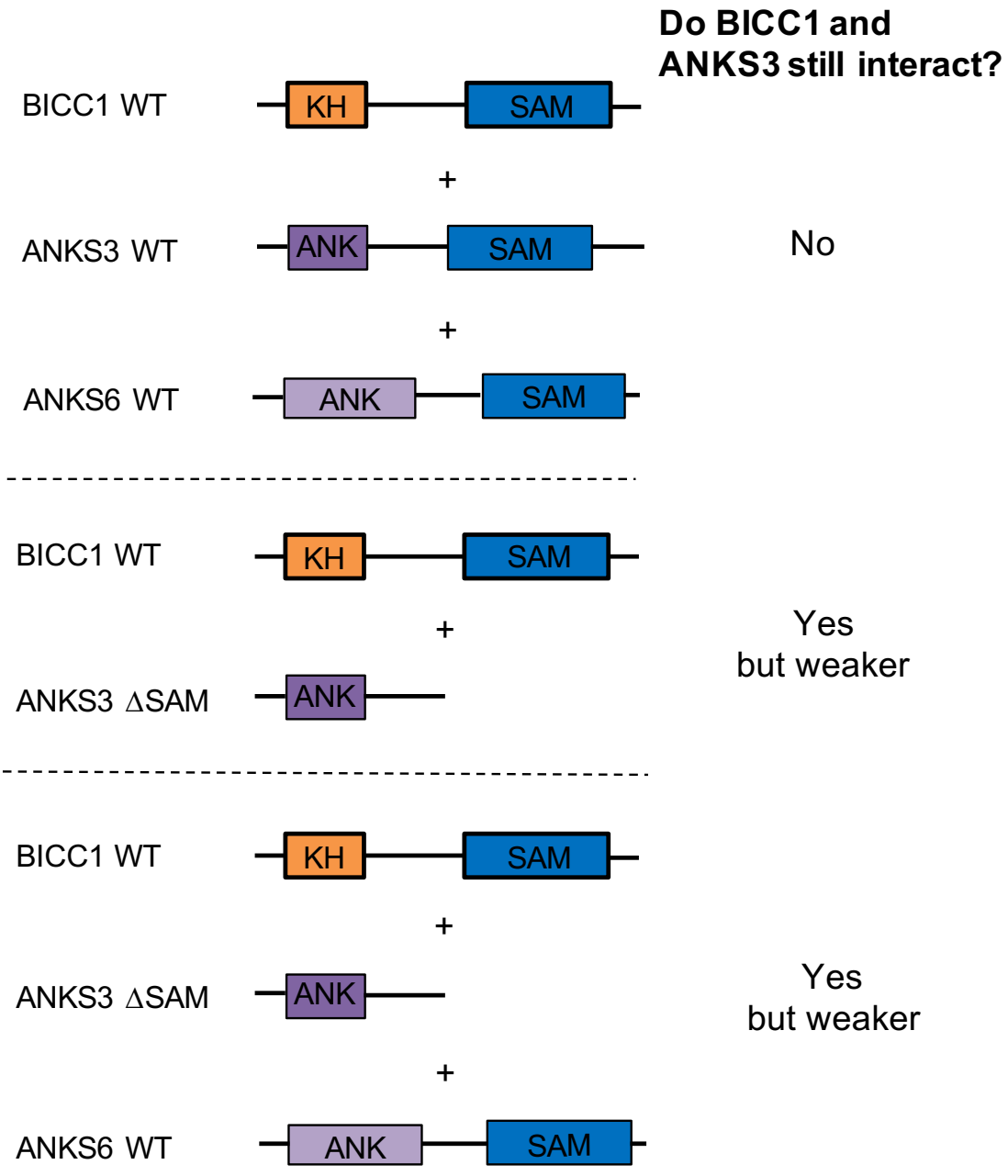

Figure 4.3.5. A schematic of the interaction complex between BICC1, ANKS3 and ANKS6. ANKS6 competitively interacts with ANKS3 over BICC1. The SAM domain of ANKS3 is important for interactions with BICC1 and ANKS6.

As discussed in section 4.1.1, a missense mutation in the SAM domain of ANKS6 (R823W) is reported to disrupt its interaction with ANKS3, while another missense mutation 6 amino acids upstream (I747N) had no effect on its interaction with ANKS3, but disrupts its interaction with BICC1. To confirm this observation, constructs containing the R823W and I747N mutations were made using mutagenesis, referred to as ANKS6-R823W and ANKS6-I817N. Note the published R823W mutation was in a rat model, while the I747N mutation was in a mouse model (the amino acid sequences differ slightly between species, hence the difference between the notation of I747N and the ANKS6-I817N construct used in this study). Co-IP experiments demonstrated that BICC1 does not interact with full-length ANKS6, as previously observed, as well as with ANKS6-R823W or ANKS6-I817N. Neither the point mutation of R823W or I817N re-established an interaction between BICC1 and ANKS3, suggesting a complete loss of ANKS6-SAM is required to reinstate this interaction. These observations are summarised in the schematic displayed in Figure 4.3.6.

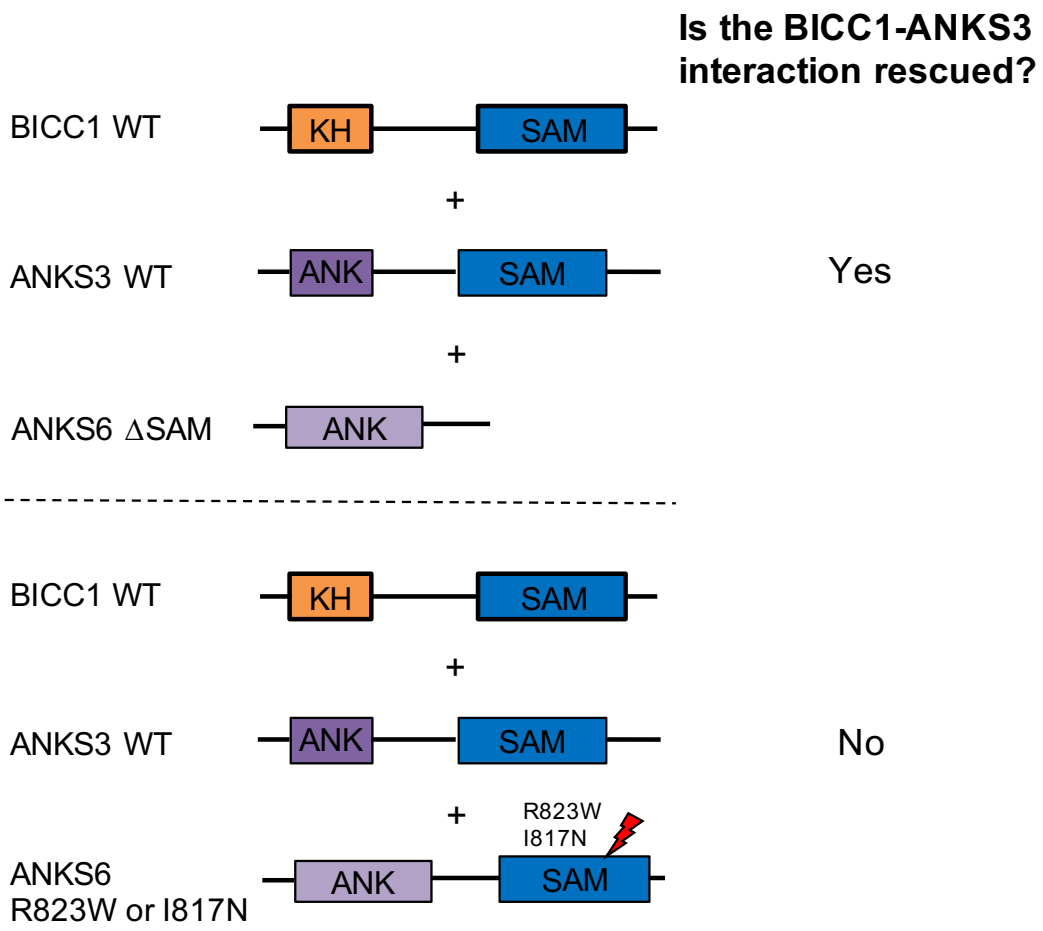

Figure 4.3.6. Deletion of the SAM domain of ANKS6 rescues the BICC1-ANKS3 interaction. Point mutations in the SAM domain of ANKS6 does not rescue the BICC1-ANKS3 interaction.

Next, we sought to identify whether ANKS3 and ANKS6 interact, as shown in published data. Co-IP experiments using ANKS3 as bait confirmed the protein-protein interaction previously observed between ANKS3 and ANKS6 in published data and also presented in this study. Furthermore, deletion domain Co-IP experiments revealed that the SAM domain of ANKS6 is not solely required to initiate an interaction with ANKS3, however the SAM domain of ANKS3 is a vital component that mediates an interaction with ANKS6. Figure 4.3.7 summarises our findings.

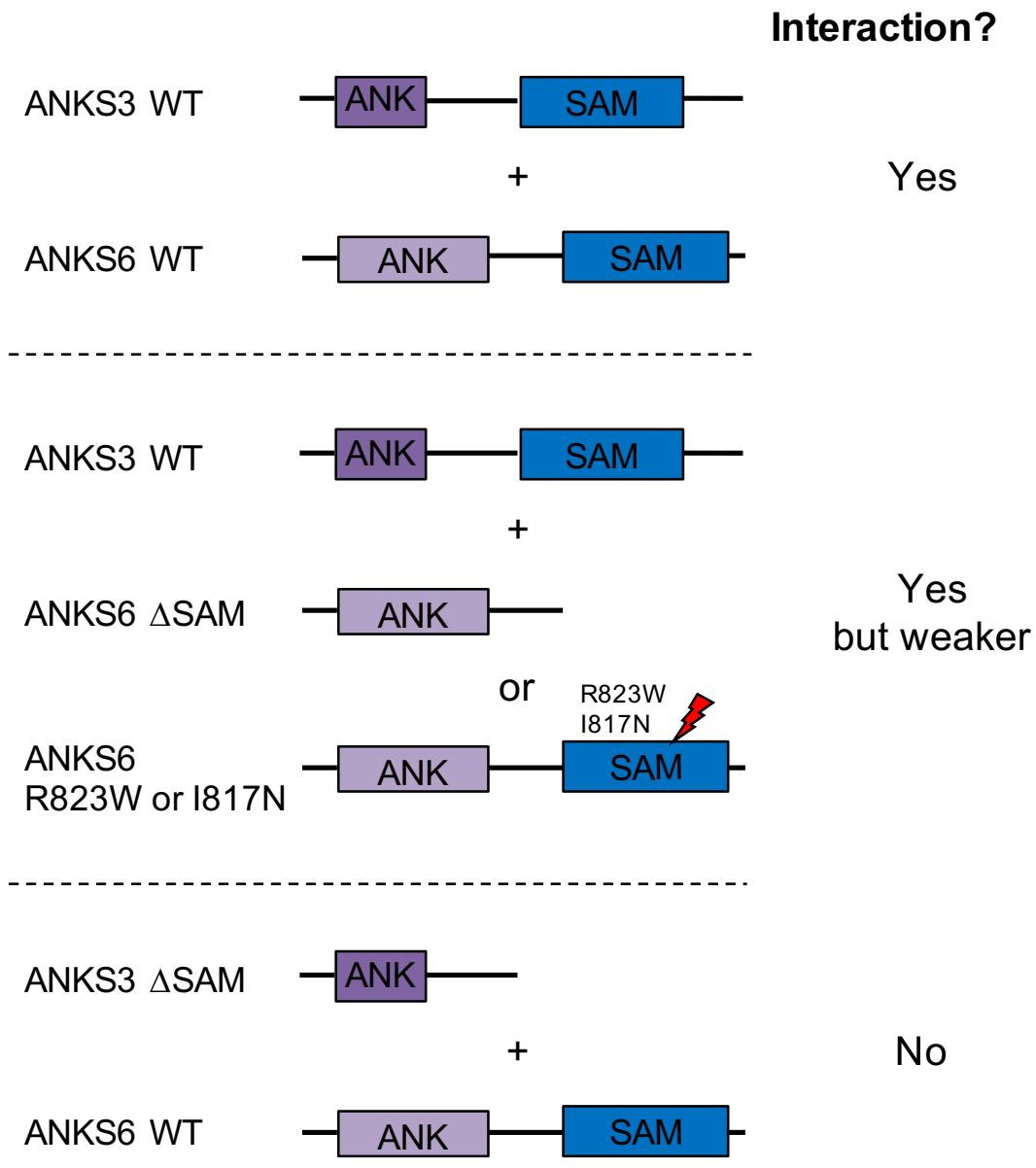

Figure 4.3.7. The SAM domain of ANKS3 but not ANKS6 is vital for an ANKS3-ANKS6 interaction.

Interestingly, endogenous Co-IP experiments between ANKS3 and ANKS6 revealed that RNase I treatment significantly decreased the interaction, by approximately 60%, which suggests that an RNA intermediate is required for an interaction between ANKS3 and ANKS6 (Figure 4.3.8).

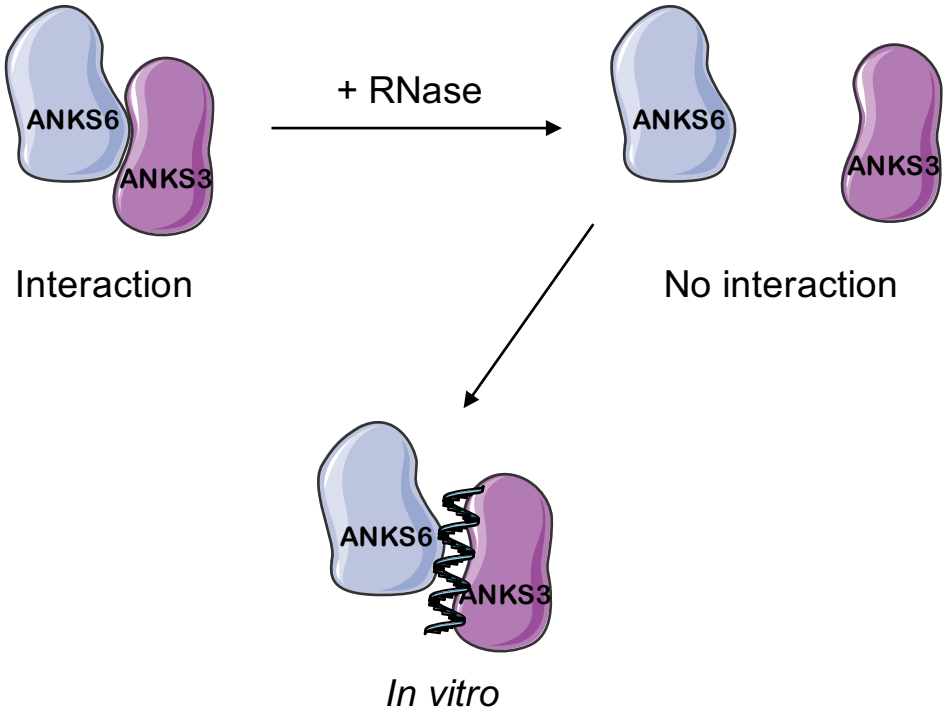

Figure 4.3.8. The ANKS3-ANKS6 interaction requires an RNA intermediate *in vitro*.

As a protein complex between BICC1 and the polycystins, as well as between BICC1 and ANKS3 was forming, we decided to investigate whether ANKS3 can interact with PC1 and PC2 at the protein level. Co-IP experiments using ANKS3 as bait revealed novel protein-protein interactions between ANKS3 and PC1 and ANKS3 and PC2. Furthermore, through deletion domain Co-IP experiments, PC1 and PC2 were shown to interact with ANKS3 through its SAM domain. As competition had been observed between BICC1 and ANKS6 for binding to ANKS3, similar Co-IP experiments were performed with ANKS3, PC1 and PC2. PC1 expression was weak when co-expressed with ANKS3 and ANKS6, therefore a conclusive observation could not be made. However, the data revealed that ANKS6 also competes with PC2 for binding to ANKS3. Figure 4.3.9 summarises our findings.

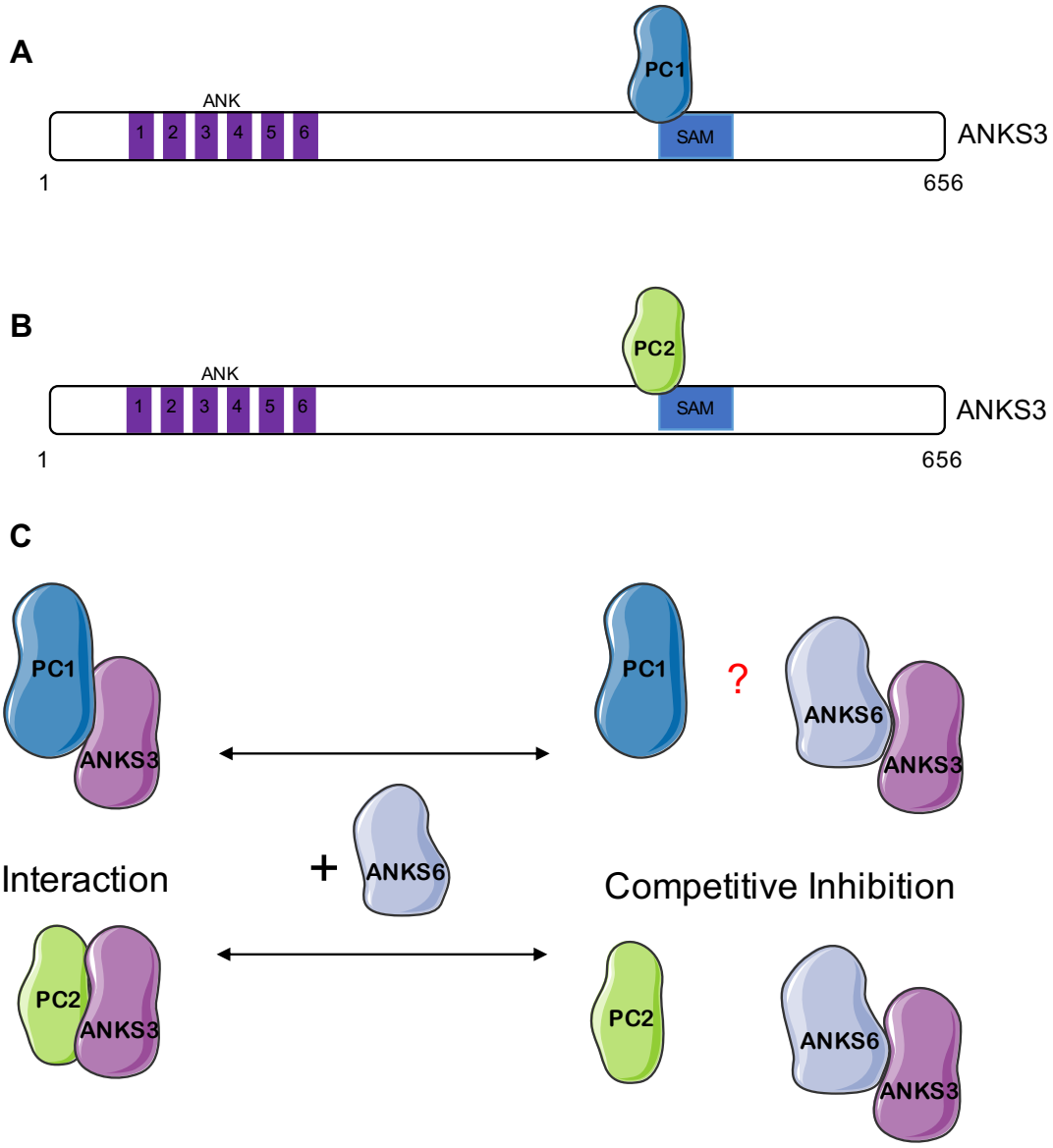

Figure 4.3.9. A schematic summary of the interaction complex between ANKS3, PC1 and PC2. A, B) Interactions between PC1 and ANKS3 and PC2 and ANKS3 require the SAM domain of ANKS3. **C)** ANKS6 competitively inhibits PC2 from interacting with ANKS3 *in vitro*.

As the previous data highlighted competition between PC2 and ANKS6 for ANKS3 binding, additional Co-IPs were performed to further investigate these interactions, the required binding domains or motifs of ANKS3 for its protein interactions, and why ANKS6 is able to interact with ANKS3 over PC2. The data demonstrated that when the SAM domain of ANKS6, but not the SAM domain of ANKS3, was deleted, the interaction between ANKS3 and PC2 was restored, albeit very weakly. These observations are summarised in the schematic displayed in Figure 4.3.10.

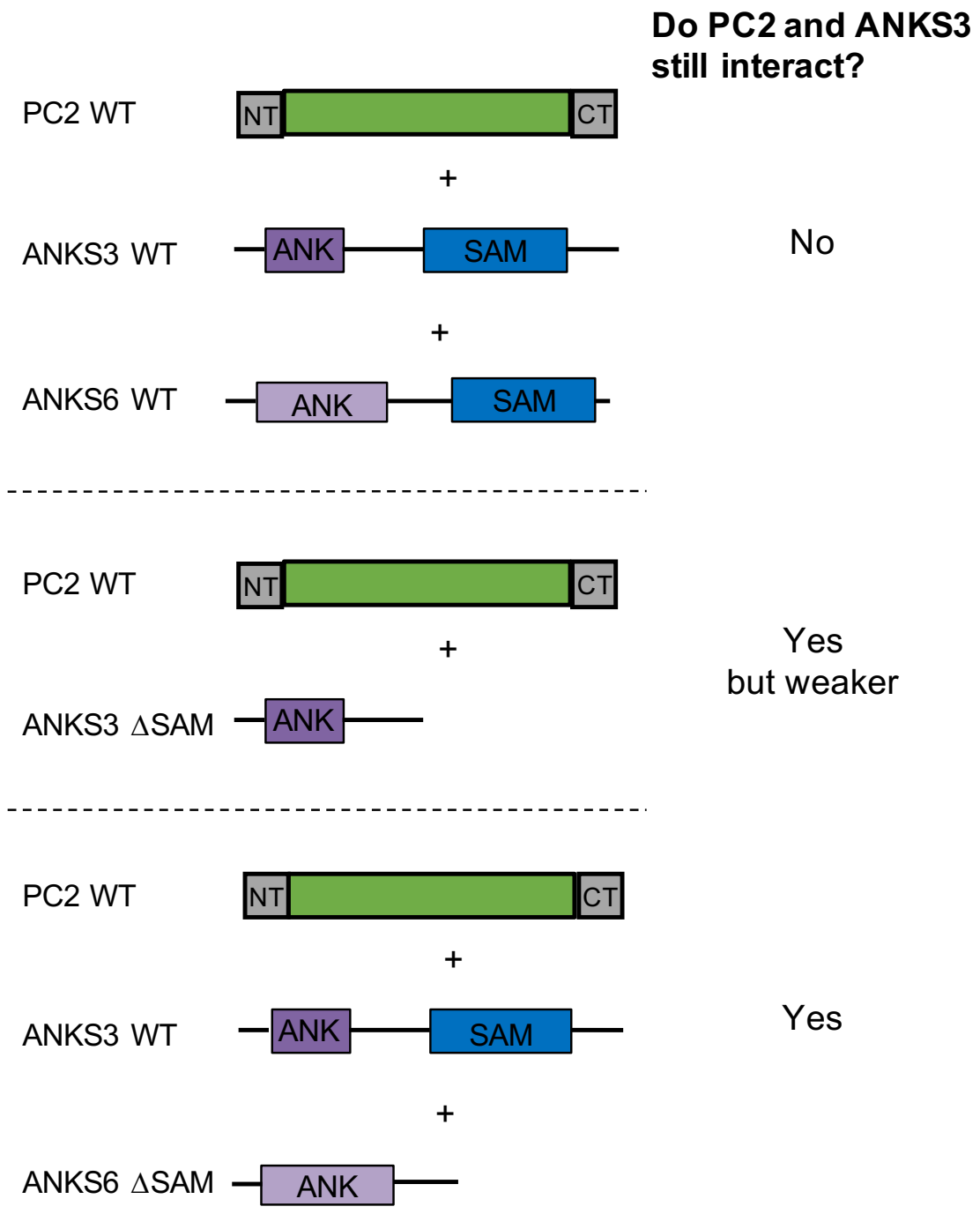

Figure 4.3.10. The SAM domain of ANKS3 is important for interactions with PC2 and ANKS6, while deletion of the SAM domain of ANKS6 rescues the PC2-ANKS3 interaction.

The final aim of this chapter sought to investigate whether BICC1 regulates the expression of ANKS3 and ANKS6, as we have demonstrated protein-protein interactions between BICC1 and ANKS3, as well as novel interactions between ANKS3, PC1 and PC2, the main proteins known to be defective in ADPKD. As previously discussed, BICC1 is a known RNA binding protein, therefore it is plausible to hypothesise that BICC1 might also regulate *ANKS3* at the RNA level. To assess the regulatory effects of BICC1 on *ANKS3*, the CRISPR-Cas9

BICC1 KO cell line was used and qPCR and western blot experiments were performed to assess the expression levels of ANKS3 and its related partner ANKS6. Table 4.3.2 summarises our findings. In brief, loss of BICC1 caused an 50% downregulation in *ANKS3 mRNA* expression and an 80% downregulation in ANKS3 protein expression. In contrast, loss of BICC1 had no effect on the expression levels of ANKS6.

CRISPR-Cas9 techniques were also used to generate stable *PKD1* and *PKD2 KO* cell lines, and the expression levels of ANKS3 and ANKS6 were assessed. Loss of PC1 caused a downregulation in both *ANKS3 mRNA* and protein expression. Loss of PC1 also caused a downregulation in ANKS6 protein expression, however the data differed between different *PKD1 KO* clones, therefore a conclusive observation could not be made. Conversely, loss of PC2 caused an approximate 1.5-fold increase in both *ANKS3 mRNA* and protein expression but had no effect on the expression levels of ANKS6.

Overexpression studies were also performed, and the data demonstrated that an overexpression of BICC1 caused a 2.5-fold increase in *ANKS3 mRNA* expression but had no effect on the mRNA expression level of *ANKS6*. Overall, this data suggests that the levels of BICC1 present in kidney epithelial cells is very important, as loss of BICC1 causes a downregulation of *ANKS3*, while an overexpression of BICC1 causes an upregulation of *ANKS3*.

Table 4.3.2. Summary of the gene expression analysis from the CRISPR-Cas9 experiments.

GENE	BICC1	ANKS3	ANKS6
BICC1 KO	-	DOWN	NO CHANGE
PKD1 KO	DOWN	DOWN	DOWN
PKD2 KO	UP	UP	NO CHANGE
BICC1 OVER	-	UP	NO CHANGE

Due to their close relationship, discussed in section 1.5.10, the regulatory effect of BICC1 upon the expression of NEK kinases and NEK protein partners transcripts was assessed. The data demonstrated that loss of BICC1 caused an average 50% downregulation of mRNA expression for most of the NEK kinases assessed. Furthermore, loss of BICC1 also caused an approximate 50% downregulation in the mRNA expression of the NEK-related genes *ACK1, NPHP3* and *INVS*, but not *CDC42*. Interestingly, NEK7 was the only NEK kinase identified as a protein binding partner of BICC1 in the MS analysis. A schematic of a hypothesised BICC1 regulatory function upon the ANKS3-ANKS6-NEK kinase network is outlined in Figure 4.3.11.

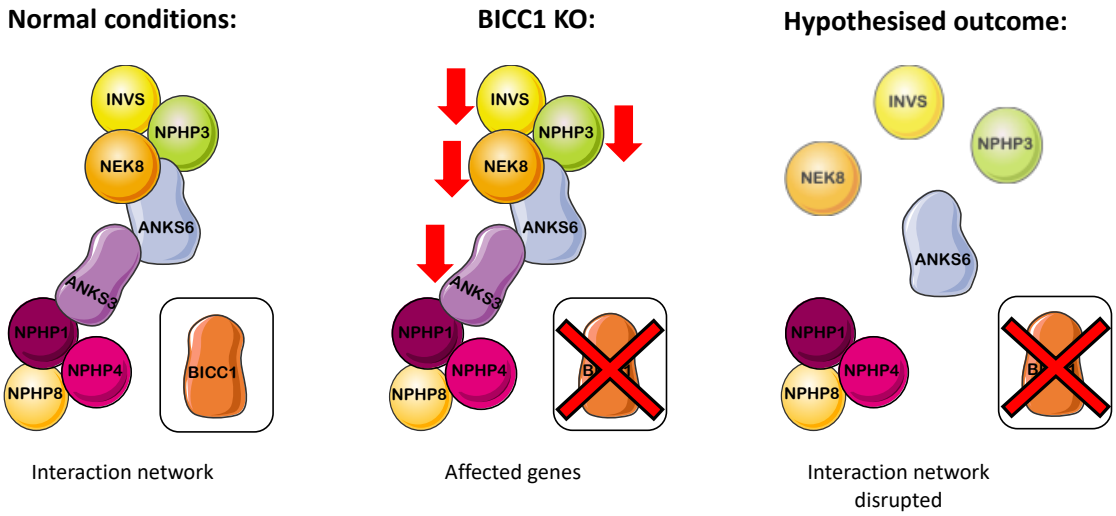

Figure 4.3.11. Loss of BICC1 negatively regulates the ANKS3-ANKS6-NEK kinase network identified in published disease models. A hypothesis could be made that states that loss of BICC1 causes a decrease in ANKS3 protein levels, which prevents the formation of the ANKS3-NPHP module and consequently prevents the module connecting with the ANKS6-NPHP module. In addition, the majority of the components of the ANKS6-NPHP module are also downregulated which might affect the assembly of this module. Without these two modules, the downstream functions of CDC42 and ACK1 in regulating actin dynamics and apical extracellular matrix remodelling might be disrupted.

Chapter 4 Summary:

- ⇒ BICC1 has several novel protein binding partners in kidney epithelial cells involved in processes such as translation initiation, cell-cell adhesion, protein binding and poly(A) binding
- ⇒ ANKS3 was identified as a binding partner of BICC1 from the MS analysis
- ⇒ BICC1 and ANKS3 interact at the protein level
- ⇒ BICC1 does not interact with ANKS6
- ⇒ ANKS3 and ANKS6 interact
- ⇒ ANKS3 interacts with PC1
- ⇒ ANKS3 interacts with PC2
- ⇒ BICC1 positively regulates *ANKS3* expression at the mRNA level
- ⇒ BICC1 does not regulate ANKS6 expression
- ⇒ Loss of *PKD1* down-regulates the expression of ANKS3
- ⇒ Loss of *PKD1* down-regulates the protein expression of ANKS6
- ⇒ Loss of *PKD2* up-regulates the expression of ANKS3
- ⇒ Loss of *PKD2* has no effect on the expression of ANKS6
- ⇒ Overexpression of *BICC1* upregulates *ANKS3* expression but has no effect on the expression of *ANKS6*
- ⇒ BICC1 positively regulates the expression of NEK kinases and NEK protein partners

Chapter 5

BICC1 BINDS AND REGULATES THE RNA OF ITS PROTEIN INTERACTOME

5.0 BICC1 binds and regulates the RNA of its protein interactome

5.1 Introduction and Aims

BICC1 is classified as an RBP responsible for post-transcriptional regulation of certain mRNA transcripts. Although the general function of BICC1 is well-known, how it regulates its mRNA targets is not fully understood. Furthermore, the specific mechanism of RNA binding, whether it is direct or indirect, and how BICC1 targets mRNA, remains unclear. Therefore, this chapter sought to further understand how BICC1 regulates the mRNA targets identified in the previous chapters, investigate whether BICC1 is able to bind to these targets, and to also discover novel BICC1-RNA interacting partners. Through the identification of novel associations within its transcriptome, we can begin to develop an improved understanding of the role of BICC1 in kidney epithelial cells and in preventing ADPKD.

Chapter Aims

1. Identify novel RNA targets of BICC1 and investigate whether BICC1 interacts with its RNA targets in kidney epithelial cells
2. Analyse the effect on global transcriptome expression in *BICC1 KO* cells and compare to WT cells through RNA-Seq
3. Investigate how BICC1 regulates the expression of its identified RNA targets by assessing mRNA stability or other methods of mRNA regulation

5.2 Results

5.2.1 BICC1 RNA immunoprecipitation optimisation

BICC1 is an RNA-binding protein known to bind and regulate several mRNA targets that function in various fundamental pathways. Data presented in Chapters 3 and 4 demonstrated that BICC1 positively regulates the expression of *PKD1*, *PKD2* and *ANKS3*, as their expression was significantly reduced in *BICC1 KO* cell models. Therefore, one could speculate that BICC1 physically interacts with these RNA transcripts, and others, to perform a regulatory function. To investigate this theory, a RIP experiment was designed. Before BICC1-RNA targets were explored, a pilot study was performed to optimise the experiment and investigate whether pre-treatment with formaldehyde would strengthen BICC1-RNA interactions for improved RNA capture downstream. Formaldehyde cross-linking has previously been shown by Hendrickson and colleagues (2016) to prevent post-lysis re-association of RNA-protein complexes and in addition, is optimal for maximal RNA and protein recovery (Hendrickson *et al.*, 2016). The pilot data indicated that addition of 0.1% formaldehyde significantly increased RNA enrichment of a known target of BICC1, its own RNA, by approximately 60-fold compared to samples treated without formaldehyde (Figure 5.2.1.1. A).

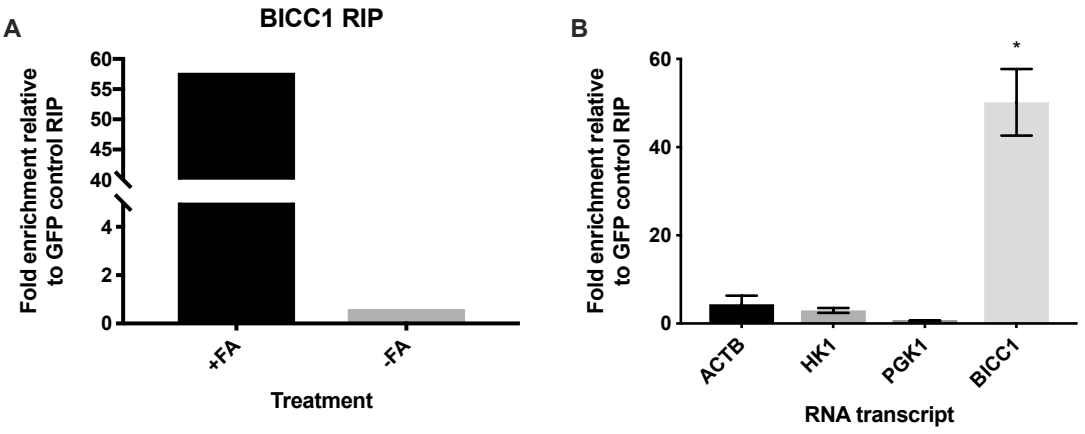

Figure 5.2.1.1. BICC1 RIP pilot data. A) qPCR was used to measure the mRNA expression of BICC1 RNA bound to BICC1 protein following RIP experiments with (+FA) or without (-FA) formaldehyde pre-treatment. **B)** *ACTB, HK1* and *PGK1* were included as negative control RNA transcripts and their fold enrichment was compared to *BICC1* (n=3). The RNA transcripts were normalised relative to control GFP RIP experiments. Paired t-tests were performed to assess statistical significance (p values * <0.05, ** = <0.01, *** = <0.001, **** = <0.0001 and ns = not significant). Error bars represent standard error of the mean.

Once established, the RIP experimental procedure was used to explore potential BICC1-RNA targets, including *PKD1*, *PKD2* and *ANKS3*. BICC1 RIP experiments were performed in UCL93 cells (healthy human patient kidney cells) and the results obtained from qPCR read-outs demonstrated that BICC1 interacts with the endogenous RNA transcripts of *PKD1*, *PKD2* and *ANKS3*, with average significant fold enrichments of 35-fold, 15-fold and 60-fold respectively (Figure 5.2.1.2). The interaction between BICC1 and *PKD2* RNA was not significant due to experimental variability; however, the fold enrichment trend is clear. An interaction with the negative control RNA transcript, *ACTB*, was not observed suggesting these RNA interactions are specific.

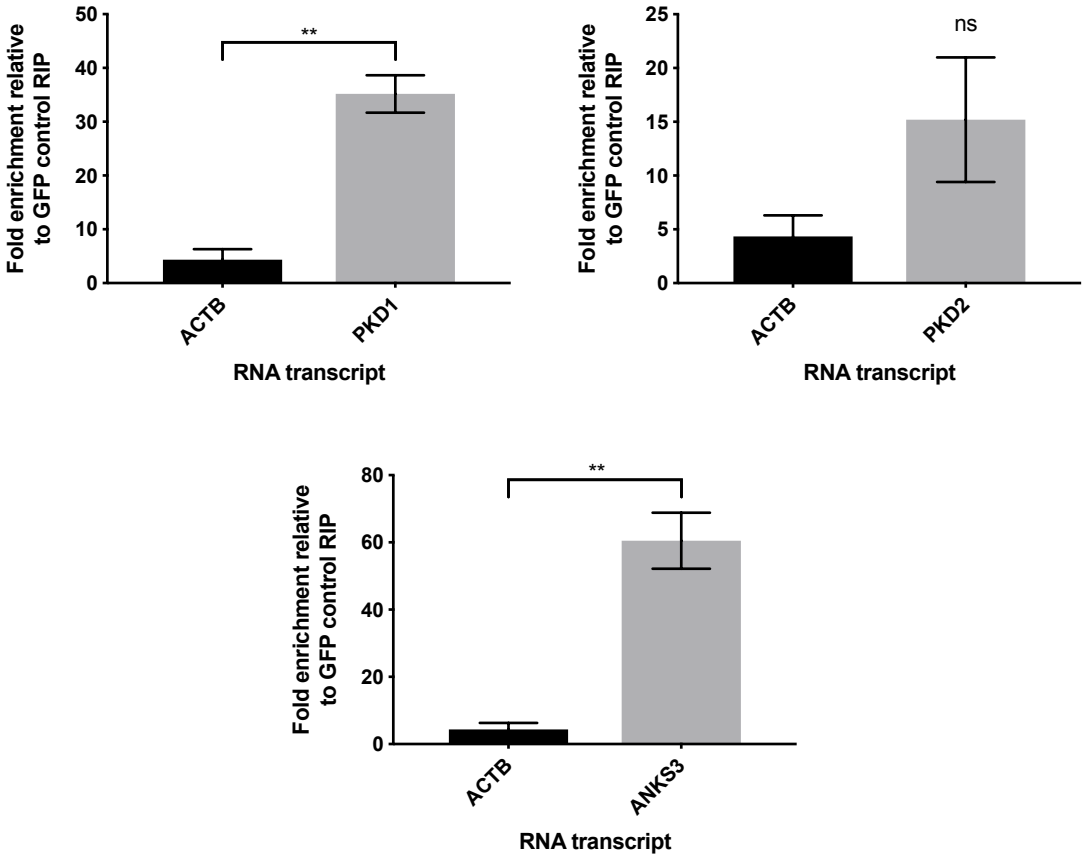

Figure 5.2.1.2. BICC1 associates with the RNA transcripts of *PKD1*, *PKD2* and *ANKS3*. qPCR was used to measure the mRNA expression of RNA transcripts associated with BICC1 following RIP experiments (n=3). The RNA transcripts were normalised relative to control GFP RIP experiments. *ACTB* was included as a negative control. Paired t-tests were performed to assess statistical significance (p values * <0.05, ** = <0.01, *** = <0.001, **** = <0.0001 and ns = not significant). Error bars represent standard error of the mean.

Recent research has identified several new RNA binding targets of BICC1, including ACDY6 and *DVL2*. Such data has also demonstrated that BICC1 regulates their mRNA transcripts through binding their 3' untranslated regions (UTR). Therefore, to assess BICC1-RNA interactions and provide spatial resolution of these associations, we designed a fragmented RIP (fRIP) experiment to assess whether BICC1 binds the 3' UTRs of all of its RNA targets. A form of sonication, known as bioruption, was selected to fragment RNA into shorter sequences to assess localised binding. Bioruption proficiently produces RNA fragments of approximately 300-400 nucleotides in length. To optimise the bioruption conditions required to efficiently fragment RNA from 10 million cells, a pilot experiment was performed. Cell lysates were subjected to bioruption for either 10 minutes, 20 minutes or 30 minutes, and an unsonicated sample was included.

Primers were designed to amplify varying lengths of an abundant RNA, *ENO1*, and referred to as amplicon 1 (A1), amplicon 2 (A2), amplicon 3 (A3) or amplicon 4 (A4). It was expected that A1 would produce an amplicon of 205 nucleotides, A2 would produce an amplicon of 301 nucleotides, A3 would produce an amplicon of 564 nucleotides and A4 would produce an amplicon of 985 nucleotides. Therefore, if bioruption was efficient at fragmenting the RNA, A3 and A4 should not be detected. Primers were also designed to the small nuclear RNA (*snRNA*) *U1* and it was included as a positive loading control, as it is a short, abundant RNA molecule of approximately 150 nucleotides and thus should be present in all of the samples.

RNA was extracted from the biorupted lysates and cDNA synthesis was performed. Following RT-PCR, the products were run on a DNA agarose gel and the data revealed that sonication of UCL93 and *BICC1 KO* cells for 30 minutes was the optimum condition, as A3 and A4 were still expressed at the 10-minute and 20-minute time-points, especially in the *BICC1 KO* cells (Figure 5.2.1.3). Expression of the *snRNA U1* was uniform, demonstrating even DNA loading of the samples, while the unsonicated condition confirmed clear expression of all the amplicons at their relevant nucleotide lengths.

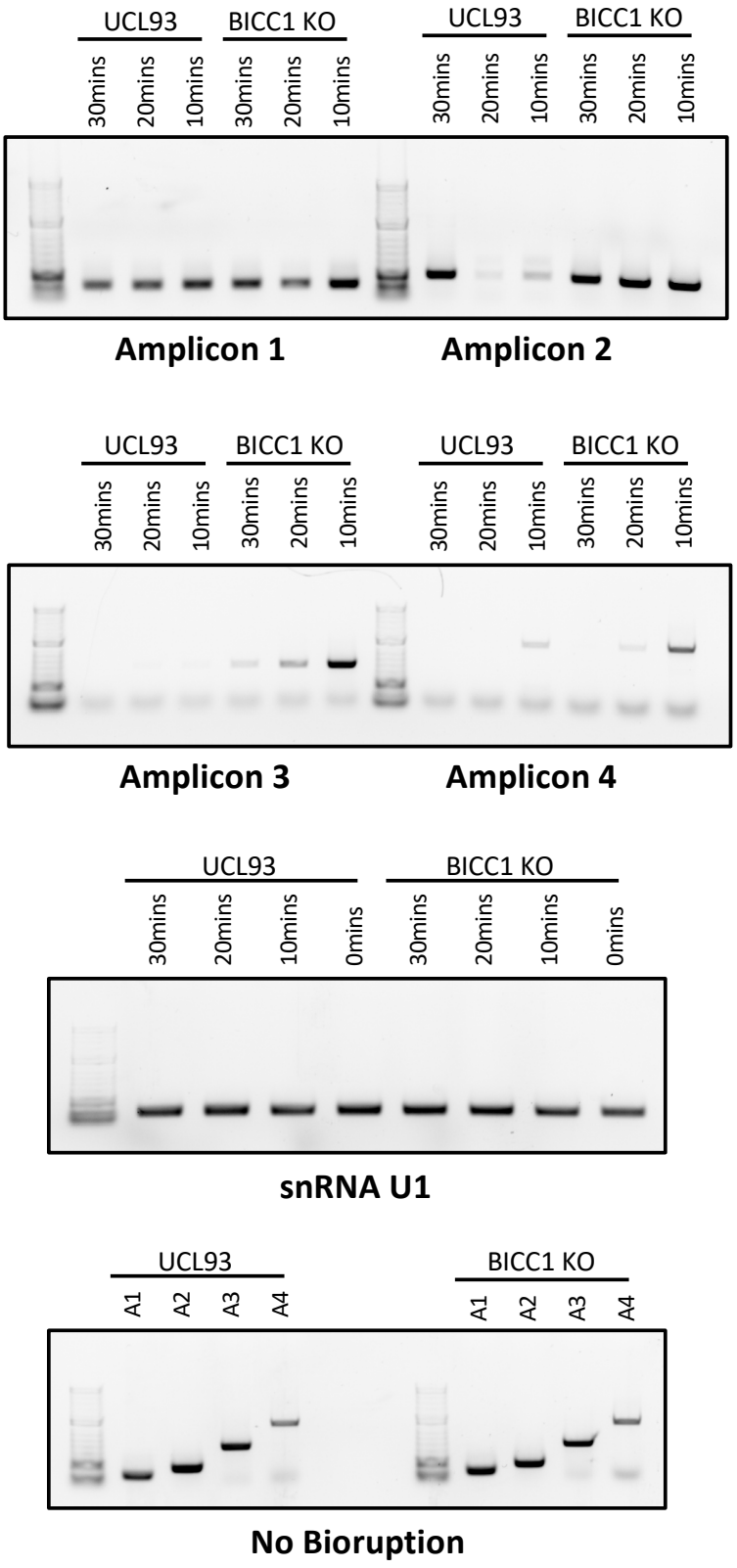

Figure 5.2.1.3. Fragmented RIP optimisation. RT-PCR and DNA agarose gels were used to assess the length of time required to successfully fragment RNA in UCL93 and *BICC1 KO* cells following bioruption. Amplicons 1-4 were subjected to no bioruption, or bioruption for either 10, 20 or 30 minutes. *snRNA U1* was included as a loading control. A 1000bp ladder was used as a loading reference. A1 = amplicon 1, A2 = amplicon, A3 = amplicon 3, A4 = amplicon 4.

5.2.2 Identification of novel BICC1-RNA interactions by fRIP and deep sequencing

To identify global BICC1-bound RNA transcripts in an unbiased manner, endogenous BICC1 was co-immunoprecipitated and associated RNAs were analysed by deep sequencing (RNA-Seq). Prior to the Co-IP, the RNA was fragmented to produce short nucleotide fragments of approximately 300-400 nucleotides to enhance spatial resolution and regional mapping of RNA association with BICC1. The enriched RNAs were normalised to the inputs from the same experiments and compared to RNA recovered from control fRIP experiments in *BICC1 KO* cells. The pair-end sequence reads were aligned and mapped to a reference human genome and transcript abundancies were analysed using the BioJupies cloud database (Torre *et al*., 2018). The BioJupies software creates an interactive notebook where various outputs can be viewed and further explored. Statistical analysis on the enriched RNA transcripts revealed there were 2313 RNAs associated with BICC1, using a false discovery rate (FDR) and adj. p-value of <0.05 (the full list was not included due to size but it is available as an excel file on request). The 2313 BICC1-enriched RNAs were not present in the control RIP performed in BICC1 KO cells.

Before BICC1-RNA enrichment analysis was performed, the fRIP-Seq dataset was subjected to various quality control (QC) checks, including hierarchical clustering by the Clustergrammer programme. The Clustergrammer plots in Figure 5.2.2.1 demonstrate that the fRIP-Seq dataset has low variance and that there is a clear difference or enrichment between the BICC1 fRIP samples and the BICC1 input samples (Figure 5.2.2.1. A) as well as between the BICC1 fRIP and the negative control *KO* fRIP samples (Figure 5.2.2.1. B). Therefore, RNA enrichment analysis could continue with the confidence that our results are reliable, for example, the RNA transcripts enriched in the BICC1 fRIP samples are clearly not enriched in the negative control samples (*KO* fRIP).

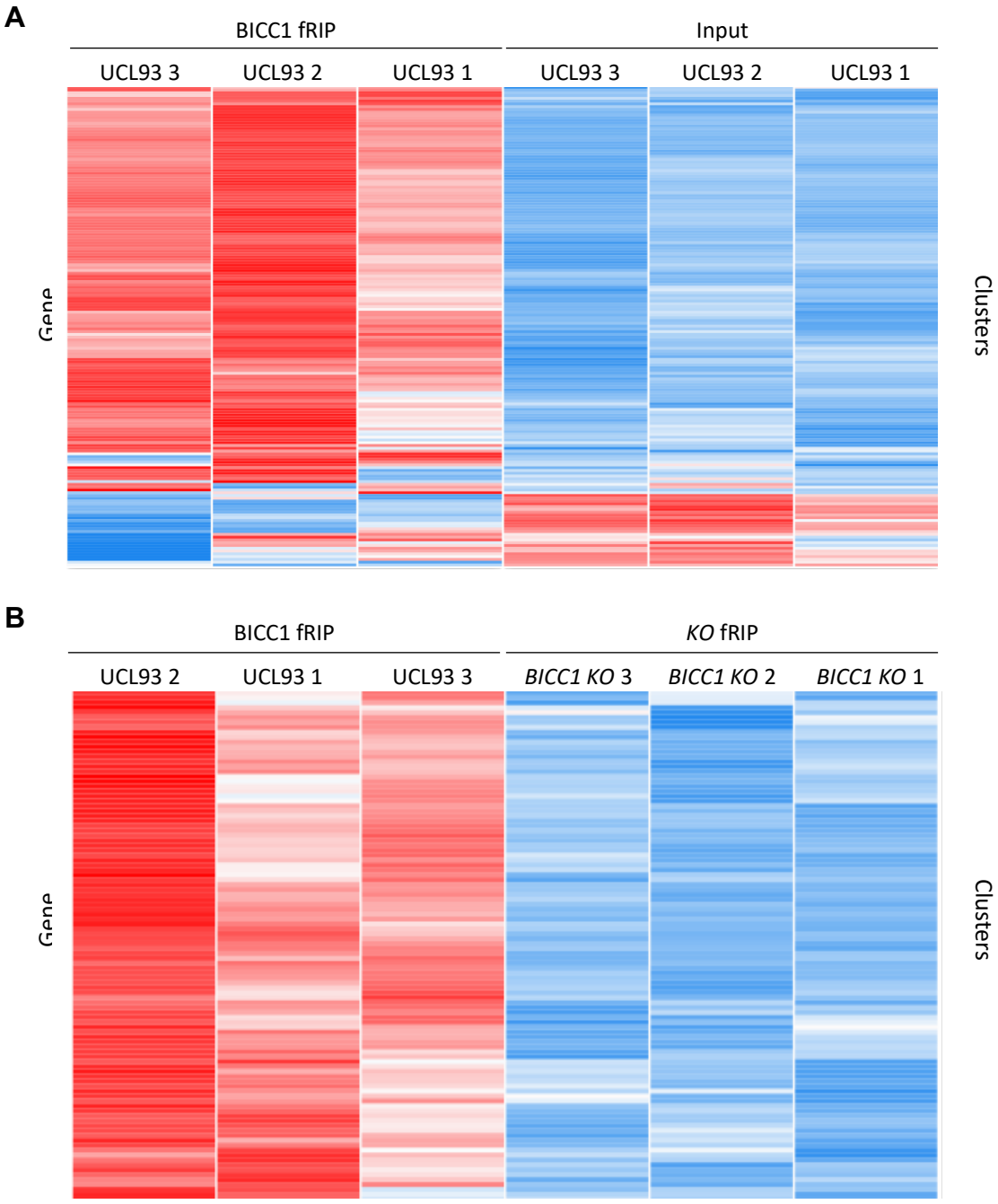

Figure 5.2.2.1. Clustergrammer analysis of the fRIP-Seq dataset. A) A clustergrammer plot to demonstrate hierarchical clustering between the BICC1 fRIP samples and the BICC1 input samples. **B)** A clustergrammer plot to demonstrate hierarchical clustering between the BICC1 fRIP samples and the negative control *BICC1 KO* fRIP samples. fRIP = fragmented RNA immunoprecipitation. *KO* = knock-out.

To assess the types of enriched RNAs associated with BICC1, the set of statistically significant enriched RNA transcripts, with adj. p-values of <0.05, were inputted into DAVID and analysed using various functional tools. As our enriched list contained 2313 RNAs, DAVID could provide a comprehensive set of functional annotation tools to aid our understanding of the biological meaning

behind the large list of gene transcripts. The results collected were also cross-checked against the PANTHER and Enrichr databases to ensure accuracy and reliability.

First, enriched UP_Keywords were explored, and the data revealed that BICC1-enriched RNAs encode various proteins which are modified, found in different cellular locations and function in important biological pathways. For example, nearly 54% of all the enriched RNAs are phosphoproteins; proteins post-translationally modified by the addition of a phosphate group. In addition, 21% of the enriched RNAs are acetylated, another form of post-translational modification. Therefore, it can be stated with confidence that the majority of BICC1-enriched RNAs are post-translationally modified. Several other significant, biologically relevant UP_Keywords can be viewed in Table 5.2.2.1.

The individual RNA transcripts enriched in the top three most significant UP Keywords were further analysed and displayed in Appendix Figure 7.4, while the Wnt signalling pathway and the endosome, UP Keywords altered in ADPKD, were further explored in Appendix Figures 7.5 and 7.6 respectively. In summary, BICC1 interacts with RNA transcripts that encode proteins involved in the regulation and induction of gene transcription and translation.

Table 5.2.2.1. The top 20 UniProtKB keywords, ranked by p-value, identified from DAVID analysis of our enriched RNA transcripts associated with BICC1. The count refers to the number of RNA transcripts enriched in function to the relevant UP_Keyword Term, and this number is also presented as a percentage of the total number of transcripts assessed (%). Significant keywords are displayed with a p-value and Benjamini (adjusted p-value) value cut off of 0.05.

UP Keyword Term	Count	%	P-Value	Benjamini
Phosphoprotein	1210	53.9	5.10E-49	2.70E-46
Acetylation	477	21.3	1.60E-10	4.30E-08
Methylation	172	7.7	3.70E-10	6.60E-08
Endoplasmic reticulum	166	7.4	7.70E-07	1.00E-04
Repressor	102	4.5	1.70E-06	1.80E-04
Growth factor binding	11	0.5	3.90E-06	3.50E-04
Golgi apparatus	129	5.8	5.20E-06	4.00E-04
Cytoplasm	601	26.8	9.50E-06	6.30E-04
Nucleus	649	28.9	1.10E-05	6.30E-04
Apoptosis	89	4	3.50E-05	1.80E-03
Prenylation	37	1.6	4.00E-05	1.90E-03
Lysosome	51	2.3	4.40E-05	2.00E-03
Endosome	81	3.6	4.90E-05	2.00E-03
Kinase	114	5.1	5.50E-05	2.10E-03
Mitochondrion	160	7.1	1.30E-04	4.60E-03
Craniosynostosis	10	0.4	2.50E-04	8.50E-03
Developmental protein	136	6.1	3.90E-04	1.20E-02
GTPase activation	38	1.7	5.20E-04	1.50E-02
Wnt signaling pathway	35	1.6	8.50E-04	2.40E-02
Lipoprotein	121	5.4	1.10E-03	3.00E-02

Second, enriched GO terms in relation to biological processes were explored, and the data revealed that BICC1-enriched RNAs encode various proteins which are involved in important biological pathways. For example, the most significantly enriched (p-value and Benjamini value <0.05) BICC1-associated RNAs encode proteins that are involved in the positive regulation of cell migration. In addition, BICC1-associated RNAs encode proteins involved in several other biological processes including the negative regulation of cell proliferation, cell cycle arrest and cell-cell adhesion. However, these biological processes have a Benjamini value higher than 0.05, but they remain statistically significant in terms of the p-value. Interestingly, the GO biological process which contains the largest percentage of enriched BICC1-asociated RNAs is the negative regulation of transcription from RNA polymerase II promoter (112 count, 5%). Several other significantly relevant GO biological processes can be viewed in Table 5.2.2.2.

The individual RNA transcripts enriched in the top three most significant GO Biological Processes were further analysed and displayed in Appendix Figure 7.7, while the cell-cell adhesion and cadherin binding, GO Biological Processes altered in ADPKD, were further explored in Appendix Figure 7.8. In summary, BICC1 interacts with RNA transcripts that encode proteins involved in the regulation of cellular proliferation, migration and adhesion.

Table 5.2.2.2. The top 20 GO biological processes, ranked by p-value, identified from DAVID analysis of our enriched RNA transcripts associated with BICC1. The count refers to the number of RNA transcripts enriched in function to the relevant GO biological process, and this number is also presented as a percentage of the total number of transcripts assessed (%). Significant keywords are displayed with a p-value and Benjamini (adjusted p-value) value cut off of 0.05, however only the first GO biological process has a Benjamini value <0.05.

GO Biological Process	Count	%	P-Value	Benjamini
positive regulation of cell migration	46	2.1	5.60E-07	2.80E-03
glycosaminoglycan catabolic process	12	0.5	6.60E-05	1.50E-01
negative regulation of cell proliferation	72	3.2	8.20E-05	1.30E-01
angiogenesis	46	2.1	1.10E-04	1.30E-01
cell cycle arrest	33	1.5	1.10E-04	1.00E-01
glycosaminoglycan biosynthetic process	15	0.7	1.50E-04	1.20E-01
semaphorin-plexin signaling pathway	13	0.6	1.80E-04	1.20E-01
cell-cell adhesion	52	2.3	2.40E-04	1.40E-01
small GTPase mediated signal transduction	48	2.1	2.90E-04	1.50E-01
neural tube development	12	0.5	3.00E-04	1.40E-01
negative regulation of transcription, DNA-templated	83	3.7	4.80E-04	2.00E-01
cell migration	36	1.6	5.10E-04	1.90E-01
positive regulation of TOR signaling	11	0.5	5.10E-04	1.80E-01
regulation of small GTPase mediated signal transduction	30	1.3	5.20E-04	1.70E-01
release of cytochrome c from mitochondria	10	0.4	6.10E-04	1.80E-01
in utero embryonic development	38	1.7	6.20E-04	1.80E-01
negative regulation of transcription from RNA polymerase II promoter	112	5	6.60E-04	1.80E-01
neural tube closure	20	0.9	8.90E-04	2.20E-01
neuron differentiation	23	1	9.20E-04	2.10E-01
canonical Wnt signaling pathway	21	0.9	9.20E-04	2.10E-01

Third, enriched GO terms in relation to molecular function were explored, and the data revealed that BICC1-enriched RNAs encode several proteins which are involved in various important biological functions. For example, the majority of enriched RNAs encode proteins that function in protein binding (1221 count, 54.4%). In addition, BICC1-associated RNAs encode proteins that have transcriptional corepressor activity (43 count, 1.9%). Both of these molecular functions have a p-value and Benjamini value of <0.05. Interestingly, BICC1-asociated RNAs encode proteins required in cadherin binding involved in cell-cell adhesion, a function previously observed in Tables 5.2.2.1 and 5.2.2.2, however this function had a Benjamini value >0.05. Several other significantly relevant GO molecular functions can be viewed in Table 5.2.2.3.

The individual RNA transcripts enriched in the top three most significant GO Molecular Function lists were further analysed and displayed in Appendix Figure 7.9, while receptor binding and GTPase activator activity, GO Molecular Functions altered in ADPKD, were further explored in Appendix Figures 7.10 and 7.11 respectively. In summary, BICC1 interacts with RNA transcripts that encode proteins that function as transcriptional regulators to control cellular growth, survival and death.

Table 5.2.2.3. The top 10 GO molecular functions, ranked by p-value, identified from DAVID analysis of our enriched RNA transcripts associated with BICC1. The count refers to the number of RNA transcripts enriched in function to the relevant GO molecular function, and this number is also presented as a percentage of the total number of transcripts assessed (%). Significant keywords are displayed with a p-value and Benjamini (adjusted p-value) value cut off of 0.05, however only the first two GO molecular functions have a Benjamini value <0.05.

GO Molecular Function	Count	%	P-Value	Benjamini
protein binding	1221	54.4	5.60E-23	8.60E-20
transcription corepressor activity	43	1.9	1.30E-04	9.40E-02
kinase activity	48	2.1	2.30E-04	1.10E-01
cadherin binding involved in cell-cell adhesion	54	2.4	5.10E-04	1.80E-01
GTPase activator activity	51	2.3	1.10E-03	2.90E-01
protein kinase binding	63	2.8	2.70E-03	4.90E-01
semaphorin receptor binding	9	0.4	3.20E-03	5.00E-01
protein C-terminus binding	35	1.6	3.30E-03	4.70E-01
receptor binding	59	2.6	3.90E-03	4.80E-01
neuropilin binding	7	0.3	4.80E-03	5.20E-01

Fourth, enriched GO terms in relation to cellular compartments were explored, and the data revealed that BICC1-enriched RNAs encode various proteins which are most significantly found in focal adhesions (88 count, 3.9%). In addition, BICC1-associated RNAs encode proteins found in the nucleoplasm (393 count, 17.7%), extracellular exosome (399 count, 17.8%) and the membrane (320 count, 14.3%). Interestingly, the cellular compartment that contains the largest percentage of BICC1-asociated RNAs is the cytosol (451 count, 20.1%). All the GO cellular compartment outputs had a p-value and Benjamini value <0.05. Several other significantly relevant GO cellular compartments can be viewed in Table 5.2.2.4. The individual RNA transcripts enriched in the top three most significant GO Cellular Compartments were further analysed and displayed in Appendix Figure 7.12. In summary, BICC1 interacts with RNA transcripts that encode proteins involved in cellular adhesion, signalling and gene transcription.

Table 5.2.2.4. The top 10 GO cellular compartments, ranked by p-value, identified from DAVID analysis of our enriched RNA transcripts associated with BICC1. The count refers to the number of RNA transcripts enriched in function to the relevant GO cellular compartment, and this number is also presented as a percentage of the total number of transcripts assessed (%). Significant keywords are displayed with a p-value and Benjamini (adjusted p-value) value cut off of 0.05.

GO Cellular Compartment	Count	%	P-Value	Benjamini
focal adhesion	88	3.9	3.40E-10	2.70E-07
nucleoplasm	396	17.7	2.50E-07	9.90E-05
extracellular exosome	399	17.8	2.70E-07	7.00E-05
membrane	320	14.3	6.20E-07	1.20E-04
endoplasmic reticulum membrane	145	6.5	8.00E-07	1.20E-04
Golgi apparatus	143	6.4	2.20E-06	2.90E-04
lysosomal membrane	58	2.6	3.60E-06	4.00E-04
cytosol	451	20.1	5.20E-06	5.10E-04
cell-cell adherens junction	61	2.7	7.30E-05	6.30E-03
mitochondrion	191	8.5	3.50E-04	2.70E-02

Fifth, enriched Interpro terms were explored, and the data revealed that BICC1-enriched RNAs encode proteins which contain various functional domains or are part of important protein super-families. For example, the most significantly enriched BICC1-associated RNAs, with a p-value and Benjamini value <0.05, encode proteins which are Semaphorins/CD100 antigens. In addition, some of the enriched RNAs are part of the insulin-like growth factor binding protein and small GTPase families. However, these Interpro terms have a Benjamini value greater than 0.05, but they remain statistically significant in terms of the p-value. Several other significant and biologically relevant Interpro terms can be viewed in Table 5.2.2.5. The individual RNA transcripts enriched in the top three most significant Interpro terms were further analysed and displayed in Appendix Figure 7.13. In summary, BICC1 interacts with RNA transcripts that encode proteins involved in cellular adhesion, signalling and cytoskeletal organisation.

Table 5.2.2.5. The top 10 Interpro terms, ranked by p-value, identified from DAVID analysis of our enriched RNA transcripts associated with BICC1. The count refers to the number of RNA transcripts enriched in function to the relevant Interpro term, and this number is also presented as a percentage of the total number of transcripts assessed (%). Significant keywords are displayed with a p-value and Benjamini (adjusted p-value) value cut off of 0.05, however only the second Interpro term has a Benjamini value <0.05.

Interpro Term	Count	%	P-Value	Benjamini
Insulin-like growth factor binding protein, N-terminal	33	1.5	5.00E-05	1.20E-01
Semaphorin/CD100 antigen	13	0.6	6.70E-05	8.20E-02
Small GTPase superfamily	31	1.4	2.90E-04	2.10E-01
Plexin	11	0.5	2.90E-04	1.70E-01
WD40/YVTN repeat-like-containing domain	58	2.6	6.00E-04	2.60E-01
Plexin-like fold	14	0.6	7.50E-04	2.70E-01
Small GTP-binding protein domain	34	1.5	7.90E-04	2.50E-01
Low-density lipoprotein (LDL) receptor class A, conserved site	12	0.5	3.50E-03	6.70E-01
Galactosyltransferase, metazoa	5	0.2	4.10E-03	6.90E-01
Semaphorin	8	0.4	4.50E-03	6.80E-01

Finally, enriched KEGG pathways were explored, and the data revealed that BICC1-enriched RNAs encode various proteins that are involved in several pathways related to cancer and signalling, some of which are significantly altered in ADPKD. For example, BICC1-associated RNAs are enriched in the following pathways; proteoglycans in cancer, HTLV-1 infection and pathways in cancer. The individual RNA transcripts enriched in the top three most significant KEGG pathways were further analysed and displayed in Appendix Figure 7.14, while endocytosis and other pathways altered in ADPKD were further explored in Appendix Figures 7.15-7.20. The pathways were downloaded from the KEGG website and displayed using Cytoscape. The BICC1-associated RNAs significantly enriched in each pathway are coloured, with blue referring to downregulated RNA transcripts, red referring to upregulated RNA transcripts and yellow referring to no change in expression in *BICC1 KO* cells (data extracted from the RNA-Seq dataset). The ErbB signalling pathway is listed as 14th most significant in Appendix Table 7.4 and was therefore included in the manual analysis due to its relevance to ADPKD. Several other significant, biologically relevant KEGG pathways can be viewed in Table 5.2.2.6.

Table 5.2.2.6. The top 10 KEGG pathways, ranked by p-value, identified from DAVID analysis of our enriched RNA transcripts associated with BICC1. The count refers to the number of RNA transcripts enriched in function to the relevant KEGG pathway, and this number is also presented as a percentage of the total number of transcripts assessed (%). Significant keywords are displayed with a p-value and Benjamini (adjusted p-value) value cut off of 0.05.

KEGG Pathway	Count	%	P-Value	Benjamini
Proteoglycans in cancer	43	1.9	4.60E-05	1.30E-02
HTLV-I infection	50	2.2	1.10E-04	1.50E-02
Pathways in cancer	69	3.1	1.90E-04	1.70E-02
MAPK signaling pathway	49	2.2	1.90E-04	1.30E-02
VEGF signaling pathway	18	0.8	3.00E-04	1.70E-02
Neurotrophin signaling pathway	28	1.2	3.30E-04	1.50E-02
Endocytosis	46	2.1	4.40E-04	1.70E-02
Hippo signaling pathway	32	1.4	6.70E-04	2.30E-02
Bladder cancer	13	0.6	1.40E-03	4.30E-02
mTOR signaling pathway	16	0.7	1.60E-03	4.30E-02

As previously stated, several signalling pathways have been found to be dysregulated or altered in ADPKD. The MAPK, VEGF, Endocytosis, Hippo, mTOR and ErbB signalling pathways have already been explored further due to their perturbation in ADPKD disease models, however, other ADPKD-related signalling pathways were also enriched within the DAVID KEGG pathway analysis displayed in Table 5.2.2.6 as well as Appendix Table 7.4. These pathways, and their ranking within the analysis, are further displayed in Table 5.2.2.7, while the logFC values of the RNA transcripts enriched within these pathways are displayed in Appendix Figures 7.21 and 7.22 (other pathways have been explored in previous appendix figures).

Table 5.2.2.7. The ADPKD-related KEGG pathways, ranked by p-value, identified from DAVID analysis of our enriched RNA transcripts associated with BICC1. The count refers to the number of RNA transcripts enriched in function to the relevant KEGG pathway, and this number is also presented as a percentage of the total number of transcripts assessed (%). From rank 31 onwards, the significance is >0.05 in regard to the p-value, while from rank 10 onwards the significance is >0.05 in regard to the Benjamini value (adjusted p-value).

Rank	Term	Count	%	P-Value	Benjamini
4	MAPK signaling pathway	49	2.2	1.90E-04	1.30E-02
5	VEGF signaling pathway	18	0.8	3.00E-04	1.70E-02
7	Endocytosis	46	2.1	4.40E-04	1.70E-02
8	Hippo signaling pathway	32	1.4	6.70E-04	2.30E-02
10	mTOR signaling pathway	16	0.7	1.60E-03	4.30E-02
14	ErbB signaling pathway	20	0.9	3.40E-03	6.60E-02
25	PI3K-Akt signaling pathway	54	2.4	1.20E-02	1.30E-01
27	TNF signaling pathway	21	0.9	1.60E-02	1.50E-01
31	Rap1 signaling pathway	35	1.6	2.00E-02	1.60E-01
58	Wnt signaling pathway	23	1	6.10E-02	2.60E-01
59	AMPK signaling pathway	21	0.9	6.10E-02	2.60E-01
62	Ras signaling pathway	34	1.5	7.50E-02	3.00E-01
64	Hedgehog signaling pathway	7	0.3	7.70E-02	3.00E-01
67	Notch signaling pathway	10	0.4	8.70E-02	3.20E-01
68	TGF-beta signaling pathway	15	0.7	8.90E-02	3.20E-01

BICC1-bound RNA transcripts were compared to a medical cystic gene panel list and there were 19 hits in common, which are displayed in Table 5.2.2.8. (Sheffield Genetics Diagnostic Service, personal communication, 2019). Interestingly, many of the significant hits are involved in various functions in regard to the primary cilium.

Table 5.2.2.8. The cystic genes, as identified by the cystic gene list significantly enriched with the BICC1 fRIP dataset, ranked by log FC. logFC = log fold change.

Gene ID	Name	OMIM Ref	Protein Type	Cellular Localisation	Function	Phenotype	fRIP logFC
GLIS2	Zinc finger protein GLIS2	608539	Transcription factor	Nucleus	Represses Hedgehog and Wnt signalling pathways	Ciliopathy gene (NPHP7) associated with cystic kidney disease	6.75
TMEM107	Transmembrane protein 107	616183	Transmembrane protein (cilia)	Plasma membrane (PM)	Ciliogenesis	?Joubert syndrome; Meckel syndrome; Orofaciodigital syndrome XVI	2.42
CFAP53/CCDC11	Cilia- and flagella-associated protein 53	614759	Dynein	Nucleus/Cytosol	Beating of primary cilia	Heterotaxy, visceral, 6, autosomal recessive	2.17
TCTEX1D2	Tctex1 domain-containing protein 2	617353	ATPase	Cytoskeleton	Retrograde ciliary transport	Short-rib thoracic dysplasia 17 with or without polydactyly; Jeune asphyxiating thoracic dystrophy; JATD	1.84
IMPDH1	Inosine-5'-monophosphate dehydrogenase 1	146690	Enzyme	Nucleus/Cytosol	Regulation of cell growth	Ciliopathies	1.81
PKD1	Polycystin-1	601313	Transmembrane glycoprotein	PM/Extracellular	Tubulogenesis and various cilia functions	Polycystic kidney disease, adult type I	1.63
INPP5E	72 kDa inositol polyphosphate 5-	613037	Phosphatase	Cytoskeleton/Cytosol	Mobilises intracellular calcium	Ciliopathy genes associated with cystic kidney disease	1.56
TCTN3	Tectonic-3	613847	Hedgehog signal transduction	PM/Nucleus	Ciliogenesis and regulator of cilia membrane composition	Orofaciodigital syndrome IV; Joubert syndrome; Meckel-Gruber; Mohr-Majewski syndrome; Joubert syndrome 18	1.56
PKD2	Polycystin-2	173910	Transmembrane protein	PM/Cytoskeleton/ Endoplasmic reticulum	Cation channel and various cilia functions	Polycystic kidney disease 2	1.38
WDR34	WD repeat-containing protein 34	613363	WD repeat protein	Cytoskeleton/Cytosol	IFT machinery and ciliary functions	Short-rib thoracic dysplasia 11 with or without polydactyly; Jeune syndrome; Short-rib thoracic dysplasia	1.34
DNAAF2	Protein kintoun	612517	Dynein	Cytosol	Cilia motility	Ciliary dyskinesia, primary;ciliopathies	1.33
CCNO	Cyclin-O	607752	Cyclin protein	Nucleus	Generation of multiciliated cells by promoting cell cycle	Ciliary dyskinesia, primary	1.33
BBS5	Bardet-Biedl syndrome 5 protein	603650	BBSome complex protein	Cytoskeleton/Cytosol	Sorts specific membrane proteins to primary cilia	Bardet Biedl syndrome 5	1.28
PRKCSH	Glucosidase 2 subunit beta	177060	N-linked glycan-processing enzyme	Endoplasmic reticulum	PKD1 biogeneis and trafficking to PM of primary cilia	Polycystic liver disease 1	1.25
DNAAF5	Dynein assembly factor 5, axonemal	614864	Dynein	Cytosol/Nucleus	Cilia motility	Ciliary dyskinesia, primary, 18	1.25
SBDS	Ribosome maturation protein SBDS	607444	Ribosomal protein	Cytoskeleton/Cytosol/ Nucleus	Ribosome biogenesis	Skeletal Ciliopathies	1.22
C21orf2/CFAP410	Cilia- and flagella-associated protein 410	603191	Mitochondrial protein	PM/Cytoskeleton/ Mitochondrion	Ciliogenesis and maintenance	Jeune asphyxiating thoracic dystrophy (JATD); Retinal dystrophy with macular staphyloma	1.22
DHCR7	7-dehydrocholesterol reductase	602858	Membrane-bound enzyme	Nucleus/Cytosol/ Endoplamic reticulum	Cholesterol biosynthesis	Smith-Lemli-Opitz syndrome	0.92
TSC2	Tuberin	191092	Tumour suppressor	Nucleus/Cytosol/Lysosom/Golgi apparatus	Negatively regulates mTORC1 signalling	?Focal cortical dysplasia, type II, somatic; Lymphangioleiomyomatosis, somatic; Tuberous sclerosis-	0.89

Our data has demonstrated that BICC1 interacts with RNA transcripts that encode proteins involved in the regulation and induction of gene transcription and translation, signal transduction pathways and the regulation of cellular proliferation, migration, adhesion and survival, which are essential to kidney homeostasis and proper function. As discussed in Chapter 4, IP experiments were performed, and the proteins bound to BICC1 were analysed and identified by mass spectrometry to assess the types of proteins associated with BICC1 and to better understand its function and its proteome. As this study has also identified RNA binding partners of BICC1, we compared the two datasets and assessed the types of pathways and biological functions they have in common.

As discussed above, the DAVID functional tool analysis was utilised for this comparison and Table 5.2.2.9 demonstrates that both datasets have significant hits in common pathways. For example, our BICC1 fRIP dataset and our MS dataset contained RNA transcripts that encode proteins that function as phosphoproteins and in acetylation. Furthermore, both datasets contained significant hits in the GO biological processes of cell-cell adhesion and negative regulation of the canonical Wnt signalling pathways. In addition, both datasets encoded proteins that are involved in protein and enzyme binding and are localised at focal adhesions, in extracellular exosomes and the nucleoplasm. Moreover, several fRIP and MS hits encode proteins that are part of the small GTPase superfamily and contain small GTP-binding protein domains and WD40/YVTN repeat-like-containing domains.

Of interest to ADPKD are the negative regulation of the canonical Wnt signalling pathway and the GTPase superfamily, as well as transcripts and proteins involved in the cell cycle and N-glycan biosynthesis, as each process has been implicated in ADPKD. The negative regulation of the canonical Wnt signalling pathway is of particular importance, as the Wnt signalling pathway has increased activity in ADPKD, therefore suggesting the regulation of its activity has been lost. The full list of pathways and biological functions can be viewed in Table 5.2.2.9 and the significantly enriched transcripts can be viewed in Figure 5.2.2.2.

Table 5.2.2.9. The comparison of enriched binding partners between our fRIP and MS datasets.

Term	fRIP		Mass Spec	
UP_Keywords	*p-value*	*Benjamini*	*p-value*	*Benjamini*
Phosphoprotein	5.10E-49	2.70E-46	1.80E-54	3.00E-52
Acetylation	1.60E-10	4.30E-08	9.80E-120	3.20E-117
Methylation	3.70E-10	6.60E-08	4.20E-22	1.70E-20
Endoplasmic reticulum	7.70E-07	1.00E-04	3.00E-09	4.80E-08
Cytoplasm	9.50E-06	6.30E-04	2.40E-22	1.10E-20
Nucleus	1.10E-05	6.30E-04	4.60E-09	6.60E-08
Mitochondrion	1.30E-04	4.60E-03	1.60E-20	6.00E-19
GO Biological Process	*p-value*	*Benjamini*	*p-value*	*Benjamini*
cell-cell adhesion	2.40E-04	1.40E-01	3.50E-21	1.00E-18
small GTPase mediated signal transduction	2.90E-04	1.50E-01	7.30E-03	1.60E-01
protein transport	2.90E-02	7.80E-01	3.20E-02	4.30E-01
negative regulation of canonical Wnt signaling pathway	3.20E-02	7.80E-01	4.60E-02	5.20E-01
GO Molecular Function	*p-value*	*Benjamini*	*p-value*	*Benjamini*
protein binding	5.60E-23	8.60E-20	1.10E-31	3.50E-29
cadherin binding involved in cell-cell adhesion	5.10E-04	1.80E-01	3.80E-26	8.30E-24
protein kinase binding	2.70E-03	4.90E-01	2.40E-04	6.80E-03
heat shock protein binding	7.00E-03	5.60E-01	3.60E-03	6.20E-02
enzyme binding	1.00E-02	6.10E-01	2.40E-04	6.80E-03
GDP binding	1.90E-02	6.90E-01	2.10E-03	4.00E-02
GO Cellular Compartment	*p-value*	*Benjamini*	*p-value*	*Benjamini*
focal adhesion	3.40E-10	2.70E-07	3.20E-19	1.60E-17
extracellular exosome	2.70E-07	7.00E-05	7.50E-44	1.90E-41
nucleoplasm	2.50E-07	9.90E-05	1.60E-17	6.70E-16
membrane	6.20E-07	1.20E-04	1.80E-83	9.00E-81
endoplasmic reticulum membrane	8.00E-07	1.20E-04	9.00E-06	1.70E-04
cytosol	5.20E-06	5.10E-04	2.80E-37	4.70E-35
cell-cell adherens junction	7.30E-05	6.30E-03	2.70E-25	2.70E-23
mitochondrion	3.50E-04	2.70E-02	5.00E-24	3.60E-22
cytoplasm	3.80E-04	2.70E-02	7.60E-14	2.70E-12
Interpro	*p-value*	*Benjamini*	*p-value*	*Benjamini*
Small GTPase superfamily	2.90E-04	2.10E-01	1.40E-02	2.60E-01
WD40/YVTN repeat-like-containing domain	6.00E-04	2.60E-01	1.90E-02	3.20E-01
Small GTP-binding protein domain	7.90E-04	2.50E-01	1.40E-02	2.60E-01
WD40 repeat, conserved site	9.80E-03	6.90E-01	1.40E-03	4.60E-02
WD40-repeat-containing domain	3.30E-02	8.90E-01	4.40E-03	1.10E-01
WD40 repeat	3.50E-02	8.80E-01	8.30E-03	1.80E-01
KEGG Pathways	*p-value*	*Benjamini*	*p-value*	*Benjamini*
Huntington's disease	2.60E-02	1.80E-01	2.20E-02	2.50E-01
Epstein-Barr virus infection	3.30E-02	2.00E-01	4.90E-04	1.50E-02
Cell cycle	3.80E-02	2.20E-01	3.50E-02	3.30E-01
N-Glycan biosynthesis	4.50E-02	2.50E-01	3.10E-02	3.30E-01

To further understand the common pathways, and the types of transcripts BICC1 may regulate, the individual enriched transcripts were explored. Of particular interest to this study, and taking into consideration the types of pathways and biological functions already identified in the analysis of the BICC1 fRIP-Seq dataset and also the BICC1 MS dataset, we chose to further analyse cell-cell adhesion (GO BP) and cadherin binding involved in cell-cell adhesion

(GO MF), small GTPase mediated signal transduction (GO MF), negative regulation of the canonical Wnt signalling pathway (GO MF), focal adhesion (GO CC), the cell cycle (KEGG) and N-glycan biosynthesis (KEGG). The common transcripts enriched in the cell-cell adhesion and cadherin binding in cell-cell adhesion GO processes included *BSG*, *EIF4G1* and *FASN*, to name but a few. The common transcripts enriched in small GTPase mediated signal transduction included *RAB2A* and *RHOT2* (Figure 5.2.2.2).

In contrast, there are no common transcripts enriched between the fRIP and the MS datasets within the negative regulation of canonical Wnt signalling pathway. Nevertheless, the top five RNA transcripts (ranked by logFC) from the fRIP dataset and all the enriched proteins from the MS dataset were explored further due to their relevance to ADPKD. Interestingly, a clear subset of proteins was enriched with BICC1, while several key players within the Wnt signalling pathway were enriched with BICC1 at the RNA level. These RNA transcripts included *FZD1*, *IGFBP4*, *AES*, *GLI1* and *RGS19*, to name but a few. The full list can be viewed in Table 5.2.2.10.

The proteins enriched with BICC1 within the negative regulation of canonical Wnt signalling pathway included *G3BP1*, *PSMC5/6*, *PSMD1-3*, *PSMD8* and *RPS27A*. The common transcripts enriched in focal adhesions included *ACTN4*, *CFL1*, *PABPC1* and *RPLP2* (Figure 5.2.2.21). Of interest is *PABPC1*, which was previously mentioned to interact with *EIF4G1* to circularise mRNA during translation. *PABPC1* binds the 3’ poly(A) tails of mRNAs and, as well as promoting translation initiation, and is also involved in the deadenylation of poly(A) tails; therefore, it has a major role in regulating mRNA stability. *YWHAH* was the only common transcript identified the KEGG cell cycle pathway when comparing the fRIP-Seq and MS datasets. Two common transcripts, *DDOST* and *MOGS*, were identified in the N-glycan biosynthesis pathway.

In summary, BICC1 interacts with RNA transcripts and proteins that are involved in the induction of translation as well as mRNA degradation, cellular energy production, cytoskeletal organisation, signal transduction and protein modification in the ER. Furthermore, the interaction of BICC1 with *BSG* suggest

BICC1 may regulate tumour or tumour-like progression. It is interesting to note that BICC1 interacts with the RNA transcripts of its proteome, which may suggest that BICC1 has a role in regulating its own proteome to ensure proper downstream function.

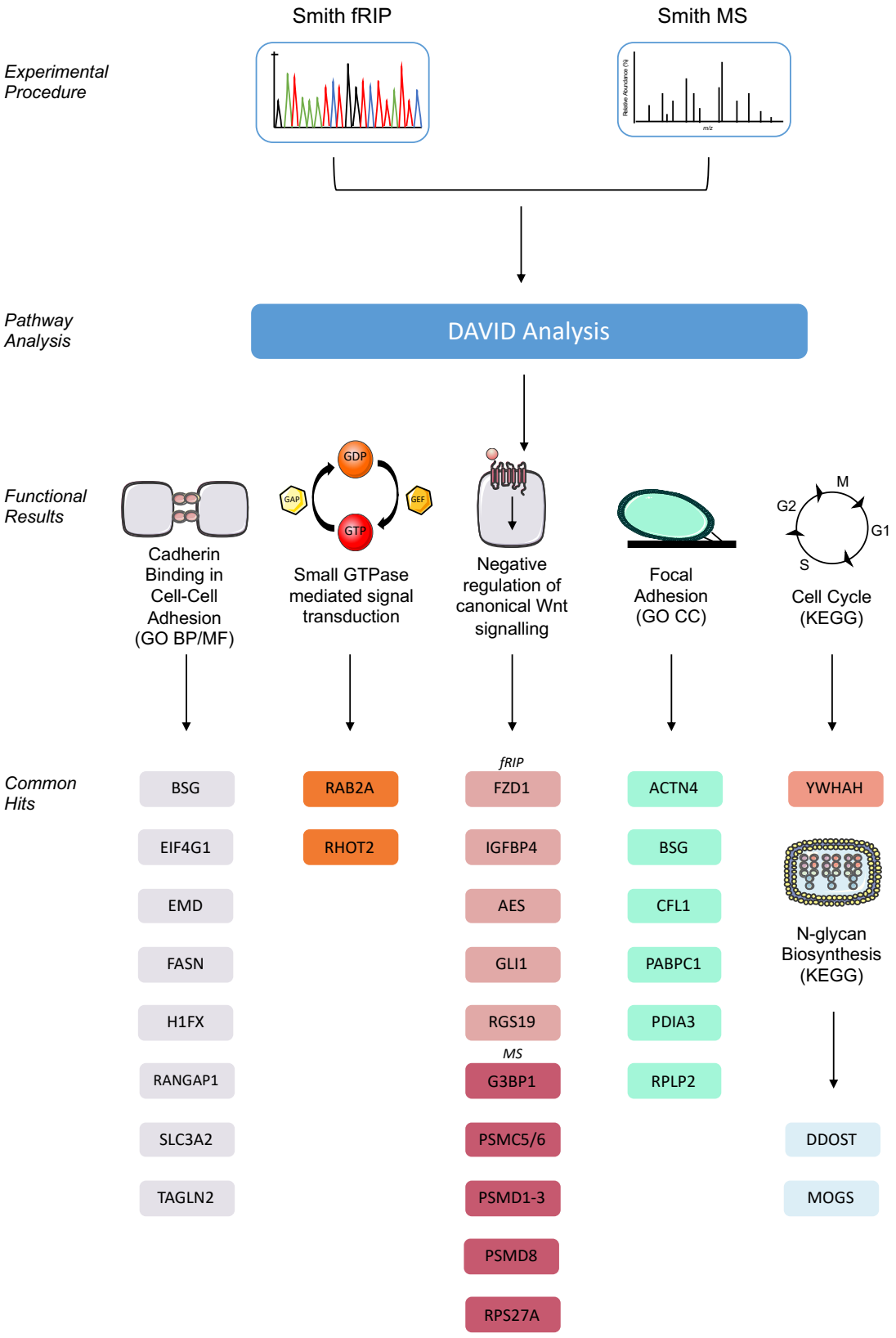

Figure 5.2.2.2. The common enriched binding partners identified in our BICC1 fRIP and MS datasets. Significantly enriched binding partners from the BICC1 fRIP and BICC1 MS datasets were compared and the common transcripts were analysed by DAVID. The individual transcripts enriched within analysed pathways were further assessed and displayed according to their functional relationship.

Table 5.2.2.10. The RNA transcripts significantly enriched within the GO Biological Process negative regulation of the canonical Wnt signalling pathway obtained from the fRIP dataset.

Gene ID	GENE NAME	logFC
FZD1	frizzled class receptor 1(FZD1)	3.25
IGFBP4	insulin like growth factor binding protein 4(IGFBP4)	2.87
AES	amino-terminal enhancer of split(AES)	2.85
GLI1	GLI family zinc finger 1(GLI1)	2.66
RGS19	regulator of G-protein signaling 19(RGS19)	2.49
KREMEN2	kringle containing transmembrane protein 2(KREMEN2)	2.15
NOG	noggin(NOG)	2.15
DVL1	dishevelled segment polarity protein 1(DVL1)	2.07
SOX17	SRY-box 17(SOX17)	2.00
IGFBP2	insulin like growth factor binding protein 2(IGFBP2)	1.82
SIAH2	siah E3 ubiquitin protein ligase 2(SIAH2)	1.75
LRP4	LDL receptor related protein 4(LRP4)	1.51
DVL2	dishevelled segment polarity protein 2(DVL2)	1.49
WNT5B	Wnt family member 5B(WNT5B)	1.39
BMP2	bone morphogenetic protein 2(BMP2)	1.31
LZTS2	leucine zipper tumor suppressor 2(LZTS2)	1.25
GSK3A	glycogen synthase kinase 3 alpha(GSK3A)	1.25
RAPGEF1	Rap guanine nucleotide exchange factor 1(RAPGEF1)	1.23
NOTCH1	notch 1(NOTCH1)	1.22
TMEM64	transmembrane protein 64(TMEM64)	1.17
DACT1	dishevelled binding antagonist of beta catenin 1(DACT1)	1.16
FOXO3	forkhead box O3(FOXO3)	1.11
AXIN1	axin 1(AXIN1)	1.10
DAB2IP	DAB2 interacting protein(DAB2IP)	1.09
DKK3	dickkopf WNT signaling pathway inhibitor 3(DKK3)	1.01
LATS2	large tumor suppressor kinase 2(LATS2)	1.00
ZNRF3	zinc and ring finger 3(ZNRF3)	0.98
CUL3	cullin 3(CUL3)	0.87

Next, we analysed the individual transcripts and proteins identified in the BICC1 fRIP and BICC1 MS datasets in regard to their enrichment with BICC1 by measurement of logFC. Figure 5.2.2.3 displays the 12 most significantly BICC1-enriched transcripts identified in both datasets, with their logFC values for each dataset presented below each transcript. The transcripts were grouped into related functional groups for ease of representation and discussion.

ANKS3 is a newly identified protein that functions in protein complexes with its related family protein ANKS6, as well as with NEK kinases including NEK7, as discussed in Chapter 4. This study has also identified ANKS3 as a binding partner of BICC1, PC1 and PC2. ANKS3 is also positively regulated by BICC1, as when BICC1 is lost, ANKS3 expression is reduced by approximately 70% (see Chapter 4 for results). The BICC1 fRIP and BICC1 MS datasets demonstrate that BICC1 interacts with ANKS3 at both the RNA and protein level, with enrichment logFC values of 3 and 5 respectively.

In summary the interacting partners of BICC1 are involved in various cellular processes to initiate and maintain proper function and homeostasis including; protein complex formation, mitochondrial and cytoplasmic protein synthesis, protein folding in the ER, cytoskeletal regulation and organisation and energy production.

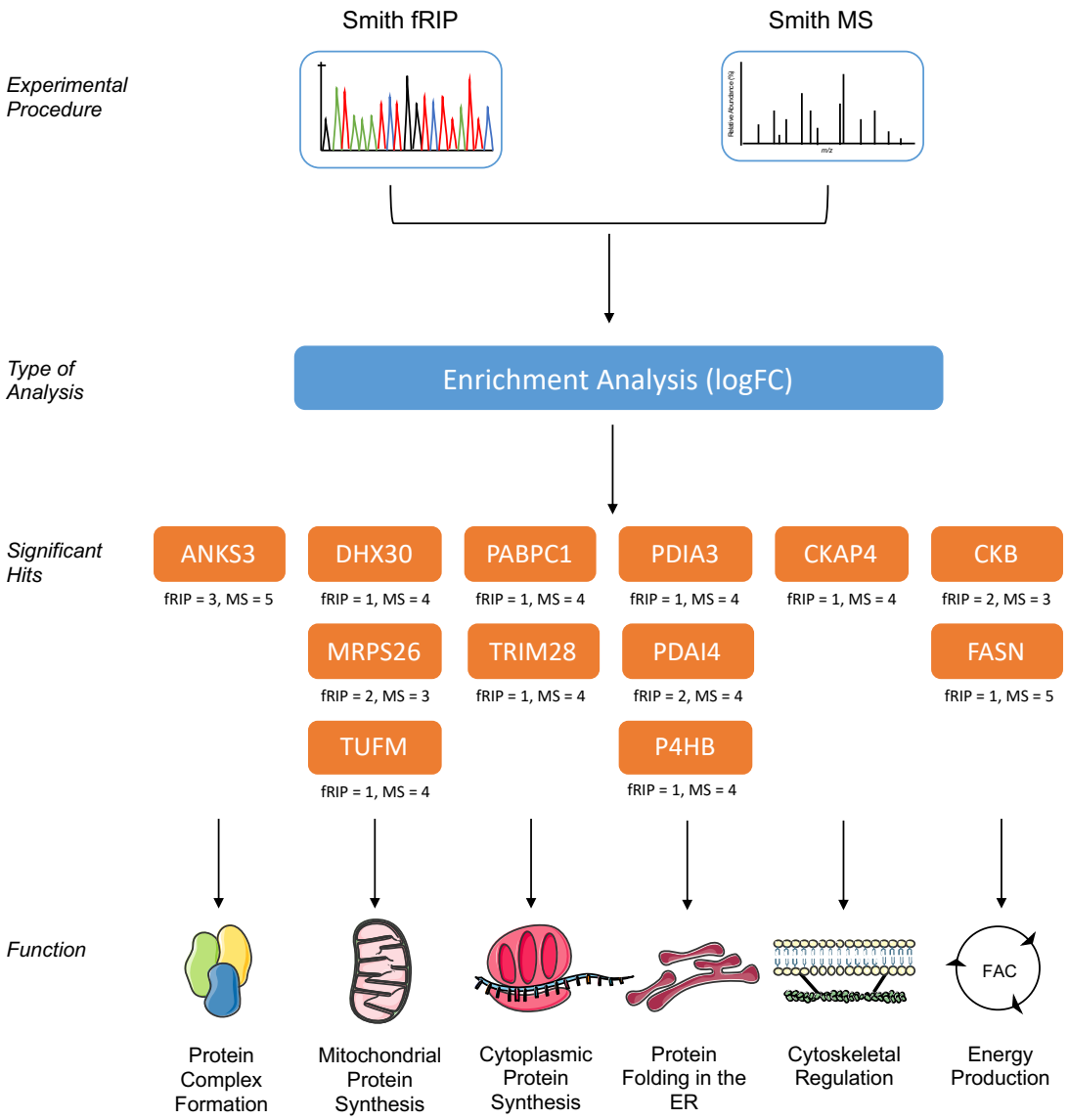

Figure 5.2.2.3. The most significantly enriched binding partners identified in our BICC1 fRIP and MS datasets. Significantly enriched binding partners identified from the BICC1 fRIP and BICC1 MS datasets were compared and the common transcripts were analysed by DAVID. Significance was measured by logFC and the values were rounded up to the nearest whole number and are displayed below each transcript. The most significantly enriched transcripts were then manually analysed and displayed according to their function. logFC = log fold change.

Following the assessment of the types of enriched RNAs associated with BICC1 using DAVID and downstream functional annotation tools, the 10 most significantly BICC1-bound RNAs (when expressed as logFC and with an adj. p-value of <0.05) were investigated further. Figure 5.2.2.4 demonstrates the 10 most significantly enriched RNAs, with *JUND* and *GLIS2* presenting with the largest logFC values of 6.70 and 6.75 respectively. Their total abundance, in terms of normalised raw gene read counts following BICC1 fRIP experiments, correlated with their logFC values and significance scores as they were the top

two most abundant RNA transcripts bound to BICC1 with gene counts of 29,583 and 12,387 respectively, closely followed by *HMGA1*, which has a gene count of 10,742.

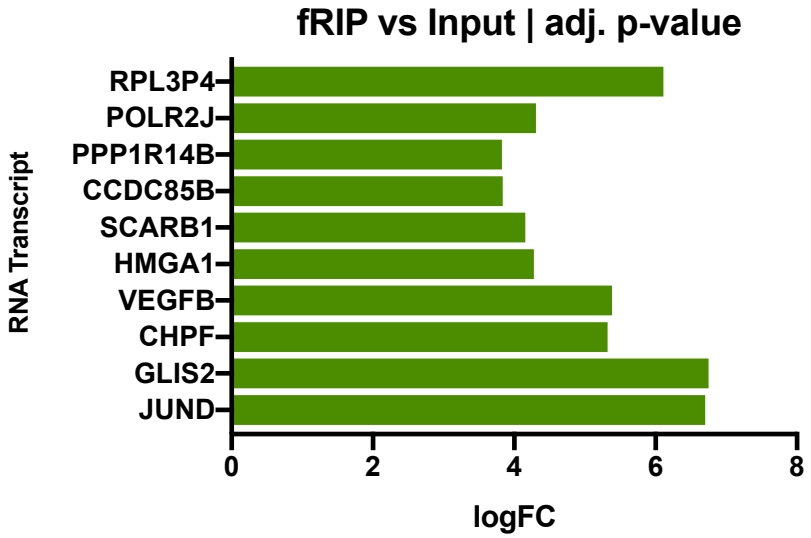

Figure 5.2.2.4. The 10 most significant BICC1-bound RNA transcripts. Significance was determined by assessing adjusted p-values (adj. p-value). The BICC1-enriched RNAs are listed in descending order in regard to significance. All adjusted p-values were <0.0001. logFC = log fold change.

To further comprehend the biological role of the most significantly BICC1-bound RNA transcripts, a table was produced to display additional information regarding the gene name of the RNA transcript and a summary of their known function (Table 5.2.2.11). Of interest is *JUND*, a proto-oncogene and transcription factor involved in the AP-1 complex. Interestingly, *GLIS2* is part of the GLIS family of zinc finger 2 and can function as a transcriptional repressor or activator. Furthermore, *GLIS2* has been linked to regulating the hedgehog-dependent expression of Wnt4 and is also associated with NPHP7 disease. More recently, *CHPF* has been linked to PKD as its gene expression was dysregulated in a *PKD1* mouse model (unpublished data). *CHPF* encodes a protein that has beta-1,3-glucuronic acid and beta-1,4-N-acetylgalactosamine transferase activity and is responsible for extending the non-reducing end of the chondroitin polymer. *HMGA1*, *CCDC85B* and several other transcripts are also involved in gene regulation. *ANKS3*, of particularly interest in this study, listed as the 25th most significantly bound RNA transcript to BICC1. Overall, the functional summaries of the 25 most significantly enriched BICC1-RNAs closely match observations made in previous figures and tables of this section.

Table 5.2.2.11. An informative table of the 25 most significant BICC1-bound RNA transcripts, ranked by adjusted p-value. A cut off of 0.05 was applied to the adjusted p-value (adj. p-value).

Gene ID	Gene Name	Summary	Interactions/Pathways Involved In	logFC	adj.p-value
JUND	JunD Proto-Oncogene, AP-1 Transcription Factor Subunit	Transcription factor which binds AP-1 sites	AP1 TF complex	6.70	9.5E-123
GLIS2	GLIS Family Zinc Finger 2	Transcriptional repressor and/or transcriptional activator	Hedgehog-dependent expression of Wnt4 - associated with NPHP7 disease	6.75	5.7E-115
CHPF	Chondroitin Polymerizing Factor	Has both beta-1,3-glucuronic acid and beta-1,4-N-acetylgalactosamine transferase activity	With PRKN may enhance cell viability and protect from oxidative stress	5.32	1.3E-63
VEGFB	Vascular Endothelial Growth Factor B	Growth factor for endothelial cells	Endothelial cell physiology	5.38	3.1E-56
HMGA1	High Mobility Group AT-Hook 1	Chromatin-associated protein involved in the regulation of gene transcription	3'-end processing of mRNA transcripts	4.28	1.6E-48
SCARB1	Scavenger Receptor Class B Member 1	Plasma membrane receptor for HDL cholesterol	Receptor for different ligands	4.16	4.7E-37
CCDC85B	Coiled-Coil Domain Containing 85B	Functions as a transcriptional repressor	CTNNB1 in a TP53-dependent manner - regulates cell growth	3.84	4.3E-33
PPP1R14B	Protein Phosphatase 1 Regulatory Inhibitor Subunit 14B	Inhibitor of PPP1CA	Beta-Adrenergic Signaling and ERK Signaling	3.82	1.3E-30
POLR2J	RNA Polymerase II Subunit J	Synthesises messenger RNA in eukaryotes	Catalysing the transcription of DNA into RNA	4.31	1.0E-29
RPL3P4	Ribosomal Protein L3 Pseudogene 4	Pseudogene	-	6.11	1.9E-29
TNFRSF12A	TNF Receptor Superfamily Member 12A	Receptor for TNFSF12/TWEAK	Proliferation of endothelial cells and cellular adhesion to matrix proteins	3.51	8.8E-29
PIK3R2	Phosphoinositide-3-Kinase Regulatory Subunit 2	Lipid kinase that phosphorylates phosphatidylinositol creating second messengers	Recruits AKT1 and PDPK1 to activate signaling cascades	3.64	2.1E-28
LTB	Lymphotoxin Beta	Type II membrane protein of the TNF family	Membrane anchor for the LTBR/TNFRSF3 complex to the cell surface	4.65	2.0E-27
TUSC1	Tumor Suppressor Candidate 1	Located within chromosome 9p that harbors tumor suppressor genes critical in carcinogenesis	An intronless gene	3.85	7.2E-26
PCSK5	Proprotein Convertase Subtilisin/Kexin Type 5	Serine endoprotease that processes proproteins	Functions in the constitutive and regulated secretory pathways	3.96	2.7E-25
SIAE	Sialic Acid Acetylesterase	An enzyme which removes 9-O-acetylation modifications from sialic acids	B lymphocyte antigen receptor signaling	3.10	3.2E-25
SEPW1	Selenoprotein W, 1	Contains a selenocysteine residue, encoded by the UGA codon, that signals translation termination	Glutathione-dependent antioxidant	3.68	1.0E-24
ZFP91-CNTF	ZFP91-CNTF Readthrough (NMD Candidate)	This gene represents a read-through transcript composed of ZFP91 and CNTF sequences	Non-coding transcript subject to NMD	6.45	1.2E-24
FOSL1	FOS Like 1, AP-1 Transcription Factor Subunit	Leucine zipper protein that can dimerize with JUN proteins, thereby forming the TF complex AP-1	Regulator of cell proliferation and differentiation	3.30	1.3E-24
KLF2	Kruppel Like Factor 2	Transcription factor that binds to the CACCC box in the promoter of target genes	Involved in development and disease including epithelial integrity	4.52	7.1E-24
H2AFZ	H2A Histone Family Member Z	Variant histone H2A which replaces conventional H2A in a subset of nucleosomes	Formation of heterochromatin and chromosome segregation	3.28	8.3E-24
ZNF354B	Zinc Finger Protein 354B	May be involved in transcriptional regulation	Belongs to the krueppel C2H2-type zinc-finger protein family	3.10	2.7E-23
MAFG	MAF BZIP Transcription Factor G	Transcriptional repressor and/or transcriptional activator dependent on dimerisation	Fos and the NFE2L2 transcription factor	3.28	2.7E-23
NSMF	NMDA Receptor Synaptonuclear Signaling And Neuronal Migration Factor	Involved in guidance of olfactory axon projections and migration of luteinizing hormone-releasing hormone neurons	Part of the CREB shut-off signaling pathway	3.21	3.6E-21
ANKS3	Ankyrin Repeat And Sterile Alpha Motif Domain Containing 3	May be involved in NPHP	ANKS6, BICC1, NPHP1, NEK8 and HIF1AN	3.33	3.9E-21

As previously stated, published research has demonstrated that BICC1 can bind and regulate several mRNA targets, including *ADCY6* and *DVL2*. BICC1 has also been linked to the regulation of *WNT11*. Therefore, this study

investigated whether *ADCY6*, *DVL2* and *WNT11* were RNA binding targets of BICC1. Data from the BICC1 fRIP demonstrated that both *ADCY6* and *DVL2* interact with BICC1, with a significant adj. p-value <0.05 (Figure 5.2.25 A). However, *WNT11* was not observed to be an interacting partner of BICC1 (data not shown), therefore a close family member, *WNT7B* (see Table 5.2.2.10), was explored and found to bind BICC1 (adj. p-value <0.05). To ensure specificity in our results, an association of BICC1 and ACTB was also explored and not found to interact with BICC1 in our study (Figure 5.2.2.24 A). Therefore, the raw read counts were assessed and represented as fold change values relative to the BICC1 fRIP input. In agreement with the logFC results, the RNA transcripts of *ADCY6*, *DVL2* and *WNT7B* presented average fold change values that suggest an interaction with BICC1 (2.3, 2.1 and 2.6 respectively), while fold change of 1 for ACTB would suggest no interaction with BICC1 (Figure 5.2.2.5 B and C).

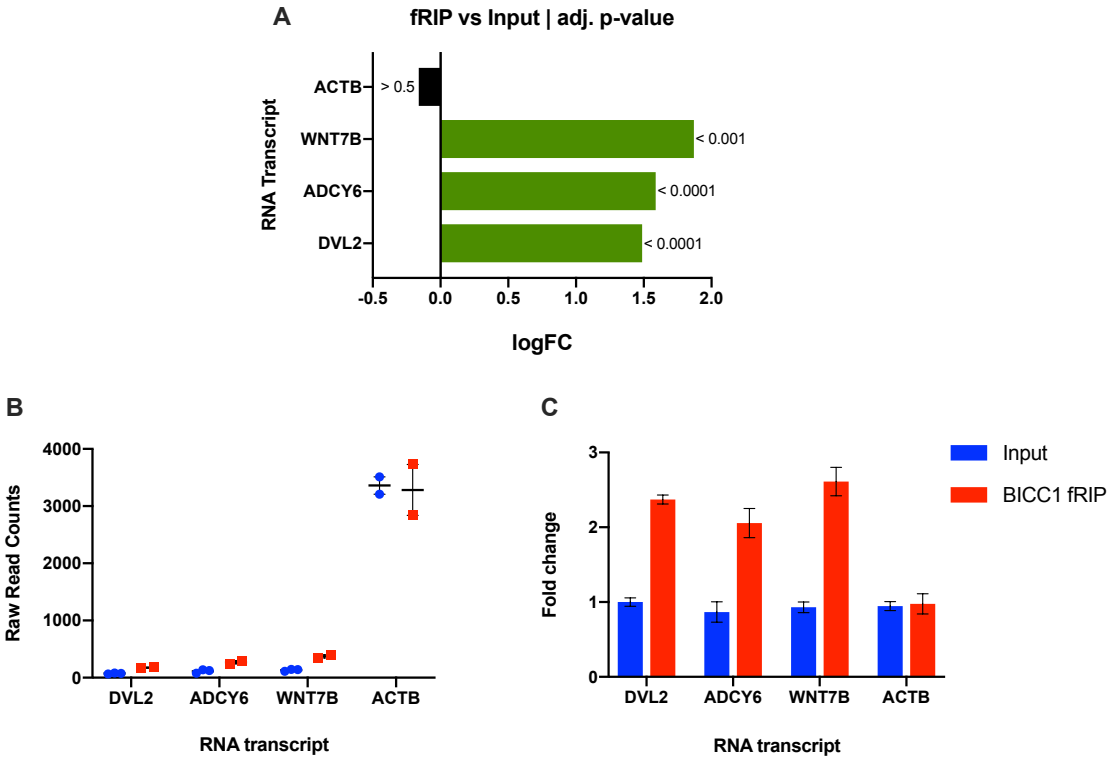

Figure 5.2.2.5. Published BICC1 RNA targets. A) The BICC1-RNA enrichment analysis of published BICC1 RNA targets expressed as logFC values. **B-C)** The raw read counts and calculated fold change values relative to the BICC1 fRIP input of published BICC1 RNA targets. *ACTB* was assessed as a negative control and no association with BICC1 was observed. The input is coloured blue while BICC1 fRIP is coloured red. Significance was determined by assessing adjusted p-values (adj. p-value) <0.05. logFC = log fold change.

In this study we have demonstrated that BICC1 can regulate several mRNAs, including *PKD1*, *PKD2* and *ANKS3*. Therefore, we investigated whether *PKD1*, *PKD2* and *ANKS3* were RNA binding targets of BICC1. Figure 5.2.2.25 A demonstrates that *PKD1*, *PKD2* and *ANKS3* interact with BICC1, with significant adj. p-values <0.05. *ANKS3* presented with the largest logFC of 3.4, while *PKD1* and *PKD2* presented of logFC values of 1.6 and 1.4 respectively. However, two control RNA transcripts, *ANKS6* and *ACTB*, were not observed to be an interacting partners of BICC1 (adj. p-value >0.05). Furthermore, the data from our study suggests that BICC1 does not interact with its own RNA, as its logFC value was the same as that of *ANKS6* and not significant (adj. p-value >0.05) (Figure 5.2.2.6 A).

The raw read counts were assessed and represented as fold change values relative to the BICC1 fRIP input. In agreement with the logFC results, the RNA transcripts of *PKD1*, *PKD2* and *ANKS3* presented average fold change values that suggest an interaction with BICC1 (3, 3.5 and 7.5 respectively), while the fold change values of *BICC1* (1.7), *ANKS6* (1.8) and *ACTB* (1) would suggest no interaction with BICC1 (Figure 5.2.2.6 B and C). Again, *ANKS3* presented with the largest fold change suggesting that *ANKS3* is a significantly enriched RNA binding partner of BICC1, which is in agreement with data presented in Table 5.2.2.10.

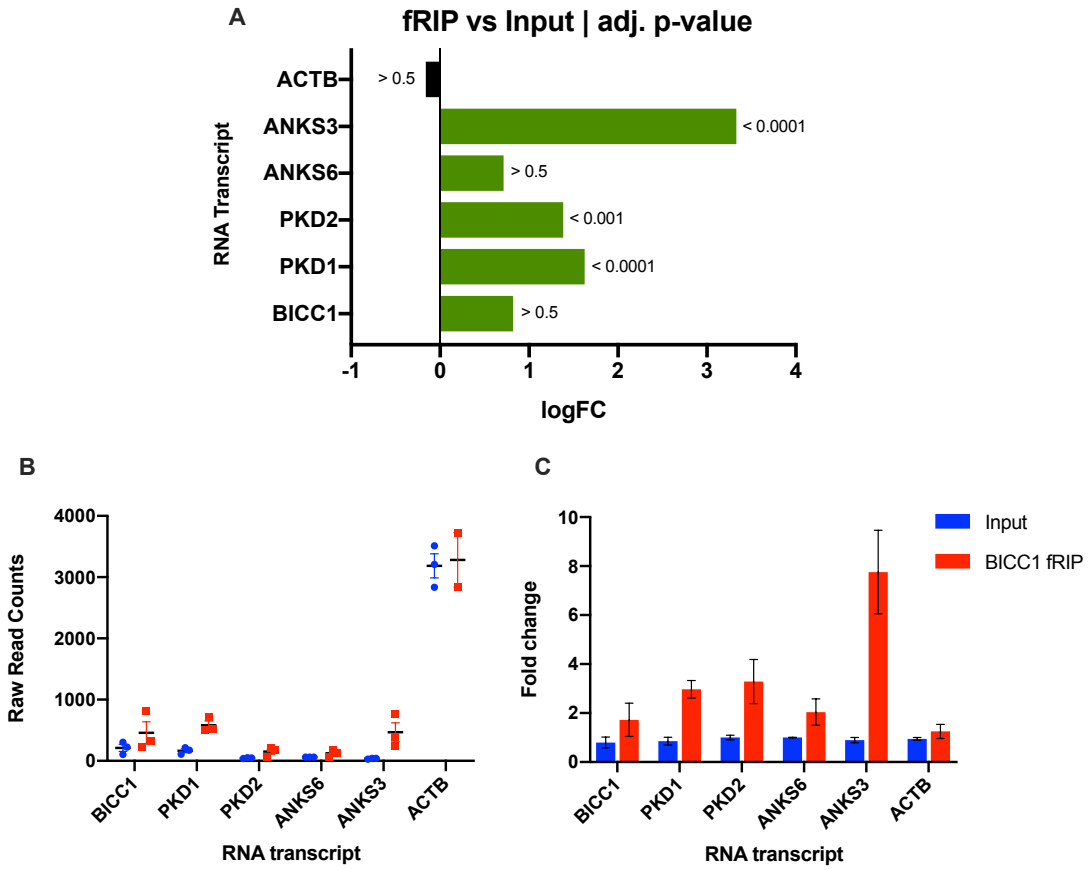

Figure 5.2.2.6. BICC1 binds *PKD1*, *PKD2* and *ANKS3* RNA transcripts *in vitro*. A) BICC1-RNA enrichment analysis expressed as logFC values. **B-C)** The raw read counts and calculated fold change values relative to the BICC1 fRIP input. The RNA transcript of *ACTB* was assessed as a negative control and no association with BICC1 was observed. The input is coloured blue while BICC1 fRIP is coloured red. Significance was determined by assessing adjusted p-values (adj. p-value) <0.05. logFC = log fold change.

5.2.3 BICC1 preferentially interacts with the 3' UTRs of its RNA targets

Due to the nature of the BICC1 fRIP, in that the cell lysates were subjected to RNA fragmentation prior to immunoprecipitation, spatial resolution and regional mapping of BICC1 binding to its RNA targets can be achieved. Therefore, aligned reads from each BICC1 fRIP replicate were analysed on the UCSC Genome Browser. First, the top three most significantly enriched BICC1-bound RNAs were assessed. Figure 5.2.3.1 demonstrates that BICC1 binds the 3' UTR of *JUND* in all of the BICC1 fRIP replicates, with a preference to the start of the 3' UTR. We can be sure that this association is specific and true, and not due to any possible background effects, as no binding is observed in the *BICC1 KO* fRIP replicates. The BICC1 fRIP input reads are displayed at the top of Figure 5.2.3.1 to demonstrate that *JUND* is normally expressed and reads are counted across the entire transcript, and therefore it must be noted that the UCSC scale for the input is lower than the fRIPs because of this.

Figure 5.2.3.2 demonstrates that BICC1 binds the 3' UTR of *GLIS2* in all of the BICC1 fRIP replicates, with a preference to the distal end of the 3' UTR. We can be sure that this association is specific and true, and not due to any possible background effects, as no binding is observed in the *BICC1 KO* fRIP replicates. The BICC1 fRIP input reads are displayed at the top of Figure 5.2.3.2 to demonstrate that *GLIS2* is normally expressed and reads are counted across the entire transcript.

Figure 5.2.3.3 demonstrates that BICC1 binds the 3' UTR of *CHPF* in all of the BICC1 fRIP replicates, with a preference to the end of the 3' UTR. We can be sure that this association is specific and true, and not due to any possible background effects, as no binding is observed in the *BICC1 KO* fRIP replicates. The BICC1 fRIP input reads are displayed at the top of Figure 5.2.3.3 to demonstrate that *CHPF* is normally expressed and reads are counted across the entire transcript.

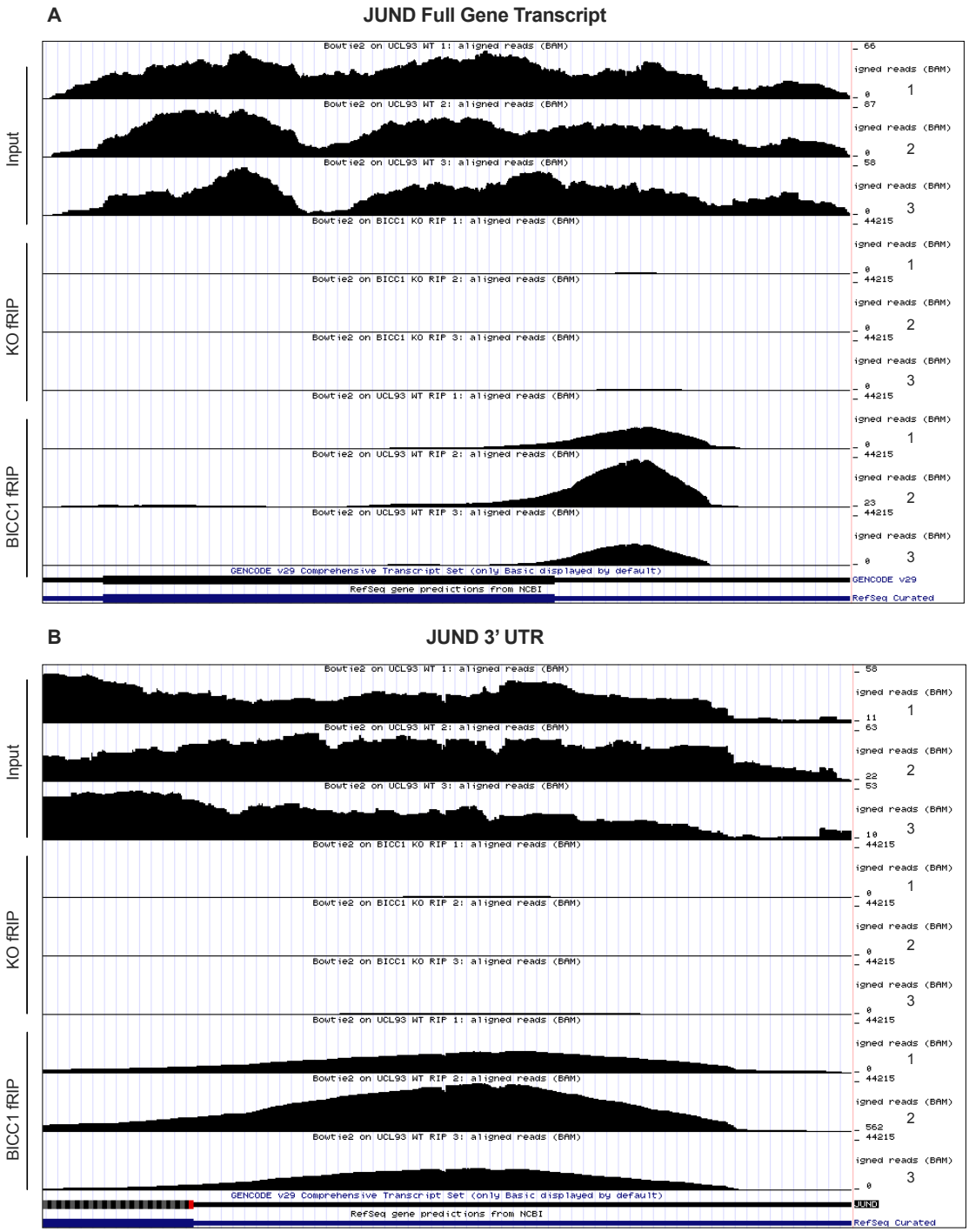

Figure 5.2.3.1. BICC1 associates with the 3' UTR of *JUND*. A) Reads from BICC1 fRIP were mapped to the known gene transcript on the UCSC Genome Browser and compared to the input and *BICC1 KO* fRIP. The maximum UCSC scale was set to 42215 for the fRIP, while the inputs were set to auto scale. **B)** A zoomed view of the 3' UTR reads. UTR = untranslated region.

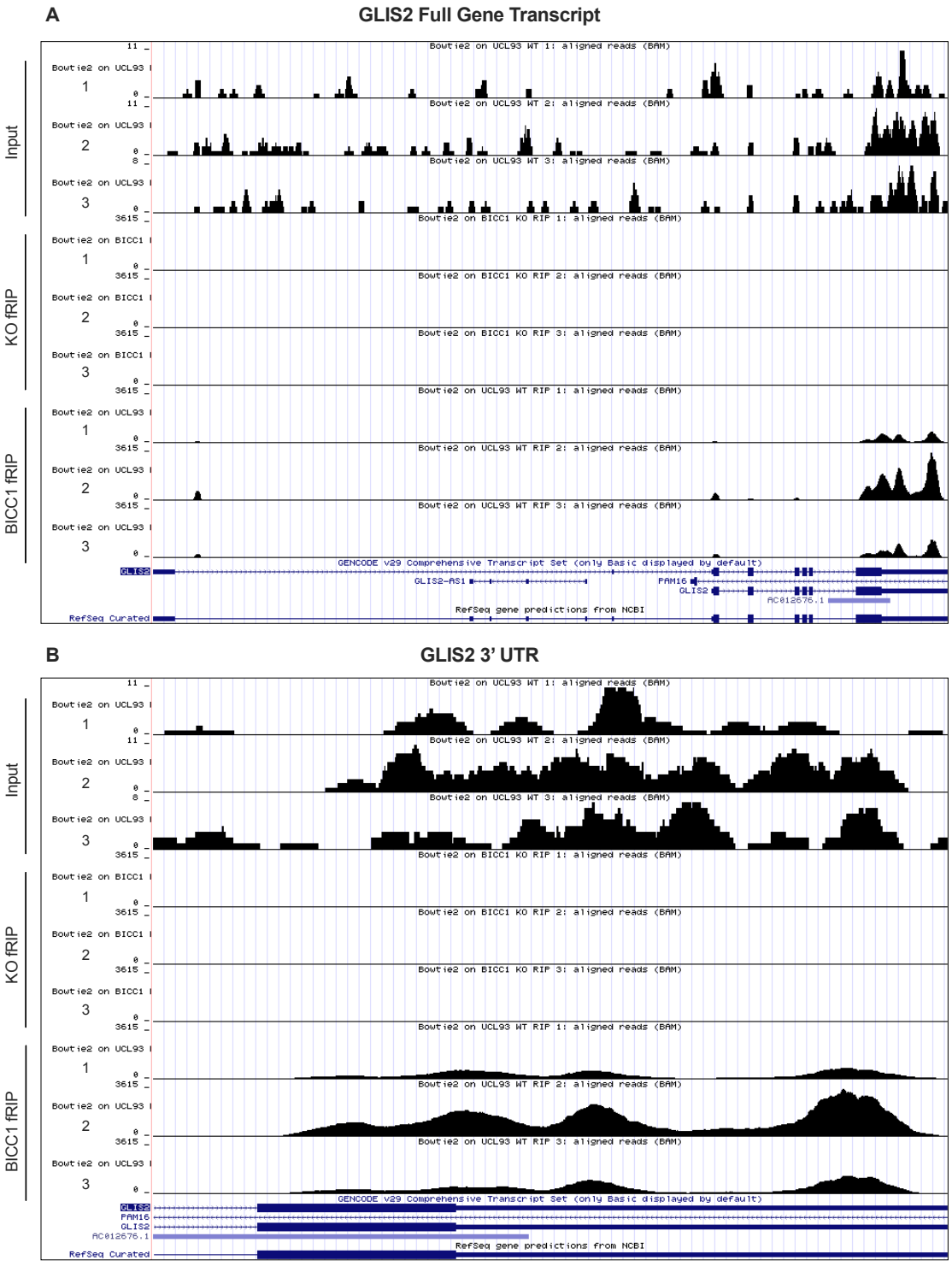

Figure 5.2.3.2. BICC1 associates with the 3' UTR of *GLIS2*. A) Reads from BICC1 fRIP were mapped to the known gene transcript on the UCSC Genome Browser and compared to the input and *BICC1 KO* fRIP. The maximum UCSC scale was set to 3615 for the fRIP, while the inputs were set to auto scale. **B)** A zoomed view of the 3' UTR reads. UTR = untranslated region.

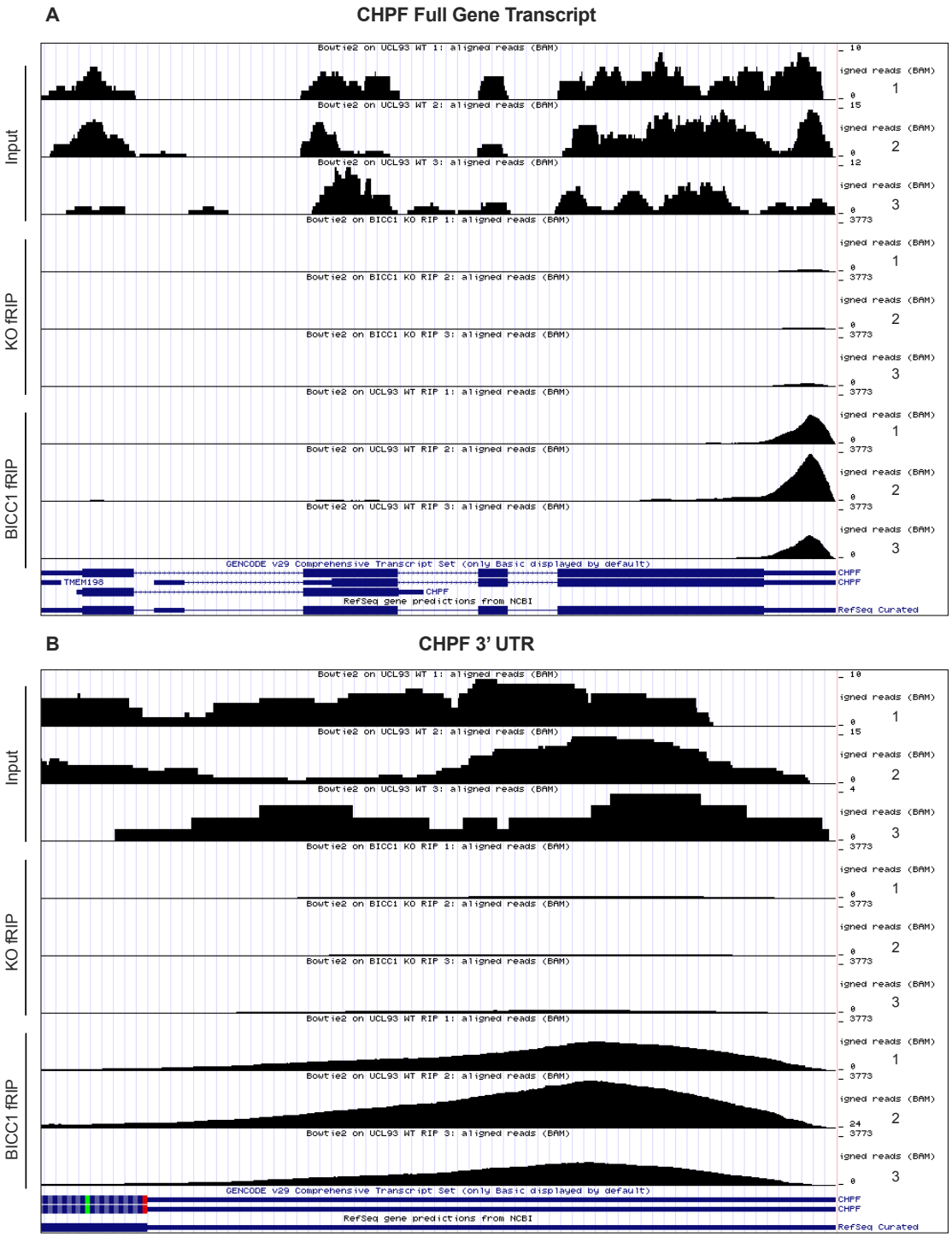

Figure 5.2.3.3. BICC1 associates with the 3' UTR of *CHPF.* A) Reads from BICC1 fRIP were mapped to the known gene transcript on the UCSC Genome Browser and compared to the input and *BICC1 KO* fRIP. The maximum UCSC scale was set to 3773 for the fRIP, while the inputs were set to auto scale. **B)** A zoomed view of the 3' UTR reads. UTR = untranslated region.

It is clear from the UCSC scales displayed Figures 5.2.3.1-3 that there is a variation between the number of reads, and therefore abundance, between each BICC1-RNA association. For example, the average number of reads for the association between BICC1 and the 3' UTR of *JUND* was 28,149, while for *GLIS2* and *CHPF* the average number of reads were 1943 and 2642 respectively (Figure 5.2.3.4). The relative average number of reads obtained from the BICC1 fRIP inputs at the 3' UTRs of *JUND*, *GLIS2* and *CHPF* were 38, 10 and 12 respectively. As the average number of reads did not greatly differ between the BICC1 fRIP inputs, it could be suggested that BICC1 has a higher interaction preference for the 3' UTR of *JUND* compared to *GLIS2* and *CHPF*.

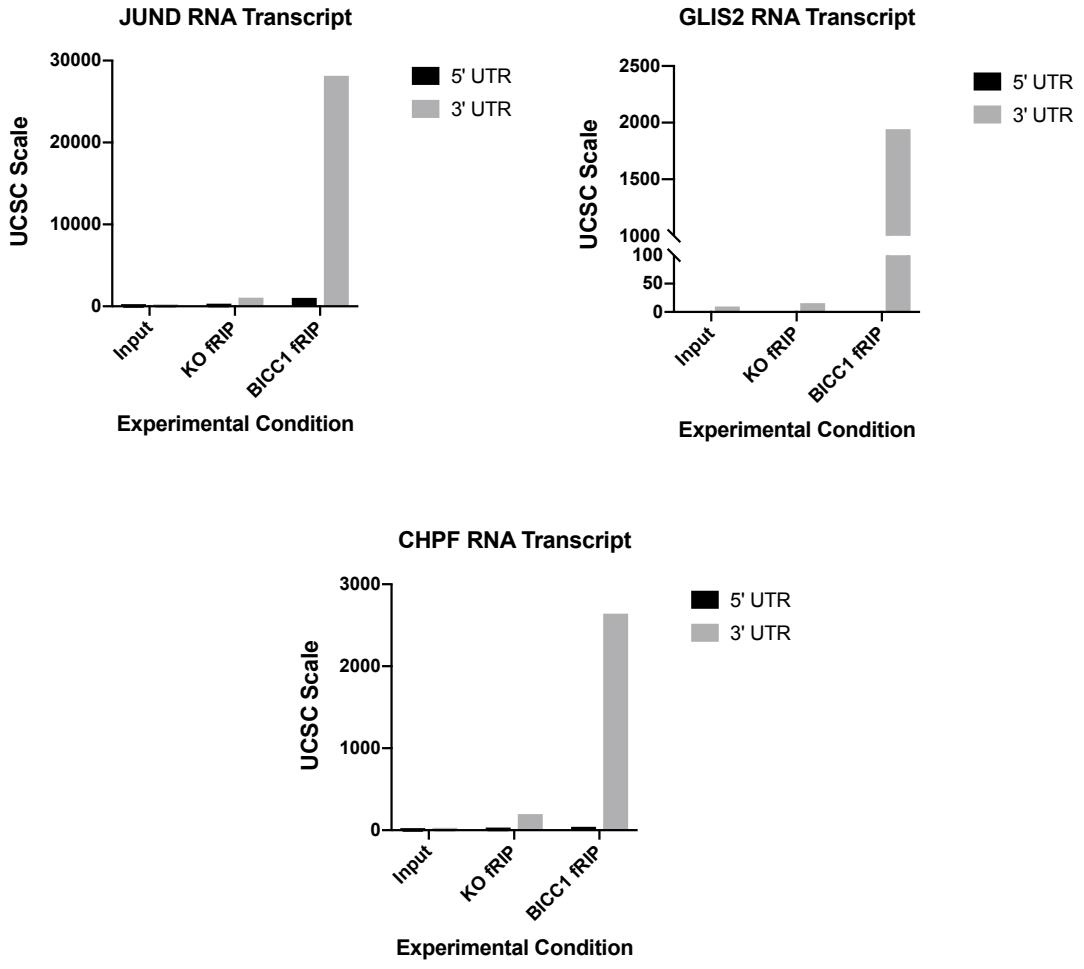

Figure 5.2.3.4. BICC1 associates with the RNA transcripts of *JUND*, *GLIS2* and *CHPF* at their 3 UTRs. Reads were mapped to the known gene transcript on UCSC Genome Browser and compared to the input and *BICC1 KO* fRIP. The data shown is the average read counts of all three replicates. The 5' UTR reads are coloured black while the 3' UTR reads are coloured grey.

Second, the published RNA targets of BICC1, discussed in section 5.2.6, were assessed. Figure 5.2.3.5 demonstrates that BICC1 binds the 3' UTR of *ADCY6* in all of the BICC1 fRIP replicates, with a preference to the end of the 3' UTR. We can be sure that this association is specific, and true and not due to any possible background effects, as no binding is observed in the 3'UTR of the *BICC1 KO* fRIP replicates. However, some reads can be observed in the first exon in both the BICC1 fRIP and the *BICC1 KO* fRIP. The reads displayed in the *BICC1 KO* fRIP suggest that the binding is unspecific in the BICC1 fRIP and should be disregarded. The BICC1 fRIP input reads for *ADCY6* are displayed at the top of Figure 5.2.3.5 to demonstrate that *ADCY6* is normally expressed and reads are counted across the entire transcript, and therefore it must be noted that the UCSC scale for the input is lower than the fRIPs because of this.

Figure 5.2.3.6 demonstrates that BICC1 binds the 5' UTR of *DVL2* in all of the BICC1 fRIP replicates. We can be sure that this association is specific and true, and not due to any possible background effects, as no binding is observed in the *BICC1 KO* fRIP replicates. The BICC1 fRIP input reads are displayed at the top of Figure 5.2.3.6 to demonstrate that *DVL2* is normally expressed and reads are counted across the entire transcript.

Figure 5.2.3.7 demonstrates that BICC1 binds the 3' UTR of *WNT7B* in all of the BICC1 fRIP replicates, with a preference to the end of the 3' UTR. We can be sure that this association is specific and true, and not due to any possible background effects, as no binding is observed in the *BICC1 KO* fRIP replicates. The BICC1 fRIP input reads are displayed at the top of Figure 5.2.3.7 to demonstrate that *WNT7B* is normally expressed and reads are counted across the entire transcript.

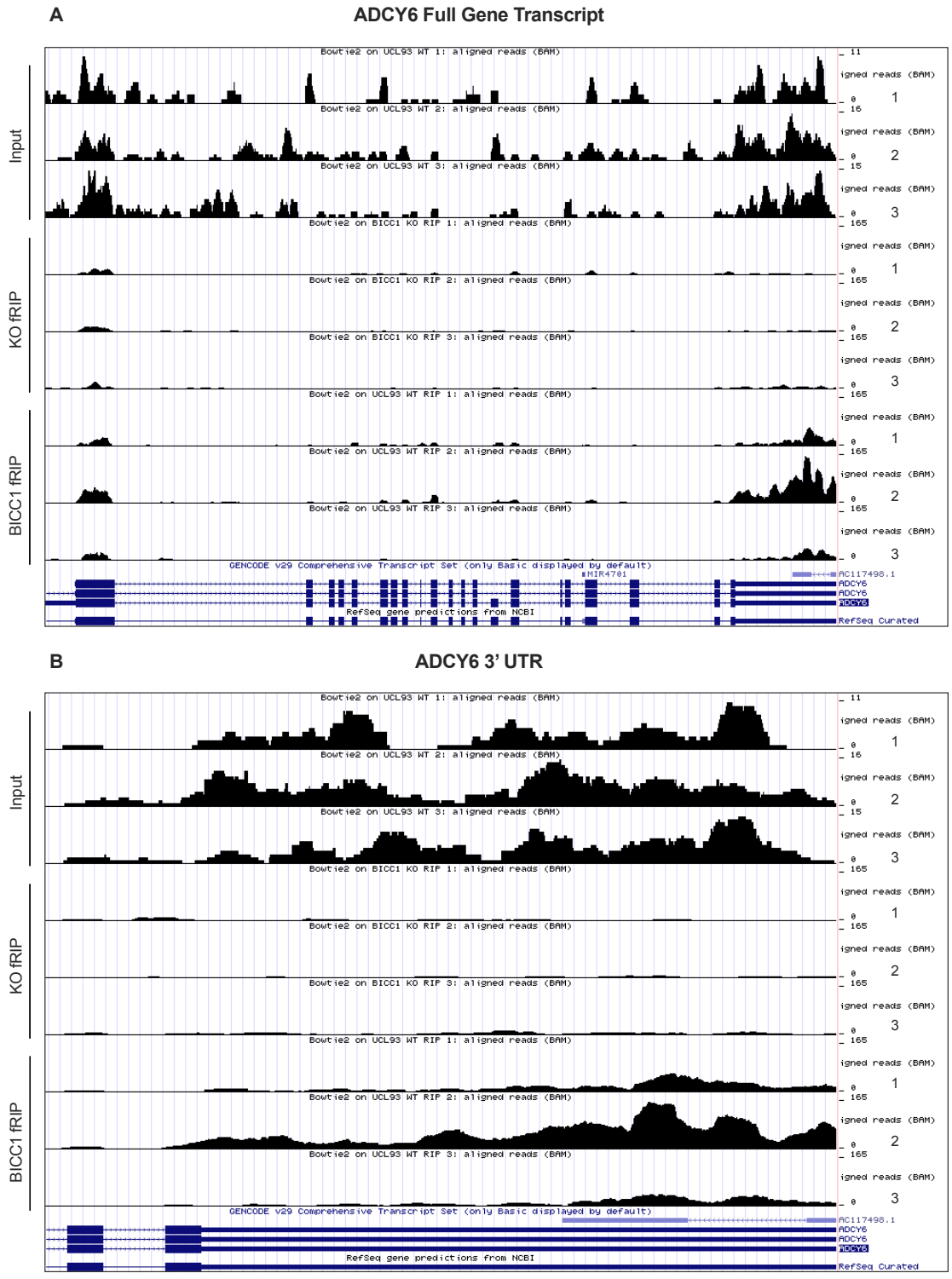

Figure 5.2.3.5. BICC1 associates with the 3' UTR of *ADCY6*. A) Reads from BICC1 fRIP were mapped to the known gene transcript on the UCSC Genome Browser and compared to the input and *BICC1 KO* fRIP. The maximum UCSC scale was set to 165 for the fRIP, while the inputs were set to auto scale. **B)** A zoomed view of the 3' UTR reads. UTR = untranslated region.

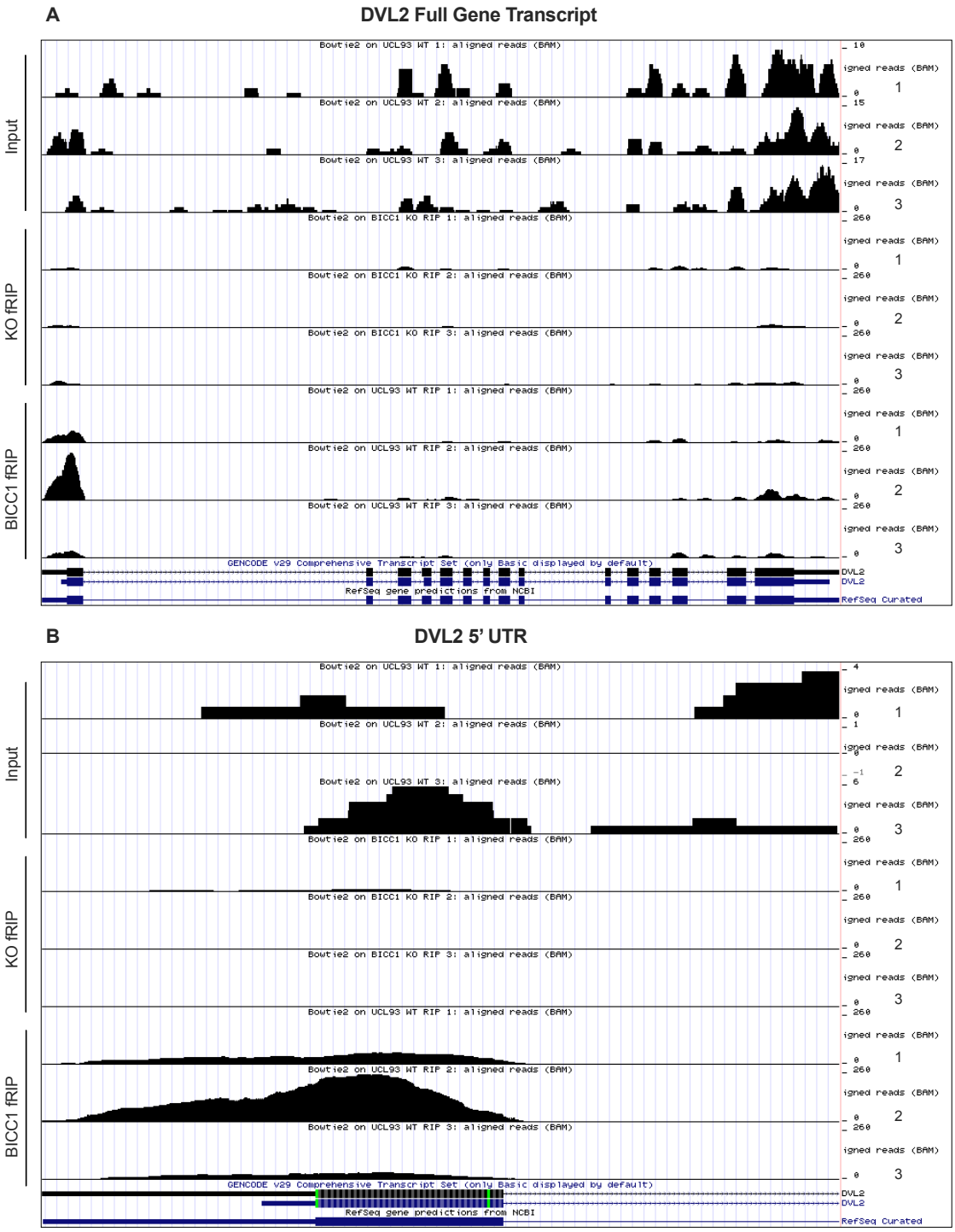

Figure 5.2.3.6. BICC1 associates with the 5' UTR of *DVL2*. A) Reads from BICC1 fRIP were mapped to the known gene transcript on the UCSC Genome Browser and compared to the input and *BICC1 KO* fRIP. The maximum UCSC scale was set to 268 for the fRIP, while the inputs were set to auto scale. **B)** A zoomed view of the 5' UTR reads. UTR = untranslated region.

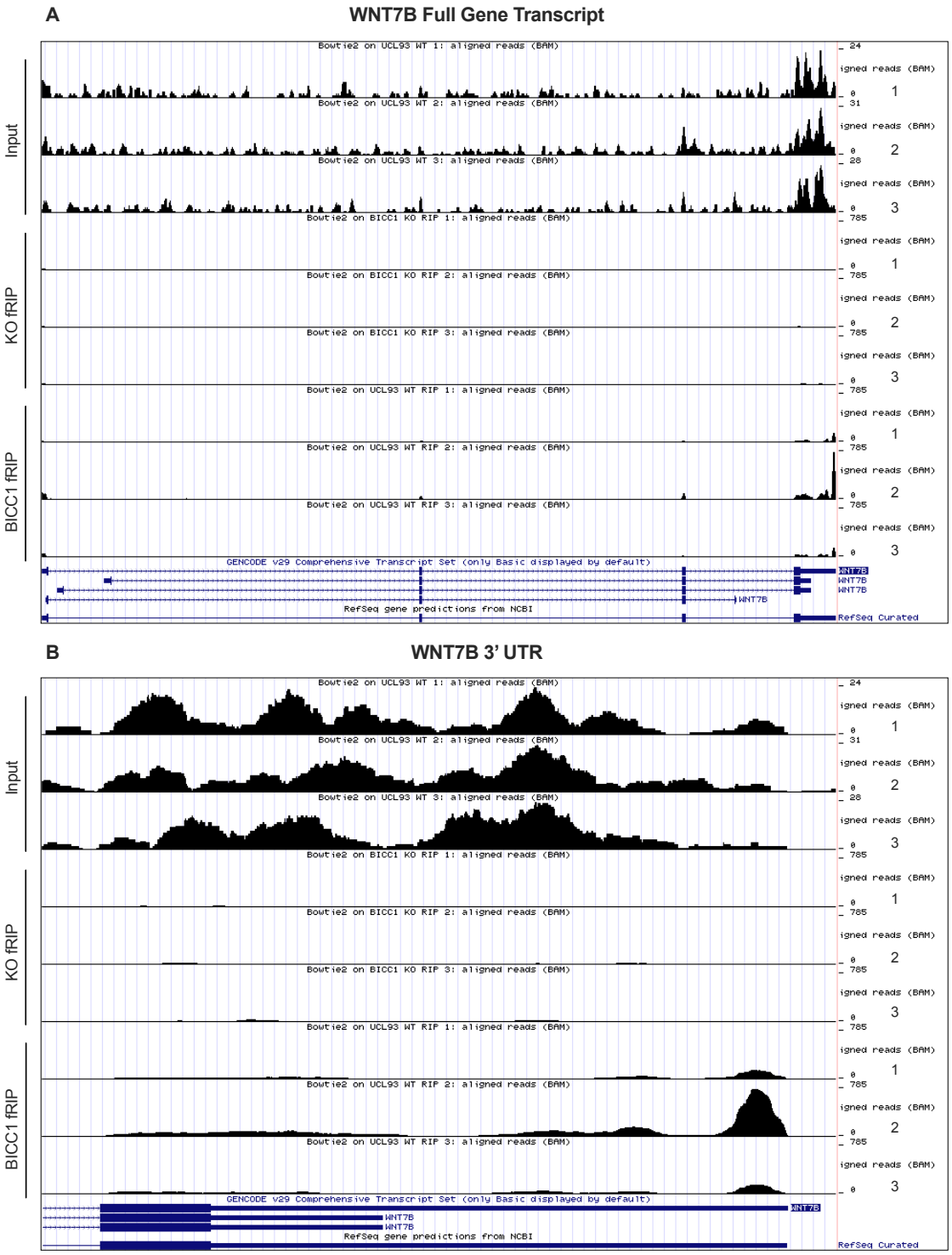

Figure 5.2.3.7. BICC1 associates with the 3' UTR of *WNT7B*. A) Reads from BICC1 fRIP were mapped to the known gene transcript on the UCSC Genome Browser and compared to the input and *BICC1 KO* fRIP. The maximum UCSC scale was set to 785 for the fRIP, while the inputs were set to auto scale. **B)** A zoomed view of the 3' UTR reads. UTR = untranslated region.

It is clear from the UCSC scales displayed Figures 5.2.3.5-7 that there is a variation between the number of reads, and therefore abundance, between each BICC1-RNA association. For example, the average number of reads for the association between BICC1 and the 5' UTR of *DVL2* was 122, while for the 3' UTRs of *ADCY6* and *WNT7B* the average number of reads were 91 and 363 respectively (Figure 5.2.3.8). The relative average number of reads obtained from the BICC1 fRIP inputs at the 5' UTR of *DVL2* and the 3' UTRs of *ADCY6* and *WNT7B* were 3, 14 and 10 respectively. As the average number of reads did not greatly differ between the BICC1 fRIP inputs, it could be suggested that BICC1 has a higher interaction preference for the 3' UTR of *WNT7B* compared to the 3' UTR of *ADCY6* and the 5' UTR of *DVL2*.

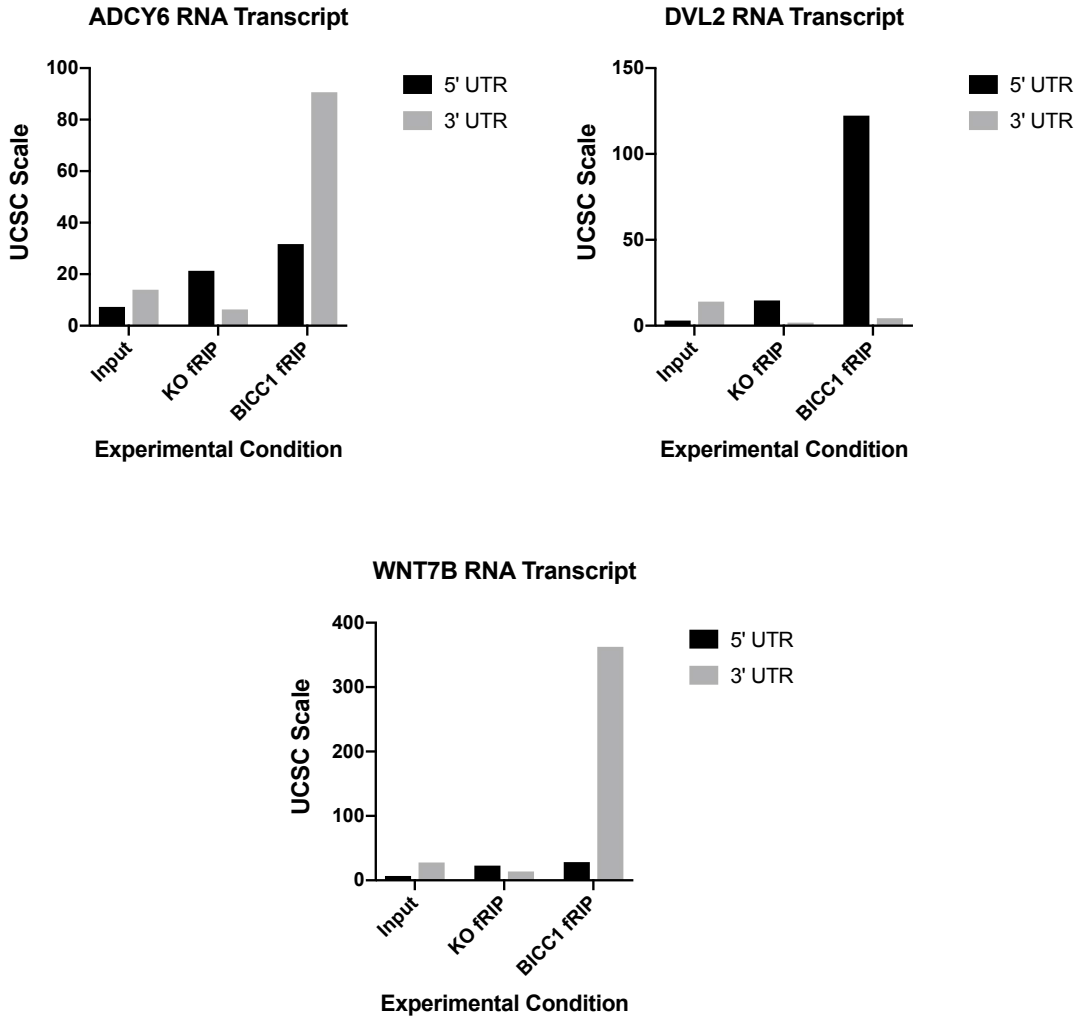

Figure 5.2.3.8. BICC1 associates with the RNA transcripts of *ADCY6* and *WNT7B* at their 3 UTRs but at the 5'UTR of *DVL2*. Reads were mapped to the known gene transcript on UCSC Genome Browser and compared to the input and *BICC1 KO* fRIP. The data shown is the average read counts of all three replicates. The 5' UTR reads are coloured black while the 3' UTR reads are coloured grey.

Third, the RNAs shown to be regulated by BICC1 in this study, as discussed in section 5.2.2, as well as its own RNA were assessed. Figure 5.2.3.9 demonstrates that BICC1 binds the 3' UTR of *PKD1* in all of the BICC1 fRIP replicates, with a preference to the end of the 3' UTR. We can be sure that this association is specific and true, and not due to any possible background effects, as no binding is observed in the 3'UTR of the *BICC1 KO* fRIP replicates. The BICC1 fRIP input reads for *PKD1* are displayed at the top of Figure 5.2.3.9 to demonstrate that *PKD1* is normally expressed and reads are counted across the entire transcript, and therefore it must be noted that the UCSC scale for the input is lower than the fRIPs because of this.

Figure 5.2.3.10 demonstrates that BICC1 binds the 3' UTR of *PKD2* in all of the BICC1 fRIP replicates, with a preference to the end of the 3' UTR. We can be sure that this association is specific and true, and not due to any possible background effects, as no binding is observed in the *BICC1 KO* fRIP replicates. However, some reads can be observed in the first exon in both the BICC1 fRIP and the *BICC1 KO* fRIP. The reads displayed in the *BICC1 KO* fRIP suggests that the binding in unspecific in the BICC1 fRIP and should be disregarded. The BICC1 fRIP input reads are displayed at the top of Figure 5.2.3.10 to demonstrate that *PKD2* is normally expressed and reads are counted across the entire transcript.

Figure 5.2.3.11 demonstrates that BICC1 binds the 3' UTR of *ANKS3* in all of the BICC1 fRIP replicates, with a preference to the start of the 3' UTR. We can be sure that this association is specific and true, and not due to any possible background effects, as no binding is observed in the *BICC1 KO* fRIP replicates. The BICC1 fRIP input reads are displayed at the top of Figure 5.2.3.11 to demonstrate that *ANKS3* is normally expressed and reads are counted across the entire transcript.

Figure 5.2.3.12 demonstrates that BICC1 does not bind its own RNA, as no significant reads can be observed. Some reads can be observed towards the 5' UTR, however, there are also reads in the *BICC1 KO* fRIP replicates, suggesting these may be sequencing adaptor reads. The BICC1 fRIP input

reads are displayed at the top of Figure 5.2.3.12 to demonstrate that BICC1 is normally expressed and reads are counted across the entire transcript.

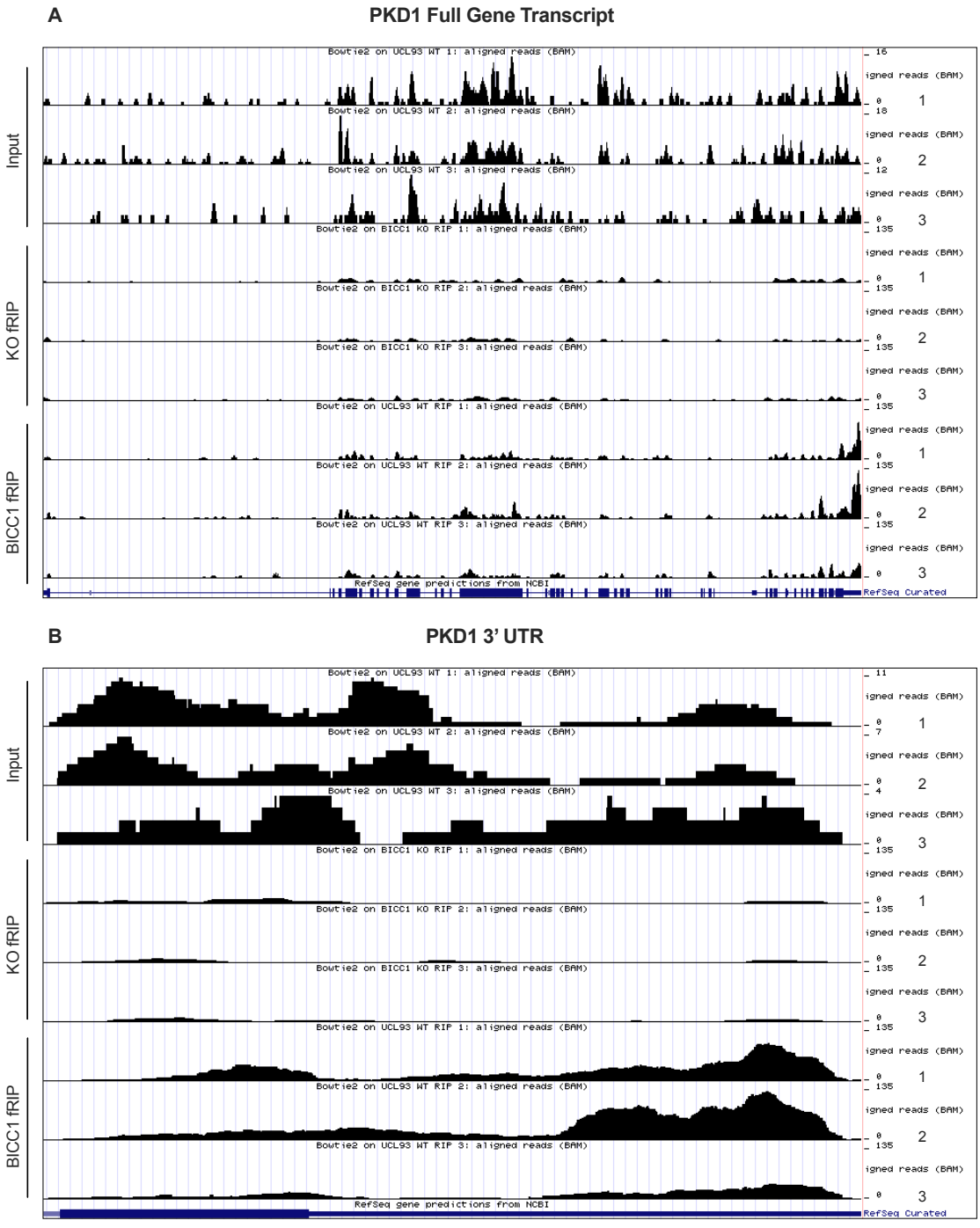

Figure 5.2.3.9. BICC1 associates with the 3' UTR of *PKD1*. A) Reads from BICC1 fRIP were mapped to the known gene transcript on the UCSC Genome Browser and compared to the input and *BICC1 KO* fRIP. The maximum UCSC scale was set to 135 for the fRIP, while the inputs were set to auto scale. **B)** A zoomed view of the 3' UTR reads. UTR = untranslated region.

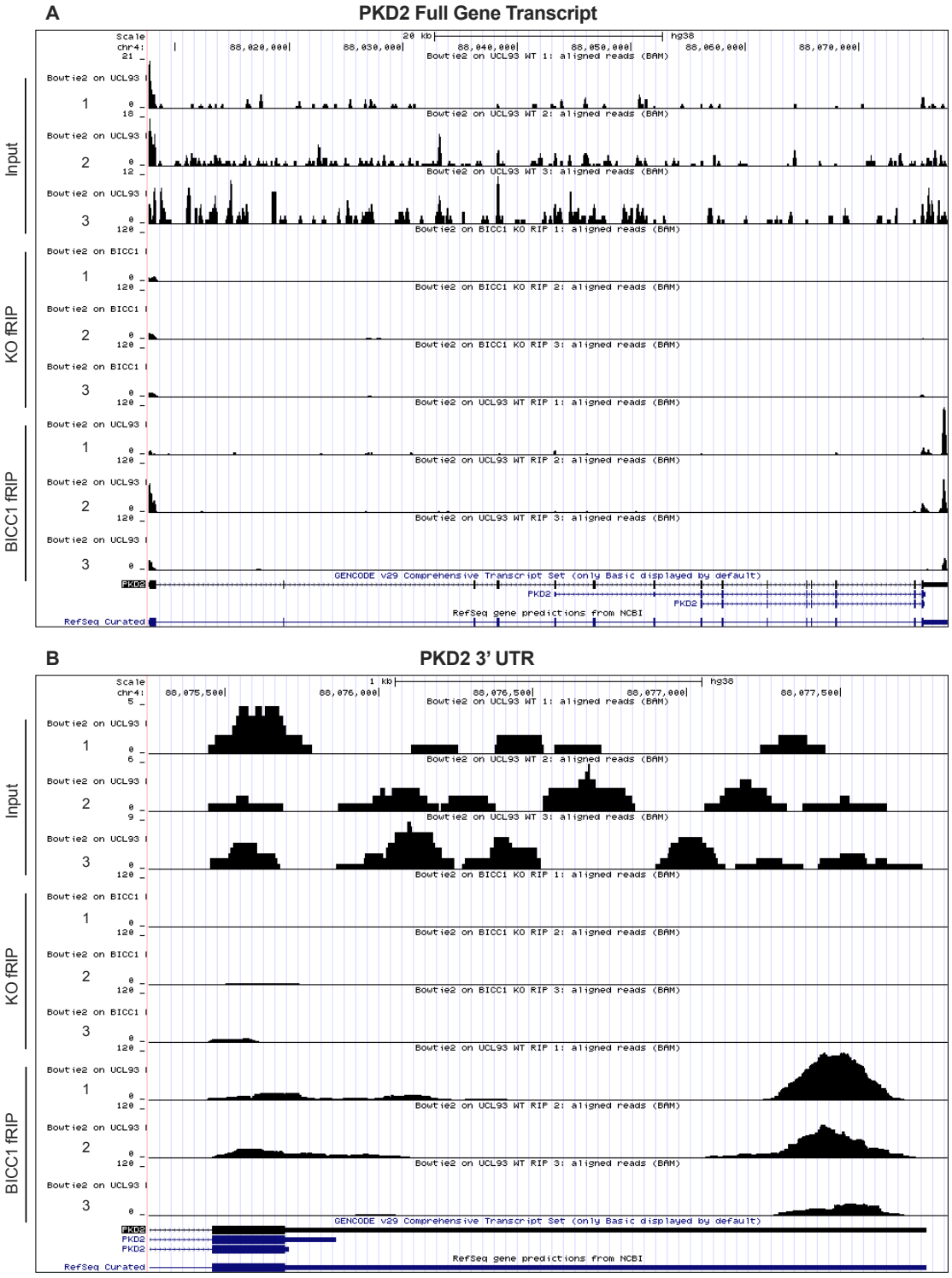

Figure 5.2.3.10. BICC1 associates with the 3' UTR of *PKD2*. A) Reads from BICC1 fRIP were mapped to the known gene transcript on the UCSC Genome Browser and compared to the input and *BICC1 KO* fRIP. The maximum UCSC scale was set to 120 for the fRIP, while the inputs were set to auto scale. **B)** A zoomed view of the 3' UTR reads. UTR = untranslated region.

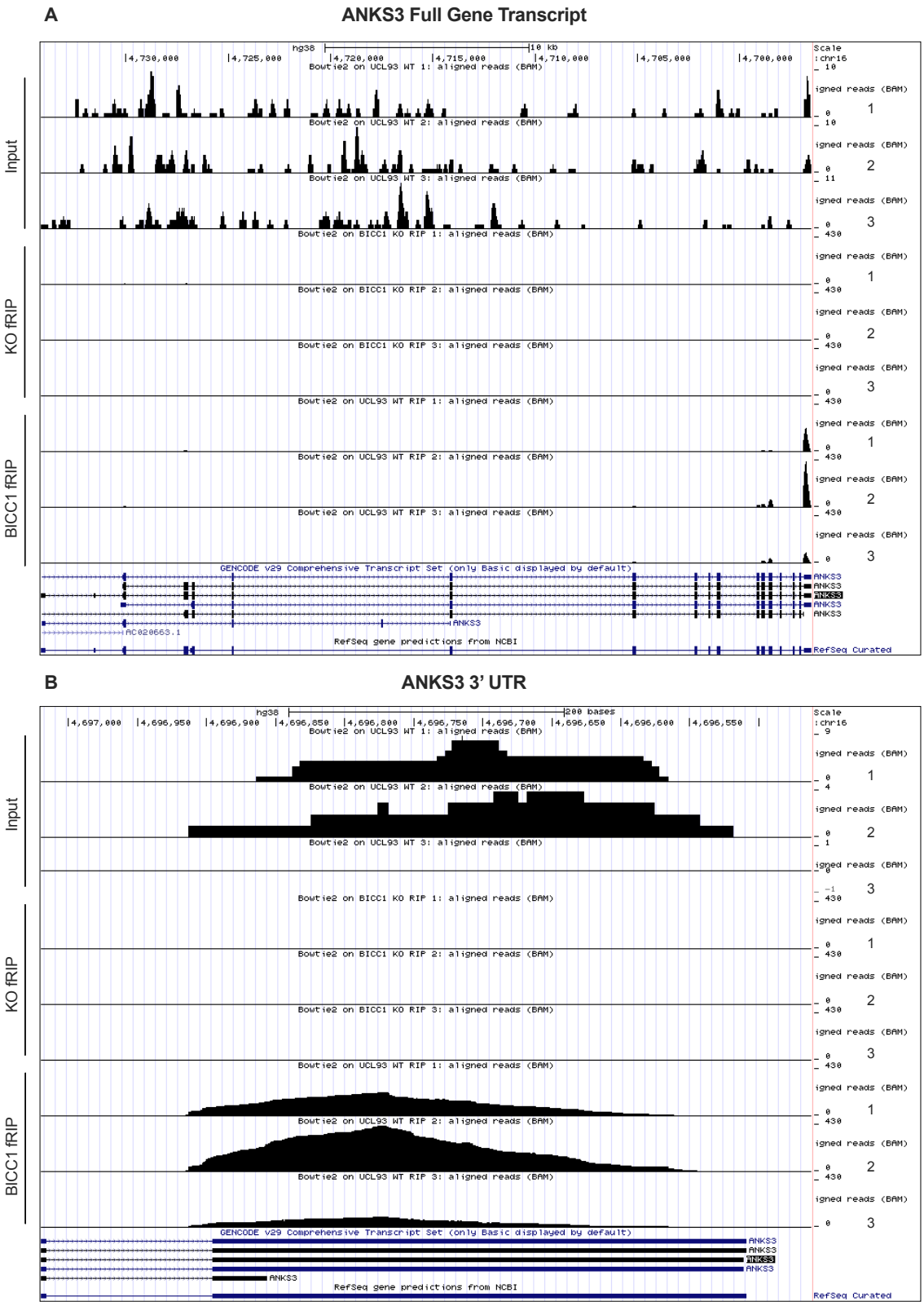

Figure 5.2.3.11. BICC1 associates with the 3' UTR of *ANKS3*. A) Reads from BICC1 fRIP were mapped to the known gene transcript on the UCSC Genome Browser and compared to the input and *BICC1 KO* fRIP. The maximum UCSC scale was set to 430 for the fRIP, while the inputs were set to auto scale. **B)** A zoomed view of the 3' UTR reads. UTR = untranslated region.

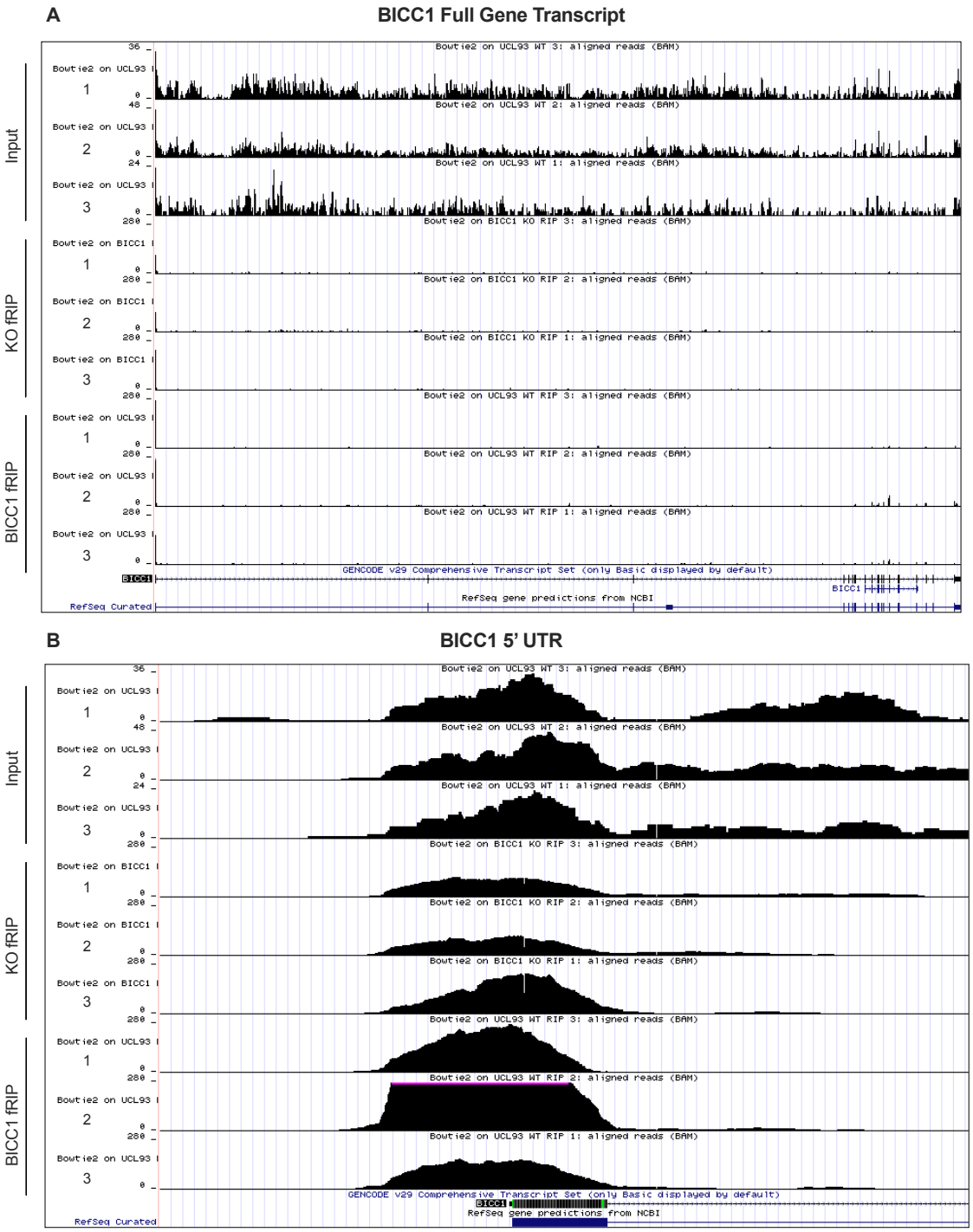

Figure 5.2.3.12. BICC1 does not associate with its own RNA transcript. A) Reads from BICC1 fRIP were mapped to the known gene transcript on the UCSC Genome Browser and compared to the input and *BICC1 KO* fRIP. The maximum UCSC scale was set to 280 for the fRIP, while the inputs were set to auto scale. **B)** A zoomed view of the 5' UTR reads. UTR = untranslated region.

It is clear from the UCSC scales displayed Figures 5.2.3.9-12 that there is a variation between the number of reads, and therefore abundance, between each BICC1-RNA association. For example, the average number of reads for the association between BICC1 and the 3' UTR of *PKD1* was 93, while for *PKD2* and *ANKS3* the average number of reads were 77 and 251 respectively (Figure 5.2.3.13). The relative average number of reads obtained from the BICC1 fRIP inputs at the 3' UTRs of *PKD1*, *PKD2* and *ANKS3* were 3, 7 and 4 respectively. As the average number of reads did not greatly differ between the BICC1 fRIP inputs, it could be suggested that BICC1 has a higher interaction preference for the 3' UTR of *ANKS3* compared to *PKD1* and *PKD2*. Data presented in Figure 5.2.3.13 also demonstrates that BICC1 does not associate with its own RNA, as the reads observed toward the 5' UTR in the BICC1 fRIP (291) were also present in the *BICC1 KO* fRIP (153) to a relative scale.

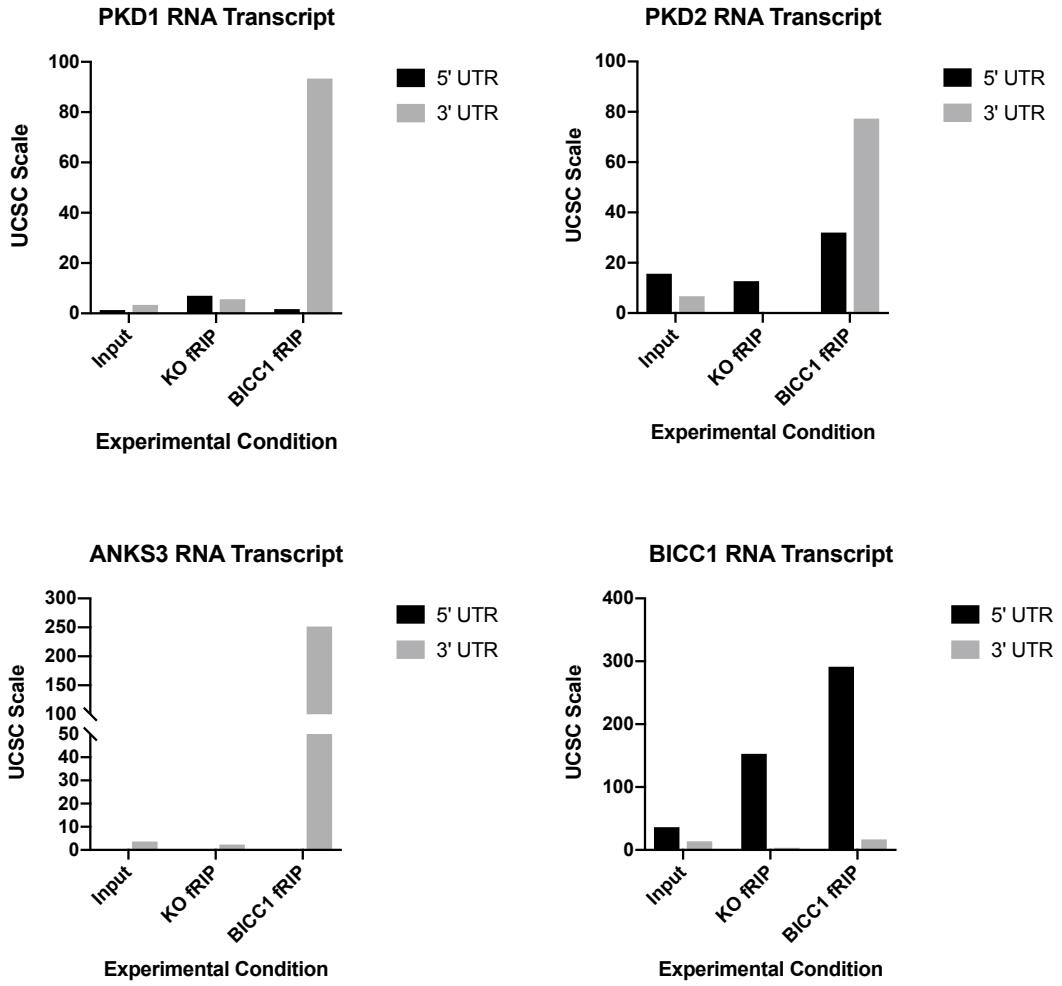

Figure 5.2.3.13. BICC1 associates with the RNA transcripts of *PKD1*, *PKD2* and *ANKS3* at their 3 UTRs. Reads were mapped to the known gene transcript on UCSC Genome Browser and compared to the input and *BICC1 KO* fRIP. The data shown is the average read counts of all three replicates. The 5' UTR reads are coloured black while the 3' UTR reads are coloured grey.

5.2.4 Whole transcriptome expression analysis of BICC1 RNA targets by RIP and deep sequencing

As discussed in section 5.2.3, following the success of the BICC1 fRIP optimisation, the experiment was repeated, and the enriched RNA transcripts associated with BICC1 were analysed and identified by deep sequencing (fRIP-Seq). RNA transcripts from the fRIP input were also analysed by RNA-Seq, to 1) control for background associations in the fRIP-Seq data set and to 2) explore any differences in global transcriptome expression levels between UCL93 and *BICC1 KO* cell lines.

The RNA-Seq analysis was performed using the cloud-based software, BioJupies (Torre *et al*., 2018). The web-based application allows for rapid alignment of the raw FASTQ, paired-end reads obtained from the deep sequencing, as well as accurate mapping and alignment (by kallisto pseudoaligner) to a reference human genome to generate a gene count matrix and gene expression levels. The BioJupies software creates an interactive notebook where various outputs can be viewed and further explored. Before differential expression analysis on the fRIP input samples was conducted, the RNA-Seq dataset was subjected to various QC checks. First, the library size was assessed to check for consistent read count distribution between the samples. Second, principal component analysis (PCA) was performed to assess the similarity between the samples. Third, the samples groups were evaluated using Clustergrammer, a programme that assesses hierarchical clustering. Finally, the samples were assessed by volcano and MA plots, which visually demonstrate any significant changes in global expression between the samples.

As shown in Figure 5.2.4.1, the RNA-Seq dataset presented high variance between the UCL93 WT samples and the *BICC1 KO* samples. Consequently, the following differential expressional analysis generated cannot be viewed as reliable and reproducible, and therefore only general expression patterns are assessed and predicted statements and outcomes are made.

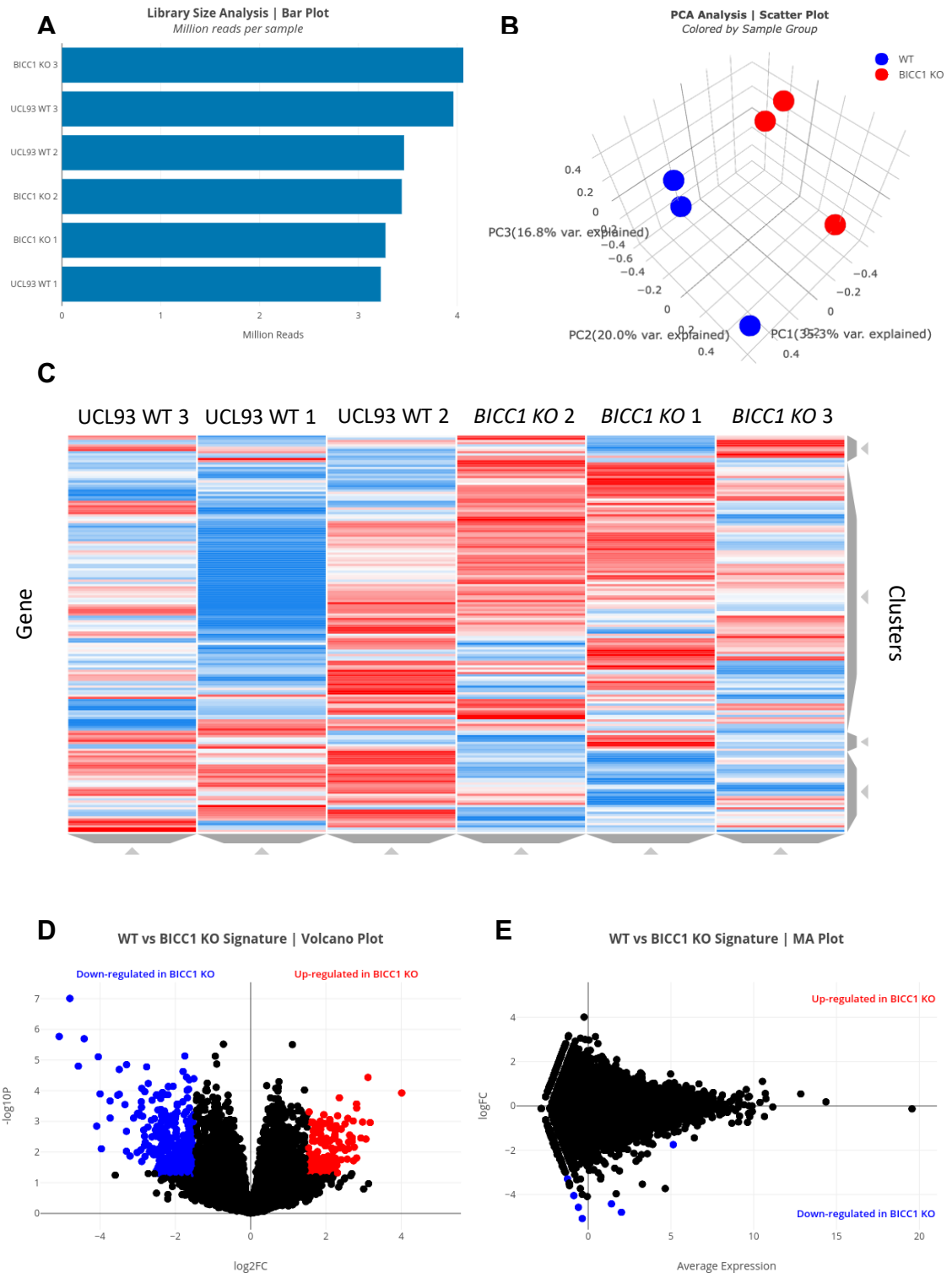

Figure 5.2.4.1. Quality control analysis of the whole transcriptome RNA-Seq dataset between UCL93 and *BICC1 KO* cell lines. A) The library size of each sample was assessed by raw read counts and shown as millions reads per sample. **B)** PCA analysis was performed to assess correlation between the samples. **C)** A clustergrammer plot to demonstrate hierarchical clustering between the samples. **D-E)** Volcano and MA plots to demonstrate significant changes in global expression between the samples. Circles coloured blue are RNA transcripts that are significantly downregulated, while circles coloured red are RNA transcripts that are significantly upregulated in *BICC1 KO* cells compared to UCL93 WT cells. PCA = principal component analysis.

The global differential expressional analysis presented in the volcano and MA plots in Figure 5.2.4.1 demonstrate that loss of BICC1 causes both an upregulation and a downregulation of various RNA transcripts, with the majority of transcript expression being downregulated. However, only 12 RNA transcripts were significantly regulated due to loss of BICC1 when expressed as logFC and with an adjusted p-value (adj. p-value) of 0.05 (Figure 5.2.4.2). Of these significantly regulated RNA transcripts, 11 were downregulated and only 1 was upregulated in *BICC1 KO* cells compared to UCL93 WT cells. The RNA transcript with the largest logFC was *CCND2* (-5.08), while the RNA transcript with the smallest logFC was *ACTN1* (-0.90). *FN1* (1.11), the only RNA transcript to be significantly upregulated in *BICC1 KO* cells, had the lowest adj. p-value (0.02), while *THBS1* (-0.72) has the lowest adj. p-value of the significantly downregulated RNA transcripts (0.02).

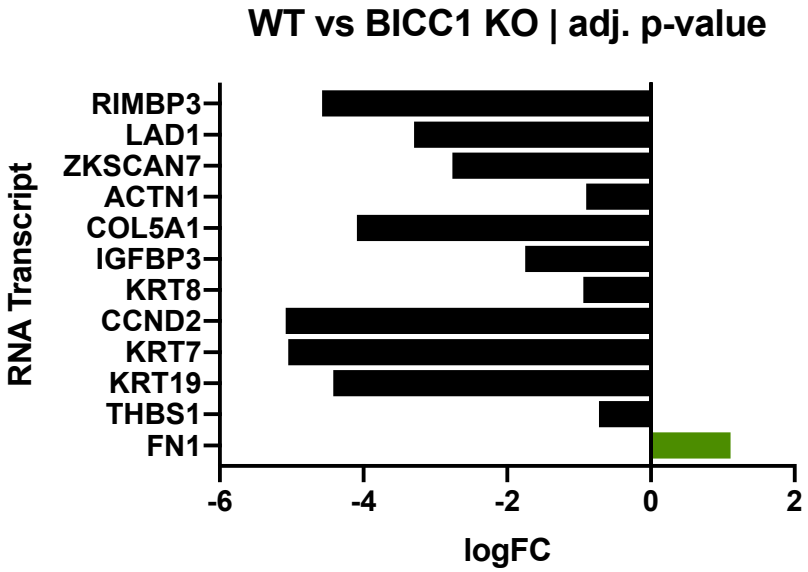

Figure 5.2.4.2. The most significant RNA transcripts differentially expressed between UCL93 and *BICC1 KO* cell lines. Significance was determined by assessing adjusted p-values and the hits are listed in descending order (0.048-0.021). logFC = log fold change.

To further understand the types of RNA transcripts BICC1 may be regulating in kidney epithelial cells, a table was produced to display further information regarding the gene name of the RNA transcripts and a summary of their known function (Table 5.2.4.1). Of interest, *FN1*, or fibronectin 1, was found to be upregulated in *BICC1 KO* cells and is a glycoprotein involved in cell adhesion and migration. In contrast, *THBS1*, or thrombospondin 1, is also a glycoprotein which mediates cell-to-cell and cell-to-matrix interactions but was found to be

downregulated in *BICC1 KO* cells. *CCND2*, or cyclin D2, forms a complex whose activity is required for cell cycle G1/S transition. Table 5.2.4.1 demonstrates that BICC1 may regulate a subset of RNA transcripts that function in cell adhesion, migration and interaction pathways, as well as the cell cycle, to maintain cellular integrity and homeostasis.

Table 5.2.4.1. An informative summary of the most significant RNA transcripts differentially expressed between UCL93 and *BICC1 KO* cell lines.

Gene ID	Gene Name	Differential Expression	Summary
FN1	Fibronectin 1	UP	A glycoprotein involved in cell adhesion and migration
THBS1	Thrombospondin 1	DOWN	An adhesive glycoprotein that mediates cell-to-cell and cell-to-matrix interactions
KRT19	Keratin 19	DOWN	Involved in the organization of myofibers
KRT7	Keratin 7	DOWN	Blocks interferon-dependent interphase and stimulates DNA synthesis in cells
CCND2	Cyclin D2	DOWN	This cyclin forms a complex with CDK4 or CDK6 and functions as a regulatory subunit of the complex, whose activity is required for cell cycle G1/S transition
KRT8	Keratin 8	DOWN	Together with KRT19, helps to link the contractile apparatus to dystrophin at the costameres of striated muscle
IGFBP3	Insulin Like Growth Factor Binding Protein 3	DOWN	Forms a ternary complex with IGFALS and either IGFs, prolonging their half-lives and altering their interaction with cell surface receptors
COL5A1	Collagen Type V Alpha 1 Chain	DOWN	This gene encodes an alpha chain for one of the low abundance fibrillar collagens
ACTN1	Actinin Alpha 1	DOWN	F-actin cross-linking protein which is thought to anchor actin to a variety of intracellular structures
ZKSCAN7	Zinc Finger With KRAB And SCAN Domains 7	DOWN	May be involved in transcriptional regulation
LAD1	Ladinin 1	DOWN	Anchoring filament protein which is a component of the basement membrane zone
RIMBP3	RIMS Binding Protein 3	DOWN	Component of the manchette, a microtubule-based structure which plays a key role in sperm head morphogenesis during late stages of sperm development

As there was high variance between the samples following RNA-Seq, the raw read counts of the RNA transcripts with significant differential expression were manually assessed. The numeric change in the raw read counts matched the differential expression analysis as for *FN1*, for example, the raw read count was much higher in *BICC1 KO* cells compared to UCL93 WT cells, while for *THBS1* the raw read count was lower in the *BICC1 KO* cells compared to the UCL93 WT cells (Figure 5.2.4.3 A). It must be noted that the number of raw read counts does vary between RNA transcripts depending on natural abundance. Therefore, the raw read counts for each individual RNA transcript were further analysed and displayed as a fold change value relative to UCL93 WT, which again were comparable to the differential expression analysis (Figure 5.2.4.3 B).

Considering the similarity between the differential expression analysis and the raw read counts of the most significant RNA transcripts, the raw read counts of *PKD1*, *PKD2*, *ANKS6* and *ANKS3* were analysed to assess whether their expression was altered between UCL93 and *BICC1 KO* cells. As observed in Figure 5.2.4.3 C, all RNA transcripts displayed a negative logFC, to varying degrees, demonstrating that they are downregulated in *BICC1 KO* cells. Their raw read counts also demonstrated a negative trend in expression, with reductions in raw reads of 50%, 45%, 20% and 25% respectively (Figure 5.2.4.3 D and E). To a certain extent, these levels of downregulated match the qPCR values obtained in Chapters 3 and 4. *SNRPA/U1* (or snRNA U1) was included as a control, as its expression levels do not change between UCL93 WT and *BICC1 KO* cells (assessed previously by qPCR in section 4.2.12 and 4.2.13). It must be noted that a high level of variation was observed for the *PKD1* RNA transcript, as well as it being the most abundant RNA transcript in this comparison.

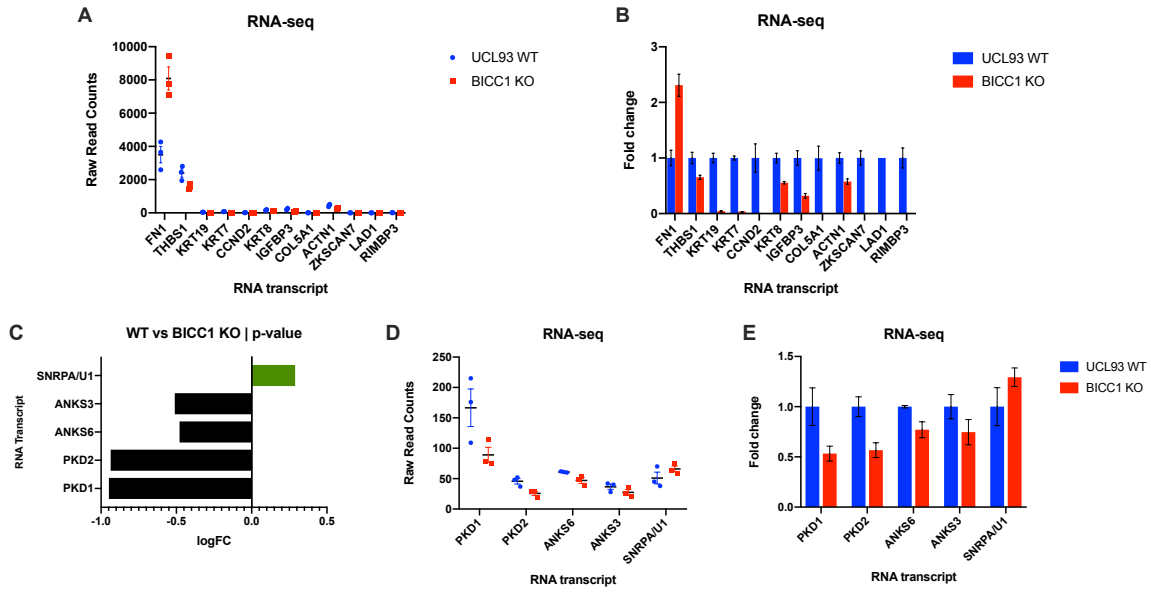

Figure 5.2.4.3. LogFC, raw read counts and calculated fold changes of RNA transcripts identified by RNA-Seq. A-B) The raw read counts and calculated fold change values of the significant RNA transcripts identified in the differential expression analysis. **C-E)** The differential expression logFC values, the raw read counts and calculated fold change values of RNA transcripts of interest to this study. Significance was determined by assessing adjusted p-values for **A-B** and p-values for **C-E** with a cut off value of 0.05. UCL93 WT cells are coloured blue while *BICC1 KO* cells are coloured red. logFC = log fold change.

To assess whether the 12 RNA transcripts significantly regulated due to loss of BICC1 are binding partners of BICC1, their BICC1 fRIP sequencing reads were aligned and mapped to a human reference genome of UCSC Genome Browser, as performed in section 5.2.3. Only two RNA transcripts, *KRT7* and *IGFBP3*, were found to be significantly enriched and bound to BICC1 when their logFC and adjusted p-value was assessed (<0.05). Figure 5.2.4.4 demonstrates that BICC1 binds both the 5' and the 3' UTR of *KRT7* in all of the BICC1 fRIP replicates, with a preference to the 5' UTR. We can be sure that this association is specific and true, and not due to any possible background effects, as no binding is observed in the *BICC1 KO* fRIP replicates. The BICC1 fRIP input reads are displayed at the top of Figure 5.2.4.4 to demonstrate that *KRT7* is normally expressed and reads are counted across the entire transcript, and therefore it must be noted that the UCSC scale for the input is lower than the fRIPs because of this.

Figure 5.2.4.5 demonstrates that BICC1 binds both the 5' UTR and the 3' UTR of *IGFBP3* in all of the BICC1 fRIP replicates, with a preference to the start of the 3' UTR. We can be sure that this association is specific and true, and not due to any possible background effects, as no binding is observed in the *BICC1 KO* fRIP replicates. The BICC1 fRIP input reads are displayed at the top of Figure 5.2.4.5 to demonstrate that *IGFBP3* is normally expressed and reads are counted across the entire transcript.

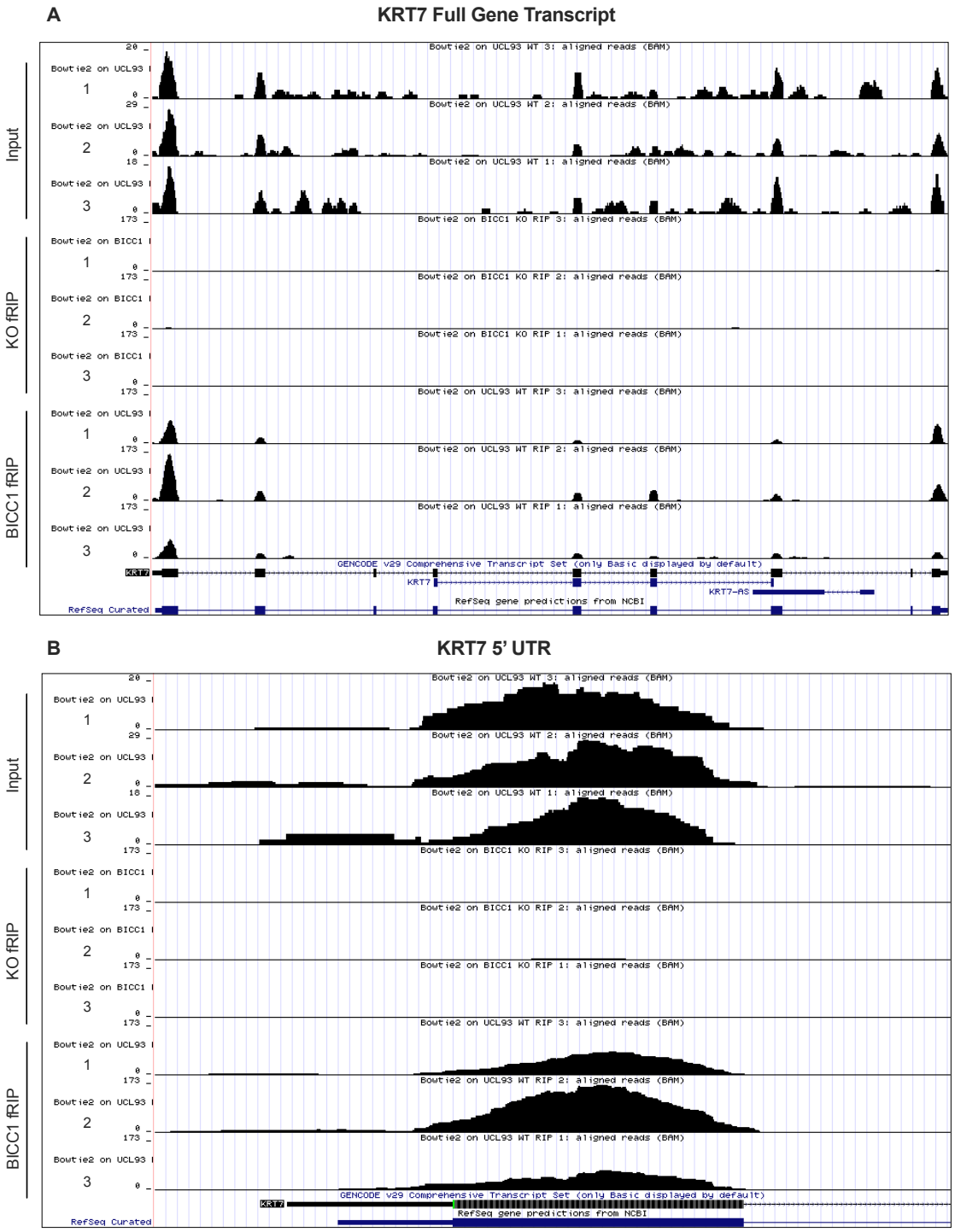

Figure 5.2.4.4. BICC1 associates with the 5' UTR of *KRT7*. A) Reads from BICC1 fRIP were mapped to the known gene transcript on the UCSC Genome Browser and compared to the input and *BICC1 KO* fRIP. The maximum UCSC scale was set to 173 for the fRIP, while the inputs were set to auto scale. **B)** A zoomed view of the 5' UTR reads. UTR = untranslated region.

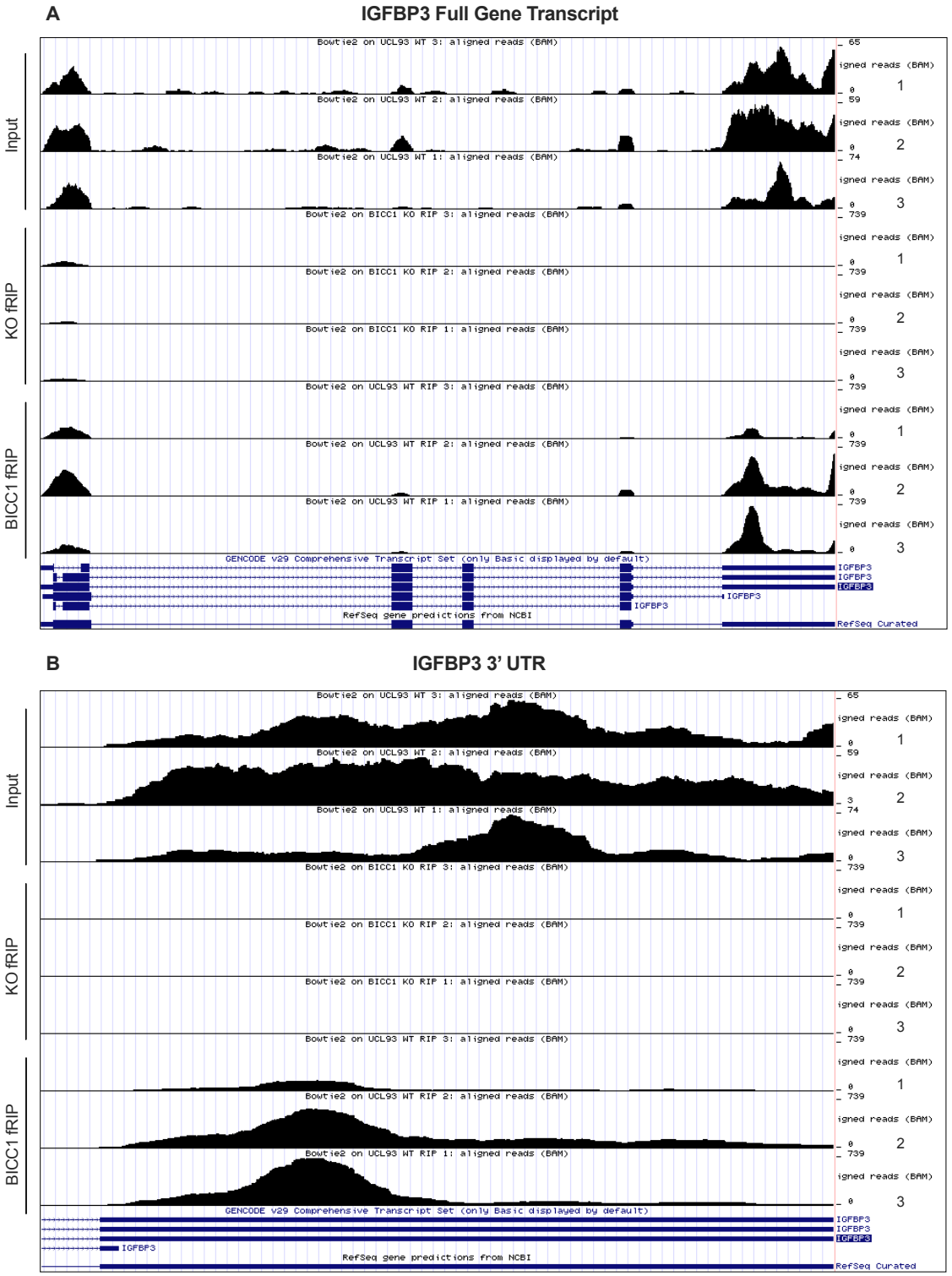

Figure 5.2.4.5. BICC1 associates with the 3' UTR of *IGFBP3*. A) Reads from BICC1 fRIP were mapped to the known gene transcript on the UCSC Genome Browser and compared to the input and *BICC1 KO* fRIP. The maximum UCSC scale was set to 739 for the fRIP, while the inputs were set to auto scale. **B)** A zoomed view of the 3' UTR reads. UTR = untranslated region.

It is clear from the UCSC scales displayed Figures 5.2.4.4 and 5.2.4.5 that there is a variation between the number of reads, and therefore abundance, between each BICC1-RNA association. For example, the average number of reads for the association between BICC1 and the 5' UTR of *KRT7* was 110, while for *IGFBP3* the average number of reads for its 3' UTR were 526 (Figure 5.2.4.6). The relative average number of reads obtained from the BICC1 fRIP inputs at the 5' UTRs of *KRT7* and *IGFBP3* were 22 and 32, while at the 3' UTRs they were 14 and 66 respectively. As the average number of reads did not greatly differ between the BICC1 fRIP inputs, it could be suggested that BICC1 has a higher interaction preference for the 3' UTR of *IGFBP3* compared to 5' UTR of *KRT7*.

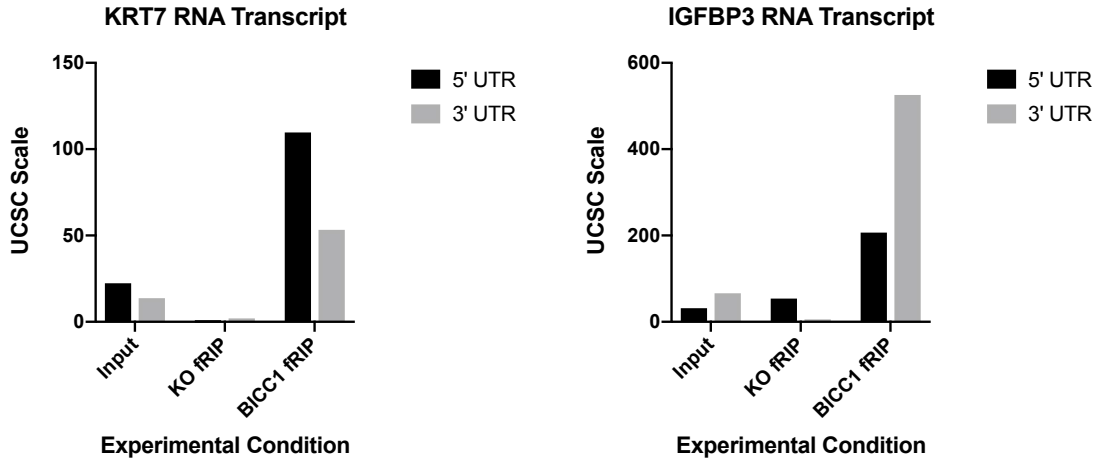

Figure 5.2.4.6. BICC1 associates with the RNA transcripts of *KRT7* and *IGFBP3* at different UTRs. Reads were mapped to the known gene transcript on UCSC Genome Browser and compared to the input and *BICC1 KO* fRIP. The data shown is the average read counts of all three replicates. The 5' UTR reads are coloured black while the 3' UTR reads are coloured grey.

Following the identification of the 10 most significantly BICC1-bound RNA transcripts in the previous section, their differential expression was assessed and is displayed in Figure 5.2.4.7. The results demonstrated that the majority of the RNA transcripts were downregulated when BICC1 expression was lost, with only *SCARB1* and *POLR2J* being upregulated, albeit with no significance. *GLIS2* was the only BICC1-bound RNA transcript that was significantly downregulated with a p-value <0.01 (Figure 5.2.4.7).

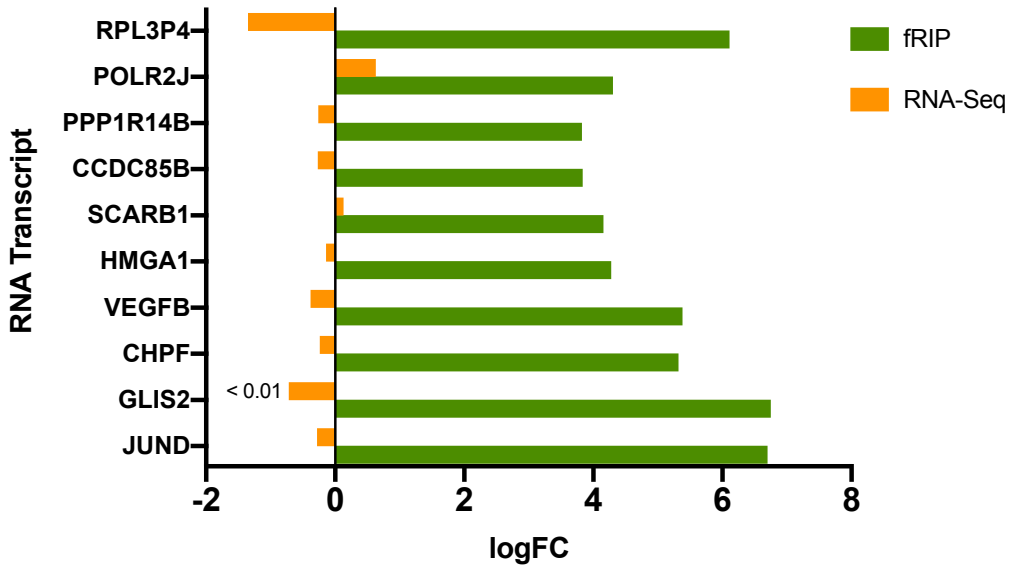

Figure 5.2.4.7. The differential expression analysis of the most significant BICC1-bound RNA transcripts. Significance was determined by assessing p-values with a cut off of 0.05. The BICC1-enriched RNAs and their corresponding expression are listed in descending order in regard to significance. The BICC1 fRIP dataset is displayed in green, while the BICC1 RNA-Seq dataset is displayed in orange. logFC = log fold change.

This study has identified novel RNA binding targets of BICC1, as well as uncovering patterns of RNA regulation when the expression of BICC1 is lost. Therefore, a comparison between the BICC1-bound RNA transcripts and their differential expression in *BICC1 KO* cells was performed. As a high level of variance was observed for the whole transcriptome dataset, only 12 RNA transcripts were significantly regulated upon loss of BICC1 when the adjusted p-value was set at a cut off of 0.05. Therefore, the dataset was re-analysed with a p-value set at a cut off of 0.05. The significant RNA transcripts were then compared to the significantly bound RNA transcripts with an adjusted p-value <0.05. In total there were 378 common transcripts identified between the BICC1 fRIP-Seq and BICC1 RNA-Seq datasets and Figure 5.2.4.8 demonstrates the 67 transcripts significantly enriched in various KEGG pathways.

The most significant pathway identified, when ranking p-values <0.05, was proteoglycans in cancer, which was also the most significant KEGG pathway identified in the BICC1 fRIP dataset. The proteoglycans in cancer pathway highlights proteoglycans and their downstream molecules that may contribute to cancer and to tumour progression through misregulation of proliferation, angiogenesis, adhesion and metastasis. Of interest, *SMO*, *WNT7B*, *ERBB2*,

MAPK12 and *VEGFA* were some of the transcripts enriched in this pathway. *SMO* is a G protein-couple receptor involved in signal transduction once activated by a hedgehog/patched protein. It is also required for the accumulation of *GLI2*, *GLI3* and *KIF7* in the cilia. *WNT7B*, or Wnt family member 7B, is a ligand for the frizzled receptor protein family which induce canonical Wnt/beta-catenin signalling. *ERBB2*, as discussed previously, is a tyrosine kinase and part of the EGF receptor family which mediate downstream signalling pathways such as the EGFR and GPCR pathways. *MAPK12* is a member of the mitogen-activated protein (MAP) kinase family and is a vital component of the MAP kinase signal transduction pathway which has been linked to the cell cycle and differentiation. *VEGFA*, as previously mentioned, is a growth factor involved in cell growth, angiogenesis and vasculogenesis.

It is important to note that although the RNA transcripts are all binding partners of BICC1, their expression is regulated by BICC1 to different extents. For example, Figure 3.4.2.9 shows that the differential expression analysis revealed *SMO* was massively downregulated compared to *MAPK12* and *VEGFA* (logFC values of -4.12, -0.40 and -0.37 respectively). *WNT7B* and *ERBB2* were also downregulated when BICC1 expression was lost, with logFC values of -1.31 and -0.85 respectively. However, BICC1 also strongly binds *PPARG*, with a fRIP logFC of 2.90, a nuclear receptor that modulates the gene transcription of fatty acids and is enriched in the transcriptional misregulation in cancer pathway. Conversely, an upregulation of *PPARG* was observed when BICC1 expression was lost (logFC 2.11). Therefore, this suggests that BICC1 binds and regulates certain RNA targets differently, possibly depending on the pathway or biological function they are involved in.

Figure 5.2.4.9 A demonstrates the logFC values of the 67 RNA transcripts in common between the BICC1 fRIP and BICC1 RNA-Seq datasets. Of interest are the RNA transcripts *AXN1*, *DVL2*, *ERBB2*, *MAPK12*, *MYC*, PLCB3, *PPARG*, *PPP2R2D*, *PPP2R3B*, *SMO*, *VEGFA* and *WNT7B* as these transcripts were highly common in several of the KEGG pathways analysed. Their enrichment logFC values is expanded in Figure 5.2.4.9 B. Furthermore, the expression data of the significantly enriched BICC1-RNA transcripts from the

cystic gene panel list discussed previously in section 5.2 and in Table 5.2.2.8 was extracted from the RNA-Seq dataset and displayed in Figure 5.2.4.9 C. There were only five transcripts significantly downregulated due to loss of BICC1 and these included *GLIS2*, *PKD1*, *PKD2*, *C21orf2* (*CFAP410*) and TSC2.

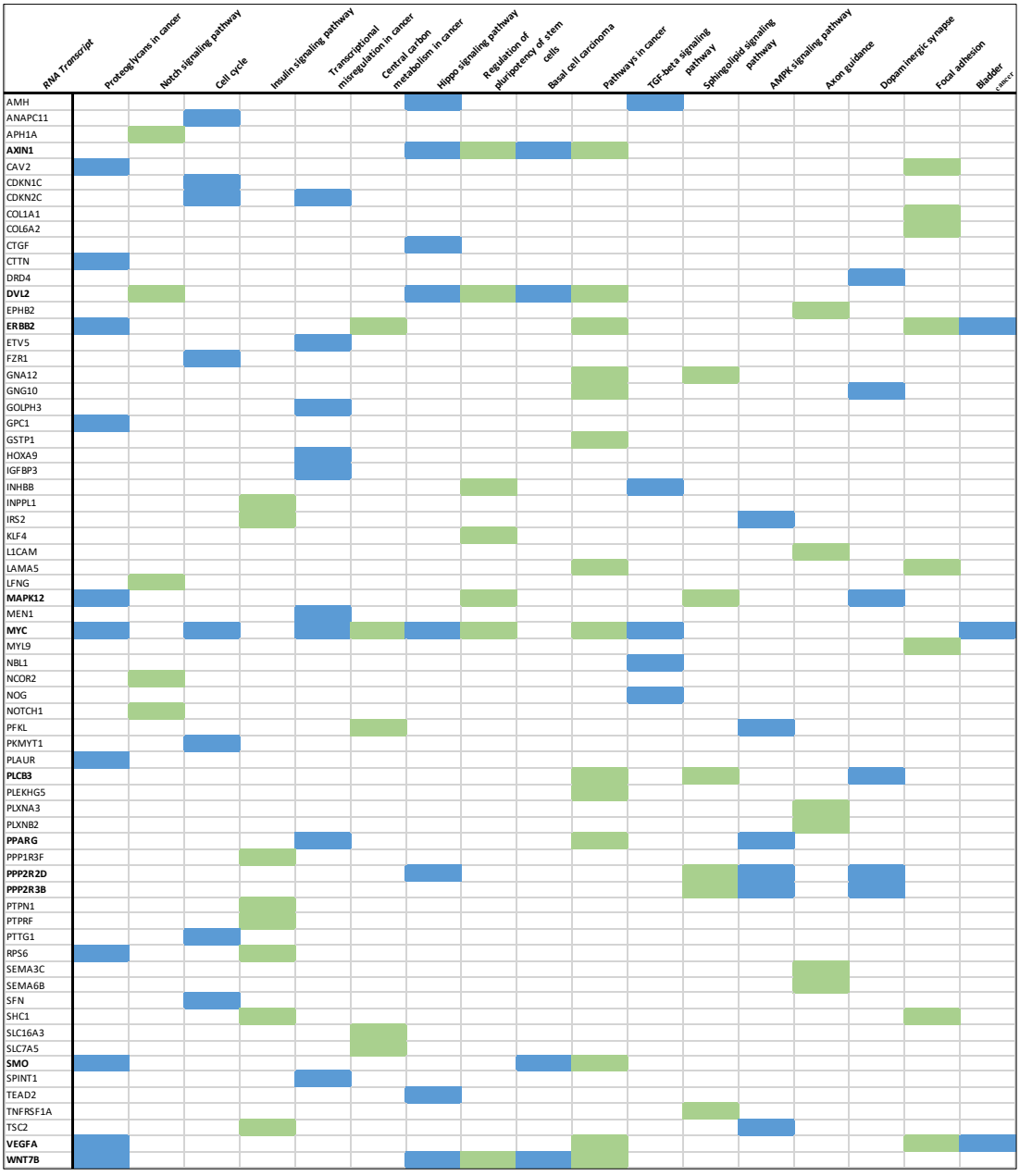

Figure 5.2.4.8. The common RNA transcripts significantly enriched in both the BICC1 fRIP and BICC1 RNA-Seq datasets identified by KEGG pathway analysis. KEGG pathway analysis was performed on the 378 common transcripts and 67 were found to be enriched within 17 significant pathways. The KEGG pathways are displayed from left to right in order of significance (p-value <0.05). The RNA transcripts highlighted in bold are transcripts that appear in three or more of the significant pathways analysed. Note: the green and blue colourings have no significance and are purely used as a visual aid.

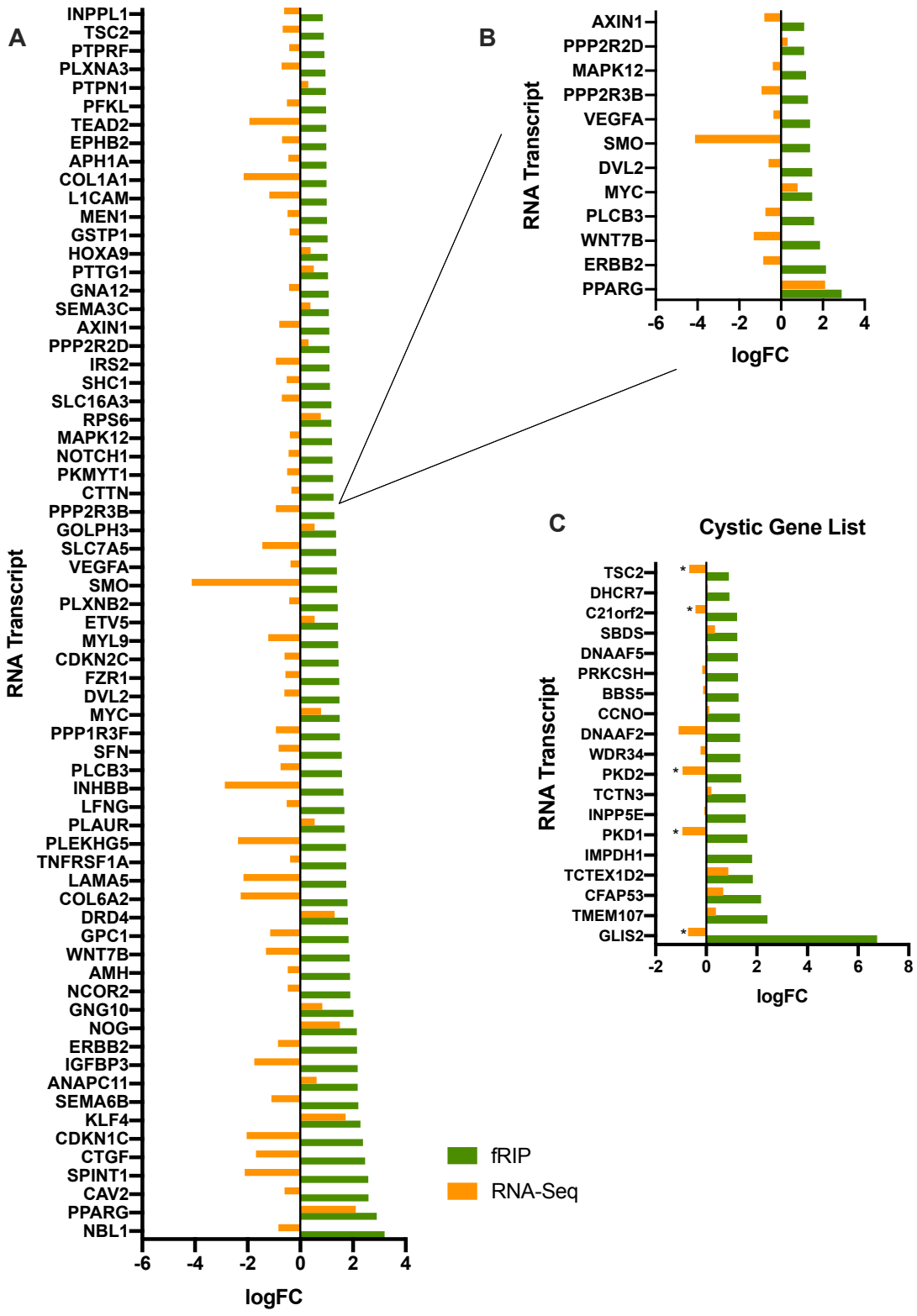

Figure 5.2.4.9. The significantly enriched RNA transcripts in common between the BICC1 fRIP and BICC1 RNA-Seq datasets. A) The 67 enriched RNA transcripts revealed in the KEGG pathway analysis. **B)** The 12 enriched transcripts that are present in three or more of the significant KEGG pathways analysed. **C)** The 19 common cystic genes when comparing the fRIP-Seq dataset to the cystic genes listed in Table 5.2.2.8. The fRIP logFC enrichments are significant in regard to the adjusted p-value while only the RNA transcripts with a * enriched in the RNA-Seq list have a significant p-value. The BICC1 fRIP dataset is displayed in green, while the BICC1 RNA-Seq dataset is displayed in orange. The enrichment is displayed as log fold change (logFC).

5.2.5 BICC1 regulates the mRNA stability of *PKD1*, *PKD2* and *ANKS3*

Data presented in Chapters 3 and 4 demonstrated that BICC1 positively regulates the expression of *PKD1*, *PKD2* and *ANKS3*, as their expression was significantly reduced in *BICC1 KO* cell models. Furthermore, data presented in sections 5.2.2-4 demonstrated that BICC1 binds and regulates *PKD1*, *PKD2* and *ANKS3 mRNA*. Therefore, this study examined a role for BICC1 in regulating the mRNA stability of *PKD1*, *PKD2* and *ANKS3* by inhibiting global transcription through treatment with actinomyosin D (ActD). ActD inhibits global transcription by preventing the elongation of the RNA chain through binding DNA at the transcription initiation complex.

RNA was extracted from UCL93 and *BICC1 KO* cell lines and assessed by qPCR following ActD treatment at regular time-points. The data demonstrated that BICC1 regulates the mRNA stability of the polycystin proteins, as loss of BICC1 caused a significant decrease in *PKD2* turnover from 17.5 hours to 7.5 hours (Figure 5.2.5.1 B, F). In contrast however, *PKD1* turnover was significantly increased from 4.2 hours to 9.1 hours (Figure 5.2.5.1 A, F). Furthermore, it is interesting to note that *PKD2* presented with a much greater half-life of 17.5 hours compared to 4.2 hours for *PKD1* (Figure 5.2.5.1 F). The data also demonstrated that BICC1 positively regulates the mRNA stability of *ANKS3*, as loss of BICC1 caused a significant decrease in *ANKS3* turnover from 6.1 hours to 3.1 hours (Figure 5.2.5.1 D, F). However, loss of BICC1 has no effect on the mRNA stability of *ANKS6*, which remained at approximately 6 hours (Figure 5.2.5.1 C, F). We can be confident that the results are specific to the genes assessed, as the mRNA turnover of *C-MYC* (a positive control) demonstrated a clear decrease in the time frame used and no difference was observed between UCL93 and *BICC1 KO* cell lines (Figure 5.2.5.1 E, F).

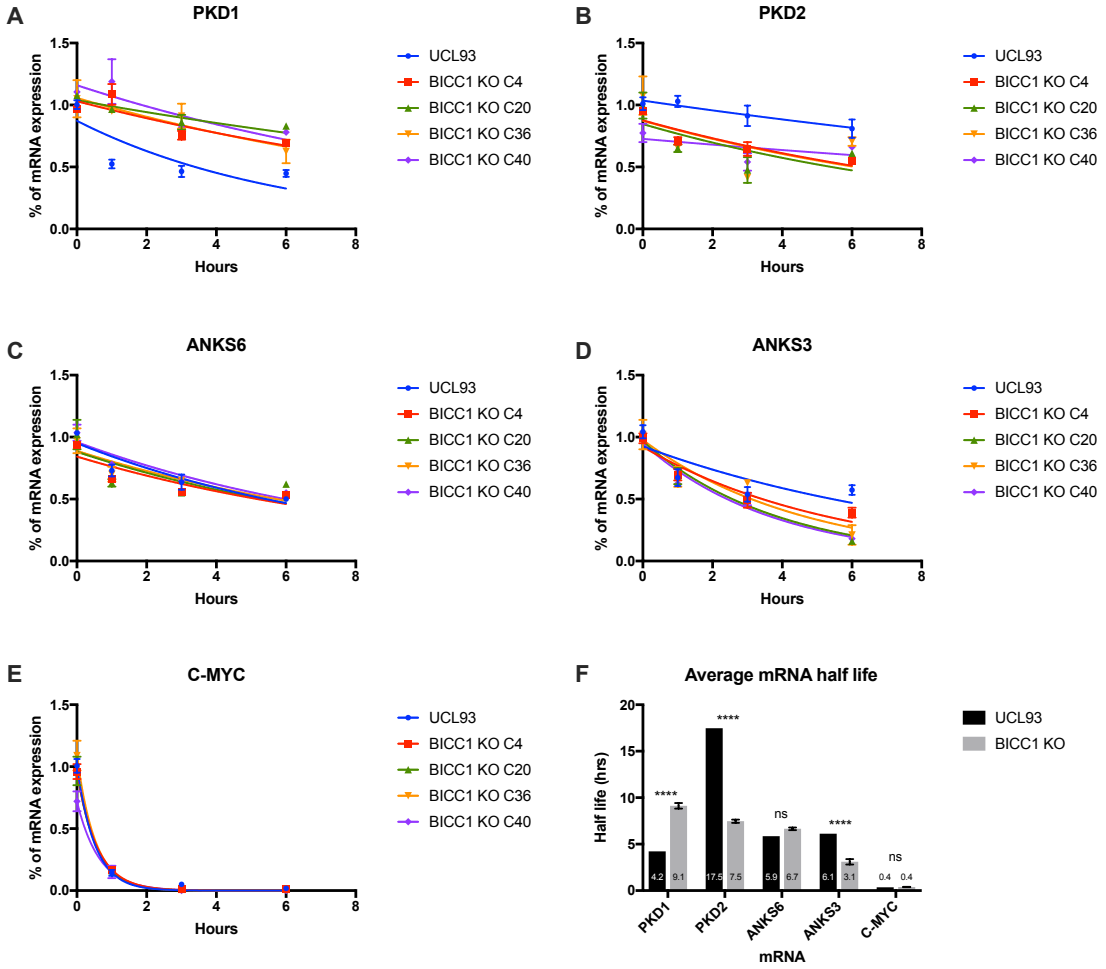

Figure 5.2.5.1. BICC1 regulates the mRNA stability of *PKD1*, *PKD2* and *ANKS3*. A-E) qPCR was used to measure the percentage of mRNA expression in *BICC1 KO* cell lines compared to a UCL93 cell line following treatment with ActD (n=3). A value of 1.0 was assigned to the level of transcript prior to treatment, and the transcript abundance at all other time points was expressed relative to this value. A non-linear regression was applied. *C-MYC* was included as a positive control. F) Average mRNA half-lives were determined using the exponential one phase decay equation and compared between the UCL93 and *BICC1 KO* cell lines. The plateau constant value was set to equal zero. A two-way ANOVA was used to measure statistical significance (p values * <0.05, ** = <0.01, *** = <0.001, **** = <0.0001 and ns = not significant). Error bars represent standard error of the mean.

5.2.6 BICC1 does not regulate *ANKS3* at the transcriptional level

To confirm the observations in section 5.2.1 and rule out other methods of RNA regulation by BICC1, such as transcriptional regulation, primers were designed across exon-intron junctions of *ANKS3* (Figure 5.2.6.1 A). *ANKS6* was included as a negative control, as its mRNA expression levels and mRNA stability were unchanged in *BICC1 KO* cell lines compared to the UCL93 cell line (Figure 4.2.6.1 and Figure 5.2.5.1). No significant changes in expression levels were observed between UCL93 and *BICC1 KO* cells for primers designed across

exon 7 and intron 7 (e7-i7) or for two sets of primers designed to the start of the 3' poly A tail sequence of *ANKS3* (Figure 5.2.6.1 B-D). In addition, no significant changes were observed for the primers designed across exon 12 and intron 12 of *ANKS6* (Figure 5.2.6.1 E). This data suggests that BICC1 does not regulate *ANKS3* at the transcriptional level, and therefore confirms a role for BICC1 in regulating mRNA stability and turnover.

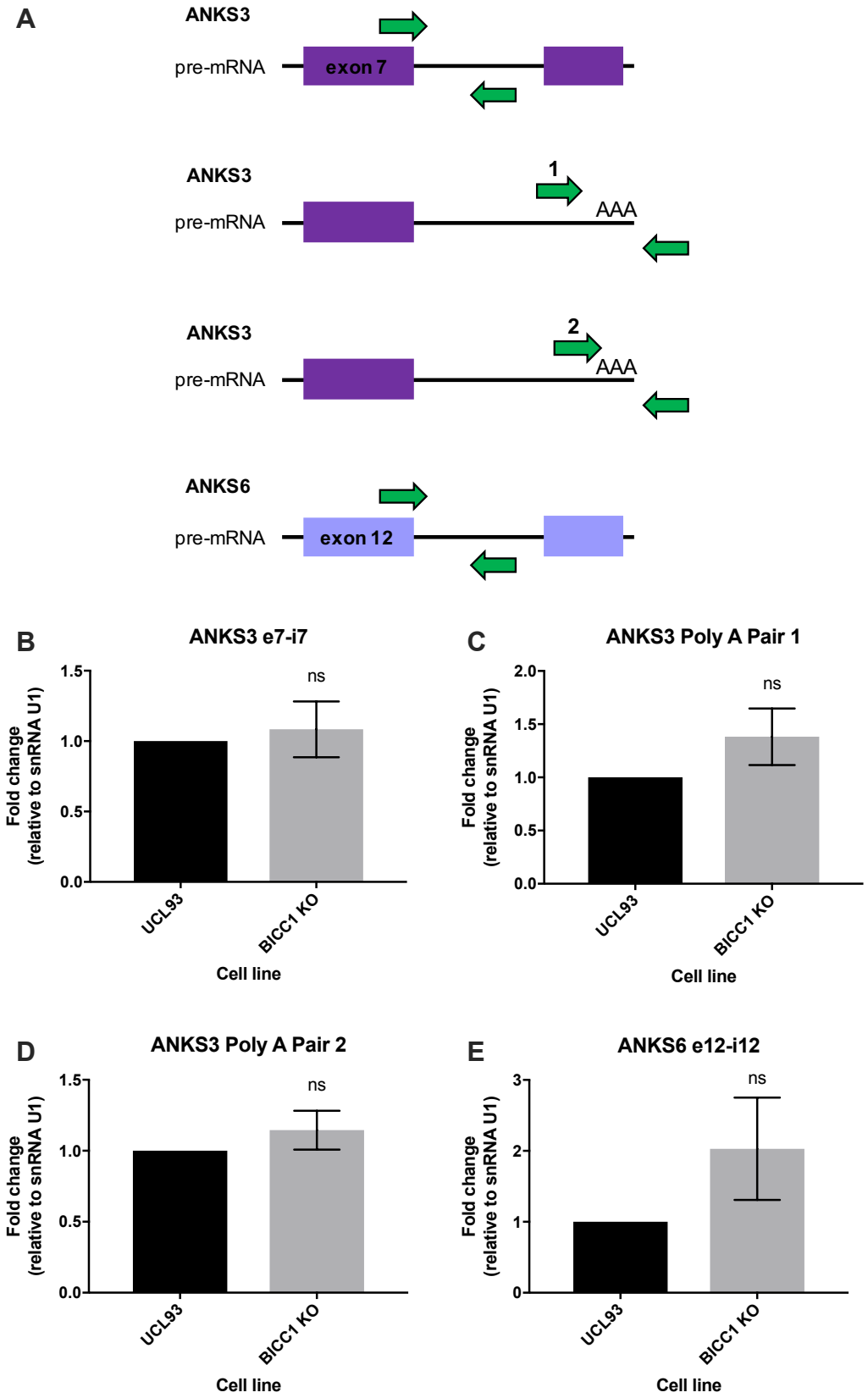

Figure 5.2.6.1. BICC1 does not regulate *ANKS3* at the transcriptional level. A) Schematic representation of the exon-intron and poly A tail primers designed for this experiment. **B-E)** qPCR was used to measure the pre-mRNA expression of *ANKS3* and *ANKS6* (unprocessed RNA transcripts) (n=3). Paired t-tests were performed to assess statistical significance (ns = not significant, p value = >0.5). Error bars represent standard error of the mean.

5.2.7 BICC1 fRIP qPCR

To validate the deep sequencing results obtained from the fRIP-Seq dataset, BICC1 fRIP experiments were repeated and RNA enrichment was assessed by qPCR. Primers were designed to the 5' and 3' UTR of RNA transcripts of interest. The results demonstrated that BICC1 preferentially interacts with 3' UTRs of *PKD1*, *PKD2* and *ANKS3*, matching results observed in the fRIP-Seq dataset. The average significant fold enrichments, relative to a negative GFP fRIP, were 6-fold, 13-fold, and 7-fold respectively (Figure 5.2.7.1). The interaction between BICC1 and *PKD1* was not significant, however the fold enrichment trend is clear.

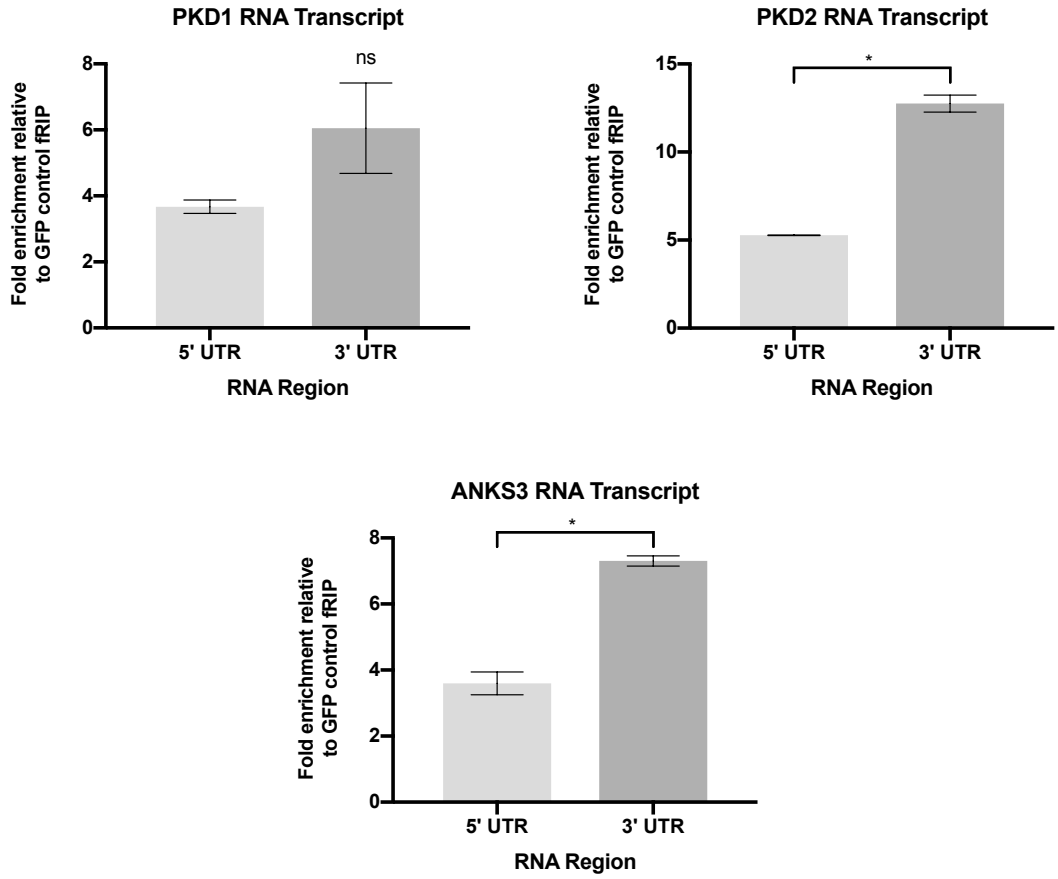

Figure 5.2.7.1. BICC1 associates with the *PKD1*, *PKD2* and *ANKS3* RNA. qPCR was used to measure the mRNA expression of RNAs bound to BICC1 protein following fRIP experiments (n=3). The RNA targets were normalised relative to control GFP fRIP experiments. Paired t-tests were performed to assess statistical significance (p values * <0.05, ** = <0.01, *** = <0.001, **** = <0.0001 and ns = not significant). Error bars represent standard error of the mean.

5.2.8 BICC1 interacts with proteins that both initiate translation and promote polyadenylation of mRNA

Data presented in the previous sections of this chapter has established that BICC1 regulates the mRNA stability of *PKD1*, *PKD2* and *ANKS3*, but how this regulation is mediated is not clear. Therefore, it was hypothesised that BICC1 might interact and potentially activate certain proteins known to either inhibit or promote mRNA stability. Several core eukaryotic translation initiation factors were observed as BICC1-protein partners from our MS study, as well as additional auxiliary factors known to induce and promote mRNA translation (Figure 5.2.8.1). However, several components of the CCR4-CNOT deadenylation complex and associated proteins known to promote deadenylation, and therefore inhibit mRNA translation, also associated with BICC1 in the MS study (Figure 5.2.8.2). CNOT1, PABP1, PABP4 and eIF3A were observed to have the greatest enrichment scores of 30-fold, 14-fold, 12-fold and 13-fold respectively. This data demonstrates that BICC1 interacts with proteins that both promote and inhibit mRNA translation, which therefore suggests that BICC1 can function as both a positive and negative regulator of mRNA stability. However, as MS analysis does not demonstrate direct interactions, we must acknowledge that some of these interactions might be indirect and occur due to being in close proximity to a direct BICC1-protein association. Furthermore, RBPs are known to form major protein complexes, therefore, some of the protein partners observed may be part of a BICC1-protein complex but not directly interact with BICC1 itself.

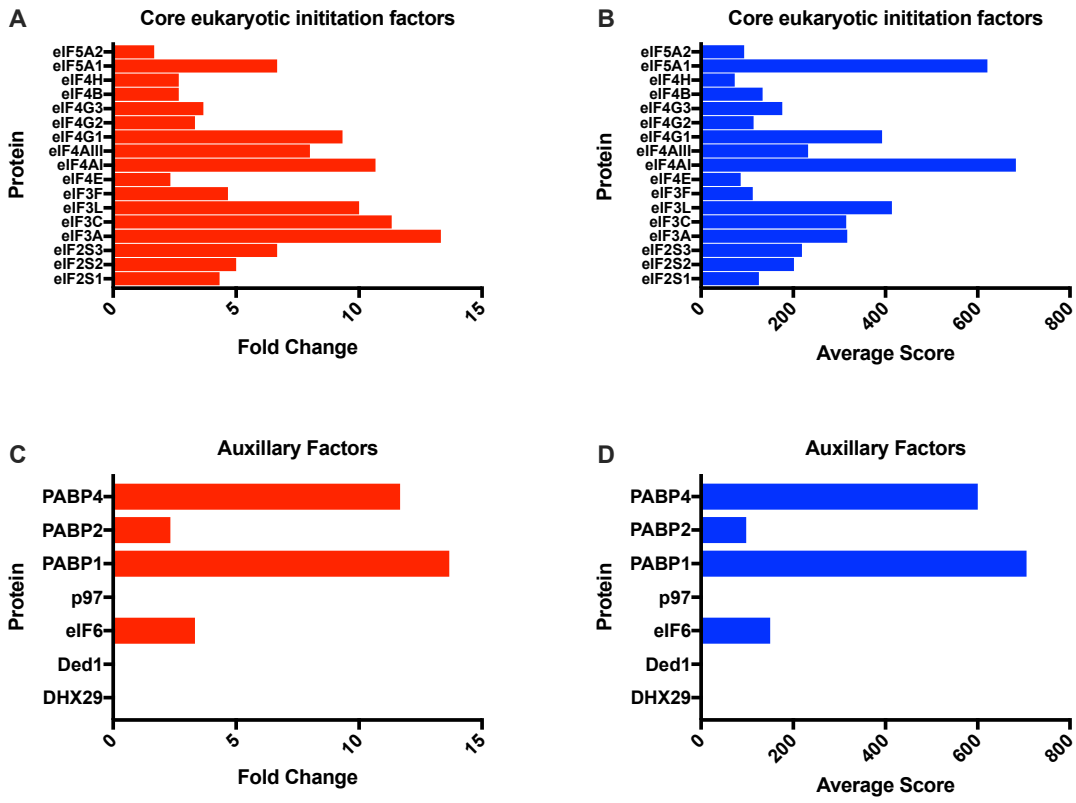

Figure 5.2.8.1. BICC1 associates with various eukaryotic initiation factors. A full list of known eukaryotic initiation factors and their relative auxiliary factors adapted from Jackson *et al*. 2010. **A-B)** Significantly enriched BICC1-protein interactions identified in the MS study as core eukaryotic initiation factors, with enrichment values displayed as either fold change (**A**) or average peptide score (**B**). **C-D)** Significantly enriched BICC1-protein interactions identified in the MS study as auxiliary factors linked to eukaryotic initiation factors, with enrichment values displayed as either fold change (**C**) or average peptide score (**D**).

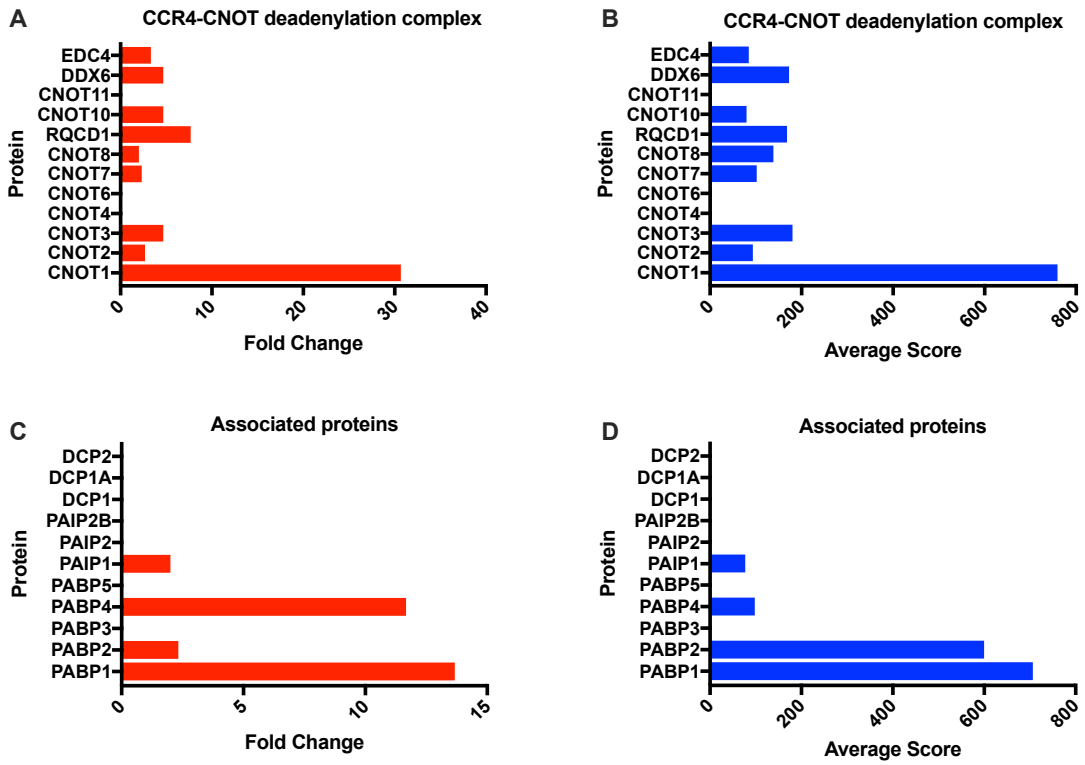

Figure 5.2.8.2. BICC1 associates with 3' polyadenylation factors. A full list of known eukaryotic initiation factors and their relative auxiliary factors adapted from Jackson *et al*. 2010. **A-B)** Significantly enriched BICC1-protein interactions identified in the MS study as members of the CCR4-CNOT deadenylation complex, with enrichment values displayed as either fold change (**A**) or average score (**B**). **C-D)** Significantly enriched BICC1-protein interactions identified in the MS study as associated proteins of the CCR4-CNOT deadenylation complex, with enrichment values displayed as either fold change (**C**) or average score (**D**).

5.3 Discussion

BICC1 is an RBP involved in the post-transcriptional regulation of mRNA transcripts. Although the general function of BICC1 is well-known, how it regulates its mRNA targets is not fully understood. Furthermore, the specific mechanism of RNA binding, whether it is direct or indirect, and how BICC1 targets mRNA, remains unclear. Therefore, this chapter aimed to further understand how BICC1 regulates the mRNA targets identified in the previous chapters, investigate whether BICC1 is able to directly bind to these targets, and to also discover novel BICC1-RNA interacting partners. Through the identification of novel associations within its transcriptome, we can begin to develop an improved understanding of the role of BICC1 in kidney epithelial cells and in preventing ADPKD.

The first aim of this chapter sought to identify novel RNA targets, as well as to investigate whether BICC1 directly interacts with its RNA targets. Therefore, a BICC1 fRIP followed by deep sequencing was performed. fRIP experiments were chosen as they provided data which suggests, but does not confirm, whether BICC1 has direct or indirect interactions with RNA; although the cross-linking would suggest any RNAs discovered are in close proximity to BICC1. The data demonstrated that BICC1 binds several RNA targets in kidney epithelial cells. Through functional annotation analysis, several BICC1-associated RNAs were identified that encode proteins mainly involved in cellular migration, adhesion, signalling and cytoskeletal organisation including, *CD33*, *SDC1*, *FZD1*, *PCSK5*, *RHOV*, *RRAS*, *RSG1*, *RAC3* and *MMP2*. Moreover, several RNA transcripts were identified as transcriptional regulators of cellular growth including *CTBP1*, *ID3* and *PIK3R2*. Furthermore, several RNAs encode proteins found in biological relevant pathways that are altered in ADPKD, including MAPK, VEGF, mTOR and ErbB signalling pathways. The biologically relevant RNA transcripts found in these pathways included, MAPK1, VEGF, TGFB1 and ERRB2.

Interestingly, the two most significantly enriched RNAs associated with BICC1 were transcription factors, suggesting BICC1 might also indirectly regulate transcription through *JUND* and *GLIS2* expression. Both *JUND* and *GLIS2* were downregulated in the whole transcriptome expression analysis (see discussion below), however their change in expression was not statistically significant in regard to the adj. p-value (>0.05). In addition, several BICC1-bound RNAs encode proteins involved in the regulation of gene expression including *EIF3CL*, *HMGA1* and *POLR2J*. *FOSL1*, another transcription factor involved in the AP-1 complex similarly to *JUND*, was also identified, as well as *GLI1*. In addition, comparisons between the BICC1 fRIP-Seq and the BICC1 MS datasets were made and several transcripts were found to be in common. These included *BSG*, *FASN*, *ACTN4*, *CFL1* and *EIF4G1*, *PABPC1* and *RPLP2*.

Further data analysis of the BICC1 fRIP-Seq confirmed published research stating BICC1 interacts with *DVL2* and *ADCY6*, at their 5' and 3' UTRs respectively, just two mRNA targets known to be regulated by BICC1 (Piazzon

et al., 2012; Rothé *et al*., 2015). These observations confirmed previous experimentation concluding BICC1 binds to the 3' UTR of *ADCY6* and presents a new interaction region between BICC1 and the 5' UTR of *DVL2*. However, in these published experiments, an interaction between BICC1 and the 3' UTR of *ADCY6* was not investigated, therefore this study had demonstrated a new link between BICC1 and *ADCY6* (Piazzon *et al*., 2012). In addition, our data has demonstrated that BICC1 interacts with *PKD1*, *PKD2* and *ANKS3* at their 3' UTRs, which might be an important observation to investigate further in order to fully elucidate the mechanistic function of regulation.

This interaction was validated by separate BICC1 fRIP and qPCR experiments. In contrast to published research, this study did not observe a statistically significant self-interaction between BICC1 and its own RNA, or an interaction with its 5' UTR, as has been discussed in published literature (adj. p-value >0.05) (Chicoine *et al*., 2007). This could be due to using the Biojupies programme, which utilises the Kallisto pseudoaligner. It has been noted that this type of genome aligner returns an alignment output in a shorter amount of time relative to other aligners. Therefore, this type of alignment may not work as well for RIP-seq data. Reanalysis of the self-interaction has been performed by the Ong group using the STAR aligner and RSEM mapper for alignment and quantification at gene and transcript level. This analysis has discovered that BICC1 was significantly enriched in the BICC1 fRIP-seq dataset compared to the BICC1 KO fRIP-seq dataset. For future publications, the STAR aligner and RSEM mapper will be used to assess and confirm BICC1-RNA interactions.

Additional spatial resolution and regional mapping analysis in the UCSC Genome Browser established that BICC1 preferentially binds the 3' UTR of many of its RNA targets, as it does for *PKD1*, *PKD2* and *ANKS3*, including the most significantly BICC1-bound RNAs *JUND*, *GLIS2*, *CHPF*, and the published RNA targets *ADCY6* and *WNT7B*. Interestingly, BICC1 preferentially interacts with the 5' UTR of *DVL2* in contrast to its other targets. Moreover, BICC1 interacts with both the 5' UTRs and 3' UTRs of *KRT7* and *IGBP3*, which could suggest an interplay of regulation between the two sites. It would be beneficial to observe regional interactions of BICC1 with its RNA targets on a global scale

to fully comprehend the binding preference of BICC1 and therefore gain a clearer understand of its function as a mRNA regulator.

The second aim of this chapter sought to analyse global transcriptome expression regulated by BICC1 in kidney epithelial cells through WT and *KO* cell models and deep sequencing methods. Unfortunately, the RNA-Seq dataset presented with high variability between samples, and therefore conclusive conclusions could not be drawn. However, general patterns and trends were observed. For example, BICC1 regulates the global expression of many RNAs in both a positive and negative manner. Furthermore, this study has shown BICC1 as a proficient positive regulator of mRNA expression over its lesser role as a negative mRNA regulator, as the majority of RNA transcripts were downregulated due to a loss of BICC1 expression. Interestingly, the most significantly regulated RNA targets suggest that BICC1 is strongly involved in regulating cell adhesion and migration as well as cellular homeostasis, as observed in the fRIP-Seq dataset. These RNA transcripts included, *FN1* (upregulated in *BICC1 KO* cells) and *THBS1* and *CCND2* (downregulated in *BICC1 KO* cells). Moreover, the role of BICC1 in positively regulating the mRNA expression of *PKD1*, *PKD2* and *ANKS3* was confirmed, correlating with data presented from previous gene expression analysis presented in chapters 3 and 4.

In addition, comparisons between the BICC1 fRIP-Seq and RNA-Seq datasets were made and the most significant KEGG pathway with common enriched transcripts was the proteoglycans in cancer pathway, which was also the most significant pathway in the BICC1 fRIP-Seq datas*et al*one. The proteoglycans in cancer pathway highlights proteoglycans and their downstream molecules that may contribute to cancer and to tumour progression through misregulation of proliferation, angiogenesis, adhesion and metastasis. The common RNA transcripts included *SMO*, *WNT7B*, *ERBB2*, *MAPK12* and *VEGFA*. The global expression of the 12 most significantly BICC1-enriched RNA transcripts was also assessed, however, only *GLIS2* was discovered to be significantly downregulated in *BICC1 KO* cells when setting an adjusted p-value cut off value of 0.05.

The final aim of this chapter sought to investigate how BICC1 regulates its identified mRNA targets. Our data demonstrated that BICC1 regulates the mRNA stability of *PKD1*, *PKD2* and *ANKS3*, but not *ANKS6* or the negative control *C-MYC*. When considering the fRIP-Seq and RNA-Seq data, it is clear that BICC1 interacts with the RNA transcripts of *PKD1*, *PKD2* and *ANKS3* to positively regulate their mRNA stability and expression in kidney epithelial cells. However, it must be noted that the mRNA stability of *PKD1* was increased in *BICC1 KO* cells, while the mRNA of stability of *PKD2* was decreased in *BICC1 KO* cells, suggesting that BICC1 regulates the mRNA stability of the polycystins in different manners. Nevertheless, this confirms our theory that BICC1 can function to regulate its RNA targets in various ways.

The function of BICC1 as a regulator of mRNA stability was confirmed by assessing whether BICC1 could regulate *ANKS3* at the transcriptional level. This study has demonstrated that BICC1 is not a transcriptional activator or regulator, as it does not regulate the transcription of *ANKS3*, therefore, confirming BICC1 as a post-transcriptional regulator. Furthermore, following further analysis of the BICC1 MS dataset, this chapter demonstrated that BICC1 interacts with proteins that both initiate mRNA translation as well as promote deadenylation of mRNA. Such data strengthens the idea that the function of BICC1 in kidney epithelial cells is to regulate mRNA stability and expression of its targets.

Overall, when considering all the data in this chapter, a strong suggestion can be made that BICC1 interacts with the RNAs it regulates, mainly through a 3' UTR binding site or secondary structure. This chapter has evidently shown that BICC1 can both positively and negatively regulate its RNA targets, so could therefore both promote translation by recruiting necessary factors, as well as regulating deadenylation by controlling the access of both deadenylation complexes and miRNA silencing complexes to the 3' UTR of target mRNAs.

Chapter 5 Summary:

- ⇒ BICC1 has several novel RNA interacting partners
- ⇒ BICC1 interacts with its novel RNA targets
- ⇒ BICC1 interacts with both the 5' and 3' UTRs of RNA targets, with a preference for 3' UTR binding
- ⇒ BICC1 RNA targets are involved in the regulation of cellular migration, adhesion, signalling and cytoskeletal organisation
- ⇒ BICC1 RNA targets are transcriptional regulators of cellular growth
- ⇒ BICC1 RNA targets are involved in gene regulation with an enrichment in the regulation of mRNA translation
- ⇒ BICC1 interacts with proteins that both initiate the translation and promote the deadenylation of mRNA
- ⇒ BICC1 binds to the 3' UTRs of *PKD1*, *PKD2* and *ANKS3*
- ⇒ BICC1 regulates the mRNA stability of *PKD1*, *PKD2* and *ANKS3*

Chapter 6

Discussion

6.0 Discussion

BICC1 mutant models, in various species, share common phenotypes with ADPKD models. The hypothesis of this study stated that BICC1 is a major interacting protein of the polycystin protein complex and is somehow involved in the pathogenesis of ADPKD. Since BICC1 is an RBP whose protein and RNA binding partners have not been fully elucidated in the human kidney, this study sought to further understand the role of BICC1 in kidney epithelial cells and ADPKD by addressing three main aims. The first aim sought to confirm a direct interaction between BICC1 and the polycystin proteins and define their likely binding domains. This study has confirmed a link between BICC1 and ADPKD through novel interactions with the polycystin proteins, PC1 and PC2, through previously unknown binding sites within the BICC1 protein. Furthermore, this study has discovered an intricate regulatory complex between BICC1 and the polycystin proteins: when BICC1 was mutated, the expression levels of *PKD1*, *PKD2* and PC2 were downregulated.

The second aim of this study set out to discover protein binding partners of BICC1 in human kidney cells by combining Co-IP with MS. A number of novel protein binding partners of BICC1 were identified, including several complexes involved in the post-transcriptional regulation of other proteins such as CNOT1 and PABPC1. ANKS3, one of the top protein binding partners identified from the BICC1-Co-IP-MS experiments, was investigated further and confirmed to be a binding partner of BICC1, as well as the polycystin proteins, building upon the hypothesis that BICC1 is a major protein of the polycystin protein complex along with other related cystoproteins. Moreover, ANKS3 expression was similarly regulated by BICC1 as was PC1 and PC2, suggesting that BICC1 controls the expression and function of this protein complex.

The third and final aim of this study endeavoured to discover global RNA binding partners of BICC1 by RNA-IP-deep-sequencing in human kidney tubular cells. Several novel RNA binding partners of BICC1 were identified, providing a deeper understanding of how BICC1 could function to regulate

normal tubular function in the human kidney. Moreover, by experimental design, novel BICC1-RNA interactions were demonstrated, and a 3' UTR binding preference of BICC1 for its RNA targets was discovered. Finally, a role for BICC1 in regulating the mRNA stability of *PKD1, PKD2* and *ANKS3* was revealed.

6.1 BICC1 is a major interacting protein of the polycystin protein complex

A loss of BICC1 in kidney epithelial cells has been shown to cause a complex PKD-like phenotype which includes defective differentiation of kidney epithelia, dysfunctional cilia and PCP, a disorganised cytoskeleton, loss of E-cadherin cell-cell adhesion, and the mis-regulation of various signalling pathways, which ultimately leads to disrupted tubulomorphogenesis and cystogenesis (Cogswell *et al*., 2003; Tran *et al*., 2007; Maisonneuve *et al*., 2009; Bouvrette *et al*., 2010; Fu *et al*., 2010; Piazzon *et al*., 2012). Previous research had demonstrated a possible functional link between BICC1 and ADPKD, as loss of PC1 was associated with a downregulation of BICC1 expression by approximately 50% at both the mRNA and protein level, suggesting that BICC1 is downstream of PC1 and its expression is regulated by PC1 in the kidney (Lian *et al*., 2014). However, how this regulation occurs is not known.

Despite this initial link between BICC1 and ADPKD through PC1, no further research into the direct relationship between BICC1 and PC1 has been published. Therefore, this study investigated whether BICC1 interacts with PC1 at the protein level. Our research has revealed a novel interaction between BICC1 and PC1 through a novel binding region within the BICC1 protein to which PC1 interacts (see Section 3.2.2). Through domain deletion Co-IPs, we discovered that PC1 binds an undefined region of BICC1 between amino acids 716 and 747, upstream of the SAM domain (see Figure 3.3.3 in Section 3.3). It must be noted, however, that the SAM domain of BICC1 may still be required to stabilise this interaction, as deletion of the SAM domain weakened, but did not abolish, the interaction between BICC1 and PC1.

Next, the region of PC1 to which BICC1 binds was investigated. This study discovered that BICC1 binds the C-terminus of PC1 (CT1), between amino

acids 4110 and 4303 (see Section 3.2.5). This study suggests two functions for BICC1 here. First, BICC1 is a central component of the polycystin complex, and possibly involved in its function, at cell membranes. Second, BICC1 binds to the C-terminus of PC1 to self-regulate its own expression and possibly that of PC1, through activation of downstream signalling pathways controlled by PC1. It would be interesting to further investigate this theory by studying the signalling pathways stimulated by PC1 that are known to regulate gene expression, such as the JAK/STAT pathway (Talbot *et al*., 2011; Kim *et al*., 2014; Dalagiorgou *et al*., 2017).

Next, this study investigated whether BICC1 interacts with PC2 at the protein level. Previous functional links have been made between BICC1 and PC2 at the RNA level, as BICC1 has been shown to positively regulate the mRNA expression of *PKD2* (Tran *et al*., 2010). In this study, a novel interaction between BICC1 and PC2 was identified through a region of BICC1 upstream of the known human KH domains, KH1 and KH2 (see Section 3.2.2). Following bioinformatic analysis of this region, this study discovered the presence of another KH domain (KH0) between amino acids 45 and 130. The results conclude that this is the sole KH domain required for an interaction between BICC1 and PC2 (see Figure 3.3.2 in Section 3.3). It is highly likely that this is a true KH domain, as its sequence is homologous to the KH1 and KH2 domains and it also contains the RNA binding motif, GXXG, commonly found within KH domains (Lewis *et al*., 2000). Furthermore, this upstream KH domain has been previously identified in other mammalian models, including mouse and rat (Cogswell *et al*., 2003; Tran *et al*., 2010; Piazzon *et al*., 2012; Rothé *et al*., 2018).

A recent screen of patients with renal abnormalities identified a nonsense mutation within exon 3, which Kraus *et al*. (2012) concluded was likely to encode the a KH domain, and through analysis of prediction models from the Interpro database this study agrees that this in the KH0 domain. Our study is the first to experimentally confirm the KH0 region as a KH domain in humans, as well as demonstrating it is functionally active. Our study observed that PC2 requires a KH domain to bind to BICC1, an unexpected result based on the fact

that KH domains commonly mediate protein-RNA interactions. However, they have been shown to mediate protein-protein interactions; but it is also possible for these interactions to occur through an RNA intermediate. With this in mind, this study investigated whether an RNA intermediate was involved in the interaction between BICC1 and PC2. Following RNase treatment, this study discovered that the interaction between BICC1 and PC2 was decreased, suggesting an RNA intermediate is required. However, endogenous Co-IPs demonstrated no RNA intermediate was required for the interaction (see Section 3.2.4). Förster resonance energy transfer (FRET) or unnatural-amino-acid-mediated photochemical crosslinking experiments could be performed to confirm whether an RNA is required to mediate an interaction between BICC1 and PC2 (Chiu *et al*., 2007; Rehman *et al*., 2014).

Next, this study investigated the binding region of PC2 to which BICC1 interacts. It was discovered that BICC1 binds both the N-terminus and C-terminus of PC2 (see Section 3.2.5). Binding to the C-terminus of PC2 is interesting, as this is the region that PC1 is thought to bind, to form the polycystin complex at cell membranes. These data further confirm that BICC1 is a central component of the polycystin complex (Giamarchi *et al*., 2010). However, an interaction with the N-terminus of PC2 was unanticipated. Previous research investigating the N-terminal protein partners of PC2 identified interactions with alpha-actinins, actin-binding and actin-bundling proteins (Li *et al*., 2005).

Li and colleagues (2005) demonstrated that alpha-actinin binds the N-terminus and C-terminus of PC2 and stimulates its channel activity. Alpha-actinins have a role in regulating cytoskeleton organisation, cell adhesion, proliferation and migration, therefore, BICC1 could be involved in this protein complex to regulate PC2 channel activity. Moreover, data collected from our BICC1 Co-IP-MS and RNA-IP-deep-sequencing datasets implicate loss of BICC1 with dysregulation of these processes. To further explore these functions, Co-IPs and lipid bilayer electrophysiology system experiments, as performed in the Li *et al*. (2005) study, should be explored.

More recently, others have demonstrated an interaction between PC2 and the retromer complex, specifically retromer-associated protein SNX3, a protein complex involved in the endo-lysosomal network and responsible for the sorting of integral membrane proteins (Feng *et al*., 2017; Tilley *et al*., 2018). This interaction occurs through the N-terminus of PC2 and the researchers suggests that this confirms PC2 as a retromer cargo protein. Interestingly, *SNX3* was identified as an RNA binding partner of BICC1 from our fRIP-Seq analysis; therefore, it would be interesting to investigate whether BICC1 is also involved in regulating this cargo complex through RIP, Co-IP and fluorescent living imaging experimentation (Feng *et al*., 2017; Tilley *et al*., 2018). In addition, *SNX12, SNX17, SNX18, SNX8* and *VPS28, VPS37B, VPS37C, VPS51* were identified as significant RNA partners of BICC1 (Appendix Table 7.5).

6.2 BICC1 is a translational activator of the polycystin complex

BICC1 has been shown to regulate various mRNA targets within the kidney. As novel protein interactions between BICC1 and the polycystin proteins have been uncovered, this study sought to investigate whether BICC1 also regulates the expression of these proteins. To investigate this possibility, stable CRISPR-Cas9 *BICC1 KO* kidney epithelial cell lines were generated to assess the mRNA and protein expression levels of PC1 and PC2 (see Section 3.2.7 and 3.2.8). In *BICC1 KO* cells, the mRNA expression of *PKD1* was significantly reduced, although its protein expression levels were unchanged. Furthermore, loss of BICC1 caused an increase in the mRNA stability of *PKD1* (see Section 5.2.5). Loss of BICC1 also caused a significant decrease in the mRNA and protein expression of PC2, as well as a significant decrease in its mRNA stability, suggesting BICC1 positively regulates the mRNA expression and stability of *PKD2*.

Together, these observations suggest that in normal epithelial cells, BICC1 binds and stabilises *PKD2* mRNA but destabilises *PKD1* mRNA. Whereas in *BICC1 KO* cells, since the BICC1 protein is absent, *PKD2* mRNA was destabilised so its mRNA and protein levels were decreased. However, *PKD1* mRNA is stabilised in *BICC1 KO* cells, without a detectable effect on its protein levels. Total transcript abundance analysis from the Human Protein Atlas (HPA)

database further supports these observations, as *PKD2* mRNA abundance in the kidneys is greater than that of *PKD1 m*RNA (55 transcripts per million (TPM) compared to 2.5 TPM respectively, obtained from RNA-seq data generated by the HPA (*PKD1* and *PKD2* available from v18.1.proteinatlas.org). Furthermore, data gathered within this study confirms greater overall *PKD2* mRNA expression levels in kidney epithelial cells compared to *PKD1* mRNA expression (data not shown).

Previous research has demonstrated a role for BICC1 in the post-transcriptional regulation of *PKD2* in a mouse model, by binding the 3' UTR of *PKD2* through its KH domains (Tran *et al*., 2010). BICC1 competitively inhibited miR-17, a repressive oncomir from the miR-17/92 gene cluster, from binding to the 3' UTR of *PKD2* to destabilise it, thereby increasing *PKD2* translation. A reduction in both the mRNA and protein expression levels of PC2 in *BICC1 KO* cells in this study suggests that BICC1 regulates PC2 by promoting mRNA stability. As previously discussed, this theory was assessed using mRNA stability assays, and this study discovered that loss of BICC1 caused a decrease in the mRNA stability of *PKD2*, therefore confirming BICC1 positively regulates *PKD2* by promoting its mRNA stability.

As discussed in Section 6.1, loss of PC1 had been reported to be associated with a downregulation in the expression of BICC1 in the kidney. To confirm this observation, this study generated stable CRISPR-Cas9 *PKD1 KO* kidney epithelial cell lines. In agreement with published data, loss of PC1 caused a significant decrease in BICC1 expression at both the mRNA and protein level (see Section 3.2.9). Expression levels of PC2 were also assessed, and a significant decrease at both the mRNA and protein level was also observed (see Section 3.2.11). At the same time, stable CRISPR-Cas9 *PKD2 KO* kidney epithelial cell lines were generated and the expression levels of PC1 and BICC1 were assessed. No change in the expression levels of PC1 were observed in *PKD2 KO* cells, whereas BICC1 expression was significantly increased (see Section 3.2.10 and 3.2.12). Overexpression studies demonstrated that a significant increase of BICC1 caused an upregulation of *PKD1* but had no effect on the mRNA expression of *PKD2* (see Section 3.2.13). The pattern in

expression levels between *BICC1*, *PKD1* and *PKD2 KO* cell lines, as well as data from the overexpression experiments, suggests a hierarchy of gene regulation. This hierarchy consists of PC1 at the top of a gene regulatory network, regulating both BICC1 and PC2, followed by BICC1, regulating PC2 and to a lesser extent PC1, and finally PC2, only regulating BICC1 expression (Table 3.3.1).

6.3 BICC1 interacts with proteins involved in mRNA regulation

Data from this study has demonstrated that BICC1 interacts with the polycystins at the protein level and regulates their mRNA expression and stability. Therefore, this study sought to identify additional novel BICC1-protein binding partners that could play a role in the pathogenesis of ADPKD, in an unbiased way, by performing BICC1 Co-IP experiments followed by mass spectrometry (Co-IP-MS). The study found that BICC1 binds several novel proteins in kidney epithelial cells (see Section 4.2.1). Through functional annotation analysis, several BICC1-associated proteins were identified, which are mainly involved in translation initiation, deadenylation, poly(A) binding, RNA transport, RNA degradation and protein processing. Furthermore, several BICC1-protein binding partners identified in this study, such as CNOT1, PABPC1 and several eukaryotic translation initiation factors, were also identified in a dataset from the Constam group (Constam MS dataset), confirming our Co-IP-MS data was reproducible and reliable (see Figure 4.2.1.2 and Appendix Table 7.6) (Leal-Esteban *et al*., 2018).

Moreover, comparative analysis demonstrated that both datasets contained enriched proteins within several KEGG pathways including the ribosome, protein processing in the ER, RNA transport, RNA degradation and aminoacyl-tRNA biosynthesis. BICC1 has been identified as an RBP involved in the post-transcriptional regulation of mRNA transcripts. As discussed previously in sections 6.1 and 6.2, BICC1 binds to the polycystin proteins and also regulates their mRNA expression and stability. How BICC1 performs this stability regulatory function, however, is unknown. Therefore, the identification of several novel protein binding partners of BICC1 that are involved in translation initiation, deadenylation, poly(A) binding and RNA degradation is of importance.

For example, BICC1 interacted with several core eukaryotic initiation factors, including eIF3A, PABPC1, PABPC4 and PAIP1. eIF3A is the RNA-binding component of the eIF3 complex responsible for the initiation of protein synthesis. The eIF3 complex is involved in several steps of translation initiation, including binding the pre-initiation complex, mRNA recruitment to the pre-initiation complex, and the scanning of mRNA for the UAG start codon. PABPC1 and PABPC4 have been shown to have dual functions, as they can bind both the 3' poly(A) tails of mRNAs as well as associate with components of the eIF3 complex. In this way, PABPC1 and PABPC4 promote translation initiation. In contrast, PABPC1 is also involved in the deadenylation of poly(A) tails; therefore, promoting mRNA degradation. PAIP1 acts as a coactivator of translation initiation of poly(A)-containing mRNAs, through binding the cap-binding complex eIF4A and activating PABPC1. Like PABPC1, PAIP1 is similarly involved in the deadenylation and degradation of mRNA in association with other RBPs and the deadenylation complex. Forming interactions with these core eukaryotic initiation factors strongly suggests a role for BICC1 in promoting or inhibiting the translation of its mRNA targets.

BICC1 is strongly associated with CNOT1, as well as other members of the CCR4-CNOT deadenylation complex including CNOT3, which had been previously identified as a binding partner of BICC1 (Piazzon *et al*., 2012). BICC1 also bound associated proteins of the CCR4-CNOT deadenylation complex, including EDC4. CNOT1 is the core subunit of the CCR4-CNOT complex and is responsible for providing a scaffold for the other subunits to bind to. CNOT3 binds to CNOT1, as well as CNOT2, to regulate RNA targeting and repression. EDC4 has been linked to the decapping of ARE-containing mRNAs and their subsequent degradation through the formation of a complex with DCP1A and DCP2, whilst stimulating the catalytic activity of the latter. When summarising the current observations from this study, it could be suggested that protein interactions between BICC1 and members of the deadenylation complex occur in an inhibitory manner to restrict access to 3' UTRs of mRNAs and prevent degradation. In this way, BICC1 protects and promotes the stability of its mRNA targets.

Overall, these novel protein interactions strongly suggest that BICC1 functions to regulate the mRNA stability and expression of its targets through the recruitment of specific translation initiation complexes to promote mRNA translation. Likewise, it is plausible for BICC1 to form protein-protein interactions with deadenylation complexes to restrict their access to target mRNAs, thereby inhibiting their function, which confirms our previous observations. However, these data could also advocate that BICC1 indirectly negatively regulates its mRNA targets through these protein interactions, as previous research groups have shown BICC1 to negatively regulate the expression of some of its mRNA targets through recruitment of the deadenylation complex and RISC, including *ADCY6* and *PKI-*α (Chicoine *et al*., 2007; Maisonneuve *et al*., 2009; Snee and Macdonald, 2009; Tran *et al*., 2010; Kraus *et al*,. 2012; Piazzon *et al*., 2012; Lian *et al*., 2014). It is possible that the function of BICC1 switches between positive regulation and negative regulation dependent upon the mRNA target, or through cellular stimulation; or BICC1 has a dual function to fine tune expression of its mRNA targets. It would be interesting to investigate whether BICC1 recruits and binds to components of the translation initiation complex or binds to members of the deadenylation complex to prevent mRNA degradation, or both, to promote the mRNA stability of *PKD2* in this study.

6.4 BICC1 forms a complex with ANKS3 and the polycystin proteins

Following the identification of novel protein binding partners of BICC1, this study sought to confirm whether BICC1 interacts with ANKS3, one of the highest enriched proteins from the MS analysis and a protein recently implicated in PKD (Yakulov *et al*., 2015; Rothé *et al*., 2018). Our research confirmed the reported interaction between BICC1 and ANKS3 but also identified a novel binding region within the BICC1 protein to which ANKS3 interacts (see Section 4.2.2). Interestingly, this region was the same binding motif (binding motif 2) to which this study discovered PC1 to bind, between amino acids 716 and 747, upstream of the SAM domain. However, the SAM domain of BICC1 may still be required to stabilise this interaction, as when the SAM domain was removed the interaction between BICC1 and ANKS3 was reduced, but not lost, as is the case for the interaction between BICC1 and

PC1. A similar observation was made by Rothé and colleagues (2018), as they observed BICC1-ANKS3 and ANKS3-ANKS6 complexes to rely on both SAM-SAM interactions, as well as additional binding surfaces involving ANK repeats and KH domains. Therefore, it is likely that the protein-protein interactions observed in this study are formed in a similar manner, and also rely on additional, previously unknown binding regions to stabilise interactions.

As both PC1 and ANKS3 bind to BICC1 in the same region, one could theorise that they do not bind BICC1 at the same time. Instead, BICC1 may act as a chaperone, delivering ANKS3 to PC1 for a particular function. To further understand this complex, BICC1, PC1 and ANKS3 could be co-expressed and interactions between BICC1 and PC1 and BICC1 and ANKS3 assessed for competitive binding. Furthermore, co-localisation studies and FRET should be performed to reveal whether these proteins do form a complex in close proximity to each other. In this way, cellular localisation of this complex would also be revealed. On the other hand, BICC1 and ANKS3 might function in a separate, but closely related, cystoprotein complex to the polycystin complex.

Next, this study investigated the region of ANKS3 to which BICC1 binds. We discovered that BICC1 required the SAM domain of ANKS3 for a stable interaction, as when the SAM domain of ANKS3 was deleted, the interaction between BICC1 and ANKS3 was greatly reduced. However, as the interaction was reduced but not completely lost, it would suggest that the SAM domain of ANKS3 is a vital, but not exclusive, element involved in mediating an interaction between BICC1 and ANKS3. Therefore, BICC1 might bind upstream or downstream of the SAM domain and link with the SAM domain in some manner to mediate an interaction, but further experimentation is required to confirm this theory, as previously discussed in this section.

In the same manner, this study investigated whether BICC1 interacts with the ANKS3 partner, ANKS6. Previous interactions have been demonstrated between BICC1 and ANKS6; however, several researchers suggest that this interaction is not direct, and an intermediate is involved (Stagner *et al*., 2009; Leettola *et al*., 2014; Bakey *et al*., 2015; Rothé *et al*., 2018). In agreement with

these research groups, our data did not demonstrate a direct interaction between BICC1 and ANKS6. Instead, we uncovered competition between BICC1 and ANKS6 for binding with ANKS3, as when ANKS3 and ANKS6 were co-expressed in HA-BICC1 cells, the interaction previously observed between BICC1 and ANKS3 was lost. These data suggest that ANKS6 has a higher binding affinity for ANKS3 over BICC1, or perhaps ANKS6 inhibits BICC1 from binding to its ANKS3 binding site.

As this study highlighted competition between BICC1 and ANKS6 for ANKS3 binding, additional experimentation was performed to further investigate these interactions, the required binding domains or motifs of ANKS3 for its protein interactions, and why ANKS6 was able to competitively interact with ANKS3 over BICC1. The data demonstrated that BICC1 interacts with full-length ANKS3 as well as ANKS3-ΔSAM, as previously observed in this study. In addition, these data confirmed that the SAM domain of ANKS3 is a vital, but not exclusive, element involved in mediating an interaction between BICC1 and ANKS3. BICC1 did not interact with ANKS6, and co-transfection of ANKS3 and ANKS6 disrupted the interaction between BICC1 and ANKS3, as formerly observed. Furthermore, no interaction was observed between BICC1 and ANKS6-ΔSAM. Moreover, co-transfection of ANKS3-ΔSAM and ANKS6-ΔSAM with BICC1 did not rescue the interaction between ANKS3 and BICC1.

Together, these data demonstrate the importance of the SAM domain of ANKS3 for initiating, but not stabilising, an interaction with BICC1, as well as controlling its interaction with ANKS6. Likewise, it also highlights the importance of the SAM domain of ANKS6 for its interaction with ANKS3, as when ANKS6-SAM is lost, ANKS6 is unable to interact with ANKS3, with or without its own SAM domain. Consequently, in this condition, BICC1 is now able to re-establish its interaction with ANKS3, through ANKS3-SAM. It is interesting to note that deletion of both of the SAM domains of ANKS3 and ANKS6 did not restore an interaction between BICC1 and ANKS3, which again confirms the necessity of the SAM domain of ANKS3 for its interaction with BICC1.

Next, this study sought to identify whether ANKS3 and ANKS6 interact, as shown in published data (Hoff *et al*., 2013; Leettola *et al*., 2014; Bakey *et al*., 2015; Delestre *et al*., 2015; Yakulov *et al*., 2015; Kan *et al*., 2016). This study confirmed a protein-protein interaction between ANKS3 and ANKS6 and also revealed that the SAM domain of ANKS6 is not solely required to initiate an interaction with ANKS3 (see Section 4.2.3). However, the SAM domain of ANKS3 is a vital component that mediates an interaction with ANKS6. Interestingly, endogenous Co-IP experiments between ANKS3 and ANKS6 revealed that RNase I treatment significantly decreased the interaction, by approximately 60%, which suggests that an RNA intermediate is required for an interaction between ANKS3 and ANKS6.

As discussed in Section 4.1.1, a missense mutation in the SAM domain of ANKS6 (R823W) was reported to disrupt its interaction with ANKS3, while another missense mutation 6 amino acids upstream (I747N) had no effect on its interaction with ANKS3, but disrupts its interaction with BICC1 (Leettola *et al*., 2014; Bakey *et al*., 2015). To confirm this observation, constructs containing the R823W and I747N mutations were made using mutagenesis, referred to as ANKS6-R823W and ANKS6-I817N. This study demonstrated that BICC1 does not interact with either ANKS6-R823W or ANKS6-I817N. Furthermore, neither the point mutation of R823W or I817N re-established an interaction between BICC1 and ANKS3, suggesting a complete loss of ANKS6-SAM is required to destabilise its interaction with ANKS3 and therefore reinstate an interaction between BICC1 and ANKS3.

6.5 ANKS3 interacts with the polycystin proteins

Our results strongly suggest a protein complex between BICC1 and the polycystins, as well as between BICC1 and ANKS3. This study also discovered novel protein-protein interactions between ANKS3 and PC1 and ANKS3 and PC2 at the protein level (see Section 4.2.4). Furthermore, through domain deletion Co-IP experiments, PC1 and PC2 were shown to interact with ANKS3 through its SAM domain. As competition had been observed between BICC1 and ANKS6 for binding to ANKS3, similar Co-IP experiments were performed with ANKS3, PC1 and PC2. PC1 expression was weak when co-expressed with

ANKS3 and ANKS6, therefore a conclusive observation could not be made. However, the data revealed that ANKS6 also competes with PC2 for binding to ANKS3, as it does with BICC1.

As competition between PC2 and ANKS6 for ANKS3 binding was observed, additional Co-IPs were performed to further investigate these interactions, the required binding domains or motifs of ANKS3 for its protein interactions, and why ANKS6 is able to interact with ANKS3 over PC2. The data demonstrated that when the SAM domain of ANKS6, but not the SAM domain of ANKS3, was deleted, the interaction between ANKS3 and PC2 was restored, albeit very weakly, in a similar manner to the interactions observed between BICC1 and ANKS3.

6.6 BICC1 has a strong, positive regulatory effect upon ANKS3

As discussed in Section 6.2, BICC1 is a known regulator of various mRNA targets within the kidney and this study has uncovered *PKD1* and *PKD2* as novel mRNA targets of BICC1 following the identification of novel protein-protein interactions. This study has also shown protein-protein interactions between BICC1 and ANKS3, as well as between ANKS3 and the polycystin proteins. Therefore, we sought to investigate whether BICC1 regulates the expression of ANKS3 and its related interacting partner ANKS6. Loss of BICC1 caused a significant 50% decrease of *ANKS3 mRNA* expression and a complete loss of ANKS3 protein expression (see Section 4.2.6). In contrast, loss of BICC1 had no effect on the expression levels of ANKS6, confirming no direct link between BICC1 and ANKS6 in kidney epithelial cells in this study.

The expression levels of ANKS3 and ANKS6 were also assessed in *PKD1* and *PKD2 KO* cell lines. Loss of PC1 caused a downregulation in both *ANKS3 mRNA* and protein expression (see Section 4.2.8). However, the level of reduced expression was not as great as observed in *BICC1 KO* cells, therefore suggesting that BICC1 is directly responsible for the regulation of *ANKS3*, perhaps initially caused by the loss of PC1 which negatively regulates the expression levels of BICC1. Unexpectedly, loss of PC1 also caused a downregulation in ANKS6 protein expression, but had no effect on *ANKS6*

mRNA expression, however; the data differed between different *PKD1 KO* clones so a conclusive observation could not be made (see Section 4.2.9). However, if these data were repeated, this could present a novel link between PC1 and ANKS6. Conversely, loss of PC2 caused an approximate 1.5-fold increase in both *ANKS3 mRNA* and protein expression but had no effect on the expression levels of ANKS6. These data suggest the presence of a close *BICC1-ANKS3-PKD2* relationship, where the expression levels of each are carefully, but perhaps indirectly, regulated by other members of the group.

Overexpression studies were also performed, and the data demonstrated that an overexpression of BICC1 caused a 2.5-fold increase in *ANKS3 mRNA* expression but had no effect on the mRNA expression level of *ANKS6*, again confirming that BICC1 has a direct and active role in *ANKS3* regulation (see Section 4.2.12). Overall, these data suggest that the levels of BICC1 present in kidney epithelial cells is very important, as loss of BICC1 causes a downregulation of *ANKS3*, while an overexpression of BICC1 causes an upregulation of *ANKS3*. Furthermore, the pattern in expression levels between *BICC1*, *PKD1* and *PKD2 KO* cell lines, as well as data from the overexpression experiments, suggests a hierarchy of gene regulation, where PC1 is at the top of the gene regulatory network followed by BICC1, ANKS3 and then PC2. To completely comprehend this gene regulatory network, assessment of expression in *ANKS3 KO* models should be performed.

The pronounced loss of ANKS3 at the protein level in *BICC1 KO* cells suggest BICC1 has a strong regulatory effect on the mRNA stability and translation of *ANKS3*. This theory was assessed using mRNA stability assays, and this study discovered that loss of BICC1 caused a decrease in the mRNA stability of *ANKS3* (see Section 5.2.5). Furthermore, the function of BICC1 as a regulator of mRNA stability was confirmed by assessing whether BICC1 could regulate *ANKS3* at the transcriptional level. This study revealed that BICC1 is not a transcriptional activator or regulator, in terms of the regulation of *ANKS3* transcription, therefore, confirming BICC1 as a post-transcriptional regulator and corroborating the theory that BICC1 positively regulates *ANKS3* by

promoting its mRNA stability, a function also observed for *PKD2* (see Section 5.2.6).

One could theorise that BICC1 regulates *ANKS3* using a similar mechanism as observed by Tran *et al*. (2010), where BICC1 binds the 3' UTR of *PKD2* through its KH domains to competitively inhibit miR-17 from binding to the 3' UTR of *PKD2* to destabilise it, thereby increasing *PKD2* translation. Following analysis of highly conserved miRNA target sequences on Target Scan, there are only two common sites between *PKD2* and *ANKS3*; miR-148 and miR-22; there was not miR-17 site present in the 3' UTR of *ANKS3* (Target Scan v6.2). However, it is possible that there is not a common miRNA between *PKD2* and ANKS3, but instead the mechanism of miRNA inhibition by BICC1 is the same. It would be interesting to further examine these sites through mutagenesis and perform experiments, such as luciferase assays, to conclude whether these miRNAs have a silencing effect upon *PKD2* and *ANKS3*, of which BICC1 inhibits in normal kidney epithelial cells.

On a related note, and due to their close relationship as discussed in Section 1.5.10, the regulatory effect of BICC1 upon the expression of NEK kinases and NEK partner transcripts was assessed. The data demonstrated that loss of BICC1 downregulated the mRNA expression of most of the *NEK* kinases assessed, by an average of 50% (see Section 3.2.13). Furthermore, loss of BICC1 also caused an approximate 50% decrease in the mRNA expression of the NEK partner genes *ACK1*, *NPHP3* and *INVS*, but not *CDC42*. Overall, BICC1 positively regulates the expression of NEK kinases and NEK partner transcripts. Interestingly, NEK7 was the only NEK kinase identified as a protein binding partner of BICC1 in the MS dataset. Following analysis of these data, a hypothesis could be formed stating that loss of BICC1 causes a complete loss of ANKS3 protein, which prevents the formation of the ANKS3-NPHP module and consequently prevents the module connecting with the ANKS6-NPHP module. In addition, the majority of the components of the ANKS6-NPHP module are also downregulated, which might affect the assembly of this module. Without the ANKS3-NPHP and ANKS6-NPHP modules, the downstream functions of CDC42 and ACK1 in regulating actin dynamics and

apical extracellular matrix remodelling might be disrupted, a common phenotype observed in PKD. Misregulation of these processes was also observed in the fRIP-Seq data, which is discussed further in Section 6.7.

6.7 BICC1 mRNA targets are involved in gene regulation processes

Data from this study, as well as published data, has demonstrated that BICC1 regulates mRNA targets within the kidney. However, how BICC1 causes various PKD-like phenotypes is still not clear. Furthermore, a comprehensive study to identify the human mRNA targets of BICC1 has not been published. Consequently, this study sought to identify, in an unbiased way, novel human BICC1-RNA partners that could play a role in the pathogenesis of ADPKD by performing BICC1 RNA-IP experiments followed by deep sequencing (fRIP-Seq). The results demonstrated that BICC1 binds several novel RNA transcripts not previously observed in kidney epithelial cells (see Section 5.2.2).

Through functional annotation analysis, several BICC1-associated RNA transcripts were identified which encode proteins mainly involved in cellular processes such as cellular migration, adhesion, signalling and cytoskeletal organisation, processes defective in ADPKD and previously discussed in preceding sections. Moreover, several RNA transcripts were identified as transcriptional regulators of cellular growth, whilst some BICC1-bound RNAs encode proteins found in biologically relevant pathways that are altered in ADPKD, including MAPK, VEGF, mTOR, ErbB and Wnt signalling pathways. Overall, these data suggest that BICC1 regulates both ciliary and non-ciliary based signalling in kidney epithelial cells.

Interestingly, the two most significantly enriched RNAs associated with BICC1 were the transcription factors, *JUND* and *GLIS2*, suggesting BICC1 might also indirectly regulate transcription through regulating their expression. In addition, several BICC1-bound RNAs encode proteins involved in the regulation of gene expression including *EIF3CL*, *HMGA1* and *POLR2J*. *FOSL1*, another transcription factor involved in the AP-1 complex (similarly to *JUND*) was also identified, as well as the transcriptional activator *GLI1*. Furthermore, comparisons between the BICC1 fRIP-Seq and the BICC1 MS datasets from

this study revealed several transcripts in common, including *BSG*, *FASN*, *ACTN4*, *CFL1* and *EIF4G1*, *PABPC1* and *RPLP2*.

Overall, these data suggest BICC1 has a key role in maintaining normal kidney epithelial cell function through regulating 1) normal cellular migration, adhesion and organisation and 2) vital signalling pathways which control various other important cellular processes. Moreover, BICC1 functions as a principal mRNA regulator within the kidney in two separate, but related ways; 1) by binding to and regulating the stability and translation of mRNA targets and 2) by binding to and regulating the expression of several transcription factors, thus indirectly regulating gene transcription. In this way, BICC1 is responsible for the regulation of a wide range of cellular processes and is a master regulator of kidney epithelial cell homeostasis.

The BICC1-bound RNAs identified in the fRIP-Seq analysis were also compared to a cystic gene panel, compiled by a medical consensus (Sheffield Genetics Diagnostic Service, personal communication, 2019). Interestingly, many of the significant RNA transcripts encode proteins which are involved in various functions in regard to the primary cilium. For example, *GLIS2* (previously discussed), *TMEM107* and *CCDC11* were the three most significantly bound RNAs and they are all involved in normal ciliogenesis and function. Therefore, one could theorise that BICC1 is involved in normal ciliogenesis and function through the regulation of a subset of vital cilia-related proteins and subsequent pathways.

6.8 BICC1 binds the RNA transcripts of the polycystin protein complex and preferentially binds the 3’ UTR of its targets

Data analysis of our BICC1 fRIP-Seq dataset confirmed published research stating BICC1 interacts with *DVL2* and *ADCY6*, just two of the mRNA targets known to be regulated by BICC1 (Piazzon *et al*., 2012; Rothé *et al*., 2015). Further spatial resolution analysis revealed that BICC1 interacts with *DVL2* and *ADCY6* at their 5’ and 3’ UTRs respectively (see Section 5.2.3). These observations confirmed previous experimentation concluding BICC1 binds to

the 3' UTR of *ADCY6* and presents a new interaction region between BICC1 and the 5' UTR of *DVL2* (Piazzon *et al*., 2012; Rothé *et al*., 2015).

In addition, this study has demonstrated that BICC1 interacts with *PKD1*, *PKD2* and *ANKS3* through their 3' UTRs, which might be an important observation to investigate further in order to fully elucidate the mechanistic function of post-transcriptional regulation (see Section 5.2.3). This interaction was validated by both BICC1 fRIP and qPCR experiments. Many RBPs bind to 3' UTRs to perform regulatory functions, so it is not surprising that BICC1 interacts with *PKD1*, *PKD2* and *ANKS3* in this way. The binding of BICC1 to the 3' UTR of *PKD2* also confirms a role for BICC1 in inhibiting miRNA-induced silencing complexes and promoting the mRNA stability of *PKD2*, as previously demonstrated by Tran *et al*. (2010) and in this study.

As discussed in Section 6.3, BICC1 forms protein interactions with members of the translation initiation complex to promote mRNA translation, as well as with components of the deadenylation complex. Furthermore, as stated in Section 1.5.4, 5' UTRs and 3' UTRs are often in close proximity to each other during mRNA translation, as the circularisation of mRNA is common due to frequent associations between the eukaryotic initiation factor eIF4G at the 5' cap and PABP proteins at the 3' UTR. Therefore, it is plausible that BICC1 influences translation initiation as well as the stability and translation of mRNA targets. Based on these data, BICC1 binds the 3' UTRs of *PKD2* and *ANKS3* to positively regulate their mRNA stability and promote their translation through novel protein-protein interactions. Further experimentation is required to fully understand the role of BICC1 upon *PKD1* mRNA regulation, as these data suggests a role for BICC1 in destabilising *PKD1* mRNA.

In contrast to published research, this study did not observe a self-interaction between BICC1 and its own RNA through its 5' UTR (see Section 5.2.3) (Chicoine *et al*., 2007). However, the observations made by others could be due to indirect interactions. For example, BICC1 might interact with other RBPs or RNPs which directly bind to the RNA transcript of BICC1. Since fragmented RIP (fRIP) experiments were not previously performed by other research groups

when investigating direct BICC1-RNA associations, this is a possible explanation.

Spatial resolution and regional mapping analysis in the UCSC Genome Browser established that BICC1 preferentially bound the 3' UTR of many of its RNA targets, including *PKD1*, *PKD2* and *ANKS3*, as well as the most significantly BICC1-bound RNAs *JUND*, *GLIS2*, *CHPF*, and the published RNA targets *ADCY6* and *WNT7B* (see Section 5.2.3). Interestingly, BICC1 preferentially bound the 5' UTR of *DVL2* in contrast to its other targets. Moreover, BICC1 interacted with both the 5' UTRs and 3' UTRs of *KRT7* and *IGBP3*, which could suggest an interplay of regulation between the two sites. It would be beneficial to observe regional interactions of BICC1 with its RNA targets on a global scale to fully comprehend the binding preference of BICC1 and therefore gain a clearer understand of its function as a mRNA regulator.

6.9 Model for BICC1 function in the human kidney

In conclusion, two models can be proposed for the mechanistic role of BICC1 in normal kidney function and in the pathogenesis of ADPKD:

1) Molecular interactions between BICC1 and cystoproteins
2) A wider role for BICC1 in kidney epithelial homeostasis

These models are summarised in Figures 6.9.1 and 6.9.2.

First, we conclude that BICC1 regulates its RNA targets, including *PKD2* and *ANKS3*, post-transcriptionally (Figure 6.9.1). This study proposes that the above regulation occurs through the protection of mRNA stability by BICC1, as whenever there is a loss of mRNA expression due to loss of BICC1, it is accompanied by a reduction in stability (Figure 6.9.1). To further confirm this function, BICC1 expression should be restored in *BICC1 KO* cells, and the mRNA stability assays repeated to assess for a change in the half-lives of *PKD2* and *ANKS3*. Furthermore, single molecule fluorescent *in situ* hybridisation (smFISH) experiments could be performed to investigate whether BICC1 promotes translation of its mRNA targets in a particular location

important for their protein function, for example, at the location where their counterpart proteins interact or form a complex, such as the cystoprotein complex observed in this study (Figure 6.9.1). Why BICC1 regulates these protein complexes and the significance of this in kidney epithelia is still unknown; therefore, further experimentation is required to completely elucidate this function.

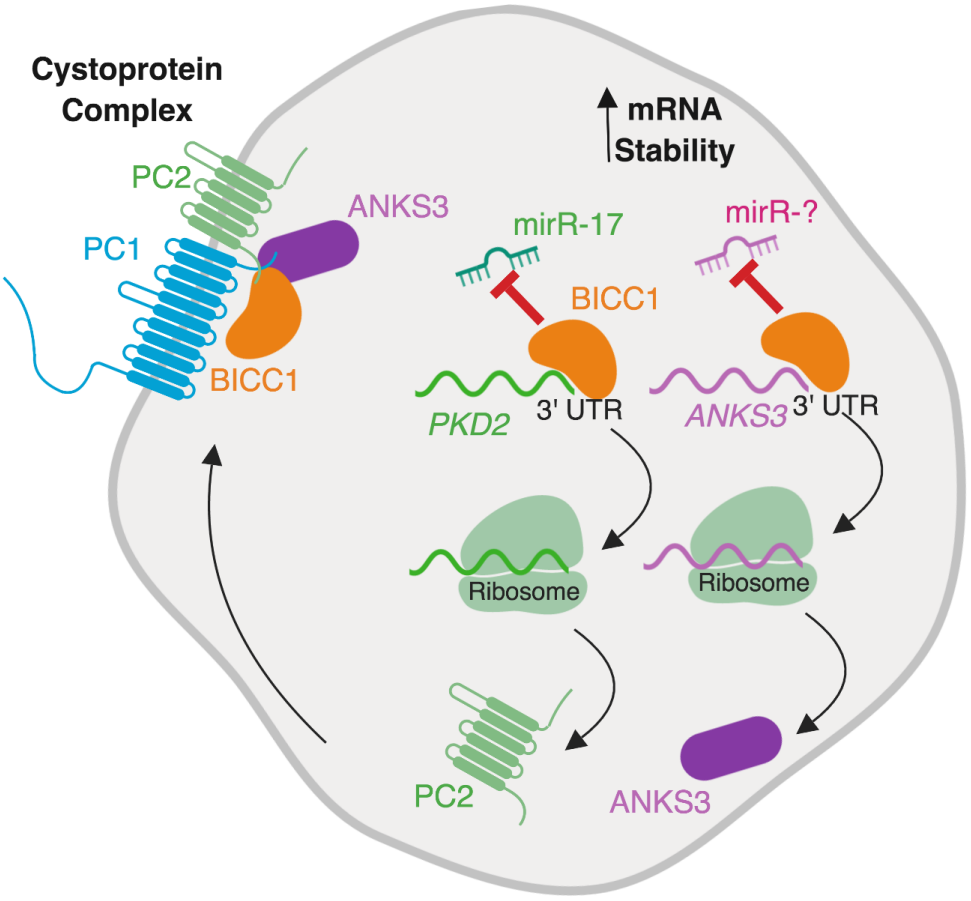

Figure 6.9.1. The molecular interactions between BICC1 and the cystoproteins. The cystoprotein complex associated with ADPKD is composed of PC1 (blue), PC2 (green), ANKS3 (purple) and BICC1 (orange). BICC1 regulates this complex on the protein and RNA level, promoting the mRNA stability of both *PKD2* and *ANKS3*.

Second, we conclude that BICC1 forms protein interactions with translation initiation complexes, to promote mRNA translation, as well as with deadenylation complexes, to inhibit mRNA degradation and protect mRNA stability (Figure 6.9.2, with more a more detailed summary in Figure 6.9.3). Furthermore, these data suggest that BICC1 is a central regulator of cystoproteins, related protein networks, cellular organisation and vital signalling

pathways, through direct or indirect interactions and modulation of both protein and RNA (Figure 6.9.2). Moreover, these data suggest that BICC1 has complex, indirect functions that contribute to the homeostasis of kidney epithelia.

It is beyond the scope of this study to investigate the latter, but the data in this study have identified said homeostatic functions as being regulated, directly or indirectly, by BICC1. Likewise, BICC1 may have a role in maintaining the normal homeostasis of kidney epithelia and may even contribute a specific function. However, this is outside of its role as a cystoprotein, and may have additional roles in organs, such as the brain and the bone.

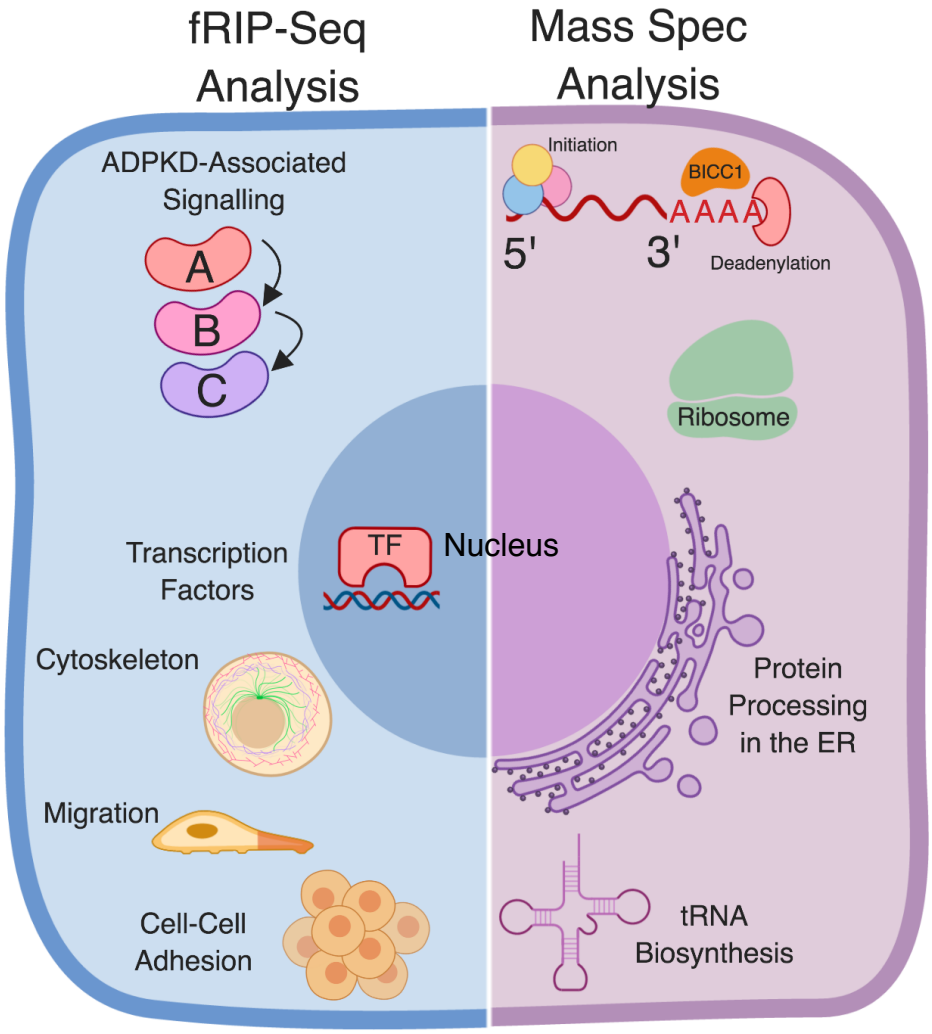

Figure 6.9.2. A wider role for BICC1 in kidney epithelial homeostasis. Based on the fRIP-Seq (left, blue) and MS (right, purple) data within this study, novel BICC1-related pathways and cellular functions have been identified. The displayed pathways and cellular functions were most significantly associated with BICC1, following GO terms and KEGG pathway analyses.

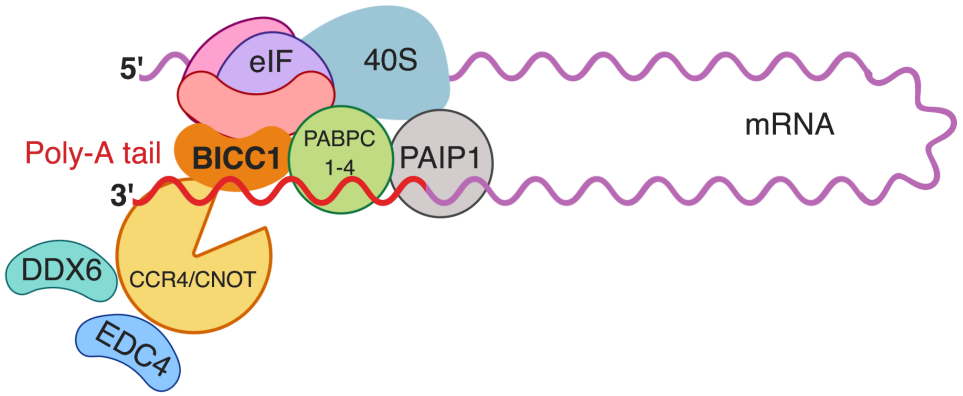

Figure 6.9.3. BICC1 interacts with proteins involved in translation initiation and the deadenylation of mRNA. Through functional annotation analysis, several BICC1-associated proteins were identified, which are mainly involved in translation initiation, deadenylation, and poly(A) binding. These proteins included several members of the eIF preinitiation complex, PABPC1, PABPC4, PAIP1, DDX6, ECD4 and several members of the CCR4-CNOT deadenylation complex. CNOT1 was of the most significantly BICC1-bound proteins identified.

Chapter 7

Appendix

7.0 Appendix

Table 7.1. The novel interacting partners of BICC1. 88 proteins enriched with BICC1 following Co-IP and MS. A cut off of 5-fold change was applied. Red = not found in all 3 Co-IPs (17 proteins). R1 = replicate 1, R2 = replicate 2, R3 = replicate 3.

Accession #	Protein Name	R1	R2	R3	Fold Change
Q9H694	Protein bicaudal C homolog 1 OS=Homo sapiens GN=BICC1 PE=1 SV=2 - [BICC1_HUMAN]	66	61	48	**59.33**
P49327	Fatty acid synthase OS=Homo sapiens GN=FASN PE=1 SV=3 - [FAS_HUMAN]	11	45	64	**41.00**
Q08211	ATP-dependent RNA helicase A OS=Homo sapiens GN=DHX9 PE=1 SV=4 - [DHX9_HUMAN]	30	34	29	**32.00**
Q00610	Clathrin heavy chain 1 OS=Homo sapiens GN=CLTC PE=1 SV=5 - [CLH1_HUMAN]	18	32	42	**31.67**
P35579	Myosin-9 OS=Homo sapiens GN=MYH9 PE=1 SV=4 - [MYH9_HUMAN]	27	26	37	**31.00**
A5YKK6	CCR4-NOT transcription complex subunit 1 OS=Homo sapiens GN=CNOT1 PE=1 SV=2 - [CNOT1_HUMAN]	34	43	12	**30.67**
P42704	Leucine-rich PPR motif-containing protein, mitochondrial OS=Homo sapiens GN=LRPPRC PE=1 SV=3 - [LPPRC_HUMAN]	13	26	46	**29.33**
P21333	Filamin-A OS=Homo sapiens GN=FLNA PE=1 SV=4 - [FLNA_HUMAN]	16	27	40	**28.67**
Q6ZW76	Ankyrin repeat and SAM domain-containing protein 3 OS=Homo sapiens GN=ANKS3 PE=2 SV=1 - [ANKS3_HUMAN]	29	32	16	**26.67**
P06733	Alpha-enolase OS=Homo sapiens GN=ENO1 PE=1 SV=2 - [ENOA_HUMAN]	12	30	33	**26.00**
P14618	Pyruvate kinase PKM OS=Homo sapiens GN=PKM PE=1 SV=4 - [KPYM_HUMAN]	10	30	33	**25.33**
Q14204	Cytoplasmic dynein 1 heavy chain 1 OS=Homo sapiens GN=DYNC1H1 PE=1 SV=5 - [DYHC1_HUMAN]	0	29	37	**23.00**
P50990	T-complex protein 1 subunit theta OS=Homo sapiens GN=CCT8 PE=1 SV=4 - [TCPQ_HUMAN]	4	23	33	**21.00**
P07814	Bifunctional glutamate/proline--tRNA ligase OS=Homo sapiens GN=EPRS PE=1 SV=5 - [SYEP_HUMAN]	10	16	33	**20.67**
P22314	Ubiquitin-like modifier-activating enzyme 1 OS=Homo sapiens GN=UBA1 PE=1 SV=3 - [UBA1_HUMAN]	5	22	32	**20.67**
Q13263	Transcription intermediary factor 1-beta OS=Homo sapiens GN=TRIM28 PE=1 SV=5 - [TIF1B_HUMAN]	11	19	26	**19.67**
P55060	Exportin-2 OS=Homo sapiens GN=CSE1L PE=1 SV=3 - [XPO2_HUMAN]	9	19	28	**19.67**
Q92616	Translational activator GCN1 OS=Homo sapiens GN=GCN1L1 PE=1 SV=6 - [GCN1L_HUMAN]	3	18	34	**19.33**
P63261	Actin, cytoplasmic 2 OS=Homo sapiens GN=ACTG1 PE=1 SV=1 - [ACTG_HUMAN]	19	23	12	**19.00**
P23396	40S ribosomal protein S3 OS=Homo sapiens GN=RPS3 PE=1 SV=2 - [RS3_HUMAN]	17	19	17	**18.67**
Q07065	Cytoskeleton-associated protein 4 OS=Homo sapiens GN=CKAP4 PE=1 SV=2 - [CKAP4_HUMAN]	7	16	30	**18.67**
P30101	Protein disulfide-isomerase A3 OS=Homo sapiens GN=PDIA3 PE=1 SV=4 - [PDIA3_HUMAN]	4	15	32	**18.00**
Q9Y490	Talin-1 OS=Homo sapiens GN=TLN1 PE=1 SV=3 - [TLN1_HUMAN]	3	19	29	**18.00**
Q93008	Probable ubiquitin carboxyl-terminal hydrolase FAF-X OS=Homo sapiens GN=USP9X PE=1 SV=3 - [USP9X_HUMAN]	19	25	6	**17.67**
Q99832	T-complex protein 1 subunit eta OS=Homo sapiens GN=CCT7 PE=1 SV=2 - [TCPH_HUMAN]	4	22	24	**17.67**
O00410	Importin-5 OS=Homo sapiens GN=IPO5 PE=1 SV=4 - [IPO5_HUMAN]	1	14	35	**17.67**
Q9Y3F4	Serine-threonine kinase receptor-associated protein OS=Homo sapiens GN=STRAP PE=1 SV=1 - [STRAP_HUMAN]	17	19	13	**17.33**
P05023	Sodium/potassium-transporting ATPase subunit alpha-1 OS=Homo sapiens GN=ATP1A1 PE=1 SV=1 - [AT1A1_HUMAN]	11	20	18	**17.33**
Q6P2Q9	Pre-mRNA-processing-splicing factor 8 OS=Homo sapiens GN=PRPF8 PE=1 SV=2 - [PRP8_HUMAN]	6	22	20	**17.00**
P00558	Phosphoglycerate kinase 1 OS=Homo sapiens GN=PGK1 PE=1 SV=3 - [PGK1_HUMAN]	4	20	24	**17.00**
P78371	T-complex protein 1 subunit beta OS=Homo sapiens GN=CCT2 PE=1 SV=4 - [TCPB_HUMAN]	0	17	31	**17.00**
Q14974	Importin subunit beta-1 OS=Homo sapiens GN=KPNB1 PE=1 SV=2 - [IMB1_HUMAN]	6	14	28	**17.00**
P50991	T-complex protein 1 subunit delta OS=Homo sapiens GN=CCT4 PE=1 SV=4 - [TCPD_HUMAN]	4	17	26	**16.67**
P04075	Fructose-bisphosphate aldolase A OS=Homo sapiens GN=ALDOA PE=1 SV=2 - [ALDOA_HUMAN]	4	19	24	**16.67**
P40939	Trifunctional enzyme subunit alpha, mitochondrial OS=Homo sapiens GN=HADHA PE=1 SV=2 - [ECHA_HUMAN]	18	16	12	**16.33**
P53396	ATP-citrate synthase OS=Homo sapiens GN=ACLY PE=1 SV=3 - [ACLY_HUMAN]	4	15	27	**16.33**
Q14697	Neutral alpha-glucosidase AB OS=Homo sapiens GN=GANAB PE=1 SV=3 - [GANAB_HUMAN]	2	15	28	**16.00**
P55072	Transitional endoplasmic reticulum ATPase OS=Homo sapiens GN=VCP PE=1 SV=4 - [TERA_HUMAN]	4	15	26	**16.00**
Q7L2E3	Putative ATP-dependent RNA helicase DHX30 OS=Homo sapiens GN=DHX30 PE=1 SV=1 - [DHX30_HUMAN]	16	18	9	**15.33**
P13667	Protein disulfide-isomerase A4 OS=Homo sapiens GN=PDIA4 PE=1 SV=2 - [PDIA4_HUMAN]	0	15	28	**15.33**
P12956	X-ray repair cross-complementing protein 6 OS=Homo sapiens GN=XRCC6 PE=1 SV=2 - [XRCC6_HUMAN]	5	13	25	**15.33**
Q9NR30	Nucleolar RNA helicase 2 OS=Homo sapiens GN=DDX21 PE=1 SV=5 - [DDX21_HUMAN]	3	24	15	**15.00**
O14654	Insulin receptor substrate 4 OS=Homo sapiens GN=IRS4 PE=1 SV=1 - [IRS4_HUMAN]	4	22	16	**15.00**
P07237	Protein disulfide-isomerase OS=Homo sapiens GN=P4HB PE=1 SV=3 - [PDIA1_HUMAN]	0	16	26	**15.00**
Q8TDX7	Serine/threonine-protein kinase Nek7 OS=Homo sapiens GN=NEK7 PE=1 SV=1 - [NEK7_HUMAN]	15	19	6	**14.33**
P05388	60S acidic ribosomal protein P0 OS=Homo sapiens GN=RPLP0 PE=1 SV=1 - [RLA0_HUMAN]	12	15	13	**14.33**
Q9Y230	RuvB-like 2 OS=Homo sapiens GN=RUVBL2 PE=1 SV=3 - [RUVB2_HUMAN]	10	12	18	**14.33**
P54886	Delta-1-pyrroline-5-carboxylate synthase OS=Homo sapiens GN=ALDH18A1 PE=1 SV=2 - [P5CS_HUMAN]	3	21	16	**14.33**
O75369	Filamin-B OS=Homo sapiens GN=FLNB PE=1 SV=2 - [FLNB_HUMAN]	0	12	28	**14.33**
P17987	T-complex protein 1 subunit alpha OS=Homo sapiens GN=TCP1 PE=1 SV=1 - [TCPA_HUMAN]	0	16	24	**14.33**
P11586	C-1-tetrahydrofolate synthase, cytoplasmic OS=Homo sapiens GN=MTHFD1 PE=1 SV=3 - [C1TC_HUMAN]	0	17	23	**14.33**
P11940	Polyadenylate-binding protein 1 OS=Homo sapiens GN=PABPC1 PE=1 SV=2 - [PABP1_HUMAN]	10	14	14	**13.67**
Q86VP6	Cullin-associated NEDD8-dissociated protein 1 OS=Homo sapiens GN=CAND1 PE=1 SV=2 - [CAND1_HUMAN]	0	15	23	**13.67**
P21796	Voltage-dependent anion-selective channel protein 1 OS=Homo sapiens GN=VDAC1 PE=1 SV=2 - [VDAC1_HUMAN]	12	11	14	**13.33**
P35580	Myosin-10 OS=Homo sapiens GN=MYH10 PE=1 SV=3 - [MYH10_HUMAN]	0	16	21	**13.33**
Q96EY7	Pentatricopeptide repeat domain-containing protein 3, mitochondrial OS=Homo sapiens GN=PTCD3 PE=1 SV=3 - [PTCD3_HUMAN]	18	10	8	**13.00**
Q9HCE1	Putative helicase MOV-10 OS=Homo sapiens GN=MOV10 PE=1 SV=2 - [MOV10_HUMAN]	10	19	7	**13.00**
P06744	Glucose-6-phosphate isomerase OS=Homo sapiens GN=GPI PE=1 SV=4 - [G6PI_HUMAN]	0	12	24	**13.00**
P56192	Methionine--tRNA ligase, cytoplasmic OS=Homo sapiens GN=MARS PE=1 SV=2 - [SYMC_HUMAN]	0	12	24	**13.00**
P62258	14-3-3 protein epsilon OS=Homo sapiens GN=YWHAE PE=1 SV=1 - [1433E_HUMAN]	0	14	22	**13.00**
Q92900	Regulator of nonsense transcripts 1 OS=Homo sapiens GN=UPF1 PE=1 SV=2 - [RENT1_HUMAN]	15	11	9	**12.67**
Q7KZF4	Staphylococcal nuclease domain-containing protein 1 OS=Homo sapiens GN=SND1 PE=1 SV=1 - [SND1_HUMAN]	0	14	21	**12.67**
P13010	X-ray repair cross-complementing protein 5 OS=Homo sapiens GN=XRCC5 PE=1 SV=3 - [XRCC5_HUMAN]	0	14	21	**12.67**
P49368	T-complex protein 1 subunit gamma OS=Homo sapiens GN=CCT3 PE=1 SV=4 - [TCPG_HUMAN]	0	14	21	**12.67**
Q12906	Interleukin enhancer-binding factor 3 OS=Homo sapiens GN=ILF3 PE=1 SV=3 - [ILF3_HUMAN]	11	11	12	**12.33**
P22102	Trifunctional purine biosynthetic protein adenosine-3 OS=Homo sapiens GN=GART PE=1 SV=1 - [PUR2_HUMAN]	0	13	21	**12.33**
P49411	Elongation factor Tu, mitochondrial OS=Homo sapiens GN=TUFM PE=1 SV=2 - [EFTU_HUMAN]	0	13	21	**12.33**
P49321	Nuclear autoantigenic sperm protein OS=Homo sapiens GN=NASP PE=1 SV=2 - [NASP_HUMAN]	0	11	22	**12.00**
Q13310	Polyadenylate-binding protein 4 OS=Homo sapiens GN=PABPC4 PE=1 SV=1 - [PABP4_HUMAN]	12	8	12	**11.67**
Q02790	Peptidyl-prolyl cis-trans isomerase FKBP4 OS=Homo sapiens GN=FKBP4 PE=1 SV=3 - [FKBP4_HUMAN]	0	11	21	**11.67**
Q6PKG0	La-related protein 1 OS=Homo sapiens GN=LARP1 PE=1 SV=2 - [LARP1_HUMAN]	12	12	7	**11.33**
Q92945	Far upstream element-binding protein 2 OS=Homo sapiens GN=KHSRP PE=1 SV=4 - [FUBP2_HUMAN]	0	8	23	**11.33**
P31948	Stress-induced-phosphoprotein 1 OS=Homo sapiens GN=STIP1 PE=1 SV=1 - [STIP1_HUMAN]	0	9	22	**11.33**
Q16531	DNA damage-binding protein 1 OS=Homo sapiens GN=DDB1 PE=1 SV=1 - [DDB1_HUMAN]	0	10	21	**11.33**
O75533	Splicing factor 3B subunit 1 OS=Homo sapiens GN=SF3B1 PE=1 SV=3 - [SF3B1_HUMAN]	0	10	21	**11.33**
P12277	Creatine kinase B-type OS=Homo sapiens GN=CKB PE=1 SV=1 - [KCRB_HUMAN]	0	9	21	**11.00**
P31939	Bifunctional purine biosynthesis protein PURH OS=Homo sapiens GN=ATIC PE=1 SV=3 - [PUR9_HUMAN]	0	9	21	**11.00**
O75643	U5 small nuclear ribonucleoprotein 200 kDa helicase OS=Homo sapiens GN=SNRNP200 PE=1 SV=2 - [U520_HUMAN]	0	9	21	**11.00**
Q86UP2	Kinectin OS=Homo sapiens GN=KTN1 PE=1 SV=1 - [KTN1_HUMAN]	0	8	21	**10.67**
Q9NZI8	Insulin-like growth factor 2 mRNA-binding protein 1 OS=Homo sapiens GN=IGF2BP1 PE=1 SV=2 - [IF2B1_HUMAN]	13	3	12	**10.33**
P12270	Nucleoprotein TPR OS=Homo sapiens GN=TPR PE=1 SV=3 - [TPR_HUMAN]	0	6	22	**10.33**
P39019	40S ribosomal protein S19 OS=Homo sapiens GN=RPS19 PE=1 SV=2 - [RS19_HUMAN]	10	9	8	**10.00**
Q92552	28S ribosomal protein S27, mitochondrial OS=Homo sapiens GN=MRPS27 PE=1 SV=3 - [RT27_HUMAN]	10	9	8	**10.00**
P82650	28S ribosomal protein S22, mitochondrial OS=Homo sapiens GN=MRPS22 PE=1 SV=1 - [RT22_HUMAN]	13	7	6	**9.67**
P51398	28S ribosomal protein S29, mitochondrial OS=Homo sapiens GN=DAP3 PE=1 SV=1 - [RT29_HUMAN]	14	7	4	**9.33**
Q13813	Spectrin alpha chain, non-erythrocytic 1 OS=Homo sapiens GN=SPTAN1 PE=1 SV=3 - [SPTN1_HUMAN]	0	3	22	**9.33**
Q9Y399	28S ribosomal protein S2, mitochondrial OS=Homo sapiens GN=MRPS2 PE=1 SV=1 - [RT02_HUMAN]	10	8	4	**8.33**
Q9BYN8	28S ribosomal protein S26, mitochondrial OS=Homo sapiens GN=MRPS26 PE=1 SV=1 - [RT26_HUMAN]	11	2	3	**6.33**

Table 7.2. The Constam-Smith MS data comparison. A cut off of 20-fold change was applied.

Constam Group

Gene	Identified Protein	Accession Number	Ctr_IP 1	IP 1	Ctr_IP 2	IP 2	Ctr_IP 3	IP 3	Fold change
CNOT1	CCR4-NOT transcription complex subunit 1 OS=Homo sapiens GN=CNOT1 PE=1 SV=2	A5YKK6	0	84	0	74	-	-	**80.0**
FLNA	Filamin-A OS=Homo sapiens GN=FLNA PE=1 SV=4	P21333 (+2)	0	36	0	18	-	-	**28.0**
ACTN4	Alpha-actinin-4 OS=Homo sapiens GN=ACTN4 PE=1 SV=2	O43707	0	29	0	23	-	-	**27.0**
CAD	CAD protein OS=Homo sapiens GN=CAD PE=1 SV=1	F8VPD4 (+1)	0	57	2	45	-	-	**26.0**
WDR26	Isoform 2 of WD repeat-containing protein 26 OS=Homo sapiens GN=WDR26	Q9H7D7-2	0	28	0	20	-	-	**25.0**
SEC16A	Protein transport protein Sec16A OS=Homo sapiens GN=SEC16A PE=1 SV=1	J3KNL6	0	24	0	23	-	-	**24.5**
GCN1	eIF-2-alpha kinase activator GCN1 OS=Homo sapiens GN=GCN1 PE=1 SV=6	Q92616	0	41	1	26	-	-	**23.0**
EPPK1	Epiplakin OS=Homo sapiens GN=EPPK1 PE=1 SV=2	A0A075B730 (+1)	0	21	0	20	-	-	**21.5**
GTF2I	General transcription factor II-I OS=Homo sapiens GN=GTF2I PE=1 SV=2	P78347 (+3)	0	21	0	18	-	-	**20.5**
FASN	Fatty acid synthase OS=Homo sapiens GN=FASN PE=1 SV=3	P49327	0	36	1	21	-	-	**19.7**
SCSDE1	Cold shock domain-containing protein E1 OS=Homo sapiens GN=CSDE1 PE=1 SV=2	O75534 (+3)	0	19	0	16	-	-	**18.5**
ANKS3	Ankyrin repeat and SAM domain-containing protein 3 OS=Homo sapiens GN=ANKS3 PE=1 SV=1	D3DUE4 (+3)	0	16	0	16	-	-	**17.0**
TCP1	T-complex protein 1 subunit alpha OS=Homo sapiens GN=TCP1 PE=1 SV=1	P17987	0	19	0	6	-	-	**13.5**
CCT8	T-complex protein 1 subunit theta OS=Homo sapiens GN=CCT8 PE=1 SV=4	P50990	1	22	0	16	-	-	**13.3**
STRAP	Serine-threonine kinase receptor-associated protein OS=Homo sapiens GN=STRAP PE=1 SV=1	Q9Y3F4	0	13	0	11	-	-	**13.0**
XPO1	Exportin-1 OS=Homo sapiens GN=XPO1 PE=1 SV=1	O14980	1	22	0	14	-	-	**12.7**
SLC25A5	ADP/ATP translocase 2 OS=Homo sapiens GN=SLC25A5 PE=1 SV=7	P05141	0	12	0	11	-	-	**12.5**
HNRNPM	Heterogeneous nuclear ribonucleoprotein M OS=Homo sapiens GN=HNRNPM PE=1 SV=1	A0A087X0X3 (+2)	0	12	0	10	-	-	**12.0**
EPRS	Bifunctional glutamate/proline--tRNA ligase OS=Homo sapiens GN=EPRS PE=1 SV=5	P07814	1	26	1	19	-	-	**11.8**
RANBP9	Ran-binding protein 9 OS=Homo sapiens GN=RANBP9 PE=1 SV=1	Q96S59	0	13	0	8	-	-	**11.5**
RUVBL1	RuvB-like 1 OS=Homo sapiens GN=RUVBL1 PE=1 SV=1	Q9Y265	0	17	1	15	-	-	**11.3**
NUP205	Nuclear pore complex protein Nup205 OS=Homo sapiens GN=NUP205 PE=1 SV=3	Q92621	0	14	0	5	-	-	**10.5**
CCT2	T-complex protein 1 subunit beta OS=Homo sapiens GN=CCT2 PE=1 SV=4	P78371	0	13	0	6	-	-	**10.5**

Smith

Gene	Identified Protein	Accession Number	Ctr_IP 1	IP 1	Ctr_IP 2	IP 2	Ctr_IP 3	IP 3	Fold change
BICC1	Protein bicaudal C homolog 1 OS=Homo sapiens GN=BICC1 PE=1 SV=2 - [BICC1_HUMAN]	Q9H694	0	66	0	61	0	48	**59.33**
FASN	Fatty acid synthase OS=Homo sapiens GN=FASN PE=1 SV=3 - [FAS_HUMAN]	P49327	0	11	0	45	0	64	**41.00**
DHX9	ATP-dependent RNA helicase A OS=Homo sapiens GN=DHX9 PE=1 SV=4 - [DHX9_HUMAN]	Q08211	0	30	0	34	0	29	**32.00**
CLTC	Clathrin heavy chain 1 OS=Homo sapiens GN=CLTC PE=1 SV=5 - [CLH1_HUMAN]	Q00610	0	18	0	32	0	42	**31.67**
MYH9	Myosin-9 OS=Homo sapiens GN=MYH9 PE=1 SV=4 - [MYH9_HUMAN]	P35579	0	27	0	26	0	37	**31.00**
CNOT1	CCR4-NOT transcription complex subunit 1 OS=Homo sapiens GN=CNOT1 PE=1 SV=2 - [CNOT1_HUMAN]	A5YKK6	0	34	0	43	0	12	**30.67**
LRPPRC	Leucine-rich PPR motif-containing protein, mitochondrial OS=Homo sapiens GN=LRPPRC PE=1 SV=3 - [LPPRC_HUMAN]	P42704	0	13	0	26	0	46	**29.33**
FLNA	Filamin-A OS=Homo sapiens GN=FLNA PE=1 SV=4 - [FLNA_HUMAN]	P21333	0	16	0	27	0	40	**28.67**
ANKS3	Ankyrin repeat and SAM domain-containing protein 3 OS=Homo sapiens GN=ANKS3 PE=2 SV=1 - [ANKS3_HUMAN]	Q6ZW76	0	29	0	32	0	16	**26.67**
ENO1	Alpha-enolase OS=Homo sapiens GN=ENO1 PE=1 SV=2 - [ENOA_HUMAN]	P06733	0	12	0	30	0	33	**26.00**
PKM	Pyruvate kinase PKM OS=Homo sapiens GN=PKM PE=1 SV=4 - [KPYM_HUMAN]	P14618	0	10	0	30	0	33	**25.33**
DYNC1H1	Cytoplasmic dynein 1 heavy chain 1 OS=Homo sapiens GN=DYNC1H1 PE=1 SV=5 - [DYHC1_HUMAN]	Q14204	0	0	0	29	0	37	**23.00**
CCT8	T-complex protein 1 subunit theta OS=Homo sapiens GN=CCT8 PE=1 SV=4 - [TCPQ_HUMAN]	P50990	0	4	0	23	0	33	**21.00**
EPRS	Bifunctional glutamate/proline--tRNA ligase OS=Homo sapiens GN=EPRS PE=1 SV=5 - [SYEP_HUMAN]	P07814	0	10	0	16	0	33	**20.67**
UBA1	Ubiquitin-like modifier-activating enzyme 1 OS=Homo sapiens GN=UBA1 PE=1 SV=3 - [UBA1_HUMAN]	P22314	0	5	0	22	0	32	**20.67**

Table 7.3. The Constam-Smith MS data comparison of the CTLH complex.

Constam Group

CTLH/GID subunit	Gene	Identified Protein	Ctr_IP 1	IP 1	Ctr_IP 2	IP 2	Ctr_IP 3	IP 3	Fold change
GID7	WDR26	WD repeat-containing protein 26	0	28	0	20	-	-	**25.00**
GID1	RanBP9	Ran-binding protein 9	0	13	0	8	-	-	**11.50**
GID9	MAEA1	Macrophage erythroblast attacher	0	11	0	4	-	-	**8.50**
GID8	TWA1	Glucose-induced degradation protein 8 homolog	0	7	0	6	-	-	**7.50**
GID2	RMND5a	Required for meiotic nuclear division 5 homolog A	0	8	0	3	-	-	**6.50**
GID5	ARMC8	Armadilo repeat-containing protein 8	1	5	0	0	-	-	**2.30**

Smith

CTLH/GID subunit	Gene	Identified Protein	Ctr_IP 1	IP 1	Ctr_IP 2	IP 2	Ctr_IP 3	IP 3	Fold change
GID7	WDR26	WD repeat-containing protein 26	0	4	0	3	0	0	**3.33**
GID1	RanBP9	Ran-binding protein 9	0	2	0	4	0	0	**3.00**
GID9	MAEA1	Macrophage erythroblast attacher	0	0	0	0	0	0	**1.00**
GID8	TWA1	Glucose-induced degradation protein 8 homolog	0	0	0	0	0	0	**1.00**
GID2	RMND5a	Required for meiotic nuclear division 5 homolog A	0	0	0	0	0	0	**1.00**
GID5	ARMC8	Armadilo repeat-containing protein 8	0	2	0	0	0	0	**1.67**

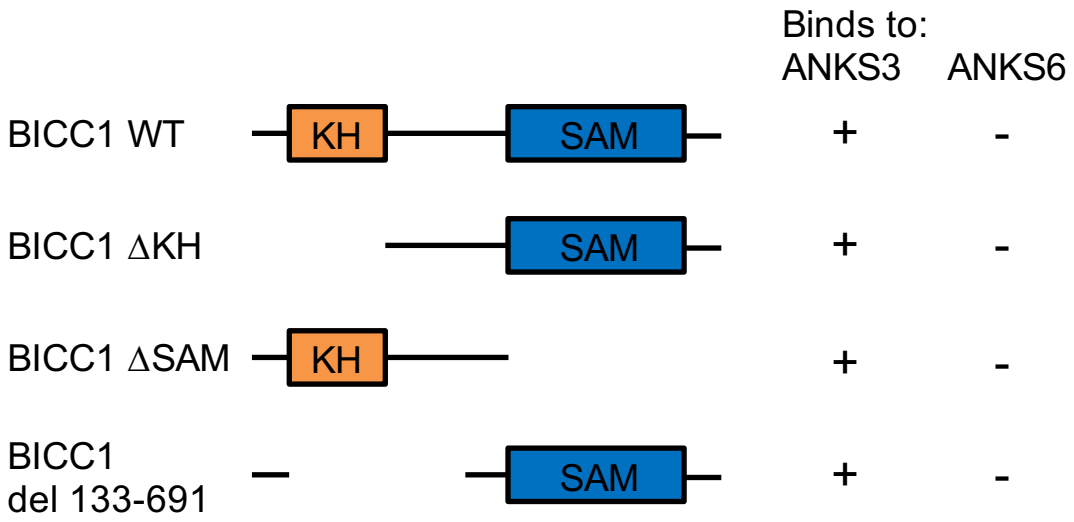

Figure 7.1. BICC1 domain interactions with ANKS3 and ANKS6.

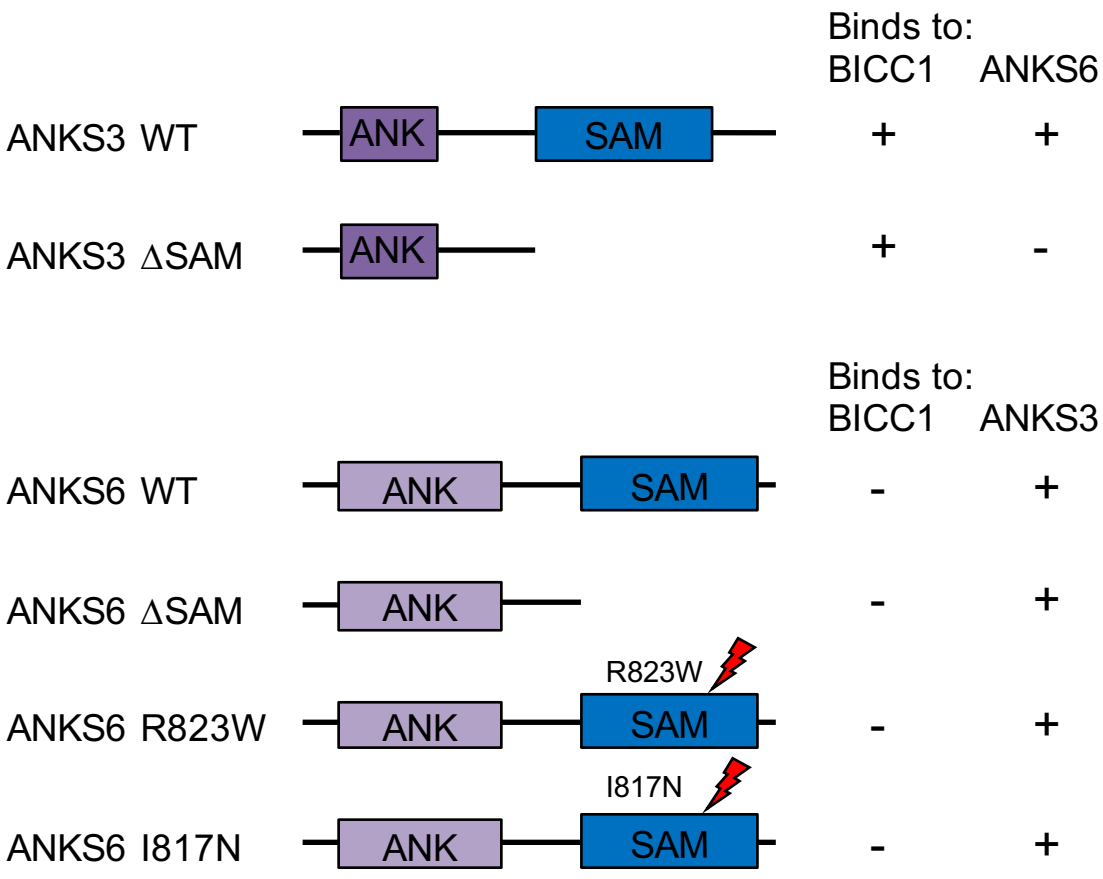

Figure 7.2. ANKS3 and ANKS6 interactions.

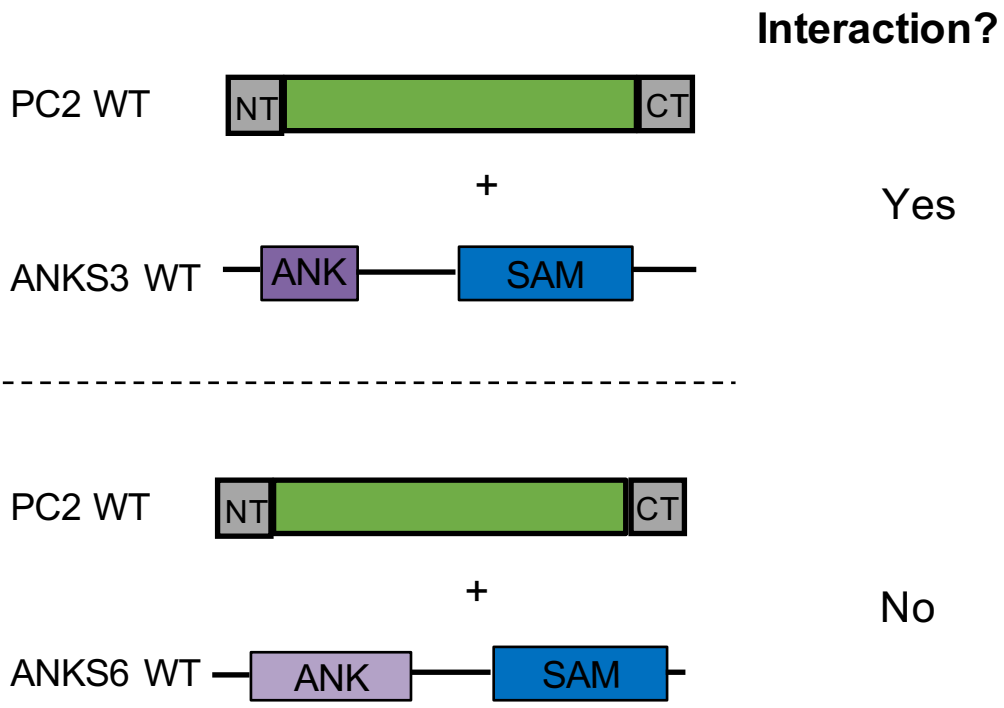

Figure 7.3. PC1 and PC2 interact with ANKS3.

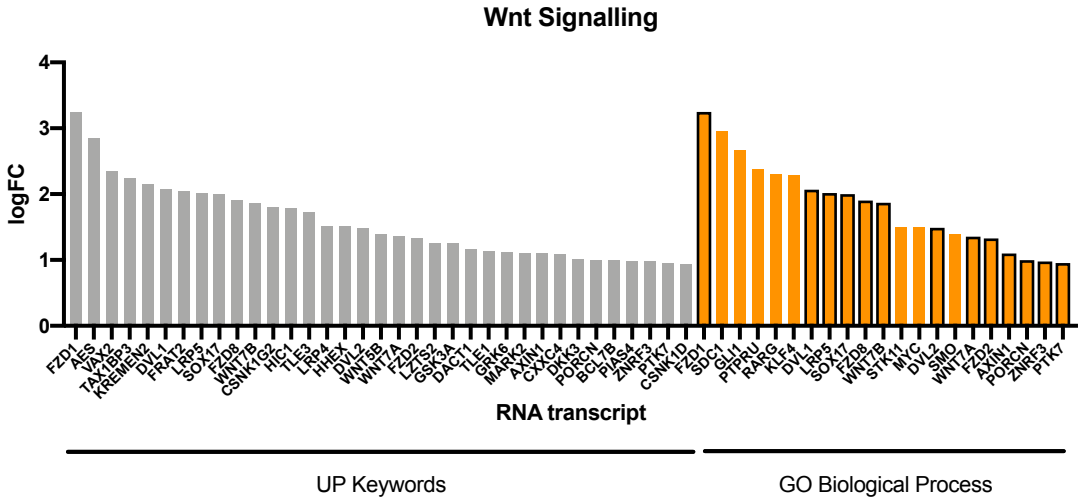

Figure 7.4. The logFC values of the individual RNA transcripts enriched within Wnt signalling following DAVID UP Keyword and GO Biological Process analysis.

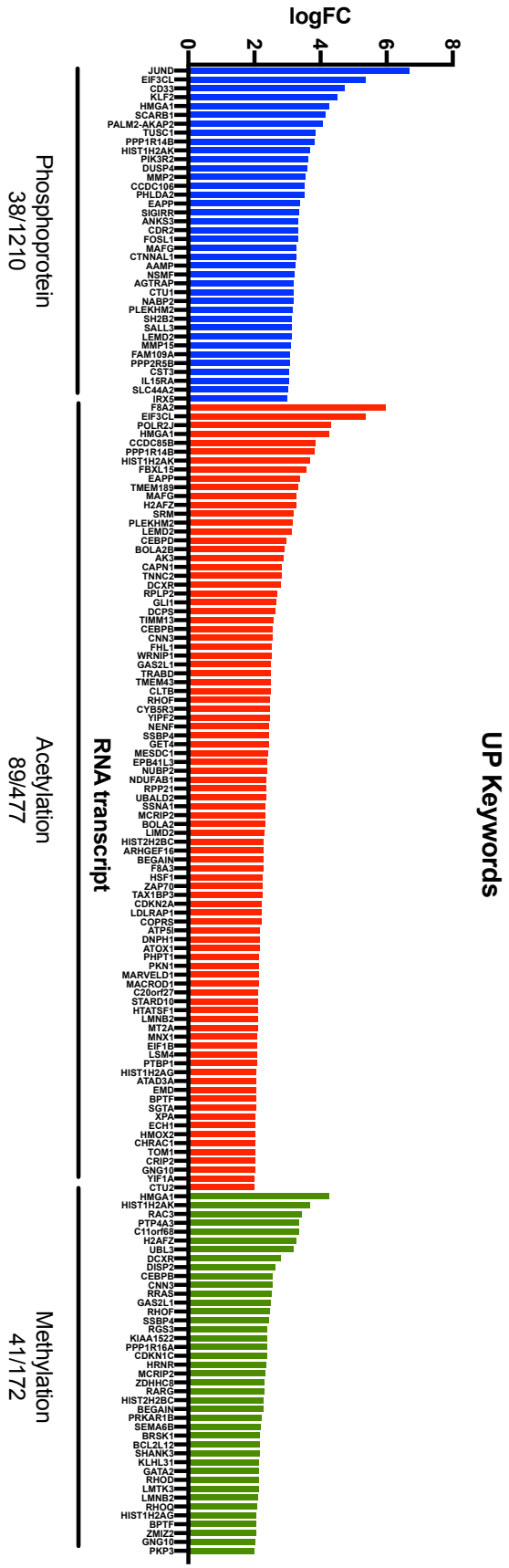

Figure 7.5. The logFC values of the individual RNA transcripts enriched within the top three most significant UP Keywords, ranked by p-value, as listed in Table 5.2.2.1.

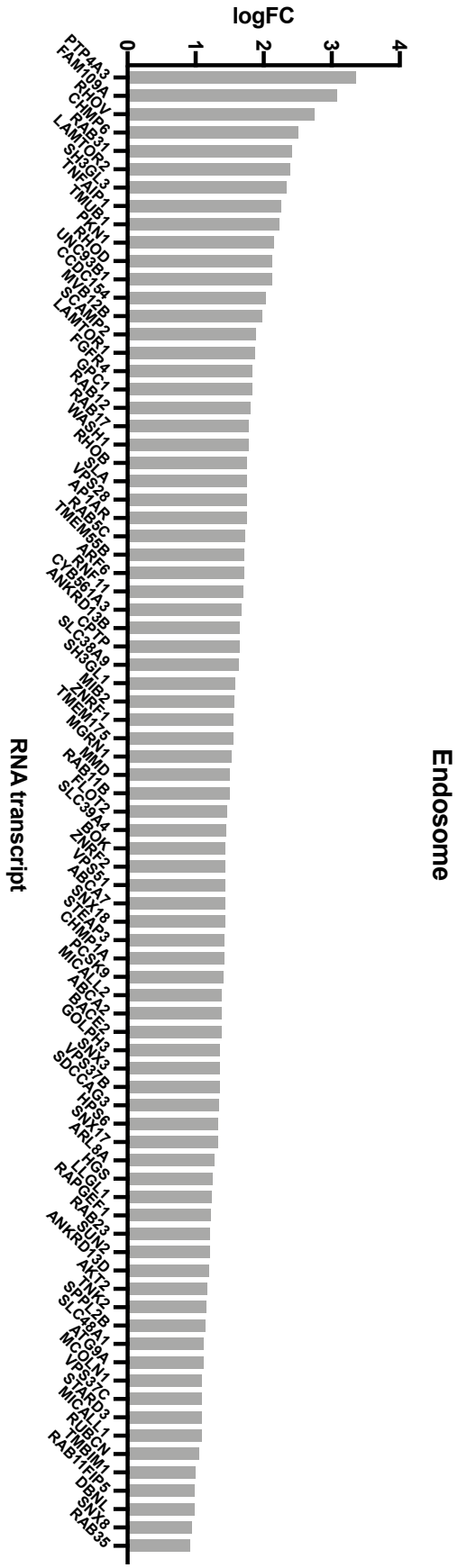

Figure 7.6. The logFC values of the individual RNA transcripts enriched within endosomes following DAVID UP Keyword analysis.

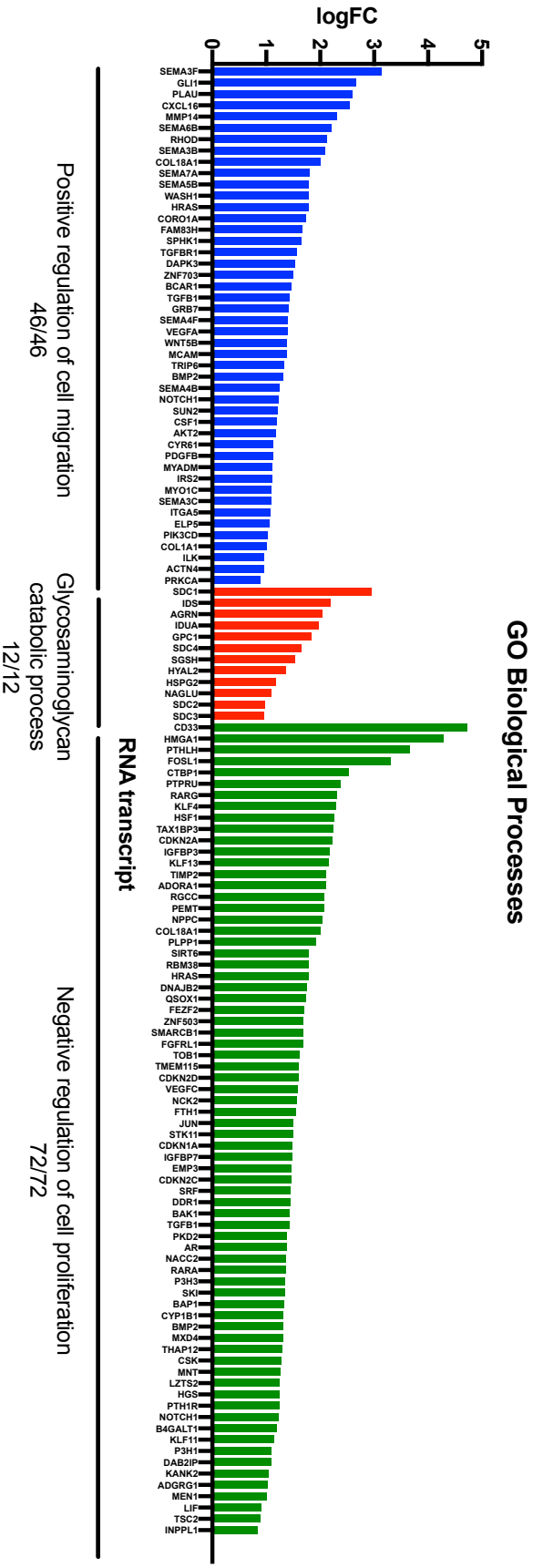

Figure 7.7. The logFC values of the individual RNA transcripts enriched within the top three most significant GO Biological Process, ranked by p-value, as listed in Table 5.2.2.2.

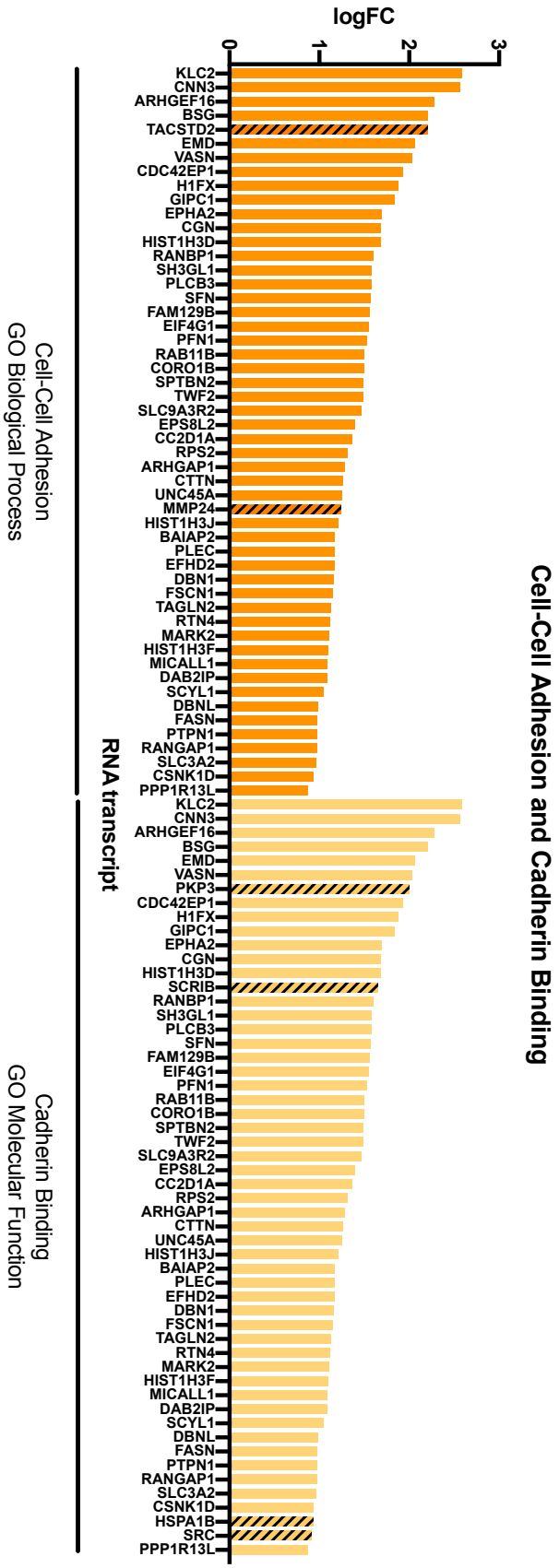

Figure 7.8. The logFC values of the individual RNA transcripts enriched within cell-cell adhesion and cadherin binding following DAVID GO Biological Process and Molecular Function analysis.

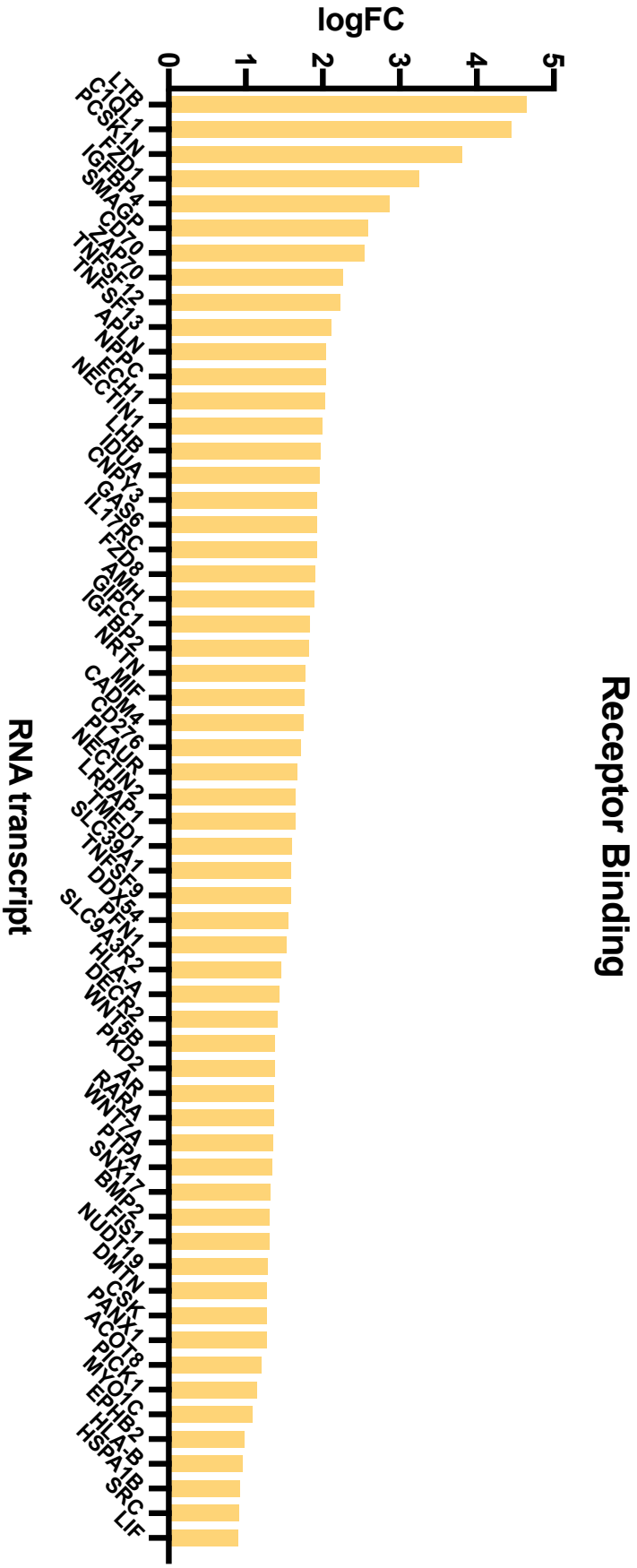

Figure 7.9. The logFC values of the individual RNA transcripts enriched within receptor binding following DAVID GO Molecular Function analysis.

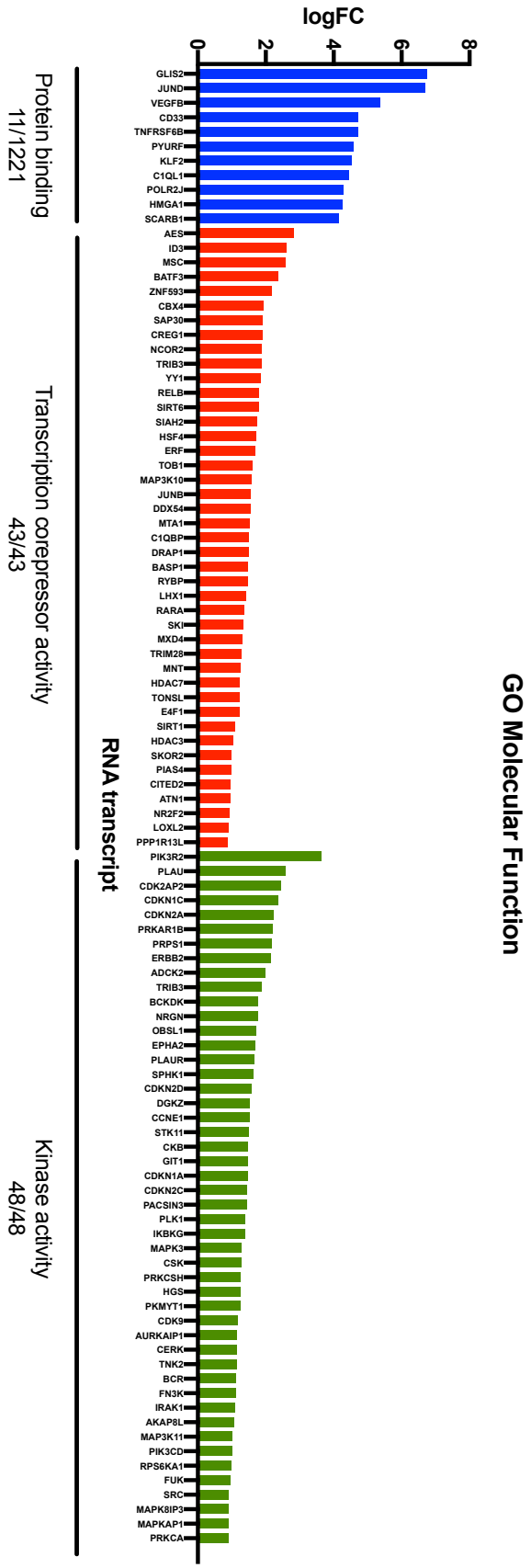

Figure 7.10. The logFC values of the individual RNA transcripts enriched within the top three most significant GO Molecular Function, ranked by p-value, as listed in Table 5.2.2.3.

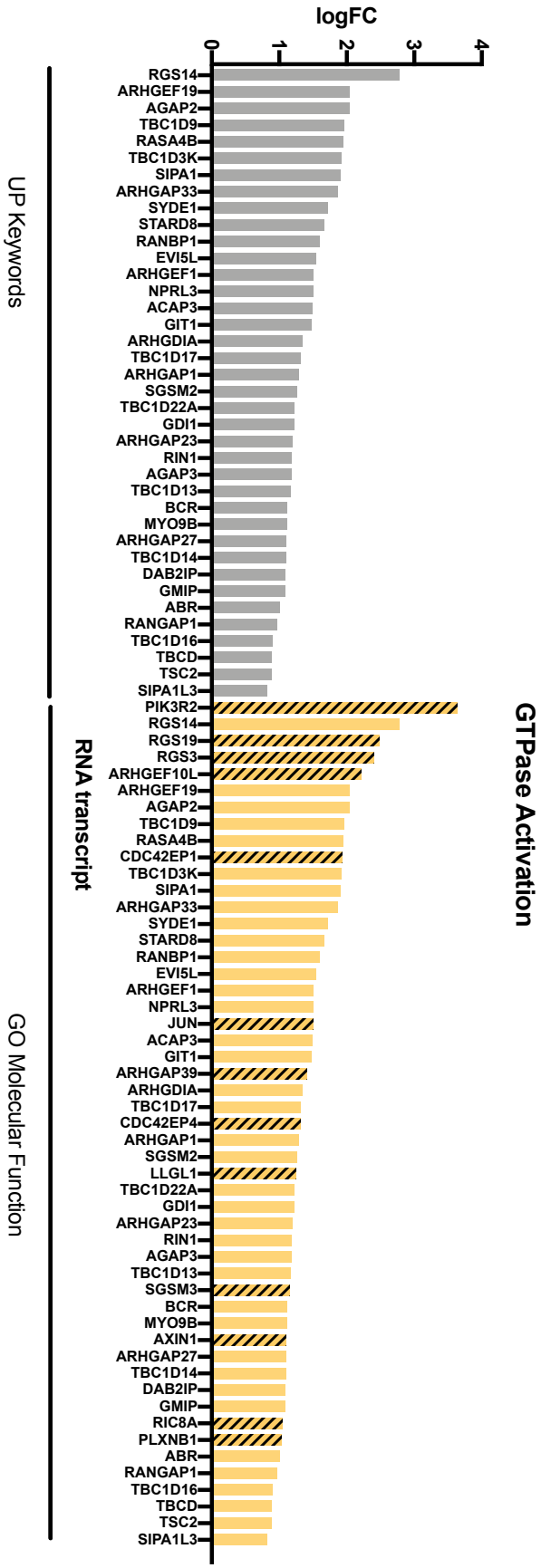

Figure 7.11. The logFC values of the individual RNA transcripts enriched within GTPase activation following DAVID UP Keyowrds GO Molecular Function analysis.

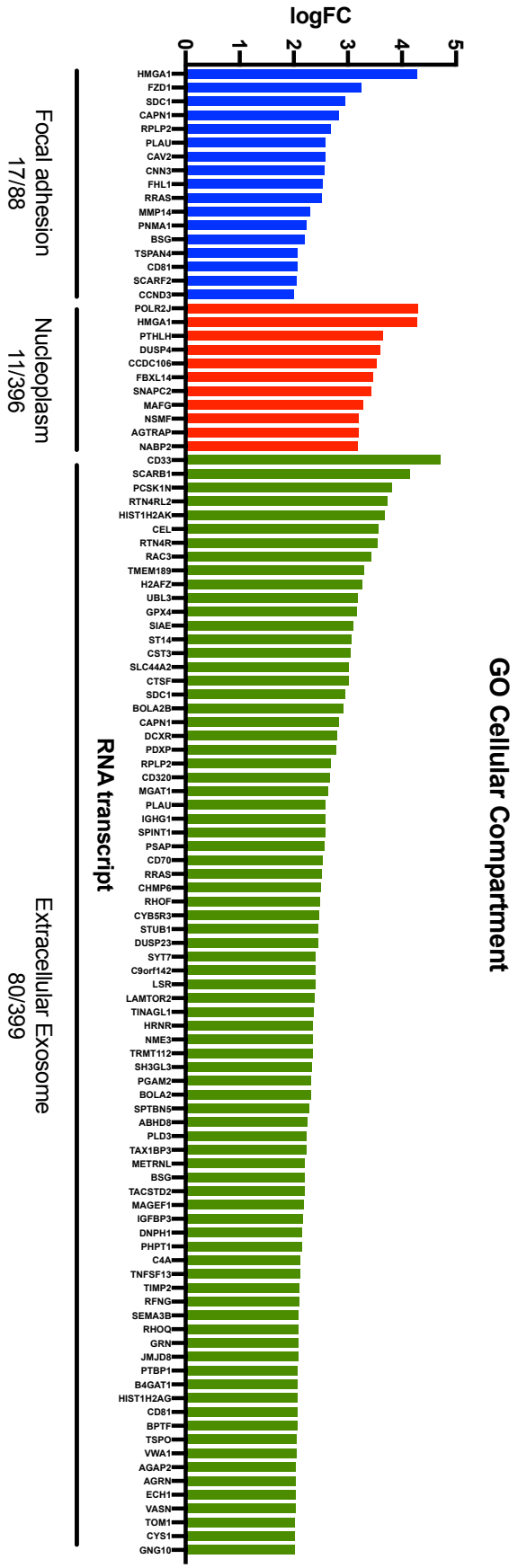

Figure 7.12. The logFC values of the individual RNA transcripts enriched within the top three most significant GO Cellular Compartment, ranked by p-value, as listed in Table 5.2.2.4.

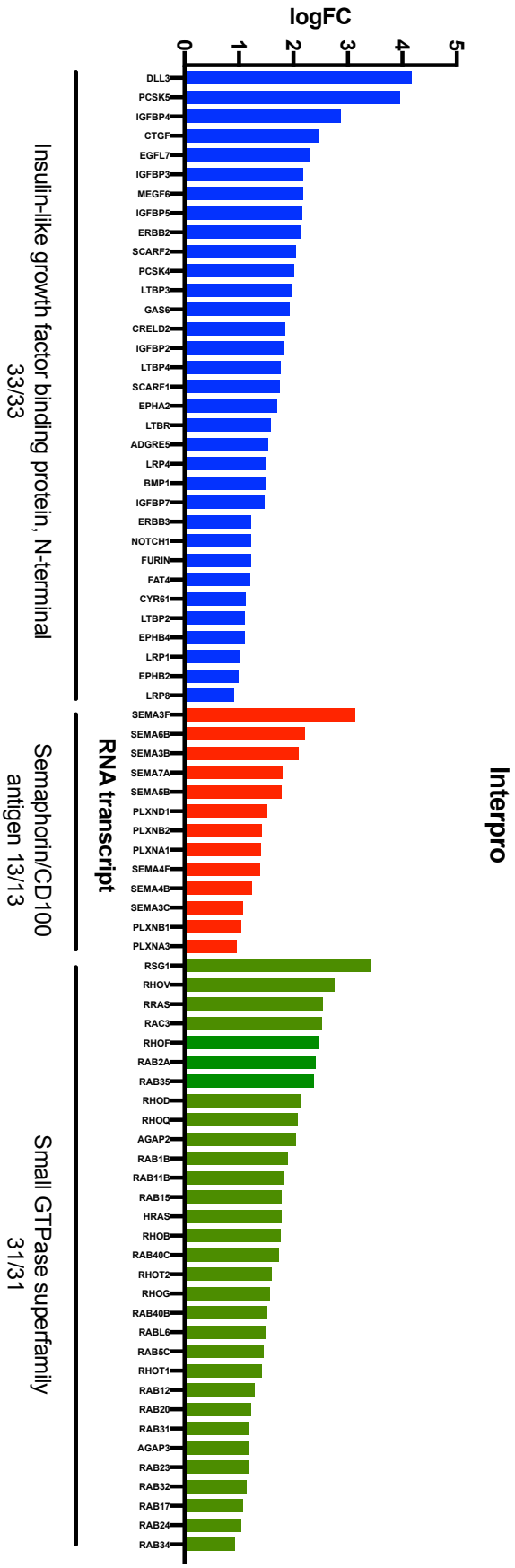

Figure 7.13. The logFC values of the individual RNA transcripts enriched within the top three most significant Interpro Terms, ranked by p-value, as listed in Table 5.2.2.5.

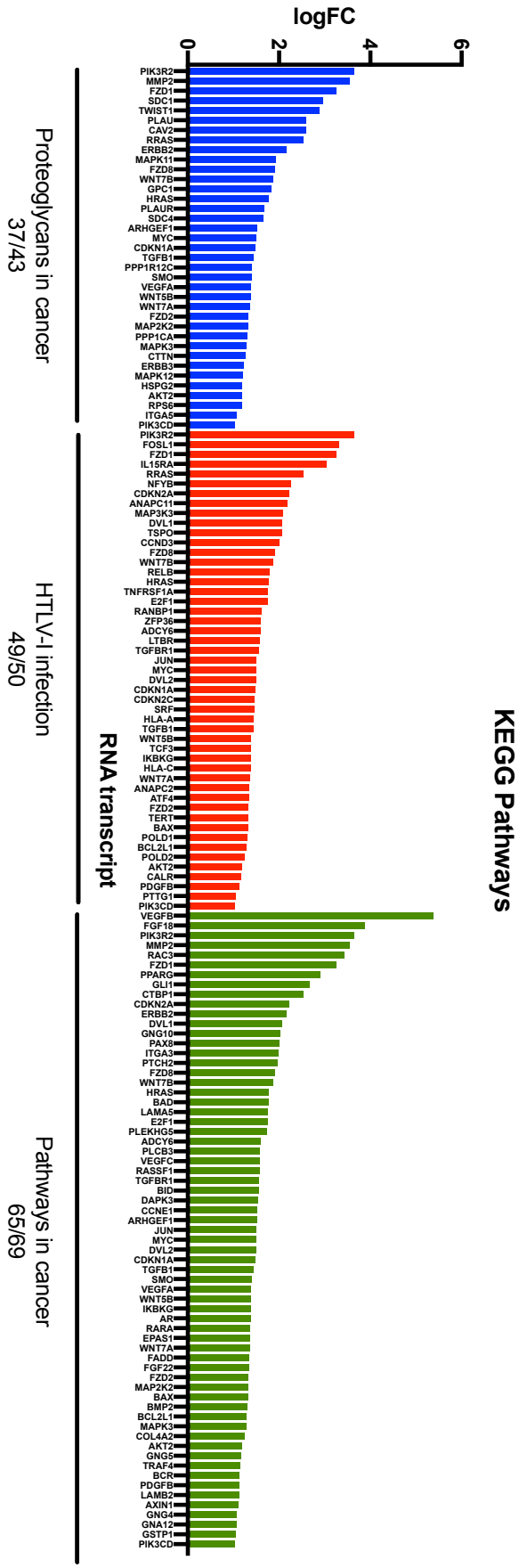

Figure 7.14. The logFC values of the individual RNA transcripts enriched within the top three most significant GO Molecular Function, ranked by p-value, as listed in Table 5.2.2.3.

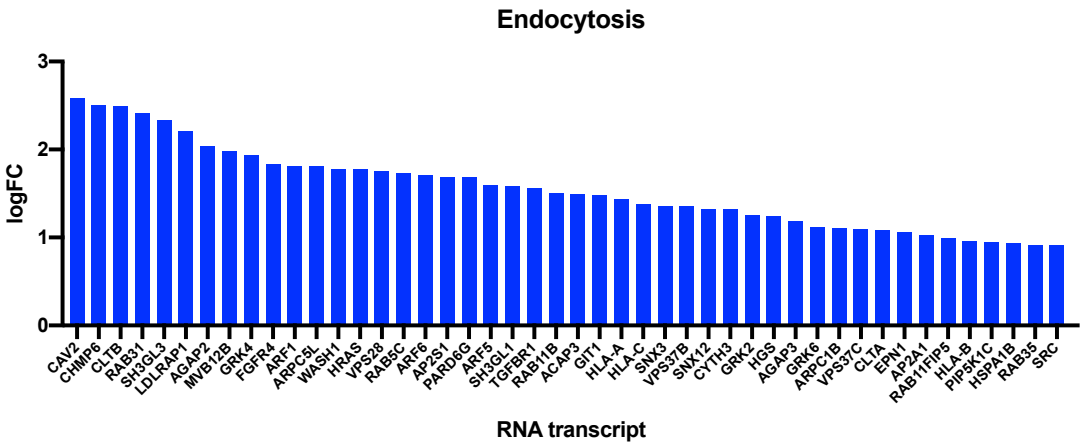

Figure 7.15. The logFC values of the individual RNA transcripts enriched within endocytosis following DAVID KEGG pathway analysis.

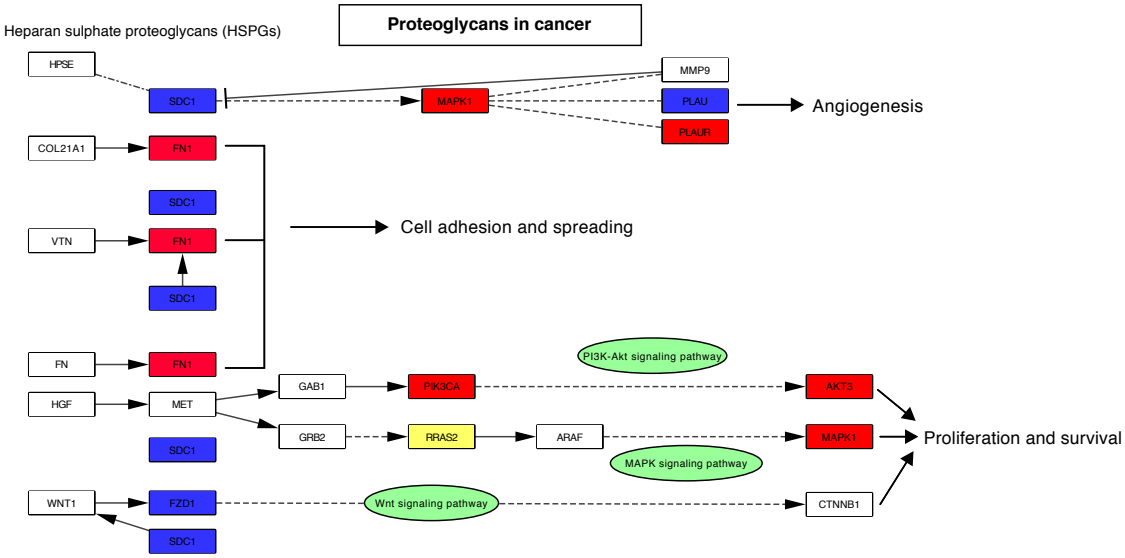

Figure 7.16. RNA transcripts bound to BICC1 enriched in the KEGG pathway proteoglycans in cancer. Significantly enriched RNAs are coloured, with blue referring to downregulated RNA transcripts, red referring to upregulated RNA transcripts and yellow referring to no change in expression in *BICC1 KO* cells (extracted from the RNA-Seq dataset which is discussed further in section 5.2.4). Additional downstream pathways of relevance to this study and ADPKD are highlighted in green.

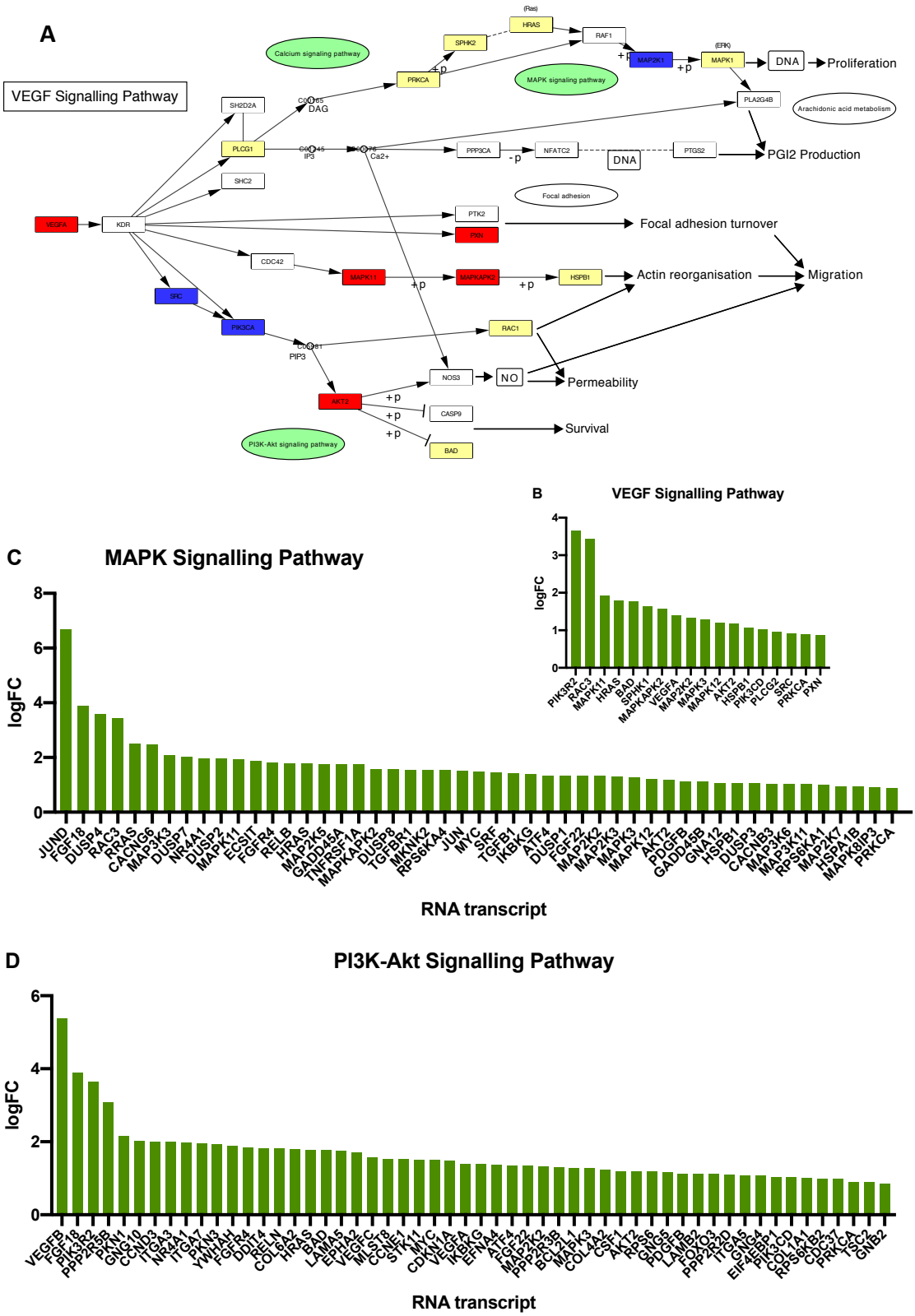

Figure 7.17. RNA transcripts bound to BICC1 enriched in the KEGG VEGF **signalling pathway. A)** Significantly enriched RNAs are coloured, with blue referring to downregulated RNA transcripts, red referring to upregulated RNA transcripts and yellow referring to no change in expression in *BICC1 KO* cells (extracted from the RNA-Seq dataset). Additional downstream pathways of relevance to this study and ADPKD are highlighted in green. **B-D)** The logFC values of the enriched RNA transcripts found in ADPKD-related KEGG Pathways are represented. logFC = log fold change.

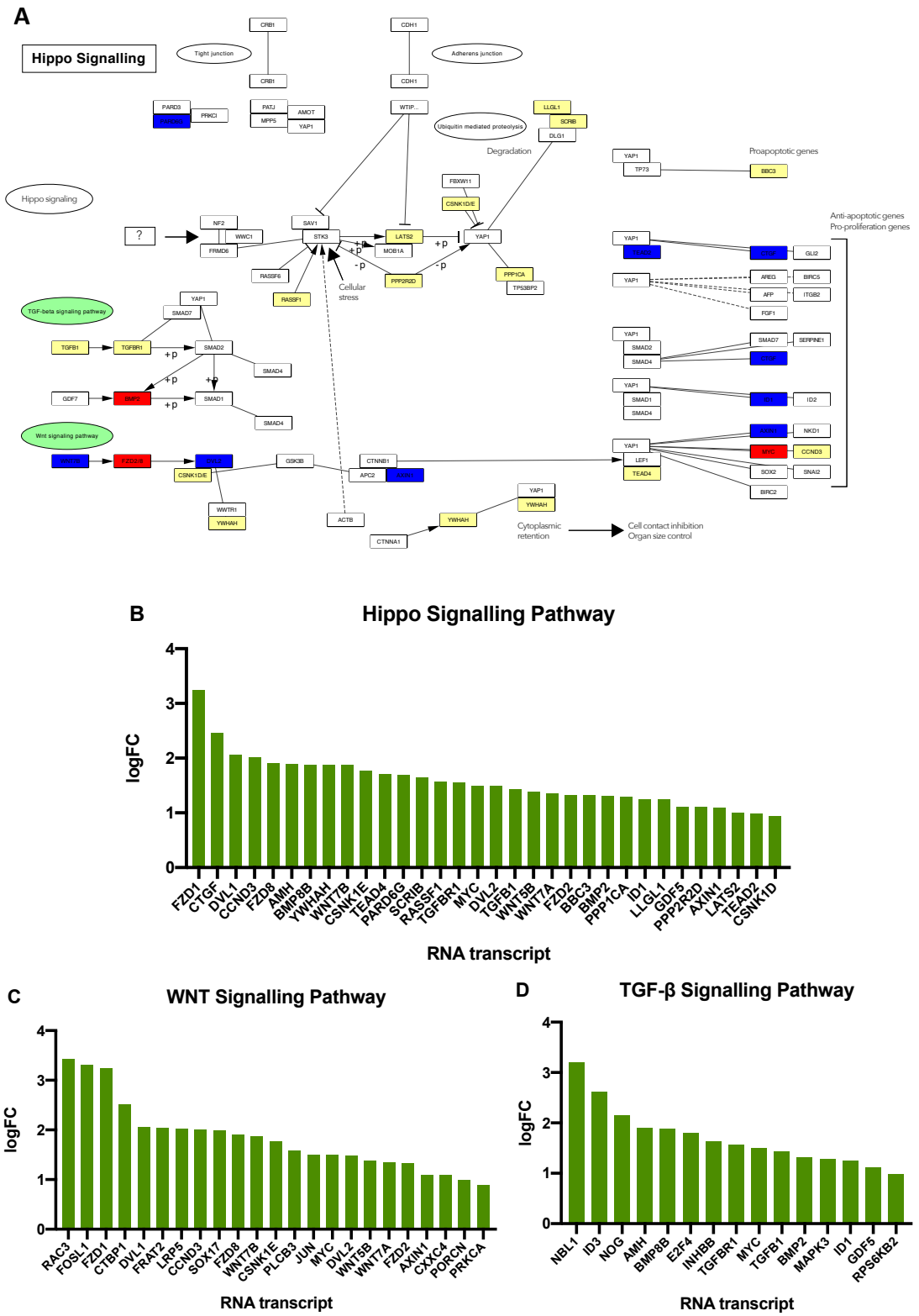

Figure 7.18. RNA transcripts bound to BICC1 enriched in the KEGG Hippo signalling pathway. A) Significantly enriched RNAs are coloured, with blue referring to downregulated RNA transcripts, red referring to upregulated RNA transcripts and yellow referring to no change in expression in *BICC1 KO* cells (extracted from the RNA-Seq dataset). Additional downstream pathways of relevance to this study and ADPKD are highlighted in green. **B-D)** The logFC values of the enriched RNA transcripts found in ADPKD-related KEGG Pathways are represented. logFC = log fold change.

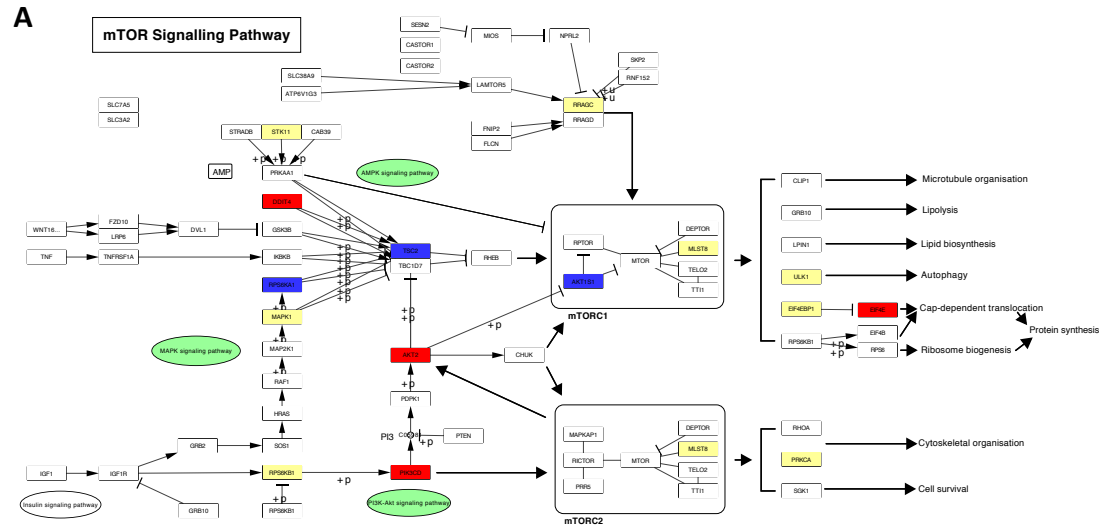

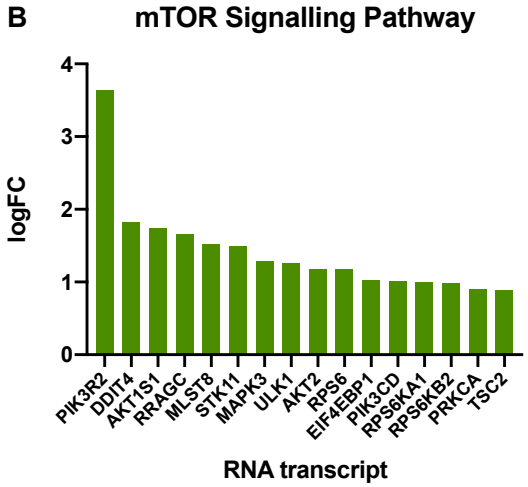

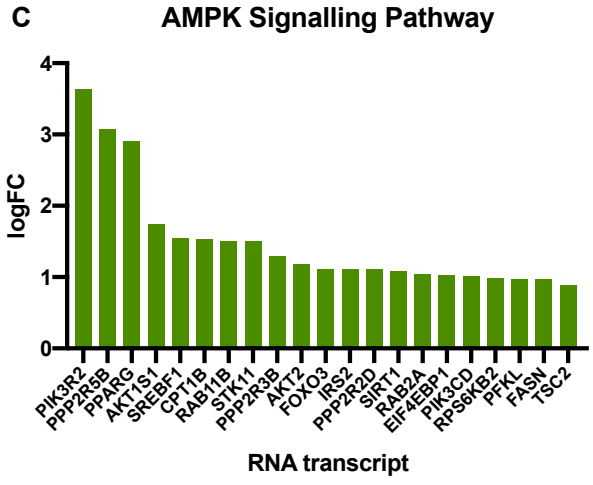

Figure 7.19. RNA transcripts bound to BICC1 enriched in the KEGG mTOR signalling pathway. A) Significantly enriched RNAs are coloured, with blue referring to downregulated RNA transcripts, red referring to upregulated RNA transcripts and yellow referring to no change in expression in *BICC1 KO* cells (extracted from the RNA-Seq dataset). Additional downstream pathways of relevance to this study and ADPKD are highlighted in green. **B-C)** The logFC values of the enriched RNA transcripts found in ADPKD-related KEGG Pathways are represented. logFC = log fold change.

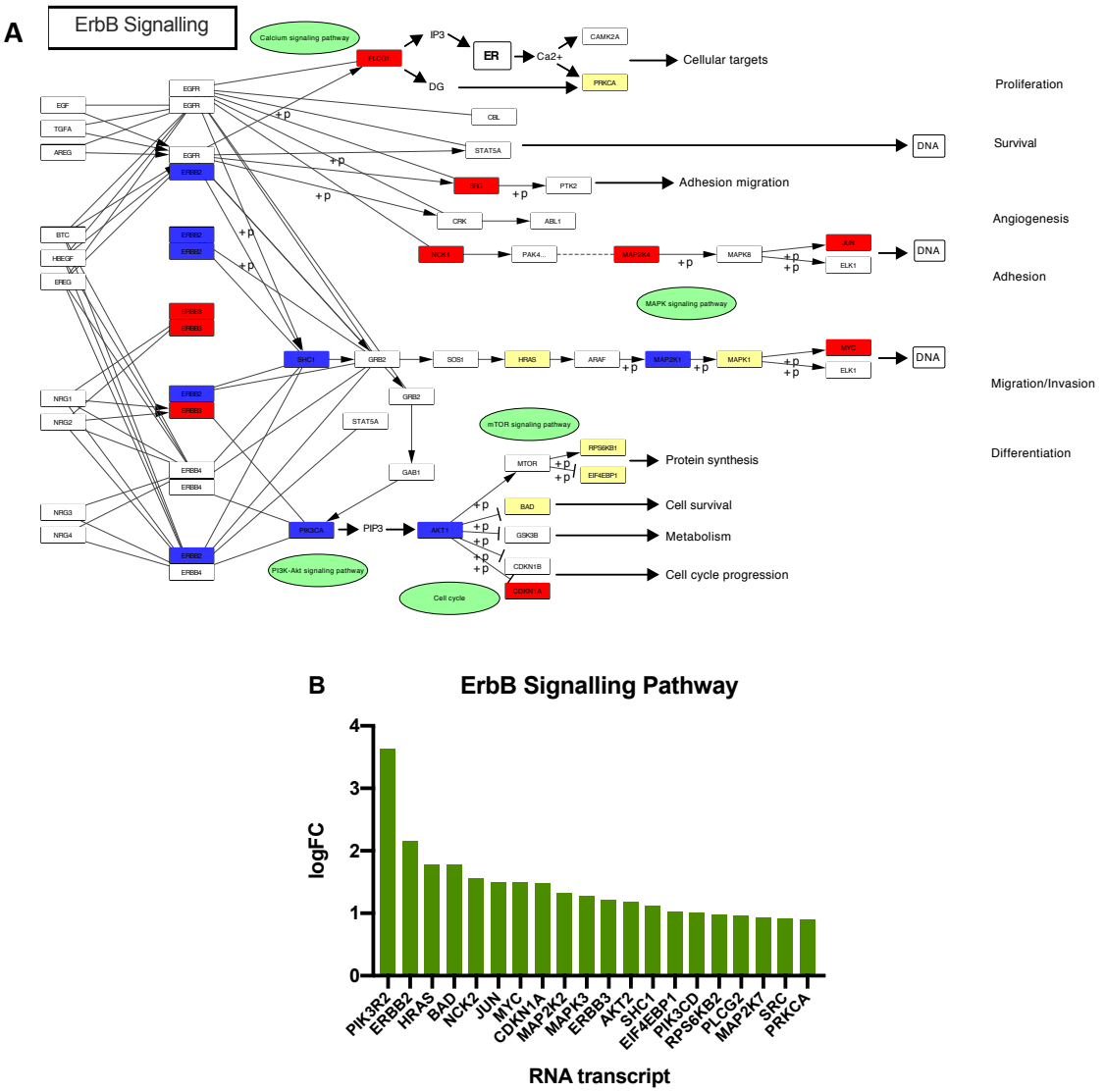

Figure 7.20. RNA transcripts bound to BICC1 enriched in the KEGG ErbB signalling pathway. A) Significantly enriched RNAs are coloured, with blue referring to downregulated RNA transcripts, red referring to upregulated RNA transcripts and yellow referring to no change in expression in *BICC1 KO* cells (extracted from the RNA-Seq dataset). Additional downstream pathways of relevance to this study and ADPKD are highlighted in green. **B)** The logFC values of the enriched RNA transcripts found in the ErbB signalling pathway, an ADPKD-related KEGG Pathway, are represented. logFC = log fold change.

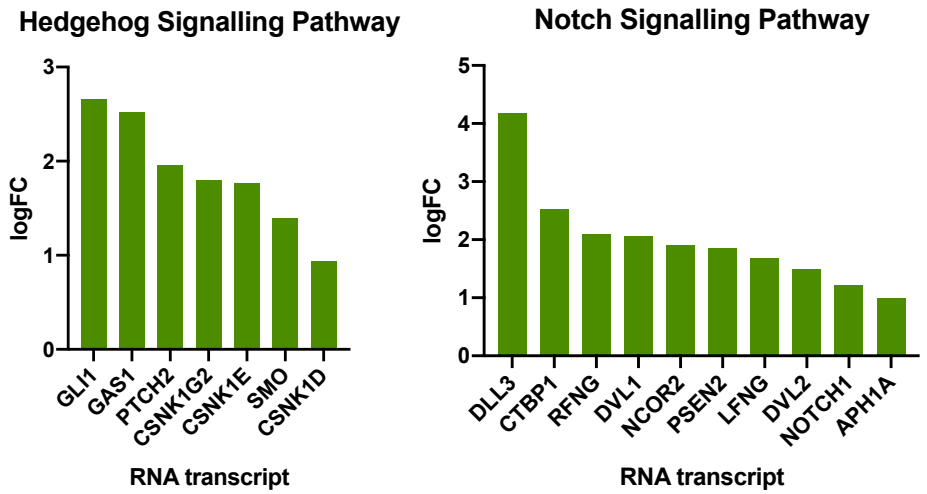

Figure 7.21. The logFC values of the individual RNA transcripts enriched within the Hedgehog and Notch signalling pathways. The logFC values of the enriched RNA transcripts found in ADPKD-related KEGG pathways are represented following DAVID analysis. logFC = log fold change.
Figure 7.21

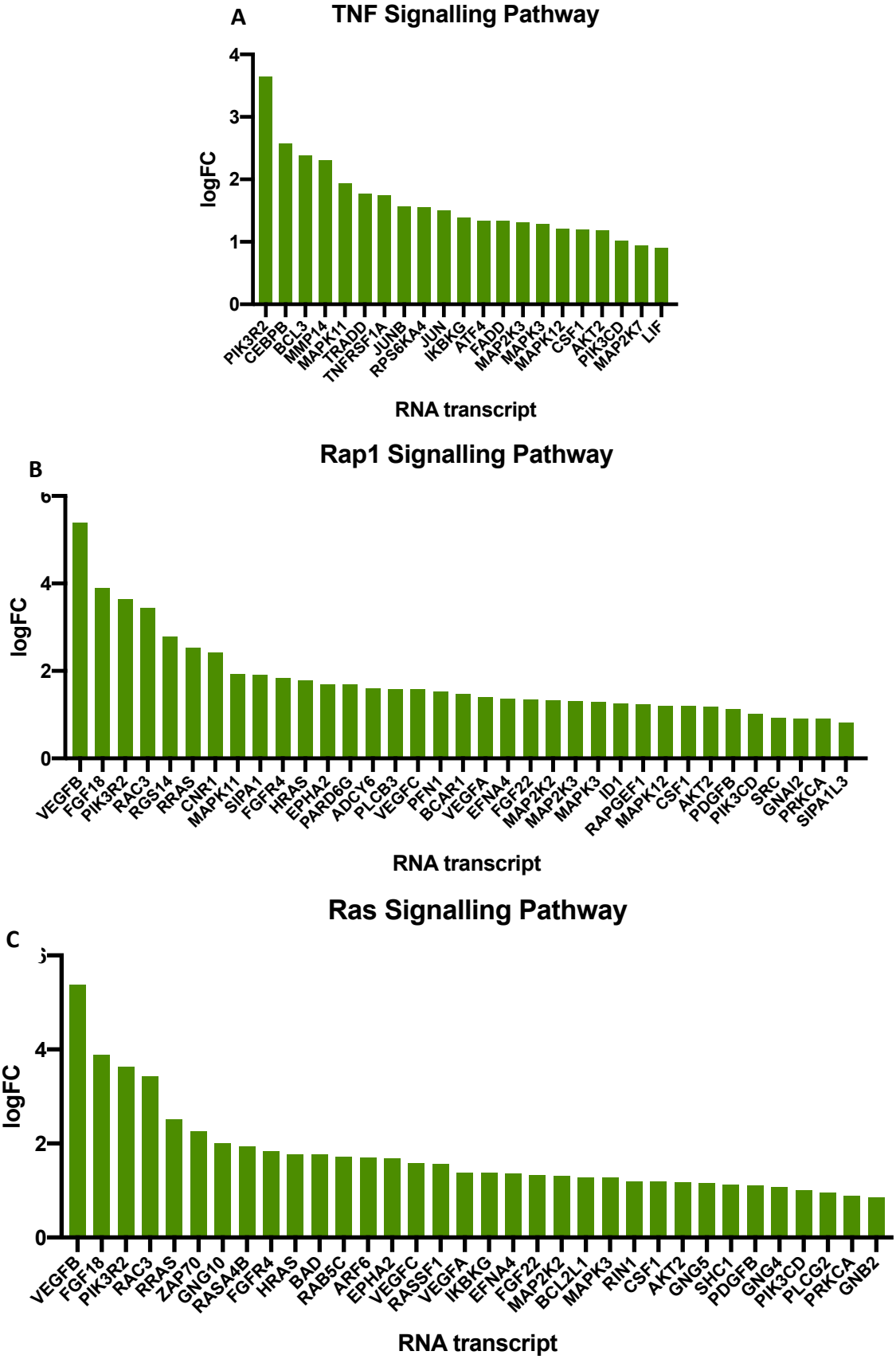

Figure 7.22. The logFC values of the individual RNA transcripts enriched within the TNF, Rap1 and Ras signalling pathways. The logFC values of the enriched RNA transcripts found in ADPKD-related KEGG pathways are represented following DAVID analysis. logFC = log fold change.

Table 7.4. The complete KEGG pathway enrichment list from the BICC1 fRIP-Seq analysis. Pathways were ranked by p-value. The ErbB signalling pathway was ranked 14th and is highlighted in grey.

Category	Term	Count	%	P-Value	Benjamini
KEGG_PATHWAY	Proteoglycans in cancer	43	1.9	4.60E-05	1.30E-02
KEGG_PATHWAY	HTLV-I infection	50	2.2	1.10E-04	1.50E-02
KEGG_PATHWAY	Pathways in cancer	69	3.1	1.90E-04	1.70E-02
KEGG_PATHWAY	MAPK signaling pathway	49	2.2	1.90E-04	1.30E-02
KEGG_PATHWAY	VEGF signaling pathway	18	0.8	3.00E-04	1.70E-02
KEGG_PATHWAY	Neurotrophin signaling pathway	28	1.2	3.30E-04	1.50E-02
KEGG_PATHWAY	Endocytosis	46	2.1	4.40E-04	1.70E-02
KEGG_PATHWAY	Hippo signaling pathway	32	1.4	6.70E-04	2.30E-02
KEGG_PATHWAY	Bladder cancer	13	0.6	1.40E-03	4.30E-02
KEGG_PATHWAY	mTOR signaling pathway	16	0.7	1.60E-03	4.30E-02
KEGG_PATHWAY	Axon guidance	27	1.2	1.80E-03	4.50E-02
KEGG_PATHWAY	Other types of O-glycan biosynthesis	9	0.4	2.00E-03	4.40E-02
KEGG_PATHWAY	Chronic myeloid leukemia	18	0.8	2.30E-03	4.80E-02
KEGG_PATHWAY	ErbB signaling pathway	20	0.9	3.40E-03	6.60E-02
KEGG_PATHWAY	Signaling pathways regulating pluripotency of stem cells	28	1.2	3.70E-03	6.60E-02
KEGG_PATHWAY	Sphingolipid signaling pathway	25	1.1	3.70E-03	6.20E-02
KEGG_PATHWAY	Lysosome	25	1.1	4.20E-03	6.60E-02
KEGG_PATHWAY	Glycosaminoglycan biosynthesis - chondroitin sulfate / dermatan sulfate	8	0.4	4.80E-03	7.10E-02
KEGG_PATHWAY	Focal adhesion	37	1.6	5.10E-03	7.10E-02
KEGG_PATHWAY	Fc gamma R-mediated phagocytosis	19	0.8	5.40E-03	7.20E-02
KEGG_PATHWAY	Insulin signaling pathway	27	1.2	6.00E-03	7.60E-02
KEGG_PATHWAY	p53 signaling pathway	16	0.7	7.00E-03	8.40E-02
KEGG_PATHWAY	Non-small cell lung cancer	14	0.6	8.50E-03	9.70E-02
KEGG_PATHWAY	B cell receptor signaling pathway	16	0.7	9.20E-03	1.00E-01
KEGG_PATHWAY	PI3K-Akt signaling pathway	54	2.4	1.20E-02	1.30E-01
KEGG_PATHWAY	Glycosaminoglycan biosynthesis - heparan sulfate / heparin	8	0.4	1.40E-02	1.40E-01
KEGG_PATHWAY	TNF signaling pathway	21	0.9	1.60E-02	1.50E-01
KEGG_PATHWAY	Basal cell carcinoma	13	0.6	1.60E-02	1.50E-01
KEGG_PATHWAY	Choline metabolism in cancer	20	0.9	1.80E-02	1.60E-01
KEGG_PATHWAY	Non-alcoholic fatty liver disease (NAFLD)	27	1.2	1.90E-02	1.60E-01
KEGG_PATHWAY	Rap1 signaling pathway	35	1.6	2.00E-02	1.60E-01
KEGG_PATHWAY	Apoptosis	14	0.6	2.00E-02	1.60E-01
KEGG_PATHWAY	Glycosaminoglycan biosynthesis - keratan sulfate	6	0.3	2.10E-02	1.60E-01
KEGG_PATHWAY	Oxidative phosphorylation	24	1.1	2.50E-02	1.90E-01
KEGG_PATHWAY	Central carbon metabolism in cancer	14	0.6	2.50E-02	1.80E-01
KEGG_PATHWAY	Huntington's disease	32	1.4	2.60E-02	1.80E-01
KEGG_PATHWAY	Bacterial invasion of epithelial cells	16	0.7	2.70E-02	1.90E-01
KEGG_PATHWAY	Pancreatic cancer	14	0.6	2.90E-02	1.90E-01
KEGG_PATHWAY	Endometrial cancer	12	0.5	2.90E-02	1.90E-01
KEGG_PATHWAY	Epstein-Barr virus infection	22	1	3.30E-02	2.00E-01
KEGG_PATHWAY	Osteoclast differentiation	23	1	3.70E-02	2.30E-01
KEGG_PATHWAY	Alzheimer's disease	28	1.2	3.80E-02	2.20E-01
KEGG_PATHWAY	Cell cycle	22	1	3.80E-02	2.20E-01
KEGG_PATHWAY	Fc epsilon RI signaling pathway	14	0.6	4.00E-02	2.20E-01
KEGG_PATHWAY	N-Glycan biosynthesis	11	0.5	4.50E-02	2.50E-01
KEGG_PATHWAY	FoxO signaling pathway	23	1	4.70E-02	2.40E-01
KEGG_PATHWAY	Acute myeloid leukemia	12	0.5	4.70E-02	2.40E-01
KEGG_PATHWAY	Galactose metabolism	8	0.4	4.70E-02	2.50E-01
KEGG_PATHWAY	Phosphatidylinositol signaling system	18	0.8	4.80E-02	2.40E-01
KEGG_PATHWAY	GnRH signaling pathway	17	0.8	4.80E-02	2.40E-01
KEGG_PATHWAY	Shigellosis	13	0.6	5.30E-02	2.60E-01
KEGG_PATHWAY	Inositol phosphate metabolism	14	0.6	5.40E-02	2.50E-01
KEGG_PATHWAY	Prolactin signaling pathway	14	0.6	5.40E-02	2.50E-01
KEGG_PATHWAY	Viral carcinogenesis	32	1.4	5.60E-02	2.60E-01
KEGG_PATHWAY	Glycosaminoglycan degradation	6	0.3	5.60E-02	2.60E-01
KEGG_PATHWAY	Hepatitis B	24	1.1	5.90E-02	2.60E-01
KEGG_PATHWAY	Glioma	13	0.6	5.90E-02	2.60E-01
KEGG_PATHWAY	Wnt signaling pathway	23	1	6.10E-02	2.60E-01
KEGG_PATHWAY	AMPK signaling pathway	21	0.9	6.10E-02	2.60E-01
KEGG_PATHWAY	Epithelial cell signaling in Helicobacter pylori infection	13	0.6	7.20E-02	2.90E-01
KEGG_PATHWAY	Regulation of actin cytoskeleton	32	1.4	7.30E-02	3.00E-01
KEGG_PATHWAY	Ras signaling pathway	34	1.5	7.50E-02	3.00E-01
KEGG_PATHWAY	Chagas disease (American trypanosomiasis)	18	0.8	7.60E-02	3.00E-01
KEGG_PATHWAY	Hedgehog signaling pathway	7	0.3	7.70E-02	3.00E-01
KEGG_PATHWAY	Metabolic pathways	154	6.9	7.80E-02	3.00E-01
KEGG_PATHWAY	Colorectal cancer	12	0.5	8.70E-02	3.20E-01
KEGG_PATHWAY	Notch signaling pathway	10	0.4	8.70E-02	3.20E-01
KEGG_PATHWAY	TGF-beta signaling pathway	15	0.7	8.90E-02	3.20E-01
KEGG_PATHWAY	T cell receptor signaling pathway	17	0.8	9.70E-02	3.40E-01

Table 7.5. The *SNX* and *VPS* RNA transcripts significantly bound to BICC1.

Gene ID	Name	fRIP logFC
SNX12	Sorting Nexin 12	1.32
SNX17	Sorting Nexin 17	1.32
SNX18	Sorting Nexin 18	1.43
SNX3	Sorting Nexin 3	1.35
SNX8	Sorting Nexin 8	0.95
VPS28	Vacuolar Protein Sorting-Associated Protein 28	1.76
VPS37B	Vacuolar Protein Sorting-Associated Protein 37B	1.35
VPS37C	Vacuolar Protein Sorting-Associated Protein 37C	1.09
VPS51	Vacuolar Protein Sorting-Associated Protein 51	1.43

Table 7.6. Comparison of the eukaryotic initiation factors and CCR4-CNOT subunits identified in our MS dataset and the Constam MS dataset. Fold change cut off was set at 20.

Gene ID	Smith FC	Constam FC
eIF3A	13.33	3.00
eIF3B	-	4.00
eIF3C	11.33	-
eIF3I	-	8.50
eIF3L	10.00	-
eIF3F	4.67	-
eIF4E	2.33	-
eIF4AI	10.67	-
eIF4AI	-	3.00
eIF4AIII	8.00	-
eIF4G1	9.33	-
eIF4G2	3.33	-
eIF4G3	3.67	-
eIF4F	-	-
eIF4B	2.67	-
eIF4H	2.67	-
CNOT1	30.67	80.00
CNOT2	2.67	6.00
CNOT3	4.67	3.50
CNOT7	2.33	0.00
CNOT8	2.00	2.00
CNOT10	4.67	4.00
CNOT11	-	2.50

8.0 Bibliography

Abeyta, A., Castella, M., Jacquemont, C., *et al*. (2017) NEK8 regulates DNA damage-induced RAD51 foci formation and replication fork protection. **Cell cycle (Georgetown, Tex.)**, 16 (4): 335–347

Aksentijevich, I., Pras, E., Gruberg, L., *et al*. (1994) The polycystic kidney disease 1 gene encodes a 14 kb transcript and lies within a duplicated region on chromosome 16. The European Polycystic Kidney Disease Consortium. **Cell**, 77 (6): 881–94

Albert, T.K., Lemaire, M., van Berkum, N.L., *et al*. (2000) Isolation and characterization of human orthologs of yeast CCR4-NOT complex subunits. **Nucleic Acids Research**, 28 (3): 809–817

Araç, D., Boucard, A.A., Bolliger, M.F., *et al*. (2012) A novel evolutionarily conserved domain of cell-adhesion GPCRs mediates autoproteolysis. **The EMBO journal**, 31 (6): 1364–78

Audrézet, M.-P., Cornec-Le Gall, E., Chen, J.-M., *et al*. (2012) Autosomal dominant polycystic kidney disease: comprehensive mutation analysis of PKD1 and PKD2 in 700 unrelated patients. **Human mutation**, 33 (8): 1239–50

Badano, J.L., Mitsuma, N., Beales, P.L., *et al*. (2006) The Ciliopathies: An Emerging Class of Human Genetic Disorders. **Annual Review of Genomics and Human Genetics**, 7 (1): 125–148

Bakey, Z., Bihoreau, M.-T., Piedagnel, R., *et al*. (2015) The SAM domain of ANKS6 has different interacting partners and mutations can induce different cystic phenotypes. **Kidney international**, 88 (2): 299–310

Bergmann, C., Fliegauf, M., Brüchle, N.O., *et al*. (2008) Loss of nephrocystin-3 function can cause embryonic lethality, Meckel-Gruber-like syndrome, situs inversus, and renal-hepatic-pancreatic dysplasia. **American journal of human genetics**, 82 (4): 959–70

Bernhardt, W.M., Wiesener, M.S., Weidemann, A., *et al*. (2007) Involvement of Hypoxia-Inducible Transcription Factors in Polycystic Kidney Disease. **The American Journal of Pathology**, 170 (3): 830–842

Bihoreau, M., Ceccherini, I., Browne, J., *et al*. (1997) Location of the first genetic locus, PKDr1, controlling autosomal dominant polycystic kidney disease in Han:SPRD cy/+ rat. **Human Molecular Genetics**, 6 (4): 609–613

Bouvrette, D.J., Price, S.J., Bryda, E.C., *et al*. (2003) Positional cloning of jcpk/bpk locus of the mouse. **Mammalian Genome**, 14 (1): 242–49

Brown, J.H., Bihoreau, M.-T., Hoffmann, S., *et al*. (2005) Missense Mutation in Sterile α Motif of Novel Protein SamCystin is Associated with Polycystic Kidney Disease in (*cy* /+) Rat. **Journal of the American Society of Nephrology**, 16 (12): 3517–3526

Bycroft, M., Bateman, A., Clarke, J., *et al*. (1999) The structure of a PKD domain from polycystin-1: implications for polycystic kidney disease. **The EMBO journal**, 18 (2): 297–305

Cai, Y., Fedeles, S. V., Dong, K., *et al*. (2014) Altered trafficking and stability of polycystins underlie polycystic kidney disease. **Journal of Clinical Investigation**, 124 (12): 5129–5144

Castello, A., Fischer, B., Eichelbaum, K., *et al*. (2012) Insights into RNA Biology from an Atlas of Mammalian mRNA-Binding Proteins. **Cell**, 149 (6): 1393–1406

Cerini, C., Kerjan, P., Astier, M., *et al*. (1991) A component of the multisynthetase complex is a multifunctional aminoacyl-tRNA synthetase. **The EMBO journal**, 10 (13): 4267–77
Chaki, M., Airik, R., Ghosh, A.K., *et al*. (2012) Exome Capture Reveals ZNF423 and CEP164 Mutations, Linking Renal Ciliopathies to DNA Damage Response Signaling. **Cell**, 150 (3): 533–548
Chang, M.-Y. and Ong, A.C.M. (2008) Autosomal Dominant Polycystic Kidney Disease: Recent Advances in Pathogenesis and Treatment Molecular Genetics of ADPKD. **Nephron Physiol**, 108: 1–7
Charron, A.J. (2000) Compromised Cytoarchitecture and Polarized Trafficking in Autosomal Dominant Polycystic Kidney Disease Cells. **The Journal of Cell Biology**, 149 (1): 111–124
Chebib, F.T., Sussman, C.R., Wang, X., *et al*. (2015) Vasopressin and disruption of calcium signalling in polycystic kidney disease. **Nature Reviews Nephrology**, 11: 451–464
Chicoine, J., Benoit, P., Gamberi, C., *et al*. (2007) Bicaudal-C Recruits CCR4-NOT Deadenylase to Target mRNAs and Regulates Oogenesis, Cytoskeletal Organization, and Its Own Expression. **Developmental Cell**, 13 (5): 691–704
Chiu, Y.-L., Cao, H. and Rana, T.M. (2007) Quantitative Analysis of RNA-mediated Protein?Protein Interactions in Living Cells by FRET. **Chemical Biology & Drug Design**, 69 (4): 233–239
Choi, H.J.C., Lin, J.-R., Vannier, J.-B., *et al*. (2013) NEK8 Links the ATR-Regulated Replication Stress Response and S Phase CDK Activity to Renal Ciliopathies. **Molecular Cell**, 51 (4): 423–439
Consugar, M.B., Wong, W.C., Lundquist, P.A., *et al*. (2008) Characterization of large rearrangements in autosomal dominant polycystic kidney disease and the PKD1/TSC2 contiguous gene syndrome. **Kidney international**, 74 (11): 1468–79
Cornec-Le Gall, E., Audrézet, M.-P., Chen, J.-M., *et al*. (2013) Type of PKD1 mutation influences renal outcome in ADPKD. **Journal of the American Society of Nephrology : JASN**, 24 (6): 1006–13
Couillard, M., Guillaume, R., Tanji, N., *et al*. (2002) c-myc-induced apoptosis in polycystic kidney disease is independent of FasL/Fas interaction. **Cancer research**, 62 (8): 2210–4
Czarnecki, P.G., Gabriel, G.C., Manning, D.K., *et al*. (2015) ANKS6 is the critical activator of NEK8 kinase in embryonic situs determination and organ patterning. **Nature Communications**, 6 (1): 6023
Dalagiorgou, G., Piperi, C., Adamopoulos, C., *et al*. (2017) Calpain-mediated proteolysis of polycystin-1 C-terminus induces JAK2 and ERK signal alterations. **Annual review of medicine**, 18 (2): e23650
Davidow, C.J., Maser, R.L., Rome, L.A., *et al*. (1996) The cystic fibrosis transmembrane conductance regulator mediates transepithelial fluid secretion by human autosomal dominant polycystic kidney disease epithelium in vitro. **Kidney International**, 50 (1): 208–218
Delestré, L., Bakey, Z., Prado, C., *et al*. (2015) ANKS3 Co-Localises with ANKS6 in Mouse Renal Cilia and Is Associated with Vasopressin Signaling and Apoptosis In Vivo in Mice Long, D. (ed.). **PLOS ONE**, 10 (9): e0136781
Delous, M., Baala, L., Salomon, R., *et al*. (2007) The ciliary gene RPGRIP1L is mutated in cerebello-oculo-renal syndrome (Joubert syndrome type B) and Meckel syndrome. **Nature Genetics**, 39 (7): 875–881
Distefano, G., Boca, M., Rowe, I., *et al*. (2009) Polycystin-1 regulates

extracellular signal-regulated kinase-dependent phosphorylation of tuberin to control cell size through mTOR and its downstream effectors S6K and 4EBP1. **Molecular and cellular biology**, 29 (9): 2359–71
Drummond, I.A. (2011) Polycystins, focal adhesions and extracellular matrix interactions. **Biochimica et Biophysica Acta (BBA) - Molecular Basis of Disease**, 1812 (10): 1322–1326
Edelstein, C.L. (2005) What is the Role of Tubular Epithelial Cell Apoptosis in Polycystic Kidney Disease (PKD)? **Cell Cycle**, 4 (11): 1550–1554
Feng, S., Okenka, G.M., Bai, C.-X., *et al*. (2008) Identification and Functional Characterization of an N-terminal Oligomerization Domain for Polycystin-2. **Journal of Biological Chemistry**, 283 (42): 28471–28479
Feng, S., Rodat-Despoix, L., Delmas, P., *et al*. (2011) A single amino acid residue constitutes the third dimerization domain essential for the assembly and function of the tetrameric polycystin-2 (TRPP2) channel. **The Journal of biological chemistry**, 286 (21): 18994–9000
Feng, S., Streets, A.J., Nesin, V., *et al*. (2017) The Sorting Nexin 3 Retromer Pathway Regulates the Cell Surface Localization and Activity of a Wnt-Activated Polycystin Channel Complex. **Journal of the American Society of Nephrology : JASN**, 28 (10): 2973–2984
Feo, S., Arcuri, D., Piddini, E., *et al*. (2000) ENO1 gene product binds to the c-myc promoter and acts as a transcriptional repressor: relationship with Myc promoter-binding protein 1 (MBP-1). **FEBS letters**, 473 (1): 47–52
Fischer, E., Legue, E., Doyen, A., *et al*. (2006) Defective planar cell polarity in polycystic kidney disease. **Nature genetics**, 38 (1): 21–3
Floege, J., Mak, R.H., Molitoris, B.A., *et al*. (2015) Nephrology research—the past, present and future. **Nature Reviews Nephrology**, 11 (11): 677–687
Fox, J.W., Lamperti, E.D., Ekşioğlu, Y.Z., *et al*. (1998) Mutations in filamin 1 prevent migration of cerebral cortical neurons in human periventricular heterotopia. **Neuron**, 21 (6): 1315–25
Fu, Y., Kim, I., Lian, P., *et al*. (2010) Loss of Bicc1 impairs tubulomorphogenesis of cultured IMCD cells by disrupting E-cadherin-based cell-cell adhesion. **European Journal of Cell Biology**, 89: 428–36
G Hendrickson, D., Kelley, D.R., Tenen, D., *et al*. (2016) Widespread RNA binding by chromatin-associated proteins. **Genome biology**, 17: 28
Gainullin, V.G., Hopp, K., Ward, C.J., *et al*. (2015) Polycystin-1 maturation requires polycystin-2 in a dose-dependent manner. **Journal of Clinical Investigation**, 125 (2): 607–620
Gattone, V.H., Wang, X., Harris, P.C., *et al*. (2003) Inhibition of renal cystic disease development and progression by a vasopressin V2 receptor antagonist. **Nature medicine**, 9 (10): 1323–6
Geng, L., Okuhara, D., Yu, Z., *et al*. (2006) Polycystin-2 traffics to cilia independently of polycystin-1 by using an N-terminal RVxP motif. **Journal of cell science**, 119 (Pt 7): 1383–95
Geng, L., Segal, Y., Peissel, B., *et al*. (1996) Identification and localizarion of polycystin, the PKD1 gene product. **J. Clin. Invest.**, 98 (12): 2674–2682
Giamarchi, A., Feng, S., Rodat-Despoix, L., *et al*. (2010) A polycystin-2 (TRPP2) dimerization domain essential for the function of heteromeric polycystin complexes. **The EMBO journal**, 29 (7): 1176–91
Gonzalez-Perrett, S. (2000) Polycystin-2, the protein mutated in autosomal dominant polycystic kidney disease (ADPKD), is a Ca2+-permeable nonselective cation channel. **Proceedings of the National Academy of**

Sciences, 98 (3): 1182–1187
Happé, H. and Peters, D.J.M. (2014) Translational research in ADPKD: lessons from animal models. **Nature Reviews Nephrology**, 10 (10): 587–601
Hoff, S., Epting, D., Falk, N., *et al*. (2018) The nucleoside-diphosphate kinase NME3 associates with nephronophthisis proteins and is required for ciliary function during renal development. **The Journal of biological chemistry**, 293 (39): 15243–15255
Hoff, S., Halbritter, J., Epting, D., *et al*. (2013) ANKS6 is a central component of a nephronophthisis module linking NEK8 to INVS and NPHP3. **Nature genetics**, 45 (8): 951–6
Hong, K.Y., Lee, S.H., Gu, S., *et al*. (2017) The bent conformation of poly(A)-binding protein induced by RNA-binding is required for its translational activation function. **RNA Biology**, 14 (3): 370–377
Iaconis, D., Monti, M., Renda, M., *et al*. (2017) The centrosomal OFD1 protein interacts with the translation machinery and regulates the synthesis of specific targets. **Scientific Reports**, 7 (1): 1–15
Iglesias, C.G., Torres, V.E., Offord, K.P., *et al*. (1983) Epidemiology of adult polycystic kidney disease, Olmsted county, Minnesota: 1935-1980. **American Journal of Kidney Diseases**, 2 (6): 630–639
Jerman, S., Ward, H.H., Lee, R., *et al*. (2014) OFD1 and Flotillins Are Integral Components of a Ciliary Signaling Protein Complex Organized by Polycystins in Renal Epithelia and Odontoblasts Lencer, W.I. (ed.). **PLoS ONE**, 9 (9): e106330
Kahvejian, A., Svitkin, Y. V, Sukarieh, R., *et al*. (2005) Mammalian poly(A)-binding protein is a eukaryotic translation initiation factor, which acts via multiple mechanisms. **Genes & Development**, 19 (1): 104–113
Kan, W., Fang, F., Chen, L., *et al*. (2016) Influence of the R823W mutation on the interaction of the ANKS6–ANKS3: insights from molecular dynamics simulation and free energy analysis. **Journal of Biomolecular Structure and Dynamics**, 34 (5): 1113–1122
Karihaloo, A., Koraishy, F., Huen, S.C., *et al*. (2011) Macrophages promote cyst growth in polycystic kidney disease. **Journal of the American Society of Nephrology : JASN**, 22 (10): 1809–14
Kaspareit-Rittinghausen, J., Deerberg, F. and Wcislo, A. (1991) Hereditary polycystic kidney disease. Adult polycystic kidney disease associated with renal hypertension, renal osteodystrophy, and uremic enteritis in SPRD rats. **The American journal of pathology**, 139 (3): 693–6
Katsura, T., Gustafson, C.E., Ausiello, D.A., *et al*. (1997) Protein kinase A phosphorylation is involved in regulated exocytosis of aquaporin-2 in transfected LLC-PK1 cells. **The American journal of physiology**, 272 (6 Pt 2): F817-22
Kim, E., Arnould, T., Sellin, L., *et al*. (1999) Interaction between RGS7 and polycystin. **Proceedings of the National Academy of Sciences**, 96 (11): 6371–6376
Kim, H., Jeong, W., Ahn, K., *et al*. (2004) Siah-1 Interacts with the Intracellular Region of Polycystin-1 and Affects Its Stability via the Ubiquitin-Proteasome Pathway. **Journal of the American Society of Nephrology**, 15 (8): 2042–2049
Kim, H., Kang, A.-Y., Ko, A., *et al*. (2014) Calpain-mediated proteolysis of polycystin-1 C-terminus induces JAK2 and ERK signal alterations. **Experimental Cell Research**, 320 (1): 62–68

Kim, S., Nie, H., Nesin, V., *et al*. (2016) The polycystin complex mediates Wnt/Ca2+ signalling. **Nature Cell Biology**, 18 (7): 752–764
Knight, M.J., Leettola, C., Gingery, M., *et al*. (2011) A human sterile alpha motif domain polymerizome. **Protein Science**, 20 (10): 1697–1706
Koulen, P., Cai, Y., Geng, L., *et al*. (2002) Polycystin-2 is an intracellular calcium release channel. **Nature cell biology**, 4 (3): 191–197
Kraus, M., Clauin, S., Pfister, Y., *et al*. (2012) Two mutations in human BICC1 resulting in Wnt pathway hyperactivity associated with cystic renal dysplasia. **Human Mutation**, 33 (1): 86–90
Kubota, H., Hynes, G. and Willison, K. (1995) The eighth Cct gene, Cctq, encoding the theta subunit of the cytosolic chaperonin containing TCP-1. **Gene**, 154 (2): 231–236
Lantinga-van Leeuwen, I.S., Leonhard, W.N., van der Wal, A., *et al*. (2007) Kidney-specific inactivation of the Pkd1 gene induces rapid cyst formation in developing kidneys and a slow onset of disease in adult mice. **Human Molecular Genetics**, 16 (24): 3188–3196
Lažetić, V. and Fay, D.S. (2017) Conserved Ankyrin Repeat Proteins and Their NIMA Kinase Partners Regulate Extracellular Matrix Remodeling and Intracellular Trafficking in *Caenorhabditis elegans*. **Genetics**, 205 (1): 273–293
Lažetić, V., Joseph, B.B., Bernazzani, S.M., *et al*. (2018) Actin organization and endocytic trafficking are controlled by a network linking NIMA-related kinases to the CDC-42-SID-3/ACK1 pathway Nance, J. (ed.). **PLOS Genetics**, 14 (4): e1007313
Leal-Esteban, L.C., Rothé, B., Fortier, S., *et al*. (2018) Role of Bicaudal C1 in renal gluconeogenesis and its novel interaction with the CTLH complex. **PLoS Genetics**, 14 (7): 1–25
Leettola, C.N., Knight, M., Cascio, D., *et al*. (2014) Characterization of the SAM domain of the PKD-related protein ANKS6 and its interaction with ANKS3. **BMC Structural Biology**, 14 (1): 17
Lemaire, L.A., Goulley, J., Kim, Y.H., *et al*. (2015) Bicaudal C1 promotes pancreatic NEUROG3 + endocrine progenitor differentiation and ductal morphogenesis. **Stem Cells and Regeneration**, 142: 858–870
Lewis, H.A., Musunuru, K., Jensen, K.B., *et al*. (2000) Sequence-specific RNA binding by a Nova KH domain: implications for paraneoplastic disease and the fragile X syndrome. **Cell**, 100 (3): 323–32
Li, A., Xu, Y., Fan, S., *et al*. (2018) Canonical Wnt inhibitors ameliorate cystogenesis in a mouse ortholog of human ADPKD. **JCI insight**, 3 (5)
Li, H., Findlay, I.A. and Sheppard, D.N. (2004) The relationship between cell proliferation, Cl− secretion, and renal cyst growth: A study using CFTR inhibitors. **Kidney International**, 66 (5): 1926–1938
Li, Q., Montalbetti, N., Shen, P.Y., *et al*. (2005) Alpha-actinin associates with polycystin-2 and regulates its channel activity. **Human Molecular Genetics**, 14 (12): 1587–1603
Lian, P., Li, A., Li, Y., *et al*. (2014) Loss of Polycystin-1 Inhibits Bicc1 Expression during Mouse Development. **PLoS ONE**, 9 (3): 1–9
Maestrini, E., Rivella, S., Tribioli, C., *et al*. (1990) Probes for CpG islands on the distal long arm of the human X chromosome are clustered in Xq24 and Xq28. **Genomics**, 8 (4): 664–70
Mahone, M., Saffman, E.E. and Lasko, P.F. (1995) Localized Bicaudal-C RNA encodes a protein containing a KH domain, the RNA binding motif of FMR1. **The EMBO Journal**, 14 (9): 2043–55

Maisonneuve, C., Guilleret, I., Vick, P., *et al*. (2009) Bicaudal C, a novel regulator of Dvl signaling abutting RNA-processing bodies, controls cilia orientation and leftward flow. **Development and Disease**, 136 (3019–30)
Manning, D.K., Sergeev, M., Heesbeen, R.G. van, *et al*. (2012) Loss of the Ciliary Kinase Nek8 Causes Left-Right Asymmetry Defects. **Journal of the American Society of Nephrology : JASN**, 24 (1): 100
Mesner, L.D., Ray, B., Hsu, Y.-H., *et al*. (2014) Bicc1 is a genetic determinant of osteoblastogenesis and bone mineral density. **The Journal of Clinical Investigation**, 124 (6): 2736–49
Mochizuki, T., Wu, G., Hayashi, T., *et al*. (1996) PKD2, a gene for polycystic kidney disease that encodes an integral membrane protein. **Science**, 272 (5266): 1339–1342
Moeller, H.B., MacAulay, N., Knepper, M.A., *et al*. (2009) Role of multiple phosphorylation sites in the COOH-terminal tail of aquaporin-2 for water transport: evidence against channel gating. **American Journal of Physiology-Renal Physiology**, 296 (3): F649–F657
Mohieldin, A.M., Haymour, H.S., Shao, Lo, T., *et al*. (2015) Protein composition and movements of membrane swellings associated with primary cilia. **Cellular and Molecular Life Sciences**, 72: 2415–29
Mollet, G., Silbermann, F., Delous, M., *et al*. (2005) Characterization of the nephrocystin/nephrocystin-4 complex and subcellular localization of nephrocystin-4 to primary cilia and centrosomes. **Human Molecular Genetics**, 14 (5): 645–656
Nakajima, Y., Kiyonari, H., Mukumoto, Y., *et al*. (2018) The Inv compartment of renal cilia is an intraciliary signal-activating center to phosphorylate ANKS6. **Kidney International**, 93 (5): 1108–1117
Nakel, K., Bonneau, F., Eckmann, C.R., *et al*. (2010) Structural basis for the activation of the C. elegans noncanonical cytoplasmic poly(A)-polymerase GLD-2 by GLD-3. **RNA**, 112 (28): 8614–19
Nakel, K., Bonneau, F., Eckmann, C.R., *et al*. (2015) Structural basis for the activation of the C. elegans noncanonical cytoplasmic poly(A)-polymerase GLD-2 by GLD-3. **PNAS**, 112 (28): 8614–19
Natoli, T. a, Smith, L. a, Rogers, K. a, *et al*. (2010) Inhibition of glucosylceramide accumulation results in effective blockade of polycystic kidney disease in mouse models. **Nature medicine**, 16 (7): 788–792
Nauli, S.M., Alenghat, F.J., Luo, Y., *et al*. (2003) Polycystins 1 and 2 mediate mechanosensation in the primary cilium of kidney cells. **Nature Genetics**, 33 (2): 129–137
Olbrich, H., Fliegauf, M., Hoefele, J., *et al*. (2003) Mutations in a novel gene, NPHP3, cause adolescent nephronophthisis, tapeto-retinal degeneration and hepatic fibrosis. **Nature Genetics**, 34 (4): 455–459
Ong, A.C.M. and Harris, P.C. (2015) A polycystin-centric view of cyst formation and disease: the polycystins revisited. **Kidney International advance online publication**, 22
Park, S., Blaser, S., Marchal, M.A., *et al*. (2016) A gradient of maternal Bicaudal-C controls vertebrate embryogenesis via translational repression of mRNAs encoding cell fate regulators. **Development (Cambridge, England)**, 143 (5): 864–71
Parker, E., Newby, L.J., Sharpe, C.C., *et al*. (2007) Hyperproliferation of PKD1 cystic cells is induced by insulin-like growth factor-1 activation of the Ras/Raf signalling system. **Kidney international**, 72 (2): 157–65

Patel, V., Li, L., Cobo-Stark, P., *et al*. (2008) Acute kidney injury and aberrant planar cell polarity induce cyst formation in mice lacking renal cilia. **Human Molecular Genetics**, 17 (11): 1578–1590
Paul, B.M., Consugar, M.B., Lee, M.R., *et al*. (2014) Evidence of a third ADPKD locus is not supported by re-analysis of designated PKD3 families. **Kidney International**, 85: 383–392
Petri, E.T., Celic, A., Kennedy, S.D., *et al*. (2010) Structure of the EF-hand domain of polycystin-2 suggests a mechanism for Ca2+-dependent regulation of polycystin-2 channel activity. **Proceedings of the National Academy of Sciences of the United States of America**, 107 (20): 9176–81
Piazzon, N., Maisonneuve, C., Guilleret, I., *et al*. (2012) Bicc1 links the regulation of cAMP signaling in polycystic kidneys to microRNA-induced gene silencing. **Journal of Molecular Cell Biology**, 4: 398–408
Piovesan, D., Tabaro, F., Paladin, L., *et al*. (2018) MobiDB 3.0: more annotations for intrinsic disorder, conformational diversity and interactions in proteins. **Nucleic Acids Research**, 46 (D1): D471–D476
Ramachandran, H., Engel, C., Müller, B., *et al*. (2015) Anks3 alters the sub-cellular localization of the Nek7 kinase. **Biochemical and Biophysical Research Communications**, 464 (3): 901–907
Rehman, S., Gladman, J.T., Periasamy, A., *et al*. (2014) Development of an AP-FRET based analysis for characterizing RNA-protein interactions in myotonic dystrophy (DM1). **PloS one**, 9 (4): e95957
Roitbak, T., Ward, C.J., Harris, P.C., *et al*. (2004) A Polycystin-1 Multiprotein Complex Is Disrupted in Polycystic Kidney Disease Cells. **Molecular Biology of the Cell**, 15: 1334–1346
Rossetti, S., Consugar, M.B., Chapman, A.B., *et al*. (2007) Comprehensive molecular diagnostics in autosomal dominant polycystic kidney disease. **Journal of the American Society of Nephrology : JASN**, 18 (7): 2143–60
Rothé, B., Leal-Esteban, L., Bernet, F., *et al*. (2015) Bicc1 Polymerization Regulates the Localization and Silencing of Bound mRNA. **Molecular and Cellular Biology**, 35 (19): 3339–53
Rothé, B., Leettola, C.N., Leal-Esteban, L., *et al*. (2018) Crystal Structure of Bicc1 SAM Polymer and Mapping of Interactions between the Ciliopathy-Associated Proteins Bicc1, ANKS3, and ANKS6. **Structure**, 26 (2): 209-224.e6
Saffman, E.E., Styhler, S., Rother, K., *et al*. (1998) Premature Translation of oskar in Oocytes Lacking the RNA-Binding Protein Bicaudal-C. **Molecular and Cellular Biology**, 18 (8): 4855–62
Schäfer, K., Gretz, N., Bader, M., *et al*. (1994) Characterization of the Han:SPRD rat model for hereditary polycystic kidney disease. **Kidney international**, 46 (1): 134–52
Shillingford, J.M., Murcia, N.S., Larson, C.H., *et al*. (2006) The mTOR pathway is regulated by polycystin-1, and its inhibition reverses renal cystogenesis in polycystic kidney disease. **Proceedings of the National Academy of Sciences of the United States of America**, 103 (14): 5466–71
Simons, M., Gloy, J., Ganner, A., *et al*. (2005) Inversin, the gene product mutated in nephronophthisis type II, functions as a molecular switch between Wnt signaling pathways. **Nature genetics**, 37 (5): 537–43
Siomi, H., Matunis, M.J., Michael, W.M., *et al*. (1993) The pre-mRNA binding K protein contains a novel evolutionary conserved motif. **Nucleic Acids Research**, 21 (5): 1193–1198
Sivasubramaniam, S., Sun, X., Pan, Y.-R., *et al*. (2008) Cep164 is a mediator

protein required for the maintenance of genomic stability through modulation of MDC1, RPA, and CHK1. **Genes & Development**, 22 (5): 587–600
Snee, M.J. and Macdonald, P.M. (2009) Bicaudal C and trailer hitch have similar roles in gurken mRNA localization and cytoskeletal organization. **Developmental Biology**, 328: 434–444
Srivastava, S., Molinari, E., Raman, S., *et al*. (2018) Many Genes—One Disease? Genetics of Nephronophthisis (NPHP) and NPHP-Associated Disorders. **Frontiers in Pediatrics**, 5: 287
Stagner, E.E., Bouvrette, D.J., Cheng, J., *et al*. (2009) The polycystic kidney disease-related proteins Bicc1 and SamCystin interact. **Biochemical and Biophysical Research Communications**, 383 (1): 16–21
Stengel, B. (2003) Trends in the incidence of renal replacement therapy for end-stage renal disease in Europe, 1990-1999. **Nephrology Dialysis Transplantation**, 18 (9): 1824–1833
Streets, A.J., Moon, D.J., Kane, M.E., *et al*. (2006) Identification of an N-terminal glycogen synthase kinase 3 phosphorylation site which regulates the functional localization of polycystin-2 in vivo and in vitro. **Human molecular genetics**, 15 (9): 1465–73
Streets, A.J., Wessely, O., Peters, D.J.M., *et al*. (2013) Hyperphosphorylation of polycystin-2 at a critical residue in disease reveals an essential role for polycystin-1-regulated dephosphorylation. **Human molecular genetics**, 22 (10): 1924–39
Strein, C., Alleaume, A.-M., Rothbauer, U., *et al*. (2014) A versatile assay for RNA-binding proteins in living cells. **RNA (New York, N.Y.)**, 20 (5): 721–31
Su, X., Wu, M., Yao, G., *et al*. (2015) Regulation of polycystin-1 ciliary trafficking by motifs at its C-terminus and polycystin-2 but not by cleavage at the GPS site. **Journal of Cell Science**, 128 (22): 4063–4073
Sullivan, L.P., Wallace, D.P. and Grantham, J.J. (1998) Epithelial transport in polycystic kidney disease. **Physiological Reviews**. 78 (4) pp. 1165–1191
Swenson-Fields, K.I., Vivian, C.J., Salah, S.M., *et al*. (2013) Macrophages promote polycystic kidney disease progression HHS Public Access. **Kidney Int**, 83446 (5): 855–864
Takakura, A., Nelson, E.A., Haque, N., *et al*. (2011) Pyrimethamine inhibits adult polycystic kidney disease by modulating STAT signaling pathways. **Human molecular genetics**, 20 (21): 4143–54
Talbot, J.J., Shillingford, J.M., Vasanth, S., *et al*. (2011) Polycystin-1 regulates STAT activity by a dual mechanism. **Proceedings of the National Academy of Sciences**, 108 (19): 7985–7990
Tilley, F.C., Gallon, M., Luo, C., *et al*. (2018) Retromer associates with the cytoplasmic amino-terminus of polycystin-2. **Journal of Cell Science**, 131 (11): jcs211342
Torres, V.E., Harris, P.C. and Pirson, Y. (2007) Autosomal dominant polycystic kidney disease. **Lancet**, 369: 1287–1301
Tran, U., Pickney, L.M., Özpolat, B.D., *et al*. (2007) Xenopus Bicaudal-C is required for the differentiation of the amphibian pronephros. **Developmental Biology**, 307: 152–164
Tran, U., Zakin, L., Schweickert, A., *et al*. (2010) The RNA-binding protein bicaudal C regulates polycystin 2 in the kidney by antagonizing miR-17 activity. **Development**, 137: 1107–16
Trudel, M., Lanoix, J., Barisoni, L., *et al*. (1997) C-MYC-induced Apoptosis in Polycystic Kidney Disease Is Bcl-2 and p53 Independent. **Journal of**

Experimental Medicine, 186 (11): 1873–1884
Wakil, S.J. (1989) Fatty acid synthase, a proficient multifunctional enzyme. **Biochemistry**, 28 (11): 4523–30
Wallace, D.P., Grantham, J.J. and Sullivan, L.P. (1996) Chloride and fluid secretion by cultured human polycystic kidney cells. **Kidney international**, 50: 1327–1336
Wang, X., Ward, C.J., Harris, P.C., *et al*. (2010) Cyclic nucleotide signaling in polycystic kidney disease. **Kidney international**, 77 (2): 129–40
Weimbs, T., Olsan, E.E. and Talbot, J.J. (2013) Regulation of STATs by polycystin-1 and their role in polycystic kidney disease. **JAK-STAT**, 2 (2): e23650
Wells, S.E., Hillner, P.E., Vale, R.D., *et al*. (1998) Circularization of mRNA by eukaryotic translation initiation factors. **Molecular cell**, 2 (1): 135–40
Wessely, O. and De Robertis, E.M. (2000) The Xenopus homologue of Bicaudal-C is a localized maternal mRNA that can induce endoderm formation. **Development**, 127: 2053–62
What are cysts? (2019). [online]. Available from: https://pkdcure.org/what-is-pkd/adpkd/what-are-cysts/ [Accessed 25 May 2019]
Wilkins, S.E., Karttunen, S., Hampton-Smith, R.J., *et al*. (2012) Factor inhibiting HIF (FIH) recognizes distinct molecular features within hypoxia-inducible factor-α (HIF-α) versus ankyrin repeat substrates. **The Journal of biological chemistry**, 287 (12): 8769–81
Xu, G.M., González-Perrett, S., Essafi, M., *et al*. (2003) Polycystin-1 activates and stabilizes the polycystin-2 channel. **Journal of Biological Chemistry**, 278 (3): 1457–1462
Xu, G.M., Sikaneta, T., Sullivan, B.M., *et al*. (2001) Polycystin-1 Interacts with Intermediate Filaments. **Journal of Biological Chemistry**, 276 (49): 46544–46552
Xu, Y., Streets, A.J., Hounslow, A.M., *et al*. (2016) The Polycystin-1, Lipoxygenase, and -Toxin Domain Regulates Polycystin-1 Trafficking. **Journal of the American Society of Nephrology**, 27 (4): 1159–1173
Yakulov, T.A., Yasunaga, T., Ramachandran, H., *et al*. (2015) Anks3 interacts with nephronophthisis proteins and is required for normal renal development. **Kidney International**, 87 (6): 1191–1200
Yamaguchi, T., Hempson, S.J., Reif, G.A., *et al*. (2006) Calcium restores a normal proliferation phenotype in human polycystic kidney disease epithelial cells. **Journal of the American Society of Nephrology : JASN**, 17 (1): 178–87
Yamaguchi, T., Nagao, S., Wallace, D.P., *et al*. (2003) Cyclic AMP activates B-Raf and ERK in cyst epithelial cells from autosomal-dominant polycystic kidneys. **Kidney international**, 63 (6): 1983–94
Yoder, B.K. (2002) The Polycystic Kidney Disease Proteins, Polycystin-1, Polycystin-2, Polaris, and Cystin, Are Co-Localized in Renal Cilia. **Journal of the American Society of Nephrology**, 13 (10): 2508–2516
Yokoyama, T., Copeland, N., Jenkins, N., *et al*. (1993) Science. **Science**, 193 (4250): 317–319
Yu, S., Hackmann, K., Gao, J., *et al*. (2007) Essential role of cleavage of Polycystin-1 at G protein-coupled receptor proteolytic site for kidney tubular structure. **Proceedings of the National Academy of Sciences of the United States of America**, 104 (47): 18688–93
Zalli, D., Bayliss, R. and Fry, A.M. (2012) The Nek8 protein kinase, mutated in

the human cystic kidney disease nephronophthisis, is both activated and degraded during ciliogenesis. **Human Molecular Genetics**, 21 (5): 1155–1171
Zhang, B.-X., Huang, H.-J., Yu, B., *et al*. (2015) Bicaudal-C plays a vital role in oogenesis in Nilaparvata lugens (Hemiptera: Delphacidae). **Journal Of Insect Physiology**, 79: 19–26
Zhang, P., Luo, Y., Chasan, B., *et al*. (2009) The multimeric structure of polycystin-2 (TRPP2): structural-functional correlates of homo- and hetero-multimers with TRPC1. **Human molecular genetics**, 18 (7): 1238–51